AD 758 978

LIBRARY
TECHNICAL REPORT SECTION
NAVAL POSTGRADUATE SCHOOL
MONTEREY, CALIFORNIA 93940

AGARD-LS-63

AGARD

ADVISORY GROUP FOR AEROSPACE RESEARCH & DEVELOPMENT

7 RUE ANCELLE 92200 NEUILLY SUR SEINE FRANCE

AGARD LECTURE SERIES No. 63

on

Helicopter Aerodynamics and Dynamics

NORTH ATLANTIC TREATY ORGANIZATION



DISTRIBUTION AND AVAILABILITY
ON BACK COVER

AGARD-LS-63

NORTH ATLANTIC TREATY ORGANIZATION

ADVISORY GROUP FOR AEROSPACE RESEARCH AND DEVELOPMENT

(ORGANISATION DU TRAITE DE L'ATLANTIQUE NORD)

AGARD Lecture Series No.63

HELICOPTER AERODYNAMICS AND DYNAMICS

The material in this book has been assembled in support of a Lecture Series presented at the von Kármán Institute (Brussels) from 2–6 April 1973, sponsored by the von Kármán Institute, and the Fluid Dynamics Panel and Consultant and Exchange Programme of AGARD.

THE MISSION OF AGARD

The mission of AGARD is to bring together the leading personalities of the NATO nations in the fields of science and technology relating to aerospace for the following purposes:

- Exchanging of scientific and technical information;
- Continuously stimulating advances in the aerospace sciences relevant to strengthening the common defence posture;
- Improving the co-operation among member nations in aerospace research and development;
- Providing scientific and technical advice and assistance to the North Atlantic Military Committee in the field of aerospace research and development;
- Rendering scientific and technical assistance, as requested, to other NATO bodies and to member nations in connection with research and development problems in the aerospace field;
- Providing assistance to member nations for the purpose of increasing their scientific and technical potential;
- Recommending effective ways for the member nations to use their research and development capabilities for the common benefit of the NATO community.

The highest authority within AGARD is the National Delegates Board consisting of officially appointed senior representatives from each member nation. The mission of AGARD is carried out through the Panels which are composed of experts appointed by the National Delegates, the Consultant and Exchange Program and the Aerospace Applications Studies Program. The results of AGARD work are reported to the member nations and the NATO Authorities through the AGARD series of publications of which this is one.

Participation in AGARD activities is by invitation only and is normally limited to citizens of the NATO nations.

The material in this publication has been reproduced
directly from copy supplied by AGARD or the author.

Published March 1973

533.661

Printed by Technical Editing and Reproduction Ltd
Harford House, 7–9 Charlotte St, London. W1P 1HD

PREFACE

This lecture series has been conceived to provide an intensive overview of the role of aerodynamics and dynamics in helicopter development from the fundamental methods and principles, through conceptual design to flight test and proof-of-concept. Few textbooks exist in this field, and this compilation of lectures provides perhaps the only publication to accomplish this objective. The lecture series is co-sponsored by the Fluid Dynamics Panel and the Consultant and Exchange Program of AGARD, and the von Kármán Institute for Fluid Dynamics. These organizations have carefully considered the timeliness and content of this series. It has been structured to meet what is considered to be a deficiency in the literature on this subject. The sponsoring agencies and the participating lecturers sincerely desire that their efforts will accomplish the purposes and intents which have been defined.

LIST OF SPEAKERS

Lecture Series Director Mr Paul F.Yaggy
Director
US Army Air Mobility Research and Development Center
Moffett Field
California 94035, USA

Mr R.Dat
Adjoint au Directeur Scientifique des Structures
ONERA
29, av. de la Division Leclerc
92329 Châtillon, France

Mr P.Fabre
Division Helicoptères
SNIAS
Usine de Marignane
B.P. 888
13221 Marseille CEDEX 1
France

Mr Franklin D.Harris
Manager, V/STOL Wind Tunnel
Mail Stop: P38-07
The Boeing Company
Vertol Division
P.O. Box 16858
Philadelphia, Pa. 19142, USA

Mr H.Huber
Messerschmitt-Bölkow-Blohm GmbH
Helicopter Division
8 München 80
Postfach 80 11 40
Germany

Dr M.V.Lowson
Reader in Fluid Mechanics
Department of Transport Technology
University of Technology
Loughborough
Leicestershire LE 11 3TU, UK

Mr K.T.McKenzie
Chief Technician
Westland Helicopters Ltd
Yeovil, Somerset, UK

Mr G.Reichert
Messerschmitt-Bölkow-Blohm GmbH
Helicopter Division
8 München 80
Postfach 80 11 40
Germany

Dr W.Z.Stepniewski
The Boeing Company
Vertol Division
P.O. Box 16858
Philadelphia, Pa. 19142, USA

CONTENTS

	Page
PREFACE	iii
LIST OF SPEAKERS	iv
	Reference
THE ROLE OF AERODYNAMICS AND DYNAMICS IN MILITARY AND CIVILIAN APPLICATIONS TO ROTARY WING AIRCRAFT by P.F.Yaggy	1
BASIC AERODYNAMICS AND PERFORMANCE OF THE HELICOPTER by W.Z.Stepniewski	2
BASIC DYNAMICS OF ROTORS: CONTROL AND STABILITY OF ROTARY WING AIRCRAFT: AERODYNAMICS AND DYNAMICS OF ADVANCED ROTARY-WING CONFIGURATIONS by G.Reichert	3
AEROELASTICITY OF ROTARY WING AIRCRAFT by R.Dat	4
HELICOPTER NOISE: ANALYSIS – PREDICTION AND METHODS OF REDUCTION by M.V.Lowson	5
PROBLEMES DE TRAINEE DES APPAREILS A VOILURES TOURNANTES par P.Fabre (Including English Translation)	6
AERODYNAMIC AND DYNAMIC ROTARY WING MODEL TESTING IN WIND TUNNELS AND OTHER FACILITIES by F.D.Harris	7
PARAMETRIC TRENDS AND OPTIMIZATION – PRELIMINARY SELECTION OF CONFIGURATION – PROTOTYPE DESIGN AND MANUFACTURE by H.Huber	8
FLIGHT TESTING FOR PERFORMANCE AND FLYING QUALITIES by K.T.McKenzie	9

THE ROLE OF AERODYNAMICS AND DYNAMICS IN MILITARY AND CIVILIAN APPLICATIONS OF ROTARY WING AIRCRAFT

by

Paul F. Yaggy
U.S. Army Air Mobility R&D Laboratory
Ames Research Center
Moffett Field, California 94035
USA

1.0 INTRODUCTION

Rotary wing aircraft have found increasingly greater applications in recent years in fulfilling both military and civil requirements for air mobility. Before we address the specific role of aerodynamics and dynamics in the design and development of these vehicles, it will be worthwhile to define these requirements -- past, present, and future. In so doing, we will identify desired performance and operational capabilities which establish the criteria to be met, not only by aerodynamics and dynamics, but by the other technologies also involved in the successful design of rotary wing aircraft. In this lecture series, however, we shall content ourselves with addressing in detail only the role of aerodynamics and dynamics.

We shall deal only briefly with the past. It is well known that prior to 1930, the helicopter and other rotary wing derivatives were viewed as oddities which could perform the unique function of vertical flight, but for which there appeared to be little practical utilization. In those early days, such men an Sir George Cayley, W. H. Phillips, Enrico Forlanini, and Thomas Edison were well-known pioneers. Paul Cornu of France constructed the first rotary wing machine to carry a pilot aloft. However, it never flew untethered. The period of 1908 to 1929 was dominated by the Berliners, father and son, who built several unique vehicles and did fly untethered. Interestingly enough, they flew both a rigid or hingeless rotor and built the predecessor of the tilt rotor concept using tilting rotors and fixed wings.

Although other well-known figures in the aeronautical world such as von Karman, Sikorsky, Pescara, de Bothezat, and von Baumhauer were active in the field, it was the pivotal effort of Juan de la Cierva in introducing the hinged rotor concept for relief of the high stresses due to cyclic loads that made vertical flight actually achievable. While Cierva did not fully achieve vertical flight in his "autogiro", this work did lay the groundwork by providing the knowledge and technology necessary for subsequent practical helicopter flight.

Work advanced rapidly in the 1930's in helicopter technology. By the end of that decade, helicopter flight had been successfully achieved. However, it took the impetus of World War II to spur development both in the United States and in Germany which made the helicopter a practical device. By the late 1940's, the general pattern of helicopter-type aircraft had been formulated, and most of the current configurations had been given serious consideration by the 1950's. These included single rotors, tandem rotors, coaxial rotors, shaft-driven and tip-driven rotors, side-by-side rotors, and the compounded rotor system with auxiliary propulsion and/or wings.

In the past, the helicopter has succeeded as an operational vehicle because no other aircraft, no matter how simple or inexpensive, has been able to compete with it in the performance of the peculiar tasks associated with vertical flight and efficient hover. Presently, the helicopter is used in operational procedures which take advantage of characteristics other than the ability to hover. The low downwash produced by the slowly turning large rotors has important implications in operating over environments where injestion due to recirculation can occur from such soil characteristics as sand and gravel, and where high downwash energies are detrimental to personnel or materiel in the operational area. The use of helicopters in great quantities, particularly in military missions, demonstrates that its mission effectiveness is worth the increase in cost because it can do something which no other aircraft can do with comparable efficiency. The utilization of the helicopter in commercial applications has been somewhat more restricted because of its cost effectiveness, which is inferior to that of fixed wing aircraft on medium stage lengths. However, the increased emphasis on short stage lengths has resulted in several recommendations by study groups to develop rotary wing aircraft capable of more efficient operation to take advantage of the unique features of vertical flight.

It is interesting to note that though a significant amount of work has taken place over the years in other concepts of VTOL aircraft, there is yet only one operational VTOL other than a rotary wing or a rotary wing derivative; this being the P-1157 Harrier direct lift fighter produced in the UK. Most applications have been pure helicopters, although in recent times efforts have been made to introduce compounded systems. Currently in the US, a tilt rotor, a rotary wing derivative in a pure sense, is being brought to the stage of demonstration of technology for potential application. This concept has been considered favorably for both military and civil application. Its unique feature is the elimination of the necessity to drive the rotor horizontally through the air which results in many complicated problems to be discussed later and which place serious limitations on hover flight efficiency due to design compromise to attain reasonable cruise efficiency.

The present utilization of helicopters finds many and varied uses. In the military role, we find helicopters employed in such tasks as light observation, light tactical transport, medium transport, armed escort, antisubmarine warfare, air/sea rescue, vertical replenishment, in-shore replenishment, heavy lift, and general utility. Examples of civil uses are short haul transportation, police patrol, aerial surveys, aerial spraying for agriculture, replenishment and support of off shore stations, aerial crane for construction, and heavy lift. For these many uses, the helicopter configuration is by no means stabilized. New technologies are continually under development such as compounds, slowed and stopped rotors (trailed or retracted), and tilt rotors. This strong interest in the rotary wing as a continuing means of both military and civilian transport is a clear indication of the realization of its utility and potential.

Thus in summary, the unique vehicles employing rotary wings which were considered as oddities of the past, have become in the present utilitarian vehicles with discreet and distinct missions to perform. Although future application appears to be assured, it is essential that a more effective and efficient machine be developed. The many unique concepts which are being pursued indicate that a strong interest exists in the future application of rotary wing aircraft. It is well for us now to examine the requirements for such vehicles in these areas of application. For this purpose, we shall identify rotary wing aircraft as those using rotating wings, unshrouded and, arbitrarily, we shall determine they shall have disc loadings of 20 pounds per square foot or less.

2.0 REQUIREMENTS

2.1 Desired Capabilities

The first and foremost capability desired of rotorcraft is that in support of its unique mission, vertical flight. It is important that the rotary wing aircraft be capable of efficient and controllable hover and vertical flight. Efficiency is imperative to permit long hover times without compromising mission accomplishment and economy. Many of the more recent projections of application have emphasized the matter of controlled hover and vertical flight to a greater degree because of the desire for precise placement of externally carried loads and operation in confined terminal areas. It is therefore imperative that not only should the vehicle be stable in the hover mode, but that it be sufficiently responsive for fine accuracy in control. These requirements sometimes run counter one to another, and challenge the designer's capabilities. In particular, the concept of heavy lift vehicles emphasizes this area.

The concept of using the helicoper or rotary wing aircraft as a civil transport demands not only a stable aircraft, but also an aircraft with a comfortable ride quality. The oscillating loads of the rotary wing must be isolated from transmission to the fuselage, and a proper level of gust response in hover must be assured.

Given a vehicle which will provide efficient performance in hover, it is also necessary that the vehicle be able to transition smoothly and to perform efficiently in the cruise mode. Not only are the ride quality and performance important, the vehicle must be capable of maneuvering in response to the peculiarities of its mission. These range from the high maneuver rates required of military gunship applications, to the precise maneuvering for heavy lifts and for operation in confined airspace.

Assuming that all of the foregoing conditions are met, one of the strongest requirements, if the rotary wing aircraft is to become competitive with its fixed-wing counterparts, is that the vehicle perform in a reliable fashion with minimum maintenance requirements. The helicopter has long been plagued with short-life components requiring frequent inspection. Mean time between failure and mean time between repair or overhaul have been extremely short. Thus, cost factors are high. If the rotary wing is to realize its full application, not only must it be made more reliable and maintainable, but fatigue failure modes must be identified and made fail-safe, and detection of incipient or impending failure must be detected by simplified diagnostic methods rather than establishing inspection and removal intervals by statistical analysis of shortest time to anticipated failure. In short, the reliability and maintainability levels of fixed-wing configurations must be approached.

Finally, one must consider requirements for increased survivability. Though one often thinks of survivability in terms of vulnerability as associated with military applications, it is also important to consider survivability for the civil application as well. For military application, vulnerability to enemy action is of course continually expected. The design must consider maximum capability to resist such action and survive. For the civil application, although one would hope never to face such circumstances, survivability in crash situations is imperative. The rotary wing aircraft has the unique feature of autorotation which increases its survivability potential in many situations. However, there are adverse circumstances in which even this feature is compromised. Whereas we can dismiss the situation in which there is no survivability potential, there is an intermediary field where proper design can improve survivability potential. It is most important, however, to recognize that adequate autorotational capability is highly dependent upon proper aerodynamics and dynamics built into the rotor system. Thus, survivability of rotorcraft is directly dependent upon an adequate comprehension of its aerodynamics and dynamics.

With this statement of requirements in general as a background, let us now turn our attention to a more specific definition of the limiting problems which are associated with the various technologies pertaining to the applications and requirements of aircraft systems utilizing rotary wings.

2.2 Performance

In our definition of rotorcraft, we limited our consideration to those systems having disc loadings of 20 pounds per square foot or less. Since the unique capability of rotary wing aircraft is vertical flight, it is well to ascertain a comprehension of the impact of disc loading on the efficiency of vertical flight. In Fig. 1 this efficiency is shown as a function of equivalent disc loading for both a figure of merit of 1.0, and a figure of merit of 0.8 which represents the current upper-bound that technology will afford. It becomes very clear from even a quick perusal of this figure why we have limited ourselves to disc loadings of 20 pounds psf, or less (the upper number being representative of tilt rotor, stopped/stowed rotor and circulation controlled rotors). It is true, of course, in a pure sense that all the vehicles represented are rotary wings, since the lift in vertical flight in each case is being produced in fact by airfoil sections rotating in a circular path. However, our definition of rotary wing shall stand as we have defined it. In Fig. 2 the impact of disc loading is further emphasized by considering the factor of time in hover. It is clear that the requirement for efficiency with long hover times demands a low disc loading. However, one cannot overlook the impact of the thrust to weight ratio as a function of hovering time as shown in Fig. 3. It becomes increasingly clear why rotorcraft have a distinct advantage for long hover times over other concepts.

It is also clear by examination of Fig. 4 that restrictions in cruise speed result from providing this hover efficiency. Design cruise speed is directly affected if the vehicle is optimized in its concept for long hovering times. Clearly, rotorcraft as we have defined them, find their primary application at cruising speeds of 300 knots or less. Thus, we see that the rotorcraft vehicles we will consider find their optimum performance within rather specifically defined operating regimes, which represent a tradeoff between hover and cruise efficiency depending on mission requirements. An example of such a tradeoff for a tilt rotor aircraft is shown in Fig. 5.

A primary influence on the performance of rotorcraft is the installed power train, including engine and transmission. In recent years, one of the most predominant influences in increasing rotorcraft efficiency has been the improvement in the power train. The conversion from the internal combustion engine to the gas turbine has accounted for much of the improvement which has led to a greater utilization of rotorcraft over the past 20 years; specific weight of engines has been reduced by a factor of 5 and specific fuel consumption by a factor of nearly 2. It is anticipated that there will be continuing improvement in both specific fuel consumption and specific weight, but at a much lower rate. Fig. 6 gives an indication of the effects of turbine inlet temperature and compressor pressure ratio on turbine engine performance. Those are probably the potential areas for further improvement. The advent of improved materials will of course have a significant impact, since increasing temperatures and pressures will overtax the capabilities of current materials. Cooling techniques are being explored, but these lead to complex machinery concepts. Consideration must be continually given to the tradeoffs between complexity and efficiency. Many believe that the time for a reevaluation is at hand and that it is time to search for engine concepts using more simple cycles to effect better total system efficiency and life cycle costs.

When considering the areas of aerodynamics and dynamics, there are two specific considerations affecting performance. These are the rotor performance and the performance of the vehicle itself in terms of the drag associated with the configuration design. There are many factors which affect rotor performance. As an example, Fig. 7 shows the ratio of cruise lift to propulsion efficiency as a function of forward speed. It is clearly indicated here how just the solidity of the helicopter rotor can have a significant influence. The interrelations of these various design features are the subject of later presentations in this lecture series. It is important, however, to recognize that a distinct requirement exists to provide both hover efficiency and cruise efficiency. These are not compatible in the general sense, and must be accommodated in an optimization parametric tradeoff study.

The second area of consideration, namely, that of power required, or in other words, equivalent drag as a function of speed is indicated in Fig. 8. It is clear from this presentation that while the induced horsepower of the rotor system is predominant in hover, as cruise speed is increased parasitic and profile power become predominant. Therefore, design features must minimize such contributing influences as poor fuselage profile, rotor hub/pylon interference drag, other appendages and bulky landing gears.

It is, of course, imperative that the empty weight to gross weight ratio be kept to a minimum if net performance is to be high. The potential for improvement in this area is largely dependent upon technological advance in materials and structural design concepts. Fig. 9 indicates the projected potential to reduce weight fraction. Fig. 10 shows where these gains may be expected to apply, and also indicates that the gain may be accompanied by higher costs at first because of high cost of new materials. Ability to predict weight also needs improvement. The potential is shown in Fig. 11. Some of the greatest gains in performance in the future can be expected from improvements in structures and materials.

In many instances, it is well to consider early in the design of the vehicle what the influences of the various technologies are on performance using a simplified performance model. This is exemplified in Fig. 12. This is a trend chart which is projected to show potential for improvement. It is clearly indicated that for the case considered, improved materials to increase the ratio of gross weight to empty weight will be the predominant influence. This projection is for a heavy lift helicopter. This will not necessarily be the case for all vehicles. However, it is important that consideration be given to such analyses in order to determine which technological improvements can be most effective in realizing performance

goals when designing aircraft. It is imperative that even the researcher in fundamental technical phenomena keep in mind that his work is only as beneficial as it has application. It should not be inferred from this example that improvements in aerodynamics and dynamics of rotary wings generally have little benefit, but it does indicate there is relativity in tradeoff among the various technologies involved in rotorcraft design. It is logical that one should direct his research and development efforts to those aerodynamic and dynamic improvements which are indicated to provide the greatest payoff. For example, in this case little performance gain is indicated for improved lift to drag ratio. Perhaps then one should concentrate on advances in technology to improve reliability by aerodynamic means to reduce oscillating airloads, or to other similar activities.

As we have indicated, there is a distinct requirement for improved performance. Fig. 13 projects improvements which are potentially achievable in the coming years for both L/D for increased aerodynamic efficiency and for increased maximum cruise speed. This figure clearly illustrates the sensitivity of performance parameters to such variables as, in this case, mission parameters. Trend charts such as these can be made to show other gains in rotor technology. The aerodynamic and dynamic problems associated with these gains and the potential for improvement will be assessed in more detail by other lecturers in this series.

Before we leave this field of performance, it might be well to detail some specific characteristics of the rotor which contribute to the performance problem. The ability to attain superior rotor performance is dependent upon an adequate definition of the flow field in which the rotor blades operate and the design of optimum blade sections to be more efficient under these conditions. In hover, problems arise predominantly as a result of the interactions between blade vortex fields shed by preceding blades and the blade which follows. In addition, the three-dimensional aspects of flow near the tip where the predominant loads are carried, require special treatment. Blades with relatively large twist are required to account for the varying velocity over the airfoil sections at the various spanwise stations along the blade. The ability to adequately model these fields and to produce airfoil sections which operate efficiently is a challenge. However, as the rotor moves into forward flight, the challenge is compounded as illustrated in Fig. 14. Now the advancing blade, which is subjected to the additive velocities of rotation plus advance, approaches or enters compressible flow. The retreating blade, whose effective velocity has been reduced by the velocity of advance, must be operated at very high angles of attack to provide the necessary lift to maintain balance of the aircraft and consequently enters the region of incipient stall. As aircraft speed or weight is increased, the retreating blade exceeds the stall limit and rapid increases in blade loads, control loads, and rotor horsepower occur. Attempts to predict these effects by using steady flow airfoil characteristics in strip theory analyses have been unsuccessful. Classic rotor theories are incapable of predicting overall rotor performance characteristics in stall. Although current efforts to improve the performance of rotary wing aircraft have resulted in an increased interest in understanding the role of viscous effects, a formidable challenge remains. The status of the situation will be a subject of discussion later by other lecturers in the series. Suffice it now to say that the aerodynamic and dynamic problems associated with the advance of a rotary wing at high speed creates severe limitations upon its performance. Thus, an important role accrues to the subject in the potential improvement of rotary wings.

2.3 Maneuver and Handling Qualities

It is essential that a rotary wing vehicle be able to maneuver as has been pointed out earlier. As the aircraft penetrates the region of high speed forward flight it is imperative that it not only be capable of lateral and longitudinal balance, but a sufficient margin must remain to induce angular moments for maneuver. The problems noted above for the retreating and advancing blades require the blade elements to generate nearly their maximum lift just to balance the aircraft. Thus, the maintenance of adequate maneuver margins is a difficulty. In addition, speed stability margins are compromised with excessive stick migration. Rotor stability is compromised, since the rotor becomes excessively susceptible to the influence of gusts. All of these factors result in major restrictions on available flight corridors. These same factors are important in the consideration of autorotation, particularly the entrance to autorotation in an emergency situation. Operation near stall conditions, of course, are a distinct compromise on the handling qualities of the vehicle. Oftentimes, unexpected penetration into regimes where stall exists can be catastrophic due to the unexpected application of moments to the vehicle which can result in pilot induced oscillations in a divergent sense.

It is clear that if the requirements for a rotary wing vehicle operating through the complete flight envelope with adequate maneuver margins and with handling qualities comparable to fixed wing aircraft are to be realized, the role of aerodynamics and dynamics is vital. The ability to provide these handling qualities, in particular, is dependent upon coping with the many aspects of a highly dynamic vehicle system which oftentimes has nonlinear characteristics. The ability to linearize the presentation of the control problem to the pilot frequently becomes a subject of parametric tradeoffs. This subject will be dealt with later by other lecturers in this series.

2.4 Dynamics and Stability and Control

In consideration of the dynamics of the rotorcraft and its influence on stability and control, one can gain some appreciation for the difficulties by examining the pictorial model of Fig. 15. In no way should this figure be considered as an exaggeration. It is purely representative of the many degrees of freedom and structural modes which exist within a typical rotorcraft. The requirement to deal with these problems, not only singularly but in their interactive modes,

taxes the full capability of both researcher and designer. The requirements placed upon a rotorcraft are that it should have stability and control characteristics at least comparable to those of fixed wing vehicles. The rotary wing itself inherently does not have this capability. The primary compromise is that due to the cyclic loads imposed upon a rotor system. Particularly in forward flight the cycles can oftentimes enter regions of nonlinearity. When these nonlinear regions are penetrated, the customary classical methods no longer apply. Thus, the representation of such systems in a mathematical sense, and their formulation for design purposes is extremely complicated. The problems of the advancing and retreating blades in nonlinear regions were described previously. The interference of the rotor wake and blade passage also was discussed previously. In addition, problems of stability arise from the various dynamic modes induced within the structure itself. It is important to note that whereas one could design a system which was statically stable, its dynamic stability might be less than adequate. For example, rotor blade stall is a dynamic phenomenon associated with the rapidly changing angle of attack which characterizes a helicopter rotor blade as it traverses the rotor disc. Particularly on the retreating side of the disc at high advance ratios, quasistatic stall theory fails to predict rotor lift for a given pitch control, shaft tilt and advance ratio. Not only does the nonsteady penetration of stall alter the lift characteristics of the airfoil, it also alters the moment characteristics as indicated in Fig. 16. Negative aerodynamic damping oftentimes occurs and results in excessive torsional loads feeding into the control system. Thus, both the aerodynamics and dynamics of the design of the rotor have an important impact on maintaining vehicle stability and control. The ability to maintain the desired steady flight platform for the applications described previously demands significant improvement over the current capability which now exists to predict and to fabricate systems which are dynamically stable and controllable.

As mentioned earlier, the rotor system inherently is a system of low stability. Oftentimes it has been found advantageous to install stability augmenting systems on rotorcraft to give better handling qualities and to improve controllability. It is likely that the need for precise maneuvering will also require such systems. Design of these systems and the ability to project their characteristics theoretically is an important field of interest which must be developed further. In such a case, the theory must adequately account for system dynamics if the system design is to be adequate.

The difficulty in maintaining adequate stability and good dynamic characteristics with high controllability in forward flight has given rise to the evolution of many rather unique concepts. Slowing the rotor obviously will reduce the compressibility effects upon the advancing tip. However, it may compound the problems on the retreating side. Stopping the rotor and stowing it eliminates the problem entirely, but creates a considerable degree of complexity and increased weight. Tilting the rotor to axial flight in the cruise mode offers high potential which is currently being investigated. Other unique concepts, such as the Sikorsky Advancing Blade Concept, unload the rotor on the retreating side and thus delay the onset of the stall problem. It is likely that the most significant advance in providing more cost effective and efficient systems for high cruise speed flight with adequate dynamics and stability and control will be a derivative of such investigations as these. The knowledgeable approach to these endeavors will be greatly dependent upon the skills of the aerodynamicist and the dynamicist in providing the parameters enabling knowledgeable tradeoff and effective utilization.

2.5 Airloads, Aeroelasticity, and Mechanical Instabilities

Along with the consideration of dynamics, stability and control, we must consider the subjects of airloads, aeroelasticity, and mechanical instabilities. These are the driving and reactive influences which create the dynamic situation. For example, a structural instability excited by an oscillating airload could result in an unsteady, and possibly divergent dynamic situation. As a case in point, coupling of structural modes in response to aerodynamic excitation is characteristic of the air resonance phenomenon. Whereas the problems of mechanical instability are from the structures and materials realm, one cannot ignore the direct coupling with aerodynamics which generate the driving force. It is important that it be recognized that the aerodynamicist and the aeroelastician must work closely together in pursuit of their technologies to assure adequate design.

Unsteady airloads result from many phenomena including, for example, blade stalling, stall flutter, tip vortex/blade interaction, and others which generate both periodic and nonperiodic loads. The ability to predict these airloads in the past has been less than adequate to meet design requirements. An indication of current prediction error and the potential for improvement is shown in Fig. 17. Note that currently, the error is extremely high in predicting both steady-state loads and transient loads. This is the direct result of the inability to properly represent the aerodynamic and dynamic conditions in mathematical model formulation. The requirements for good design to meet the vehicle application requirements are highly dependent upon realizing the improvement goals which are indicated. It is important that mechanisms be established for alleviating oscillating airloads. Whereas vibration absorbers can be utilized, a more effective mechanism is to reduce the driving force at its source. A better comprehension of the aerodynamics of rotating wings, particularly near the stall, is imperative if these goals are to be realized.

Although outside the scope of this lecture series, it is well to appreciate the major considerations of structural dynamics which couple to the problems of aeroelasticity and mechanical instability. These include response characteristics of the elastic system, fatigue and fracture problems of materials, stress and vibration levels, and adequate description of the many degrees of freedom, including the instabilities that may occur from both singular and coupled modes of oscillation. The interdependence of these various factors and airloads will be discussed more fully in Session 4 of this lecture series.

2.6 Noise

Although rotorcraft are not particularly noisy in the sense of their maximum level of decibels, rotorcraft have signatures which are characteristic in nature. Furthermore, because of the desire to use the vertical lift capability in military uses for close support, and in civil uses near population centers, noise becomes an important consideration. It is urgent that for military uses the noise level be as low as possible and as nondistinct as possible to minimize detection and to preserve the element of surprise in offensive actions. Aural detectors are often used for sighting of more sophisticated weapons of greater threat. To deny potential enemies the capability of such detection greatly enhances the survivability of the vehicle. Civil applications require that not only the overall decibel level be sufficiently low as to be compatible with the ambient level, but that the characteristic signature be such that it blend with the background noise. It has been ascertained on several occasions that it is the characteristic signature of rotorcraft which is detected rather than the overall noise level and which brings many complaints from the surrounding areas.

It is important in our consideration that we distinguish between the two classifications of noise sources. The first is the aerodynamically generated noise resulting from the passage of the rotor blades through the air. The second is that associated with the power train and structural vibration. It will not be our intent to discuss in any detail the noise levels generated by the power train. These are not aerodynamic or dynamic in nature and are outside of the detail of our consideration. However, it is appropriate to mention that power train noise is an important factor in both passenger comfort and disturbance to the surrounding community.

The source of aerodynamic noise is a subject of considerable effort at this time. It is elemental that the rotating system will generate noise simply because it is a pulsating source. In addition, it is clear that vortex noise will be generated as result of passage of the blades through the air. However, there are characteristic signatures of the rotary wing which result because of aerodynamic situations existing which are not fully comprehended or explained. The high level of impulsive noise generated by some rotors remains yet to be defined. It is speculated that interference between the blade passage and the preceding shed tip vortex may account for some of this effect. In addition, compressibility effects on the advancing blade are also suspect. Regardless of the source, it is essential that it be identified and that the aerodynamicist evolve design techniques which will lessen its impact.

It is important to recognize also that much structural noise which is a matter of great discomfort to pilots and passengers results from pulsating pressure fields impinging on various portions of the rotorcraft structure. Analyses to date have indicated that very high orders of oscillating airloading are involved in the generation of audible noise and these pulsating pressure fields. The only apparent resolution of these problems appears to be through a better comprehension of the aerodynamics and dynamics situations to effect design changes for improvement.

It is important to note that the ability to reduce noise signature levels and characteristics may require tradeoffs in design which affect performance and operating costs. It is extremely important, therefore, that the technologies which are derived in support of this effort not only identify those parameters which are significant in noise reduction, but carefully relate these parameters to the aerodynamic and dynamic parameters which affect performance, controllability, stability, and other factors. It is only in this manner that knowledgeable tradeoffs can be made between these various parameters to optimize the design. Again, it is a fundamental concept that the ultimate goal of effecting efficient design must be considered even at the fundamental levels of generating technology. It is this fundamental issue that often is overlooked and results in efforts being expended in areas of lower priority and lower payoff potential.

The session set aside for discussing noise factors in this series is indeed comprehensive. It relates to the basic mechanisms and the potential for their improvements. It also indicates the extreme complexity of the problem as it now exists, and the difficulty to clearly identify the areas of improvement. Thus, requirements would appear to be difficult to meet. However, the driving influence of reduced detectability for survivability and reduced noise emission for acceptance in surrounding communities for military and civil applications, respectively, will assure that a continued effort will be made to solve these problems.

3.0 PROOF OF TECHNOLOGY

In previous sections we have discussed several characteristics of vehicles that are desired to produce capabilities within the rotorcraft systems. Many technologies are involved in evolving these capabilities. Orderly analyses contribute extensively to generating the mathematical models necessary to represent the parametric structures of the physical phenomena and to exercise them over a matrix for optimization. However, it has been factually ascertained that it is essential that technology derived from these models be demonstrated by experiment and proven before system development is begun. This demonstration can be at component level or it can be an assemblage of components, even in a demonstrator flying vehicle of prototype class. It is essentially important that it be done in an orderly manner to identify the priorities to be applied in the resolution of technical void areas and to reduce risk in later systems development to a reasonable level. It is only in this manner that the various components can be integrated systematically into the resultant weapon system or transportation system which is desired. Cost effectiveness in the current market is extremely important. Increased vehicle sophistication has driven costs continually higher. Therefore, an embarkation on programs which

are not fully cost effective generally is no longer tolerated. Proof of technology is accomplished in many ways. Some of the characteristic experiments which are performed in support of technology proof are component bench tests, wind tunnel tests, tests on tracts, whirl towers, and other devices, and finally, integration into experimental prototypes.

The relative importance of these mechanisms for testing depends to a great extent upon the type of technology which is to be proven. For example, little is learned from component bench testing regarding the aerodynamic aspects of a component. but much is learned regarding its dynamics. Structural dynamics are extremely important, however, in relation to aerodynamics both in the static and dynamic sense. This point is stressed, since often the appreciation of the interrelative and interactive facets of technologies, particularly aerodynamics and dynamics, are overlooked in the design of rotorcraft.

Wind tunnel testing, when properly performed, gains insight into both aerodynamic and dynamic problems. Whereas it is not possible to fully represent all of the degrees of freedom in the wind tunnel tests, broad parametric studies can be made at low cost using small scale models representing lower investment. Generally, however, it is desirable to simulate at larger scale at least some of the testing to verify the scaling laws which are involved and to account for such factors as Reynolds number, Strouhal number, and Froude number. The essentiality of large scale testing is a matter of some controversy and will be dealt with in some detail in the session devoted to this subject. Nevertheless, an important factor is to be appreciated; the ability to test in wind tunnels has been considered less of a factor in rotorcraft design than in the design of fixed wing vehicles to date. It is important to recognize that this situation is changing as the more sophisticated theories evolve. The impact of the high-speed computer has been great in bringing this about. It has removed much of the cut-and-try empiricism which has characterized the development of rotorcraft in the past. Such knowledgeable approach is essential, since we have realized already much of the improvement in performance which is possible from aerodynamics and dynamics within the rotorcraft concept and must now concentrate on applying the principles of aerodynamics and dynamics to produce a more effective reduction in the adverse attributes of the vehicle such as vibration, high maintenance cost, and low reliability. Gains in these areas come hard and only as a result of fundamental comprehension of the phenomena involved.

Wind tunnel research is aided by the use of tracks, towers, and other such devices. As an example of the specialized use of these devices, whirl towers are used to obtain hover data for rotors since the wall constraints within a wind tunnel adversely affect the flow conditions making the obtaining of adequate data impossible. In addition, tracks are often useful, since rapid variation in track speed is obtainable to effect the dynamic velocity conditions important to assessing the dynamic characteristics. In summary, all of these various devices are important in simulating as nearly as possible the flight environment to obtain an assessment of the technology and to prove that which has been evolved through analytical methods.

The concept of cyclic research is easily envisioned from this discussion. The proof of technology many times reveals additional voids which have not been appreciated. Thus, it is essential to return to the analytical procedures to improve the mathematical models which have been generated. It is only in this manner that confidence can be gained in the design methods evolving from the analyses. Cut-and-try efforts in rotorcraft have become so costly that knowledgeable design methods must be obtained if further improvement is to be realized. As gains become smaller for effort expended, this factor becomes increasingly important.

Prototypes, that is, an assemblage of components involving technology for which proof is desired, into a flying vehicle are receiving increasing interest. These prototypes may be derived in less than a full system sense to test high risk items before embarking upon the total integration of systems. This is especially important in the military application where a significant quantity of subsystems are involved. In such programs where development is underway for full systems capability, it is extremely costly and oftentimes results in aborting a development effort if fundamental problems arise in the airframe aerodynamic and dynamic systems which delay orderly development.

4.0 PROTOTYPE DESIGN AND MANUFACTURE

It has been intimated in several instances in the preceding, that the fundamental purpose of generating technology in aerodynamics and dynamics for rotorcraft is to effect adequate design techniques which will enable knowledgeable design of systems to meet the desired capabilities set forth in requirements. For this purpose, it is essential that the aerodynamics and dynamics, along with other technologies, be characterized in a parametric sense where trends can be indicated and where tradeoff studies can be made in a knowledgeable fashion. It is only in this manner that design optimization for any given requirement may be accomplished with confidence. The preliminary selection of configuration results from such tradeoff studies, constrained by the requiring document. The designers are limited by knowledge available to them. An indication of available knowledge in aerodynamics and dynamics is shown in Fig. 18.

Not only is the basic knowledge important, but the appreciation of interactive effects is also of significant concern. The complexity of these interactive effects is illustrated in Fig. 18, which illustrates the interaction between the basic sciences, interdisciplinary sciences, subsystems, and support technologies, all leading to the design of a new airmobile system. Life cycle elements are illustrated on the bottom of this figure beginning with technology studies

through concept formulation into the contract definition, development and production, and, finally, operations and disposal. All of these are important in the appreciation of factors affecting selection of configuration.

If it is to be assured that the design will meet all of the specified requirements, it is obvious that a great deal of confidence must exist in the design techniques which are employed. The extreme complexity illustrated by the model shown in Fig. 18 has in the past resulted in a great deal of empiricism. However, the advent of computer-aided design has had a significant impact on the accomplishment of this task. It is clear from the model presented that it would be highly desirable to conduct the parametric studies in the many areas to be considered in a parallel fashion rather than in sequence. Indeed, this is what has been accomplished in computer-aided design techniques. It is only by this knowledgeable approach that full advantage can be taken of the technological advances which are continually appearing. It is stressed that if the model shown in Fig. 18 fails in representing the complexity of interaction, it is because it is too simple.

This important area of parametric design has been accorded a full session in this lecture series. Its purpose will be to demonstrate how the design methods are applied to meet the requirements and, specifically, how this is impacted by considerations of aerodynamics and dynamics. It should be appreciated that this is the heart of the various mechanisms which convert technology into usable systems. In the vernacular, this is what it is all about.

5.0 FLIGHT TESTING

To assure the ability of the system to meet the requirements, it is necessary to prove the system in the flight environment. As has been discussed, this is possible either through prototyping or ultimately, through the preproduction vehicle itself. It is only in the actual environment that the final proof of the designed performance and flying qualities can be made. This is a most costly effort and, therefore, advantage must be taken of all the techniques and methodology discussed previously to minimize this cost. One area which has not yet been mentioned, is that of simulation. Advanced simulators are becoming available in many parts of the industrial community. These simulators are capable of sophisticated representation not only of vehicle characteristics, but of the environmental situation in which these vehicles will operate. It is important, of course, that the simulation is known to be accurate or at least that reasonable confidence can be realized. Correlation of simulation and flight is a continuing area of research and is reaching a high level of sophistication.

Flight testing must also deal with subjective ratings by the pilots who will operate the vehicles. It is at this point that pilot ratings properly quantitized become significantly effective. Not only may these pilot ratings be established on existing systems, but these may also be used to confirm simulation of the systems. The ability to simulate these systems gives added credence to the simulation of advanced systems through orderly projection of trends and data. Pilot rating oftentimes is authenticated by instrumented results from the vehicle in flight, which more clearly indicate what parametric factors are most significant in affecting pilot rating. The use of subjective pilot ratings in flight testing is generally accepted and oftentimes is an overriding factor to the instrumented results. However, flight testing must carefully utilize instrumentation for factual evaluation of the characteristics being tested. It is only through the acquisition of these instrumented results that an orderly procedure may be employed for vehicle improvement.

Flight testing for rotorcraft is extremely important since it is at this point that the full dynamics of the system may be evaluated. The many degrees of freedom and their coupled modes are not possible of full duplication in other than the flight environment. Therefore, flight testing of rotorcraft must be done in a carefully controlled and knowledgeably expanded flight envelope. Because of its peculiar characteristics, the rotorcraft is subject to many resonant conditions throughout its operating range. Though these have been knowledgeably assessed in the development cycle, it is often possible that a divergent situation which has not been anticipated may occur. Although new theories are being generated to more adequately represent these characteristics, flight test still is a predominant factor in the evaluation of rotorcraft configurations. The session set aside for discussion of these flight testing techniques will deal in detail with the important aspects of aerodynamics and dynamics as they relate to flight characteristics and demonstration.

6.0 SUMMARIZATION

It is clear from the matters which we have considered that aerodynamics and dynamics play a key role in the meeting of requirements for application to military and civil uses of rotary wing aircraft. Also, it has been indicated that though it has not been clearly assessed, potential does exist for decided improvements in rotorcraft resulting from improved technologies in aerodynamics and dynamics. The poor assessment results primarily from the fact that these are perhaps the most complex of all technologies involved in rotorcraft design. The complexity of the flow field in which the rotor operates, the complexity of its dynamics and its oscillating modes, and the difficulty in representing these factors in properly assessed mathematical models all contribute to this unfortunate circumstance. Among the various technologies which apply to rotorcraft, only structures and materials offer a competing potential for improvement. It is important to note that aerodynamics and dynamics no longer hold great hope

for significant performance improvement. However, there is great opportunity to improve the operating characteristics so that the full performance characteristics inherent in the designs may be realized. Many current systems fail in the utilization of their full performance as a result of high vibrational levels and reduced reliability, accompanied by extremely high maintenance requirements. The field of aerodynamics and dynamics offer great potential for improving this situation through knowledgeable approach based on a solid foundation of technological advance.

It is perhaps most significant to note that the requirements for utilization of rotorcraft are valid and demanding, and that the field is open to further advance in aerodynamics and dynamics, which will render solutions to these problems. These solutions are expected to come hard after considerable expenditure of research effort. Nevertheless, a knowledgeable attack on the problems, prioritized according to a full appreciation of the pacing technical voids, can be expected to result in much improvement. Based on the long-range projected use of rotorcraft and derivatives, the effort is well worthwhile. The detailed sessions of this lecture series are formulated to provide the necessary understanding which will enable an appreciation of the task. Coupled with this overview of the general consideration, a full comprehension should result.

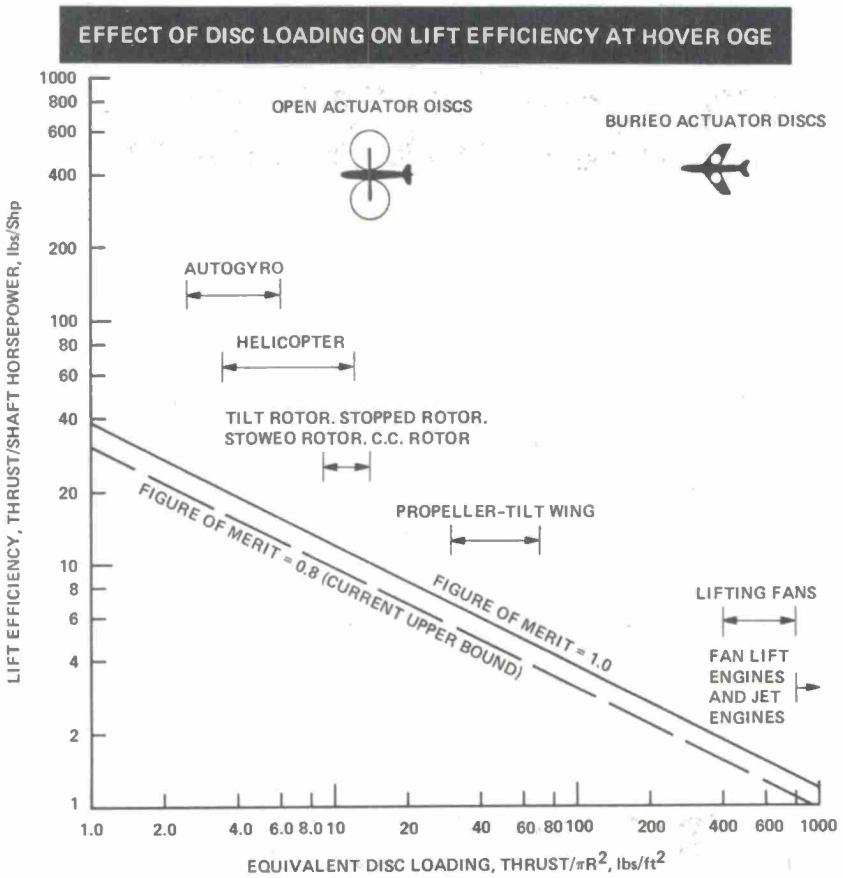


Fig. 1

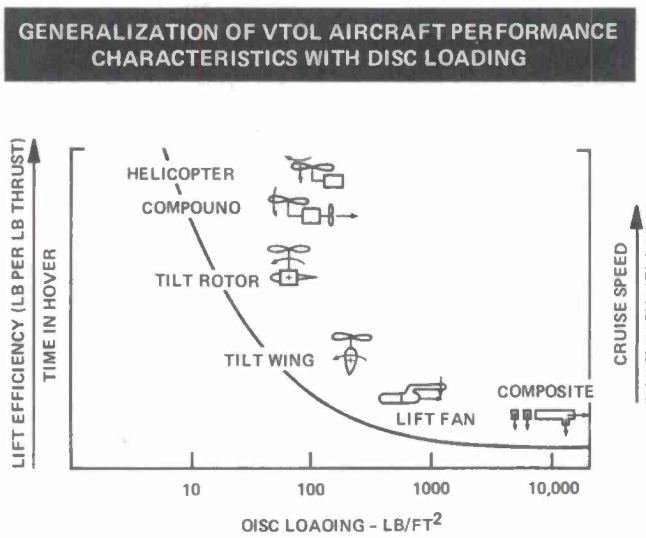


Fig. 2

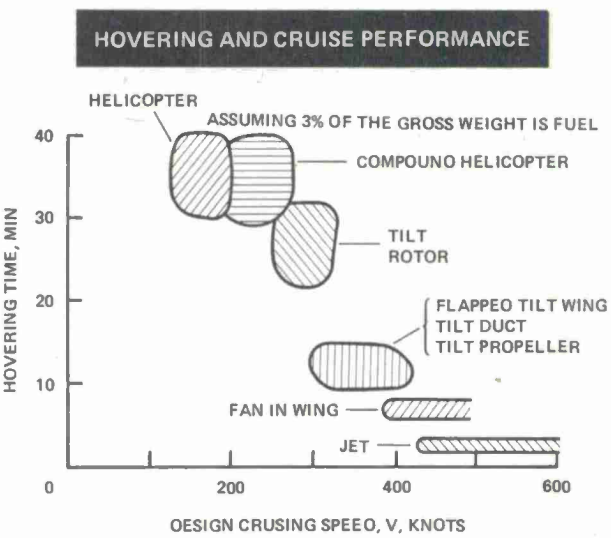


Fig. 3

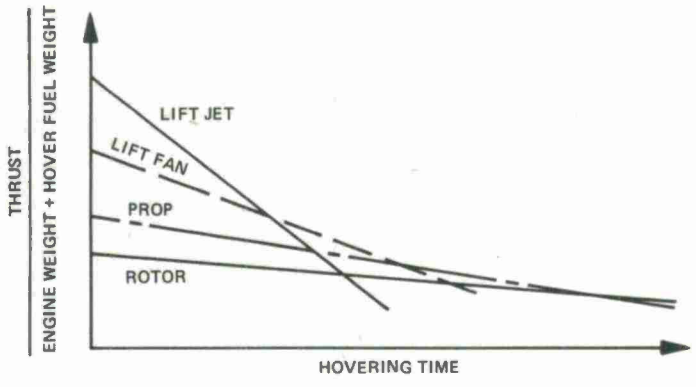


Fig. 4

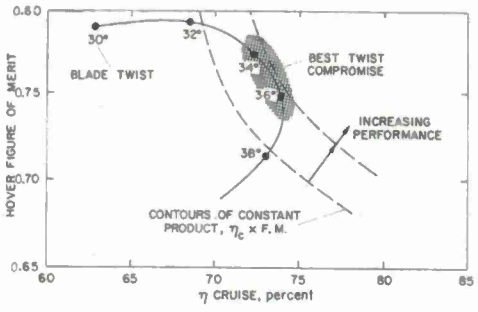


Fig. 5

INFLUENCE OF TURBINE-INLET TEMPERATURE AND COMPRESSOR PRESSURE RATIO ON ENGINE PERFORMANCE

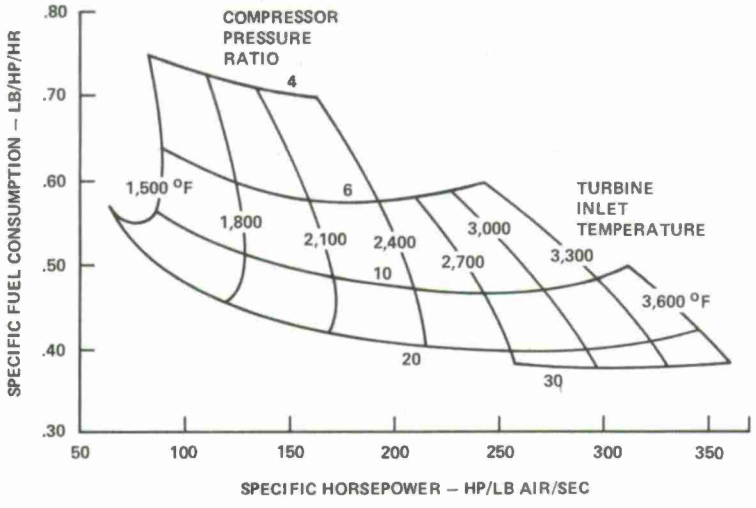


Fig. 6

CRUISE LIFT/PROPULSTION EFFICIENCY VERSUS SPEED

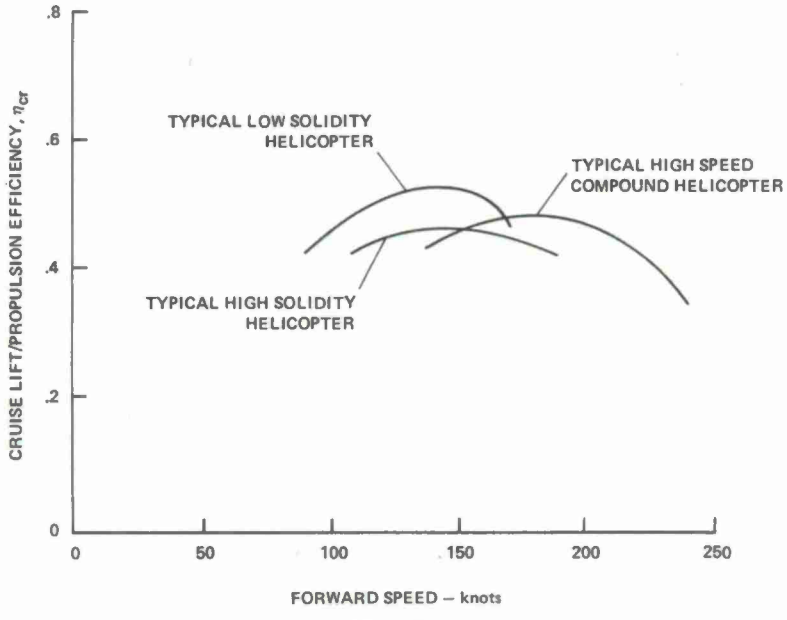


Fig. 7

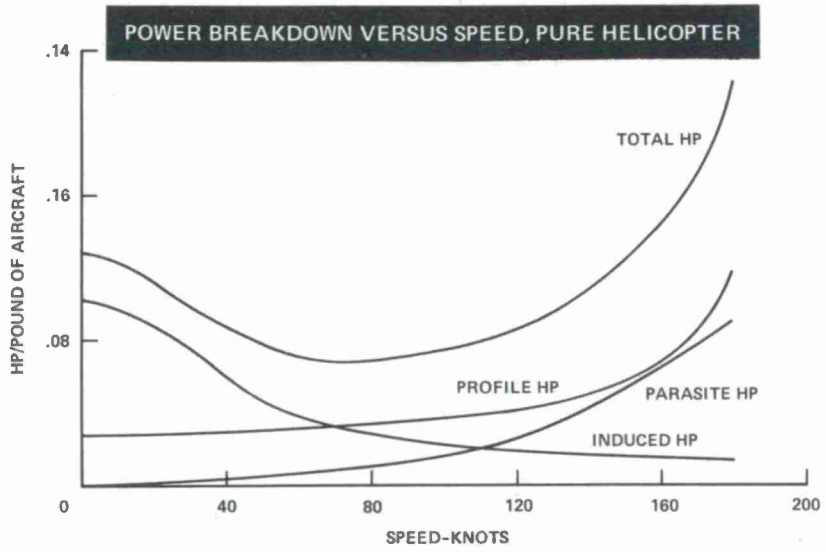


Fig. 8

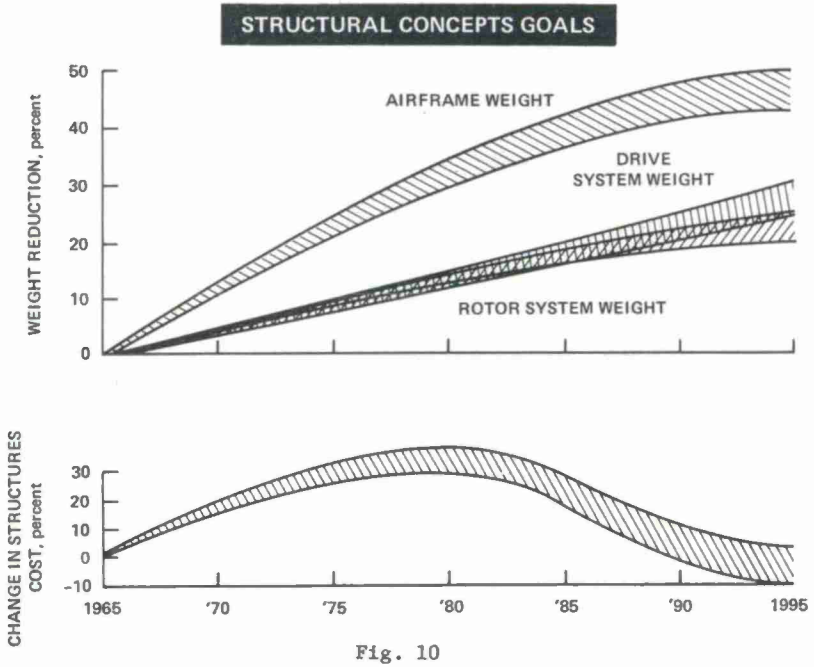


Fig. 10

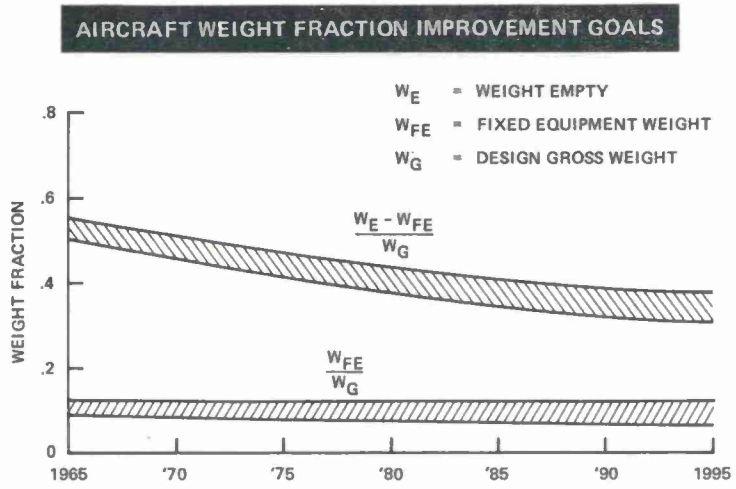


Fig. 9

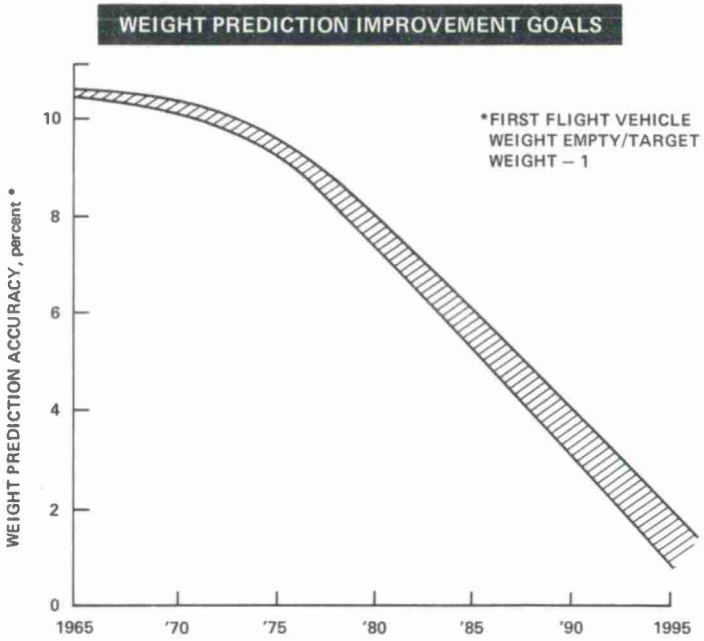


Fig. 11

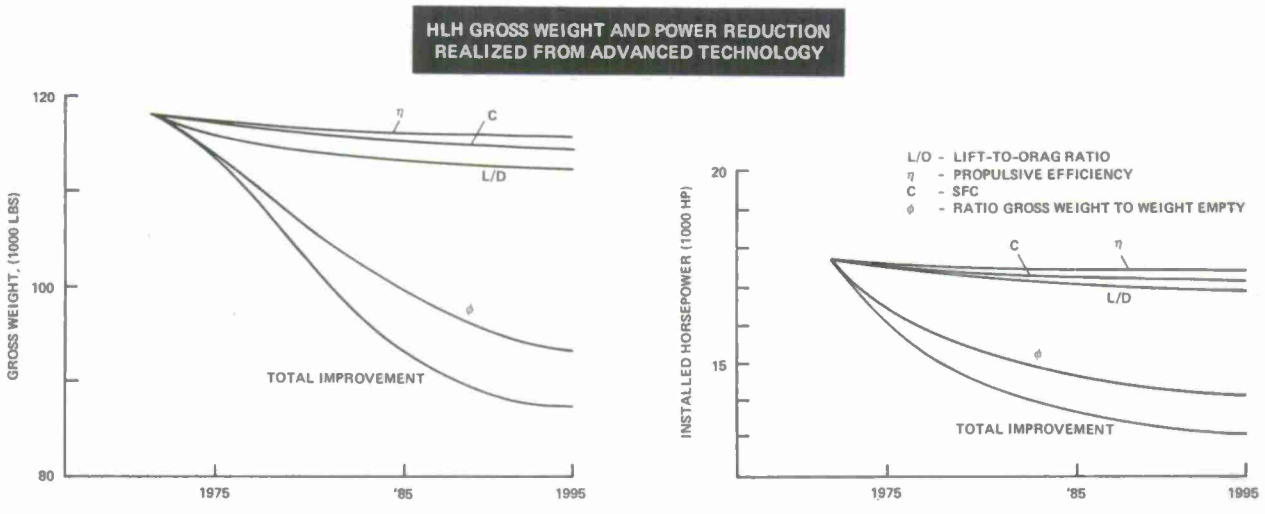

HLH GROSS WEIGHT AND POWER REDUCTION REALIZED FROM ADVANCED TECHNOLOGY
GROSS WEIGHT, (1000 LBS)
120
100
80
η
C
L/D
ϕ
TOTAL IMPROVEMENT
1975
'85
1995
INSTALLED HORSEPOWER (1000 HP)
20
15
L/D - LIFT-TO-DRAG RATIO
η - PROPULSIVE EFFICIENCY
C - SFC
ϕ - RATIO GROSS WEIGHT TO WEIGHT EMPTY
C
η
L/D
ϕ
TOTAL IMPROVEMENT
1975
'85
1995

Fig. 12

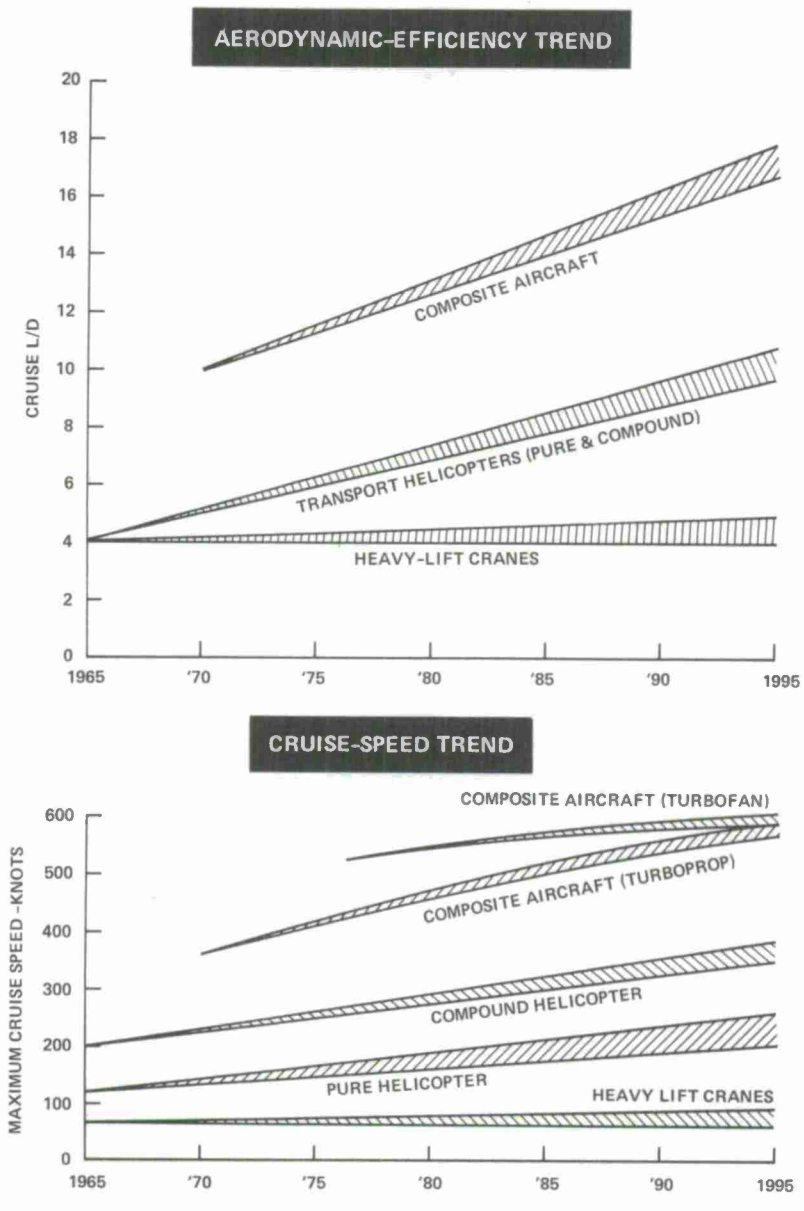

AERODYNAMIC-EFFICIENCY TREND
CRUISE L/D
20
18
16
14
12
10
8
6
4
2
0
COMPOSITE AIRCRAFT
TRANSPORT HELICOPTERS (PURE & COMPOUND)
HEAVY-LIFT CRANES
1965
'70
'75
'80
'85
'90
1995
CRUISE-SPEED TREND
MAXIMUM CRUISE SPEED - KNOTS
600
500
400
300
200
100
0
COMPOSITE AIRCRAFT (TURBOFAN)
COMPOSITE AIRCRAFT (TURBOPROP)
COMPOUND HELICOPTER
PURE HELICOPTER
HEAVY LIFT CRANES
1965
'70
'75
'80
'85
'90
1995

Fig. 13

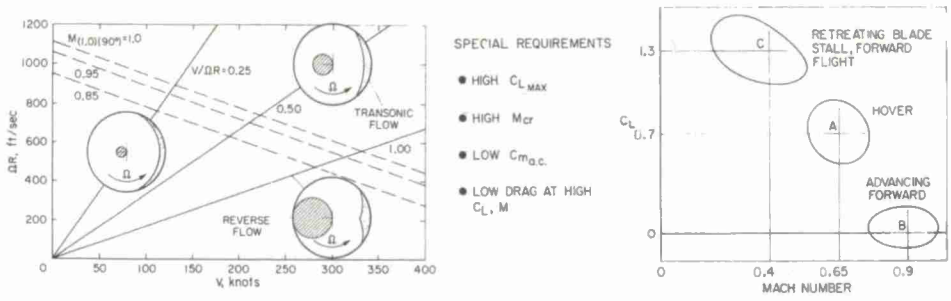


Fig. 14

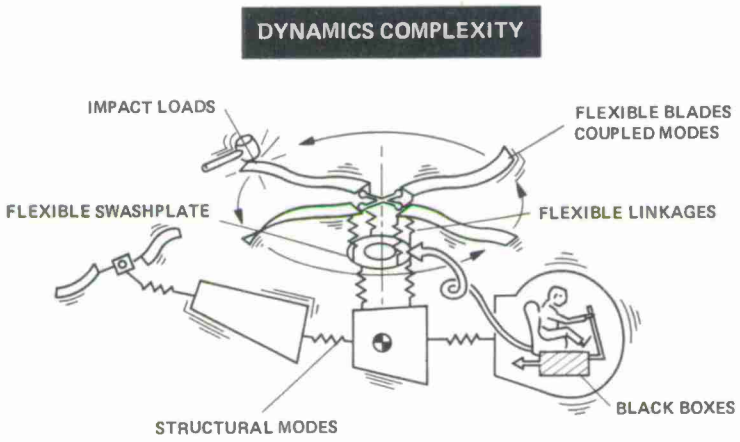
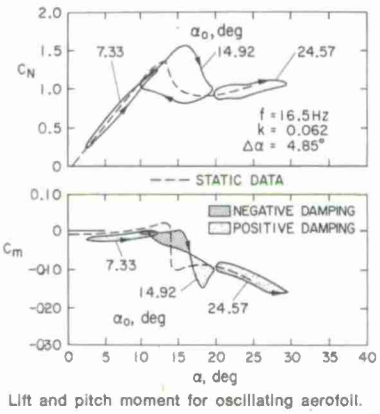


Fig. 15



Lift and pitch moment for oscillating aerofoil.

Fig. 16

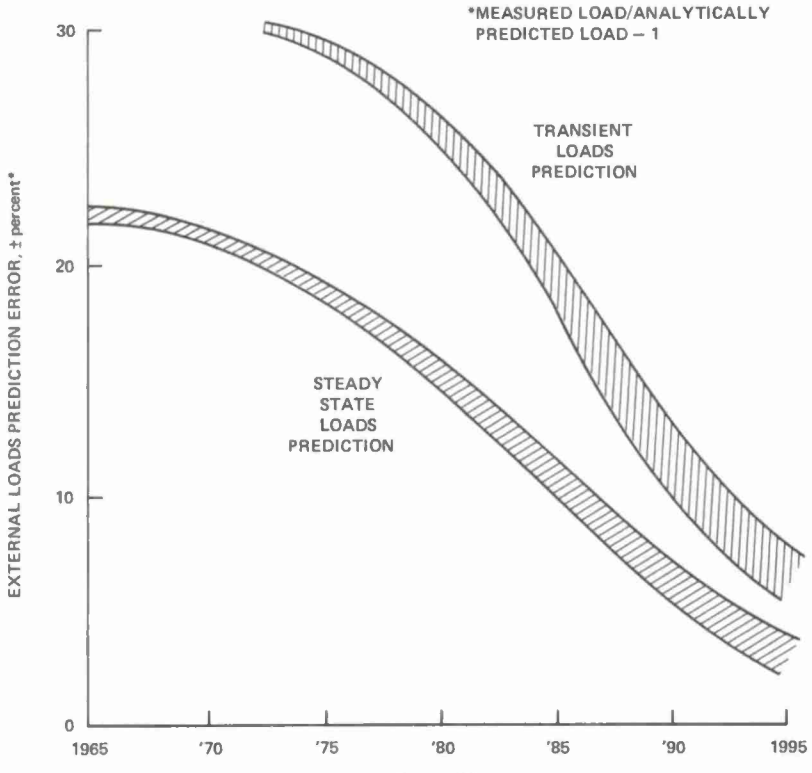


Fig. 17

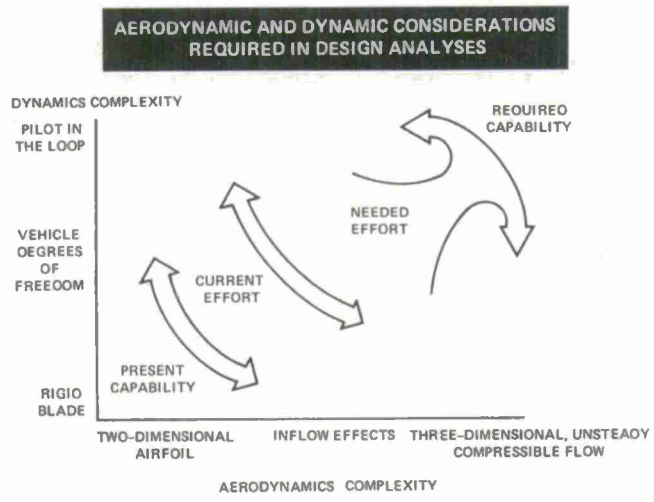

AERODYNAMIC AND DYNAMIC CONSIDERATIONS REQUIRED IN DESIGN ANALYSES
DYNAMICS COMPLEXITY
PILOT IN THE LOOP
VEHICLE DEGREES OF FREEDOM
RIGID BLADE
REQUIRED CAPABILITY
NEEDED EFFORT
CURRENT EFFORT
PRESENT CAPABILITY
TWO-DIMENSIONAL AIRFOIL
INFLOW EFFECTS
THREE-DIMENSIONAL, UNSTEADY COMPRESSIBLE FLOW
AERODYNAMICS COMPLEXITY

Fig. 18

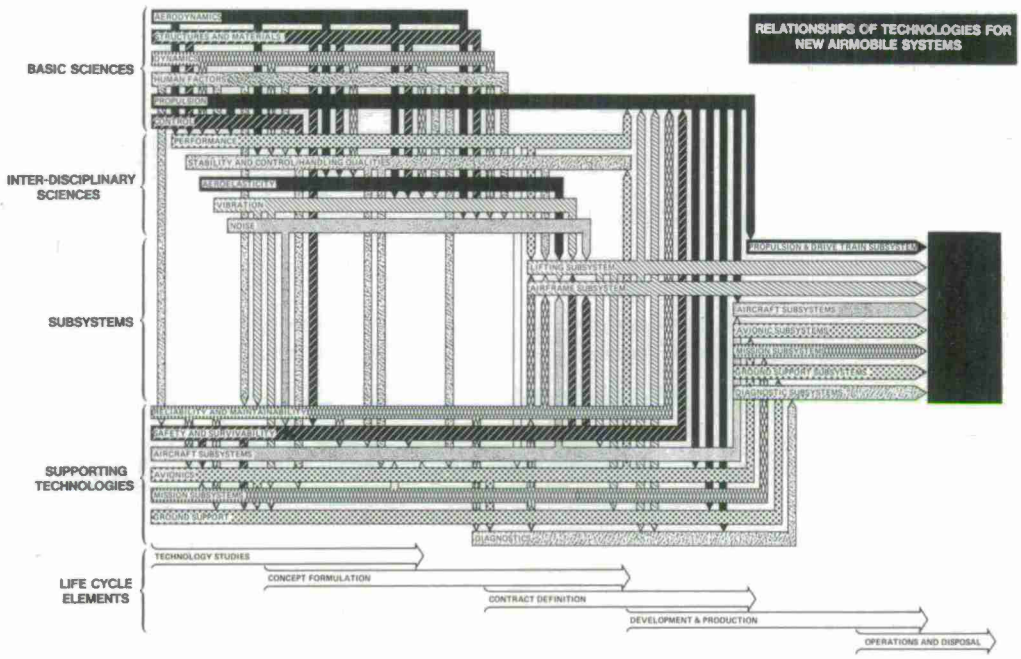

RELATIONSHIPS OF TECHNOLOGIES FOR NEW AIRMOBILE SYSTEMS
BASIC SCIENCES
INTER-DISCIPLINARY SCIENCES
SUBSYSTEMS
SUPPORTING TECHNOLOGIES
LIFE CYCLE ELEMENTS
AERODYNAMICS
STRUCTURES AND MATERIALS
DYNAMICS
HUMAN FACTORS
PROPULSION
CONTROL
PERFORMANCE
STABILITY AND CONTROL/HANDLING QUALITIES
RELIABILITY AND MAINTAINABILITY
VIBRATION
NOISE
PROPULSION & DRIVE TRAIN SUBSYSTEM
LIFTING SUBSYSTEM
AIRFRAME SUBSYSTEM
AIRCRAFT SUBSYSTEMS
AVIONICS SUBSYSTEMS
MISSION SUBSYSTEMS
GROUND SUPPORT
SAFETY AND SURVIVABILITY
DIAGNOSTIC SUBSYSTEMS
TECHNOLOGY STUDIES
CONCEPT FORMULATION
CONTRACT DEFINITION
DEVELOPMENT & PRODUCTION
OPERATIONS AND DISPOSAL

Fig. 19

BASIC AERODYNAMICS & PERFORMANCE OF THE HELICOPTER

by

W. Z. Stepniewski
The Boeing Vertol Company
Philadelphia, Pennsylvania 19142, USA

SUMMARY

In this part of the course, emphasis is placed on the fundamentals of rotary-wing aerodynamics and their application to performance considerations of classical helicopters. This approach was dictated by: (1) an apparent need for assembling, under one cover, a concise presentation of rotary-wing aerodynamics that is presently scattered throughout various publications - many of them being out-of-print, and (2) to provide methods and procedures that would not necessarily require high-speed computers. The latter aspect may be especially helpful for establishing general trends, design philosophies and to provide means for scrutinizing and checking more complicated computer-based programs. This goal dictated the selection of the subject material which is presented in separate chapters covering the following aspects: (1) momentum theory, (2) blade element theory in general and in particular, the combined momentum and blade element theory, (3) fundamentals of vortex theory and current programs in that domain, (4) applications of the presented material to some facets of design of new rotary-wing aircraft and performance optimization of those already defined, and (5) an example of helicopter performance prediction based on current industrial practice.

1. INTRODUCTION

The main purpose of this section of the course is to provide an understanding of aerodynamic phenomena of the rotor as well as to furnish tools for their quantitative evaluation. The second of these aims will be chiefly directed toward prediction of helicopter performance. It is hoped, however, that the whole presentation will also contribute to a better insight into other fields of rotary-wing aircraft analysis.

In order to achieve this double aim of understanding and quantitative evaluation, various conceptual models will be developed. The models would, on one hand, reflect physical aspects of the considered phenomena while on the other, they would permit establishment of a mathematical treatment. To emphasize more strongly this duality of purpose, an adjective "physicomathematical" instead of the more customary "mathematical" will be used in this text whenever referring to these models.

It should be realized at this point that similar to other fields of engineering analysis, these models, no matter how complicated in detail will still represent a simplified picture of the physical reality. It is obvious, hence, that the degree of sophistication of the physicomathematical models should be geared to the purpose for which they are intended. When faced with the task of defining such a model, one may be advised to first ask the following two questions: (1) whether the introduction of new complexities truly contributes to a better understanding of the physics of the considered phenomena and its qualitative and quantitative evaluation, and (2) whether the possible accuracy of the data inputs is sufficiently high to justify those additional complexities.

In other words, one should honestly consider whether a more complex model would truly lead to a more accurate quantitative analysis of the investigated phenomena or just, perhaps, only the procedure would look more impressive (especially to the ignorant), while mathematical manipulation would consume more time and money. Furthermore, it should be realized that often in the more complex approach, neither intermediate steps nor final results can be easily scrutinized.

With respect to rotary-wing aerodynamics in general, and performance prediction in particular, one should realize that aerodynamic phenomena associated with the various regimes of flight of an even idealized, completely rigid rotor are very complicated. Furthermore, the level of complexity increases due to the fact that in reality, every rotor is non-rigid because of the elasticity of its components and/or due to the built-in articulations. As a result, it is subjected to various time-dependent deformation from its neutral state. This leads to a continuous interaction between aerodynamics and dynamics, thus introducing new potential complexities to the task of predicting aerodynamic characteristics of the rotor. Fortunately, even some conceptually very simple physicomathematical models would enable one to get either accurate trends or acceptable approximate answers to many rotary-wing performance problems.

By following the development of the basic rotor theories, from the simple momentum through the combined momentum and blade element and finally, the vortex theory, the reader would be able to watch the evolution of the physicomathematical model of the rotor from its simplest form to more complex ones. He will also be able to see how the need for an understanding or explanation of the newly encountered phenomena would require modifications and additions and sometimes, a completely new approach to the representation of the actual rotor by its physicomathematical model. By the same token, he would be able to develop a better feel with respect to the circumstances under which the

simpler approach may still suffice. Furthermore, as long as the shortcomings and limitations of the simplified approaches are understood, they may be used for approximate performance predictions. Finally, these simpler and easier to scrutinize methods may serve as a reliable means of checking the validity of the results obtained in potentially more accurate, but complicated, ways which may be prone to computational errors.

In Chapters 2 to 4, methods applicable to performance prediction in various regimes of flight of an isolated rotor and rotary-wing aircraft as a whole will be outlined. In Chapter 5, some very basic aspects of performance tradeoffs in the preliminary design stage and later, performance optimization of a helicopter within a defined flight envelope will be discussed. Finally, in Chapter 6, performance prediction methods for a single-rotor helicopter will be illustrated by an example based on actual industrial practices.

2. SIMPLE MOMENTUM THEORY

2.1 SIMPLEST MODEL OF THRUST GENERATOR

Basic relationships of Newtonian mechanics can lead to the development of a simple, but at the same time, quite universal physicomathematical model of a thrust generator. Without going into any details regarding either geometric or other characteristics of the thrust generator itself, it is simply assumed that in translation with velocity $\vec{V}$ with respect to the fluid, as well as under static conditions, it is somehow capable of imparting linear momentum to that ideal (frictionless and incompressible) fluid of density ρ and pressure p_o. For simplicity, let it be assumed that this completely general thrust-generating device remains stationary while a very large mass of fluid moves past it with a uniform velocity $(-\vec{V})$, (Fig 2-1). Let it also be assumed that the thrust coincides with the positive axis of a coordinate system with its origin at the "center" of the thrust generator.

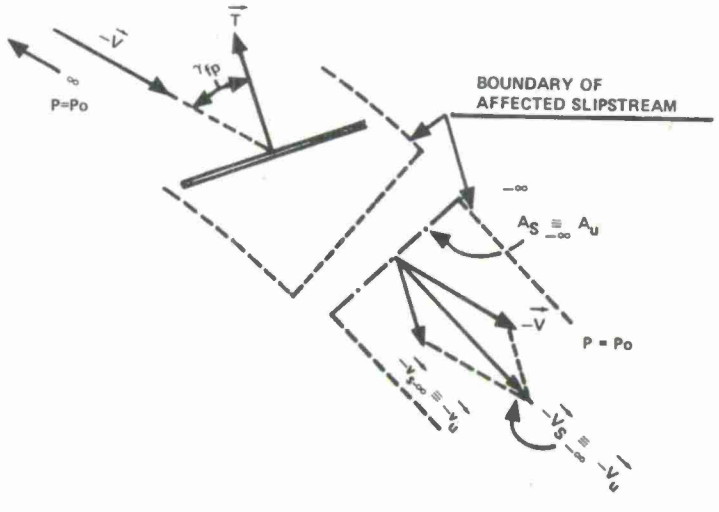


Figure 2-1. Simplest Physicomathematical Model of a Thrust Generator

The thrust generator interacts with the fluid by imparting uniformly distributed linear momentum to a distinct streamtube of fluid (passing close to it) and bound by a separating surface preventing an exchange of mass through it. This means that by the law of continuity, the mass flow within the tube is the same at every section, while both velocity and pressure of the fluid alter. However, somewhere far downstream, the pressure returns to p_o, while the incremental velocity variation reaches its ultimate value of $-\vec{v}_u$ uniformly distributed over the tube cross-section area, A_u.

Knowledge of $\vec{v}_u$ and A_u, in addition to the already known $\vec{V}$ and ρ, represents all the necessary information for determining the thrust $\vec{T}$ generated by that very simple physicomathematical model, as well as the power required in that process.

According to the laws of classical mechanics, the direction of the thrust-generated $(\vec{T})$ will be opposite to that of $\vec{v}_u$, while its magnitude will be equal to the rate of momentum change within the streamtube between its final and initial value. Denoting the rate of mass flow by $\dot{m}$, the force $\vec{T}$ becomes

$$\vec{T} = -\dot{m}(\vec{V}_u - \vec{V}) \tag{1}$$

where the resultant velocity of flow far downstream $(\vec{V}_u)$ is $\vec{V}_u = \vec{V} + \vec{v}_u$. Consequently, Eq (1) becomes

$$\vec{T} = -\dot{m}\,\vec{v}_u. \tag{1a}$$

Furthermore, since $\dot{m} = V_u A_u$, the above equation can be rewritten as

$$\vec{T} = -|\vec{V} + \vec{v}_u| A_u\, \rho\, \vec{v}_u \tag{1b}$$

where $||$ denotes absolute (scalar) value of the resultant vector, $\vec{V}_u$; while $\vec{v}_u$ from now on, will be called the fully-developed induced velocity.

Inspection of Eqs (1a) and (1b) can teach us that in dynamic generation of a given thrust $(\vec{T})$, a tradeoff can be made between the magnitude of a fully-developed induced velocity $(\vec{v}_u)$ and the mass flow which, in turn, depends on: (a) a cross-section of the streamtube far downstream, A_u; (b) absolute value of the resultant velocity of flow within the tube itself far downstream, V_u; and (c) density of fluid, ρ. This, of course, would permit further tradeoffs between the above parameters within a constant $\dot{m}$.

The above general conclusions already contribute to some understanding of dynamic thrust generation, but in order to get a still deeper insight into this matter, it is also necessary to consider power (P) required in this process. This can be done by examining the difference in the rate of flow of kinetic energy through a cross-section of the streamtube far downstream in the ultimate wake $(\dot{E}_u)$ and far upstream $(\dot{E}_{up})$

$$P = \dot{E}_u - \dot{E}_{up} = \frac{1}{2}\dot{m}(\vec{V}_u^{\,2} - \vec{V}^2). \tag{2}$$

Remembering that $\vec{V}_u = \vec{V} + \vec{v}_u$, and performing subtraction as indicated in Eq (2), one obtains

$$P = \frac{1}{2}\dot{m}\,\vec{v}_u \cdot (2\vec{V} + \vec{v}_u), \tag{2a}$$

but $\dot{m}\vec{v} = -\vec{T}$; hence, Eq (2a) can be rewritten as follows:

$$P = -(\vec{T}\cdot\vec{V} + \frac{1}{2}\vec{T}\cdot\vec{v}_u). \tag{2b}$$

The above equation shows that power required by our simple thrust generator is equal to minus the sum of a dot (scalar) product of the velocity of flow and the developed thrust, and one-half of another dot product of thrust and fully-developed induced velocity.

Since $\vec{T}$ and $\vec{v}_u$ are in the opposite directions (they form a 180° angle between each other), their dot product $(\vec{T}\cdot\vec{v}_u)$ is negative. Hence, the second term in the brackets in Eq (2) is always negative and in view of the minus sign in front of the bracket, contribution of that product to the power required is always positive. In other words, a power input is always required to cover energy losses associated with the induced velocity needed in the process of dynamic thrust generation.

As to the first term $(\vec{T}\cdot\vec{V})$ in the brackets of Eq (2b), it should be realized that γ_{fp} angles between thrust $(\vec{T})$ and flight path $(\vec{V})$ may vary from $0°$ to $180°$. For $90° \leq \gamma_{fp} < 180°$, the $\vec{T}\cdot\vec{V}$ is negative; hence, its contribution to the power required would be positive as in the case of the $\vec{T}\cdot\vec{v}_u$ product. By contrast, for $0° \leq \gamma_{fp} < 90°$, the sign of the $\vec{T}\cdot\vec{V}$ product will be positive and consequently, the total amount of power required to be inputted into the thrust generator may be decreased, reduced to zero, or even become negative as in the case of a windmill.

For the case of actual flight, Eq (2b) can be rewritten in nonvectorial notations:

$$P = TV\cos\gamma_{fp} + \frac{1}{2}Tv_u. \tag{2c}$$

It should be noted at this point that in developing our simplest physicomathematical model, an ideal fluid was assumed, with no dissipation of energy through friction or energy transfer to the fluid under the form of turbulent wakes. Furthermore, a uniform distribution of the fully-developed induced velocity has been assumed.

It can be shown that this condition of uniformity of the fully-developed downwash velocity is synonymous with minimization of the power required to generate a given thrust under assumed conditions of flight velocity, air density, and the cross-section area of the fully-developed slipstream. Thus, the power expressed by Eqs (2b) or (2c) may be called the ideal power (P_{id}) required, while its part related to the thrust-generating process and represented by the second term in Eqs (2b) or (2c) may be named the ideal induced power (P_{iid}). It should also be noted that the assumption of a steady-state motion signifies that the thrust T is in balance with all of the other forces (aerodynamic, gravitational, etc.) acting on the thrust generator.

It may be of interest to find out that even this simplest physicomathematical model of a thrust generator may be helpful in understanding some important trends in the VTOL field. For instance, Eq (2c) indicates that for the case of static thrust generation which for VTOL is synonymous with hovering, the ideal power required would be:

$$P_{id_h} = \frac{1}{2}Tv_u \qquad ft.lbs/sec \tag{3}$$

or

$$T/P_{id_h} = 1100/v_u \qquad lbs/hp. \tag{3a}$$

The above expression clearly shows that in order to obtain the highest possible power economy (maximum thrust per horsepower) in the static thrust generation, one should strive for the lowest possible induced velocity in the fully-developed slipstream. The relationship given in Eq (3a) is plotted in Fig 2-2 (reproduced from Ref 1) and it remarkably well indicates the actual trend in static power loading, from helicopters to rockets.

In the previously considered simplest model of the thrust generator, no attempt was made to describe its geometry nor to explain the actual process of imparting linear momentum to the fluid. For this reason, our simplest model, although helpful in predicting some general trends, would not be sufficient in dealing with practical problems of design and performance predictions of rotary-wing aircraft. Thus, another model, reflecting at least some geometric characteristics of open airscrews (rotors and propellers) would be required.

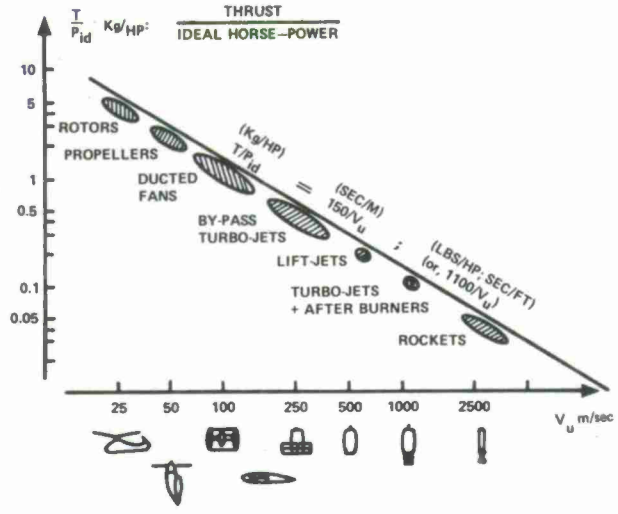


Figure 2-2. Trend in Static Thrust to Ideal Power Ratios for Various VTOL Concepts

2.2 ACTUATOR DISC

The actuator disc concept still represents a very simple physicomathematical model, but it is better suited to simulate an open airscrew. In this case, a disc perpendicular to the generated thrust and capable of imparting axial momentum to the fluid and sustaining pressure differential between its upper and lower surface, is substituted for an actual rotor-propeller. This concept may be considered as a sublimation of the idea of a rotor-propeller with a very large number of blades.

As in the previous section, motion of the disc with velocity $\vec{V}$ through air of density ρ and pressure p_o may be replaced by the flow of air with velocity $-\vec{V}$, while the disc itself remains stationary. Under these conditions, the mechanism of thrust generation is explained as follows: Fluid passing either through the disc or in its vicinity acquires induced velocity, v, which is uniform over the entire disc and is directed opposite to the thrust. It is again assumed that the actuator disc operates in an ideal fluid; i.e., its rotation does not encounter any friction or form drag as the fluid is passing through it. It is also assumed that the disc imparts only linear momentum to the passing fluid; i.e., there is no rotation of the slipstream.

2.2.1 Induced Velocity and Thrust in Axial Translation

Axial translation can obviously be either in the thrust direction as in vertical climb of a rotorcraft, or in the opposite one as in vertical descent. As the first case, let us consider a rotor or propeller developing a thrust T and moving up (climbing) along its axis with a constant velocity V_c. For this type of motion, an equivalent one is substituted with the thrust generator being stationary while the air flows past it in the axial direction with a speed (far from the rotor) of $-V_c$ (Fig 2-3).

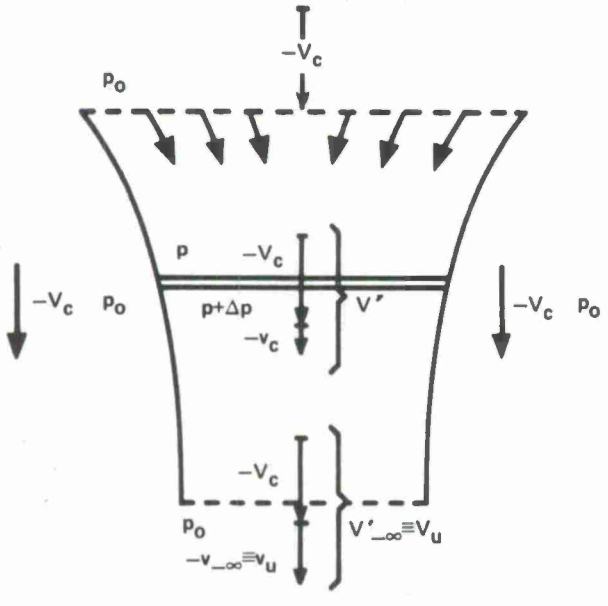


Figure 2-3. Scheme of Flow Corresponding to Vertical Climb

Similar to the previously considered simple model, a single-axis coordinate system is selected with its positive direction coinciding with that of the thrust T. Air particles approaching the actuator disc acquire some additional axial velocity that reaches a $-v_c$ value at the disc itself.

After passing through the disc, the speed of flow increases still further until far downstream, the induced velocity reaches its ultimate value of $-v_u$, while the resultant velocity of flow becomes $V_u = -V_c - v_u$, and pressure returns to that of the surrounding air; i.e., it becomes p_o. Remembering that the mass flow within the streamtube is constant, its probable shape can be anticipated as in Fig 2-3.

In order to physically explain the thrust-generating mechanism of the actuator disc, it may be assumed that pressure above the disc is lower than that below it. Because of this discontinuity in pressure, Bernoulli's equation can only be applied separately to the upstream and downstream parts of the flow tube. For the upstream

part of the tube, the total H_o should be the same.

$$H_o = p_o + \frac{1}{2}\rho V_c^2 = p + \frac{1}{2}\rho(V_c + v_c)^2 \tag{4}$$

where $-v_c$ is the induced velocity at the disc and p is the pressure just above the disc surface.

The same is true for the total head (H_d) of the downstream part:

$$H_d = p_o + \frac{1}{2}\rho(V_c + v_u)^2 = p + \Delta p + \frac{1}{2}\rho(V_c + v_c)^2 \tag{5}$$

where $p + \Delta p$ represent the pressure just below the disc, with Δp being the pressure differential at the disc.

Subtracting H_o from H_d, one obtains:

$$\Delta p = \rho\left(V_c + \frac{1}{2}v_u\right)v_u. \tag{6}$$

Consequently, thrust developed by a disc of radius R can be expressed as $T = \pi R^2 \Delta p$ or, in terms of Eq (6):

$$T = \pi R^2 \rho\left(V_c + \frac{1}{2}v_u\right)v_u. \tag{7}$$

On the other hand, according to Eq (1a), the total thrust T can be expressed in this case as

$$T = \pi R^2 \rho(V_c + v_c)v_u. \tag{8}$$

Equating the right-hand sides of Eqs (7) and (8), one finds that

$$v_c = \frac{1}{2}v_u \tag{9}$$

or

$$v_u = 2v_c. \tag{9a}$$

Substitution of this new value of v_u into Eq (8) results in

$$T = 2\pi R^2 \rho(V_c + v_c)v_c \tag{10}$$

or denoting the total thrust-generating area of any actuator disc-like device by A, Eq (10) may be rewritten more generally as

$$T = 2A\rho(V_c + v_c)v_c. \tag{10a}$$

Eq (10a) can be solved for v, thus obtaining an expression for induced velocity at the disc

$$v_c = -\frac{1}{2}V_c + \sqrt{\frac{1}{4}V_c^2 + \frac{T}{2A\rho}} \tag{11}$$

or, remembering that $T/A \equiv w$ is the disc loading or, in more general terms, the thrust area loading, it can be rewritten as follows:

$$v_c = -\frac{1}{2}V_c + \sqrt{\frac{1}{4}V_c^2 + \frac{w}{2\rho}}\,. \tag{11a}$$

In a particular case, when the speed $V_c = 0$; i.e., in hovering or under any static conditions:

$$T = 2A\rho v^2 \tag{12}$$

while the induced velocity (v_h) becomes

$$v_h = \sqrt{w/2\rho}. \tag{13}$$

It can now be seen that the last term under the square root sign in Eq (11a) is the square of induced velocity in hovering. Eq (11a) can be rewritten, hence, as follows:

$$v_c = -\frac{1}{2}V_c + \sqrt{\frac{1}{4}V_c^2 + v_h^2}\,. \tag{14}$$

The above expression can be nondimensionalized by dividing both sides by v_h and defining two nondimensional velocities: (1) the nondimensional induced velocity $\overline{v}_c \equiv v_c/v_h$, and (2) the nondimensional rate of climb $\overline{V}_c \equiv \overline{V}_c/\overline{v}_h$ or, more generally, the nondimensional rate of axial translation in the direction of thrust $\overline{V}_{ax} \equiv V_{ax}/v_h$. For the case of climb, Eq (14) can now be rewritten as follows:

$$\bar{v}_c = -\frac{1}{2}\bar{V}_c + \sqrt{\frac{1}{4}\bar{V}_c^2 + 1}\,. \tag{14a}$$

The above equation shows how the nondimensional induced velocity varies (decreases) from its maximum value of 1.0 in hover, with the increasing velocity of the axial translation in the direction of thrust as measured by the ratio V_c/v_h or V_{ax}/v_h. The relationship expressed by Eq (14a) is shown graphically in Fig 2-4.

Knowledge of the fully-developed induced velocity ($v_u = 2v_c$) would permit determination of the slipstream contraction (ratio of the radius of the fully-developed slipstream, R_u, to that of the actuator disc, R) for the case of climb, or more generally, axial translation in the thrust direction:

$$R_u/R = \sqrt{[1 + (V_c/v_c)]/[2 + (V_c/v_c)]} \tag{15}$$

It can be seen from Eq (15) that for $V_c = 0$ (i.e., in hovering), $Ruh/R = .707$. As V_c/v_c increases, so does the R_u/R ratio, and for $V_c >> v_c$, contraction of the slipstream tends to disappear (Fig 2-5).

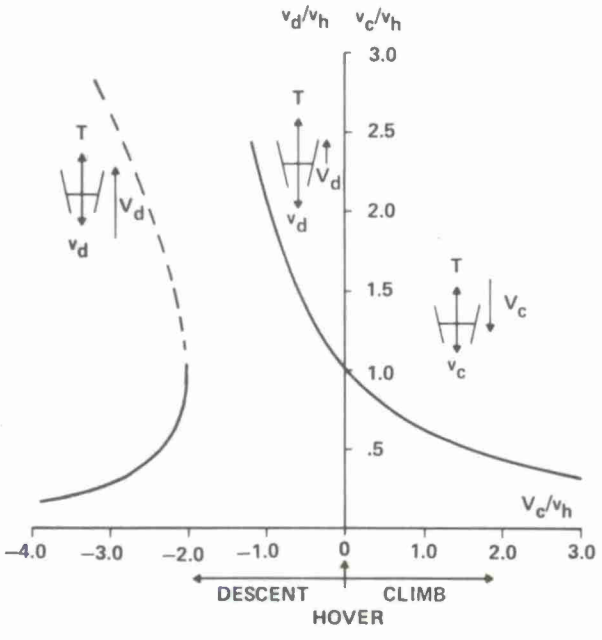


Figure 2-4. Nondimensional Induced Velocity vs Nondimensional Rate of Climb or Descent

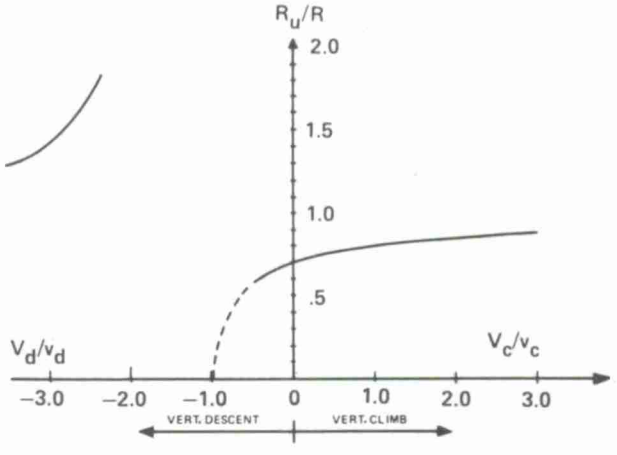


Figure 2-5. Ratios of Fully-Developed Wake Radius to That of the Actuator Disc vs V_c/v_c

As V_c/v_c becomes negative, $[(V_c/v_c) < 0]$; i.e., when vertical climb is replaced by vertical descent (far-away flow in Fig 2-3 directed upward), the R_u/R ratio tends to further decrease with the increasing absolute values of $-(V_c/v_c)$ until for $V_c/v_c = -1.0$, it would become zero (Fig 2-5).

However, as $(V_c/v_c) \to -1.0$, the rate of flow through the disc also approaches zero $[\pi R^2 \rho (v_c - V_c) \to 0]$. Thus, for $V_c/v_c \to -1.0$, the whole concept of the actuator disc acting on the air passing through it becomes meaningless. Furthermore, for $(-V_c/v_c)$ being within -1.0 to -2.0 limits, the R_u/R ratio (Eq (15)) is imaginary. At $(-V_c/v_c) = -2.0$, $R_u/R = \infty$ and only for $(-V_c/v_c) < -2.0$ does it again become real and positive. It becomes clear, hence, that the mathematical trend as indicated by Eq (15) loses a physical sense for $-2.0 \leq -V_c/v_c \leq -1.0$. Thus, the validity of the physicomathematical model based on the actuator disc concept, although apparently satisfactory for the case of vertical climb, hovering and moderate rates of vertical descent, should be reexamined.

This will be done by considering a case of vertical descent at rates so high that an unbroken flow can be expected within the whole streamtube. The necessary condition would obviously be that $|V_d/v_d| > 2.0$, where the symbol v_d is used for induced velocity to emphasize that it refers to the distinct case of (vertical) descent.

When the above condition is fulfilled, the following shape of the airstream affected by the rotor action (Fig 2-6) can be imagined. Far below the rotor, the airstream velocity is $V_d \equiv -(-V_c)$. As the flow approaches the rotor, this velocity is reduced (the airstream widens), since it encounters the downwash produced by the rotor.

If the downwash at the rotor itself is $-v_d$, then the rate of flow through the rotor disc will obviously be $V' = V_d - v$. It can be shown, as for the case of climb, that the downwash downstream of the rotor (in this case, above the rotor) can reach a maximum value equal to twice the induced velocity at the disc: $v_u = -2v_d$.

As to the R_u/R ratios, they can still be determined from Eq (15), remembering that $V_d \equiv -V_c$ as shown in Fig 2-5. It can be seen from this equation that with $|-V_c/v_c|$ ratios, the widening of the slipstream in the ultimate wake begins to disappear when $(V_c/v_c) \to -\infty, (R_u/R) \to 1.0$. By contrast, as $|V_d/v_d| \to -2.0$; $R_u/R \to \infty$, while $V_d - 2v_d \to 0$. This would mean that the air flow in the streamtube (Fig 2-6) would come to rest with respect to the rotor disc, while the whole mass of air (outside of the tube) would still flow upward at a speed equal to V_d. Of course, this situation is not acceptable from a physical point of view, and it is more reasonable to assume that before this ultimate state of air coming to rest is reached, a new flow pattern would be created.

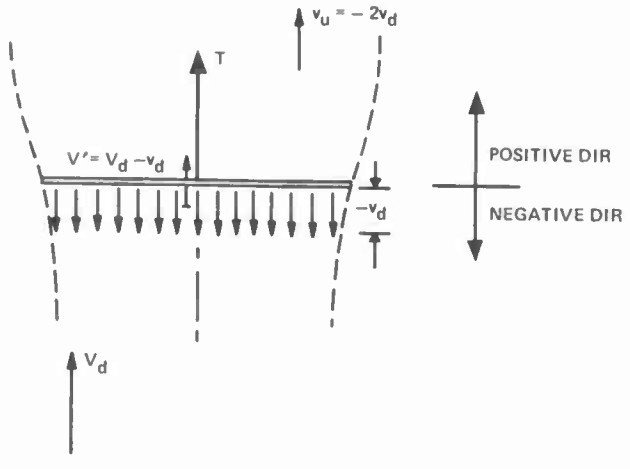


Figure 2-6. Flow Patterns in Vertical Descent

To establish a relationship between the thrust and induced velocity for the case of low rates of vertical descent, $|(V_d \equiv -V_c)/v| < 1.0$, Eqs (11) to (14a) can be modified by substituting the rate of descent V_d and $\bar{V}_d$ for the negative rate of climb $-V_c$ and $-\bar{V}_c$, thus obtaining the following:

$$v_d = \frac{1}{2} V_d + \sqrt{\frac{1}{4} V_d^2 + \frac{T}{2A\rho}} \tag{16}$$

or

$$v_d = \frac{1}{2} V_d + \sqrt{\frac{1}{4} V_d^2 + \frac{w}{2\rho}} \tag{16a}$$

or

$$v_d = \frac{1}{2} V_d + \sqrt{\frac{1}{4} V_d^2 + v_h^2} \tag{16b}$$

and finally, in the nondimensional form with $\bar{v}_d \equiv v_d/v_h$ and $V_d \equiv \bar{V}_d/v_h$:

$$\bar{v}_d = \frac{1}{2} \bar{V}_d + \sqrt{\frac{1}{4} \bar{V}_d^2 + 1}. \tag{16c}$$

A plot representing Eq (16c) is added to Fig 2-4.

For the case of $|V_d/v_d| > 2.0$ (Fig 6), the relationship for thrust can be written as follows:

$$T = 2\pi R^2 \rho (V_d - v_d) v_d.$$

Substituting $v_h^2 = T/2\pi R^2 \rho$ and solving the above equation for v_d, one obtains:

$$v_d = \frac{1}{2} V_d - \sqrt{\frac{1}{4} V_d^2 - v_h^2} \tag{17}$$

or in a nondimensional form ($\bar{v}_d \equiv v_d/v_h$ and $\bar{V}_d \equiv V_d/v_h$),

$$\bar{v}_d = \frac{1}{2} \bar{V}_d - \sqrt{\frac{1}{4} \bar{V}_d^2 - 1}. \tag{17a}$$

A plot representing Eq (17a) is also added to Fig 2-4.

2.2.2 Ideal Power in Axial Translation

As in the case of the simplest thrust generator model, power required by the actuator disc either for climb or in hovering may again be called the ideal power. This is justified by the previously made assumptions that (a) there are no friction or form drag losses, (b) the whole disc up to the limit of its geometric dimensions is participating in the thrust generation, and (c) the downwash velocity is uniform at any slipstream cross-section.

Expressions for the ideal power in vertical climb (P_{cid}) can readily be obtained from the relationship previously established for the simplest model. When a proper value of the fully-developed downwash velocity $(v_u = 2v_c)$ and $\cos \gamma_{fp} = 1.0$ are introduced into Eq (2c), then P_{cid}, in horsepower becomes:

$$P_{cid} = T(V_c + v_c)/550. \tag{18}$$

Eq (18) shows that for an idealized rotor as modeled by the actuator disc developing a thrust T, the power required in steady climb at a rate V_c is equal to the product of the thrust and the sum of the rate of climb (V_c) and induced velocity at the disc (v_c).

Thus, in the case of a steady vertical ascent when $T = W$ (W being the weight of the aircraft), the total ideal power required to climb is equal to the power required to overcome gravity ($V_c W$) plus the ideal induced power (Wv_c).

By substituting into Eq (18), an expression for v_c from Eq (11a), the following explicit relationship between power required (in HP) and rate of climb V_c (for $T = W$) is obtained:

$$P_{c_{id}} = W\left(\frac{1}{2}V_c + \sqrt{\frac{1}{4}V_c^2 + \frac{W}{2A\rho}}\right)\Big/550 \tag{19}$$

Eq (19) is also valid for an axial motion in the direction of thrust when V_{ax} is substituted for V_c and T for W).

Remembering that $W/2A\rho \equiv w/2\rho = v_h^2$, Eq (19) can be rewritten as follows:

$$P_{c_{id}} = W\left(\frac{1}{2}V_c + \sqrt{\frac{1}{4}V_c^2 + v_h^2}\right)\Big/550 \tag{19a}$$

or in terms of nondimensional rate of climb $\bar{V}_c \equiv V_c/v_h$, it becomes:

$$P_{c_{id}} = Wv_h\left(\frac{1}{2}\bar{V}_c + \sqrt{\frac{1}{4}\bar{V}_c^2 + 1}\right)\Big/550 \tag{19b}$$

However, $P_{c_{id}}$ can be expressed as the ideal power required in hovering $P_{h_{id}}$ times a factor κ_c: $P_{c_{id}} \equiv \kappa_c P_{h_{id}}$ where, in turn, $P_{h_{id}}$ in HP is $P_{h_{id}} = Wv_h/550$. Substituting the above expressions into Eq (19b), one obtains:

$$\kappa_c = \frac{1}{2}\bar{V}_c + \sqrt{\frac{1}{4}\bar{V}_c^2 + 1} \tag{19c}$$

Eq (19c) can also be solved for $\bar{V}_c$:

$$\bar{V}_c = \kappa_c - (1/\kappa_c). \tag{20}$$

The above relationship is shown graphically in Fig 2-7.

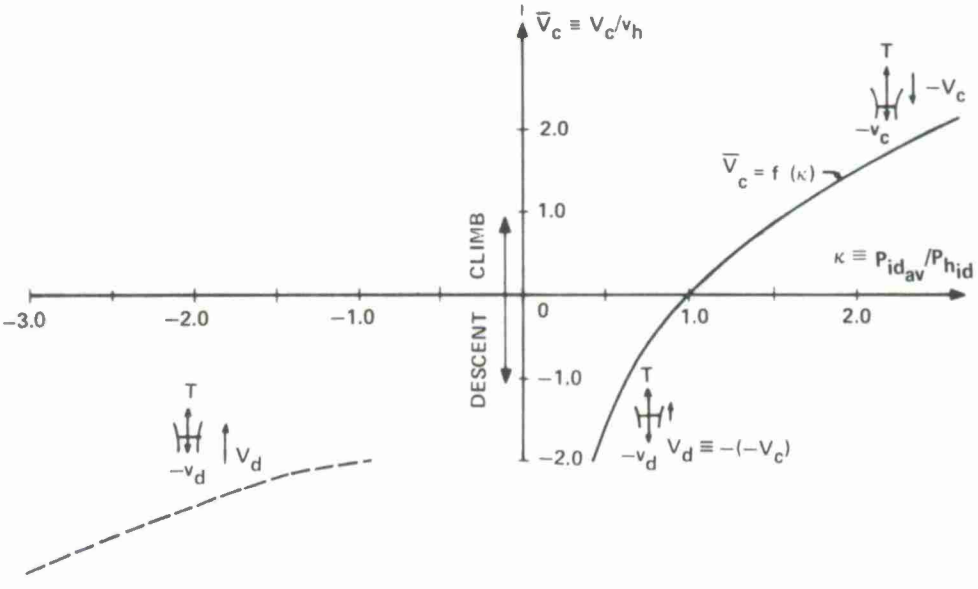


Figure 2-7. Nondimensional Rate of Climb and Descent vs Power Setting

For a particular case of hovering or static thrust conditions in general, $V_c = 0$, and Eq (18) would reduce to the following expression for the power required in HP:

$$P_{h_{id}} = Tv/550 \tag{21}$$

The above result could have been obtained directly from Eq (3), remembering that for the actuator disc, $v_u = 2v_h$.

Substituting for v_h, its value from Eq (13) and rewriting Eq (17) in terms of the reciprocal of the power loading (T/P); i.e., $(P/T)_h$ and disc loading w, one obtains:

$$(P/T)_h = \sqrt{w/2\rho}/550 \tag{21a}$$

where for the case of hovering with no download, $T = W$ and thus, $w \equiv T/A = W/A$.

Eq (21a) indicates that if a physicomathematical model based on the actuator disc concept could truly represent practical rotor-propellers, there would be no lower limit for the power required to produce a given static thrust. It would only be necessary to make the disc loading (w) as low as possible. It will be shown later, however, that the existence of profile drag, which has been completely neglected in the simple-momentum-theory approach will considerably modify this conclusion.

It will be shown later that practical problems of predicting rate of vertical ascent as well as absolute and/or operational ceiling (corresponding to a prescribed rate of climb value) can be reduced to the case of the ideal actuator disc considerations. For this reason, a way of determining the dimensional rate of climb vs altitude is discussed below.

When $T = W$, the total axial flow through the disc $V' = V_c + v_c$ can be found from Eq (18) as

$$V' = 550P_{id_{av}}/W, \tag{22}$$

where $P_{id_{av}}$ is the ideal horsepower available at the rotor. On the other hand, the induced velocity (v_c) can be found from Eq (10):

$$v_c = W/2\pi R^2\rho V'.$$

Substituting into this last expression, the value of V' as given by Eq (22), we obtain the following:

$$v_c = W^2/1100\pi R^2\rho P_{id_{av}}. \tag{23}$$

Since the rate of climb in this case is

$$V_c = V' - v_c,$$

then, from Eqs (22) and (23), one obtains

$$V_c = (550P_{id_{av}}/W) - (W^2/1100\pi R^2\rho P_{id_{av}}). \tag{24}$$

As the variation of $P_{id_{av}}$ with altitude should be known, then $550P_{id_{av}}/W$ can easily be computed for any altitude h. The same applies to $W^2/1100\pi R^2\rho P_{id_{av}}$, and the vertical rate of climb at any altitude can readily be obtained from Eq (24).

If the relationship between the power available from the rotor $(P_{id_{av}})$ and air density, ρ, can be expressed as a simple algebraic function, then by setting $V_c = 0$, Eq (24) can be solved for ρ_H; i.e., the density corresponding to the absolute ceiling. From this value of ρ_H, the absolute ceiling can readily be found from tables for standard atmosphere. When there is a defined requirement for rate of vertical climb at the operational hovering altitude (say, $V_c = 500\ fpm \approx 8.3\ fps$); the hovering ceiling can be found by substituting the desired value of V_c into Eq (24) and solving it for ρ. Usually, the relationship between engine power and density cannot be expressed simply, and a suitable computer program for solving Eq (24) through an iteration process has to be established, or a graphical method can be used (Fig 2-8).

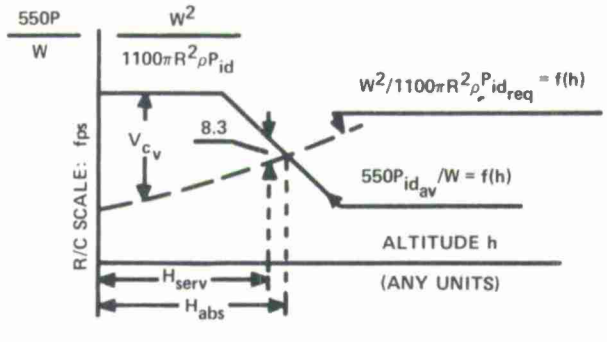


Figure 2-8. Absolute and Service Ceiling in Vertical Climb

Rates in partial-power descent will be considered first for the $|V_d/v_d| < 1.0$ case. Under these conditions, the general flow is still down and, according to the previously developed rules, the ideal power (in HP) required for this process according to Eq (2b) with $T \cdot V_d$ being negative, will be as follows:

$$Pd_{id} = T(v_d - V_d)/550 \tag{25}$$

or, assuming $T = W$,

$$P_{d_{id}} = W(v_d - V_d)/550 \tag{25a}$$

Substituting into Eq (25a), the v_d value from Eq (16a), relationships similar to those given by Eqs (19) to (20) can be obtained.

$$P_{d_{id}} = W\left(-\frac{1}{2} V_d + \sqrt{\frac{1}{4} V_d^2 + \frac{W}{2A\rho}}\right)\Big/550 \tag{26}$$

or

$$P_{d_{id}} = W\left(-\frac{1}{2} V_d + \sqrt{\frac{1}{4} V_d^2 + v_h^2}\right)\Big/550 \tag{26a}$$

In substituting $\bar{V}_d \equiv |V_d/v_h|$ and defining, as in the case of climb, $P_{d_{id}} \equiv \kappa_d P_{h_{id}}$, where $0 \leq \kappa_d \leq 1.0$, one obtains:

$$\kappa_d = -\frac{1}{2}\bar{V}_d + \sqrt{\frac{1}{4}\bar{V}_d^2 + 1} \tag{26b}$$

Solution for Eq (26b) for $\bar{V}_d$ in terms of κ_d gives

$$\bar{V}_d = -\kappa_d + (1/\kappa_d) \tag{27}$$

The above relationship is added to Fig 2-7. It can be seen from this figure that as the actuator disc starts to descend at some nondimensional rate $\bar{V}_d$ or, in other words, when $\bar{V}_c$ changes its sign from the positive to the negative, power required to produce a given amount of thrust becomes lower than that required in hovering ($\kappa < 1.0$). Conversely, when power supplied to the rotor is reduced below the hovering level, it starts to descend in the so-called vertical partial-power descent. It should be noted, however, that both Fig 2-7 and Eq (26b) indicate that no-power required ($\kappa = 0$) can only be approached at very high $\bar{V}_d$ values ($\kappa \to 0$ when $\bar{V}_d \to -\infty$, or $-\bar{V}_c \to -\infty$). It may be recalled at this point that the relationships given in Eqs (26) to (27) were based on a physical concept, assuming that within the whole slipstream tube, the resultant flow is everywhere in the direction of the downwash at the disc (down, as dictated by the condition of $|2v_d| > |V_d|$), while the flow outside of the tube itself moves in the direction of thrust (up).

Let us now look at the other concept of flow; namely, when $|V_d| \geq |2v_d|$; hence, the flow within the streamtube is always in the direction of thrust (up), just as the movement of the whole mass of air. In this case, since $|V_d| \geq |2v_d|$, $P_{d_{id}}$ as given by Eq (25) and (25a) will be negative.

$$P_{i_d} = -T(V_d - v_d)/550 \tag{28}$$

or

$$P_{i_d} = -W(V_d - v_d)/550. \tag{28a}$$

Eqs (28) and (28a) now indicate that power is delivered by the actuator disc and thus, this particular stage of vertical descent or, more generally, of exposure to the airflow with velocity $|V_d| \geq |2v_d|$ in the thrust direction is called the windmill state. Substituting into Eq (28a), the induced velocity value (v_d) as given by Eq (17) and making rearrangements as in the previous case, one obtains

$$P_{d_{id}} = -W\left(\frac{1}{2} V_d - \sqrt{\frac{1}{4} V_d^2 - v_h^2}\right)\Big/ 550 \tag{29}$$

or, in a nondimensional form,

$$\kappa_d = -\frac{1}{2}\bar{V}_d + \sqrt{\frac{1}{4}\bar{V}_d^2 - 1} \tag{29a}$$

and

$$\bar{V}_d = -[\kappa + (1/\kappa)]. \tag{30}$$

It can be seen from Eq (29a) that for $\bar{V}_d > 2$, the κ_d is negative; i.e., power is delivered by the rotor. When $\bar{V}_d < 2$, there is no real solution to Eq (29a), which means that the assumed physical concept of the model as pictured in Fig 2-6 is not applicable any more. For the limiting case of $\bar{V}_d = 2$, the power ratio reaches its lowest value for the windmill state; namely, $\kappa = -1.0$, and the corresponding rate of descent also attains its lowest value, $\bar{V}_d = 2$. In order to maintain a steady-state operation, energy delivered by the rotor should be consumed or dissipated at the rate of its generation. Actual rotors dissipate energy because of the existance of profile power. However, the rotor profile power of such rotary-wing aircraft as helicopters and tilt-rotors does not usually exceed 30 percent of the ideal hovering power. This obviously means that even for the limiting case of the lowest power delivered in the windmill stage ($\kappa = -1$), all of that power cannot be dissipated as profile power losses. It may be expected, hence, that the corresponding rate of descent of $\bar{V}_d = 2.0$ or, in other words, $V_d = 2\sqrt{w/2\rho}$ would be too conservative. Indeed, the above velocity is higher than those usually observed in actual flight tests. It should also be pointed out that the requirement of air coming to rest in the slipstream above the rotor while the remaining mass moves at

steady velocity V_d is difficult to explain physically. One may expect that before this physically doubtful stage is reached, a different pattern of flow would be established.

It appears that the actuator disc concept, when applied to the cases of vertical ascent and hovering does not encounter any logical difficulties. By contrast, in vertical descent, inadequacies of the assumed model become quite obvious. It may be expected, hence, that the actuator disc approach may provide reasonably good guidance for both understanding and even approximate performance predictions in vertical climb and in hover and, perhaps, at partial power descents with power levels only slightly lower than that required in hover. However, even in the latter case, wind-tunnel tests performed by Yaggy[2] with a tilt-wing propeller, and discussed by this author[3], leave some doubts regarding the validity of Eq (30). As to the whole spectrum of vertical descent; i.e., from those at partial power to pure autorotation ($\kappa = 0$), a search still continues for a completely satisfactory physicomathematical model. In the meantime, analytical gaps are being plugged by experimental results. The theoretical and experimental efforts that started with classical presentations of Lock[4] and Glauert[5] continued through the efforts of Bennett[6], Nikolsky and Seckel[7], Castles and Gray[8,9], and are still continuing as examplified by the more recent works of Washizu[10], Azuma[11], Wolkovitch[12] and Zimmer[13].

2.2.3 Induced Velocity and Thrust in Nonaxial Translation

Through application of the actuator disc concept to the case of axial translation, a basic relationship for thrust in this type of motion was established which may be expressed as follows:

> The thrust developed by a rotor moving along its axis with a speed $\vec{V}_{ax}$ is equal to the rate of flow through the disc times the doubled induced velocity at the disc. In this case, the rate of flow is clearly defined as a product of the disc area ($A \equiv \pi R^2$) times the air density ρ, times the resultant speed of flow through the disc: $\vec{V}' = (\vec{V}_{ax} + \vec{v})$ (which, in axial translation, is identical with an algebraic sum).

The accuracy of the above relationship has been proven (within the limits of validity of the theory itself). Unfortunately, as far as exposure of an actuator disc to a velocity $-\vec{V}$ (opposite to the flight speed) with an inplane velocity component is concerned (Fig 2-9), no rigorous development of the formula for thrust can be offered as yet. Nevertheless, a relationship proposed by Glauert[14,15] when expressed in words, sounds exactly the same as that for axial translation. However, in a nonaxial translation, the resultant speed of flow through the disc should always be interpreted as a vectorial sum of $-\vec{V}$ and $-\vec{v}_f$.

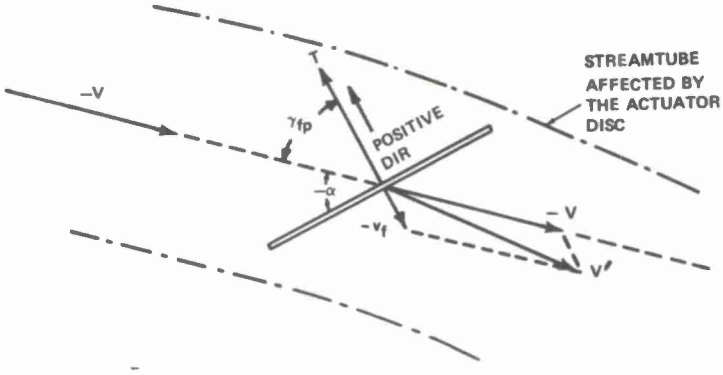


Figure 2-9. Actuator Disc in an Oblique Flow

Denoting the scalar value of the resultant speed of flow at the disc by V', the formula for thrust established for axial translation (Eq (10)) can now be generalized into the following expression by substituting V' for $(V_c + v_c)$:

$$T = 2\pi R^2 \rho V' v_f \tag{31}$$

By analogy with Eq (10), it is postulated that far downstream, the induced velocity v_f is doubled; i.e., $v_u = 2v_f$. By making this assumption, $\pi R^2 \rho V'$ becomes the mass flow through the streamtube (affected by action of the rotor), whose cross-section is πR^2.

An indirect support for the validity of Eq (31) can be found by comparing it with a formula giving thrust developed by a wing with a $2R$ span and having a downwash v distributed uniformly along the span. In this case, the lift developed in horizontal flight is expressed by exactly the same formula as Eq (31).

Accepting the validity of Eq (31), the induced velocity in forward flight can readily be expressed as:

$$v_f = T/2\pi R^2 \rho V'. \tag{32}$$

It should be noted, however, that the above expression in its present form does not permit determination of the v_f value explicitly since V' is also dependent on v_f, $(\vec{V}' = \vec{V} + \vec{v}_f)$. In order to solve Eq (32) for v_f, V' must be expressed first in terms of V and v_f.

With notations as in Fig 2-9, V' becomes:

$$V' = \sqrt{(v_f - V \sin \alpha)^2 + (V \cos \alpha)^2}\,.$$

Substituting the above value into Eq (32), and performing the necessary manipulation, remembering that $T/\pi R^2 \equiv w$ (disc loading), the following fourth-degree equation, in v_f, is

obtained:

$$v_f^4 - 2Vv_f^3 \sin\alpha + V^2v_f^2 - (w/2\rho)^2 = 0. \tag{33}$$

However, $(w/2\rho)^2 = v_h^4$ where v_h is the induced velocity in hovering (or under static thrust conditions in general), and Eq (33) can be presented in nondimensional form:

$$\bar{v}_f^4 - 2\bar{V}\bar{v}_f^3 \sin\alpha + \bar{V}^2\bar{v}_f^2 - 1 = 0. \tag{33a}$$

Where $\bar{V} \equiv V/v_h$ and $\bar{v}_f \equiv v_f/v_h$. Either Eq (33) or (33a) can be solved by Newton's method, and its more modern derivatives adapted to computer techniques. Also, graphical solutions may be quite useful in that respect.

It should be noted that for the axial translation in the direction of thrust; i.e., when $\alpha = -90°$, and $V = V'_{ax}$ or $V = V_c$, Eq (33a) can be reduced to a quadratic form with its solution identical with that of Eq (14a). Also of interest may be another limiting condition; namely, when $\alpha = 0$. In the latter case, Eq (33a) is reduced to a biquadratic form and a solution for $\bar{v}_f$ can also easily be obtained.

$$(\bar{V}_f)_{\alpha=0} = \sqrt{-\tfrac{1}{2}\bar{V}^2 + \sqrt{\tfrac{1}{4}\bar{V}^4 + 1}} \tag{34}$$

$\bar{v} = f(\bar{V})$ for $\alpha = -90°$ and $\alpha = 0°$ are plotted in Fig 10. Thus, these two curves represent the limiting cases of the nondimensional induced velocity, $\bar{v}_f$, vs nondimensional speed of flow, $\bar{V}$ (speed of flight with the opposite sign). All other cases corresponding to the intermediate α values will be included within these two curves. Of course, for horizontal flight when absolute values of the angle of attack (α) are small, the trend indicated by the $\alpha = 0$ curve should be quite representative. By examining Fig 2-10, it should also be noted that for $\bar{V} \geq 3.0$, $\bar{v}$ values tend to converge to a common limit, regardless of the magnitude of α. Furthermore, starting from $\bar{V} \geq 3.0$, the nondimensional induced velocities can be well approximated by the simple relationship

$$\bar{v}_f = 1/\bar{V} \tag{35}$$

Eq (35) can be directly derived from Eq (31) by assuming that $V' \approx V$. Then Eq (31) becomes:

$$T = 2\pi R^2 \rho V v_f \tag{36}$$

and consequently,

$$v_f = T/2\pi R^2 \rho V \tag{37}$$

which can be easily transformed into the Form of Eq (35).

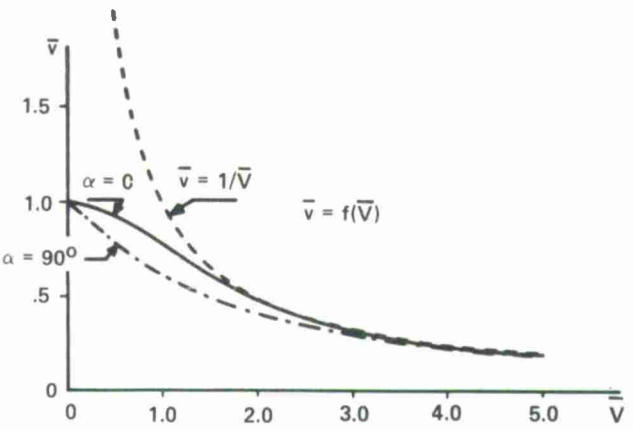


Figure 2-10. Nondimensional Induced Velocity vs Nondimensional Speed of Flow

2.2.3 Power Required in Nonaxial Translation

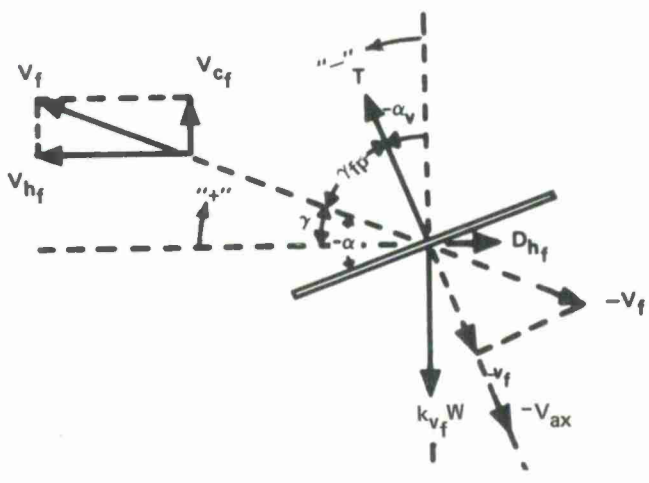


Figure 2-11. Rotary-Wing Aircraft (Modeled by the Actuator Disc) in Forward Flight

Using the notations in Fig 2-11, and substituting into Eq (2b) the proper quantities for $\vec{T}\cdot\vec{V}$ and $(1/2)\vec{T}\cdot\vec{V}_u$, the ideal power required (P_{fid}; ft.lbs/sec) in the nonaxial translation (forward flight) can be obtained:

$$P_{fid} = -T(V_f \sin\alpha - v_f) \tag{38}$$

where the expression in the parentheses represents the axial component (V'_{ax}) of the resultant flow (V') at the disc: $V'_{ax} = V \sin\alpha - v_f$. It can be seen that when $\alpha < 0$, Eq (38) is positive; i.e., power must be delivered to the actuator disc (modeling an actual rotor) in this type of flow.

For a helicopter modeled by the actuator disc and moving in the gravitational coordinate system with velocity of flight V_f, P_{fid} can be obtained by rewriting eq (38).

$$P_{f_{id}} = -(T V_f \cos \gamma_{fp} - v_f). \tag{38a}$$

However, $\gamma_{fp} = 90° - (\gamma + \alpha_v)$ and Eq (38a) can be presented in the following form:

$$P_{f_{id}} = V_f \sin \gamma \; T \cos \alpha_v + V_f \cos \gamma \; T \sin \alpha_v + T v_f \tag{39}$$

It should be realized that

$V_f \sin \gamma \equiv V_{c_f}$ rate of climb in forward flight

$V_f \cos \gamma \equiv V_{h_f}$ horizontal component of the speed of flight

and in a steady-state flight:

$T \cos \alpha_v = k_{v_f} W$ vertical thrust component, balancing aircraft gross weight times k_{v_f} coefficient, accounting for the vertical drag in forward flight

$T \sin \alpha_v = D_{h_f}$ horizontal thrust component required to overcome the horizontal component of the total drag.

Taking into consideration the above relationships, the ideal power required in forward flight can be expressed as follows:

$$P_{f_{id}} = V_{h_f} D_{h_f} + V_{c_f} k_{v_f} W + T v_f \tag{40}$$

where $T = \sqrt{(k_{v_f} W)^2 + D_{h_f}{}^2}$ or $T = W\sqrt{k_{v_f}{}^2 + (D_{h_f}/W)}$ and D_{h_f}/W is the horizontal drag-to-weight ratio of the aircraft as a whole at the considered speed. For those cases when $k_{v_f} \approx 1.0$ and (D_{h_f}/W) may be considered small, it may be assumed that $T \approx W$, and Eq (40) may be written as follows:

$$P_{f_{id}} = W[(D_{h_f}/W) V_{h_f} + V_{c_f} + v_f] \tag{40a}$$

Thus, the ideal power required by a helicopter modeled by the actuator disc is a sum of three distinct (also ideal) terms: (a) power required to overcome the horizontal component of the total drag, (b) power required to perform the work against gravity in climb, and (c) the induced power associated with the process of thrust generation.

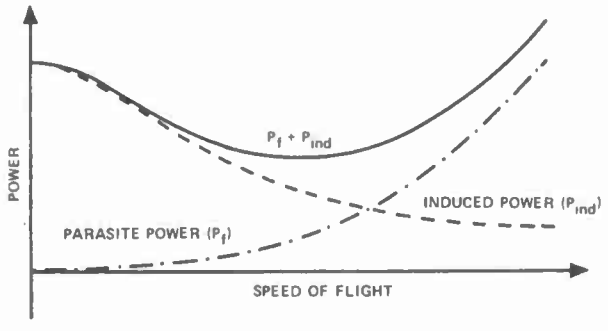


Figure 2-12. Parasite & Induced Power vs Speed of Flight

For the particular case of horizontal flight, the ideal power required would be composed of the drag and the induced terms only. With the induced velocity and hence, the induced power, decreasing with the speed of flight from its maximum value in hovering (Fig 2-10) and the drag power increasing roughly as the cube of forward speed, the resulting total ideal power required curve should resemble that shown in Fig 2-12.

2.2.5 Thrust Tilt in Forward Flight

In the pure helicopter, the rotor performs the dual function of lifting and propelling in all regimes of powered flight. Using the notations of Fig 2-11, the horizontal forces equilibrium condition can be expressed as:

$$T \tan \alpha_v = D_{h_f}$$

or

$$\alpha_v = \tan^{-1}(D_{h_f}/T) \tag{41}$$

Probably for almost all practical conditions, small angle assumption as well as the $W \approx T$ condition can be justified. Thus, Eq (41) can be simplified to the following form:

$$\alpha_v \approx (D_{h_f}/W). \tag{41a}$$

2.2.6 Determination of Induced Power in Horizontal Flight

Eq (33) or (33a) permit, in principle, calculation of induced velocity at any speed of flight (V_{h_f}) once the tilt of the thrust vector (α_v) and hence, the α angle $(\alpha = \alpha_v)$ corresponding to that speed is computed from Eqs (41) or (41a). However, the iteration method required to solve Eqs (33) and (33a) may be tedious unless a suitable computer

program is available. For this reason, simpler approaches may be of some value.

At low flying speeds, the assumption $V_{hf} = V'$ is no longer acceptable and thus, Eqs (35) and (37) cannot be used. However, the rotor tilt $\alpha_v = -\alpha$ required in steady flight at low velocities will be so small that $\alpha_v \approx 0$. This implies that the induced velocity v_{hf} is perpendicular to the flying speed V_{hf} (see Fig 2-13).

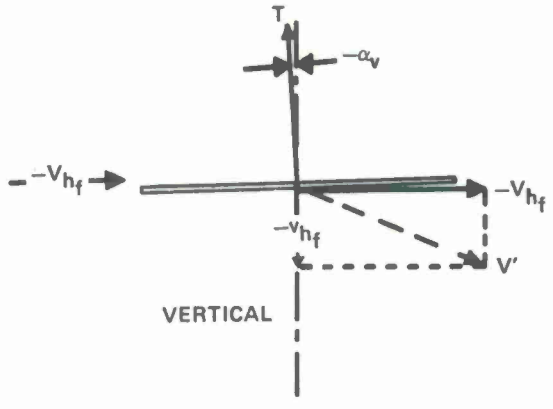


Figure 2-13. Velocity at the Disc at a Low Horizontal Speed

Under the foregoing assumptions, Eq (34) can be used. Also, approximate values of v_{hf} can be obtained from the nondimensional graph of Fig 2-10. However, for those cases when the $\alpha_v \approx 0$ assumption is not acceptable, the following graphical method can be used which permits consideration of the existence of the tilt angle, $\alpha_v \neq 0$.

A curve giving $v = f(V')$ is drawn from Eq (32) using the scale for the ordinate and the abscissa axes. This will obviously be a hyperbola whose point $v = V'$ will correspond to the hovering condition.

The value of the induced velocity must satisfy Eq (32) as given by the graph in Fig 2-14, as well as the other relationship of

$$\vec{V}' = \vec{V}_{hf} + \vec{v}_{hf}.$$

By referring to Figs 2-13 and 2-14, one can see the simple graphical method which can be employed in finding the downwash velocity v in horizontal flight.

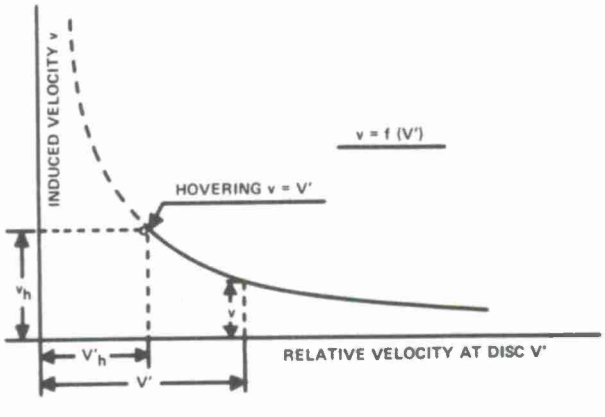


Figure 2-14. Induced Velocity vs Relative Velocity at the Disc

The value of V_{hf} and the direction of v_{hf} (tilt of the rotor α_v) are known. Assuming a value of V', the corresponding value of v_{hf} is found from Fig 2-14. These values of V' and v must also satisfy the vectorial relationship shown in Fig 2-15. This means that the head of the vector V' must lie on line a-b parallel to the rotor axis, while the length of a-b must be equal to the value of v_{hf} corresponding to the assumed V'. If the V' and v_{hf} chosen the first time do not fulfill these conditions, a new value of V' should be assumed and the whole procedure repeated. By cutting and trying, the correct pair of values of V' and v_{hf} satisfying both Eq (32) and the vectorial sum condition can easily be found.

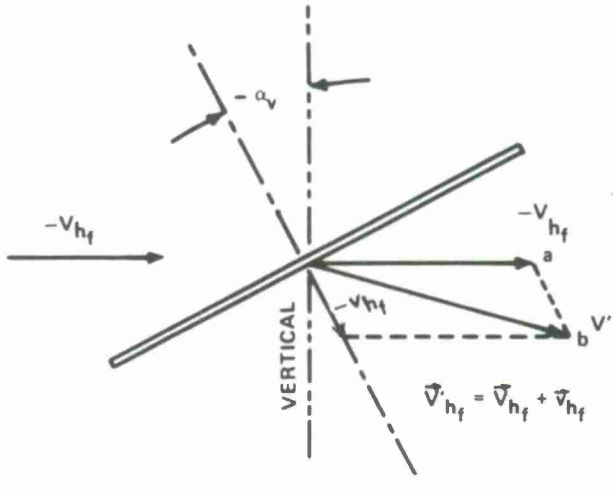


Figure 2-15. Velocities at the Disc in Horizontal Flight at High-Thrust Inclination

2.2.7 Rate of Climb in Forward Flight

When the total power available at the actuator disc modeling a rotor ($P_{id_{av}}$) is known, the rate of climb can be found in the following manner.

It is assumed that the rotor inclination α_v remains the same in ascending flight as it would be in horizontal flight at a speed V_{hf} equal to the horizontal component of the actual flying speed V_f. Hence, if the drag as a function of forward speed of the helicopter is known, then the rotor tilt α_v can readily be computed. Also, since the power available at the rotor $P_{id_{av}}$ in HP is known, the total rate of axial flow through the disc U can be found from Eq (38), where U is substituted for the axial component V'_{ax}.

$$U = 550\, P_{id_{av}}/k_{v_f} W \tag{42}$$

On the other hand, the rate of climb can be expressed (see Fig 2-16) as:

$$V_c = U - (V_f \alpha_v + v_f) \tag{43}$$

and, substituting Eq (42) for U,

$$V_c = (550\ P_{id_{av}}/k_{v_f} W) - (V_f \alpha_v + v_f). \quad (44)$$

The value of v_f in Eq (44) is yet unknown; but it may readily be found with the help of a simple graph as shown in Fig 2-16. From the head of vector Vh_f, a line parallel to the disc axis is drawn. Again, from the head of vector U, a line normal to the disc axis is drawn, intersecting the first line. By approximation, point A may be considered as the head of a vector representing the relative velocity of the slipstream V'. 0-A indicates the magnitude of V', and from the graph, $v_f = f(V')$, (Fig 2-14), the corresponding v_f can be found easily. When this latter value is introduced into Eq (44), the rate of climb will be obtained.

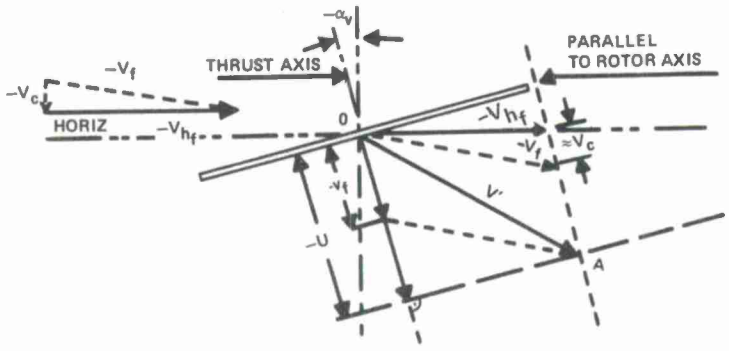


Figure 2-16. Velocity Scheme in Forward Flight Climb

In finding the induced velocity v_f at altitude, it must be remembered that v_f is inversely proportional to the air density (see Eq 32). A graph of $v_f = f$ (altitude) with the scale of V' remaining constant, could be helpful for altitude calculations. However, a procedure based on the principle of excess power is usually accurate enough for all practical purposes in determining the rate of climb. It can be seen from Eq (40) that

$$V_c = [P_{id_{av}} - (Vh_f Dh_f + T v_f)]/k_{v_f} W .$$

In the above equation, the expression in the parentheses represents the power required in horizontal flight $(P_{id_f})_{req}$ at a speed Vh_f, while $P_{id_{av}}$ should be interpreted as the ideal power available at the actuator disc (rotor). When both powers are in HP, V_c in fps can be expressed as follows:

$$V_c = 550(P_{id_{av}} - P_{id_{f_{req}}})k_{v_f} W . \quad (45)$$

In many cases, it may be assumed that the vertical load factor $k_{v_f} = 1.0$.

Service and absolute ceilings in forward flight can be obtained from Eq (45) by finding the maximum rate of climb (Vc_{max}) at several altitudes and plotting Vc_{max} values versus altitude. It is obvious that the altitude at which Vc_{max} reaches some prescribed value; say, $Vc_{max} = 200\ fpm$ will yield the service ceiling (see Fig 2-17).

The method of finding the rate of climb from the excess power can be accepted for higher flying speeds (V_e and higher) when climbing would not appreciably change the rate of flow through the disc. For low forward speeds, the graphical method previously outlined is more suitable.

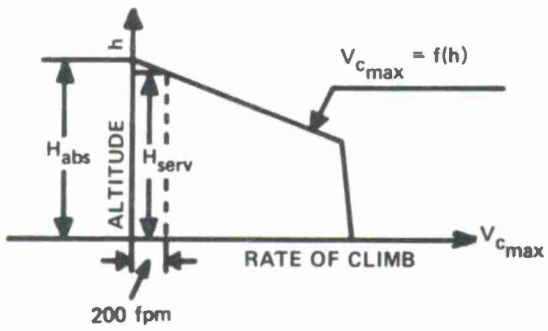


Figure 2-17 Maximum Forward Climb Diagram & Determination of Absolute and Service Ceilings

2.3 NONUNIFORM INDUCED VELOCITY AND TIP LOSSES

Up to this point, physicomathematical models based on the actuator disc concept have been used. It has been assumed that the induced velocity is uniform both at the disc and in the fully established wake. Furthermore, it has also been assumed that the disc is equally effective in thrust generation up to the limit of its geometric dimension; i.e., up to its radius R. However, it may be expected that actual thrust generators may produce nonuniform induced velocity distributions, and also various aerodynamic phenomena occurring at the outer rim of the disc may reduce its thrust-generating effectiveness in that region. In other words, it may be expected that the effective disc radius $R_e < R$, or $R_e/R \equiv x_e < 1.0$ where x is a new symbol that will be used from now on to denote the nondimensional disc radius $x \equiv r/R$, r being the geometric radius.

Since the induced power corresponding to the uniform downwash distribution and full effectiveness of the actuator disc area represents a minimum of power needed for generation of a given thrust T by a rotor of radius R, that power has been called ideal (P_{id}) as well as the associated induced velocity v_{id}. However, due to a nonuniform downwash and reduced thrust-generating effectiveness of the disc, the actual induced power P_{ind} required for generating thrust T will be higher than the ideal one. These deviations of the actual induced power from its ideal level can be evaluated through the k_{ind} factor, defined as:

$$k_{ind} \equiv P_{ind}/P_{id}. \tag{46}$$

Momentum theory can help in developing some feeling regarding the magnitude of the k_{ind} factor corresponding to various patterns of induced velocity distribution, the nondimensional effective radius (x_e) values, as well as other aerodynamic interferences. An illustration of those aspects will be provided by two examples: one, dealing with a single rotor under static conditions (hovering) and another, by examining the induced power of a tandem in horizontal translation.

2.3.1 The k Factor in Hovering

2.3.1.1 Rectangular Downwash with Tip Losses

Let it be assumed that the induced velocity is uniform over the disc area within the limits of $0 \leq x \leq x_e$ and equal to v_{ind} (Fig 2-18b). For $x > x_e$, $v_{ind} = 0$, it is easy to show that in order to produce the same thrust as for the ideal case (Fig 17a) the induced velocity should be

$$v_{ind} = v_{id}/x_e \tag{47}$$

and consequently,

$$k_{ind_h} = 1/x_e. \tag{48}$$

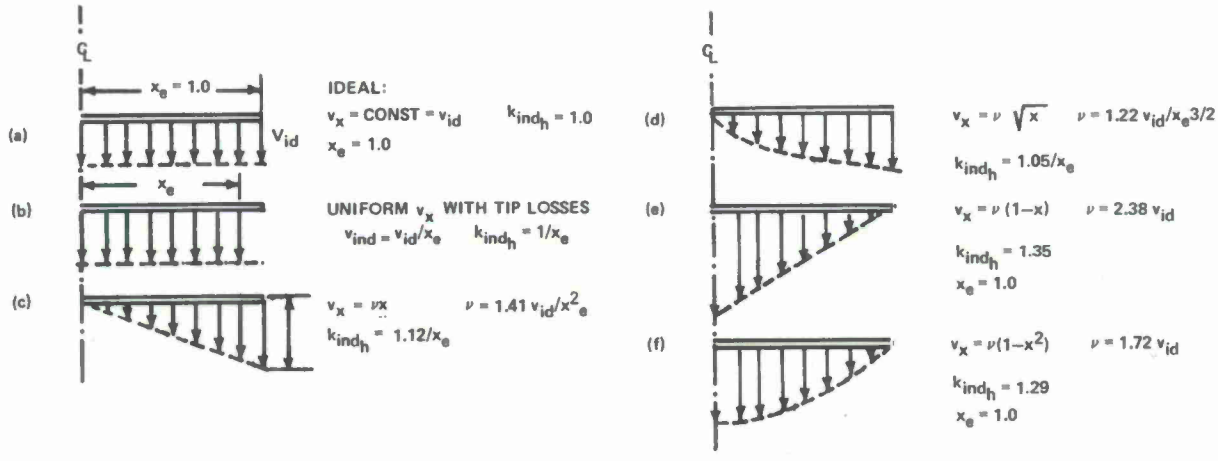


Figure 2-18. Examples of Induced Velocity Distributions

2.3.1.2 Triangular and Other Patterns of Downwash Distribution

In this case, the induced velocity at any nondimensional radial station $x \equiv r/R$ is expressed as follows:

$$v_x = \nu x \tag{49}$$

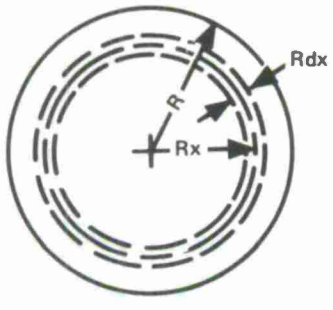


Figure 2-19. Elementary Ring at the Actuator Disc

where ν is the induced velocity at $x = 1.0$.

A ring of radius $r \equiv Rx$ and width $dr \equiv Rdx$ (Fig 2-19), with induced velocity $v_r \equiv v_x$, should produce an elementary thrust

$$dT_x = 4\pi R^2 \rho v_x^2 x\, dx. \tag{50}$$

Substituting into Eq (50), the v_x value from Ea (49), and integrating from $x = 0$ to $x = x_e$, the following expression for the total thrust (T) is obtained.

$$T = 4\pi R^2 \rho \nu^2 \int_0^{x_e} x^3\, dx = \pi R^2 \rho \nu^2 x_e^4. \tag{51}$$

Equating the above obtained expression for thrust to that of the ideal case ($T = 2\pi R^2 \rho v_{id}^2$), one obtains

$$v = 1.41\ v_{id}/x_e^2. \tag{52}$$

Induced power can now be found by considering first, its elementary value dP_{ind} corresponding to the previously considered ring (Fig 2-19).

$$dP_{ind_x} = dT_x\, v_x \tag{53}$$

Substituting Eq (50) for dT_x, and Eq (49) for v_x and then Eq (52) for v, Eq (53) becomes:

$$dP_{ind_x} = 4\pi R^2 \rho (1.41\, v_{id}/x_e^2)^3\, x^4\, dx. \tag{53a}$$

Integrating Eq (53a) within the $x = 0$ to $x = x_e$ limits, the following is obtained:

$$P_{ind} = 2.24\pi R^2 \rho\, v_{id}^3/x_e. \tag{54}$$

Finally, by dividing Eq (54) by the ideal induced power value, the expression for the k_{ind_h} factor becomes

$$k_{ind_h} = 1.12/x_e. \tag{55}$$

Using procedures similar to the above-described one, it is possible to obtain the k_{ind_h} factor values for other assumed shapes of the induced velocity distribution. Two of them, a triangular one with maximum induced velocity at the disc center and a parabolic one, again, with $v_{x=0} = v_{max} \equiv v$, are shown in Fig 2-18. It should be noted from that figure that in the two latter cases, the x_e does not appear either in the expression for v or for k_{ind_h}. This is obviously due to the fact that because of the low induced velocities of the outer disc rim, variation of the x_e values within practical limits ($.9 \leq x_e \leq 1.0$) has very little influence on the level of v and k_{ind_h}.

By reviewing Fig 2-18, one may conclude that when the induced velocity distribution deviates from its ideal uniform shape, noticeable increases in the induced power over its ideal value can be expected. It also becomes clear that especially unfavorable are the $v_x = f(x)$ shapes where maximum downwash velocity is at the central portion of the disc ($k_{ind_h} = 1.29$ for the parabolic, and $k_{ind_h} = 1.35$ for the triangular downwash distribution). It also can be seen from Fig 2-18 that the importance of the x_e values is not the same for all types of the induced velocity distribution. However, for more practical shapes (e.g., Cases (b), (c) and (d)), its value should be $x_e \geq .95$ in order to keep the resulting induced power losses within a few percent of the ideal power.

2.4 INDUCED VELOCITY AND INDUCED POWER OF THE TANDEM CONFIGURATION IN HORIZONTAL FLIGHT

Physicomathematical models based on the actuator-disc concept can also be helpful in understanding the induced velocity and induced power aspects of the non-overlapping tandem configurations* in horizontal flight.

It may be anticipated that, in general, the most important parameters as far as induced velocity and induced power are concerned will probably be: (a) geometrical position of the rotors, and (b) relative value of forward speed with respect to the average induced velocity. As to the first factor, attention will be focused on the relative elevation, h_{re}, of the rear rotor over the front one (Fig 2-20).

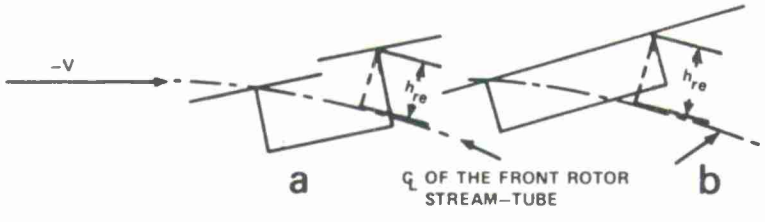


Figure 2-20. Relative Elevation of the Rear Rotor

With regard to the second factor, it will be assumed that the forward speed is high enough to justify the small angle assumption in determining deflection of the flow due to the induced velocity. Furthermore, it will be assumed that the rate of flow through the rotor is almost equal to the speed of flight ($V' \approx V$) and finally, that both rotors are of the same radius R.

Analogy with a tandem biplane, as well as some experimental evidence, indicates that the influence of the rear rotor on the front one can be neglected. This means that the average induced velocity of the front rotor (v_{fr}), developing thrust T_{fr} can be expressed in the same way as for the isolated rotor:

---

*It will become clear later from the example of overlapping and/or intermeshing tandems in hovering that for this particular configuration, additional information about rotor geometry is necessary which cannot be incorporated in the simple momentum approach.

$$v_{fr} = T_{fr}/2\pi R^2 \rho V. \tag{56}$$

It will be shown in the following chapter that the downwash velocity at the trailing edge of the rotor reaches its full far-downstream value of twice the average induced velocity. It is logical to assume, hence, that the air approaching the rear rotor has already a downward component equal to $2v_{fr}$.

Induced velocity associated with thrust T_{re} of the rear rotor will be

$$v_{re} = T_{re}/2\pi R^2 \rho V. \tag{57}$$

Should the rear rotor be completely submerged in the slipstream of the front one, then the total axial component of the rate of flow through its disc associated only with lift generation by both rotors will be

$$V_{ax_{re}} = 2v_{fr} + v_{re}. \tag{58}$$

Consequently, the induced power in HP associated with thrust generation by the rear rotor will be

$$P_{ind_{re}} = T_{re}(2v_{fr} + v_{re})/550 \tag{59}$$

and the total induced power of both rotors would be

$$P_{ind} = [T_{fr}v_{fr} + T_{re}(2v_{fr} + v_{re})]/550. \tag{60}$$

For the particular case when the front and rear rotor are producing the same thrust, and the latter is fully submerged in the slipstream of the front one, the induced power of the tandem would be equal to twice that of the two isolated rotors producing the same thrust: $T = T_{fr} + T_{re}$.

However, in numerous practical cases, the rear rotor is not fully submerged in the streamtube affected by the front rotor. This may be due to the geometry of the aircraft, the trim position of the ship in flight, and finally, the downward deflection of the front rotor slipstream. In order to deal with all of these cases, a simplified picture of the interaction between the slipstream of the front and rear rotor is conceived, imagining that the airstreams penetrate each other in the manner shown in Fig 2-21.

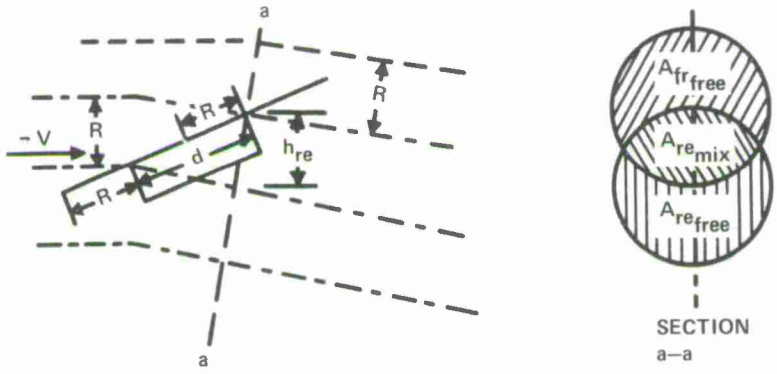


Figure 2-21. Mixing of the Streamtubes of 2 Rotors

It may be anticipated that within those regions where the streamtube affected by the front rotor does not penetrate into that influenced by the rear rotor, the downwash in the non-mixed part of the rear rotor streamtube will remain as given by Eq (57). In those regions where the airstream influenced by the front rotor penetrates that influenced by the rear one, Eq (58) is assumed to be valid.

Consequently, the induced power of the whole helicopter can be broken down into three components and computed separately. The first one will be of the whole front rotor, and will remain the same as in the previously discussed case.

$$P_{ind_{fr}} = v_{fr} T_{fr} \tag{61}$$

As far as the rear rotor is concerned, the part of its induced power that may be "credited" to the non-mixed part of the rear-rotor airstream can be expressed as:

$$P_{ind_{re_{free}}} = T_{re}v_{re}(A_{re_{free}}/\pi R^2)/550. \tag{62}$$

For that part where the two streams mix together, the induced power can be determined as:

$$P_{ind_{re_{mix}}} = T_{re} v_{re} (A_{re_{mix}}/\pi R^2)/550 \tag{63}$$

where $A_{re_{mix}}$ is the area of the mixed, and $A_{re_{free}}$ of the free, stream (Fig 2-21).

The total induced power of the helicopter will be a sum of all three components:

$$P_{ind} = \left\{ T_{fr} v_{fr} + (T_{re}/\pi R^2) \left[v_{re} A_{re_{free}} + (2v_{fr} + v_{re}) A_{re_{mix}} \right] \right\} / 550. \tag{64}$$

For the particular case of rotors producing the same thrust equal to $T/2$, the expression for induced power is reduced to the following:

$$P_{ind} = \frac{T^2}{\pi R^2 \rho V} \left[\frac{1}{4} + \frac{1}{4\pi R^2} \left(A_{re_{free}} + 3A_{re_{mix}} \right) \right] / 1100 \tag{65}$$

It should be realized that the above-considered induced power of the tandem configuration is still for an idealized case, as it assumes uniform downwash distribution and no tip losses. However, P_{ind}, as given by Eq (65) will be higher than the truly ideal one, corresponding to two isolated rotors, each developing a thrust of one-half T. Similar to the preceding section, the k_{ind_f} factor can be defined as a ratio of the induced power as given by Eq (65) to that of the ideal induced power of two isolated rotors of the same radius, each developing a thrust of one-half T:

$$k_{ind_f} \equiv P_{ind}/2P_{id}\big|_{(1/2)T}.$$

Performing the necessary substitution, one obtains:

$$k_{ind_f} = 2 \left[\frac{1}{4} + \frac{1}{4\pi R^2} \left(A_{re_{free}} + 3A_{re_{mix}} \right) \right] \tag{66}$$

It can be seen that for rotors so located that the centerline of the front rotor airstream passes through the hub of the rear rotor ($h_{re} = 0$), the k would become equal to 2. However, when corrections resulting from tip losses are introduced, the k_{ind_f} factor for the case of $h_{re} = 0$ becomes higher than 2.0.

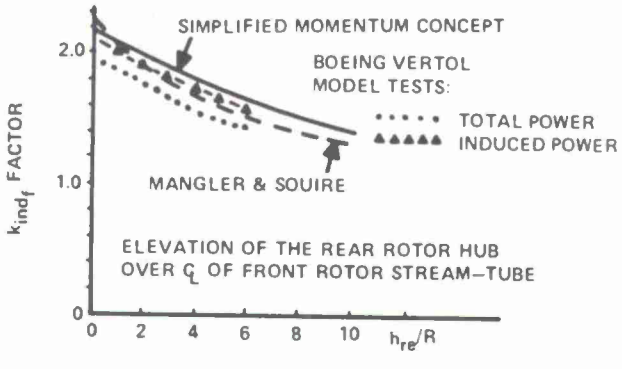


Figure 2-22. The k_{ind_f} Factor for a Tandem in Forward Flight vs Rear Rotor Elevation

In Fig 2-22, a graph is plotted showing the variation in the k_{ind_f} factor vs elevation of the hub of the rear rotor over the centerline of the front rotor airstream tube, as predicted by the momentum approach (including tip losses)[16].

For comparison, values of the k_{ind_f} factor are shown as computed for a non-overlapped tandem on the basis of the Mangler-Squire theory[17].

In addition, results representing an average of over 60 points obtained by Boeing Vertol in wind-tunnel tests of a universal tandem helicopter model are also shown in this figure. The lower of the two Boeing curves represents direct total power measurements (including blade profile drag contribution). The upper curve gives the induced power ratios (the true k_{ind_f} factor values) which were computed by assuming that profile power amounts to 25 percent of the total power. It can be seen from Fig 2-22 that k_{ind_f} values predicted by the momentum approach agree quite well with those obtained from the wind-tunnel model tests.

2.5 CONCLUDING REMARKS RE SIMPLE MOMENTUM THEORY

Physicomathematical models of rotary-wing aircraft, based on the simple momentum approach have been applied to the aerodynamic phenomena, both in an axial as well as an oblique translation of the thrust generators. In this way, an insight has been obtained into basic relationships between such important design parameters as disc loading (w) and power required per pound of thrust (P/T). An understanding of the power requirements for climb, both in vertical ascent and in forward translation, has been reached. Some understanding of the partial power and no-power vertical descent phenomena has been achieved, although it became clear that in this particular case the physical assumptions required in the structure of the model based on the simple momentum approach are not completely convincing. Finally, some idea regarding the importance of nonuniform induced velocity distribution, tip losses in hovering, and aerodynamic interference of tandem rotors in forward flight has been examined. It may be stated that, indeed, the simple momentum theory contributed to a better understanding of many basic aspects of performance of rotary-wing aircraft. Furthermore, many performance aspects of actual helicopters (e.g., vertical and forward flight, average downwash velocity at various tilt angles of the

rotor, etc.) can be reduced to the simple conceptual models based on the simple momentum theory. This may provide a clarity of the overall picture that could be lacking in other approaches. However, as far as providing guidance for design of the rotor, the presently discussed theory encounters serious limitations. It singles out disc loading as the only important parameter. It does not provide any insight into such aspects as ratio of the blade area to the disc area (solidity ratio: σ), blade airfoil characteristics, tip speed values with all the associated phenomena of compressibility, etc. Even when discussing the influence of the nonuniformity of induced velocity and tip losses on the k_{ind} factor in hovering, the simple momentum approach did not provide a physical concept that could explain the reason for nonuniformities of downwash velocities or presence of tip losses.

In order to be able to investigate such rotor design parameters of blade geometry (planform, airfoils, and twist), airfoil characteristics, solidity ratio and tip speed, a new physicomathematical model that would somehow reflect all these quantities must be conceived. The combined blade element and momentum theory that will be considered in the next chapter should provide the desired, more refined model.

References for Chapter 2

1. Poisson-Quinton, P., Introduction to V/STOL Aircraft Concepts and Categories, AGARDograph 126, May 1968.

2. Yaggy, P.F. and K. W. Mort, Wind-Tunnel Tests of Two VTOL Propellers in Descent, NASA TN D-1766, 1963.

3. Stepniewski, W.Z., The Subsonic VTOL and GETOL in Perspective, Aerospace Engineering, Vol. 21, No 4, April 1962.

4. Lock, C.N.H., H. Bateman, and H.C.H. Townsend, An Extension of the Vortex Theory of Airscrews with Application to Airscrews of Small Pitch, Including Experimental Results, Br. R&M 1014, 1925.

5. Glauert, H., The Analysis of Experimental Results in the Windmill Brake and Vortex Ring States of an Airscrew, Br. R&M 1026, 1926

6. Bennett, J.A.J., Rotary-Wing Aircraft, Aircraft Engineering, January to August 1940.

7. Nikolsky, A.A. and E. Seckel, An Analytical Study of the Steady Vertical Descent in Autorotation of Single-Rotor Helicopter, NACA TN 1906, 1949.

8. Castles, W., Jr. and R. B. Gray, Experimental Relation between Induced Velocity, Thrust and Rate of Descent of a Helicopter Rotor as Determined by Wind-Tunnel Tests on Four Model Rotors, TN 2474, 1951, NACA

9. Castles, W., Jr., Flow Induced by a Rotor in Power-On Vertical Descent, NACA TN 4330, 1958.

10. Washizu, K., A. Azuma, J. Kōo and T. Oka, Experiments on a Model Helicopter Rotor Operating in the Vortex Ring State, Journal of Aircraft, Vol. 3, No 3, May-June 1966.

11. Azuma, A. and A. Obata, Induced Flow Variation of the Helicopter Rotor Operating in the Vortex Ring State, Journal of Aircraft, Vol. 5, No 4, July-August 1968.

12. Wolkowitch, J., Analytical Prediction of Vortex-Ring Boundaries for Helicopters in Steep Descent, AHS Journal, Vol. 17, No. 3, July 1972.

13. Zimmer, Herbert, The Rotor in Axial Flow, AGARD-CPP-111, September 1972.

14. Durand, W.F., Aerodynamic Theory, Vol. IV, Div. L: Airplane Propellers by H. Glauert, Durand Reprinting Committee, CIT (California Institute of Technology), 1943.

15. Stepniewski, W.Z., A Simplified Approach to the Aerodynamic Rotor Interference of Tandem Helicopters, Proceedings of the West Coast American Helicopter Society Meeting, September 21 and 22, 1955.

16. Mangler, K.W. and H.B. Squire, The Induced Velocity Field of a Rotor, R&M No. 2642, 1953.

3. BLADE ELEMENT THEORY

In order to overcome the previously discussed limitations of the momentum theory, a physicomathematical model of the rotor is needed that would depict the aerodynamic phenomena occurring at the blade itself. This would permit various geometric and aerodynamic characteristics of the blade to be introduced into the model; thus, leading to a more representative picture of the action of all the blades belonging to a single rotor or a combination of rotors.

The blade element theory represents one of the first attempts to solve these problems. In its initial simplified form, sometimes known as the "Primitive Blade Element Theory," it was developed almost entirely by S. Drzewiecki between 1892 and 1920 (see p. 211, Ref. 1). At that time, no attempt was made to account for all the velocity components in the immediate vicinity of a considered blade element. In particular, the influence of the induced velocity on the flow patterns and thus, the sectional angle of an attack of the blade element was not considered.

As one possible way of overcoming these difficulties in predicting thrust and torque of propellers and rotors, lift (C_L) and drag (C_D) coefficients for the above calculations were obtained in three-dimensional wind-tunnel tests at some rather arbitrary aspect ratios. For instance, some authors proposed $AR = 6$; others, $AR = 12$. In other cases, the actual aspect ratio of the blade was suggested. This uncertainty of the actual angle of attack at every element of the blade constituted a serious logical drawback of the rotor model based on the "primitive" blade element theory.

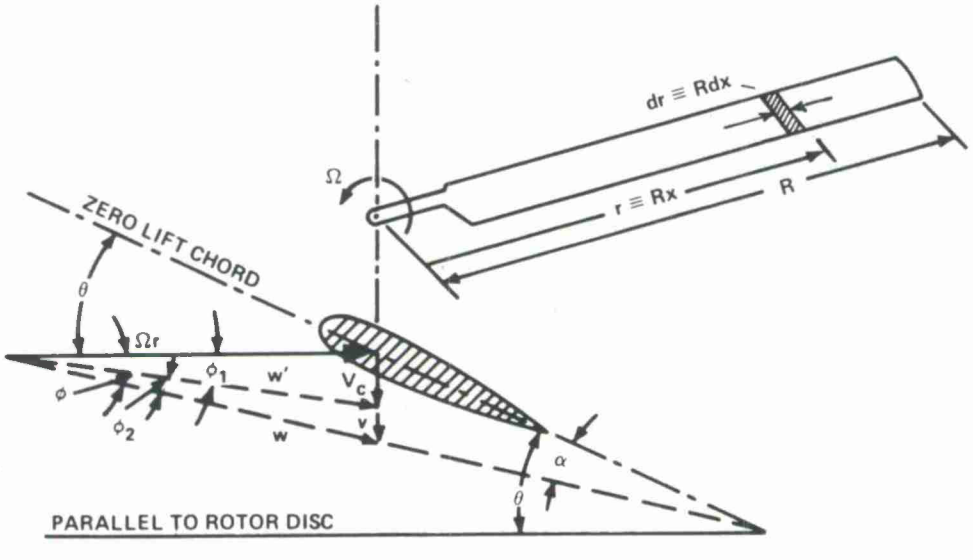
However, should the pattern of air flow in the immediate vicinity of the blade element be known, the thrust and torque produced by it could be more accurately predicted. Indeed, the whole current philosophy of predicting rotor performance strives to depict, as accurately as possible, the flow patterns at the blade element, including their variation with time. Once the above information is known, then sectional (two-dimensional) aerodynamic coefficients (c_ℓ, c_d and c_m) for either steady or unsteady flow can be used.

3.1 AXIAL TRANSLATION AND HOVERING

3.1.1 Basic Considerations of Thrust and Torque Predictions

By analogy with the momentum theory, basic concepts of the blade element theory will be initially examined on the case of a rotor in axial translation in the direction of thrust (climb).

Consider that the blade of a rotor of radius R is composed of narrow elements $dr \equiv Rdx$ wide, having a chord c, and a defined airfoil section. In general, both the chord c and airfoil section may vary along the blade span, or in other words, may depend on the radial position of the blade element as defined by $r \equiv Rx$ (Fig 3-1).



NOTE: In this figure, the blade element is shown stationary, while the air flows past it.

Figure 3-1. Blade Element Concept

The whole rotor is composed of b blades, and is assumed to be turning at a rotational velocity $\Omega \equiv V_t/R$ (where V_t is the tip speed) while moving along its axis (in the direction of thrust) with a speed V_c.

If the pitch angle (i.e., the angle between the zero lift-line of the element and the rotor disc) of an element located at radius r is θ_r; then, its angle of attack α_r, will be (see Fig 3-1):

$$\alpha_r = \theta_r - (\phi_{1_r} + \phi_{2_r})$$

where ϕ_{1_r} is the angle due to the rate of climb $\phi_{1_r} = tan^{-1}(V_c/\Omega r)$ and ϕ_{2_r} is the induced angle: $\phi_{2_r} = tan^{-1}(v_r/\Omega r)$.

The angle of attack of the element at station r can now be expressed as:

$$\alpha_r = \theta_r - tan^{-1}[(V_c + v_r)/\Omega r] \tag{1}$$

or in those cases where V_c and v_r are small in comparison to Ωr,

$$\alpha_r = \theta_r - (V_c + v_r)/\Omega r \tag{1a}$$

where, of course, all angles are expressed in radians.

If the induced velocity at some radius r were known, it would be possible to estimate accurately the lift and drag of the blade element using section coefficients. The section lift coefficient $c_{\ell_r} = a_r \alpha_r$, where a_r is the slope of the lift curve for the airfoil of the blade element under consideration. The a_r value, of course, should correspond to the operational conditions of that particular blade element; i.e., its Mach and Reynolds numbers as well as special aspects of unsteady aerodynamics should be considered. Readers interested in the influence of unsteady aerodynamics on sectional airfoil characteristics are directed to a recent review paper by Ward and Young[2] as well as reports on experimental investigations by Liiva, et al[3,4], Philippe and Sagner[5], Valensi et al[6], etc. An insight into theoretical aspects of unsteady aerodynamics phenomena can be gained from papers of Hammond and Pierce[7], McCroskey[8], and others.

The magnitude of the lift $(dL_r \perp w_r)$ experienced by the blade element of width dr and chord c_r will be:

$$dL_r = \frac{1}{2} \rho\, a_r\, \alpha_r\, w_r^2\, c_r\, dr$$

When V_c and v_r are small in comparison to Ωr (which is often true for the working part of the blade), $w_r \approx \Omega r$. Therefore, substituting Eq (1a) for α_r, Eq (2) becomes:

$$dL_r = \frac{1}{2}\, a_r \rho \left(\theta_r - \frac{V_c + v_r}{\Omega r}\right) c_r (\Omega r)^2 dr. \tag{3}$$

The elementary profile drag $(dD_{pr_r} /\!/ w_r)$ experienced by the blade element at radius r will be

$$dD_{pr_r} = \frac{1}{2} \rho\, c_{d_{O_r}}\, w_r^2\, c_r\, dr \tag{4}$$

or, assuming $\Omega r \approx w_r$:

$$dD_{pr_r} = \frac{1}{2} c_{d_{O_r}}\, \rho\, (\Omega r)^2\, c_r\, d_r. \tag{5}$$

Consequently, the elementary thrust (dT_r) will be

$$dT_r = dL_r\, cos\, \phi_r - dD_{pr_r}\, sin\, \phi_r \tag{6}$$

and the corresponding elementary torque:

$$dQ_r = (dL_r\, sin\, \phi_r + dD_{pr_r}\, cos\, \phi_r) r \tag{7}$$

where ϕ_r is given by the relationship

$$tan\, \phi_r = (V_c + v_r)/\Omega r.$$

When ϕ_r is small,

$$tan\, \phi_r \approx sin\, \phi_r \approx \phi_r$$

and

$$dT_r = dL_r - dD_r[(V_c + v_r)/\Omega r] \tag{8}$$

For the working part of the blade, usually, $dD[(V_c + v)/\Omega r] \ll dL_r$, and Eq (8) becomes:

$$dT_r \approx dL_r. \tag{8a}$$

Similarly, the simplest formula for the elementary torque will be:

$$dQ_r = [dL_r (V_c + v_r)/\Omega r + dD_{pr_r}] r \tag{9}$$

or, in light of Eq (8a):

$$dQ_r = [dT_r (V_c + v_r)/\Omega r + dD_{pr_r}] r. \tag{9a}$$

Remembering that elementary power (dP_r *in ft.lbs/sec*) required by the considered blade element is

$$dP_r = dQ_r \Omega$$

and substituting Eq (9a) into the above relationship, dP_r can be expressed as follows:

$$dP_r = dT_r(V_c + v_r) + dD_{pr_r} r\Omega \,. \tag{10}$$

It can be noticed from Eq (10) that the power required by a blade element in axial translation in the direction of thrust (climb) contains two terms previously identified in the momentum theory; namely, $dT_r V_c$: i.e., power associated with an axial translation at a speed V_c, and $dT_r v_r$, i.e., power associated with induced velocity or in other words, the induced power. However, a third term that was not present in the momentum considerations appears in Eq (10). This is $dD_{pr_r} r\Omega$ which, of course, represents the profile power required by the blade element moving through the air at a velocity $r\Omega$.

3.1.2 Combined Blade Element and Momentum Theory

By combining blade element and momentum theories as probably proposed originally by Klemin[9], it becomes possible to determine induced velocity (v_r) for various values of r. This would provide the missing link for a more accurate estimation of dT_r, dQ_r and hence, dP_r values.

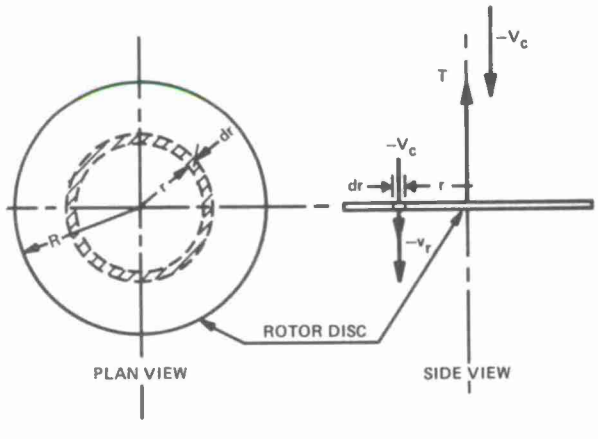


Figure 3-2. Elementary Ring of the Rotor Disc

Using the notations in Fig 3-2, thrust (dT_r) produced by an elementary ring of width dr and radius r can be expressed according to the momentum theory (see Section 2.3.1) as:

$$dT_r = 4\pi\rho(V_c + v_r)v_r\, r\, dr \tag{11}$$

where v_r is the induced velocity at the rotor disc.

On the other hand, according to the blade element theory and under the assumptions discussed in the preceding paragraphs, the elementary thrust experienced by b number of blades can be expressed as:

$$dT_r = \frac{1}{2} c_{\ell_r} (\Omega r)^2 \rho b c_r\, dr. \tag{12}$$

The location of a blade element can also be defined by a nondimensional ratio of $x \equiv r/R$. Then,

$$\left.\begin{aligned} r &= Rx \\ dr &= R dx \\ r\Omega &= V_t x \end{aligned}\right\} \tag{13}$$

where $V_t \equiv R\Omega$ is the tip speed.

Equating the right sides of Eqs (11) and (12), introducing the notations as given in Eq (13), and remembering that if the pitch angle at station x is θ_x, then $c_{\ell_x} = a_x[\theta_x - (V_c + v_x)/V_t x]$, and the following basic equation can be obtained:

$$8\pi R v_x^2 + (V_t a_x b c_x + 8\pi R V_c) v_x + V_t V_c a_x b c_x - V_t^2 a_x b c_x \theta_x = 0. \tag{14}$$

In Eq (14), c_x is the blade chord at station x. The above equation can be solved for the induced velocity at station x:

$$v_x = V_t \left[-\left(\frac{a_x b c_x}{16\pi R} + \frac{V_c}{2V_t}\right) + \sqrt{\left(\frac{a_x b c_x}{16\pi R} + \frac{V_c}{2V_t}\right)^2 + \frac{a_x b c_x \theta_x}{8\pi R} - \frac{a_x b c_x V_c}{8\pi R V_t}} \right] \tag{15}$$

In hovering, when $V_c = 0$, Eq (15) is simplified to the following:

$$v_x = V_t \left[-\frac{a_x b c_x}{16\pi R} + \sqrt{\left(\frac{a_x b c_x}{16\pi R}\right)^2 + \frac{a_x b c_x \theta_x}{8\pi R}} \right] \tag{16}$$

If, in addition, the blade is of rectangular shape (chord c is constant), then the rotor solidity σ can be expressed as follows:

$$\sigma = bcR/\pi R^2 = bc/\pi R$$

hence, $$bc = \sigma\pi R.$$

Further assuming that the lift slope a may be considered the same for the whole blade span, Eq (16) becomes:

$$v_x = V_t \left[- \frac{a\sigma}{16} + \sqrt{\left(\frac{a\sigma}{16}\right)^2 + \frac{a\sigma x \theta_x}{8}} \right] \tag{17}$$

Knowing the variation of the blade twist angle with its span, $\theta_t(x)$, the blade pitch angle at any station x can be expressed analytically. For example, in the case of a linear twist,

$$\theta_x = \theta_0 - \theta_t x$$

where θ_0 is the pitch angle at zero station, while θ_t expresses the total angle of washout. Substituting the above expression into Eq (17), the formula for downwash distribution of a linearly twisted rectangular blade is obtained:

$$v_x = V_t \left[- \frac{a\sigma}{16} + \sqrt{\left(\frac{a\sigma}{16}\right)^2 + \frac{a\sigma x}{8}\left(\theta_0 - \theta_t x\right)} \right] \tag{17a}$$

Eqs (15) to (17a) permit the computation of downwash velocity (v_x) in vertical ascent, or in hovering for a rotor with any number of blades (b) of any planform and any pitch distribution. Knowing the true downwash value at any blade station x, it is possible to find (with the help of two-dimensional airfoil characteristics) the true values of thrust and torque experienced by every blade element (see Eqs (3), (4), (8) and (9)). Furthermore, one may get some feeling regarding performance advantages (magnitude of the k_{ind} factor) either in hovering or in climb resulting from particular combinations of the chord (planform) and twist distribution. It would also be possible to learn about the sectional lift coefficient variation along the blade span $[c_\ell = f(x)]$. All these aspects are illustrated on the following example of the hover case for a rotor with rectangular, untwisted blades. For $\theta_t = 0$, Eq (17a) can be presented in a nondimensional form as $(v_x/V_t) = f(x)$.

$$v_x/V_t = - \frac{a\sigma}{16} + \sqrt{\left(\frac{a\sigma}{16}\right)^2 + \frac{a\sigma}{8}\,\theta_0 x} \tag{18}$$

Assuming $a = 5.73/rad$, several values of θ_0 ($\theta_0 = 4° \approx .07\ rad$, $8° \approx .14\ rad$, and $12 \approx .21\ rad$), and two solidity ratios, $\sigma = .05$ and $.10$; (v_x/V_t) is computed from Eq (18) and shown in the lower part of Fig 3-3.

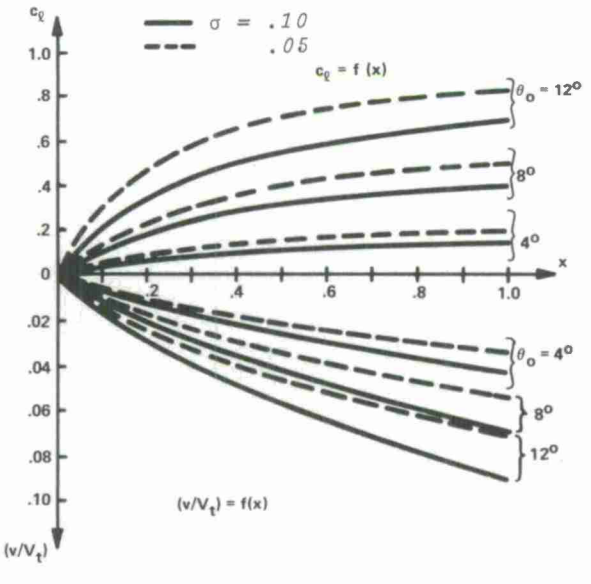


Figure 3-3. Examples of Sectional Lift Coefficient & Relative Induced Velocity Distribution along the Blade

Knowing the $(v_x/V_t) = f(x)$, the angle of attack at a station x can be obtained from Eq (1)

$$a_x = \theta_0 - \tan^{-1}(v_x/V_t)/x$$

and consequently,

$$c_{\ell_x} = a\alpha_x = a[\theta_0 - \tan^{-1}(v_x/V_t)/x] \tag{19}$$

Section lift coefficients thus calculated are shown in the upper part of Fig 3-3.

It should be noted at this point that the physicomathematical model of the rotor based on the combined momentum and blade element theory indeed provided the means for establishing induced velocity distribution along the blade of a rotor with defined geometry and known airfoil section characteristics. This, in turn, would permit calculation of the thrust developed by the rotor, both in hovering and climb, as well as the corresponding power required in those regimes of flight. Also, knowledge of the section-lift distribution along the blade span at various θ_0 values should give some idea regarding the appearance of stall as the collective pitch angle is further increased.

However, the above-discussed model has not given any indication regarding the existence of tip losses. Also, as far as the inflow and wake structure is concerned, it gives only time average of induced velocity distribution in the wake. Its shape still remains undetermined except for its contraction far downstream due to the increase of the induced velocity to twice that of its "at the disc value."

Nevertheless, in spite of all the above shortcomings, the combined momentum and blade element theory provides enough insight into the operation of real-life rotors to serve on one hand, as a guide in design of rotary-wing aircraft while on the other, in

helping to estimate their performance. Some aspects of application of the combined momentum and blade element theory to performance and design problems of rotors in axial translation but especially, in hovering, are discussed in the following sections.

3.1.3 Nondimensional Coefficients

Similar to fixed-wing practice, nondimensional thrust and torque or power coefficients of a rotor can be defined on the basis of: (1) area (either disc or total blade area), (2) air density, and (3) the square of characteristic velocity (tip speed V_t) and in the case of torque, (4) rotor radius (R). Nondimensional coefficients based on the disc area (πR^2) are defined as follows:

$$\textit{Thrust Coefficient} \qquad C_T = T/\pi R^2 \rho V_t^2$$

$$\textit{Torque Coefficient} \qquad C_Q = Q/\pi R^3 \rho V_t^2$$

$$\textit{Power Coefficient} \qquad C_P = P/\pi R^2 \rho V_t^3 \qquad (\textit{power in ft.lbs/sec})$$

and those referred to the blade area (A_b):

$$\textit{Thrust Coefficient} \qquad c_t = T/A_b \rho V_t^2 \equiv C_T/\sigma$$

$$\textit{Torque Coefficient} \qquad c_q = Q/A_b R \rho V_t^2 \equiv C_Q/\sigma$$

$$\textit{Power Coefficient} \qquad c_p = P/A_b \rho V_t^3 \equiv C_P/\sigma.$$

In hovering, it is easy to develop expressions for the following: the average lift coefficient, $\bar{c}_{\ell_h}$; the average profile drag coefficient, $\bar{c}_{d_o}$; and the average total drag coefficient, $\bar{C}_{D_h}$.* Within the validity of small angle assumptions $(dT = dL)$, the thrust of a blade element $cRdx$ located at $r = Rx$ can be expressed as:

$$dT = \frac{1}{2} \rho b c R c_\ell V_t^2 x^2 dx .$$

Assuming that c_ℓ along the span is constant and equal to $\bar{c}_{\ell_h}$, the above expression can be integrated from $x = 0$ to $x = 1.0$; leading to

$$\bar{c}_{\ell_h} = \frac{6T}{\sigma \pi R^2 V_t^2} = \frac{6C_T}{\sigma} = 6c_t. \tag{20}$$

Assuming uniform distribution of downwash velocity over the entire disc, still another useful expression for $\bar{c}_{\ell_h}$ can be developed by substituting for T in Eq (20), its expression based on ideal induced velocity (v_{id}): i.e., $T = 2\pi R^2 \rho v_{id}^2$.

$$\bar{c}_{\ell_h} = 12(v_{id}/V_t)^2/\sigma \tag{21}$$

and conversely, for a selected value of the average lift coefficient, the corresponding (v_{id}/V_t) ratio would be:

$$(v_{id}/V_t) = .288\sqrt{\bar{c}_{\ell_h}\sigma} . \tag{21a}$$

Similar to the average lift coefficient, the average profile $(\bar{c}_{d_o})$ and total drag $(\bar{C}_D)$ coefficients can be defined. Contribution to the rotor profile power (in ft.lbs/sec) of b blade elements located at xR will be

$$dP_{pr} = \frac{1}{2} \rho b c R^2 c_{d_o} V_t^3 x^3 dx \tag{22}$$

Again assuming that c_{d_o} is constant along the blade and equal to $\bar{c}_{d_o}$, the above equation is integrated within $x = 0$ to $x = 1.0$ limits to obtain profile power in hovering $(P_{pr_o}$ in ft.lbs/sec).

$$P_{pr_o} = \frac{1}{8} \sigma \pi R^2 \rho V_t^3 \bar{c}_{d_o} \tag{22a}$$

and consequently,

$$\bar{c}_{d_o} = 8P_{pr_o}/\sigma \pi R^2 \rho V_t^3. \tag{23}$$

The total average drag coefficient $(\bar{C}_{D_h})$ will (by analogy with Eq (23) be

$$\bar{C}_{D_h} = 8P_{R_h}/\sigma \pi R^2 \rho V_t^3 \tag{24}$$

where P_{R_h} represents the total rotor power in hovering (in ft.lbs/sec).

---

*Lower case letters are used for $\bar{c}_{\ell_h}$ and $\bar{c}_{d_o}$ in order to emphasize their relationship to the section coefficients, while the $\bar{C}_{D_h}$ is obviously based on the total drag of the blade; i.e., including the induced drag.

3.1.4 Rotor Profile Power in Axial Translation

To develop a better understanding of the rotor-profile problems in axially symmetrical regimes of flight, the following discussion is provided.

Quite often, the blade chord, c, and almost always, the profile drag coefficient, c_{d_o}, vary along the blade span. At any particular station x, $c_{d_{ox}} = f(RN_x, M_x, c_{\ell x}$, etc.) where the *etc* could mean airfoil section geometry; surface roughness, special boundary layer conditions as influenced by the centrifugal accleration field of rotating blade; possibly, BLC schemes and probably a few additional parameters. All of the above parameters are, in turn, dependent on x; thus, $c_{d_{ox}} = f(x)$ as well. Under these circumstances, integration of Eq (22) would lead to

$$P_{pr_o} = bR\rho V_t^3 \int_0^{1.0} c_x c_{d_{ox}} x^3 dx \tag{25}$$

where the above indicated integration should usually be performed either numerically or graphically.

When $c_x = c = const$, equating the right sides of Eqs (22a) and (25) would lead to the following expression for the average profile drag coefficient:

$$\bar{c}_{d_o} = 8 \int_0^{1.0} c_{d_{ox}} x^3 dx. \tag{26}$$

It was mentioned above that blade surface roughness is one of the parameters influencing the $c_{d_{ox}}$ values. Some allowance should be made, hence, for the increase in profile drag by multiplying the $c_{d_{o_{min}}}$ values from airfoil wind-tunnel data by a roughness coefficient. Depending on the blade construction and state of the blade surface, the value of the roughness coefficient may vary within rather wide limits; from *1.15* for smooth blades to *1.5* or even more, for sand and/or rain-eroded ones. For laminar airfoil sections which are very sensitive to surface roughness, roughness correction factors may exceed *1.5* whenever the blades are not kept in perfect condition.

As a practical short-cut in estimating approximate profile power of rectangular, untwisted blades, the following procedure is indicated:

1. For given conditions of pitch angle, tip speed, and air density, the section lift coefficient $c_{\ell_{.75}}$ is determined at $x = .75$.
2. Assume that this lift coefficient (obtained in *1*) also exists at $x = 0.8$. Then compute the c_{d_o} value, taking into account the Reynolds and Mach numbers existing at $x = 0.8$ and the above $c_{\ell_{.75}}$.
3. Correct the c_{d_o} thus obtained for roughness (multiplying the $c_{d_{o_{min}}}$ component of the total profile drag coefficient by a suitable correction factor) and further assuming that this c_{d_o} value exists along the whole blade, compute the profile power from Eq (22a).

It should be emphasized, however, that since the profile power increases due to compressibility may be quite considerable, the short-cut method may not be sufficiently accurate. Whenever there is a possibility that an unfavorable combination of lift coefficient and Mach number may exist for any extended part of the blade (mostly outboard), the problem of compressible drag rise should be investigated more thoroughly. This should be done throughout the whole operational range of the rotor and especially for the combinations of high thrust and tip speed *(rpm)* with low air density and temperature.

However, in some cases, a combination of a given thrust, air density and temperature with a lower tip speed may be more critical. This obviously could happen when higher blade-element lift coefficients ($c_{\ell x}$ resulting from a reduced V_t) in combination with lower Mach numbers produce higher drag coefficients than those corresponding to the original combinations of higher Mach numbers and lower $c_{\ell x}$ values.

3.1.5 Tip Losses

Vortex theory provides an insight into tip losses. Nevertheless, these losses should still be considered when the rotor thrust is calculated by the combined momentum blade element theory. This is usually done by assuming that the predicted aerodynamic lift extends up to some blade station; i.e., to the so-called effective blade radius, $R_e = Rx_e$ and ends abruptly at that station. The blade tip itself $[R(1 - x_e)]$ is assumed not to contribute to the thrust generation at all.

There are numerous either theoretical or empirical formulae for tip losses. For instance, for propellers, Prandtl gives a simple, but only approximate, formula based on the vortex theory (see Ref 1, p. 265):

$$x_e = 1 - (1.386\lambda/b\sqrt{1 + \lambda^2}) \tag{27}$$

where b is the number of blades, λ is the inflow ratio of the propeller, $\lambda \equiv V_{ax}/V_t$; V_{ax} being the axial velocity at the disc.

Some authors simply recommend expressing the effective radius as:

$$R_e = R - .5\,\bar{c}$$

where $\bar{c}$ is the average blade chord.

By dividing the above equation by R, the following is obtained:

$$x_e = 1 - .5(\pi\sigma/b). \tag{28}$$

Sissingh[10] proposes the following expression:

$$x_e = 1 - c_r[1 + .7(tr)]/1.5R$$

where c_r is the chord length at the root and (tr) is the blade taper ratio.

By analogy with the preceding case, the above expression for rectangular blades can be presented as follows:

$$x_e = 1 - 3.54\sigma/b. \tag{29}$$

Wald[11] recommends another expression which, for a rotor with rectangular blades, can be written as follows:

$$x_e = 1 - 1.96\sqrt{C_T/b}\ . \tag{30}$$

For comparison, tip losses, as given by Eqs (27) to (30) are computed for a hovering rotor (at *SL STD*, out-of-ground effect) with the following characteristics: $w = 8$ *psf*; $V_t = 650$ *fps*; $b = 4$; $\sigma = .10$. The results are shown in Table I.

EQUATION	x_e
(27)	.978
(28)	.961
(29)	.912
(30)	.956

TABLE I

It can be seen from Table I that x_e values calculated by different formulae are somewhat different. However, their average amounts to $x_e = .952$, and this, or an even slightly higher value $(x_e = .96)$, appears as reasonable numbers for estimating tip losses of practical rotors in hovering.

3.1.6 Rotor Thrust and Power in Climb and Hovering

Knowledge of induced velocity distribution along the blade and hence, of sectional lift coefficients permits calculation of the thrust of the rotor using the blade element approach. However, quite often, once $v = f(x)$ has been established, it may be more convenient to use the momentum theory in estimating the total thrust T.

After substituting Rx for r, and Rdx for dr, Eq (11) becomes

$$dT = 4\pi R^2 \rho (V_c + v) v x\, dx$$

and consequently,

$$T_c = 4\pi R^2 \rho \int_{x_i}^{x_e} (V_c + v) v x\, dx\ . \tag{31}$$

In hovering,

$$T_h = 4\pi R^2 \int_{x_i}^{x_e} v^2 x\, dx \tag{32}$$

When induced velocity vs blade span is given in a nondimensional form of (v/V_t), Eq (32) becomes

$$T_h = 4\pi R^2 \rho V_t^2 \int_{x_i}^{x_e} (v/V_t) x\, dx \tag{32a}$$

In all of the above 3 equations, x_i is the inboard station where the actual blade begins. Since the analytical relations between v and x are rather complicated, a computerized or graphical integration is more suitable for practical purposes.

In the case of a rotor having rectangular untwisted blades, the $(v/V_t) = f(x)$ is expressed by a relatively simple relationship (Eq (18)). If, in addition, the influence of *MN* and *RN* on the variation of the lift slope along the blade radius can be neglected (i.e., it may be assumed that $a = const$ for all stations); then introducing Eq (18) into Eq (32a), performing the indicated integration (for simplicity, within the limits of

$x_i = 0$; $x = x_e$) and neglecting the term $2A^{5/2}$, the following formula can be obtained:

$$T = 4\pi R^2 \rho V_t^2 \left[A^2 x_e^2 + \frac{1}{3} B x_e^3 + \frac{4A(2A^2 - 3Bx_e)\sqrt{(A^2 + Bx_e)^3}}{15B^2} \right] \tag{33}$$

where $A = \sigma a/16$ $B = \sigma a \theta_o/8$

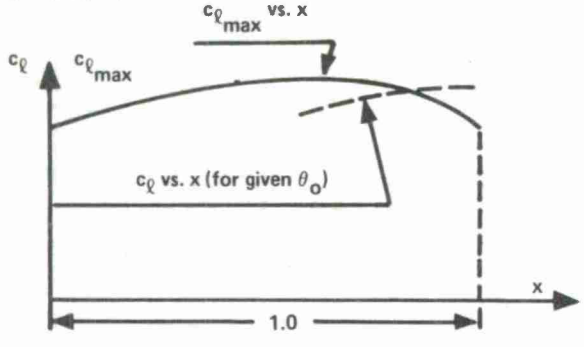
or

$$C_T = 4 \left[A^2 x_e^2 + \frac{1}{3} B x_e^2 + \frac{4A(2A^2 - 3Bx_e)\sqrt{(A^2 + Bx_e)^3}}{15B^2} \right] \tag{33a}$$

For a rotor having linearly twisted blades, expressions for T and C_T can be obtained similarly to the preceding case.

3.1.6.1 Maximum Thrust in Hovering

In some practical problems, it may be important to know what maximum thrust can be obtained from a given rotor, assuming that the power available is sufficient to retain a given tip speed. To solve this problem, it would be necessary to figure out which sections of the blade would stall first and at what pitch angle. The blade pitch angle corresponding to the beginning of stall can easily be found by the following procedure.



The maximum section lift coefficient $(c_{\ell_{max}})$ at various stations x should be estimated first by taking into consideration the blade airfoil sections, the effect of Reynolds and Mach numbers and finally, all other secondary effects as, for instance, unsteady aerodynamic phenomena (should this be justified by the rate of the pitch change), boundary layer interaction, etc. (see Fig 3-4).

Figure 3-4. Determination of the Blade Stall Regions

By equating right sides of Eqs (11) and (12), assuming $V_c = 0$, and remembering that $r \equiv Rx$ and $dr \equiv Rdx$, the following relationship between induced velocity at a station x, (v_x) and lift coefficient of that blade element $(c\ell_x)$ is obtained.

$$v_x = V_t \sqrt{\left(\frac{1}{8\pi}\right)\left(\frac{bc}{R}\right) c\ell_x \, x} \tag{34}$$

or

$$\frac{v_x}{V_t} = \sqrt{\left(\frac{1}{8\pi}\right)\left(\frac{bc}{R}\right) c\ell_x \, x} \tag{34a}$$

For rectangular blades $[(bc/R) = \pi\sigma]$, Eq (34a) becomes

$$\frac{v_x}{V_t} = \sqrt{\frac{1}{8} \sigma c\ell_x \, x} \tag{34b}$$

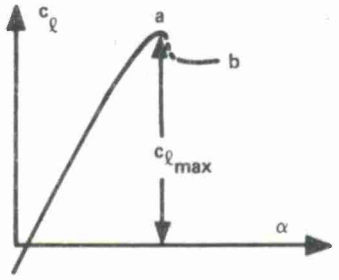
When $c_{\ell_{max}}$ reaches its maximum value $(c_{\ell_{max_x}})$, so does the (v_x/V_t) ratio. Consequently, within limits of validity of small angle assumptions, the pitch angle of the blade element at station x corresponding to the beginning of stall will be:

$$\theta_{x_{st}} = c_{\ell_{max_x}}/a_x + (v_x/V_t)_{max}/x \tag{35}$$

After the $\theta_{x_{st}}$ values have been calculated for several blade stations, one can have a fairly clear picture as to what pitch angle (of the blade as a whole) that stall begins. Should there be a requirement to obtain maximum possible thrust from a blade of a given planform and airfoil section, then it would be possible to select such twist distribution that the section lift coefficients simultaneously reach their maximum values over the largest possible part of the blade. When the blade is non-twisted (no washout), it is obvious that the lowest value of $\theta_{x_{st}}$ is, at the same time, the blade pitch angle at which stall begins.

Using the previously established formulae, the T_{max} value can now be calculated from the known $(v_x/V_t) = f(x)$ relationship at the beginning of stall. A more thorough study of T_{max} can be made when T is calculated for several values of θ_o greater than the θ_o at the beginning of stall. In this case, it must be taken into consideration that at those blade stations where the local stall pitch angle $\theta_{x_{st}}$ has been exceeded, the downwash velocity v_x should be computed by Eqs (34a) or (34b) using (instead of $c_{\ell_{max}}$) the

suitable c_ℓ value after stalling (Region a-b, Fig 3-5).



After the above discussion of the hovering case, it should not be difficult for the reader to find the thrust in vertical flight at a given rate of climb, as well as the pitch angle corresponding to the beginning of stall, and maximum thrust under these conditions.

Figure 3-5. Typical c_ℓ vs α Curve

3.1.6.2 Induced Power in Axial Translation

In axial translation (vertical climb or vertical descent) as well as in hovering, the induced power can be estimated as shown in Section 2.3.1. Once the v_x values or the (v_x/V_t) ratios are computed as a function of x, the whole procedure of finding the induced power (either in hover, P_{ind_h} or in climb, P_{ind_c}) becomes quite simple. As shown in Section 2.3.1,

$$dP_{ind_x} = 4\pi R^2 \rho v_x{}^3 x\, dx$$

and consequently,

$$P_{ind} = 4\pi R^2 \rho \int_{x_i}^{x_e} v_x{}^3 x\, dx. \tag{36}$$

or

$$P_{ind} = 4\pi R^2 V_t{}^3 \rho \int_{x_i}^{x_e} (v_x/V_t)^3 x\, dx \quad (ft.lbs/sec). \tag{36a}$$

Because of the complexity of the expressions for $v_x = f(x)$ or $(v_x/V_t) = f(x)$, the most practical procedure for finding P will be to perform the above indicated integration either on a computer or graphically. The latter procedure is illustrated in Fig 3-6.

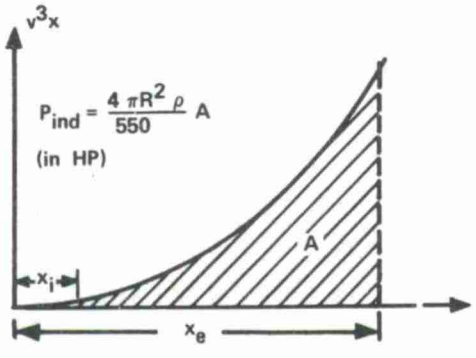


Figure 3-6. Graphical Integration of Induced Power

Now, the induced power k factor $k_{ind} \equiv (P_{ind}/P_{id})$ can be determined. As an example, this will be done for the case of rotor hovering with rectangular blades where closed form formulae for P_{ind_h} can easily be obtained. Substituting the (v_x/V_t) ratio as given in Eq (18) into Eq (36a); defining $(a\sigma/16) \equiv A$ and $(a\sigma\theta_o/8) \equiv B$; and integrating within the limits of $x_i = 0$ to x_e; and neglecting the terms $2A^5$ and $4A^7$, the following is obtained:

$$P_{ind} = 4\pi R^2 V_t{}^3 \rho \left\{ \frac{2}{5} \frac{(3Bx_e - 2A^2)\left(\sqrt{A^2 + Bx_e}\right)^3}{B^2} + \frac{2}{35} \frac{5\left(\sqrt{A^2 + Bx_e}\right)^7 - 7A^2\left(\sqrt{A^2 + Bx_e}\right)^5}{B^2} - 2A^3 x_e{}^2 - ABx_e{}^3 \right\}$$

(37)

Equating thrust expressed in terms of ideal induced power (v_{id}) to thrust given by Eq (33), the following formula for the equivalent $v_{id_{eq}}$ is obtained,

$$v_{id_{eq}} = 1.41\, V_t \sqrt{A^2 x_e{}^2 + \frac{1}{3} Bx_e{}^3 + \frac{4}{15} \frac{A\left(2A^2 - 3Bx_e\right)\left(\sqrt{A^2 + Bx_e}\right)^3}{B^2}} \tag{38}$$

and consequently, the k_{ind_h} factor:

$$k_{ind_h} = P_{ind}/2\pi R^2 \rho v_{id_{eq}}{}^3$$

where P_{ind} is given by Eq (37) and $v_{id_{eq}}$ by Eq (38).

3.1.6.3 Blade Twist and Chord Distribution for Uniform Downwash in Hovering

The problem consists of finding a blade twist and/or chord distribution that under assumed operating conditions would produce a uniform downwash over the largest possible part of the blade. These operating conditions can be specified either in terms of the effective disc loading $w_{ef} \equiv T/\pi x_e{}^2 R^2$, tip speed V_t and air density (ρ), or simply as the average lift coefficient, $\bar{c}_{\ell_h}$ and V_t (especially for rectangular blades). In the first case, the induced velocity, which we try to make uniform, would be $v = \sqrt{w_{ef}/2\rho}$ while in the second case, it can be expressed from Eq (21a) as

$$v = \left(.288 V_t \sqrt{\bar{c}_{\ell_h} \sigma}\right)/x_e$$

However, from Eq (34), the lift coefficient which should exist at station x in order to produce the required uniform downwash is:

$$c_{\ell_x} = 8\pi R (v/V_t)^2/b c_x x \tag{40}$$

or for a rectangular blade, with the (v/V_t) ratio substituted from Eq (21a), the c_{ℓ_x} distribution in terms of $\bar{c}_{\ell_h}$ becomes

$$c_{\ell_x} = \frac{2}{3} \frac{\bar{c}_{\ell_h}}{x} . \tag{40a}$$

It is clear from Eqs (40) and (40a) that the required c_{ℓ_x} increases toward the root of the blade (as x decreases). For a nonrectangular blade, this need for an increase in c_{ℓ_x} can be at least partially offset by the chord enlargement (Eq (40)). Nevertheless, it is obvious that the special condition of a uniform downwash can only be fulfilled down to the value of x where the required c_{ℓ_x} does not exceed the maximum section lift coefficient $c_{\ell_{max}}$.

The blade pitch angle (θ_x) at station x required to produce downwash v can now be readily obtained:

$$\theta_x = (c_{\ell_x}/a_x) + (v/V_t x). \tag{41}$$

For rectangular blades, the right side of Eq (40a) can be substituted for c_{ℓ_x} in Eq (41) and v/V_t can be expressed in terms of $\bar{c}_{\ell_h}$; thus, Eq (41) becomes:

$$\theta_x = \left(\frac{2}{3} \bar{c}_{\ell_h}/a_x x\right) + (.288\sqrt{\bar{c}_{\ell_h} \sigma})/x_e x \tag{41a}$$

For $\sigma = .1$ and $\bar{c}_{\ell_h} = .3$, $.4$, and $.5$, the $\theta_x = f(x)$ is computed from Eq (41a) and plotted in Fig 3-7, and c_{ℓ_x} from Eq (40a) is also shown, thus giving some idea of approximate limits (under small angle assumptions) for those blade stations where uniform downwash in hovering can be achieved without encountering stall.

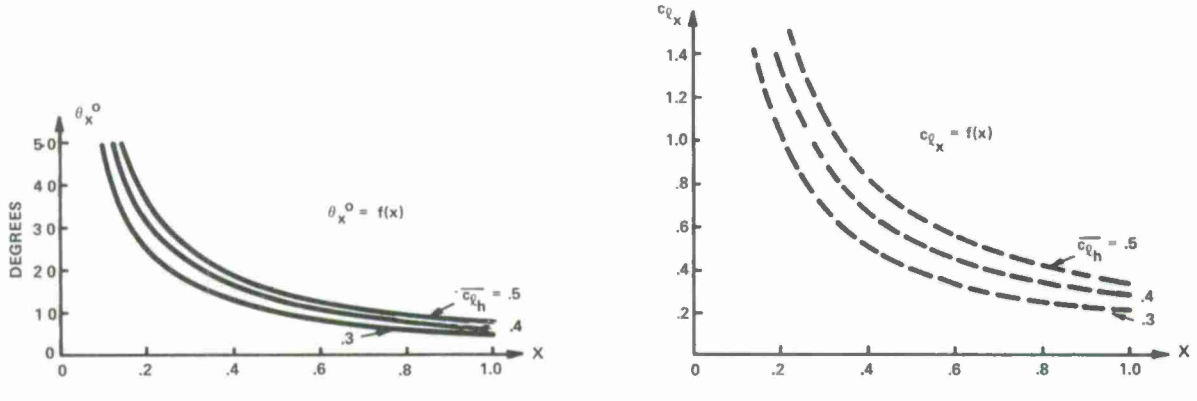


Figure 3-7. Blade Twist and Section Lift Distribution Required for Uniform Downwash

It can be seen from Fig 3-7 that because of the twist angles and section blade lift coefficient requirements, achieving a uniform induced velocity over almost the entire blade (down to say, $x = .1$ station) is not practical. By the same token, it appears that even linear twist (amounting to $\theta_t \approx -10°$) should well approximate the ideal twist distribution for blade stations $.4 \leq x \leq 1.0$.

3.1.6.4 Power Losses Due to the Slipstream Rotation

In the momentum theory, no slipstream rotation was considered. However, it can be seen that lift generation by the blade elements may introduce some rotation to the slipstream which, although not contributing to the lift, will create a new requirement for

power as additional energy is carried away in the wake.

In a nonviscous fluid, slipstream rotation is due to the fact that downwash v_L produced by the blade element is not parallel to the rotor axis, but perpendicular to the resultant flow at the lifting line of the element (see Fig 3-8). It can be seen from this figure that $v_{rot}/v = v_L/V_{res}$. Assuming that $v_L \approx v$ and $V_{res} \approx V_t x$, the following is obtained:

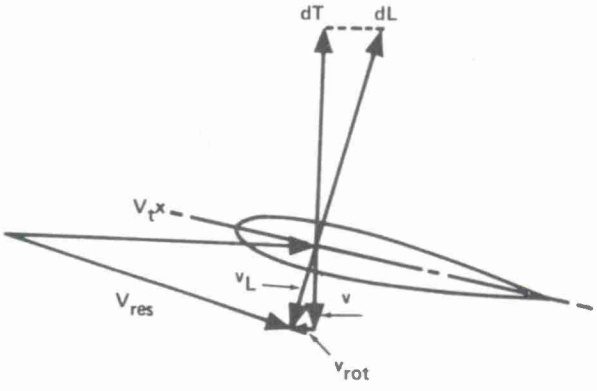


Figure 3-8. Slipstream-Rotating Component (v_{rot}) of Lift Induced Velocity (v_L)

$$v_{rot} = v(v/V_t x). \tag{42}$$

The power loss (in ft.lbs/sec) due to the rotation of the fluid passing at a rate of $2\pi R^2 \rho v x\, dx$ through an annular ring located in the ultimate wake and having a radius $R_u x$ and width $R_u dx$ will be:

$$dP_{rot} = \pi R^2 R_u^2 \rho v \omega_u^2 x^3\, dx \tag{43}$$

where ω_u is the angular speed of the slipstream rotation in the fully-developed wake. Defining the speed of slipstream rotation in the disc plane by ω, remembering that $R_u = R/\sqrt{2}$, and applying the principle of conservation of angular momentum, one can find that:

$$\omega_u = 2\omega \tag{44}$$

and Eq (43) can be rewritten as follows:

$$dP_{rot} = 2\pi R^2 v \rho (Rx\omega)^2 x\, dx \tag{45}$$

but $Rx\omega \equiv v_{rot} = v^2/V_t x$ (Eq (42)); hence,

$$dP_{rot} = [2\pi R^2 \rho v^3 (v/V_t)^2/x]dx. \tag{45a}$$

Assuming next that the induced velocity v is constant over the disc and performing integration from x_i to x_e, the following is obtained:

$$P_{rot} = 2\pi R^2 \rho v^3 (v/V_t)^2 \ell n(x_e/x_i). \tag{46}$$

However, $2\pi R^2 \rho v^3$ is the ideal induced power in hovering, P_{id}, hence

$$P_{rot} = P_{id}(v/V_t)^2 \ell n(x_e/x_i). \tag{47}$$

For the limits $x_i = 0.25$ and $x_e = 0.97$;

$$P_{rot} \approx 1.36 P_{id}(v/V_t)^2. \tag{48}$$

Since for contemporary helicopters, usually, $v/V_t \leq 0.07$; power losses due to the slipstream rotation should not exceed .7 percent.

3.1.6.5 Thrust and Induced Power of Intermeshing and Overlapping Rotors

Definition of Overlap: In multirotored aircraft, the rotors may be arranged in such a way that the distance (d) between the axes of any two rotors (1 and 2) may be smaller than the sum of their respective radii (R_1 and R_2). In this case ($d < R_1 + R_2$), mutual interference would lead to aerodynamic characteristics of such rotors different from the isolated ones.

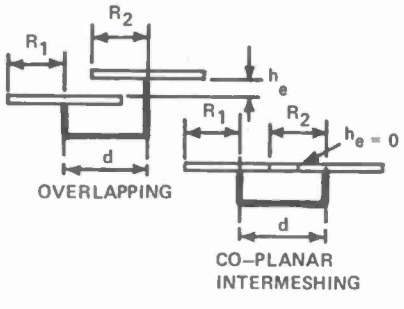


Figure 3-9. Overlapping and Intermeshing Rotors

As to the arrangement of rotors having $d < R_1 + R_2$, they may be either coplanar (pure intermeshing), or one may be elevated above the other, thus forming an overlapping configuration (Figure 3-9).

The amount of overlap (ov) for $R_1 = R_2$ can be expressed as a nondimensional number (or in percent) as follows:

$$ov = [1 - (d/D)]. \tag{49}$$

A physicomathematical model based on the combined momentum and blade element theory may be helpful in understanding aerodynamic interference of intermeshing and overlapping rotors in hovering and other regimes of flight.

The philosophy of this approach and the obtained results will be briefly discussed here, while details of the presented approach can be found in Ref 12.

The considered case will be limited to either truly coplanar rotors, or those of relatively small vertical displacement (say, $h_e \leq .10R$). This would permit treating them as the intermeshing ones. Thus, it will be assumed that a common rate of flow is established within the overlapped area.

Induced Velocity: The induced velocity (v_{ov}) at any point of the overlapped region can be obtained by considering an elementary area dA of diameter dr (Fig 3-10), the location of which is determined by r_1 and r_2.

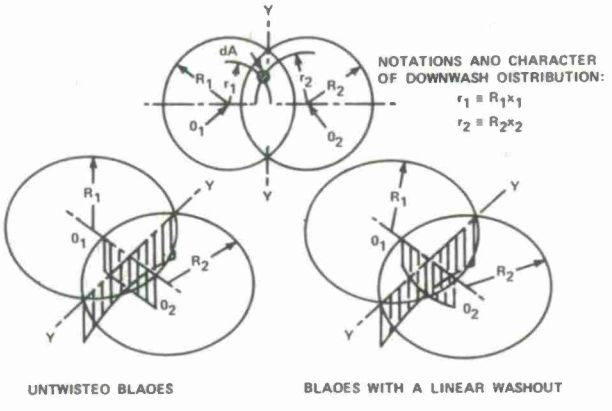


Figure 3-10. Theoretical Character of Downwash Distribution of Overlapping Rotors in Hovering

The rate of flow through the element dA will be $v_{ov}\,\rho\,(1/4)\pi dr^2$, and the thrust produced (according to the momentum theory):

$$dT = (\pi/4)2\rho v_{ov}^2 dr^2 \tag{50}$$

On the other hand, the elementary thrust due to the action of Rotor *1*, expressed according to the blade element theory, will be:

$$dT_1 = (1/16)\rho(\Omega r_1)^2 c_{\ell_1} bc(dr^2/r_1) \tag{51}$$

And similarly, for Rotor *2*,

$$dT_2 = (1/16)\rho(\Omega r_2)^2 c_{\ell_2} bc(dr^2/r_2) \tag{52}$$

where c_ℓ, with a suitable subscript, is the section lift coefficient at the corresponding radius ($r_1 \equiv x_1 R$ or $r_2 \equiv x_2 R$). But the elementary thrust produced, according to the momentum theory, should be equal to the sum of those produced by Rotors *1* and *2*:

$$dT = dT_1 + dT_2 \tag{53}$$

Substituting Eqs (50), (51) and (52) into Eq (53) and further simplifying under the assumption that the blades have uniform chord, the following formula for the downwash velocity at any point of the overlapped area is obtained:

$$v_{ov} = V_t \left\{ -\frac{1}{8}\sigma a + \sqrt{\left(\frac{1}{8}a\sigma\right)^2 + \frac{1}{8}a\sigma\left[\theta_0(x_1 + x_2) + \theta_t(x_1^2 + x_2^2)\right]} \right\} \tag{54}$$

When the blade is non-twisted, Eq (54) becomes

$$v_{ov} = V_t \left[-\frac{1}{8}\sigma a + \sqrt{\left(\frac{1}{8}a\sigma\right)^2 + \frac{1}{8}a\sigma\theta_0(x_1 + x_2)} \right] \tag{54a}$$

Along the axis ($O_1 - O_2$) (joining centers of the rotors), the sum $x_1 + x_2$ is constant at all points. This means that for rotors with untwisted blades, the downwash velocity is constant along this axis within the overlapped area. Along the axis y-y, the sum $x_1 + x_2$ increases with the distance from the $O_1 - O_2$ axis. This implies that the downwash velocity for flat blades increases toward the sharp edges of the overlapped area (Fig 3-10a). Fig 3-10b shows the character of induced velocity distribution for blades with a linear washout.

In the limiting case, when the overlap amounts to *100%* (i.e., when the rotors are coaxial and hence, $x_1 = x_2 = x$), Eqs (54) and (54a) become identical with those expressing the downwash for an isolated rotor with the exception that the solidity of this single rotor is equal to the sum of solidities making a coaxial arrangement.

Experimental results[12] from direct induced velocity measurements with a bank of pitot-static anemomenters in model tests of coplanar, or slightly vertically displaced overlapping rotors (with an overlap of up to *40%*) seem to confirm the predicted trend (Fig 3-11).

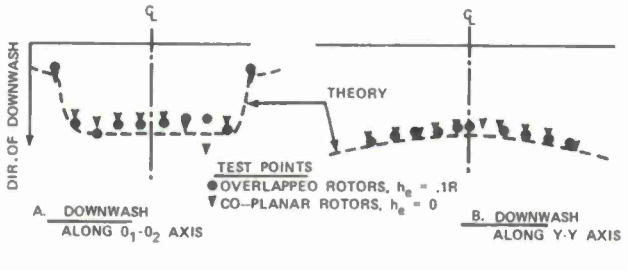


Figure 3-11. Examples of Predicted and Measured Downwash of Overlapping and Intermeshing Rotors Incorporating *37-1/2%* Overlap

Determination of Thrust and Induced Power: Knowing the induced velocity at all points of the overlapped area and remembering the expressions that give the value in the non-overlapped portion, it is easy to calculate the thrust and induced power for each part of the total projected area of the overlapped rotor configurations. Fig 3-12 shows a relative reduction in thrust of the overlapped configuration with respect to that of two isolated rotors. This figure also gives a comparison with test results.

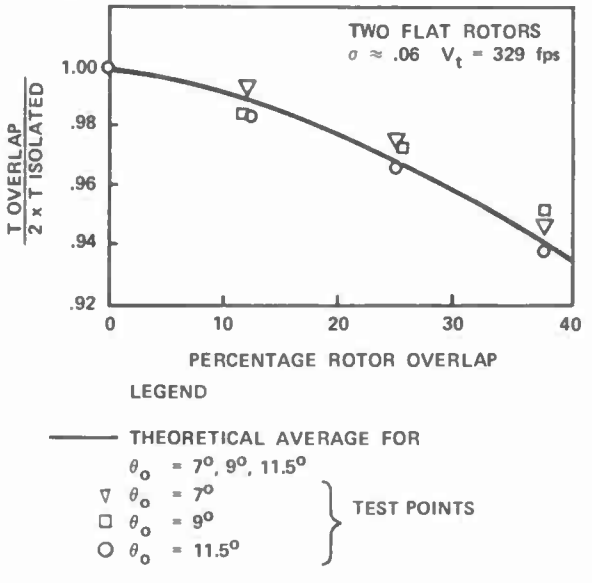


Figure 3-12. Thrust Ratio vs Percentage of Rotor Overlap

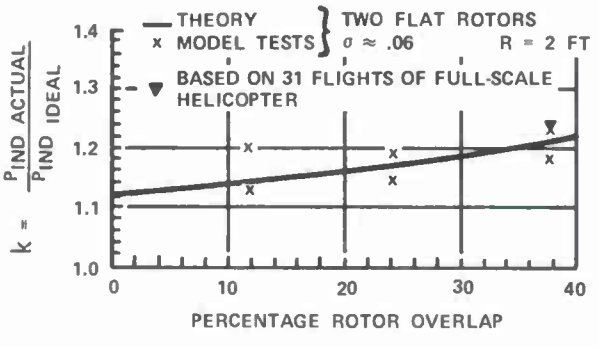


Figure 3-13. Ratio of Actual-to-Ideal Induced Power vs Percentage of Rotor Overlap

In Fig 3-13, the k_{ind_h} factor of the overlapped configuration is plotted vs percentage of overlap. It may be noticed at this point that for a helicopter having *37-1/2%* overlap, the increase in induced power would amount to about *10%* over that required by two isolated rotors jointly producing the same thrust.

3.1.6.6 Aerodynamic and Overall Efficiencies in Hover

The combined blade element theory helped us to develop physicomathematical models of the rotor in axially symmetrical regimes of flight. It accounted for the profile power and nonuniform induced velocity distribution. In addition, it was also indicated that in the actual rotor, tip losses should also be expected. In view of all of this, it may be desirable to develop quantative means of comparing the performance of the actual rotor with that of its idealized values as given by the actuator-disc model. The so-called *figure of merit (FM)*, which this author prefers to call the aerodynamic efficiency (η_a) is usually referred to the static thrust case (hovering), and it can be defined as follows:

$$\eta_a = P_{id}/P_R \tag{55}$$

where P_{id} is the ideal and P_R is the actual power required by the rotor at a given level of the thrust generator loading as defined by either the total thrust T per rotor, or more generally, by the nominal disc loading $w \equiv T/\pi R^2$.

Remembering that $P_{id} = T\sqrt{w/2\rho}$, while $P_R = k_{ind}P_{id} + (1/8)\sigma\pi R^2\bar{c}_{d_o}V_t^3$, and $\bar{c}_{\ell_h} = 6w/\sigma\rho V_t^2$, the above P_{id} and P_R values can be substituted into Eq (55), then the numerator and denominator of this equation is divided by $T/\sqrt{w/2\rho}$; thus leading to the following:

$$\eta_{a_h} = 1\Big/\left[k_{ind} + \frac{3}{4}\left(\bar{c}_{d_o}/\bar{c}_{\ell_h}\right)\left(V_t/\sqrt{w/2\rho}\right)\right] \tag{56}$$

or, since $\sqrt{w/2\rho} = v_{id_h}$, Eq (56) becomes

$$\eta_{a_h} = 1\Big/\left[k_{ind} + \frac{3}{4}\left(\bar{c}_{d_o}/\bar{c}_{\ell_h}\right)V_t/v_{id_h}\right] \tag{56a}$$

$50 \leq (\bar{c}_{\ell_h}/\bar{c}_{d_o}) \leq 70$ would probably represent the limits for the contemporary helicopters. Assuming, in addition, $k_{ind_h} = 1.12$, the η_a values were computed from Eq (56a) and plotted vs (V_t/v_{id_h}) in Fig 3-14.

From this figure, it can be seen that for disc loading $w = 8$ *psf* and $V_t = 700$ *fps*, $[(V_t/v_{id_h}) \approx 17]$, aerodynamic efficiencies as high as $\eta_a \approx .78$ may be expected. But for $w = 4$ *psf* and the same $V_t = 700$ *fps* $[(V_t/v_{id_h}) \approx 24]$, η_a may drop to $\eta_a \approx .7$.

The aerodynamic efficiency obviously provides a measure to evaluate only the aerodynamic aspect of the excellence of design. In order to compare the overall efficiency of various rotary-wing aircraft (both shaft and tip-jet driven) in hovering, a method based on a comparison of the ideal power required to the thermal energy input per unit

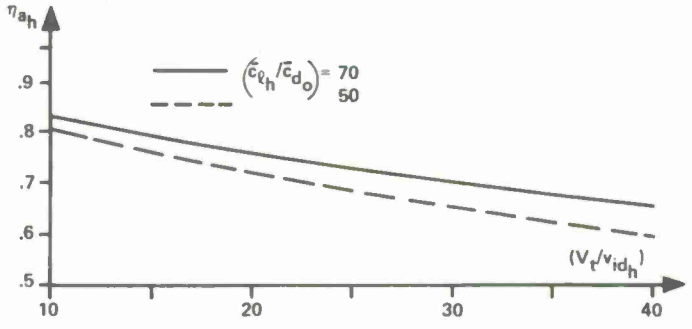


Figure 3-14. Aerodynamic Efficiency in Hovering (η_{a_h}) vs (V_t/v_{id_h}) Ratio

of time may be more suitable[13]. As long as jet fuels with a heat capacity of about 18,500 BTU/lb are in common use, the thermal energy input per second and pound of thrust generated can be defined as follows:

$$\eta_{ov} = \sqrt{w/2\rho}/4{,}000\ tsfc \tag{57}$$

or

$$\eta_{ov} = v_{id_h}/4{,}000\ tsfc \tag{57a}$$

where the symbol *tsfc* is used to denote the thrust specific fuel consumption (lbs/hr;lb) with respect to the total rotor thrust T. For instance, it can be seen that for a helicopter with $w = 7.0\ psf$ ($v_{id} \approx 38\ psf$) developing $10\ lbs/HP$, and having a fuel consumption of $.5\ lb/HP;hr.$, the $tsfc \approx .05\ lb/lb;hr.$, and consequently, $\eta_{ov} \approx .19$.

3.2 FORWARD FLIGHT

As in the case of vertical ascent and hovering, the blade element theory could provide a proper means for predicting forces acting on the blade in forward flight. It is obvious that a correct prediction of elementary forces should be based on the two-dimensional (section) airfoil characteristics, including all of the aspects of unsteady aerodynamics and, if possible, proper corrections for oblique flow at various azimuth angles, effect of blade centrifugal field on the boundary layer, etc[8]. In addition, it is necessary to know the magnitude and direction of the relative air flow in the immediate vicinity of the investigated element of the blade.

In the general case of a steady-state flight of a helicopter, the rotor axis is tilted from the vertical through an angle α_v, while the aircraft is moving at constant speed V_f along the inclined path where V_c is the vertical component (rate of climb) and V is the horizontal component.

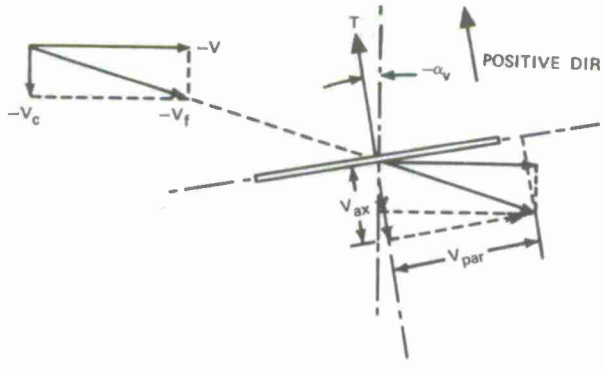


Figure 3-15. Air Flows at the Disc in Forward Translation

Using the concept of a stationary rotor as in Fig 3-15, the speed V_f can be resolved into two components - the axial (perpendicular to the airscrew disc) and another parallel to the disc. The axial components obviously, will be:

$$V_{ax} = -V_c \cos \alpha_v + V \sin \alpha_v . \tag{58}$$

The parallel component will be:

$$V_{par} = -V \cos \alpha_v + V_c \sin \alpha_v \tag{59}$$

In those cases when the tilt angle α_v is small (as it usually is in all helicopter flight regimes), Eqs (58) and (59) can be simplified as follows:

$$V_{ax} = -V_c + V\alpha_v \tag{58a}$$

and

$$V_{par} = -V + V_c \alpha_v . \tag{59a}$$

As the first approximation, only the component of V_{par} perpendicular to the blade axis will be considered for computing forces acting on the element. Measuring azimuth angle from the blade downwind position (Figure 3-16) and following this convention, the perpendicular component (V_b) will obviously be:

$$V_b = V_{par} \sin \psi . \tag{60}$$

In the case of horizontal flight (which is most often analyzed in detail), V_{par} may be considered (for small α_v) as identical with the speed of flight V, and Eq (60) becomes:

$$V_b = V \sin \psi . \tag{60a}$$

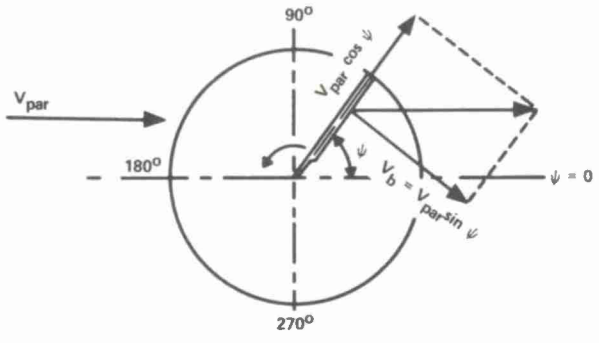


Figure 3-16. Air Velocities at the Blade Due to Translation in the Disc Plane

Consequently, for a blade situated at a distance $r \equiv Rx$, the total resultant velocity w_{par} experienced in the plane of the disc will be;

$$w_{par} = V_{tx} + V \sin \psi. \tag{61}$$

Assuming that the blade does not change its position with respect to the plane of the rotor disc, the air flow in the immediate neighborhood of a blade element located at a station x on the blade and at an azimuth angle ψ will be shown in Fig 3-17. Designating the pitch angle of a blade element as $\theta_{\psi x}$, the corresponding angle of attack $\alpha_{\psi x}$, will be

$$\alpha_{\psi x} = \theta_{\psi x} - \phi_{\psi x}. \tag{62}$$

Where $\phi_{\psi x}$ is the total inflow angle,

$$\tan^{-1} \phi_{\psi x} = V_{ax_{tot_{\psi x}}} / w_{par_{\psi x}}, \tag{63}$$

and, in turn, $V_{ax_{tot}}$ is the sum of V_{ax} is defined by Eq (58a) and the induced velocity $v_{\psi x}$ at the considered element.

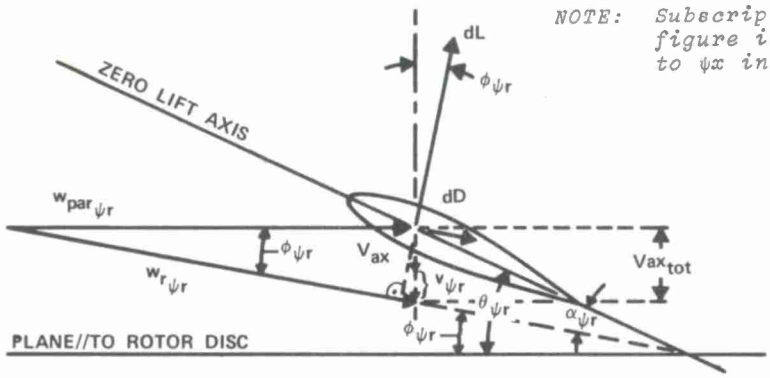


Figure 3-17. Air Velocities at a Blade Element

If the true value of the $V_{ax_{tot}}$ for a blade element at a station x and azimuth angle ψ were known, then it would be possible to compute the elementary lift $(dL_{\psi x})$ and elementary profile $(dDpr_{\psi x})$ or total drag $(dD_{\psi x})$ experienced by this element.

Within the limits of the small angle assumptions (the validity of which should always be checked prior to starting the actual calculations), these elementary aerodynamic forces and moments $(dQ_{\psi x}$ and $dQpr_{\psi x})$ can be expressed as follows:

$$\left.\begin{aligned}
dT_{\psi x} \approx dL_{\psi x} &= \tfrac{1}{2} R\rho \left[(V_{tx} + V \sin \psi)^2 a_{\psi x} (\theta_{\psi x} - \phi_{\psi x}) c_x\right] dx \\
dD_{\psi x} &= dL_{\psi x}\, \phi_{\psi x} + \tfrac{1}{2} R\rho \left[(V_{tx} + V \sin \psi)^2 c_x\, c d_{o\psi x}\right] dx \\
dDpr_{\psi x} &= \tfrac{1}{2} R\,\rho \left[(V_{tx} + V \sin \psi)^2\, c_x\, c d_{o\psi x}\right] dx \\
dQ_{\psi x} &= Rx\, dD_{\psi x} \\
dQpr_{\psi x} &= Rx\, dD_{pr\psi x}
\end{aligned}\right\} \tag{64}$$

Now, thrust (T) as well as either total (Q) or profile drag (Q_{pr}) torque and rotor total (P_R) or profile drag $(P_{R_{pr}})$ power can be evaluated. For the case of rectangular blades, they may be presented as follows:

$$T = \frac{1}{4}\sigma R^2 \rho \int_{x_i}^{x_e} \int_{0}^{2\pi} \left[(V_t x + V \sin\psi)^2 \, a_{\psi x}(\theta_{\psi x} - \phi_{\psi x})\right] dx \, d\psi$$

$$Q = \frac{R}{2\pi} \int_{x_i}^{x_e} \int_{0}^{2\pi} \phi_{\psi x} \, x \, dL_{\psi x} \, d\psi + \frac{1}{4}\sigma R^3 \rho \int_{x_i}^{1.0} \int_{0}^{2\pi} \left[(V_t x + V \sin\psi)^2 \, c_{d_{o\psi x}}\right] dx \, d\psi \qquad (65)$$

$$Q_{pr} = \frac{1}{4}\sigma R^3 \rho \int_{x_i}^{1.0} \int_{0}^{2\pi} (V_t x + V \sin\psi)^2 \, c_{d_{o\psi x}} \, dx \, d\psi$$

$$P_R = Q\Omega$$

$$P_{R_{pr}} = Q_{pr}\,\Omega$$

where Ω is the angular velocity of the rotor.

Integration indicated by Eq (65) usually have to be performed either on a computer or graphically. In either case, the thrust and/or torque for the whole blade is computed for selected azimuth angles, then the average for a complete revolution is found and the result multiplied by the number of blades. However, in order to apply the above-described procedure, the downwash velocity $v_{\psi x}$ (Fig 3-17) at each point of the rotor disc must be known. Methods of obtaining $v_{\psi x}$ with the help of the vortex theory will be described in Chapter 4, but an approach based on the combined momentum and blade element theory can also be of some help in that respect[14].

In those cases when the induced part represents only a small fraction of the total axial inflow velocity $(V_{ax_{tot}})$, the deviations of the actual induced velocity (at various points of the rotor or propeller disc) from the average value becomes less important. Hence, it becomes permissible to assume that the downwash is uniform over the whole disc, and can be computed according to the simple momentum theory. Further analysis of the aerodynamic forces acting on the blade may be carried out along the lines presented in this paragraph.

3.2.1 Blade Profile Drag Contribution to Rotor Power and Drag (Simple Approach)

The blade element theory may be quite helpful in developing physicomathematical rotor models permitting one to gain a better insight into problems of the blade profile drag contributions to the rotor power required in forward flight as well as rotor overall drag.

The elementary profile drag experienced by an element of the blade, $dr = Rdx$ wide, and located at a distance $r = Rx$ from the rotor axis when the blade is at an azimuth angle ψ, will be:

$$dD_{x\psi} = \frac{1}{2} R \rho \, c_x \, c_{d_{ox\psi}} \, w_{x\psi}^2 \, dx \qquad (66)$$

where $w_{x\psi}$ is the component of total air velocity perpendicular to the blade at x,ψ. The corresponding elementary torque $(dQ_{x\psi})$ is:

$$dQ_{x\psi} = Rx\,dD_{x\psi} \qquad (67)$$

and the drag component in the direction of flight $(dD_{f_{x\psi}})$ becomes:

$$dD_{f_{x\psi}} = dD_{x\psi} \sin\psi. \qquad (68)$$

In the simple approach, only the component of the resultant air velocity perpendicular to the blade at the x,ψ coordinates $(w_{x\psi})$ is considered, while the influence of the velocity component parallel to the blade is neglected.

Using the notations from Fig 3-18, $w_{x\psi}$ becomes:

$$w_{x\psi} = V_t x + V \sin\psi \qquad (69)$$

or, with $\mu \equiv V/V_t$,

$$w_{x\psi} = V_t(x + \mu \sin\psi). \qquad (69a)$$

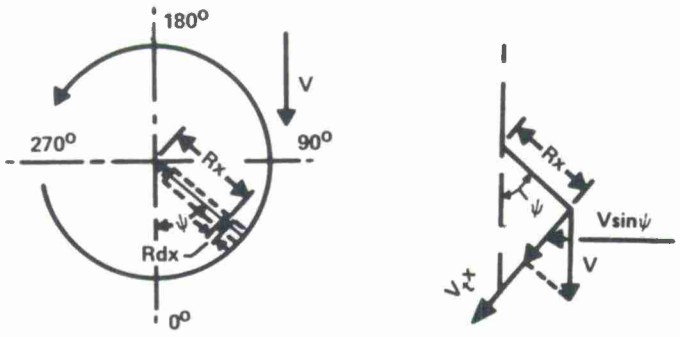


Figure 3-18. Air Velocity Perpendicular to the Blade

Since, in general, $dD_{x\psi}$ varies with the azimuth angle (ψ) as well as the blade element position (x), values of both the torque (Q) and the drag contribution $(D_{f_{pr}})$ of all b blades averaged over one full rotor revolution must be obtained by an integration with respect to x as well as ψ.

Substituting in Eqs (67) and (68), the value for $w_{x\psi}$ from Eq (69a), the following is obtained:

$$Q_{pr} = \frac{bR^2 \rho V_t^2}{4\pi} \int_0^{1.0} \int_0^{2\pi} c_x \, cd_{o_{x\psi}} (x + \mu \sin\psi)^2 \, dx \, d\psi \tag{70}$$

Usually, the Q_{pr} values must be obtained either through numerical procedures on the computer or graphically, but it can be easily integrated with the following simplifying assumptions:

1. The drag coefficient is constant along the blade; and equal to $\bar{c}_{d_o}$.
2. The drag coefficient does not vary as the blade changes its azimuth.
3. The blade chord is constant.

Then, Eq (70) is reduced to

$$Q_{pr} = \frac{1}{8} \sigma\pi R^3 \rho V_t^2 \bar{c}_{d_o} (1 + \mu^2) \tag{71}$$

and the corresponding profile power, in *HP*, is

$$P_{pr} = \sigma\pi R^2 \rho V_t^3 \bar{c}_{d_o} (1 + \mu^2)/4400 \tag{71a}$$

but $\sigma\pi R^2 \rho V_t^3 \bar{c}_{d_o}/4400 = P_{pr_o}$; i.e., the power required in hovering; hence,

$$P_{pr} = P_{pr_o} (1 + \mu^2). \tag{71b}$$

Similarly,

$$D_{pr} = \frac{bR \rho V_t^2}{4\pi} \int_0^{1.0} \int_0^{2\pi} c_x \, cd_{o_{x\psi}} (x + \mu \sin\psi)^2 \sin\psi \, dx \, d\psi \tag{72}$$

and under the simplifying assumptions (1) to (3):

$$D_{pr} = \frac{1}{4} \sigma\pi R^2 \rho V_t^2 \mu \bar{c}_{d_o}. \tag{72a}$$

The corresponding power, in *HP*, is

$$P_{D_{pr}} = \mu^2 \rho \sigma\pi R^2 V_t^3 \bar{c}_{d_o}/2200. \tag{73}$$

3.2.2 Contribution of Blade Element Induced Drag to Rotor Torque (Power) and Drag

In performance predictions of helicopters in forward flight, it is usually sufficient to estimate the induced power from the momentum theory and then correct those estimates through proper factors (k_{indf}). However, there are also cases where more detailed studies of the induced power in forward flight of helicopters are required. To provide the necessary insight into those problems, a simplified approach to the estimation of the rotor torque (Q_{ind}) due to the blade element induced drag is briefly outlined. This is supplemented with considerations of the blade element induced drag contribution to the total drag of the rotor.

Let $dL_{x\psi}$ be the lift generated by a blade element located at a station x, while the blade itself is at an azimuth ψ; then for those flight conditions and x values where the small angle assumptions are valid, the elementary induced drag (due to lift $dL_{x\psi}$) may be expressed as follows (Fig 3-19):

$$dD_{L_{x\psi}} = \left[(v_{x\psi}/V_t)/(x + \mu \sin\psi)\right] dL_{x\psi}. \tag{74}$$

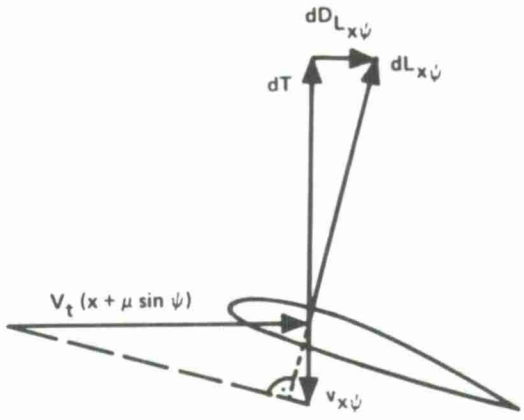


Figure 3-19 Forces & Velocities at a Blade Element

The corresponding elementary torque for all b blades $(dQ_{ind_{x\psi}})$ will be

$$dQ_{ind_{x\psi}} = bR\left[(v_{x\psi}/V_t)/(x + \mu \sin\psi)\right] x\,dL_{x\psi} \tag{75}$$

and the elementary power in ft.lbs/sec: $dP_{ind_{x\psi}} = \Omega dQ_{ind_{x\psi}}$ or, $(\Omega R = V_t)$,

$$dP_{ind_{x\psi}} = b\left[v_{x\psi}/(x + \mu \sin\psi)\right] x\,dL_{x\psi}. \tag{76}$$

However, once $v_{x\psi}$ values over the whole disc area, $v_{x\psi} = f(x,\psi)$, as well as the actual or equivalent blade pitch angle $\theta_{x\psi} = f(x,\psi)$, are known, then $dL_{x\psi}$ can be estimated. Now, both Q_{ind} and P_{ind} can be obtained by evaluating the following integral, either on the computer or graphically:

$$Q_{ind} = \frac{b}{2\pi R} \int_{x_i}^{x_e} \int_{0}^{2\pi} \left[v_{x\psi}/(x + \mu \sin\psi)\right] x\,dL_{x\psi}\,d\psi \tag{77}$$

while

$$P_{ind} = \Omega Q_{ind}.$$

As to the contribution of the blade element induced drag $(dD_{L_{x\psi}})$ to the total drag of the rotor $(dD_{ind_{x\psi}})$, it should be noted that similar to the profile drag case, the latter can be expressed as follows:

$$dD_{ind_{x\psi}} = \left[(v_{x\psi}/V_t)/(x + \mu \sin\psi)\right] \sin\psi\; dL_{x\psi}. \tag{78}$$

Again, the induced part of the rotor drag (D_{ind}) would be obtained as a double integral of Eq (78) within the limits $x = x_i$ to $x = x_e$, and $\psi = 0$ to $\psi = 2\pi$. However, in order to give some insight into this subject, it will be assumed that at some representative blade station $x = x_r$, both the induced velocity and the elementary lift remain constant throughout a complete rotor revolution; i.e., $v_{x\psi} = v_{x_r} = const$ and $dL_{x\psi} = dL_{x_r} = const$. Under these assumptions, Eq (78) can be integrated from $\psi = 0$ to $\psi = 2\pi$, thus giving the contribution $(dD_{ind_{x_r}})$ to the rotor drag:

$$dD_{ind_{x_r}} = \frac{dL_{x_r}}{2\pi} (v_{x_r}/V_t) \int_{0}^{2\pi} \left[\sin\psi/(x_r + \mu \sin\psi)\right] d\psi \tag{79}$$

As an example, the $(dD_{ind_{x_r}}/dL_{x_r})$ ratio has been evaluated from Eq (79) for the following conditions: $x_r = .7$, $\mu = .3$, $V_t = 650$ fps, $w = 8$ psf, and consequently, $v_{ind} \approx 8$ fps and $(V_{ind}/V_t) \approx .0123$. Under the above assumptions, $\left(dD_{ind_{.7}}/dL_{.7}\right) \approx -.005$.

It can be seen from the above example that probably under normal operating conditions of helicopters, the contribution of the blade element induced drag to the total drag of the rotor may be neglected.

3.2.3 Further Study of Blade Profile Drag Contribution to Rotor Power and Drag

Equations expressing the contribution of the blade profile drag to the rotor power (Eq (71b)) and drag (Eq (73)) were developed under the following simplifying assumptions:

1. Influence of oblique flow on the profile drag coefficient of the blade airfoil was neglected.

2. In determining the drag of any blade element, only the flow components perpendicular to the blade were considered.

3. Influence of the reversed flow region on the retreating side, and differences in profile drag coefficients associated with this type of flow were neglected.

In order to perform a more realistic evaluation of the profile drag and power problem, a new study is performed without the above limiting constraints.

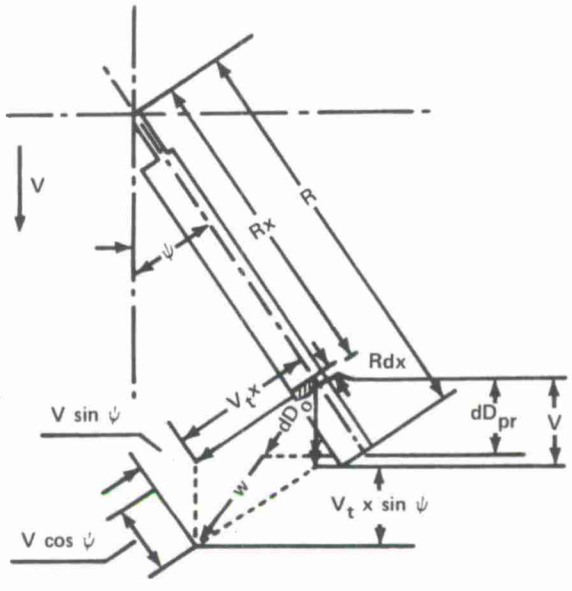


Figure 3-20. Flow Directions and Drag Components at Blade Element

Using notations as in Fig 3-20, it is possible to express the total resultant speed $(w_{x\psi})$ at any blade element located at station x and being at an azimuth ψ by the following:

$$w_{x\psi} = V_t\sqrt{(x + \mu \sin\psi)^2 + \mu^2 \cos^2\psi}\ . \tag{80}$$

Consequently, the total profile drag $(dD_{o_{x\psi}})$ of the blade element in the direction of the resultant local air flow becomes:

$$dD_{o_{x\psi}} = \frac{1}{2}\rho V_t^2\left[(x + \mu \sin\psi)^2 + \mu^2 \cos^2\psi\right] c d_{o_{x\psi}}\ c R\, dx \tag{81}$$

where $cd_{o_{x\psi}}$ stands for the profile drag coefficient at station x and azimuth ψ, with due consideration of the actual flow conditions; i.e., direction of flow (oblique, reversed) in addition to the usually considered influences of Reynolds and Mach numbers.

The contribution of $dD_{o_{x\psi}}$ to the rotor drag component $(dD_{pr_{x\psi}})$ can be expressed as follows (see Fig 3-20):

$$dD_{pr_{x\psi}} = \frac{V_t x \sin\psi + V}{w_{x\psi}}\, dD_{o_{x\psi}} \tag{82}$$

Making proper substitutions from Eqs (80) and (81), Eq (82) becomes:

$$dD_{pr_{x\psi}} = \frac{1}{2}\rho c R V_t^2\, c d_{o_{x\psi}}\left(x \sin\psi + \mu\right)\sqrt{(x + \mu \sin\psi)^2 + \mu^2 \cos^2\psi}\ dx\,. \tag{83}$$

The total contribution to the parasite drag of a rotor equipped with b blades will be:

$$D_{pr} = \frac{1}{4\pi}\rho\, b c R\, V_t^2 \int_0^1 \int_0^{2\pi} c d_{o_{x\psi}}\left(x \sin\psi + \mu\right)\sqrt{(x + \mu \sin\psi)^2 + \mu^2 \cos^2\psi}\, dx\, d\psi \tag{84}$$

For rotors with constant chord blades, $\sigma\pi R^2$ is substituted for bcR, and Eq (84) is rewritten in a form similar to Eq (72a):

$$D_{pr} = \frac{1}{4}\rho\,\sigma\,\pi R^2 \mu V_t^2 \frac{1}{\pi\mu}\int_0^1 \int_0^{2\pi} c d_{o_{x\psi}}\left(x \sin\psi + \mu\right)\sqrt{(x + \mu \sin\psi)^2 + \mu^2 \cos^2\psi}\, dx\, d\psi \tag{85}$$

Power (in *HP*) required to overcome this drag will be:

$$P_{D_{pr}} = \frac{\mu^2}{2200}\rho\sigma\pi R^2 V_t^3 \frac{1}{\pi\mu}\int_0^1\int_0^{2\pi} c_{d_{o_{x\psi}}}(x\sin\psi + \mu)\sqrt{(x+\mu\sin\psi)^2 + \mu^2\cos^2\psi}\,dx\,d\psi \qquad (86)$$

By examining Eqs (85) and (86), it can readily be seen that the expression $(1/\pi\mu)$ times the double integral, etc., replaces the $\bar{c}_{d_o}$ term in Eqs (72a) and (73). Thus, it may be considered as a true average drag coefficient $(\bar{c}_{d_{pr}})$ as far as rotor contribution to the power and parasite drag is concerned.

$$\bar{c}_{d_{pr}} = \frac{1}{\pi\mu}\int_0^1\int_0^{2\pi} c_{d_{o_{x\psi}}}(x\sin\psi + \mu)\sqrt{(x+\mu\sin\psi)^2 + \mu^2\cos^2\psi}\,dx\,d\psi \qquad (87)$$

Because of the difficulties which may be encountered in expressing the variation of c_{d_o} with x and ψ under an analytical form, it will probably be more practical to perform the integration in Eq (87) either on a computer or graphically.

Comparing the values of $\bar{c}_{d_{pr}}$ as determined from Eq (87) with those of $\bar{c}_{d_o}$, some feeling may be developed as to the order of magnitude of error occurring when skin friction and all other effects of the skewed air flow with respect to the blade axis are neglected.

As an illustrative example, the variation of $\bar{c}_{d_{pr}}$ coefficient (from Eq (87)) was computed vs μ. It was assumed in this simplified example that no compressibility effects are encountered and variations in the blade lift coefficient are such that $c_{d_{o_{x\psi}}}$ values are influenced only by the direction of flow with respect to the blade radial axis.

The following numerical values were used in the present example: airfoil thickness $t/c = 15$ percent, the profile drag at the "sweep-back" angle $\Gamma = 0°$, $c_{d_o} = 0.009$, the friction drag at $\Gamma = 90°$ is $c_f = 0.0067$ and the drag coefficient in the completely reversed flow; i.e., at $\Gamma = 180°$ is $c_{d_{180}} = 0.035$. Furthermore, it was assumed that for the oblique flow, the profile drag coefficient varies according to the following formula (given on p. 211 of Ref 15):

$$c_{d_r} = c_f[1 + 2(t/c)\cos\Gamma + 60(t/c)^4\cos\Gamma].$$

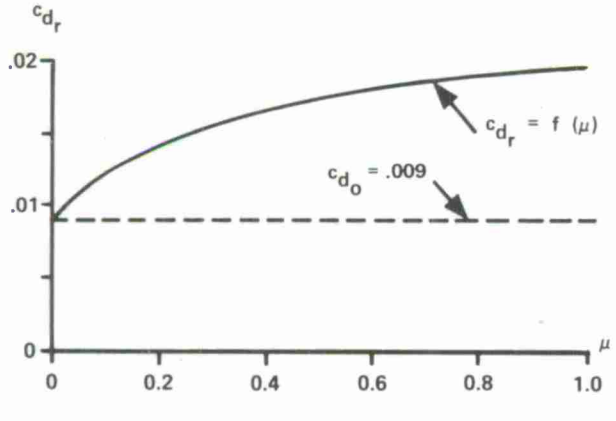


Figure 3-21. Total Equivalent Profile Drag Coefficient versus μ

Results of the computation of $\bar{c}_{d_{pr}}$ are shown in Fig 3-21. A glance at this figure will show that the blade profile drag contribution to the parasite drag increases at first, rather rapidly with μ and then very slowly as it approaches assymptotically the average drag coefficient of the stopped rotor $(\mu = \infty)$. For the range of medium μ values (say, about $\mu = .35$), it may be assumed that on the average,

$$\bar{c}_{d_{pr}} = 1.5\,\bar{c}_{d_o}.$$

Substituting the above value instead of $(1/\pi\mu)$ times the double integral, etc., into Eq (85), the following is obtained:

$$D_{pr} = \frac{3}{8}\rho\sigma\pi R^2 V_t{}^2\mu\bar{c}_{d_o} \qquad (88)$$

and

$$P_{D_{pr}} = (3/4400)\rho\sigma\pi R^2 V_t{}^3\mu^2\bar{c}_{d_o} \qquad (89)$$

but $(1/4400)\rho\sigma\pi R^2 V_t{}^3\bar{c}_{d_o}$ is the profile power in hovering, P_{pr_o}; hence, Eq (89) can be rewritten as follows:

$$P_{D_{pr}} = 3\mu^2 P_{pr_o}. \qquad (90)$$

Considerations similar to the preceding ones would indicate that the profile power in forward flight (P_{pr}) increases more rapidly than indicated by Eq (71b). The following expression probably describes this power rise more correctly.

$$P_{pr} = P_{pr_o}(1 + 1.7\mu^2) \qquad (91)$$

Consequently, total power required to overcome the blade profile drag will be the sum of Eqs (90) and (91).

$$P_{pr_{tot}} = P_{pr_o}(1 + 4.7\mu^2). \qquad (92)$$

3.2.4 Propulsive Thrust and Power Required in Horizontal Flight

Let it be assumed that f stands for the equivalent flat plate area of the helicopter as a whole except for the actual blades. This means that in addition to the airframe drag, f would also represent the drag of the hub and tail rotor (if present).

It was shown in Section 3.2.2 that contributions of the blade element induced drag to the rotor drag may usually be neglected. Hence, the total drag of a helicopter in forward flight will be

$$D = D_{par} + D_{pr}$$

where $D_{par} = \rho V^2 f$. Expressing D_{pr} as in Eq (88) for a helicopter with n identical rotors, D becomes:

$$D = \frac{1}{2}\rho V^2 f + \frac{3}{8} n\rho\sigma\pi R^2 \mu V_t^2 \bar{c}_{d_o} . \tag{93}$$

Magnitude of Thrust Inclination in Forward Flight (within the validity of small angle assumptions) can now be expressed as:

$$-a_v \equiv D/W = \left(\frac{1}{2}\rho f V^2 + \frac{3}{8} n\rho\sigma\pi R^2 \mu V_t^2 \bar{c}_{d_o}\right)/W. \tag{94}$$

Defining $W/f \equiv w_f$ as the equivalent flat plate area loading and remembering that $W/\sigma\pi R^2 \equiv w_b$ is the blade loading, Eq (94) can be rewritten as follows:

$$-a_v = \frac{1}{2}\rho V_t^2 \mu\left(\frac{\mu}{w_f} + \frac{3}{4}\frac{\sigma}{w}\bar{c}_{d_o}\right) \tag{94a}$$

or

$$-a_v = \frac{1}{2}\rho V_t^2 \mu\left(\frac{\mu}{w_f} + \frac{3}{4}\frac{\bar{c}_{d_o}}{w_b}\right) . \tag{94b}$$

It is apparent from Eq (94b) that reduction of the blade area (high w_b) without a corresponding increase in the $\bar{c}_{d_o}$ values would be beneficial for reducing a_v. Reduction of the parasite drag (increase of w_f) is obviously also beneficial.

Total rotor horsepower required in horizontal flight of the helicopter will be the sum of the induced, profile, and parasite powers. Thus, assuming that the gross weight $W \approx T$, and disc loading is w, the total power (in HP) becomes:

$$RHP = \frac{k_f}{1100}\frac{Ww}{\rho V} + (1 + 4.7\mu^2)\frac{n}{4400}\sigma\pi R^2\rho\bar{c}_{d_o}V_t^3 + \frac{1}{1100}\rho f V^3 . \tag{95}$$

3.3 CONCLUDING REMARKS RE BLADE ELEMENT THEORY

Basic philosophy of the blade element theory consists of the idea of investigating aerodynamic phenomena occurring within a narrow strip of the blade. Once all the flow conditions in the immediate neighborhood of the element as well as its aerodynamic coefficients under these particular circumstances are known, then at least in principle, it should be possible to predict aerodynamic forces and moments acting on that blade element. Indeed, physicomathematical models based on the blade-element approach still form the foundation of the analytical methods of predicting, not only performance, but structural aerodynamic loads as well. They are also applied in the investigation of aeroelastic problems.

The pure momentum approach (Chapter 2) recognized the disc loading (w) as the only design parameter influencing the performance of a rotor. By contrast, the blade element theory permits one to recognize the importance of such additional design parameters as: tip speed (V_t): blade loading (w_b); blade airfoil characteristics $(c_\ell$ and $c_{d_o})$; blade planform $(c_x = f(x))$ and blade twist distribution $(\theta_t = f(x))$. Availability of this tool permits the designer to investigate the interplay between all of the above-quoted design parameters plus the previously mentioned disc loading; thus opening a new road toward rotor and/or helicopter optimization with respect to the defined mission requirements.

The importance of a detailed knowledge of the flow conditions at the considered blade element was emphasized at the beginning of this chapter. Obviously, the ability to determine the induced velocity at the blade element is essential for the definition of the flow at the blade element. In this respect, the combined momentum and blade element theory provides one of the possible means of achieving the goal of predicting induced velocity with due consideration of the important design parameters of the rotor. However, it should be noted that the picture of aerodynamic events thus obtained, although much more detailed than that provided by the momentum theory, is still somewhat idealized. This is chiefly due to the fact that air movements associated with thrust generation are represented as time-average flows.

If one would investigate the rotor wake with not-too-sensitive anemometers (pitot-static tubes for instance) he would probably find that indeed, the measured flows are in good agreement with those predicted by the combined momentum blade-element theory, especially inboard from the blade tip regions. However, should more sensitive velocity measuring devices such as the hot-wire anemometers be used, or the actual flow in the wake visualized by smoke or other means, then one would realize that the flow in the wake is actually time-dependent and subjected to various fluctuations. The combined momentum and blade-element theory is, unfortunately, unable to explain many of those time-dependent events. This limitation may not be too important from the performance point of view, but may become significant as far as predictions of blade air loads, vibratory excitations and understanding of noise generation are concerned.

The so-called vortex theories, which will be reviewed in the following chapter, should provide a more suitable physical representation of aerodynamic events and thus, permit development of models more suitable for deeper investigations of such aspects as blade airloads, vibratory forces, aeroelastic phenomena and noise in addition to performance. Nevertheless, there is still a place for the combined momentum and blade-element theory. This theory may be especially useful in establishing general design and performance trends and philosophies, as well as to indicate the proper direction toward design optimization. This is due to the fact that through the combined momentum and blade-element theory, one is permitted to watch more closely the consequences of varying the different design and operational parameters. Thus, the whole functional dependence between the parameter change and its effect on performance becomes more clearly visible. Due to this, the combined theory is especially suitable for the preliminary design and requirements formulation when basic concepts of the aircraft or even the whole operational system are being formed and various design and operational tradeoffs investigated.

References for Chapter 3

1. Glauert, H., Airplane Propellers, Div. L, Vol. IV of Durand's Aerodynamic Theory, Durand Reprinting Committee, Cal. Tech., 1943.

2. Ward, J.F. and W.H. Young, Jr., A Summary of Current Research in Rotor Unsteady Aerodynamics with Emphasis on Work at Langley Research Center, AGARD-CPP-111, September 1972.

3. Liiva, J., F. Davenport, L. Gray and I. Walton, Two-Dimensional Tests of Airfoils Oscillating Near Stall, USAAVLABS Tech. Report 68-13A, Vols. I & II, 1968.

4. Liiva, J., Unsteady Aerodynamic and Stall Effects on Helicopter Rotor Blade Airfoil Sections, Paper 68-58 presented at the 6th Aerospace Science Meeting of the AIAA, January 1968.

5. Philippe, J.J. and M. Sagner, Calcul et des Forces Aerodynamiques sur Un Profil Oscillant, Avec et Sans Decrochage, AGARD-CPP-111, September 1972.

6. Valensi, J., J.M. Rebont, J. Renaud and G. Vingut, Efforts Aerodynamiques sur Un Profil D'Aile Anime D'Un Mouvement Harmonique Parallele A L'Ecoulement de Tamis, AGARD-CPP-111, September 1972.

7. Hammond, C.E., and G.A. Pierce, A Compressible Unsteady Aerodynamic Theory for Helicopter Rotors, AGARD-CPP-111, September 1972.

8. McCroskey, W.J., The Inviscid Flowfield of an Unsteady Airfoil, AIAA Paper No. 72-681, June 1972.

9. Klemin, A., Principles of Rotary-Wing Aircraft, AERO Digest, May 1 and June 1, 1945.

10. Sissingh, G., Contribution to the Aerodynamics of Rotary-Wing Aircraft, NACA TM No. 921, 1939.

11. Wald, Q., The Effect of Planform on Static Thrust Performance, Sikorsky Aircraft, SER 442, November 1944.

12. Stepniewski, W.Z., A Simplified Approach to the Aerodynamic Rotor Interference of Tandem Helicopters, Proceedings of the West Coast AHS Forum, September 1955.

13. Stepniewski, W.Z., Suggested Ways of Comparing Overall Efficiency of Helicopters, Journal of Aeronautical Sciences, Vol. 19, June 1952.

14. Stepniewski, W.Z., Introduction to Helicopter Aerodynamics, Rotorcraft Puablishing Committee, Morton, Pa. 19070, Second Edition, 1958.

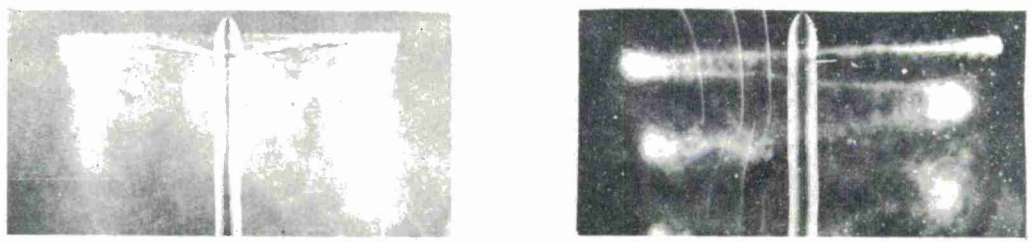
15. Hoerner, S.F., Aerodynamic Drag, published by the author, 1952.

4. VORTEX THEORY

Vortex theory represents another of the classical approaches to rotor aerodynamic . During the last decade, it has been widely applied to rotary-wing problems and thus, suitable references are readily available through various publications; for example, the recent AGARD report[1]. For this reason, the current presentation of vortex theory will be chiefly limited to a general review of the field, while for details, the reader will be directed to the references.

4.1 FUNDAMENTALS OF VORTEX THEORY

It was indicated in the preceding chapter that there are design problems (e.g., the significance of the number of blades) and aerodynamic phenomena (e.g., tip losses, upwash, impulsive loading, impulsive noise generation, etc.) that cannot be properly handled with the help of physicomathematical models based on either the momentum or combined momentum and blade-element theories. In particular, when one starts to think about large rotors with a small number of blades rotating at 2 rps or even less, the whole concept of a continuous steady flow within a well-defined stream that may be acceptable for a multibladed confiquration (Fig 4-1a), does not now appear to properly model the actual physical phenomena (Fig 4-1b). Various techniques of flow visualization reveal



(a) (b)

Figure 4-1. Examples of Flow Visualization for:
(a) Six-Bladed and, (b) One-Bladed Rotors in Hover[2]

the presence of vortices in the wake in all regimes of flight (Figs 4-1 and 4-2)[2]. It should also be noticed that vortices springing from the blade tips seem to dominate the flow picture. It is understandable, hence, why the early physicomathematical models of the rotor had their logical structures built around the tip vortices.

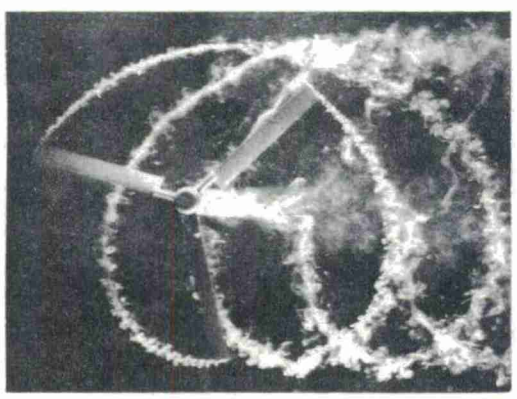


Figure 4-2. An example of Flow Visualization of a Rotor in Forward Translation[2]

All early attempts in the development of the vortex theory were based on the classical approach, treating air as an incompressible frictionless fluid. Furthermore, all the assumptions of classical hydro and aero mechanics regarding vortices were retained. In any textbook on this subject (e.g., Ref 3), one can find that fluid motion associated with the existence of a vortex can be broken down into (a) rotation of the vortex core (filament), and (b) irrotational (potential) flow outside of the core itself. Two-dimensional flow induced by a vortex of strength Γ occurs in concentric circles and tangential velocity (v_t) at any point of a given circle of a radius r is constant and equal to

$$v_t = \Gamma/2\pi r. \qquad (1)$$

Because of the existence of the core, v_t does not increase to infinity at $r \to 0$, but only reaches its (finite) maximum value at the border of the core which is assumed to rotate as a rigid body. The character of the tangential velocity distribution (v_t) around the vortex may be expected to be as shown in Fig 4-3.

As to the vortex filaments, their behavior is governed by the following theorems of Helmholtz and Kelvin:

1. "No fluid particle can have a rotation if it did not originally rotate."

2. "Fluid particles which at any time are part of a vortex line (filament) always belong to the same vortex line."

3. "Vortex filaments must be either closed lines or end on the boundaries of the fluid."

It may be expected that in such a real fluid as air, the above should be considered as only approximate rules. Because of the existence of friction, the vortex filaments undergo changes with time. Such investigations as those of McCormick, et al[4], Cook[5], and others considerably improved our understanding of the behavior of real vortices.

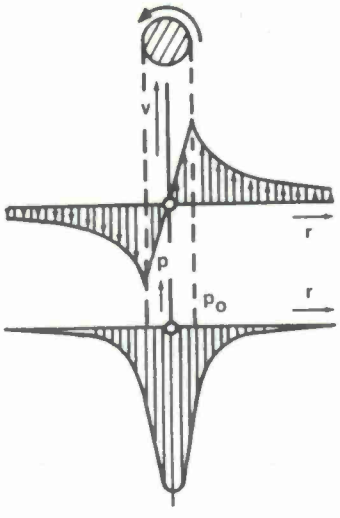


Figure 4-3. Velocity and Pressure Distribution in the Interior, and in the Neighborhood of a Rectilinear Vortex[3]

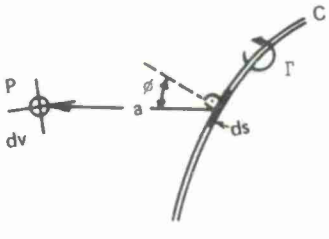


Figure 4-4. Induction of Velocity dv at a Point P

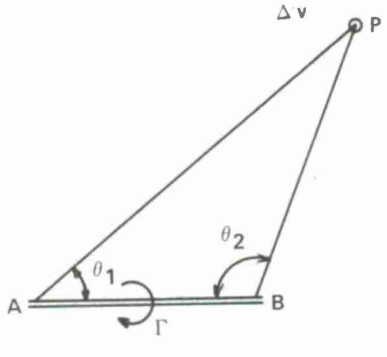


Figure 4-5. Increment of Velocity Δv Induced by Vortex Segment A-B

Biot-Savart Law is one of the principle tools for determination of the flow field induced by a system of vortex filaments. For this reason, its basic aspects are recalled here. In vectorial notations, velocity $\vec{v}$ induced by a filament C of strength Γ can be expressed as follows:

$$\vec{v} = \oint^{C} \frac{d\vec{s} \times \vec{a}}{a^3} \qquad (2)$$

where the integral sign indicates that an integration is carried along the line of the filament C. $d\vec{s}$ represents an element of that filament and $\vec{a}$ is the distance between the point in space where we want to determine velocity $\vec{v}$, and the element $d\vec{s}$. The cross-product $d\vec{s} \times \vec{a}$ has a value of $ds\, a\, sin(ds,a)$ and has a direction perpendicular to $d\vec{s}$ and $\vec{a}$. In Ref 3, the following wording is used to describe $\vec{v}$:

"The velocity $\vec{v}$ is obtained by adding together the contributions of the individual filament elements ds, and the contribution of this element is perpendicular to ds and a, and is inversely proportional to the square of the distance a from the point in question. This, however, is exactly the law of Biot and Savart in electrodynamics from which the magnetic field in the neighborhood of a current-carrying wire can be calculated. If the vortex filament lies in a plane (Fig 4-4), the above equation simplifies to

$$v = \frac{\Gamma}{4\pi} \oint^{C} \frac{ds}{a^2} \sin\phi \,." \qquad (3)$$

For the particular case of an infinite rectangular vortex of strength Γ, Eq (3) reduces to the previously mentioned Eq (1).

In those cases when the actual shape of the vortex filament can be approximated by rectilinear segments, Eq (3) may be used by taking the line integral within each segment. In some cases, the following formulae may be more convenient for determination of the velocity induced by a straight-line segment $(A\text{-}B)$ of a vortex filament of circulation Γ (Fig 4-5):

$$v = (\Gamma/4\pi r)(\cos\theta_1 + \cos\theta_2) \,. \qquad (4)$$

Although vortices induce velocities within the fluid they, in turn, may be subjected to the action of the fluid. According to Helmholtz's theorem, there is no exchange of either mass or momentum between the vortex core and the rest of the fluid; hence, if a vortex filament were located in the mass of the moving fluid, it would move with the fluid. This obviously means that velocity fields induced by more than one vortex can produce a motion of one vortex with respect to another.

Kutta-Joukowski Law relating lift (ℓ) per unit length of a wing or blade in a two-dimensional flow to the strength of circulation at a particular station of the wing, or blade, provides another important building-block in the development of the vortex theory. This basic formula is:

$$\ell = \rho w \Gamma \qquad (5)$$

where Γ is the strength of circulation around the airfoil section, ρ is the air density, and w is the air velocity at the considered section.

If c is the chord and c_ℓ is the lift coefficient at the considered section, then Eq (5) can be rewritten as follows:

$$c_\ell = 2\Gamma/wc \tag{6}$$

or

$$\Gamma = \frac{1}{2} c_\ell w c. \tag{7}$$

Consideration of the Helmholtz and Kutta-Joukowski Laws would indicate that whenever the product of c_ℓ, w_ℓ and c varies along the rotor blades or, in other words, the circulation around the blade changes, then a vortex filament of strength $\Delta\Gamma$ equal to the change in the circulation should leave the blade. By the same token, if the circulation around the blade remains constant along its entire span, then the vortex bound to the blade would leave it at the tip and at the root only (Fig 4-6).

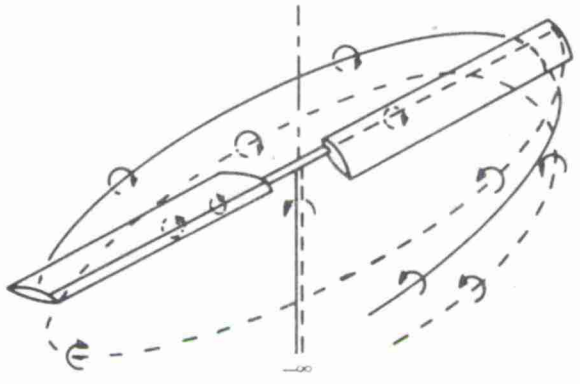


Figure 4-6. Vorticity Scheme in Axial Translation for Constant Circulation along the Blades

As to the root vortex, it is apparent that since Ωr is zero at the rotor axis, the only remaining velocity (in the case of vertical flight or hovering) is axial. Hence, it is not difficult to imagine that each vortex leaving the blade at the root combines with those of the other blades to form one common vortex line along the rotor axis (Fig 4-6). Vortices springing out from the tip will form approximately a helical line (also, see Fig 4-1b).

For the case of hovering or axial translation at such speeds that velocity (w_x) experienced at various blade stations x may be considered as $w_x \approx V_t x$, it is easy to express the constant blade circulation in terms of the rotor thrust coefficient (C_T), tip speed (V_t), rotor radius (R) and number of blades (b).

Since $w = V_t x$, according to Eq (5), the load distribution along the blade is triangular, reaching its maximum value per running foot $\ell_{max} = \Gamma_b \rho V_t$ at the tip, where Γ_b is the circulation along the blade. The total load (thrust) per blade T_b, hence, will be $T_b = \Gamma_b \rho V_t R/2$. However, $T_b = T/b$ where T is the total thrust. Consequently,

$$\Gamma_b = 2T/b \rho V_t R. \tag{8}$$

Multiplying the numerator and denominator of the above expression by $\pi R V_t$, the following is obtained:

$$\Gamma_b = 2C_T \pi R V_t / b. \tag{8a}$$

4.2 EARLY DEVELOPMENTS OF THE VORTEX THEORY

4.2.1 Hovering Rotor with a Single Cylinder of Tip-Shed Vorticity

The vortex theory has found wide application in propeller analysis, starting with the pioneering work of Goldstein[6] in 1929.

However, as far as lifting rotors are concerned, attempts at its application can probably be traced to the early works of Knight and Hefner in 1937[7]. These and similar studies were performed before the advent of high-speed computing devices and thus, required some simplifying assumptions. For instance, it was assumed that the rotor has a very large number of blades. This implies that distances between the consecutive vortex helixes are so small that instead of having either helical vortex sheets or helixes of tip vortices corresponding to the number of blades, the whole wake below the rotor may be considered as filled with vorticity (physical concept somewhat similar to that of Fig 4-1a).

Under these assumptions, the wake may be sliced into horizontal circular vortex rings and longitudinal vortex lines extending along the rotor streamtube. The vortices directed along the wake will contribute to the rotation of the slipstream, while the ring vortices will produce the downward movement of the air (downwash). As to the contribution of the bound vortices to the creation of downwash in the plane of the disc, the sum of their contribution (under the assumption of a large number of blades) will be zero. This can be proven by selecting an arbitrary point on the disc. The tendency to create downwash by the sum of all vortices located to one side of a line through the chosen point and the center of the disc will be exactly equal in magnitude and opposite in sign to the sum of those located at the other side of the line. It is obvious, hence, that under these assumptions, no downwash can be created by the bound vortices.

Following the above reasoning, Knight and Hefner assumed an infinite number of blades and thus determined the induced velocity normal to the plane of the rotor by a cylindrical surface of vorticity, starting at the rotor disc and extending downward to infinity (Fig 4-7)

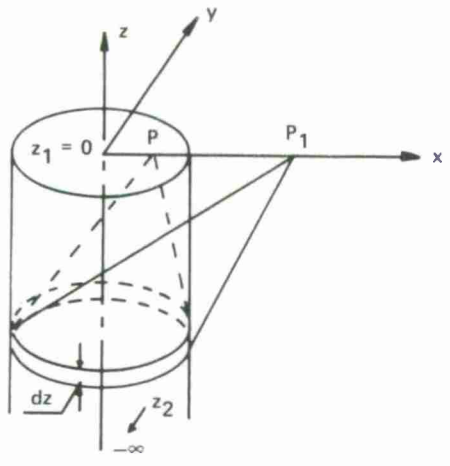


Figure 4-7. Scheme of Cylindrical Vorticity of a Stationary Rotor

The Biot-Savart Law indicates that at a point P, the velocity potential Φ_p corresponding to a closed vortex filament of strength Γ, will be (Ref 3, p. 204):

$$\Phi_p = (\Gamma/4\pi)\omega$$

where ω is the solid angle subtended by that closed vortex line. The velocity (v_p) induced at that point will be:

$$v_p = grad\ \Phi = \frac{1}{4\pi}\, grad\ \Gamma\omega. \tag{9}$$

In view of the above, the induced velocity (i.e., in the direction of the z axis) will be obtained by differentiating $\Gamma\omega$ with respect to z. However, under the assumption of a cylindrical wake with no slipstream contraction, the intensity of the ring velocity along the z axis is expressed by $d\Gamma/dz = const$.

As to the gradient of the angle ω, it may be assumed that between the two coordinates z_2 and z_1, it can simply be expressed as the difference of the $\omega(z_2)$ and $\omega(z_1)$ values. Now, Eq (9) can be rewritten as follows:

$$v_p = \frac{1}{4\pi}(d\Gamma/dz)\ \omega(z_2) - \omega(z_1). \tag{10}$$

Let it be assumed that the rotor is far from the ground and thus, its wake extends far below: $z_2 = -\infty$ (Fig 4-7). For any point P, located in the plane of the rotor disc but inside the circle of the vortex cylinder, $\omega(z_2) = 0$ since the supporting ring is infinitely far away from the point P. As to the value of $\omega(z_1)$, it will be $\omega(z_1) = 2\pi$, since the point P lies in the plane of the supporting ring $(z_1 = 0)$. This means that the induced velocity in the plane of the disc (v_p) becomes

$$v_p = -\frac{1}{2}(d\Gamma/dz) = const. \tag{10a}$$

Since the above equation was established for an arbitrary point of the rotor disc, the induced velocity should be constant over the whole disc area.

Should point P be located outside of the rotor disc, then in addition to $\omega(z_2) = 0$, also $\omega(z_1) = 0$; thus, according to Eq (10), no flow (at least in the z direction) would be induced by the assumed wake.

The downwash velocity far below the rotor $(v_{-\infty})$ can also be found with the help of Eq (10): If point P is moved far below the rotor, then obviously, $\omega(z_2)$ still remains equal to zero, but $\omega(z_1) = 4\pi$ and thus,

$$v_{-\infty} = -(d\Gamma/dz). \tag{10b}$$

Comparing Eqs (10a) and (10b), one sees immediately that $v_{-\infty} = 2v$; as previously indicated by the momentum theory.

Taking Eq (8) into consideration, the total value of the circulation corresponding to one revolution of the rotor becomes:

$$\Delta\Gamma = 2T/\rho V_t R \tag{11}$$

and

$$d\Gamma/dz = -\Delta\Gamma/\Delta z \tag{12}$$

where $\Delta z = v\Delta t$ is the distance traveled by the wake during the time Δt corresponding to one complete rotor revolution; however, $\Delta t = 2\pi R/V_t$. Making the necessary substitutions for $\Delta\Gamma$ and Δz in Eq (12), the following is obtained:

$$d\Gamma/dz = -T/\pi R^2 \rho v_{ind}. \tag{13}$$

where v_{ind} is the induced velocity at the disc. Substituting Eq (13) into Eq (10a) where v_p is now identical to v_{ind}, and solving for v_{ind} results in the following:

$$v_{ind} = \sqrt{T/2\pi R^2 \rho}.$$

The above expression is immediately recognized as the formula for induced velocity previously obtained in the momentum theory.

Although the above results appear to be correct, nevertheless, the whole idea of the physicomathematical model based on a uniform cylindrical vorticity distribution contains some logical contradictions: the increase of velocity in the downstream direction, as

postulated by Eq (10b), should cause contraction of the wake supporting the shed vorticity, but in spite of this, a constant cross-section of the slipstream is still assumed.

4.2.2 Circulation Varying Along the Blade Radius

Cases when circulation is varying along the blade should be of greater interest from the point of view of practical applications. In the simplest physicomathematical model of a hovering rotor with varying circulation, it may be assumed that a vortex filament leaving the blade at a particular station moves (as in the preceding case) along a circular cylinder of the radius equal to that of the blade station from which the filament originated. The strength of each vortex filament leaving the blade is equal to the corresponding variation of circulation along the radius.

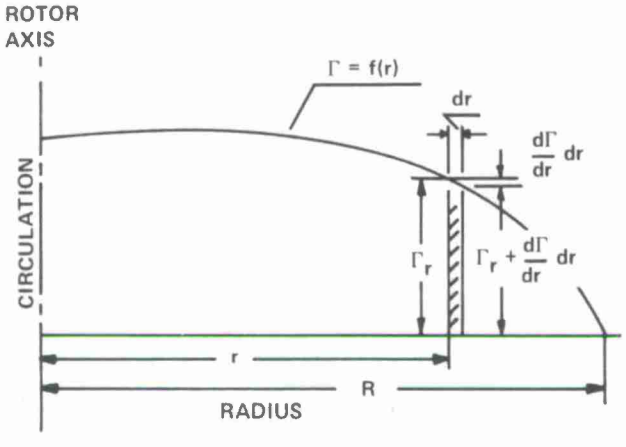


Fig 4-8. Circulation Varying Along the Blade

Assuming that $\Gamma = f(r)$ for the blade is known (Fig 4-8), the variation of circulation for a blade element dr wide and located at a distance r from the rotor axis will be $(d\Gamma/dr)dr$. Thus, a vortex of this strength should leave the blade at station $r + dr$. It has been shown in the preceding paragraph that vortices springing out at a given radius do not produce any downwash in the place of the disc outside of the radius at which they separate from the blade. This means that the considered vortex of strength $(d\Gamma/dr)dr$ and leaving the blade at station $r + dr$, has no influence on the downwash velocities of blade elements outboard of this station. The vortex, however, may affect the inboard elements, and this influence can be easily estimated.

As shown in the previous paragraph, the induced velocity in the plane of the rotor disc is:

$$v = -\frac{1}{2} d\Gamma/dz .$$

Hence, the downwash produced by the blade element dr will be

$$v = -\frac{1}{2} \frac{d[\Gamma_r + (d\Gamma/dr)dr]}{dz} . \tag{14}$$

Neglecting the infinitesimals of higher order, this equation becomes, as before:

$$v = -\frac{1}{2} (d\Gamma/dz) . \tag{14a}$$

The downwash created by the inboard elements to station r, $(0$ to $r)$ will be:

$$v_{0-r} = -\frac{d[\Gamma_r + (d\Gamma/dr)dr - \Gamma_r]}{dz} . \tag{15}$$

Neglecting the infinitesimals of higher order, Eq (15) reduces to zero.

These results indicate that the circulation existing at any blade element influences the downwash at that particular element only. Thus, it proves that the blade elements are reciprocally independent, as was assumed in the combined momentum and blade-element theory.

For each blade station, it is now possible to establish certain relationships existing between the circulation, the geometry of the rotor (chord, number of blades, etc.) and the characteristics of the airfoil section at this station, without worrying about any possible ramifications from any other point along the blade.

The lift coefficient of a blade section at a given radius r is:

$$c_{\ell_r} = a_r(\theta_r - \phi_r) .$$

In hovering, where θ_r is the pitch angle at this station, and ϕ_r is the total inflow angle which, under the small angle assumptions, becomes $\phi_r = v_r/\Omega r$,

$$c_{\ell_r} = a_r[\theta_r - (v_r/\Omega r)] . \tag{16}$$

Substituting Ωr in Eq (7) for the velocity of flow w, and expressing c_ℓ according to Eq (16), the total circulation at station r for b number of blades is readily obtained:

$$\Gamma_r = \frac{1}{2} a_r \, bc_r \, [\theta_r - (v_r/\Omega r)] \Omega r. \tag{17}$$

In the case of hovering, as the vortex filaments spring out from each blade station and move down with the slipstream, it is clear that the distance (d_z) measured along the rotor axis *(z axis)* between successive filaments will be:

$$d_z = (2\pi r/b)(v_r/\Omega r) = 2\pi v_r/b\Omega. \tag{18}$$

Now, the average change of circulation along the rotor axis (z) in the negative direction, $-(d\Gamma/dz)$ can be obtained by dividing Eq (17) by Eq (18):

$$-(d\Gamma/dz)_r = \frac{1}{4\pi} a_r \, bc_r \left[\theta_r - (v_r/\Omega r)\right] \Omega^2 r/v_r. \tag{19}$$

Remembering from Eq (10a) that $v_r = -(1/2)(d\Gamma/dz)_r$; expressing this derivative according to Eq (19) and switching to the x notations $(r \equiv Rx)$ for determining the position of the considered element on the blade, the following equation, now in v_x is obtained:

$$8\pi R \; v_x^2 + V_t \, a_x \, bc_x \, v_x - V_t^2 \, a_x \, bc_x \, x \, \theta_x = 0. \tag{20}$$

A glance at the above equation will indicate that it is identical to Eq (14) in Chapter 3, with $V_c = 0$; obtained from the combined momentum and blade-element theory.

4.3 FURTHER DEVELOPMENTS OF VORTEX THEORY

It can be seen from Sections 4.1 and 4.2 that basic analytical building blocks of the vortex theory are rather simple. However, computational difficulties start to mount when one tries to develop a meaningful physical model of a rotor, and attempts to account for the mutual interaction of all the vortices, both bound and free forming the vorticity system of a rotor in various regimes of axial (including hovering) and oblique translation. This mutual interaction generates a field of flow on which an additional inflow due to the translatory movement of the rotor may be superimposed, leading to computational difficulties that in general, can be attacked only through the use of high-speed computers. However, even in simplified cases when only tip vortices are considered, those computational difficulties still remain quite high, especially in oblique flow.

Striking a proper balance between physical representations of the model and reduction of computational complexities to such a level that programs can be manageable even for large-capacity computers, forms the essence of many programs currently being used by industry and research institutions. However, because of the limitations imposed by the capacity of computational facilities, there seems to be, as yet, no physicomathematical model of the rotor that would be completely satisfactory in all regimes of flight (especially when aeroelastic phenomena are also incorporated). In order to cover these conceptual inadequacies of the model, in some programs one would find various "fudge factors," which may be determined experimentally in an attempt to get a better agreement between the predicted and tested values. Determination of the wake goemetry with the help of experimentally obtained inputs may be cited as an example of such "doctoring" of the model.

In other cases, one would find rather artificial, and physically unjustified assumptions as, for instance, those of excessive diameters of the vortex cores, etc. For this reason, some vortex-theory-based programs that give experimentally justified results for one range of applications may become less satisfactory when extrapolated beyond those areas. One would be advised, hence, to check the whole program for both explicit and hidden "fudge factors" before using it outside of its proven limits of reliability.

Some aspects of the extension of the vortex theory beyond its fundamentals and especially, attempts to apply it to rotary-wing aerodynamics will be briefly reviewed. This will be done by relying on the material presented in Ref 1 in general, and in particular, this review will closely follow the treatment of this subject by Landgrebe and Cheney[8]. Consequently, when considering works already discussed by them, no separate references will be made to the original publications, since the reader will be able to obtain them from Ref 8.

4.3.1 Review of Rotor Wake Models

Similar to the previously discussed model of the rotor in hovering proposed by Knight and Hefner, undistorted wake geometry was assumed in forward flight. However, this time, the wake itself is assumed skewed, as shown in Fig 4-9, although a concept of the uniform vorticity along the blade (vorticity shed at the tips only as in Fig 4-9a) was retained by the original investigators.

The methods of Coleman, et al; Castles and DeLeeuw; and Castles and Durham were based on this concept. Further evolution of this approach consisted of removing uniform loading assumptions by Hayson and Katzoff who modeled the wake as a number of parallel and concentric vortex cylinders (Fig 4-9b). However, all of the above discussed approaches described aerodynamic phenomena of the rotor in terms of time-average steady flows.

In order to remove this limitation, it was necessary to develop physicomathematical models with wakes containing vorticity systems generated by the individual blades. Goldstein, with his propeller model based on a system of tip vortices pointed out the direction to follow. However, especially in forward flight, the wake geometry is quite complicated from the computational point of view and many attempts have been made to simplify this approach[8]. The initial attempts were based on various modifications of the rigid-wake concept whose definition can be formulated as follows: "The undistorted or rigid-wake assumption means that the inplane wake coordinates (inplane parallel to the tip-path plane) are determined by the rotor rotational and translational velocities, and the axial coordinates (normal to the tip-path plane) are determined by a mean-flow velocity which is generally the momentum inflow value." Fig 4-10 shows a model of a rather complete, but still undistorted wake as used by Piziali and DeWaldt, where each blade is represented by a mesh of segmented vortex filaments. Miller used a similar approach and that technique was later extended to tandem configurations by Davenport and Balcerak.

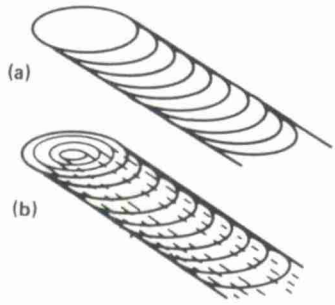


Figure 4-9. Concepts of Rotor Vorticity Distribution in an Oblique Translation

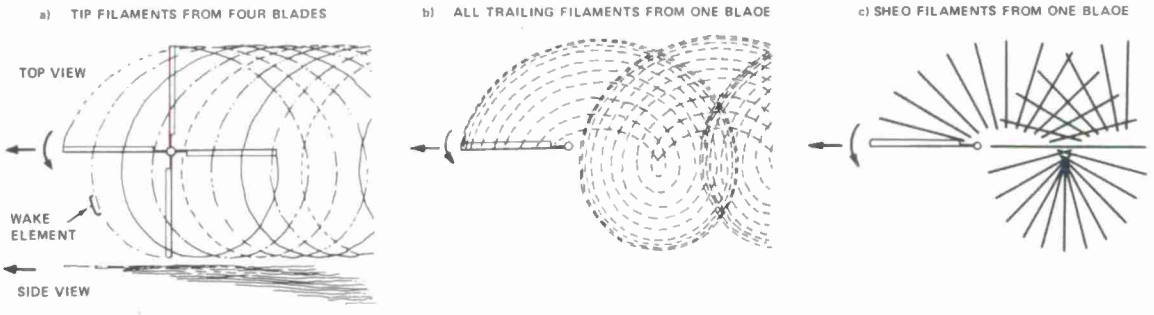


Figure 4-10. Rotor Undistorted Wake Model[8]

Using the undistorted vortex sheet approach, Ichikawa even succeeded in obtaining closed-form solutions for blade spanwise lift distribution.

In spite of some computational attractiveness of the undistorted wake geometry, it was recognized and stated by Miller, Piziali and others "that the sensitivity of blade inflow and associated airloading to wake distortions could be significant[8]." Thus, Miller introduced the concept of the "semi-rigid" wake. It consists of replacing the constant axial velocity, assumed in the rigid wake, with the instantaneous axial velocity associated with each vortex element. This should lead to a distorted spiral wake; however, "changes in the vortex element with time, due to interaction with the wake and blades are neglected..." Other investigators (Piziali, Brandt, Ham, etc.) also used the semi-rigid wake concept, but a comparison of that method with experimental results showed major discrepancies between predicted and measured wake coordinates. Attempts of several investigators to properly account for the wake contraction are reviewed in some detail in Ref 8.

In principle, the most realistic physicomathematical model would be obtained by using as many stations as possible on each blade to account for vortex filaments leaving the blade. They should be allowed "to freely distort until a converged wake results." However, this is obviously the most computer-time-consuming approach. For this reason, actual computer programs still incorporate some simplifications. For instance, methods developed by Langrebe describe reduction of the wake geometry methods to actual practice (for references to these methods, see p. 1-5 of Ref 8). For instance, a method is discussed which consists of "grouping the vortices from each blade into: (1) a strong, rolled-up tip vortex filament, and (2) several weaker trailing vortex filaments representing the inboard vortex sheet" (Fig 4-11). The complete mutual interaction of these vortices may be calculated, or the geometry of the inboard vortices may be prescribed and the distortions of the tip vortex computed.

The computation of the wake geometry is accomplished by the following procedures:

1. "The circulation strength in the wake is estimated from a previous solution of the bound circulation distribution on the blade (lifting line).

2. "An initial wake geometry is specified.

3. "The classical Biot-Savart Law is applied to compute the velocities induced by each vortex segment in the wake at the end points of the assigned distorting

segments.

4. "These velocities are integrated over a small increment in time to define a new wake geometry.

5. "Steps (3) and (4) are repeated alternately until a converged wake geometry corresponding to the initial estimate of blade bound circulation is obtained.

6. "A new estimate of the blade bound circulation distribution is computed using the calculated wake.

7. "Steps (2) through (6) are repeated, iterating until a compatible wake geometry-circulation solution is obtained[8]."

The desire to develop realistic physico-mathematical models of rotors based on the vortex theory produced still another approach to that problem. It may be called a method based on prescribed empirical wake geometry which is chiefly directed toward static thrust conditions. In this approach, the actual shape of the wake is obtained by flow visualization. Within the defined wake geometry, a model for vorticity distribution is conceived. For instance, Gray assumed a vortex structure consisting of a rolled-up tip vortex filament and a separate inboard vortex sheet (Fig 4-12)[8]. Studies of the vortex wake of a single-bladed hovering rotor have been further expanded by Gray and Brown[9]. Other investigators used either empirical or semiempirical inputs in order to obtain on one hand, the desired wake shape while on the other, to achieve a good correlation between the predicted and measured results. Magee, Maisel and Davenport obtained wake contraction partially from a theoretical model of Brady and Crimi, and partially from the experimentally determined slipstream acceleration parameter[8].

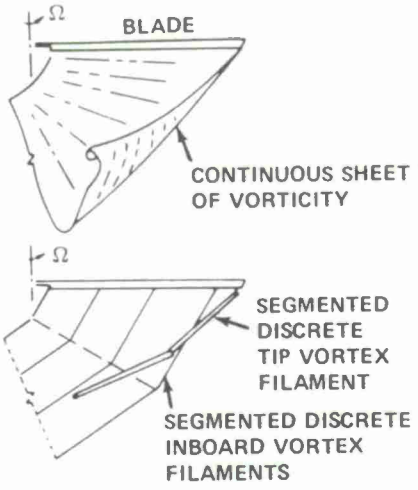


Figure 4-11 Representation of a Vortexx Sheet by Discrete Tip and Inboard Vortex Filaments

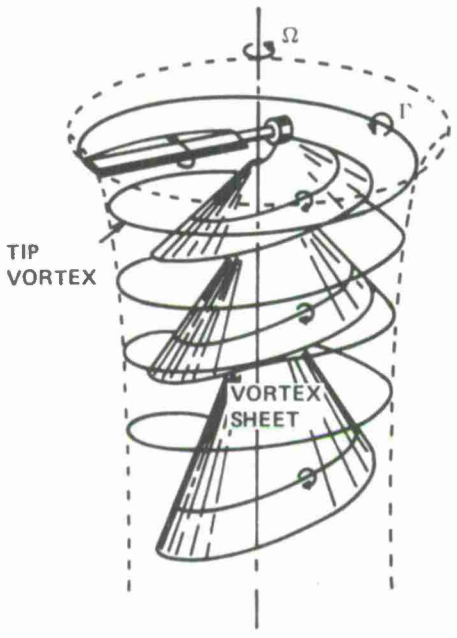


Figure 4-12 Schematic of Hovering Rotor Wake Structure Proposed by Gray[8]

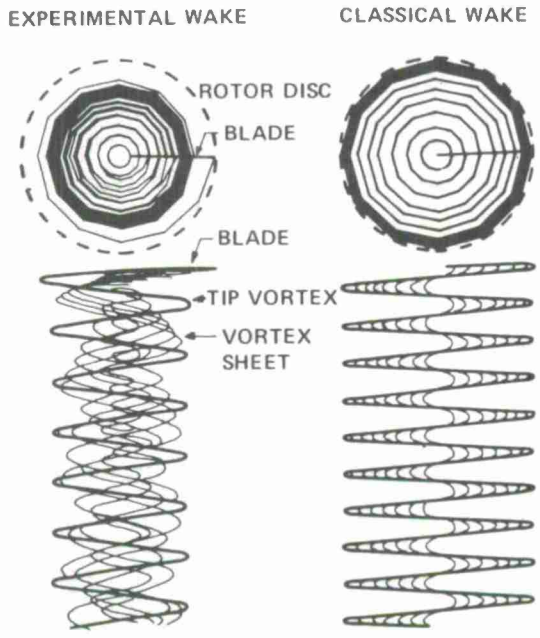


Figure 4-13. Computer Wake Patterns for One Blade[8]

One of the most recent additions to methods based on the prescribed wake geometry is that developed by Landgrebe at the United Aircraft Research Lab for hovering rotors with any number of blades. It permits computation of the blade circulation and inflow distribution and the corresponding rotor performance based on the prescribed wake geometry (for example, see Fig 4-13)[8].

In order to gain a still deeper insight into phenomena occurring in the wake, one must account for the fact that actual vortex filaments do not behave according to Helmholtz's theorem. Because of friction, they undergo the modifications that were mentioned before[4,5]. Cook[5], in his studies of the structure of the rotor blade tip vortex indicates that (a) the vortex can be assumed

to be effectively rolled up after about 70 degrees of rotation of the rotor, (b) the effective size of the vortex core is considerably larger than suggested by simple theories, but the viscous core is significantly smaller, (c) the velocity distribution through the vortex was different from that obtained on semi-span wings in a wind tunnel (smaller viscous core and a fuller velocity profile), (d) circulation contained in the tip vortex was approximately one-half the value expected, and (e) higher blade loadings caused a marked change in the vortex structure (possibly due to a stall in the tip region.

It should be mentioned that in addition to the vortex theory applications discussed by Landgrebe and Cheney in Ref 8, there is also an effort sponsored by NASA Langley that is directed toward improved calculation methods of determining the wake flow. Ward and Young[10] show (Fig 4-14) an example of rotor wake geometry prediction obtained by the method of Sadler. According to Ref 10 in Sadler's method, "the rotor wake is calculated by a process similar to the startup of a rotor in a freestream.

"An array of discrete trailing and shed vortices is generated. Vortex strengths corresponded to stepwise radial and azimuthal blade circulations, and this array is limited to an arbitrary number of azimuthal steps behind each blade. The remainder of the wake model for each blade is an arbitrary number of trailed vortices. Vortex element end points are allowed to be transported by the freestream and vortex-induced velocities. Wake geometries, wake flows, and wake induced velocity influence coefficients for use in blade loads calculations are determined. Wake geometries can be calculated for various rotor configurations, including rotor systems having shaftwise separation, nonuniform azimuth spacing (as in Fig 4-14), counter-rotating blades, and rotors with blade length and other physical differences.

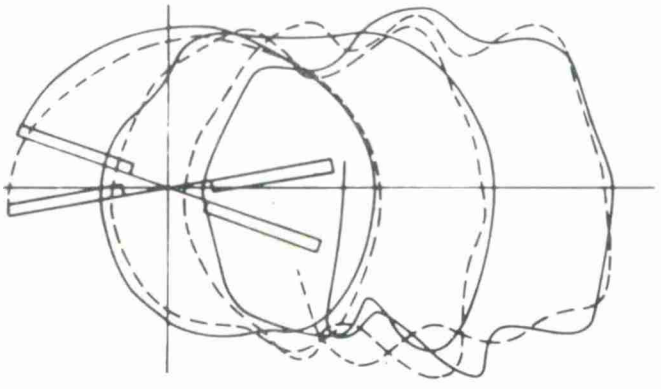


Figure 4-14 Rotor Wake Geometry Prediction Computer Program Output at $\mu = 1$ (Ref 8)

"The computer program also includes a blade loads program which allows the computation of the response of flexible rotor blades to the applied airloads. The wake geometry and blade response computer program has recently been extended to handle steady-state maneuvers."

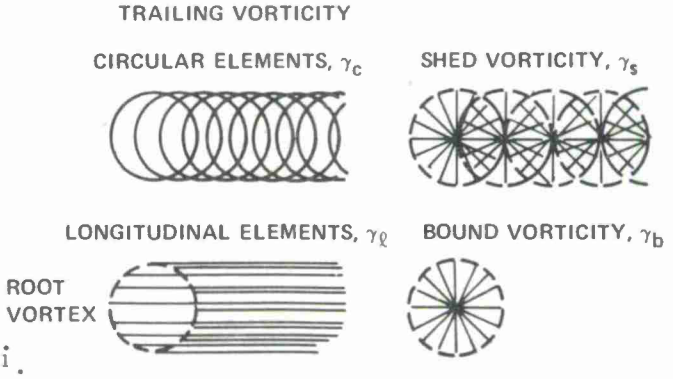


Figure 4-15 Schematic of Vorticity Decomposition in Flat Planar Wake[11]

At the conclusion of this review, it should be noted that in addition to the previously discussed methods basically dealing with discrete vortex filaments, efforts are also being made to further develop physicomathematical models reflecting the concept of the actuator disc and continuous wake. These methods should be less complex from a computational point of view and thus, may be more suitable for application to the preliminary-design phase. One such approach is presented by Ormiston[11]. In this case, the model is developed along the line of fixed-wing, lifting-line theory. Considerable computational simplifications are achieved through an assumption that for a wide range of flight conditions, the rotor wake vorticity can be considered to lie in a flat planar wake. Next, the vorticity elements are, in turn, decomposed into simpler circular, (γ_c), and longitudinal, (γ_ℓ) elements of trailing vorticity (Fig 4-15). There are also elements of shed vorticity (γ_s) and the bound circulation distribution (γ_b). For constant bound circulation, γ_s vanishes and γ_b does not contribute to the downwash generation (see Section 4.2.1). However, in general, all four types of vorticity plus the root vortex should be considered. Eventually, the solution for the rotor downwash is obtained as a Fourier Series.

References for Chapter 4

1. AGARD Conference on Aerodynamics of Rotary Wings, AGARD-CPP-111, September 1972

2. Werle, H. and C. Armand, Mesures et Visualisations Instationnaires sur les Rotors, ONERA, T.P. No. 777, 1969.

3. Prandtl, L. and O.G. Tietjens, Fundamentals of Hydro- and Aeromechanics (translated by L. Rosenhead), Dover Publications, 1957.

4. McCormick, B.W., J.L. Tangler and H.E. Sherrier, Structure of Trailing Vortices, Journal of Aircraft, Vol. 5, June 1968.

5. Cook, C.V., The Structure of the Rotor Blade Tip Vortex, AGARD-CPP, September 1972.

6. Goldstein, S., On Vortex Theory of Screw Propellers, Royal Society Proceedings, (a)123, 1929.

7. Knight, M. and R. A. Hefner, Static Thrust Analysis of the Lifting Airscrew, NACA TN 626, 1937.

8. Landgrebe, A.J. and M.C. Cheney, Jr., Rotor Wakes - Key to Performance Prediction, AGARD-CPP-111, September 1972.

9. Gray, R.B. and G.W. Brown, A Vortex-Wake Analysis of a Single-Bladed Hovering Rotor and a Comparison with Experimental Data, AGARD-CPP-111, September 1972

10. Ward, J.F. and W.H. Young, Jr., A Summary of Current Research in Rotor Unsteady Aerodynamics with Emphasis on Work at Langley Research Center, AGARD-CPP-111, September 1972.

11. Ormiston, R.A., An Actuator Disc Theory for Rotor Wake Induced Velocities, AGARD-CPP-111, September 1972.

5. SOME PERFORMANCE CONSIDERATIONS IN THE DESIGN OF HELICOPTERS AND PERFORMANCE OPTIMIZATION WITHIN DEFINED FLIGHT ENVELOPE

As far as performance is concerned, there seems to be two aspects of the application of rotary-wing aerodynamics to engineering practice: (1) performance prediction and/or optimization during various design stages of new helicopters, and (2) operational performance optimization within an already established flight envelope.

In principle, the problem of aircraft performance optimization could be formulated very precisely, either by the customer or by the designer himself. This could be done by defining on one hand, hard constraints in the form of an acceptable minima for various performance items (V_{max}, V_{cr}, $V_{c_{max_F}}$, $V_{c_{max_V}}$, Payload, Range, etc.) and perhaps, also for the noise level; while on the other, by specifying various weighted merits for exceeding these requirements. Under these circumstances, the process of selecting the best possible design parameters (e.g., disc loading, operational $\bar{c}_\ell$, tip speed, etc.) could have been formulated as a rigorous maximization process of a payoff function (J) representing the sum of all the properly weighted performance excesses over their specified acceptable minima.

$$J = \xi_1 f_1(x_1, x_2, \ldots x_n) + \xi_2 f_2(x_1, x_2, \ldots x_n) \ldots + \xi_k f_k(x_1, x_2, \ldots x_n) \qquad (1)$$

where $\xi_1 \ldots \xi_k$ are the proper weighting factors, while f_1, f_2, etc., represent functional dependencies of the excesses over their lowest acceptable minima of various performance items (V_{max}, V_{cr}, $V_{c_{max}}$, etc.) on the design parameters x_1, $x_2 \ldots$, etc. (disc loading, operational $\bar{c}_\ell$, tip speed, etc.). Once Eq (1) was established, then a search for an optimum set of parameters, x_1, $x_2 \ldots x_n$, maximizing Eq (1) could have been performed, using various optimization techniques; for instance, the Multivariable Search[1].

Unfortunately, it is almost impossible as yet to formulate performance requirements for a helicopter as a whole so precisely that they can be expressed in a form as clear-cut as that of Eq (1). For this reason, selection of the proper (optimum) values of design parameters still remains an art. However, there are specific performance problems where payoff functions, or functionals, can be properly defined and various available optimization techniques can be used to identify optimum values of design parameters. Furthermore, the whole process of selecting optimum design parameters can be guided by establishing and studying the trends existing between variations in values of these parameters and corresponding changes in performance aspects. Some aerodynamic considerations that may be of some help in formulating design philosophy from the performance point of view are sketched in this chapter.

Once the design of a rotary-wing aircraft as well as its flight envelope is fixed, then another problem arises as to what flight control technique would optimize operational performance within the limits of the defined flight envelope. The following tasks can be cited as typical: (a) optimization of takeoff of overloaded helicopters with forward run; (b) minimization of time and/or fuel in climb to a prescribed altitude; (c) minimization of fuel consumed between two points; (d) maximization of productivity (payload transported times block speed); etc.

All of the above tasks can usually be described by a system of ordinary differential equations:

$$dx_i/dt = f_i(x_1, \ldots x_n; u_1, \ldots u_r) \qquad i = 1, \ldots n$$

where the $x_1, \ldots x_n$ are the so-called state, or phase variables describing the state of the object itself, while $u_1, \ldots u_r$ are the control variables, or control parameters

(often called simply, controls) which influence the course of the process.

The goal of optimization[2b] is usually expressed as a requirement to find a control variation with time (within a certain time interval t), $\bar{u}_j(t)$, $j = 1,\ldots r$, that would extremize a functional expressing some payoff quantity (J) associated with the transfer of the object itself from a given initial phase state $x_i(t_o) = x_{i_o}$, $i = 1,\ldots n$; to a prescribed terminal phase state $x_{i_1}(t_1) = x_{i_1}$, $i = 1,\ldots n$:

$$J = \int_{t_o}^{t_1} f_o(x_1,\ldots x_n;\ u_1,\ldots u_r)dt = opt. \tag{2}$$

There is considerable literature dealing with the type of problems defined by Eq (2). Some of the textbooks that may be helpful in this respect are listed in Ref 2. In some cases, dynamic problems can be represented in the parametric form and the search technique as outlined in Ref 1, or similar ones, may be used in the optimization process.

In this chapter, only a few performance optimization problems of helicopters will be mentioned, and the reader will be directed to the available literature on that subject.

5.1 PERFORMANCE CONSIDERATIONS

5.1.1 Weight-to-Equivalent Drag Ratio

The weight-to-equivalent-drag ratio is defined as follows:

$$(W/D_e) = WV_h/325\ SHP$$

where SHP is the total shaft horsepower required in horizontal flight at a speed V_h in knots, and W is the gross weight of the aircraft in considered flight. (W/D_e) is a convenient yardstick for comparing the overall aerodynamic perfection of various shaft-powered rotary-wing aircraft. It is obvious that maximization of this value (or minimization of D_e/W) especially in the operational regimes of flight should be considered as one of the prime objectives of a proper aerodynamic design. In order to indicate the parameters which may influence the D_e/W levels, the equivalent drag-to-weight ratio is expressed by the following relationship based on the blade-element theory:

$$\frac{D_e}{W} = \frac{1}{\eta_{tr}}\left[\frac{1}{2}\rho\frac{V_h^2}{w_f} + \frac{k_f w}{2\rho V_h^2} + \frac{1}{8}\rho V_t^2\frac{\bar{c}d_o}{w_b\mu}\left(1 + 4.7\mu^2\right)\right] \tag{3}$$

where η_{tr} is the transmission efficiency, also covering power losses resulting from running the accessories and all other mechanical devices on the aircraft that consume the engine power; w_f is the equivalent flat plate area (f) loading $w_f \equiv W/f$; and w_b is the blade loading $(w_b \equiv w/\sigma)$. However, from Eq (20) on p. 25, the blade loading (assuming $x_e = 1.0$) can be expressed as follows:

$$w_b = \frac{1}{6}\bar{c}_{\ell_h}\rho_h V_{t_h}^2 \tag{4}$$

where c_{ℓ_h}, ρ_h and $V_{t_h}^2$ refer to the design hovering conditions. Substituting Eq (4) into (3), the latter becomes:

$$\frac{D_e}{W} = \frac{1}{\eta_{tr}}\left[\frac{q_f}{w_f} + \frac{k_f w}{4q_f} + \frac{3}{4\mu}\left(\frac{\bar{c}d_{o_f}}{\bar{c}_{\ell_h}}\right)\left(\frac{\rho_f}{\rho_h}\right)\left(\frac{V_{t_f}}{V_{t_h}}\right)^2\left(1 + 4.7\mu^2\right)\right] \tag{5}$$

where a new symbol, q_f, is the dynamic pressure of forward (horizontal) flight. The first term in the square brackets represents the contribution of the parasite drag power (P_{par}) and, obviously, its value (at any given q_f) can be decreased by making w_f as high as possible. The second term reflects the input due to the induced power (P_{ind}) and here, the low disc loading (w) and the k_f factor as close as possible to its maximum limit of $k_f = 1.0$ are the tools for reducing the P_{ind} contribution. It should also be noted that in contrast to the first term, the importance of the second one decreases with the increasing q_f (square of the speed of flight). As to the third term, it represents contributions due to the total blade profile drag power (P_{pr}). It can be seen from Eq (5) that a high value of the c_{ℓ_h}/cd_o is desirable as well as the possibility of reducing the tip speed in forward flight (V_{t_f}) below its hovering value (V_{t_h}). However, it should be remembered that at a fixed forward velocity (V_f), a decrease in V_{t_f} causes an increase in the tip speed ratio (μ). Since this latter quantity appears in Eq (5) both in the numerator and the denominator, it is not apparent at first sight whether an increase in μ would counterbalance the gains resulting from the (V_{t_f}/V_{t_h}) reduction. Fig 5-1 should clarify this question. From this figure, it can be seen that at high speeds of flight, the blade drag contribution to D_e/W is quite considerable, unless the rotor is slowed down. This explains why, in many advanced concepts of compound helicopters, the rotor is "unloaded" by a fixed-wing and then slowed down to the limit (usually $\mu \leq .9$) dictated by the aeroelastic instabilities. Complete stopping of the rotor (without retraction) would result in slight additional improvements of the D_e/W values.

In order to provide a deeper insight into the importance of the individual contributions of P_{par}, P_{ind} and P_{pr} to the overall (D_e/W) or (W/D_e) level, $(W/D_e) = f(V)$ is computed first for a hypothetical classic helicopter, representative of the present state of the art for the 15,000-pound gross-weight class. In this case, the following values for the quantities appearing in Eq (5) have been assumed: $w = 8$ psf; $k_f = 1.1$; $w_f = 750$ psf; $\bar{c}_{d_o}/\bar{c}_{\ell_h} = 1.45$; $\rho_{5000} = .00205$ slugs/ft^3; $\eta_{tr} = .94$; $\rho_{5000} = \rho_h$ and $V_{t_f} = V_{t_h}$. $(W/D_e) = f(V)$, computed under the above assumptions, is shown in Fig 5-2. In addition, three additional plots are also shown in this figure. In these plots, it has been alternatively assumed that one of the three main components (induced, profile, and parasite) of the total power becomes zero, while the other two retain their previous values. By examining this figure, one should realize where the potentially most profitable areas are for improvement of the overall aerodynamic characteristics of the classic helicopter.

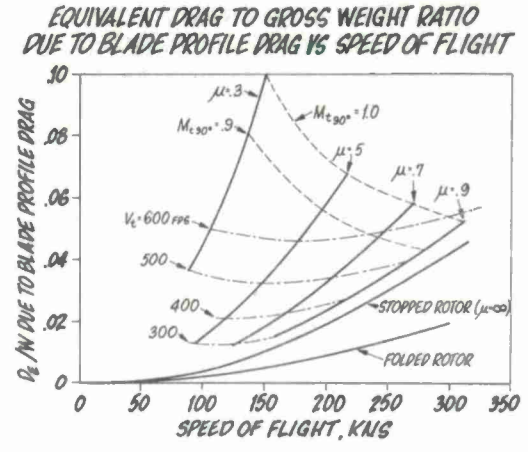


Figure 5-1 Contribution of Blade Profile Drag to Equivalent Drag-to-Gross-Weight Ratio

It can be seen from Fig 5-2 that even a complete elimination of the induced power would considerably improve the (W/D_e) values only in the low (60-80 knots) and medium (up to 120 knots) speed range. Its influence in the high-speed range ($V_f > 160$ knots) is less significant. Obviously, a complete elimination of P_{ind} is impossible; however, its level can be reduced and in order to achieve this goal, the designer can do the following: (a) reduce the disc loading (w), and (b) make the k_{ind_f} factor approach unity. As far as (a) is concerned, usually other considerations such as dimensions of the aircraft, weight, etc., constrain the designers freedom to make w low. With Respect to (b), there is a need of making the k_{ind_f} values as close to 1.0 as possible. This can be done by reducing tip losses and approaching a uniform induced velocity distribution. However, any additional gains from the current state-of-the-art level are not very probable and furthermore, the payoff for achieving even the ideal level of $k_{ind_f} = 1.0$ still would not be very high.

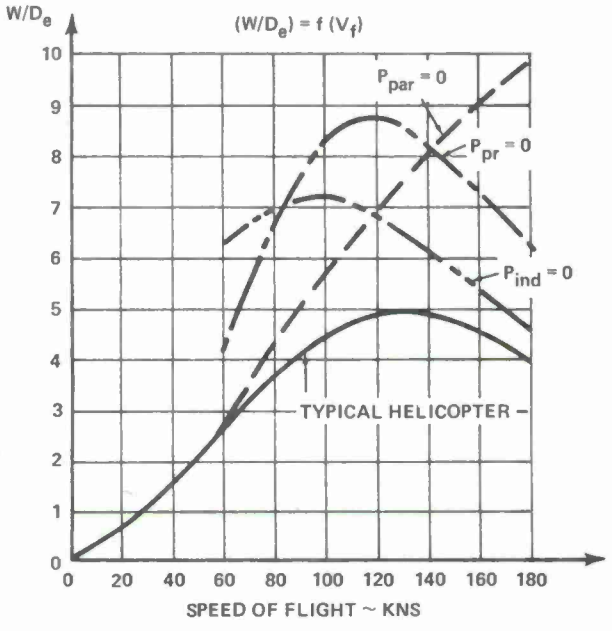


Figure 5-2 Weight-to-Equivalent-Drag Ratios

It may be concluded, hence, that although aerodynamic characteristics of a helicopter can be degraded by not paying enough attention to the k_{ind_f} values, concentration of design and research efforts on P_{ind_f} does not represent a profitable road toward significant improvements of W/D_e in the high-speed regions.

By contrast, a fight against the blade profile power appears more promising (see Fig 5-2) as far as improvement of the overall level of the W/D_e is concerned, especially in the high-speed region. Although a complete elimination of P_{pr} in forward flight is only possible through retraction of the blades, some gains from the current state-of-the-art appear possible, even for classical helicopters as well as those with additional propulsive thrust. It appears from Eq (5) that minimization of

$$(\bar{c}_{d_o}/\bar{c}_{\ell_h})(\rho_f/\rho_h)(V_{t_f}/V_{t_h})^2 = (\bar{c}_{d_{of}}/\bar{c}_{\ell_f})$$

is the necessary condition for reducing the P_{pr} contribution. Development of special airfoil sections, still acceptable from the point of view of aeroelastic requirements (zero, or very low c_m, favorable stalling characteristics, etc.), but combining high c_ℓ's with the corresponding low c_{d_o}'s represents one promising avenue. Indeed, it appears that there is a renewed interest, both within industry[3,4] and research institutions[5,6], in the development of such airfoils and a better understanding of the particular problems of their operation in regard to rotors. Application of lift-increasing devices, including circulation control[7], probably also represents a potential source of improvements. Possibilities of improving the $(\bar{c}_{d_{of}}/\bar{c}_{\ell_f})$ ratio by a radical reduction of the c_{d_o} coefficient through BLC (suction) along the line attempted by Pfenninger[8] appear more remote, especially due to the high turbulence of the environment in which the rotor operates.

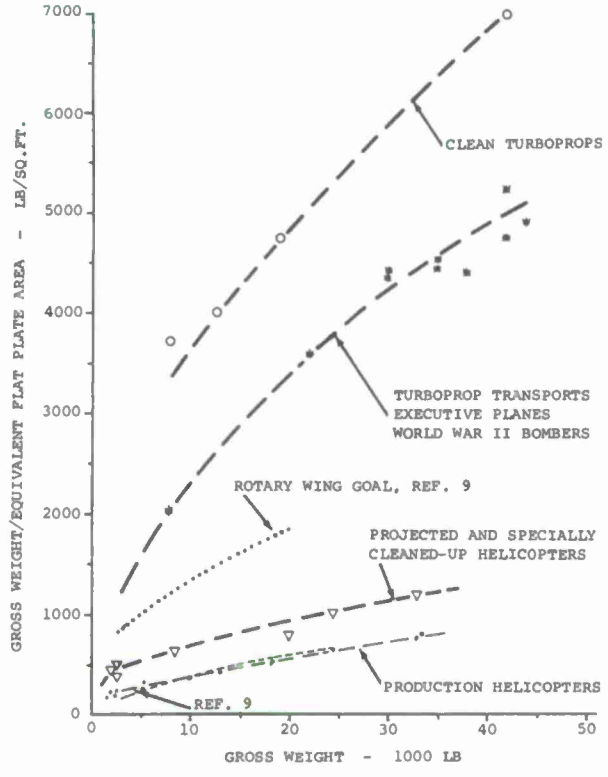


Figure 5-3 Trends with Gross Weight of Equivalent Flat Plate Area Loading of Helicopters (Hubs Included) and Fixed-Wing Aircraft (Profile Drag of Wings and Empennages Excluded)

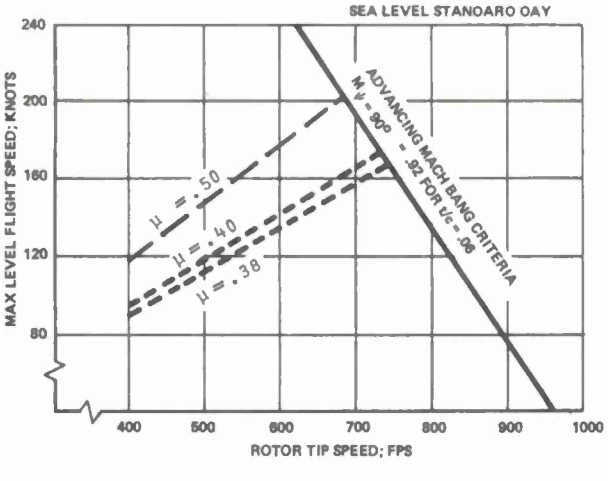


Figure 5-4 High-Speed Band and μ Limits

Fig 5-2 indicates that the highest gains in (W/D_e) in the high-speed regimes of flight can be achieved through reduction of the parasite component of the total power. This obviously, is synonymous with reduction of the parasite drag of all nonrotating components, rotor hubs, various interference drags, powerplant installation drag, etc. The need for a radical parasite drag reduction of helicopters in order to make them competitive with fixed-wing aircraft as far as (W/D_e) is concerned, has been recognized for a long time[9]. Nevertheless, progress in that respect has been slow and it appears that only the current generation of helicopters seems to follow the trend marked in Fig 5-3 as "projected and specially cleaned-up helicopters" (also see Fig 6-12 in the following chapter). However, the current trend is quite far from the "rotary-wing goal"[9] and still further from the aerodynamic cleanness of turboprop transports.

5.1.2 Maximum Speed Capabilities

The previously discussed low (W/D_e) values in the high-speed region lead to high-power requirements which may be called the power barrier to maximum speed capability of classical helicopters. However, there are other limits as well that have been recognized and frequently discussed from the early stages of helicopter development. They are compressibility effects of the advancing blades and stall problems of the retreating ones.

As far as the compressibility limits are concerned, they may become even more restrictive than in the past. In the past, only purely aerodynamic (drag divergence, c.p. movement, etc.) and associated aeroelastic phenomena were considered in establishing these limits. However, recent emphasis on the noise aspects seems to introduce one more strong constraint on the upper limit of the resultant Mach number of the advancing blade $(M_{t_{90°}})$. It appears[10] that in order to avoid the "high-speed bang", $M_{t_{90°}} \leq .92$. For $S/L\ STD$ conditions (with speed of sound $a = 1116\ fps$) this would lead to $V_{max}\ vs\ V_t$ restrictions as in Fig 5-4.

Although Harris and Pruyn[11] express some doubt whether, under the three-dimensional time-variable conditions of skewed flow, lift stall in the classical sense actually appears at high μ's on the retreating blades; nevertheless, there definitely are other speed-limiting phenomena present. They point out that rapid increase of the sectional drag and pitching moment coefficient (leading to high pitch-link loads) as well as stall flutter phenomena still represent an important constraint for high μ values.

Furthermore, it should be remembered that at μ .5, propulsive capabilities of conventional rotors start to deteriorate rapidly. In view of this, even if the currently acceptable operational limits of $\mu \approx .4$ (dictated mostly by vibrations, stall flutter, pitch link loads, etc.) are exceeded, those improvements would probably still not push the classical (uncompounded) helicopter beyond $\mu \approx .5$. Consequently, the high-speed capabilities for the noise and μ constrained helicopters would presumably be as shown in Fig 5-4.

5.2 OPERATIONAL PERFORMANCE OPTIMIZATION WITHIN ESTABLISHED FLIGHT ENVELOPE

Optimization of takeoff performance of a helicopter overloaded beyond its vertical climb capacity represents an important operational task (Fig 5-5). Schmitz[12] considered that problem analytically using optimal control theory. He formulated his task as finding flight trajectories that maximize the terminal height for a fixed horizontal distance. Flight tests later confirmed[13] that trajectory control suggested by the

analytical approach actually improves take-off performance within the practical limits.

Some physical aspects of time and fuel minimization in reaching a given altitude as well as descending from it, are discussed in Appendix D of Ref 14. In this case, a simplified kinematic model is used in application to trajectory optimization problems of a tilt-rotor aircraft. However, general strategies can also be applied to pure helicopters as well. Among others, it was indicated that minimization of the time for climb, both in vertical as well as forward flight ascent, is synonymous with the optimization of fuel required in those maneuvers. This, in turn, implies that in principle, throughout the whole climb, maximum power available should be used (some special final boundary conditions; e.g., a priori defined value of horizontal velocity at the target altitude, may modify that statement).

The kinemetic model of Ref 14 was also helpful in establishing trends for optimum strategies (minimum fuel and time) in descents terminating with a vertical landing at a prescribed touch-down speed.

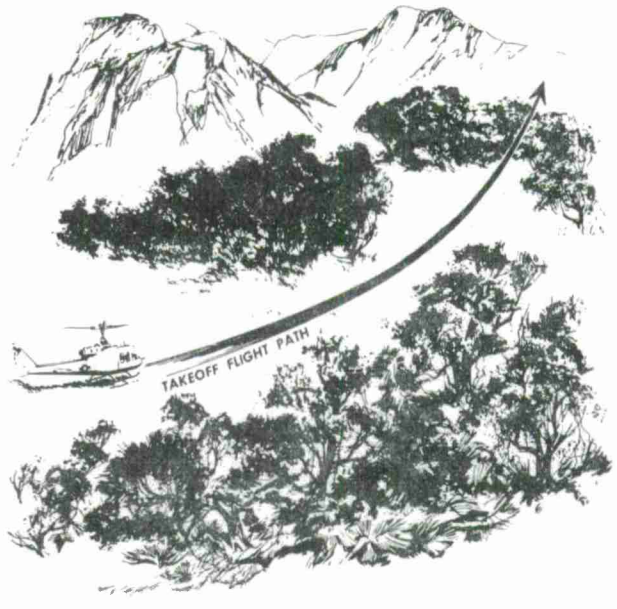


Figure 5-5 Example of Scenario for Take-off in Overloaded Conditions

References for Chapter 5

1. Stepniewski, W.Z. & C.F. Kalmbach, Jr., Multivariable Search and Its Application to Aircraft Design Optimization, The Aeronautical Journal, Vol. 74, No. 713, May 1970.
2. Textbooks that may be helpful in performance optimization problems:
   a. Bellman, R.E., Dynamic Programming, Princeton Univ. Press, 1957.
   b. Pontryagin, L.S., et al, The Mathematical Theory of Optimal Processes, Interscience Publishers, 1962.
   c. Bellman, R. and S.E. Dreyfus, Applied Dynamic Programming, Princeton Univ. Press, 1962.
   d. Leitman, G., Optimization Techniques, Academic Press, 1962.
   e. Fan, Liang-Tseng and Chiu-Sen Wang, The Discrete Maximum Principle, John Wiley & Sons, 1964.
   f. Fan, Liang-Tseng, The Continuous Maximum Principle, John Wiley & Sons, 1964.
   g. Wilde, D.J. and C.S. Beightler, Foundations of Optimization, Prentice-Hall, 1967.
   h. Bryson, A.E. and Y.C. Ho, Applied Optimal Control, Blaisdell, 1969.
   i. Luenberger, David G., Optimization by Vector Space Methods, Wiley-Interscience, 1969.
3. Benson, G.R., L.V. Dadone, R.E. Gormont and G.R. Kohler, Influence of Airfoils on Stall Flutter Boundaries of Articulated Rotors, Preprint 621, AHS 28th National Forum, May 1972.
4. Reichert, G. and S.N. Wagner, Some Aspects of the Design of Rotor Airfoil Shapes, AGARD CPP-111, September 1972.
5. McCroskey, W.J., Recent Developments in Rotor Blade Stall, AGARD CPP-111, Sept. 1972.
6. Wilby, P.G., and H.H. Pearcey, Some Aspects of the Aerodynamic Design of Profile Shapes for the Blades of Helicopter Rotors, AGARD CPP-111, September 1972.
7. Williams, R.M., Recent Developments in Circulation Control Rotor Technology, AGARD CPP-111, September 1972.
8. Pfenninger, W., Flow Problems of Swept Low-Drag Suction Wings of Practical Construction at High Reynolds Numbers, Annals of the New York Academy of Sciences, Vol. 154, Art. 2, November 1968.
9. Wachs, M. and J. Rabbott, Jr., Rotary-Wing Aircraft Design Trends, AIAA Proceedings of USAF Vehicle Design & Propulsion Meeting, Nov. 4-6 1963, pp. 24-36.
10. Stepniewski, W.Z. and F.H. Schmitz, Possibilities and Problems of Achieving Community Noise Acceptance of VTOL, ICAS Paper No. 72-34, September 1972.

11. Harris, F.D. and R.R. Pruyn, Blade Stall - Half Fact, Half Fiction, Proceedings of the 23rd Annual National Forum of the AHS, Washington, D.C., May 10-12, 1967.

12. Schmitz, F.H., Optimal Takeoff Trajectories of a Heavily Loaded Helicopter, Journal of Aircraft, Vol. 8, No. 9, September 1971.

13. Vause, R.C. and F.H. Schmitz, Near Optimal Performance of a Heavily Loaded Helicopter in Ground Effect, Army Air Mobility R&D Lab, Moffett Field, Calif. 94035, June 1972.

14. Schmitz, F.H., W.Z. Stepniewski, J. Gibs, and E. Hinterkeuser, A Comparison of Optimal and Noise Abatement Trajectories of a Tilt-Rotor Aircraft, NASA CR-2034, May 1972.

6. EXAMPLE OF HELICOPTER PERFORMANCE PREDICTION

(Based on inputs by C.N. Keys of Boeing Vertol Company)

In order to complete this presentation on the fundamentals of rotary-wing aerodynamics, an example is given showing the steps that can be taken in actual performance predictions of a classical helicopter. Although this example is chiefly based on procedures used by a particular company (Boeing Vertol Company), it is believed that it is quite representative of current engineering practices of the industry.

6.1 BASIC INPUTS

6.1.1 Aircraft Data

The considered aircraft is assumed to be a twin-engine, single-rotor helicopter of the 15,000-pound design gross weight class suitable for the military and/or civilian utility, or light-transport applications. This helicopter is equipped with a four-bladed hingeless main rotor. Its aerodynamic lines and external dimensions can be seen from the three-view drawing (Fig 6-1), while additional inputs required for this configuration definition are given in Table 6-I.

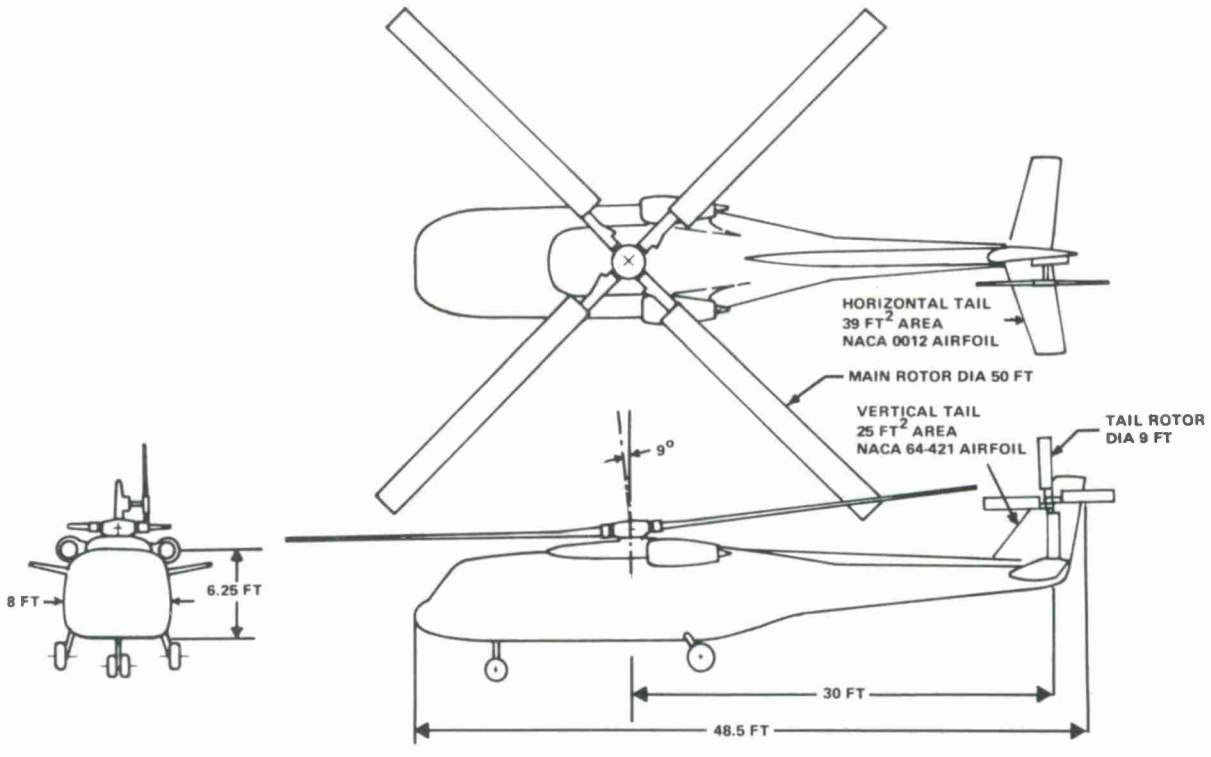


Figure 6-1 Three-View Drawing of a Hypothetical Helicopter

Additional important inputs needed for performance predictions are (a) airfoil characteristics throughout the anticipated ranges of Mach and Reynolds numbers, and (b) engine data under various altitude and power-setting conditions.

Some of the important characteristics for the selected airfoil are shown in Figs 6-2, 6-3 and 6-4, while basic data of the assumed powerplant are given in Figs 6-5, 6-6 and 6-7.

WEIGHTS:	
Design Gross Weight (DGW)	15,000 lbs
Disc Loading & DGW	7.65 lb/ft^2
Maximum GW	18,000 lbs
Weight Empty (WE)	9,450 lbs
WE/DGW	.630
Fixed Useful Load	430 lbs
(2 Crew @ 200 lbs ea., + 30 lbs trapped liquid)	
Fuel Capacity *(2300 lbs JP-4)*	354 gal
MAIN ROTOR:	
Diameter	50 ft
Chord	24 in
Solidity	.101
Tip Speed	700 ft/sec
No. of Blades	4
Airfoil	Vsrtol 23010 - 1.58
Twist	-10°
Cutout *(r/R)*	20%
RPM	267.5
TAIL ROTOR:	
Type	Pusher
Diameter	9 ft
Chord	9 in
Solidity	.213
Tip Speed	700 ft/sec
No. of Blades	4
Airfoil	Vertol 23010 - 1.58
Twist,	-8°
Cutout *(r/R)*	20%
AIRFRAME:	
Parasita Drag	19.0 ft^2
Landing Gear	Fixed
ENGINES:	
Number	2
Rating SL/STD (Military/Normal)	1600/1300
Lapse Rate	6.0 HP/°F
Installation Losses	1%
TRANSMISSION RATINGS:	
Dual Engine (SL/80°F - MIL Power)	2900 SHP
Single Engine (SL/STD - MIL Power)	1600 SHP

Table 6-I Configuration Definition

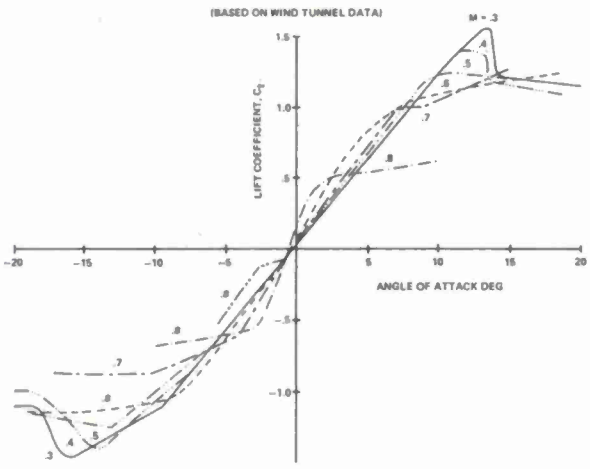


Figure 6-2 Variation of Section-Lift Characteristics with Mach Number

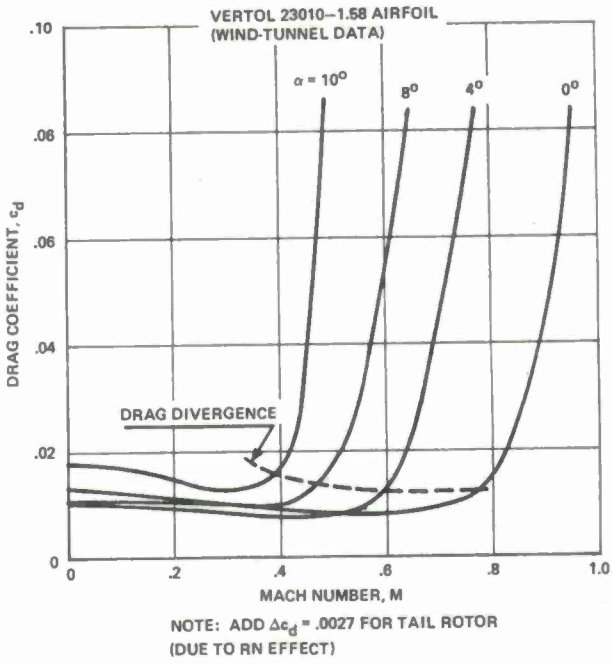


Figure 6-3 Variation of Section-Lift Characteristics with Mach Number

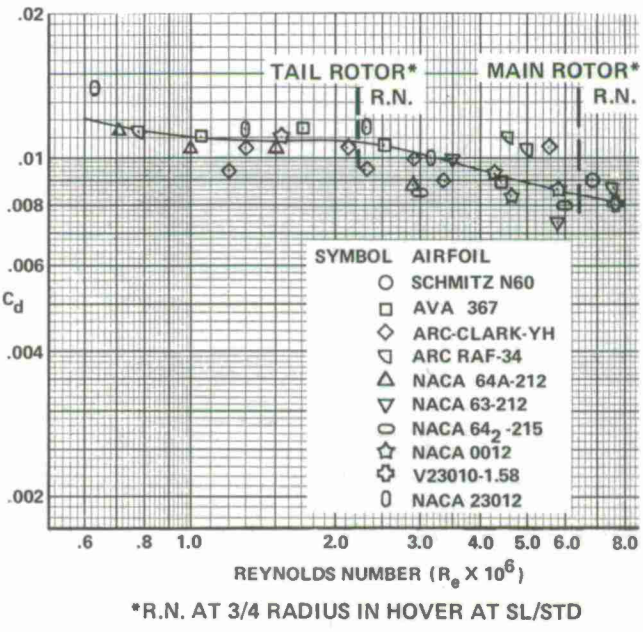


Figure 6-4 Reynolds Number Effect on Airfoil Section Drag

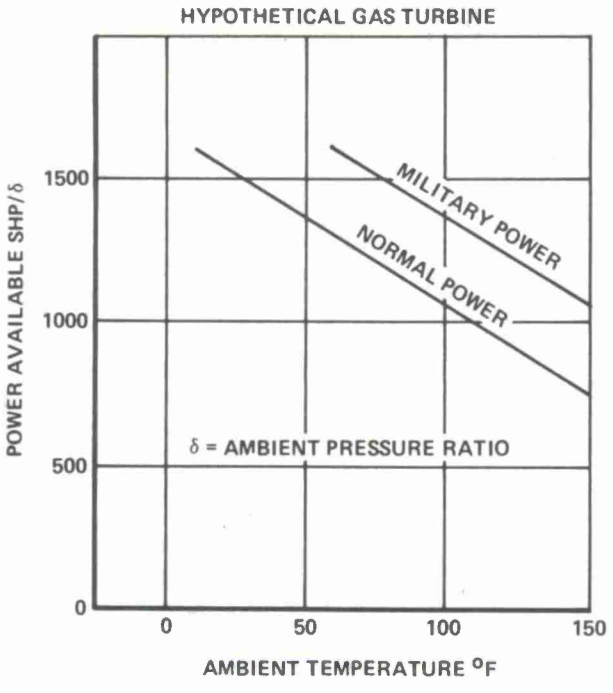


Figure 6-5 Power vs Temperature at SL/STD

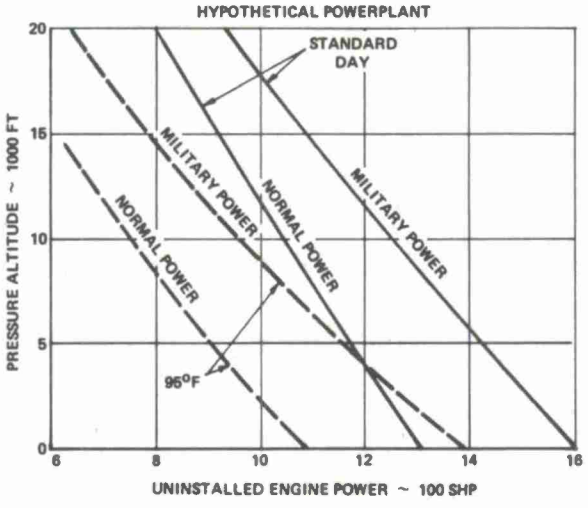


Figure 6-6 Power vs Pressure Altitude

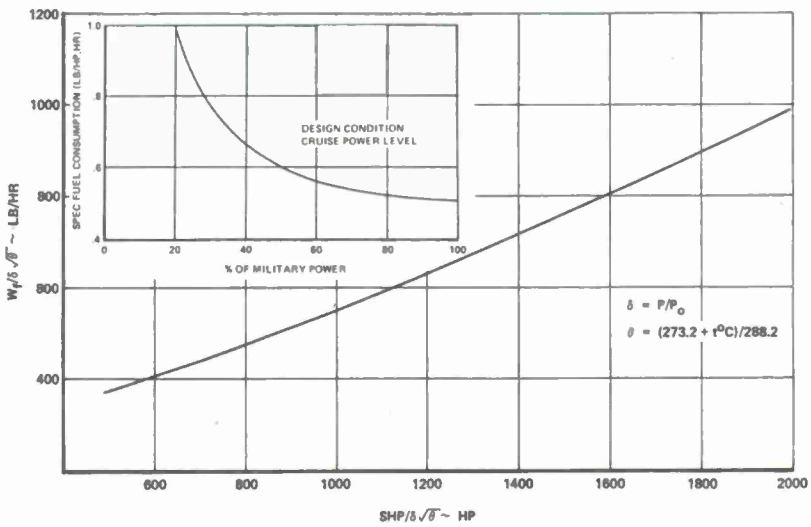


Figure 6-7 SFC Trend vs Partial Power Setting and Fuel Flow for One Engine

6.2 OUTLINE OF PERFORMANCE PREDICTION PROCEDURE

6.2.1 Hovering (In-and-Out-of-Ground Effect) and Vertical Climb

Various steps required in performance calculations for hovering outside of ground effect are shown in the flow chart presented in Fig 6-8.

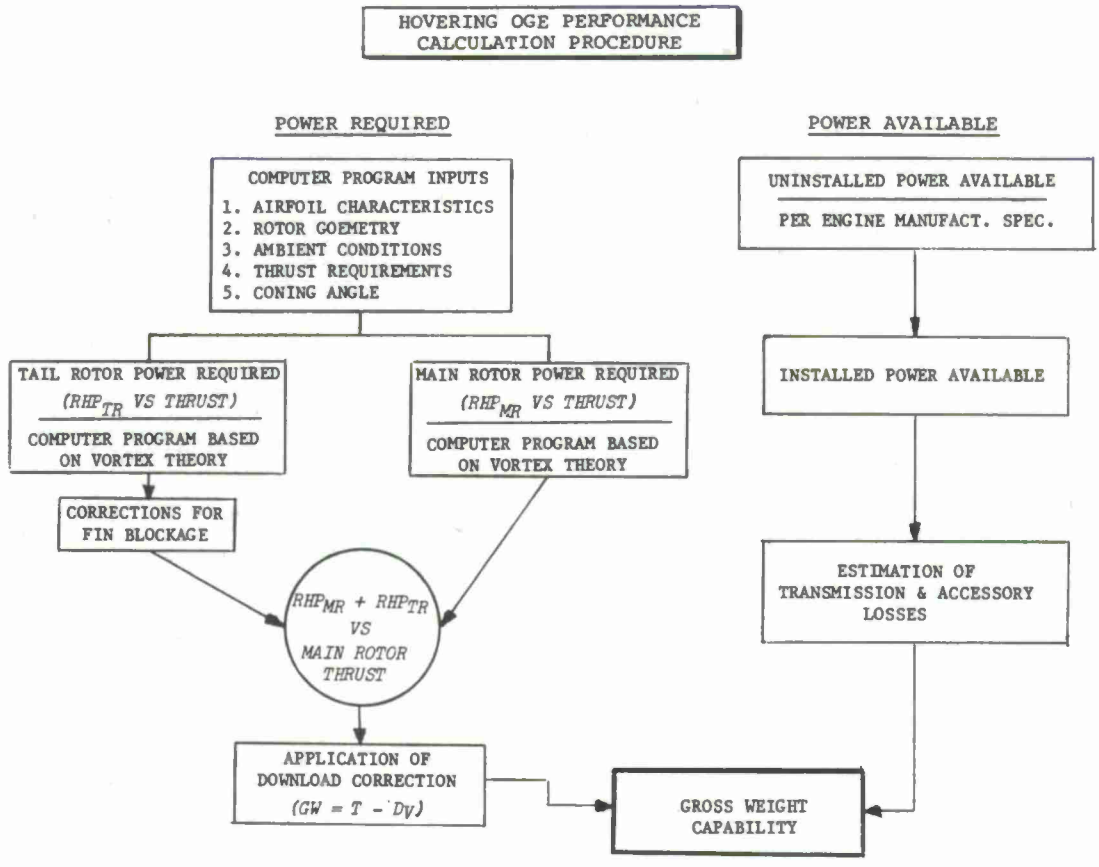


Figure 6-8 Flow Chart of Performance Calculations for Hovering OGE

The main and tail-rotor power required for OGE was predicted, using the Boeing Vertol Company's computer program based on vortex theory. Methodology of this program is similar to that described by Magee, et al[1]. Rotor induced and profile power obtained from this program is shown as Fig 6-9. For comparison, ideal induced and profile power (based on a constant value of $\bar{c}_{d_o} = .008$) are also plotted. In addition, k_{ind_h} is also shown in this figure. Finally, total rotor horsepower required to hover is shown in a nondimensional form (C_T vs C_p) in Fig 6-10.

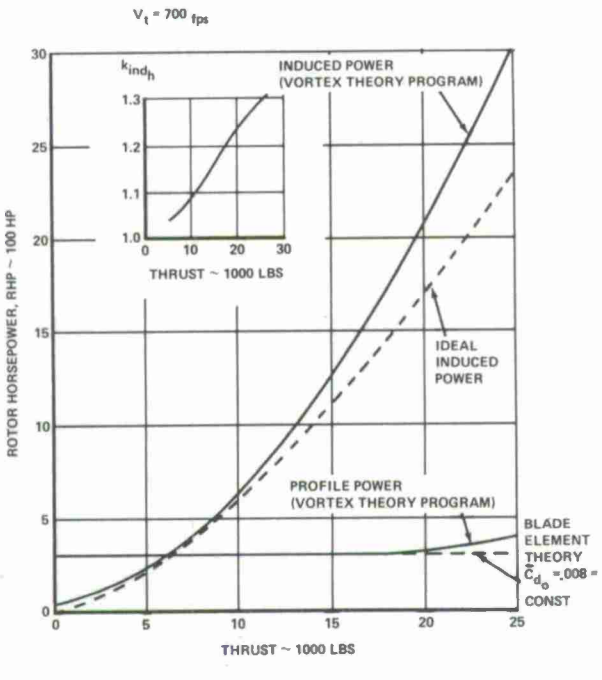


Figure 6-9 Main Rotor Induced and Profile Power

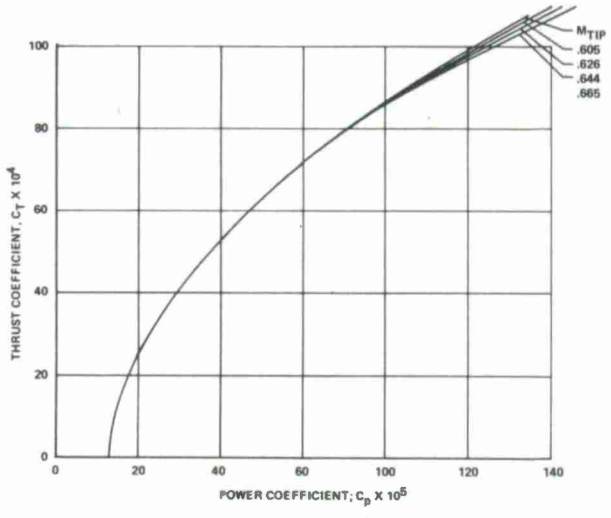


Figure 6-10 Main Rotor Performance Characteristics in Hover OGE

The same computer program was used for determination of the tail rotor performance characteristics.

Download or vertical drag (D_V) was estimated by considering the main rotor flow velocity distribution and proper drag coefficients of various parts of the airframe exposed to the downwash which was determined from wind-tunnel measurements.

As far as power available is concerned, transmission, accessories and powerplant installation losses were estimated in addition to the power lapse due to the ambient conditions of pressure and temperature.

Ground effects on hovering performance were evaluated using empirical corrections based on the relative elevation of the main rotor from the ground.

On the basis of the above inputs, a graph was prepared (Fig 6-11) giving hovering ceiling vs gross weight in, and out of, ground effect for the military power setting and two temperature conditions (Sea Level Std., and 95°F days).

Rate of Vertical climb was calculated by first determining inflow effects on download in this regime of flight, which permits one to estimate ideal power required vs rate of climb. Next, ideal power available was obtained by subtracting profile power and induced power losses from the engine power transmitted to the rotor. Further procedure was basically as outlined in Section 2.2.2.

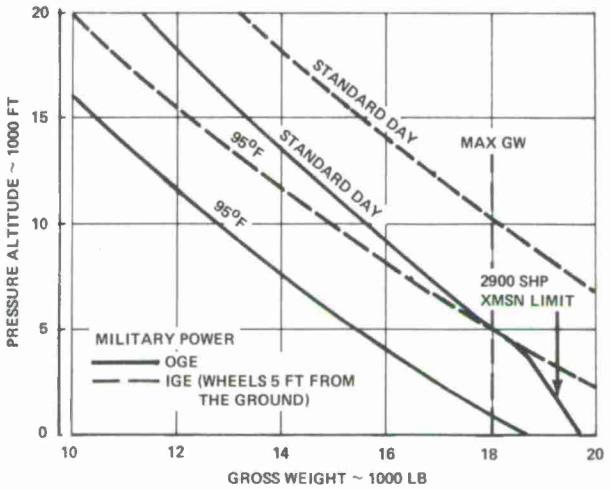


Figure 6-11 Hovering Ceiling In-and-Out-of-Ground Effect

6.2.2 Forward Flight

The basic approach to performance prediction in forward flight is somewhat different from that in hover. The more accurate but, at the same time, more complex procedures incorpoating vortex theory are replaced here by methods based on a uniform induced velocity distribution. The more important aspects of these calculations are outlined below:

1. Determination of the airframe drag. This is normally done in two steps: (a) analytical estimates (first column of Table 6-II), and (b) wind-tunnel tests of a usually unpowered, the so-called drag and stability model (second column of Table 6-II). In addition, the results may be checked against statistical trends as, for instance, those shown in Fig 2-12, where $w_f \equiv (GW)/f = f(GW)$ is related to maximum gross weight. Also, some insight into the aerodynamics of nonrotating parts of a helicopter can be gained from Ref 2.

ITEM	ESTIMATE f; ft^2	WIND TUNNEL TEST RESULTS f; ft^2
BASIC FUSELAGE & PYLON	2.35	2.5
LANDING GEAR	4.56	4.9
Main	*(2.82)*	*(2.9)*
Nose	*(1.74)*	*(2.0)*
MAIN ROTOR HUB	5.22	4.3
ENGINE NACELLES	1.09	1.7
VERTICAL & HORIZONTAL TAIL	.83	.7
TAIL ROTOR HUB ASSEMBLY	1.19	1.4
TRIM DRAG	.80	.7
SUBTOTAL	16.04	16.2
ESTIMATED ITEMS:		
Roughness & Leakage	*(1.0)*	*(1.0)*
Protuberances	*(1.6)*	*(1.6)*
Cooling Losses	*(.3)*	*(.3)*
	2.90	2.90
GRAND TOTAL	18.94	19.1

Table 6-II Parasite Drag Estimates

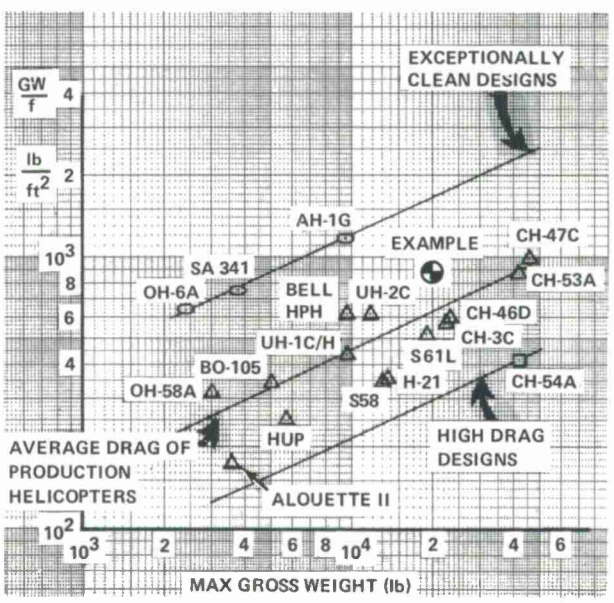


Figure 6-12 Equivalent Flat Plate Area Loading Based on Maximum GW

2. Determination of power required in horizontal flight at higher speeds by using the uniform induced velocity approach (Eq (32) from Chapter 2) and correcting the results for downwash nonuniformities and tip effects. Separate power-required estimates are made for the region of low speeds down to hovering (see Section 2.2.6).

3. Computations of maximum rate of climb at various altitudes using the excess power available concept (Section 2.2.7).

4. Determination of aerodynamic (stall) and/or aeroelastic (stall flutter, excessive pitch link loads, etc.) limits to V_{max}.

Once the complete spectrum of performance both in vertical and forward flight is covered, the level of confidence in obtaining these performance figures is examined and on that basis, the guaranteed performance figures for submittal to the customer are obtained.

References to Chapter 6

1. Magee, J.P., M.D. Maisel, and F.J. Davenport, The Design and Performance Prediction of Propeller/Rotor for VTOL Applications, Proceedings of the 25th Annual AHS Forum, No. 325, May 1969.

2. Bosco, A., Aerodynamics of Helicopter Components Other than Rotors, AGARD CPP-111, September 1972.

ACKNOWLEDGEMENTS

The author wishes to express his indebtedness to Mr. C.N. Keys, from Boeing Vertol Company for the material he provided for Chapter 6.

Special thanks go to Mrs. W. L. Metz, also from Boeing Vertol Company, who cooperated with this author from the early stage of literature search through the consecutive steps leading to the complete manuscript. In particular, Mrs. Metz provided valuable editorial help and also typed (including transcription of the formulae) and graphically arranged the final text.

BASIC DYNAMICS OF ROTORS
CONTROL AND STABILITY OF ROTARY WING AIRCRAFT
AERODYNAMICS AND DYNAMICS OF ADVANCED ROTARY-WING CONFIGURATIONS

by

G. Reichert

Messerschmitt-Bölkow-Blohm GmbH

8012 Ottobrunn, Germany

OUTLINE

Introduction: Various rotor systems as teetering, articulated, elastomeric-bearing rotor hub, hingeless systems.

Basic dynamics of rotors: Fundamentals of blade dynamics; elementary forces on a blade element, air velocity components. Motion of articulated, rigid blades; flapping motion, lagging motion, feathering motion and rotor control. Motion of rigidly attached blades; definition of an equivalent hinged rotor, flapping behaviour, influence of inplane stiffness, elastic coupling effects.

Mechanics of helicopter flight: Principles of helicopter control; trim calculation, control characteristics and requirements. Dynamics of helicopter flight; introduction to stability, helicopter static stability, helicopter dynamic stability, maneuver capability. Stability and control augmentation systems; general remarks, mechanical devices, modern stability and control augmentation systems.

Aerodynamics and dynamics of advanced rotary-wing configurations: Advanced rotor systems. Advanced rotary-wing configurations; compound helicopter; advanced convertible configurations

1. INTRODUCTION

The aerodynamic flow situation of a helicopter rotor is determined by the rotation of the rotor. In forward flight - see Figure 1 - the speed of flight will be superimposed to the rotational velocity, resulting in periodically changing velocities for the blades with opposite characteristics at the advancing and at the retreating side. That means, that a helicopter, even in steady flight conditions, is submitted to unsteady rotor conditions. The periodically changing velocities cause alternating forces and moments at the blades and at the rotor hub resulting in many dynamic effects which are determining the special characteristics of a helicopter.

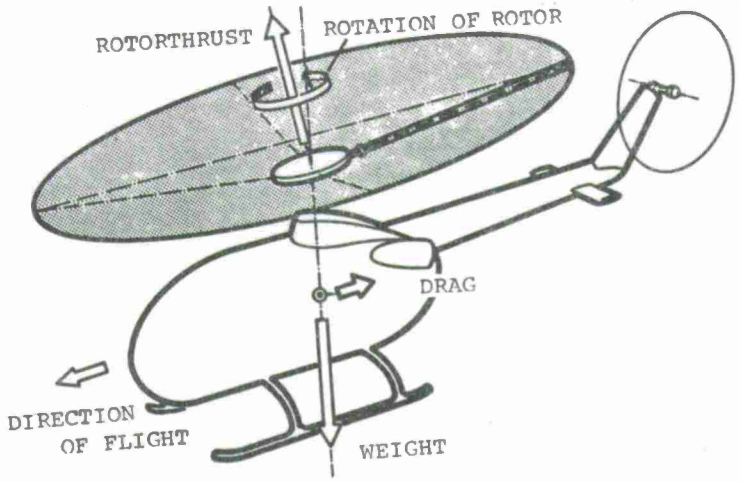


Figure 1 Helicopter in forward flight

The historical story of the helicopter is marked by the struggle against the dynamic forces at the blades and the dynamic characteristics of the whole helicopter. The concept of using air screws for vertical lift and vertical flight is very old, and the first flight trails of helicopters were about the same time as the first flights of fixed wing aircrafts, but these early attempts with rotating-wing aircrafts were without success. The predominating opinion of this era was that there will be no future for rotating-wing aircraft for technical reasons, and that it makes no sense to work in this field. In the following years, engineering effort concentrated on developing the fixed-wing aircrafts, but, not withstanding the development of the fixed-wing aircraft, men have been aware that they had still to achieve complete mastery of the air; namely, the ability to stay aloft without maintaining forward speed and to ascend and land vertically in restricted areas. Development of the helicopter continued to this end.



Figure 2 Cierva - Autogiro C19 Mk IV

The most pivotal effort in the attempt to achieve vertical flight was the work of Juan de la Cierva in the 1920's in developing the first truly successful rotary wing aircraft which he called the "Autogiro" (Figure 2). This aircraft employed a propeller for forward motion, as in an airplane, and a freely rotating rotor for lift. The Autogiro did

not actually achieve truly vertical flight; it required small forward speeds to maintain its lift and could take off and land within extremely short distances. Autogyro development continued in Europe and in America for more than a decade and reached a state of considerable advancement, but there was no commercial breaking through and the progress come almost to a standstill (1). However, the autogyro layed the groundwork necessary for practical helicopter flight by providing the knowledge and technology necessary for subsequent practical helicopter flight. It was only with the introduction of the articulated blade attachment done by de la Cierva that the prerequisites for a realization of technically satisfactory helicopter projects were created. At that time, with the insufficient knowledge of the physical-technical correlation the blade attachment hinges were the only way to overcome the mechanical strength difficulties at the blades and the control problems of the helicopter caused by the dissymmetry of the relative velocities on the two sides of the rotor disc. All helicopters of the following period and still most of today's helicopters have articulated blade attachment in one of the many possible variants.

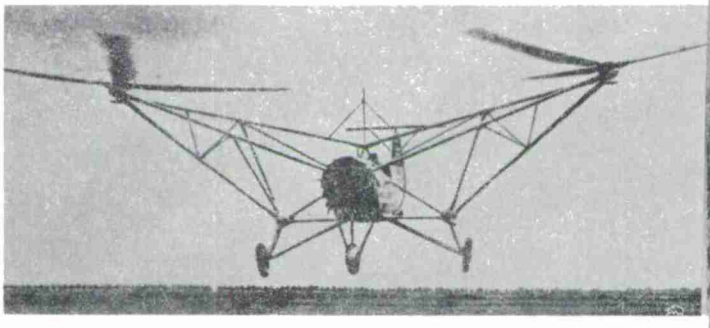


Figure 3 Focke side-by-side helicopter FW 61

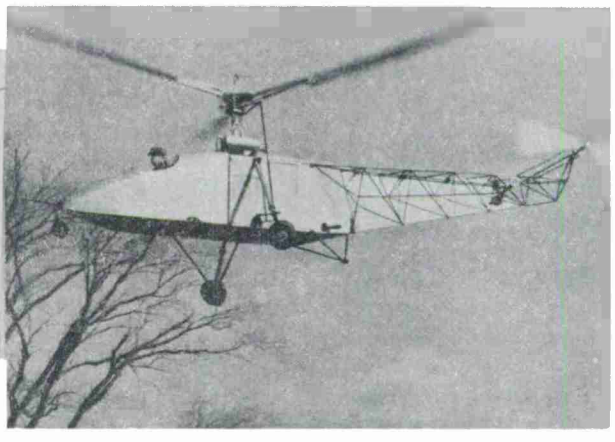


Figure 4 Sikorsky helicopter VS-300

Following autogyro development, progress was being made toward successful helicopters. By 1936 Focke in Germany demonstrated a successful side-by-side, two-rotor machine (Figure 3), and in 1939 - 1940 Sikorsky introduced the VS-300 (Figure 4), a single lifting rotor machine with a vertical tailrotor for torque counteraction. These both designs are the real beginning of the successful helicopter era, they gave tremendous impetus to the development. In the following years more than forty serious and independent developments sprang up. In the late 1940's the general pattern of helicopter-type aircraft had been formulated to a rather complete degree and most of the current configurations had been given serious consideration by the 1950's. These included single rotors, tandem rotors, coaxial rotors, shaft driven and tip driven rotors, side-by-side rotors, and compounded rotor systems.

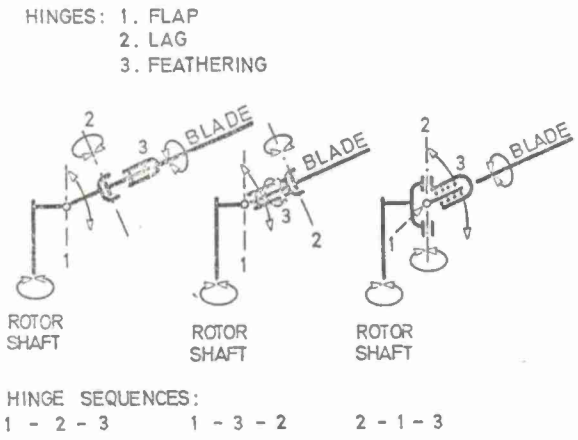
In the more recent era, general advance in helicopter knowledge - in its flight mechanics, its dynamics and structural properties - has progressed and designers returned to projects with rigid blade attachment as in the beginning of the helicopter history. Almost simultaneously, aircraft manufacturers such as Bell, Lockheed, and Bölkow started theoretical and practical work on mechanical simplification of helicopters by elimination of blade attachment hinges, and now the first helicopters with hingeless rotors are in production. However, such developments cannot be considered as "rigid rotors", as is done frequently but erroneously. It is more accurate to speak of "hingeless rotors" since the conventional flapping and lagging hinges are absent. Only the blade torsional or feathering hinges for blade control are provided. The flapping and lagging motions of the rotor blades, prevailing in articulated rotors, are replaced by elastic blade deformations.

Regarding the dynamic behaviour of rotor systems, there are differences for the various types, and an accurate mathematical representation is necessary for theoretical studies. The primary characteristics concern the manner in which the rotor blade is attached to the hub of the rotor mast as well as the stiffness characteristics of the system involved for that attachment. For the type of attachment, the two ends of the spectrum are represented by the fully articulated blade and the rigidly attached blade as a cantilever to the hub. The stiffness of attachment of the blade to the mast in the several variations in this spectrum can be represented by the pinned joint for essentially zero stiffness and a maximum stiffness joint represented by the inherent bending of a beam which is the blade itself.

Each of these statements applies to the basic modes of blade motion relative to the mast which are considered in design: flapping, inplane (lead-lag), and feathering. In any of these directions the amound of stiffness determines the level of articulation. Also, the relationship of stiffness in one direction to another can be different for

different design approaches. Finally, another variation in design among these possibilities is the location, in terms of the radial distance outboard from the center of the rotor shaft, at which the stiffness for a particular mode of blade motion is introduced.

Three basic variations of position of stiffness introduction or position of articulation are illustrated in Figure 5. Examples of fully articulated blade systems are those which have been used by Sikorsky and also by Boeing-Vertol as well as others. In all three directions pinned joints are used to approach a condition of zero stiffness. The differences among the fully articulated designs lie in the relative locations of the hinges in the three basic directions. In the first arrangement, used for some Boeing-Vertol designs as CH 46 or BV-107 and for the Westland Scout and the SNIAS Alouette, the pitch change of the blade occurs outboard of both flap and lag hinges, and the pitch arm leads and lags with the blade. The hinge pin does not tilt with pitch change. In the second arrangement, used for instance in the Boeing-Vertol Chinook, the Hughes OH6 and the SNIAS SA-341, the pitch change occurs between the flap and lag hinges, and the pitch arm does not lead and lag with the blade. The lag hinge pin tilts with pitch change. The third system shown in Figure 5 is used in current Sikorsky helicopters. It also has the three hinges with the lag hinge inboard, next the flap hinge at the same distance from the center of the rotor, with the pitch axis outboard. The pitch arm flaps, leads and lags with the blade.



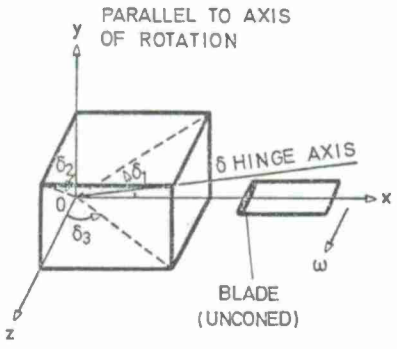
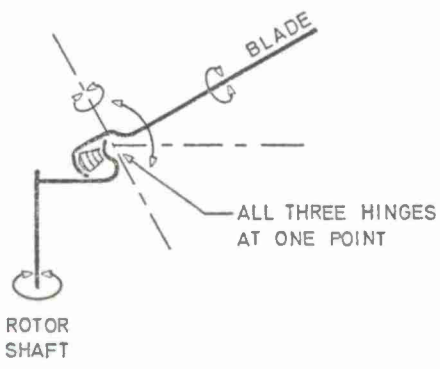


Figure 5 Typical articulated rotor system

Figure 6 Definition of hinge inclination

Additional possibilities for variation are the angles of inclination of the hinges. The flapping and the lagging hinge can be inclined with respect to their normal axes, as is shown in Figure 6, thereby causing displacements about the hinge to have feathering components from flapping or inplane motions. Thus new terminology has to be introduced, the inboard flapping hinge becoming known as the "delta hinge" and the outboard inplane hinge as the "alpha hinge". The projections of the delta hinge on the three planes make angles δ_1, δ_2 and δ_3 respectively with the axes O_x, O_y and O_z. The best known inclined hinge is the "delta-three hinge" which, being inclined in plane zOx only, causes cyclic pitch change or periodic feathering of the blade in combination with periodic flapping. In former times, mainly in the era of the autogyro, many combinations of inclined delta and alpha hinges were studied; with the helicopter of today there are nearly no hinge inclinations except a slight δ_3, normally.



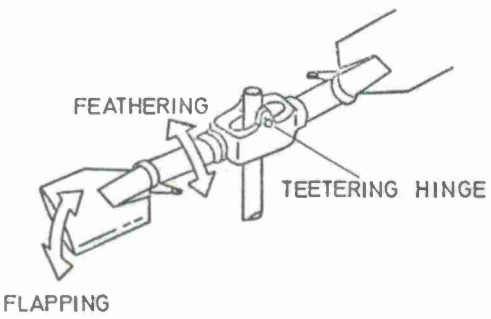


Figure 7 Elastomeric-bearing rotor hub system

Figure 8 Teetering or see-saw rotor

The socalled elastomeric-bearing rotor hub, which is in an experimental status, uses a single spherical bearing per blade to provide blade motion in the flap, lag and pitch directions, as is shown schematically in Figure 7. The elastomeric bearing consists of concentric spherical laminations of an elastomer and metal bounded together in thin alternate layers. The bearing is mounted so that the centrifugal force exerted by the blade results in compression of the elastomer, while pitch, lag, and flap motions results in shear deflection of the elastomer. The elastomeric bearing is working as a universal hinge that gives all three degrees of freedom in a highly simplified mechanical design (2).

The teetering two bladed rotor system as used by the Bell helicopters is an example of partial articulation. The two blades configured as a continuous beam from tip to tip and attached to the rotor mast by trunnion pivots provide for a quasi-flapping articulation, a rigid in-plane characteristic and a zero stiffness feathering characteristic, see Figure 8.

For the socalled rigid or hingeless rotor types the blades are attached to the mast as a cantilever and in all but the feathering axis direction an attempt is made to obtain a stiffness considerably higher than that for the hinged joint of full articulation. As is illustrated in Figure 9 several variations are possible. The first arrangement, used in the MBB - BO 105, has a very stiff hub with the feathering hinges located at stiff hub arms; the elastic blade deflections in flapping and inplane directions are outboard the feathering hinges. In the second arrangement, used for the Westland WG-13, the hub arms allow deflections in flapping directions; inplane deflections occur at the blade, and the feathering hinges are outboard the main flapping but inboard of the inplane deflections. The third system, used for the Lockheed design, has flapping flexibility at the hub but nearly no inplane flexibility. The feathering hinges are outside the main flapping deflections.

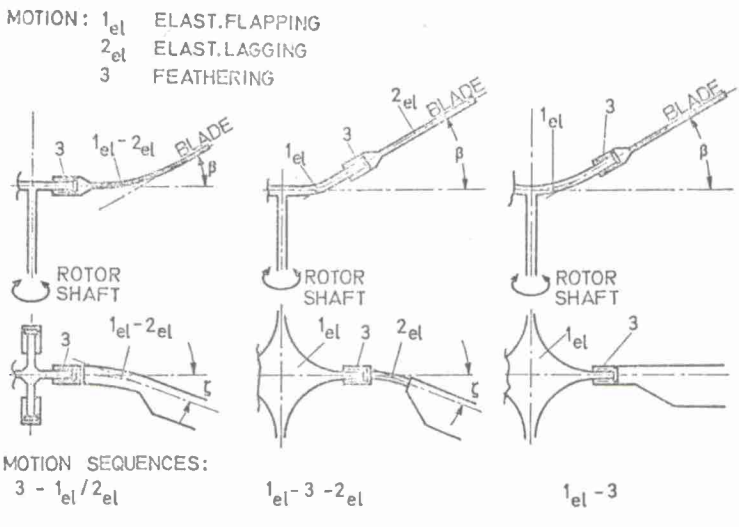


Figure 9 Various hingeless rotor systems

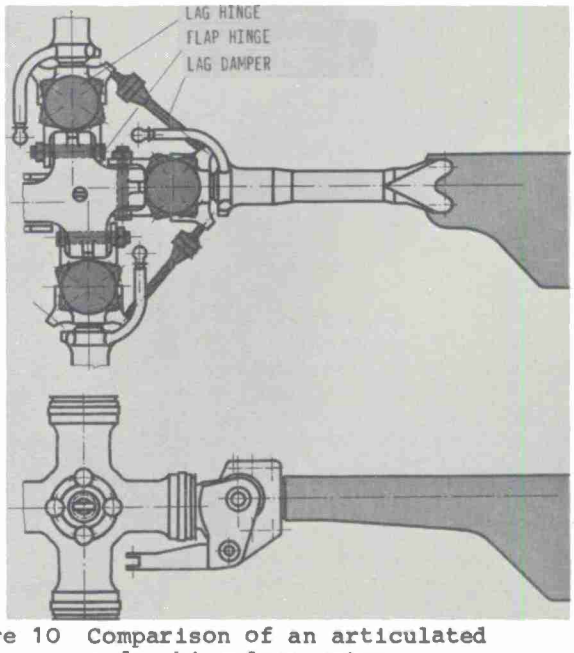


Figure 10 Comparison of an articulated and a hingeless rotor

Compared to articulated rotors a hingeless rotor design causes a mechanical simplification and offers marked improvements in handling qualities, in addition. As is illustrated in Figure 10, showing a comparison of an articulated and a hingeless rotor, the hingeless rotor will need only about 20 percent of the parts of an articulated rotor. It needs no flapping and no lagging hinges and no lag dampers. In addition, the lubrication system is much more simple.

The behaviour of a helicopter is primarily influenced by the behaviour of its rotors - one or more - in the various conditions of flight, but the helicopter has to be considered as a whole - its fuselage, its source of power and its means of control. There are many helicopter configurations possible, as is illustrated in Figure 11. Each type has its unique characteristics, advantages, and disadvantages. The first classification is into shaft-driven systems and reaction tip driven systems. Today, nearly all helicopters are using shaft-driven rotor systems because of their better efficiency and performance characteristics compared to helicopters with reaction driven rotors.

Shaft-driven rotors need special precaution for torque-counteraction. Always a controversey has been on the most favourable configuration - a controversy which, even today, has not reached a unanimous conclusion. In terms of the number of machines in operation today, the single lifting rotor machine with tail rotor is by far the most common type. In selecting twin rotors, the two rotors can be arranged one behind the other in the tandem configuration as in the Boeing-Vertol Chinook. Alternatively, the rotors could be placed side-by-side. In other arrangements, two rotors were closely intermeshed or were superimposed, one above the other, in contrarotation. Throughout the years, the single and twin rotor tandem helicopters have formed the main lines of development. Although, at various

times, one or the other has been selected as best satisfying specifications for military or civil purposes, the differences have been so small that invariably the decision was reached on considerations other than that of configuration. Even today, where single and tandem helicopters of the same weight and powered by the same engine installation can be compared, there is little to choose between them. Nowadays, there is a renewed discussion for very large helicopters as the Heavy Lift Helicopter, which is in development for the US Armed Forces. One school of thought intends to continue the single rotor layout to larger sizes and could see no basic objections to following this course. On the other hand, there are those who have reservations on the ability to construct rotors of sufficient size and considered a twin-rotor arrangement, which can use proven technology, to be a more realistic approach. The closely intermeshing rotors have survived in the Kaman helicopters, but the latest products of this firm have also moved away from this arrangement (3).

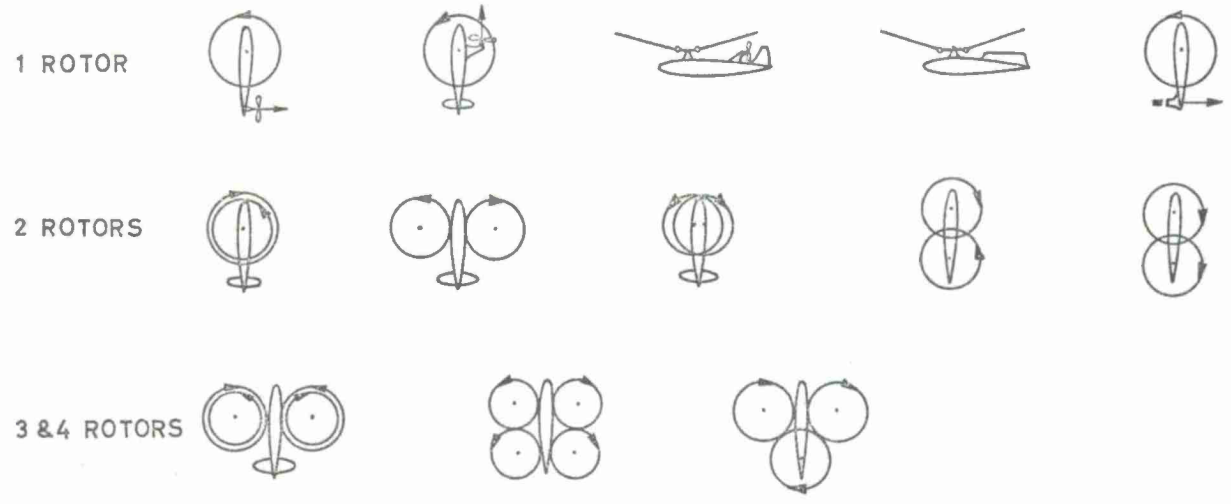
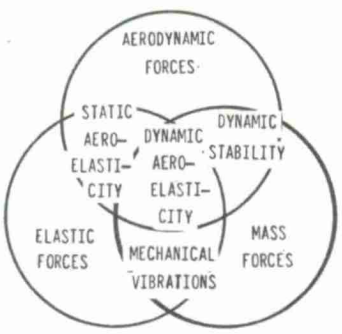


Figure 11 Helicopter configurations

Theoretical investigations for helicopters are rather complicated because of their highly complicated mechanical system and the dissimmetry in the flow conditions of the rotating blades in forward flight. The dynamic equations of motion have periodic coefficients, normally. Therefore, a special treatment is neccessary. In addition, all helicopter investigations have to consider static and dynamic interaction between aerodynamic forces and the motions of the rotor blades induced thereby. In the case of the articulated rotor, the motions of the articulated blades without additional flexibility are most important, but for the hingeless rotor - even for very simple calculations - the elastic deformations of the blades have to be considered. All helicopter phenomena can be related to the triangle of forces, representing aerodynamic, inertial and elastic forces, which is wellknown in the field of aeroelasticity (Figure 12). As a first approximation, the helicopter with articulated rotor blades can be considered as a system of several rigid bodies, which are combined by inertial and aerodynamic forces determining blade motions and flight dynamics. The rotation of the rotor causes a centrifugal restraint between airframe and rotor. Therefore in a helicopter with an articulated rotor many phenomena are similar to aeroelastic phenomena without structural deflections. In the case of a helicopter with a rigid or hingeless rotor the flapping and inplane movements of the rotor blades are elastic deflections. The control of the helicopter is achieved by controlling the flapping blades, also dynamic stability is mainly influenced by the behaviour of the flapping rotor. Therefore all the flight dynamics are of aeroelastic origin.



STATIC AEROELASTICITY
- Blade divergenz

DYNAMIC AEROELASTICITY
- Elastic blade motion
- Blade stability
- Flight mechanics of hingeless rotors
- Dynamic response (vibrations)
- Air resonance

MECHANICAL VIBRATIONS
- Ground resonance
- Engine vibrations
- Critical speeds

DYNAMIC STABILITY
- Rigid blade motion
- Flight mechanics for articulated rotors

Figure 12 Triangle of forces at a helicopter

Perhaps, this full interaction between aerodynamic, dynamic and elastic forces, which is much stronger for helicopters than for fixed-wing aircrafts, could be the reason why in the classical textbooks of aeronautical sciences and engineering so little attention is paid to helicopter phenomena. Helicopter theories and engineering went their own way. Unfortunately, there are no modern textbooks reviewing the knowledge and the

methods of today, most of which are pure numerical methods set up for the computers of today. Normally, the methods are engineering tools, developed in the industry for its purposes, and they are only published partly in special papers. However, about the fundamental theories and methods, there are some good older textbooks, which still today can give an excellent introduction, and the next chapter follows partially these textbooks (4 ÷ 9).

2. BASIC DYNAMICS OF ROTORS

2.1 FUNDAMENTALS OF BLADE DYNAMICS

Knowledge of the principles of blade dynamics demands a thorough analysis of blade forces and motions. The analysis requires mathematical treatment. Though the mathematical methods are relatively simple, the execution of the analytical procedure is laborious. Therefore only the physical foundations and some important results will be discussed.

Elementary forces on a blade element

The basis of rotor dynamics is the analysis of the forces acting on a blade element. The motion of the blade element is part of the motion of the blade, which will be considered to be articulated but without elastic deformations.

From the physical point of view there are only three sources of external forces acting on a blade element: (a) aerodynamic loads, (b) gravity loads, (c) dynamic loads. It is useful to distinguish between several systems of rectangular velocities at a blade element, see Figure 13. The first is the "hinge system" based on the rigid blade. One axis coincides with torsion axis, the second is parallel with the lagging hinge and hence normal to the flapping hinge, and the third is normal to the lagging hinge. Another rotating system of co-ordinates is the "rotor or hub system" based on the plane of the rotor, which is defined normal to the mechanical axis of rotation. The basic directions in this hub system are: radial R, normal N and tangential T. Other co-ordinate systems are useful in specific cases. When the blade is of symmetrical profile, of symmetrical construction and is untwisted, the axis of symmetry of the blade profile, together with the span axis and axis normal to both, form a system which can be called the "blade system". Its coordinates can be called the spanwise, chordwise and beamwise directions. Without a constant blade angle along the span one section is used to represent the blade and defines in this case the blade system. In addition, "blade section co-ordinates" can be distinguished, which vary from section to section.

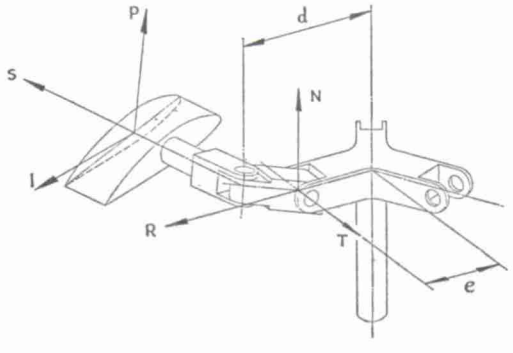


Figure 13 Rotating system of co-ordinates

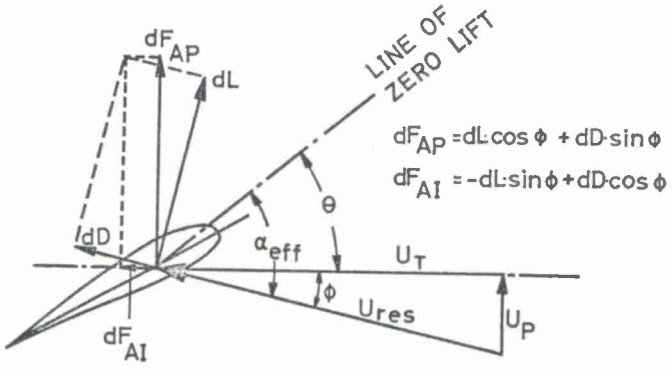


Figure 14 Blade element in forward flight

The external aerodynamic forces acting on the blade element are pressures distributed over its surface and the gravity and dynamic forces distributed throughout its mass. The aerodynamic force system is customarily described by the three quantities:

$$dL = \frac{1}{2}\rho\, C_l \Omega^2 R^2 (U_T^2 + U_p^2)\, c\, dr ,$$

$$dD = \frac{1}{2}\rho\, C_d \Omega^2 R^2 (U_T^2 + U_p^2)\, c\, dr ,$$

$$dM = \frac{1}{2}\rho\, C_m \Omega^2 R^2 (U_T^2 + U_p^2)\, c^2 dr ,$$

where the tangential component U_T and the perpendicular component U_p are referred to the tip speed ΩR, see Figure 14. Lift dL and drag dD are the two components in a plane normal to the blade span of the force acting through the aerodynamic center of the blade section assuming that there is no spanwise force component of importance. The moment dM is the component of pure aerodynamic moment acting about an axis parallel to the span. In the analysis of rotors it is normally advantageous to use the force components in

axial direction (thrust) and tangential in direction of rotation.

Gravity forces are represented by the weight of the blade element acting in its c.g.. They are acting along the gravity axis, and would require a further system of co-ordinates for its accurate description. Numerically, the weight component is of no importance, normally.

The calculation of the dynamic forces requires a knowledge of the absolute accelerations. The velocity and acceleration of a blade element are described by the components of linear motion of the c.g. of the element, and by the components of the rotational motion about the c.g.. In principle, a large number of acceleration terms results, which all have to be related to the parameters of blade motion, such as flapping angle, lagging angle and feathering angle, and to the parameters describing the motion of the complete helicopter with its rotor. The more general case, not limited to straight uniform flight is illustrated in Figure 15. The determination of the velocities and accelerations can be done using the wellknown methods of classical analytical mechanics.

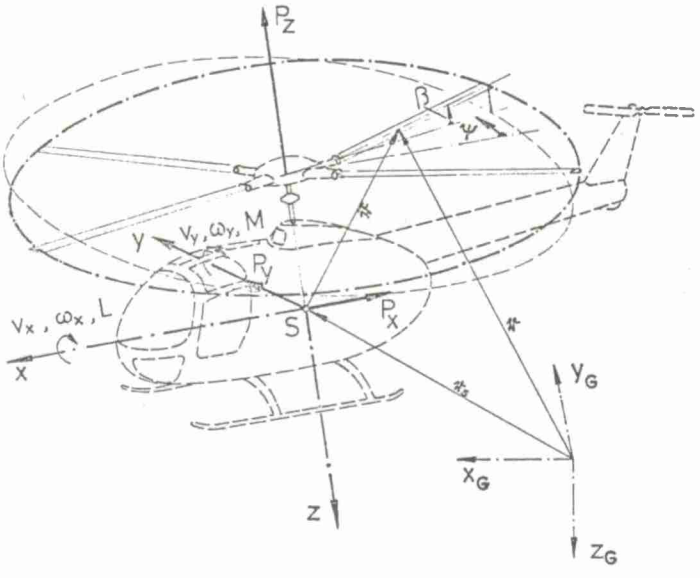


Figure 15 The systems of co-ordinates of a helicopter in forward flight

In the following, only the most significant components of dynamic forces and moments will be discussed, and the condition of flight will be limited to straight uniform flight. Most important are the centrifugal forces acting at the c.g. of the section in radial direction

$$d\ (C.F.) = m\ dr\ \Omega^2\ r\ .$$

The inertia forces due to relative acceleration of the blade in its motion about the flapping and lagging hinges are

$$d\ (J.F.)_\beta = -\ m\ dr\ \frac{d^2\beta}{dt^2}\ (r-e);\ d\ (J.F.)_\zeta = -\ m\ dr\ \frac{d^2\zeta}{dt^2}\ (r-d)\ .$$

Both components act through the c.g. of the section. The Coriolis force, which also acts through the c.g., has a purely tangential component, if the rotor axis is stationary or subject to translational motion only,

$$d\ F_{Co_R} = 2m\ dr\ \Omega\ \frac{d\beta}{dt}\ \beta\ (r-e)\ .$$

Coriolis forces are fundamental in rotor dynamics, as the lead-lag motion of the blades is mainly influenced by them. A tangential Coriolis force will be experienced whenever a mass moves radially in a rotating plane, it is proportional to the rotational velocity and the radial velocity of the mass. The radial movement of the mass is caused by the flapping of the blade. An effect, which should be insignificant by a first view, which, however, cannot be neglected.

Air velocity components

The air velocity components can be derived from Figure 16. For rough calculations it is customary to ignore the difference between the inplane and tangential components and to use the assumptions $\sin\beta \approx \beta$ and $\cos\beta \approx 1$. The components of the velocities at a blade element referred to the tip speed ΩR may be written as

$$U_T = x + V\cos\alpha\ \sin\psi\ ,$$

$$U_P = (V\sin\alpha - v)\ \cos\beta - \frac{r}{\Omega}\ \frac{d\beta}{dt}\ V\cos\alpha\ \cos\psi\ \sin\beta\ .$$

Or with the tangential advance ratio $\mu = \frac{V\cos\alpha}{\Omega R}$, the uniform inflow ratio $\lambda = \frac{V\sin\alpha - v}{\Omega R}$

and $\frac{d\beta}{dt} = \Omega \frac{d\beta}{d\psi}$

$$U_T = x + \mu \sin\psi$$

$$U_P = \lambda - (x - \frac{e}{R}) \frac{d\beta}{d\psi} - \mu\beta \cos\psi \ .$$

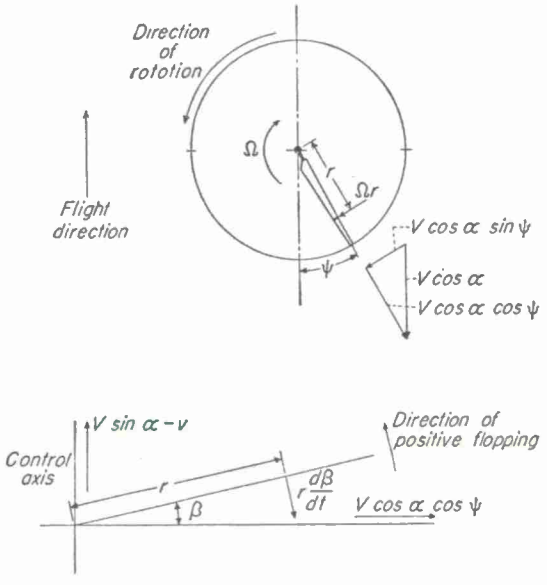


Figure 16 Velocities at a blade element

In Figure 16 it is assumed that only the flapping motion but not the inplane motion will contribute significantly to the air velocity components. There is no fundamental problem to derive the velocity components without neglections for the general case of a fully articulated rotor, the hub of which is preconed inside the flapping hinge, has a "pre-lag" angle inside the lead-lag hinge and has no mass symmetry in the blade itself, as is sketched in Figure 17 with the different systems of co-ordinates to be considered. The expressions for the velocity components, but without the components due the translational and rotational velocities of the helicopter, are now

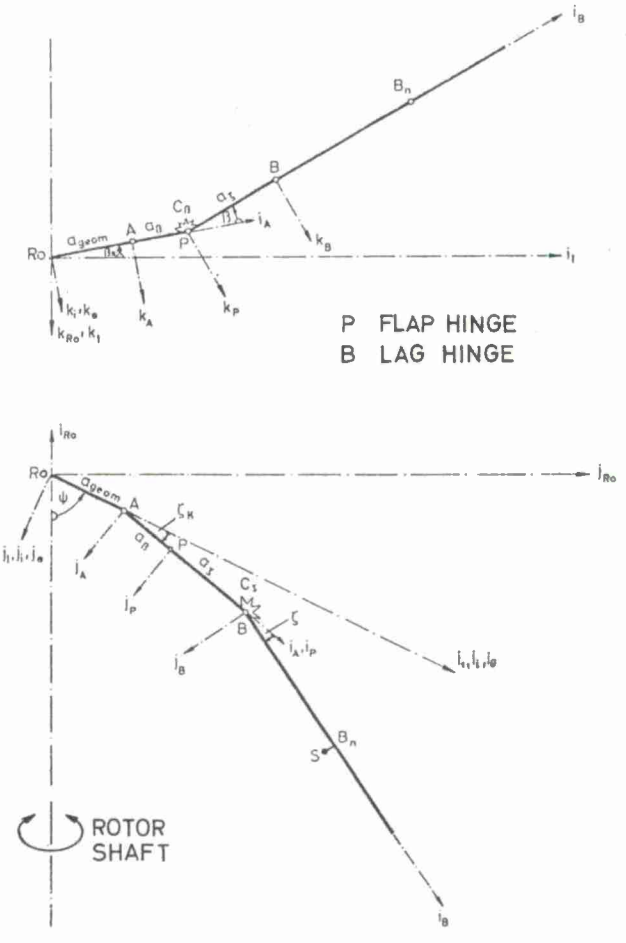


Figure 17 Systems of co-ordinates of a fully articulated rotor

$$\begin{aligned}
U_T \cdot R\Omega = \Omega \{ & b [- \sin\beta_k \cos\zeta_k \sin\beta + \cos\beta_k \sin\theta \sin\zeta_k \sin\beta + \\
& + \cos\beta_k \cos\theta \cos\beta] + \\
& + a_{geom} [\cos\beta_k \cos\zeta_k \cos\theta \cos\zeta - \cos\beta_k \sin\theta \sin\beta \sin\zeta - \\
& - \cos\beta_k \cos\theta \sin\zeta_k \cos\beta \sin\zeta] + \\
& + a_\beta [\cos\beta_k \cos\theta \cos\zeta - \sin\beta_k \sin\zeta_k \sin\beta \sin\zeta - \\
& - \cos\beta_k \sin\theta \cos\zeta_k \sin\beta \sin\zeta] + \\
& + a_\zeta [- \sin\beta_k \cos\zeta_k \sin\beta \cos\zeta + \cos\beta_k \sin\theta \sin\zeta_k \sin\beta \cos\zeta + \\
& + \cos\beta_k \cos\theta \cos\beta \cos\zeta] \} + \\
& + \dot{\theta} \{- b \cos\zeta_k \sin\beta - a_\beta \sin\zeta_k \sin\beta \sin\zeta - a_\zeta \cos\zeta_k \sin\beta \cos\zeta\} - \\
& - \dot{\zeta} \cdot b \\
& + v_i [\sin\beta_k \cos\zeta_k \cos\beta \sin\zeta - \cos\beta_k \sin\theta \sin\zeta_k \cos\beta \sin\zeta + \\
& + \cos\beta_k \cos\theta \sin\beta \sin\zeta + \sin\beta_k \sin\zeta_k \cos\zeta + \cos\beta_k \cdot \\
& \cdot \sin\theta \cos\zeta_k \cos\zeta]
\end{aligned}$$

$$U_p \cdot R\Omega = \Omega \{ b [\sin\beta_k \cos\zeta_k \cos\beta \sin\zeta - \cos\beta_k \sin\theta \sin\zeta_k \cos\beta \sin\zeta +$$
$$+ \cos\beta_k \cos\theta \sin\beta \sin\zeta + \sin\beta_k \sin\zeta_k \cos\zeta +$$
$$+ \cos\beta_k \sin\theta \cos\zeta_k \cos\zeta] +$$
$$+ a_{geom} [- \cos\beta_k \cos\theta \sin\zeta_k \sin\beta + \cos\beta_k \sin\theta \cos\beta] +$$
$$+ a_\beta [\sin\beta_k \sin\zeta_k \cos\beta + \cos\beta_k \sin\theta \cos\zeta_k \cos\beta] +$$
$$+ a_\zeta [\sin\beta_k \sin\zeta_k + \cos\beta_k \sin\theta \cos\zeta_k] \} +$$
$$+ \dot{\theta} \{ b [\cos\zeta_k \cos\beta \sin\zeta + \sin\zeta_k \cos\zeta] + a_\beta \sin\zeta_k \cos\beta + a_\zeta \sin\zeta_k \} +$$
$$+ \dot{\beta} \{ - b \cos\zeta - a_\zeta \} +$$
$$+ v_i [\sin\beta_k \cos\zeta_k \sin\beta - \cos\beta_k \sin\theta \sin\zeta_k \sin\beta - \cos\beta_k \cos\theta \cos\beta] .$$

They are rather lengthy and less clear. Normally, they are used in such a form in modern computer programs.

2.2 MOTION OF ARTICULATED, RIGID BLADES

Flapping motion

The most general conception of the motion of a fully articulated rigid blade is a movement about all the hinges, a motion with three degrees of freedom, which is somewhat difficult to analyze. In normal rotor systems, motion about the torsion hinge is not free, but either prevented or controlled by the rotor control linkage. Fortunately, the flapping motion, which is the most component, is virtually independent of lagging motion. Therefore, the flapping motion is a motion with a single degree of freedom, and is determined mathematically by a single equation which states that the sum of all moments about the flapping hinge, including the inertia moment, is zero (see Figure 18):

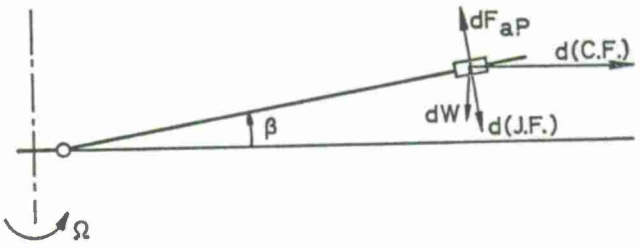


Figure 18 Forces acting on a flapping blade element

$$M_A + M_I + M_{CF} + M_G = 0 .$$

The moments will be found by integration of the aerodynamic forces and the mass forces, which can be done easily:

Aerodynamic moment
$$M_A = \int_e^R (r-e)\, dF_{AP}$$
$$= M_{Ao} + M_{AC1} \cos\psi + M_{AS1} \sin\psi + M_{AC2} \cos 2\psi + M_{AS2} \sin 2\psi + \ldots\ldots$$

Moment of inertia forces
$$M_I = \int (r-e) \frac{d(J.F.)}{dr} \ddot{\beta} = -\frac{d^2\beta}{dt^2} \int_o^R m\, (r-e)^2\, dr = -\frac{d^2\beta}{dt^2} J_f$$
(J_F = mass moment of inertia)

Centrifugal moment
$$M_{CF} = -\sin\beta \int_e^R (r-e) \frac{d(CF)}{dr}\, dr = -\sin\beta\, \Omega^2 \int_e^R m\, r\, (r-e)\, dr .$$

When the flapping hinge offset e is zero and the flapping β is small, the flapping moment of the forces can be equated to

$$M_{CF} = -\beta\, \Omega^2\, J_F .$$

The flapping equation is a differential equation in the flapping angle β, because each of the moments, including the aerodynamic moment, is a function of β of its time derivatives. For zero hinge offset and small angles, it is the linear differential equation

$$J_f \ddot{\beta} + \Omega^2 J_f \beta = M_{AO} + M_{AC1} \cos\psi + M_{AS1} \sin\psi + M_{AC2} \cos 2\psi + M_{AS2} \sin 2\psi \ldots\ldots,$$

in which the right side is the aerodynamic moment being a function of β too. Without aerodynamic forces it is the wellknown equation of a mechanical system with one degree of freedom without damping. The natural frequency of the flapping is Ω and equals the rotational frequency, it is independent of mass or geometric properties of the blade.

The aerodynamic moment gives a forcing function and in addition a damping moment since the velocity components at the blade element are depending on $\dot{\beta}$. The harmonic for-

cing function

$$M_{AO} + M_{AC1} \cos\psi + M_{AS1} \sin\psi + M_{AC2} \cos 2\psi + M_{AS2} \sin 2\psi + \ldots\ldots$$

will induce a flapping motion of the same frequency, and hence a steady-state solution

$$\beta = a_o - a_1 \cos\psi - b_1 \sin\psi - a_2 \cos 2\psi - b_2 \sin 2\psi + \ldots\ldots$$

is naturally expected to describe the motion.

In hovering and axial flight the flapping equation becomes simply an equation with constant coefficients, because there exists no periodic disturbance. The resulting nonperiodic flapping angle which is called the cone angle is determined by equating the lift and the centrifugal force moments. High lift causes a larger angle, heavy blades or high rotational frequency a small angle.

In translational flight there is a periodic excitation caused by the different flow situation at the advancing and at the retreating side of the rotor. Without cyclic blade control the aerodynamic forces as well as the aerodynamic moment are in a first approximation proportional to the square of velocity at the blade, which is approximately

$$U_P^2 + U_T^2 \approx U_T^2 = (x + \mu\sin\psi)^2 = x + 2\mu x + \mu^2 \sin^2\psi$$

$$= x + \frac{1}{2}\mu^2 + 2x\,\mu\,\sin\psi - \frac{1}{2}\mu^2 \cos 2\psi \ .$$

A first harmonic change in velocity therefore imposes first and second harmonic disturbances. In flight conditions without acceleration, the blade must be at all times in equilibrium; that is, no unbalanced forces may exist. The forward flight situation is described approximately in Figure 19. A blade in the rearward position encounters no added velocity due to forward speed. As the blade advances, however, the velocity and thus the lift are increased. As the blade experiences this first increased force it immediately moves upwards. In flapping upward, the direction of the relative wind changes so as to decrease the angle of attack and thus the lift. With no inertia forces, the flapping velocity has to be of such a magnitude as to decrease the angle of attack enough so that the moment of the lift will remain constant during revolution. The maximum upward flapping occurs at $\psi = 90^\circ$ where it is needed most. Following the blade around, then the flapping velocity is zero at $\psi = 0^\circ$, maximum upward at $\psi = 270^\circ$ and again zero at $\psi = 360^\circ$. The rotor is therefore high in front and low in back.

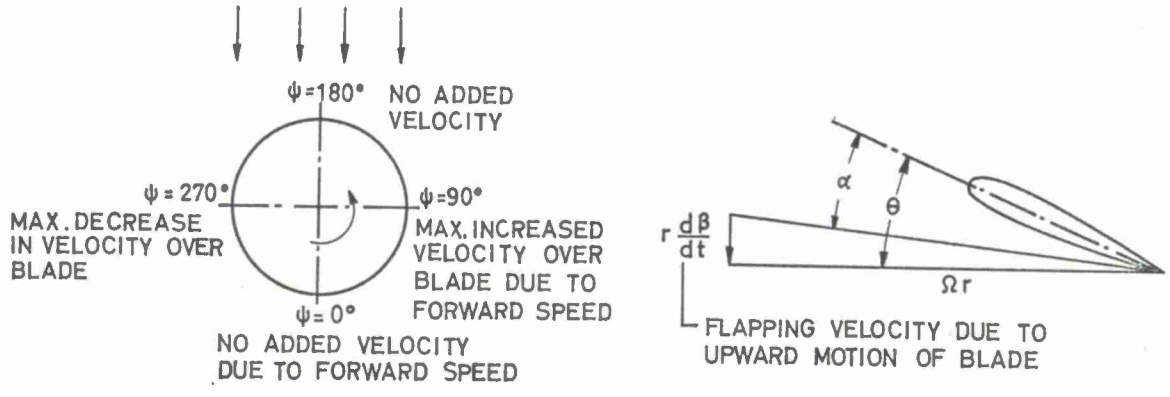


Figure 19 Effect of forward speed and of blade flapping

To examine the effects of blade mass and of air damping on the flapping motion more exactly, it is necessary to consider the blade as a dynamic system. The flapping blade is mechanically equivalent to a system with one degree of freedom with some damping and which is forced to vibrate by a periodically varying forcing function. The equivalent system is shown in Figure 20. The mass is analoguos to the flapping blade and the spring restoring forces to the centrifugal forces; the forced vibration is supplied by the air force, and the damping is air damping proportional to the flapping velocity.

For such a system the phase between force and displacement is related to the forcing frequency as shown in Figure 21. In the figure, ω_n is the natural frequency of the system, ω is the frequency of the forced vibration, and ϕ is the phase angle between the maximum applied force and the maximum displacement (that is the angle by which the force leads the displacement). C/C_c is the ratio of actual damping to critical damping. The displacement-force phase angle at any value of ω/ω_n is a function of the amount of damping,

except when the force is applied at the natural frequency of the system. In this case, the phase angle is 90° and is independent of the amount of damping.

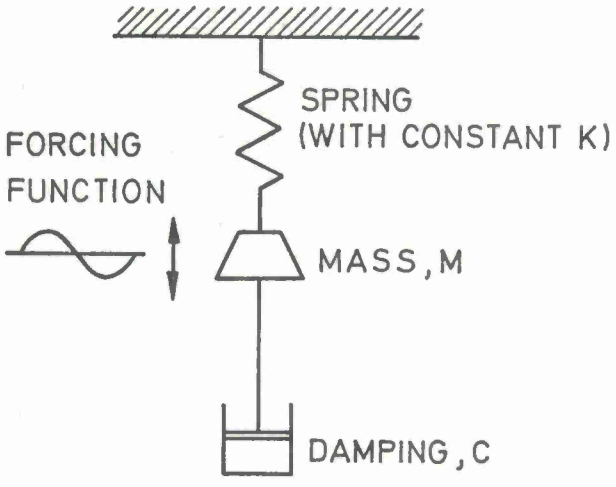


Figure 20 Mechanical analogy to a flapping blade

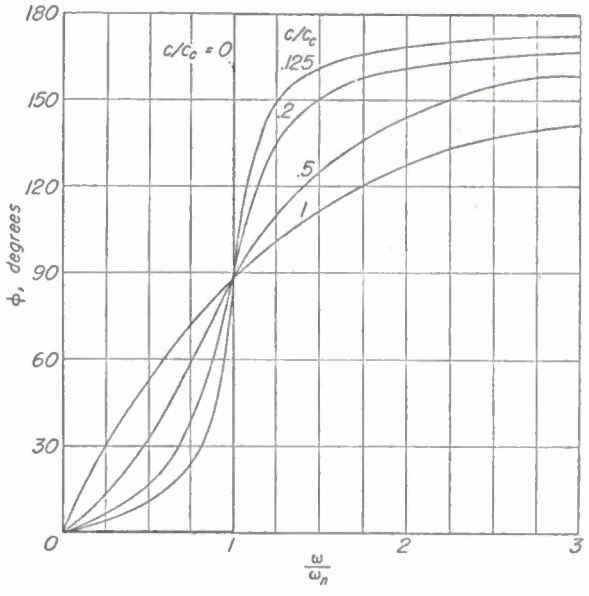


Figure 21 Relation between force-displacement phase and frequency

In the case of the centrally hinged rotor the natural frequency and the frequency of the exciting air force are the same (neglecting higher harmonic components). The force-displacement phase is 90° and is independent of the amount of damping. As already shown, the natural flapping frequency is independent of the blade,too, so that for the simple rotor neither blade mass nor damping affect the 90° phase shift between force and displacement. Thus, the results of the initial approach to the longitudinal flapping a_1 (asuming no inertia forces and no damping) are unchanged in the real case. The exciting forces act on a system in resonance, which by definition is a system in which the mass forces are in equilibrium with the spring forces, and in which external forces are in equilibrium with the damping forces.

The sideward tilting of the rotor by the lateral flapping b_1 may be viewed as arising from coning a_o. For the coned rotor in Figure 22 it may be seen that there is a difference in angle of attack of the blades at the front and rear of the rotor because of the forward speed, whereas with no coning, the effect of the forward velocity is indentical in the fore and aft positions. For the coned rotor a periodic air force is produced which has a maximum at the front of the rotor ($\psi = 180°$) and a minimum at the rear of the rotor ($\psi = 0°$). This airforce is in addition to the already known force in forward flight producing the longitudinal tilt a_1. The coning causes a lateral tilt b_1. The b_1 flapping can be of the same order of magnitude as the a_1 flapping.

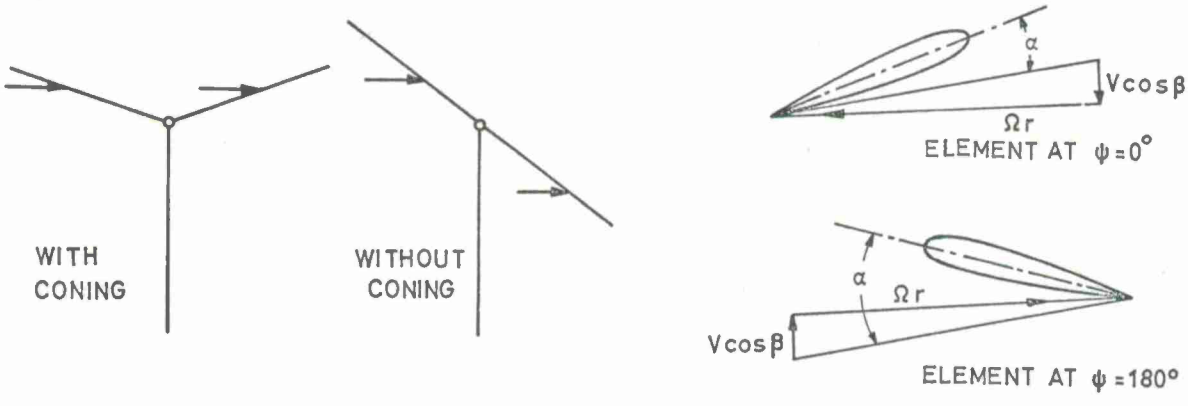


Figure 22 Effect of rotor coning on velocity distribution and blade section angles of attack

It should be noted that the b_1 tilt is very sensitive to variations in inflow from the front to the rear of the disk. For rough estimations it is usually assumed in forward flight analysis that the induced flow is uniform. At low forward speed, however, the induced velocities are still quite large; there is an inflow distribution with a lower inflow in the front of the rotor and a higher inflow at the rear of the rotor, thus increasing the b_1 flapping. The asymmetry of the inflow increases from zero in hovering to a maximum at some low forward speed then decreases steadily as speed increases. At high

speeds the inflow is again almost uniform inasmuch as the bulk of the inflow is due to the flight velocity acting through the tilted rotor.

As in the hovering case, the coning angle a_o depends upon the non-periodic magnitudes of the two primary moments about the flapping hinge - the aerodynamic lift moment and the centrifugal moment. It is not very much changed in forward flight. The most significant effect is coming from the variation of the rotor inflow. The coning angle is directly affected by the blade mass. The sideward flapping b_1 involves in the same way as the longitudinal flapping a_1 a system in resonance, and in this respect it would be independent of blade mass. The exciting forces for the b_1 motion, however, have been shown to be primarily proportional to the coning angle a_o which is proportional to blade mass. The amplitude of any oscillation of the system with damping and in resonance is, of course, proportional to the magnitude of the excitation. Therefore, b_1 is depending on blade mass, contrary to a_1.

The higher harmonics a_2, b_2, a_3, b_3, etc. may be viewed as a weaving of the blade in and out of the surface of the cone formed by the coning angle and the first harmonic motions of the blades. The sources of higher harmonic flapping lie in the forces produced by the periodically changing velocities at the blades, in higher harmonic components of nonuniform downwash, and in effects of reverse flow on the retreating side of the rotor. The higher harmonic motions do not involve a system in resonance, but a forced vibration well above resonance, wherein the exciting force is opposed almost entirely by the mass forces. The amplitudes of motion are therefore inversely proportional to blade mass. The higher harmonic blade motions are small and of little importance in problems of rotor control and rotor performance but may be extremely important in problems of rotor vibration and blade stress.

If the flapping hinge does not lie on the axis of rotation, the flapping is no longer in resonance with the rotor angular velocity. When the flapping hinge is at distance e from the axis of rotation, the natural flapping frequency is given as

$$\omega_f = \Omega \sqrt{\frac{\int m\,(r-e)\,r dr}{\int m\,(r-e)^2 dr}} = \Omega \sqrt{1 + \frac{e \int m\,(r-e)\,dr}{m \int (r-e)^2 dr}} \approx \Omega \sqrt{1 + \frac{3}{2}\frac{e}{R}} \quad .$$

For normal hinge offset (about 2% of radius) the natural frequency is only slightly modified, and there is nearly no difference in the flapping behaviour of the rotor, but for more accurate calculations the equations are largely extended.

Lagging motion

The introduction of flapping hinges usually necessitates hinging the blade in the inplane direction, that it can execute a lead-lag motion. This lagging motion is evaluated in a manner similar to the motion about the flapping hinge. The equation of lagging motion in general terms is obtained by equating the sum of all the moments about the drag hinge to zero

$$M_A + M_I + M_{CF} + M_{COR} + M_D = 0 \quad ,$$

where M_D is the moment exerted on the blade by a damper element which will be regarded as a linear damper, so that

$$M_D = K_D \dot{\zeta} \quad .$$

In principle, the moments will be the same as considered before, but there is a difference for the resulting centrifugal moment compared to flapping, as can be derived from Figure 23. The moment about the drag hinge of the lagging components of centrifugal forces can be represented by the following integral

$$M_{CF} = -\zeta\,\Omega^2\,d \int_d^R m\,(r-d)\,dr \quad .$$

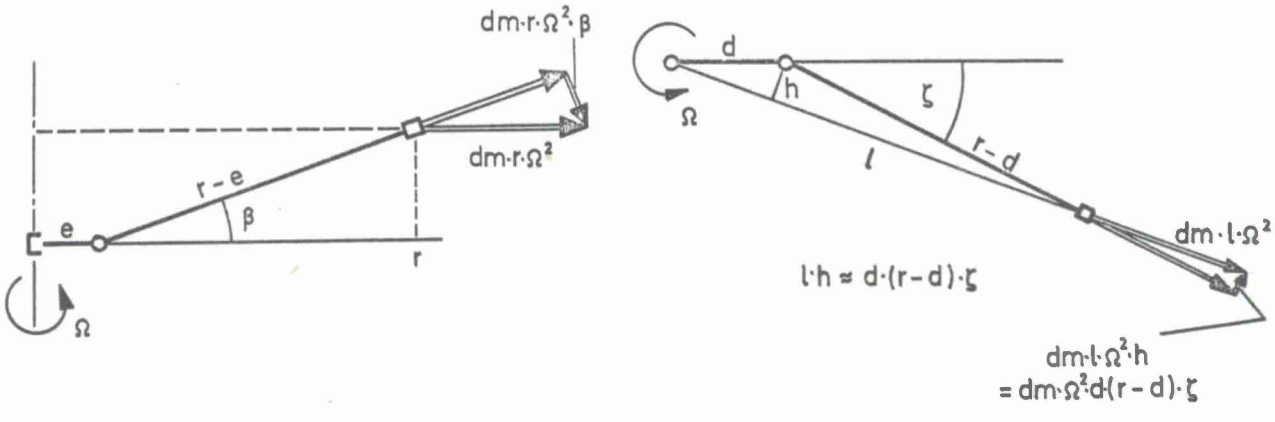


Figure 23 Comparison of centrifugal moments for flapping and for lagging motion

Comparing the centrifugal moments about the flapping hinge and about the lagging hinge there is to observe that the functional relation $\int r \cdot (r-e) \cdot dr$ is replaced by $\int \cdot (r-d) \cdot dr$, resulting in a much smaller restoring centrifugal moment for the lagging motion compared to the flapping motion.

The Coriolis forces acting at the blade elements cause the Coriolis moment

$$M_{COR} = 2\Omega \beta \frac{d\beta}{dt} \int_o^R m\,(r-e)(r-d)\,dr \quad ,$$

thus introducing a coupling between flapping motion and lagging motion.

M_I and M_A can be expressed in a similar way as for the flapping equation. The equation of lagging motion can be obtained in the form

$$A\ddot{\zeta} + B\dot{\zeta} + C\zeta + D = 0 \; .$$

The steady-state solution of this equation, similarly to the flapping motion is a harmonic function in ψ and can be expressed by the lagging motion coefficients

$$\zeta = e_o - e_1 \cos\psi - f_1 \sin\psi - e_2 \cos 2\psi - f_2 \sin 2\psi - \ldots$$

The major component of lagging moment is due to the Coriolis moment and therefore depending on the flapping motion. In approximate investigations it is customary to evaluate the Coriolis effect only and to neglect the variation of aerodynamic lagging moment altogether. The amplitude of the drag motion due to Coriolis moments can reach several degrees in a rotor with a high coning angle. The Coriolis moment is proportional to

$$\beta \cdot \frac{d\beta}{dt} = \Omega\,(a_o - a_1 \cos\psi - b_1 \sin\psi - \ldots) \cdot (a_1 \sin\psi - b_1 \cos\psi + \ldots)$$

$$= \Omega\,(a_o\, a_1 \sin\psi - a_o\, b_1 \cos\psi + a_1\, b_1 \cos 2\psi + \frac{1}{2}\,(-a_1^2 + b_1^2) \sin 2\psi) + \ldots$$

First harmonic inplane motion, therefore, only will be for a coned rotor (a_o). A purely first harmonic flapping rotor (a_1; b_1) would produce second harmonic inplane motion. Without the drag hinge these Coriolis moments could cause a high stress loading at the blade root section.

As long as the periodic lagging motions remain small and slow, the aerodynamic lagging moments do not depend on lagging motion. The periodically varying airforces in the drag direction therefore, do not change the restoring and damping coefficients in the equation of motion; they purely generate periodic impulses resulting, of course, in additional periodic lagging motions. The exact expressions for the aerodynamic lagging moment are exceedingly lengthy, and a rigorous treatment of blade lagging motion is equally laborious. In Figure 24, lagging motions considering Coriolis moment only and considering all moments are compared for a normal level flight condition and for a maneuver case. As easily can be seen, the direct influence of aerodynamic inplane moments to the alternating lagging motion is very small. The mean value of lagging, which is the constant coefficient e_o, is proportional to the rotor torque. It is changing with power, and therefore different in powered helicopter flight from power-off flight in autorotation.

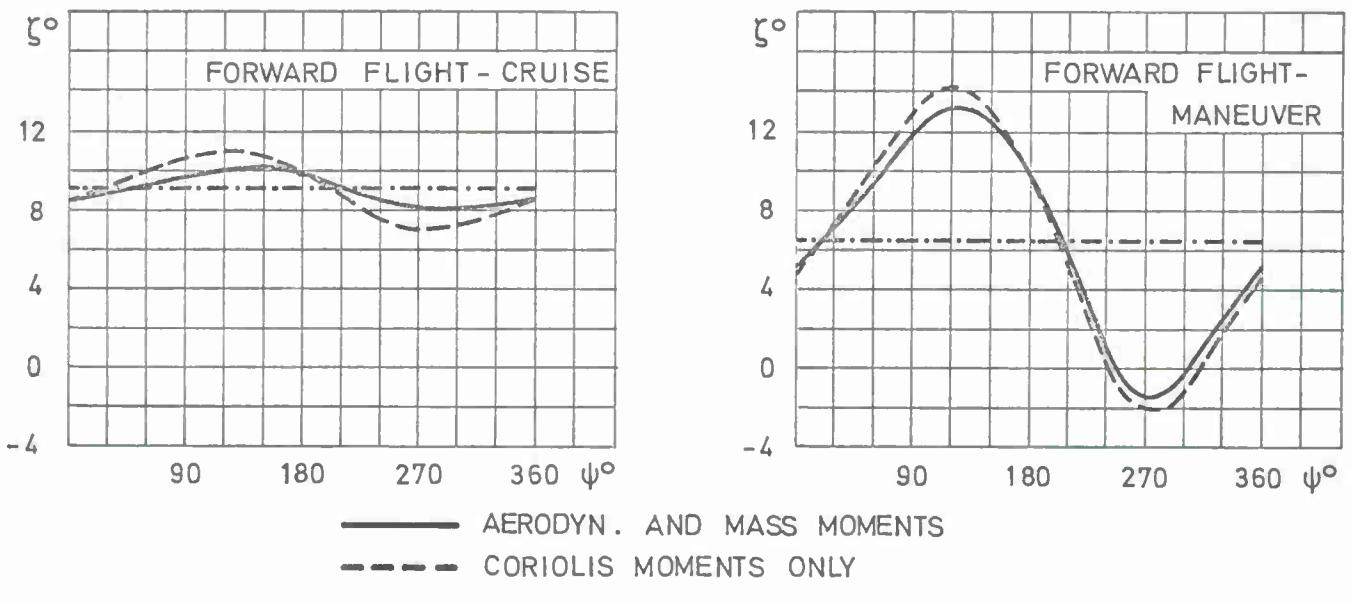


Figure 24 Lagging motion in forward flight

It is important to note that while blade flapping motion is essentially a resonant phenomenon, lagging motion has a natural frequency well below the rotational speed for normal lag-hinge offset. The natural frequency of the lagging motion wherein spring forces are always in equilibrium with mass forces, depends on the inertia moment and the centrifugal moment, which is different from that for flapping

$$\omega_e = \Omega \sqrt{\frac{d\int m\,(r-d)\,dr}{\int m\,(r-d)^2 dr}} \approx \Omega \sqrt{\frac{3}{2}\frac{d}{R}} \quad .$$

For normal lag-hinge distances, the natural frequency of the blade in lagging is about one-third to one-fourth of the rotational speed.

Under certain circumstances, the inplane motion of the blades can get unstable. The most extreme example is that of ground resonance, a divergent and often destructive oscillation which is self-excited, and which usually occurs whilst the helicopter is in contact with the ground. It is not a pure rotor phenomenon, since it must be coupled with a translational movement. Ground-resonance will be discussed in Session 4.

Feathering motion and rotor control

In a torsionally rigid blade, which will be considered here, the moment equilibrium about the torsion hinge does not determine the feathering motion of the blade. In most rotors the blades are constraint in pitch by the control linkage and the problem of evaluating free feathering motion does not arise, since the feathering motion is imposed.

Whatever type of control linkage is used, it allows to impose collective feathering A_o and each of the cyclic components A_1, B_1, independently. As a result the blade control is given by

$$\theta = A_o - A_1 \cos\psi - B_1 \sin\psi \quad .$$

The selection of the three magnitudes A_o, A_1 and B_1 is dictated by the desired state of flight. A_o depends substantially on the performance of the rotor, whereas A_1 and B_1 are determined neither by the performance of the rotor nor even by the dynamics of the rotor alone but are dictated by the mechanics of flight of the whole helicopter. Whatever the state of flight, the rotor by itself can be flown with any amount of cyclic feathering.

The magnitude of cyclic feathering actually selected is due to the relation between cyclic feathering and cyclic flapping. Cyclic flapping determines the direction of the total rotor force and hence must be so chosen, that the required equilibrium of forces and moments on a machine is maintained (see Chapter 3.1). It is also desirable that excessive cyclic flapping should not occur in any state of flight. In this sence it can be said that cyclic feathering is introduced to suppress cyclic flapping. Whether the suppression can be applied depends, however, on the moment equilibrium of the machine at different flying speeds.

The relation between cyclic feathering and cyclic flapping therefore occupies an equivalence of cyclic feathering and cyclic flapping, and an amount of cyclic feathering replaces an equal amount of flapping. This can be shown easily by introducing the cyclic feathering in the air force moment for the flapping equation, but the equivalence of flapping and feathering can be demonstrated graphically, too. Consider a rotor in forward flight as in Figure 25, which is assumed to be a simple flapping rotor without feathering. Its control axis, or axis of no cyclic pitch change, is vertical and the tip-path plane tilts rearward by an amount a_1. An observer riding on the control axis and rotating with the blades observes that the blades flap up and down each revolution but they do not change pitch. At the same time an observer who sits in the plane of the tips rotating with the blades, observes that the blades do not flap at all but do change their pitch - high, then low - one each revolution. The pitch is low on the advancing side of the rotor and high on the retreating side. The amount of blade feathering with respect to the plane of the tip is equal in degrees to the amount of blade flapping with respect to the control axis. Fore and aft flapping (a_1) with respect to the control axis is therefore equal to lateral feathering (B_1) with the axis perpendicular to the plane of the tips, as can be seen from Figure 26. The control axis is the axis of no feathering; the axis perpendicular to the plane of the tips is the axis of no flapping (except for higher harmonics).

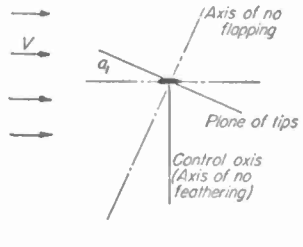
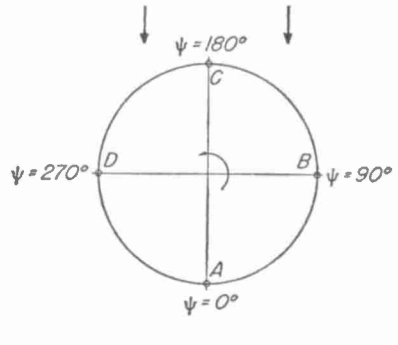


Figure 25 Flapping rotor in forward flight



With respect to tip-path plane

Feathering zero
Feathering max. down
Feathering zero
Feathering max. up

With respect to control axis

A = Flapping full down
B = Flapping zero
C = Flapping full up
D = Flapping zero

Figure 26 Blade positions with respect to control axis and tip-path plane

With the so-called direct control, the control axis is located in space by physically tilting the rotor shaft, or the hub with respect to the shaft, to the desired position with respect to the fuselage, as illustrated in Figure 27. For the commonly used control by cyclically changing blade pitch, the hub may remain fixed to the shaft, and the blade pitch will be varying cyclically by special means. Such a system is shown in Figure 28. The system consists of blades attached to the hub which are free to flap and free to change their pitch angles. The blades are held in pitch through a linkage connecting them to the swashplate. If simple feathering control is defined as a swash-plate system with a 1:1 linkage ratio, then the pitch of the blade is always constant with respect to the plane of the swash-plate, hence the axis is perpendicular to the physical shaft; both flapping and feathering motions exist.

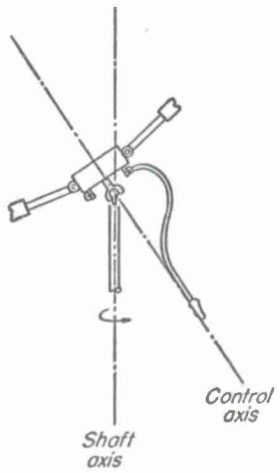


Figure 27 Control by tilting hub with respect to shaft

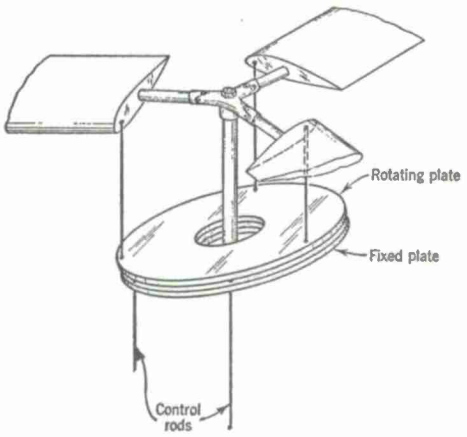


Figure 28 Control by cyclic pitch - swashplate assembly

2.3 MOTION OF RIGIDLY ATTACHED BLADES

For the socalled hingeless or rigid rotors it is not quite correct to use the designation "rigid rotor". The rigidity is only in the hub. The cantilevered blades eliminate the flap and the lead-lag hinges. The blades are flexible, therefore they execute elastic deformations equivalent to the flapping and lagging motions of articulated blades. In general, the equations which describe the flap bending, lead-lag bending, and torsion of such cantilevered blades are nonlinear, partial integro-differential equations, whereas the equations of articulated rigid blades are ordinary differential equations.

The characteristics of a rotor with rigidly attached blades is determined by its aeroelastic behaviour; but even with the means of modern computer mathematics the solution of the governing exact nonlinear, partial integro-differential equations would be rather difficult and laborious. For engineering investigations, therefore, a simplified treatment is commonly used, assuming that the elastic cantilevered blade can be represented by a hinged, spring restrained, rigid blade. Such an approximation method was first developed by Allen (10), who placed the entire flexure at the blade root and considered the blade itself as being rigid. The blade elasticity thus was reduced to a spring at the blade root and thus to an elastic blade attachment. The resulting flapping motion corresponds to the flexure. Payne used in his textbook (7) a similar analytical procedure. He introduced an effective hinge stiffness which simultaneously takes care of a flapping hinge offset or vice versa. The best way to understand a rotor with rigidly attached, flexible blades is to regard it as a successful attempt to produce a rotor whose flapping and lagging hinges are replaced by the elastic deformation of the flexible rotor blades. Such a rotor behaves similarly as an articulated rotor with a relatively large hinge offset.

Definition of an equivalent hinged rotor

In the analytical development one can see that practical rotor blades are quite flexible, in the sense that their first beamwise bending frequency is not very much greater than the once per revolution flapping frequency of an articulated rotor. A simplified theory, therefore, can be utilized for describing the elastic flapping response in terms of the fundamental blade beamwise mode. This can be done using the fundamental beamwise mode directly or by approximating it by a straight line approximation, leading to the concept of a virtual offset flapping hinge, permitting the use of conventional analytical methods for articulated rotors with offset flapping hinges.

The viewpoints that must be considered in determining the equivalent system, i.e. the equivalent hinge offset and the equivalent stiffness, have been discussed by Young (11), and now there are many papers reporting about rotor theories using such equivalent systems, for instance (12 ÷ 15).

It is necessary, that an equivalent system simulates both the aerodynamic and the dynamic behaviour adequately. For simple studies, it can be assumed that the blades have flexibility only in the flapwise direction and are infinitely stiff in the chordwise and

torsional directions. The main features of such a flapping equivalent system are shown in Figure 29; practically, it is a flapwise articulated rotor with a large hinge offset. In Figure 30 the moment distribution over the blade span is illustrated for a typical flight condition. It can be seen that the moment raises mainly in the very stiff parts of the root section and the rotor hub; and it seems well justified to represent this rotor blade configuration by an equivalent flapping system. Hingeless rotor systems allow the transfer of large moments from the rotor to the fuselage which results in a substantial improvement of the flight mechanical behaviour of the whole helicopter. An equivalent system has to simulate the moment loading of the rotor adequately, therefore. Experience has shown that the simple equivalent flapping system can model the rotor well enough for stability and control calculations as well as for the prediction of the determining loads including steady-state flight, maneuver and gust conditions.

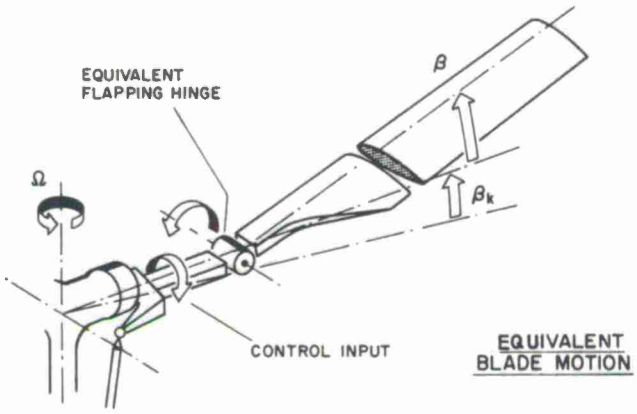


Figure 29 Model of an equivalent rotor blade

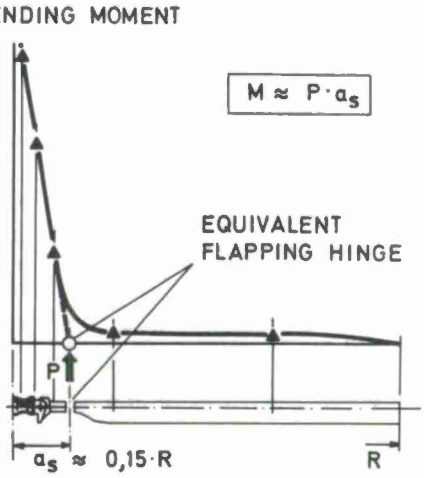


Figure 30 Distribution of flapwise bending moment on a rigid rotor blade

In selecting the equivalent system, first, the natural frequency and the fundamental mode of flapwise bending have to be determined. The governing differential equation for flapwise bending is

$$(EJw'')'' + m\Omega^2\ddot{w} + \Omega^2 \left[mrw' - w'' \int_r^R mr\, dr\right] = F(r, \psi) .$$

The deflection is denoted by w, the stiffness by EJ . F is the loading function including centrifugal and aerodynamic loads as well as the damping terms. The deflection can be represented by a superposition of modal deflection functions $w_j(r)$

$$w(r, t) = \sum_{j=1}^{J} w_j(r) \cdot \beta_j(t) .$$

It is customary to use the bending modes of the blade as the modal deflection functions. They can be evaluated in the common way. The $\beta_j(t)$ are generalized coordinates or mode participation factors.

Substituting the deflection w(r, t) by a superposition of modal deflection functions into the partial differential equation reduces this,by the use of Galerkin's method, to a system of ordinary differential equations in terms of β_j. The equations which define the mode participation factors are of the form

$$A\ddot{\beta}_j + A\dot{\beta}_j\, \beta\, C\beta_j + D = 0 .$$

They are very similar to the equation of the flapping motion of an articulated, rigid blade. For approximate calculation it is sufficient to consider only the first bending mode. With further neglections this can be replaced by the motion of an equivalent articulated, rigid blade. The equivalence becomes evident by comparing the equations for the mode participation factor and for the flapping rigid blade. The equivalent system, as far as possible, has the same dynamic properties as the real system, i.e. it has the same natural frequency. In addition, it should have similar aerodynamic properties and should react similarly to exciting forces. The natural frequency of the equivalent articulated blade with offset hinge e and hinge restraint (c_β) is determined by

$$\left(\frac{\omega_f}{\Omega}\right)^2 = 1 + \frac{\int mr(r-e)\,dr}{\int m(r-e)^2\,dr} + \frac{C_F}{\int m(r-e)^2\,dr} = 1 + \frac{3}{2}\frac{e}{R} + \frac{C_\beta}{J_f} .$$

The equivalent flapping hinge offset is commonly defined by the best straight line approximation of the fundamental bending mode, as illustrated in Figure 31. Bending line and the equivalent flapping blade coincide substantially; deviations at the outermost blade points should be as small as possible. This approximation will yield a suitable value for the equivalent flapping hinge offset.

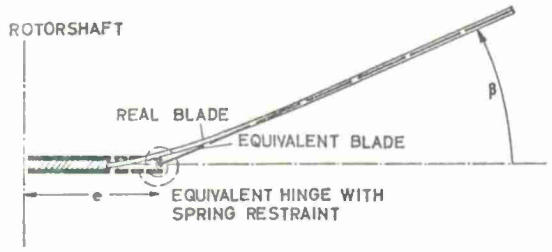


Figure 31 Equivalent system for a rigidly attached elastic blade

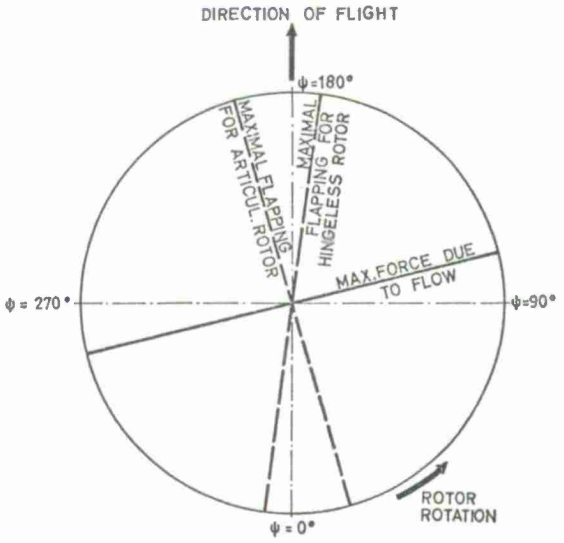


Figure 32 Phase shift between aerodynamic force and flapping motion

Flapping behaviour

The flapping frequencies of hingeless rotor systems are about in the region of 1.1 to 1.2 of the rotor frequency; the equivalent hinge offsets are 12% to 22% of radius. In this case, flapping is no longer a resonance phenomenon, and the phase relationsship between exciting force and the displacement will move to a value lower than 90°. The ratio of flapping angle to cyclic control angle, which is one for the resonance rotor, is not greatly influenced, also the flapping situation in forward flight changes not much. The conditions can be illustrated on the rotor disk shown in Figure 32. As already mentioned, a cone angle effect will produce no symmetry of relative flow. The effect is such that, in a standard rotor in which the phase angle of the flapping motion is 90°, a lateral inclination is added to the longitudinal inclination of the rotor. For hingeless rotors the asymmetry of the relative flow may be compensated partly during the flapping motion because of the smaller phase angle. This would be optimal with respect to the rotor control, because only longitudinal control would be needed; but it should be mentioned that final control phasing has to be chosen for best dynamic flight behaviour without critical pitch-roll cross coupling effects, which will be discussed in Chapter 3.2

Influence of inplane stiffness

Inplane flexibility of rigidly attached blades can be treated in a similar way as flapping. A refined equivalent system, which is an extension of the pure flapping system and has an additional degree of freedom in chordwise direction, can be introduced. For the definition of the equivalent system, similar conditions as for flapping can be used. The lagging motion, itself, behaves similar as in the case of articulation.

The chordwise bending stiffness of the rotor is an important parameter. Due to the different influence of the centrifugal forces in comparison to the flapping motion, the possible range of inplane frequencies is much more extended. While typical articulated rotors lie in an inplane frequency range of 0.2 ÷ 0.3 of rotor frequency, hingeless rotor concepts can be handled from 0.3 up to 1.5 of rotor frequency, depending on the flexibility of the root and the blade section. There are soft inplane rotors and stiff inplane rotors.

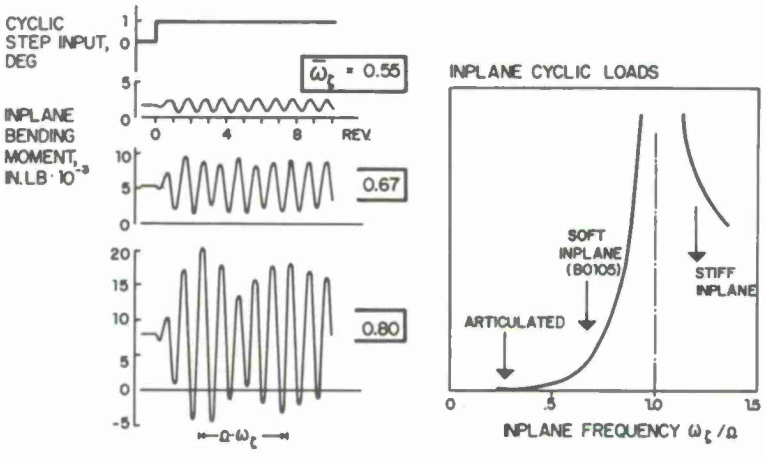


Figure 33 Effect of inplane natural frequency on structural loads

The soft inplane rotors show similar behaviour as rotors with lag hinges. They are susceptible to air or ground resonance instability, while stiff inplane rotors are not. This instability is not as serious as it is for articulated rotors because of the relatively high inplane frequency, and there are successful rotors without mechanical lead-lag dampers.

As a mechanical system in which exciting forces are governing the deflections, the chordwise deflecting blade will be sensitive approaching resonance between exciting frequency and natural frequency. In Figure 33, the variation of oscillatory inplane loads versus the inplane frequency are shown. In the left part of the picture records of the chordwise moments are presented for a cyclic step input in hover. Three typical "soft in-plane" frequencies are shown and it is indicated that the chordwise loads strongly increase with increasing inplane stiffness. Soft inplane rotors with frequencies of about 0.6 to 0.75 seem to be a good solution, their loads are lower than that of stiff inplane rotors.

Elastic coupling effects

For fundamental studies, a system as described in Figure 34 with degrees in flapping, in chordwise and torsional direction with additional control system flexibility, should be considered. While inplane bending of the blade has nearly no direct influence on aeroeynamic loading, it may effect the control system dynamics, if control flexibility is considered. Torsionally elastic motions of the blades are included as they act directly as control inputs and thus can have an influence on aerodynamic loading and on flight behaviour. Effects of different positions of the aerodynamic center, the elastic axis and the c.g. of the blade profile sections as a function of blade span can be calculated (16 ÷ 18).

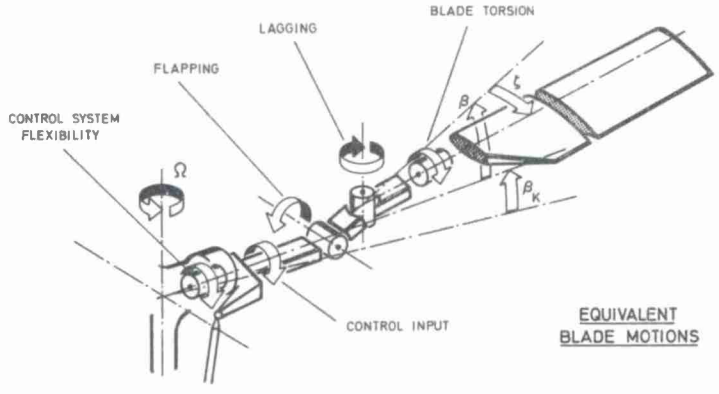


Figure 34 Model of rotor blade with flapping, lagging and torsion degrees of freedom

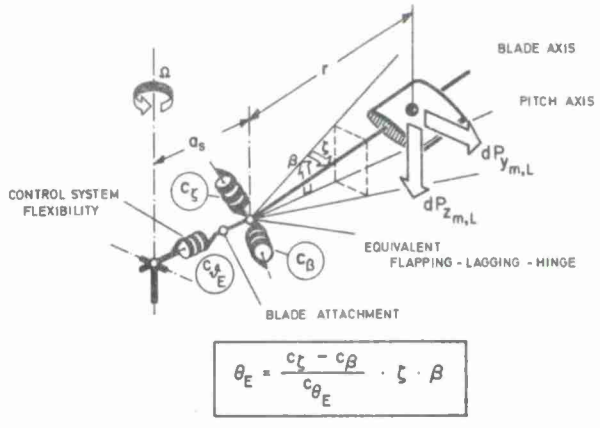


Figure 35 Elastic pitch-flap-lag coupling

Hingeless rotors with feathering hinges fixed to a stiff hub and with blades deflecting out of this axis show coupling effects, as illustrated in Figure 35, when control flexibility is present. The elastic control deflection is

$$\theta \cdot c_{\theta_E} = (c_\zeta - c_\beta)\ \zeta \cdot \beta ,$$

thus introducing a coupling between the components of blade motion.

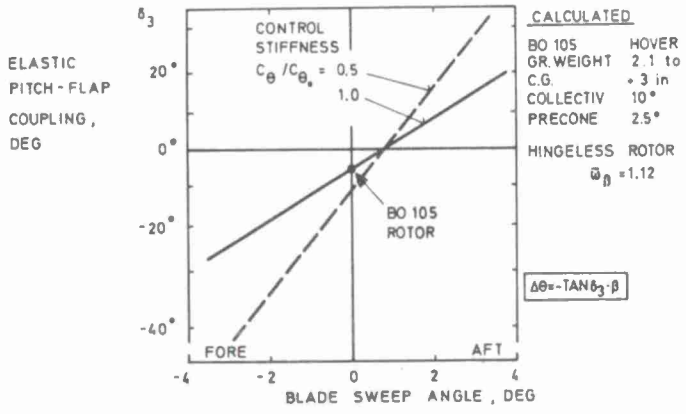


Figure 36 Effect of blade sweep on elastic δ_3-coupling

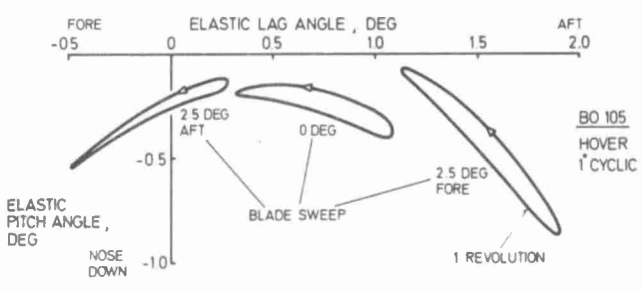


Figure 37 Elastic pitch-lag coupling

The most common parameter, which can result in this type of coupling, are precone of the feathering axis, blade sweep, flapping and inplane stiffness, and control system flexibility. It is indicated that the elastic couplings are comparable to pitch-flap-coupling hinges. Figure 36 shows some results illustrating the effective δ_3-angle obtained at a hover cyclic control condition. The elastic coupling angle is shown as a function of the blade sweep angle. Forward sweep of the blade results in negative δ_3, rearward sweep in positive δ_3. The influence of the control system stiffness proves to be almost linear. Similarly, the elastic δ_3-behaviour of hingeless rotors can be influenced by precone of the feathering axis and by the chordwise flexibilities of the blade, both changing the blade position relative to the pitch axis.

In addition to these coupling effects specific interactions between the inplane and pitching motions can be observed at hingeless rotor blades. In order to illustrate this type of coupling, typical variations of elastic blade pitch angle with lag angle are shown in Figure 37. There is indeed an elastic pitch-lag-coupling, as shown by the slope of the curves. In the case of forward swept blades the coupling becomes negative, aft swept blades result in a positive coupling.

The phenomenon of pitch-lag coupling can be favourable or unfavourable for rotors, depending on the amount and sign of the coupling. It may have a stabilizing or destabilizing influence on the flap-lag oscillations. Therefore accurate investigations are necessary for hingeless rotors.

An analysis of the torsional equation of motion indicates that the torsion of rotor blades is strongly influenced by chordwise distribution of mass. It can be shown that both inertia forces and centrifugal forces can produce nose-up and nose-down moments, depending on blade position in relation to the plane of rotation. Considering a blade with c.g. shifted toward leading edge, centrifugal forces will produce a nose-down twist, if blade bending is upwards. The amount of twist is proportional to the blade deflection. This means that a strong coupling of flapwise bending and torsion of the blade exists, if the blade is unbalanced in chordwise direction. In order to give a rough impression of its efficiency, the dynamic blade response to a discrete gust is shown in Figure 38. The figure shows the elastic deflection of the blade tip, as an observer at the center of the hub would see it, when looking toward the blade tip and rotating with the blade. There is a strong difference in blade response between the blades with different chordwise c.g. position.

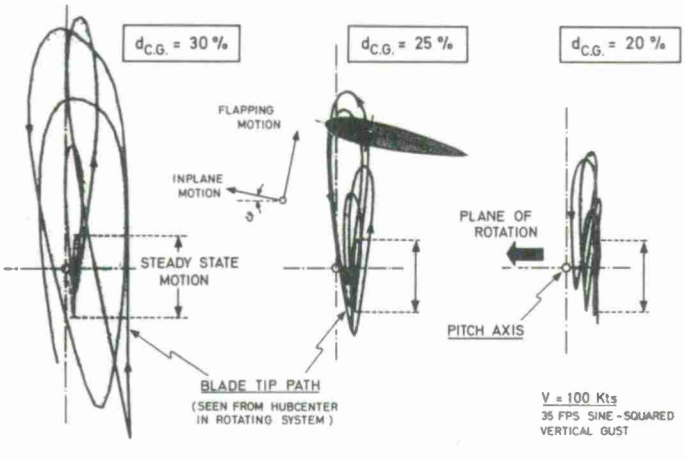


Figure 38 Influence of blade c.g.-position on blade gust response

A good understanding of hingeless rotor characteristics necessitates the understanding of the elastic coupling effects. It has become apparent that these coupling will probably be useful in a rotor design in which all the design parameters are optimized.

3. MECHANICS OF HELICOPTER FLIGHT

3.1 PRINCIPLES OF HELICOPTER CONTROL

In Chapter 2 the motions of the rotor blades have been discussed. Controlling the feathering motion of the blades causes a cyclic flapping of the blades and thus an inclination of the rotor tip-path plane and the thrust vector of the rotor with respect to the airframe. The overall aerodynamic force of the rotor is approximately perpendicular to the tip-path plane. This may appear to be reasonable, since the blade lift is perpendicular to blade span, so that its average direction over the disc is normal to the tip-path plane, as illustrated in Figure 39.

The control of the whole helicopter is, in the case of normally articulated rotor blades, mainly done by this inclination of the thrust vector, thus producing a moment around the center of gravity of the helicopter. For a helicopter with a hingeless rotor system an inclination of the thrust vector is combined with a very strong hub moment, and the moment around the helicopter c.g. is a combination of the hub moment and the moment due to the thrust inclination. Figure 40 compares the moment capability of a rotor with articulated blades and a small hinge offset and of a hingeless rotor having a relatively high equivalent hinge offset. As is shown in Figure 41, the same amount of cyclic control input results in nearly the same amount of cyclic flapping, and therefore the same thrust vector inclination; but for the hingeless rotor the flapping motion is combined with a large hub moment. The total control moment about the helicopter c.g. is about 3 to 4 times higher for the hingeless rotor than for the articulated rotor. The possibility to transfer high moments from the rotor blades to the hub and the airframe improves remarkably control and trim behaviour of a hingeless rotor.

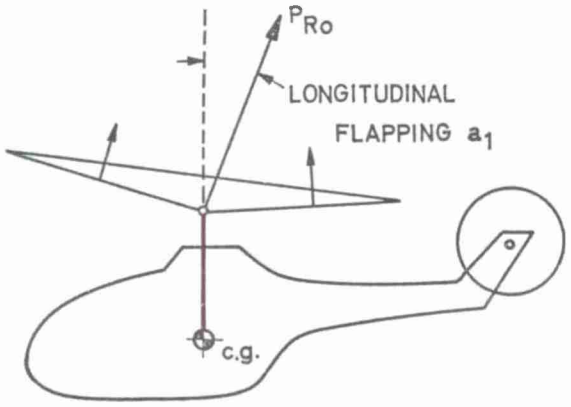


Figure 39 Longitudinal flapping - view from side

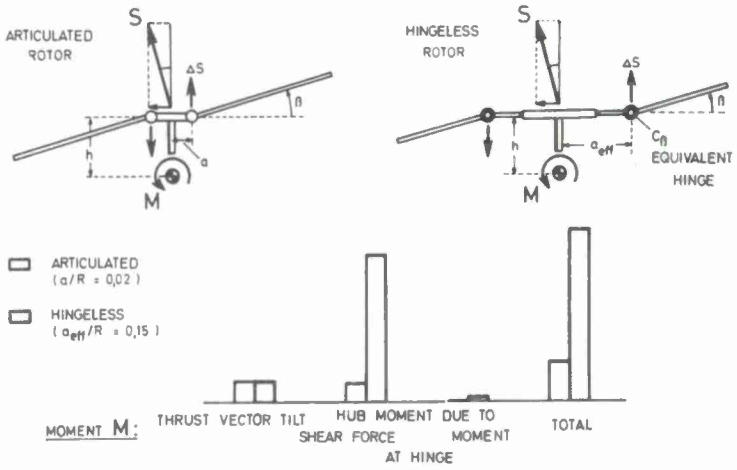


Figure 40 Rotor control moment capability

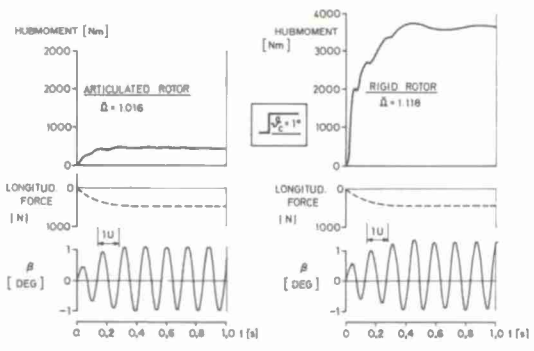


Figure 41 Hub moment due to cyclic control

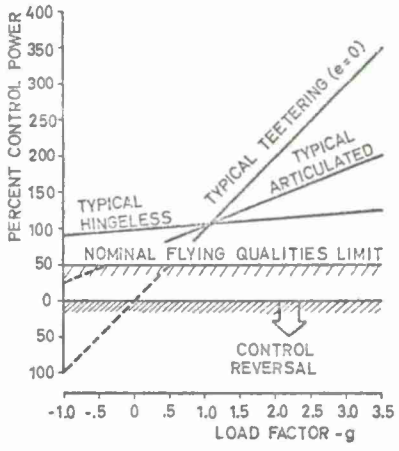


Figure 42 Control power during maneuvers

The design parameters influencing directly the control moment of a helicopter are the height of the rotor above the helicopter c.g., the hinge offset or the equivalent stiffness of hingeless rotors and, of course, the rotor thrust itself. For the centrally hinged rotor without thrust, it is possible to incline the tip-path plane by cyclic control, but there will be no moment around the helicopter c.g.. For the articulated rotor with relatively small offset, the moment capability of the unloaded rotor is small; only the hingeless rotor has a moment capability which is relatively independent of thrust. Offset flapping hinges introduce moments at the hub, which are approximately proportional to the flapping angle times the centrifugal force. These relations may be of special importance in special maneuver flight conditions resulting in zero or negative load factors as is illustrated in Figure 42. The articulated rotor looses its controllability.

Trim calculation

The control moment, which has to be applied with the rotor, depends on the equilibrium conditions of the different flight conditions. It is required to determine values of the flight variables which would result in lift, drag, and moment equilibrium (see for instance Figure 1). Lift, drag, and moment are coupled. Therefore, because all three are controlled by the rotor and because of certain algebraic complications, no simple closed-form expression can be used to calculate the trim variables. The controls of a helicopter with automatic power and r.p.m. control are collective pitch and cyclic pitch, controlling the attitude of the rotor and the helicopter, collective pitch mainly the rotor thrust and the power; but there is a relatively strong coupling between all of them influencing the flight variables in combination.

A rotor in forward flight without cyclic control will execute a flapping motion with respect to the helicopter as described in Chapter 2.2. This flapping can be suppressed by cyclic control as long as it is possible to maintain the condition of equilibrium of the moments around the helicopter c.g.. There has to be a balance of the forces which are weight of the helicopter, drag of the helicopter and the rotor thrust to overcome them. The thrust has to produce the lift component and the propulsion component to overcome drag.

The balance of the forces determines the position of the tip-path plane with re-

spect to the directions of flight and gravity, independently of its position against the helicopter. The attitude of the helicopter itself and the inclination of the tip-path plane against the helicopter axis are determined by the equilibrium of the moments around the helicopter c.g., which can be influenced by the amount of flapping with respect to the helicopter axis and can be changed by cyclic control. For this equilibrium of moments all the different moments of all helicopter components have to be considered: c.g. position, moment of the rotor, aerodynamic moment of the fuselage and moments of stabilization or control planes. The different components, which have to be considered, are illustrated in Figure 43. The calculation of these moments raises no problems if the velocity and the angle of attack are known. The complete calculation has to consider all three axis between which a relatively strong coupling is existing since the helicopter is not a symmetrical aircraft, as indicated in Figure 44 showing a hovering helicopter.

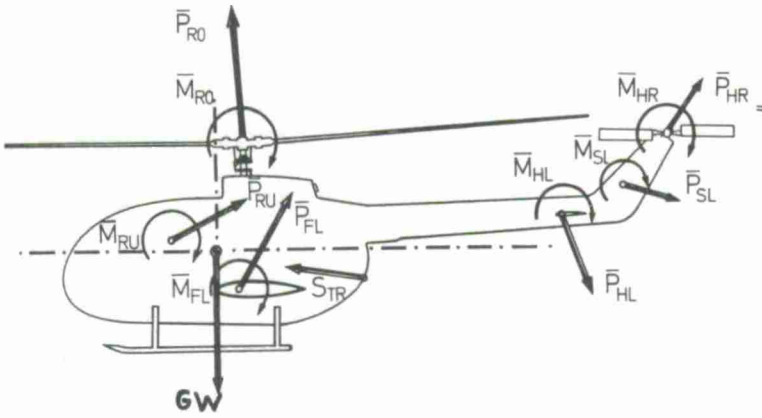


Figure 43 Forces and moments acting on a helicopter

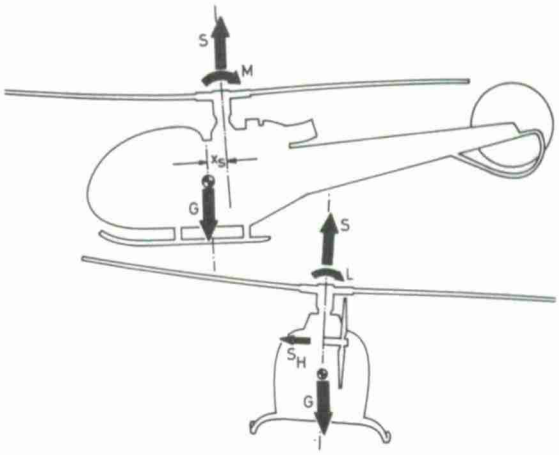


Figure 44 Helicopter in stationary hover flight

The calculation of the trim position fulfilling balance of forces and equilibrium of moments can accurately be done only iteratively in a numerical way as indicated in Figure 45.

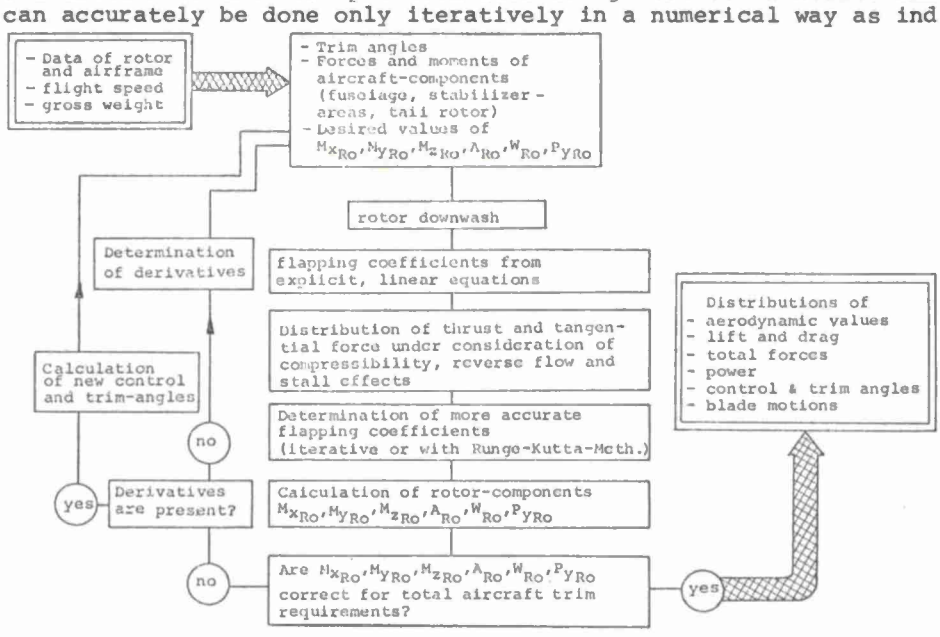


Figure 45 Trim calculation flow chart

Input for the calculation are the basic data of rotor airframe and the data determining the condition of flight (flight speed, altitude, gross weight). In a first step, the desired values of the rotor forces and rotor moments, which will result in equilibrium considering the forces and moments of the other components as fuselage, stabilizer, tail-rotor etc. are calculated. The rotor inflow - at first uniformly or trapeziodally distributed - is determined by flight speed, rotor thrust and rotor angle of attack. In the next step, the flapping behaviour of the rotor has to be considered, as there is an essential influence on the aerodynamics. In the first approximation, this can be done using linear, closed form equations. Blade lift and drag distributions are calculated in the common way using twodimensional airfoil data considering stall, reverse flow and compressibility effects. A refined calculation using the accurate equations for the blade motion is done in a pure numerical way, iteratively or in an azimuthal step-by-step numerical integration. With the knowledge of the blade loads and of blade motion, it is possible to calcu-

late the forces and moments at the rotor hub. If these forces and moments do not meet the trim requirements, an iteration process will be necessary. This is done using force and moment derivatives with respect to the control angles and the helicopter attitudes. These derivatives can be calculated with the same program changing only one control or attitude angle. Using the derivatives,refined input values for control and for the attitudes can be found. Changed helicopter attitudes as well as a change in the rotor downwash will influence the forces and moments of all helicopter components. The iteration process will be repeated until convergency is obtained. The final results of the combined trim and rotor aerodynamic calculation are the control angles, the attitudes of the helicopter, the required power, the total forces and moments of all components, load distribution at the blades and the blade motion.

Such accurate trim calculations are relatively lengthy and complex. For rough estimations it is possible to use a more simple approach considering the relations between the flight variables and the control parameters. The relations for the forces and moments can be expressed in dimensionless form in diagrams. The trim solution will be found in an iterative procedure also in this approximation, see for instance (19; 20).

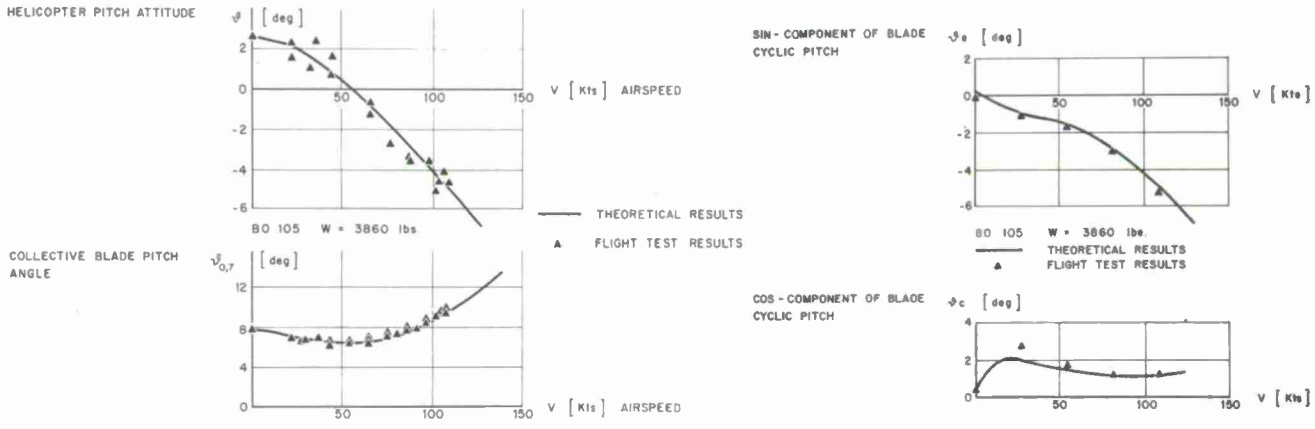


Figure 46 Helicopter pitch attitude and rotor control angles versus speed

In Figure 46 typical results of a trim calculation for a helicopter in forward flight are shown. For a helicopter with an articulated rotor and for a helicopter with a hingeless rotor there are only small differences. If there would be equilibrium of moments without the rotor moment there would be no difference at all. In this case cyclic rotor control would be only used to overcome effects from the asymmetry of the flow conditions, which are not influenced by the type of rotor blade attachment. Such conditions of moment equilibrium would be desirable; they would result in practically no flapping with respect to the shaft, which is adventageous for vibrations and for the loads; but, normally, it is not possible to keep such conditions in a larger regime of forward speeds.

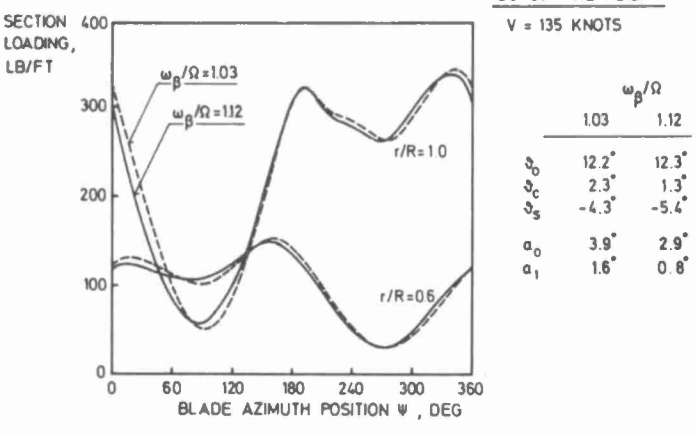


Figure 47 Blade section loading in trimmed flight with different rotors

Figure 47 illustrates azimuthal blade section loading in trimmed flight for different rotors. The fluctuations in the aerodynamic forces during blade revolution nearly are not influenced by the flapping frequency. The corresponding control angles of the two rotors are fixed by the flow conditions and the trim requirements of the helicopter. The small difference in cyclic control is due to the slightly different flapping. The differences in the control angles in the Figure 47 are resulting from a different flapping of the two rotors. Trim conditions which need a rotor produced moment to overcome c.g.-travel or slope landing conditions, for instance, require an cyclic first harmonic moment in the rotating system for the hingeless rotor, whereas in the case of an articulated rotor because of the pure equivalence of cyclic control and blade flapping only an inclination of the thrust is necessary. Inasmuch as the amount of control displacement is limited for mechanical reasons, an increase in the amount of control power through the use of off-

set flapping hinges or rigid blade attachment is the feasible way to allow for greater moments as needed for a greater c.g. travel for instance.

Control characteristics and requirements

In addition to the pure trim behaviour, the effects obtainable with a certain control deflection and the corresponding time behaviour are the most important parameters in evaluating the control characteristics. Changing the control settings is necessary when going from one condition of equilibrium to another or from one flight condition to another. All maneuvers and all the stabilization work to hold a certain flight condition are done using the control means.

A control input causes changed rotor forces and moments, which are no longer in equilibrium. The response of the rotor tip-path plane to a change of cyclic control is very rapid and heavily damped. In fact the time of response is usually a fraction of a revolution time for a blade. This is very short compared to any characteristic motions of the helicopter as a whole, and for practical purposes it may be assumed that the rotor responds instantly and without overshoot to cyclic input. Following the inclined tip-path plane the helicopter will start to move translationally and rotationally. The time behaviour of this reaction is most important considering handling qualities, Commonly, the control efficiency will be expressed by the initial acceleration per unit stick deflection, which is equal to the ratio of the control moment obtainable with the stick deflection to the moment of inertia of the helicopter. Numerous investigations have shown, that, for a satisfactory control behaviour, a definite correlation should exist between the control moment or the initial acceleration and the damping of the resulting motion. This characteristic is called control sensitivity and may be defined in three alternate ways, which are equivalent, as follows - see for instance (5)-

$$\text{Control sensitivity} = \frac{\text{control power}}{\text{rotor damping}} = \frac{\dfrac{\text{control moment}}{\text{stick displacement}}}{\dfrac{\text{damping moment}}{\text{angular velocity}}} = \frac{\text{angular velocity}}{\text{stick displacement}} \quad .$$

Physically, the manner in which control power and damping determine control sensitivity may be understood from the following argument. If the control stick is displaced (laterally, for example) and held, the helicopter will initially accelerate angularly at a constant rate that is inversely proportional to the moment of inertia of the helicopter following the law

$$M = J \cdot \frac{d\omega}{dt} \quad .$$

As the angular velocity builts up, an opposing damping moment builts up increasing in proportion until an angular velocity is reached at which the damping moment is equal to the control moment. The helicopter is therefore stabilized at that angular velocity, because the resultant moment on the helicopter is zero. It is thus apparent that, if the rotor damping is large with respect to the control power, then the maximum rate of roll reached by the helicopter by a given stick displacement would be small, inasmuch as a sufficiently large damping moment would be produced at a small rolling velocity to balance the control moment. Alternately, it is clear that, if rotor damping is small with respect to the control power, then the maximum angular velocity attained by a given stick displacement would be large.

The rotor damping has its physical origin in the inertia of the rotor blades causing some delay between a rapid shaft tilt and the realignment of the rotor with the shaft. Thus, if the shaft continues to tilt, the tip-path plane will continue to lag behind the rotor shaft and in so doing supplies the aerodynamic moment necessary to overcome continuously the flapping inertia of the rotor during steady pitching or rolling. If the aerodynamic and inertia flapping moments are equated, the following result for the angular displacement of the rotor plane with respect to the shaft per unit tilting velocity of the shaft is obtained for the hovering case

$$\frac{\delta}{\omega} = \frac{16}{\gamma\Omega} \quad \left(\text{with the blade mass factor } \gamma = \frac{c\ \rho\ a\ R^4}{J_f}\right) \quad .$$

The quantity $16/\gamma\Omega$, which has the units of time, can be interpreted physically as follows: if the rotor shaft is tilting at any constant angular velocity, the thrust vector reaches a given attitude in space $16/\gamma\Omega$ seconds after the rotor shaft has reached that attitude.

If a helicopter is tilted at an angular velocity ω, as shown in Figure 48, the ensuring lag of the rotor plane displaces the thrust vector and thus produces a moment about the helicopter c.g.. If offset hinges are present, there is an additional moment caused by the tilt, see Figure 49. Moments attributable to tilting velocity M_ω are known as damping in pitch or damping in roll. Because this moment is opposite to the tilting velocity, it is stabilizing.

In numerous investigations limits of satisfactory and insufficient properties for the control characteristics have been established, as illustrated in Figure 50 in a plot of the damping versus the control moment for pitching of the helicopter. Along straight lines through the origin, there is the same control sensitivity, meaning the same angular velocity per stick displacement. In the figure the critical curves found by Salmirs and

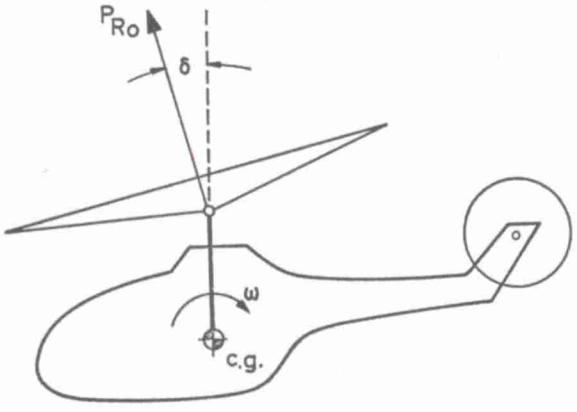


Figure 48 Damping moment arising from pitching velocity

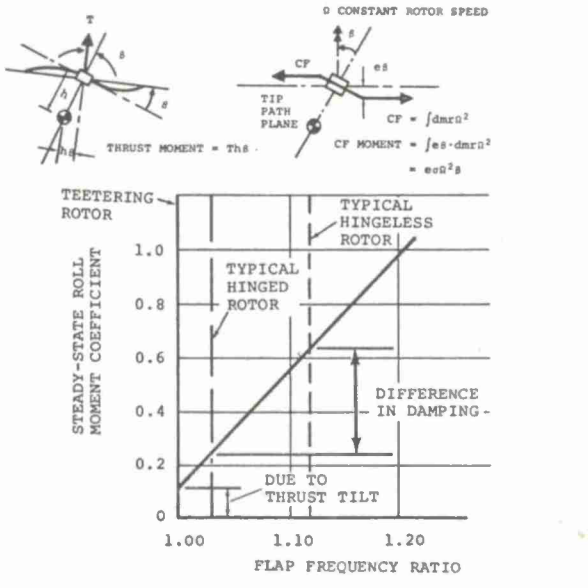


Figure 49 Damping moment of articulated and hingeless rotor

Tapscott (21) are compared with the Military Specifications for Handling Qualities (22), and in addition recommendations especially for armed helicopters (23) are given. Not only the control sensitivity is of importance. As already known, a discrepancy exists between the various recommendations and specifications. Most likely, the reason lies in the fact that these were established on the basis of pilot evaluations from limited flight tests or simulation studies. In addition, the figure gives the values obtained for a helicopter with hingeless rotor and for a helicopter with an articulated rotor of about 2% flapping. hinge offset. Both helicopters have about the same control sensitivity, because of the fact that offset flapping hinges or rigid blade attachment increase both, control moment and damping moment. The helicopter with the articulated rotor is about in the range of the curves of Salmirs and Tapscott, only it seems, that the control ratio of stick movement to blade cyclic pitch is somewhat to high. Reducing this ratio causes a shift towards left in the diagram or towards reduced control sensitivity. The helicopter with the hingeless rotor is within quite another range than usual for conventional helicopters. The control moment for the same stick deflection is about three times the value of the articulated rotor; for damping a similar relation exists. This is still more important than the control moment, which can be influenced to a certain amount by the control ratio to get within the recommended region.

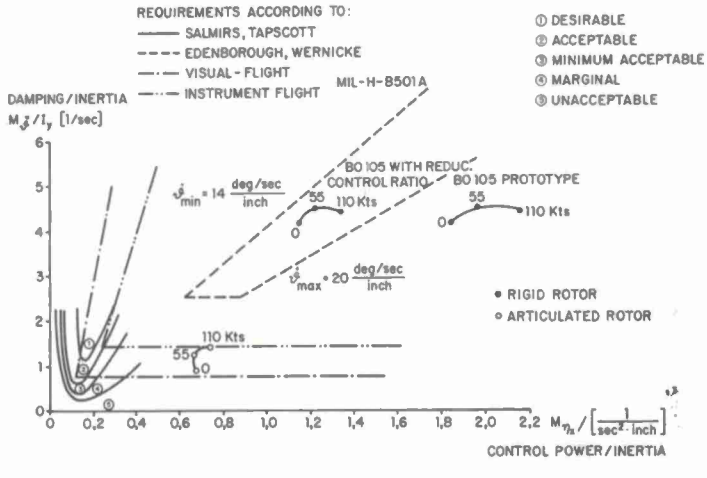


Figure 50 Control characteristics pitching

By assuming that the control is influencing the rotary motions of the helicopter primarily, it can be shown that the reciprocal values of the damping moments, referred to the moment of inertia represent the time constants of the system. The equation of the moments

$$J \cdot \dot{\omega} + M_{\omega} \cdot \omega = M_{\eta} \cdot \eta$$

has the corresponding transfer function

$$\frac{\omega}{\eta} = \frac{M_\eta}{M_\omega} \quad \frac{1}{1+(M_\omega/J)\cdot s} = \frac{M_\eta}{M_\omega} \frac{1}{1+\tau\cdot s} \text{ with } \tau = \text{time constant .}$$

The time constant is defined as the time required for reaching 63% of the stationary angular velocity after a control step input, see Figure 51. A high damping moment is resulting in a low time constant. Figure 51 gives an impression of the different time constants with the hingeless rotor and with an articulated rotor. For pitching the values are about 1.2 sec for the articulated rotor and about 0.2 sec for the hingeless rotor; the corresponding values for rolling are 0.3 sec and 0.05 sec, respectively. The times are shorter in rolling because of the smaller moment of inertia. When the time constant is short, the helicopter follows control motions more directly, i.e. the final angular velocity for a step input will be reached sooner, or for a harmonic control input the angular velocity will be better in phase with the control displacement. Figure 52 illustrates the phase angle of roll rate response as a function of the stick input frequency. For comparison, it is shown, that for fast stick motions, the roll rate of the H-13 is about 90° out of phase with the lateral stick motion (23). That means that the stick has to be to the right when the ship is banked to the left, still reacting from the previous left stick input. This lag makes the helicopter difficult to stabilize and to control during maneuvers. The hingeless rotor greatly reduces this lag. The phase angle is very small and therefore the pilot's control is nearly a rate type control, which is desirable. The frequency of the test points of about 0.3 to 0.4 is a normal frequency in controlling or stabilizing a helicopter.

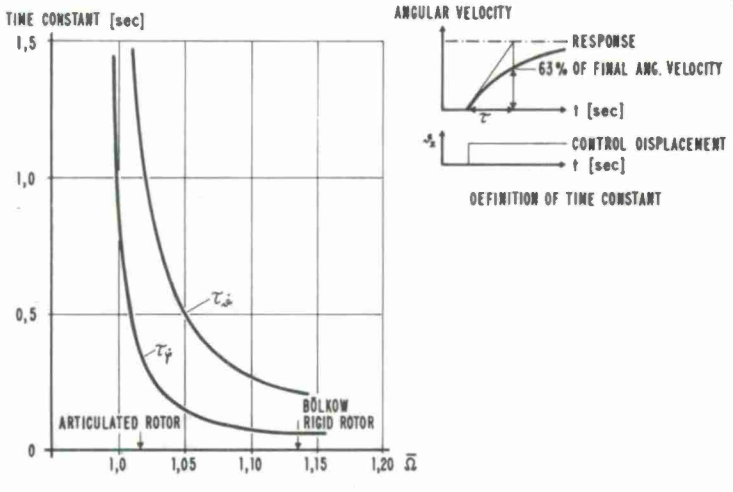


Figure 51 Time constants as a function of flapwise frequency

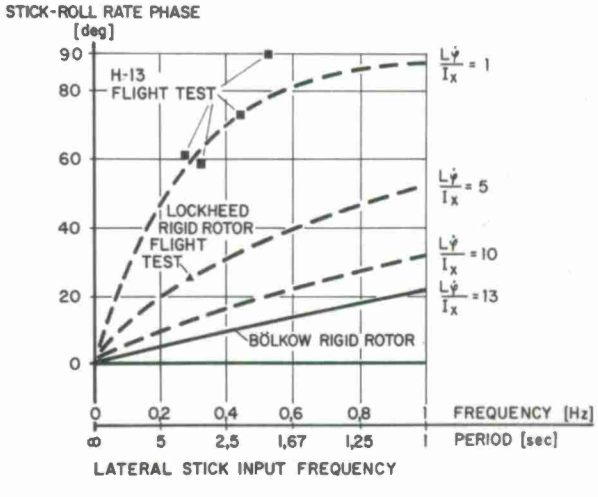


Figure 52 Stick-roll rate phase vs. control input frequency

Crosscoupling effects

Due to the dynamics of the rotor, there is a pronounced crosscoupling between pitching and rolling. By an optimization of the control phase between stick deflection and inclination of the swashplate, these crosscoupling effects have to be minimized. Figure 53 illustrates that such effects should not be critical neither for an articulated rotor (with flapping frequency ratio of 1.016) nor for a hingeless rotor (with a frequency ratio of 1.135). The figure depicts roll and pitch attitude response to the same control input for the articulated and the hingeless rotor. Results for different values of control phase angles are shown, i.e. the angle between stick motion and azimuth position of maximum cyclic pitch. It does not seem practical to choose the control phase angle corresponding to the lag angle of flapping following cyclic control, which is about 90° for the articulated rotor and about 70° for the hingeless rotor. The optimum control phase angle to achieve a pure pitch motion will be about 75° for the hingeless rotor and nearly the same for the articu-

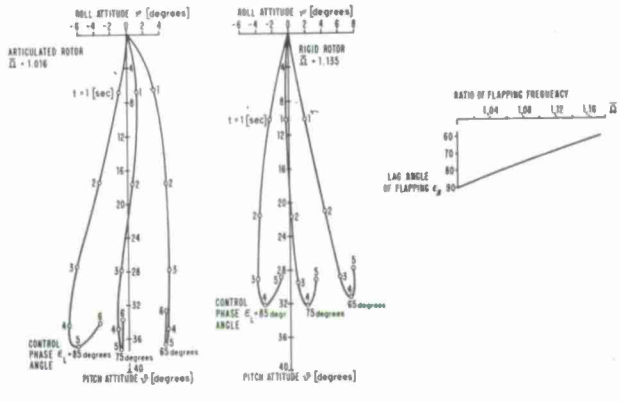


Figure 53 Crosscoupling effects at different control angles

lated rotor. Flight test experience using such control phase angles has shown that there are practically no problems with crosscoupling effects (24).

3.2 DYNAMICS OF FLIGHT

The aim of stability and control theory is to enable an aircraft to be designed with satisfactory flying qualities. The flying, or handling, qualities of an aircraft have been defined as the stability and control characteristics that have an important bearing on the safety of flight and on the pilot's impression of the ease of flying and maneuvering an aircraft. An introductory survey of helicopter stability would therefore most profitably concern itself with those factors that directly affect helicopter flying qualities. In addition to the control characteristics, which already have been reviewed in Chapter 3.1, the static and dynamic stability of the helicopter are determining the handling qualities. The dynamic behaviour of the helicopter is to a large extent affected by the stability parameters.

Because the mathematical theory of helicopter stability is a complex subject to the non-specialist, it is considered desirable to separate the fundamental ideas of helicopter dynamics from the mathematics to explain them in a rather general fashion. The discussion will follow some helicopter textbooks and reviewing reports, in parts directly, which can give a good introduction (4 ÷ 7; 19; 20; 25). There is a very large number of special papers dealing with helicopter flight dynamics, but only a few of them can be referenced here.

Introduction to stability

An aircraft is statically stable if there is an initial tendency for it to return to its trim condition after an angular displacement or after a change in translational velocity from that condition; it is unstable if it tends to diverge from trim after being displaced. An aircraft is neutrally stable if it tends to remain in the condition to which it has been displaced.

The dynamic stability of an aircraft deals with the oscillation of the aircraft about its trim position following a disturbance from trim. Figure 54 illustrates a stable and an unstable variation of amplitude. The period of the oszillation is defined as the time required for the oszillation to go through one cycle. The time to double or half the amplitude of the oszillation is defined as the time necessary for the amplitude of the envelope to double or half. This quantity is a measure of the degree of stability or instability.

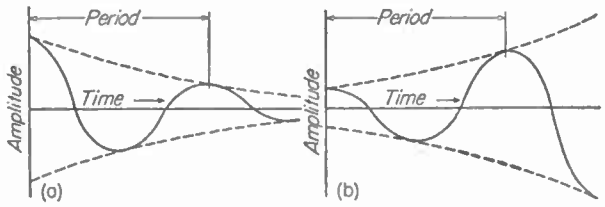


Figure 54 Stable and unstable oscillations

The dynamic motion of an aircraft after a disturbance or a control input is expressed by the following equations of forces and moments in a system of the co-ordinates fixed to aircraft

$$
\begin{aligned}
X:\quad & -m\cdot\dot{v}_{xG}\cdot d_{11} - m\cdot\dot{v}_{yG}\cdot d_{21} - m\cdot\dot{v}_{zG}\cdot d_{31} = -G_1\\
Y:\quad & -m\cdot\dot{v}_{xG}\cdot d_{12} - m\cdot\dot{v}_{yG}\cdot d_{22} - m\cdot\dot{v}_{zG}\cdot d_{32} = -G_2\\
Z:\quad & -m\cdot\dot{v}_{xG}\cdot d_{13} - m\cdot\dot{v}_{yG}\cdot d_{23} - m\cdot\dot{v}_{zG}\cdot d_{33} = -G_3\\
L:\quad & -I_{xx}\cdot\dot{\omega}_x + I_{xy}\cdot\dot{\omega}_y + I_{xz}\cdot\dot{\omega}_z = -G_4\\
M:\quad & +I_{xy}\cdot\dot{\omega}_x - I_{yy}\cdot\dot{\omega}_y + I_{yz}\cdot\dot{\omega}_z = -G_5\\
N:\quad & +I_{xz}\cdot\dot{\omega}_x + I_{yz}\cdot\dot{\omega}_y - I_{zz}\cdot\dot{\omega}_z = -G_6 \ .
\end{aligned}
$$

These equations are explicit with respect to the translational and rotational accelerations; the right sides G_i contain the lower time derivatives of the variables of flight and in addition the forcing forces and moments. The relation to the system of gravity axes is determined by the matrix of transformation

$$
\left[M_{GS}\right] = \begin{bmatrix} d_{11} & d_{21} & d_{31} \\ d_{12} & d_{22} & d_{32} \\ d_{13} & d_{23} & d_{33} \end{bmatrix} = \begin{bmatrix} \cos\psi_L\cos\theta_L & \sin\psi_L\cos\theta_L & \sin\theta_L \\ -\sin\psi_L\cos\phi_L + \cos\psi_L\sin\theta_L\sin\phi_L & \cos\psi_L\cos\phi_L + \sin\psi_L\sin\theta_L\sin\phi_L & \cos\theta_L\sin\phi_L \\ \cos\psi_L\sin\theta_L\cos\phi_L + \sin\psi_L\sin\phi_L & \sin\psi_L\sin\theta_L\cos\phi_L - \cos\psi_L\sin\phi_L & \cos\theta_L\cos\phi_L \end{bmatrix}
$$

in which the angles ϕ_L, θ_L and ψ_L define the attitudes of the aircraft. There is the relation

$$\begin{aligned}\omega_x &= \dot{\phi}_L - \dot{\psi}_L \cdot \sin\theta_L \\ \omega_y &= \dot{\theta}_L \cdot \cos\phi_L + \dot{\psi}_L \cos\theta_L \cdot \sin\phi_L \\ \omega_z &= \dot{\psi}_L \cos\theta_L \cos\phi_L - \dot{\theta}_L \cdot \sin\phi_L \quad .\end{aligned}$$

The choice of co-ordinate axes for the equations of motion is arbitrary. Since it is more convenient to express the aerodynamic and gravitational forces and moments with respect to body axes than to express inertia forces and moments with respect to wind or gravity axes, a body axis co-ordinate system is used commonly.

In the case of a helicopter, the equations of the blade motion have to be considered, in addition to the equations of motion of the helicopter itself.

By integrating the equations of motion numerically by a step-by-step approach, the motion of the aircraft following a disturbance or control input can be calculated. For pure stability investigations the equations will be linearized using the small-perturbation assumption that the variables of flight are small quantities and that their second and higher-order terms are neglegible. The forces and the moments are expressed in a Taylor series using only first order terms, e.g.

$$\begin{aligned}M = M_o &+ \frac{\partial M}{\partial v_x}\Delta v_x + \frac{\partial M}{\partial v_y}\Delta v_y + \frac{\partial M}{\partial v_z}\Delta v_z \\ &+ \frac{\partial M}{\partial \dot{\theta}_L}\Delta\dot{\theta}_L + \frac{\partial M}{\partial \dot{\phi}_L}\Delta\dot{\phi}_L + \frac{\partial M}{\partial \dot{\psi}_L}\Delta\dot{\psi}_L \\ &+ \frac{\partial M}{\partial \theta_L}\Delta\theta_L + \frac{\partial M}{\partial \phi_L}\Delta\phi_L + \frac{\partial M}{\partial \psi_L}\Delta\psi_L \quad .\end{aligned}$$

There are terms for every variable and its time derivatives. The dynamic derivatives of the aircraft are simply its mass and the components of its moment of inertia. In principle, aerodynamic derivatives exist with regard to displacements and accelerations as well as velocities. In practice, linear displacements of the aircraft have no effect on its forces and moments, and it can be shown that aerodynamic acceleration derivatives are insignificant under normal conditions of flight.

The linearized system has natural solutions of the form

$$\Delta x = x_o e^{\lambda t}; \quad \Delta y = y_o e^{\lambda t}; \quad \ldots$$

in which λ is the generalized frequency and is found from the characteristic equation

$$A_n\lambda^n + A_{n-1}\lambda^{n-1} + \ldots + A_3\lambda^3 + A_2\lambda^2 + A_1\lambda + A_o = 0 \quad .$$

This equation is obtained by the substitution of the solutions into the homogeneous equations of motion, and the coefficients A_J are expressions in terms of the derivatives and other machine constants.

The values of the roots λ may be positive, negative or complex occuring in pairs. A positive solution denotes physically a divergence, by which is meant an increasing departure from the equilibrium position. A negative solution means convergence - a gradual return to the equilibrium position. In the complex solution $\lambda = \delta \pm i\nu$ the combination gives an oscillatory motion with a frequency ν and a damping coefficient δ. The period of the oscillation may be expressed by $T = 2\pi/\nu$ and the time to half or double amplitude by $t_{H/D} = \ln 2/\delta. = 0.693/\delta.$

The general solution of the free motion of the aircraft is given in the following form

$$\begin{aligned}\Delta v_x &= v_1 e^{\lambda_1 t} + v_2 e^{\lambda_2 t} + \ldots \\ &\vdots \\ \Delta\psi &= \psi_1 e^{\lambda_1 t} + \psi_2 e^{\lambda_2 t} + \ldots \quad .\end{aligned}$$

Each solution λ_J of the frequency equation represents a mode of motion characterized by the constants $v_J \ldots \psi_J$. In practise it is often found that some of the coefficients are very small, and in this sense it can be said that a solution of the frequency equation is physically equivalent to a simple motion involving predominantly only one or two variables.

The frequency equation gives rise to get another definition of static stability. It is determined by the sign and magnitude of the coefficient A_o in the frequency equation. A positiv A_o means positive static stability, a negative A_o static instability. It can be shown mathematically that a positiv A_o is a necessary though not sufficient condition for

dynamic stability. It is worthwile to mention that for a positive all-round static stability A_o, it is not necessary for all static stabilities describing the restoring moments and forces to be positive.

Most helicopters are dynamically unstable. Dynamic stability is not essential; but it is generally assumed that dynamic stability is desirable, though it is not fully clear which of the parameters describing the oscillation after a disturbance is most significant. The natural period and the damping (or amplification) factor may have an independent significance, or may be combined in a third parameter expressing the time taken to double or half the amplitude of the disturbance.

The reviewed methods and assumptions in the study of the free motion are following the methods of classical mechanics and the classical theory of differential equations; but the language and the methods of modern control theory can be used as well. The pilot usually flies the airplane by the feedback method - that is, he senses by sight or feel the motion of the aircraft, and moves the control so as to reduce the difference between actual and some desired motion. The pilot "closes the loop". The free motion of an aircraft is determined by the "open-loop" characteristics.

By taking the Laplace transform of the equations of motion and expanding the necessary determinants, the transfer functions relating the variables of flight (x) to control inputs (y) or other disturbances may be written in the form e.g.

$$\mathcal{L}\{\frac{x}{y}\} = \frac{B_n\lambda^n + \ldots + B_1\lambda + B_o}{A_n\lambda^n + \ldots + A_2\lambda^2 + A_1 + A_o} \quad .$$

The roots of the numerator and denominator of this expression are known respectively as its zeros and poles. It develops that poles of the transfer function determine the modes which can be considered to make up the response, they are the roots of the characteristic equation or so-called stability equation derived from the homogeneous equations of motion. As such, the poles are common to the transfer function of all variables whereas the zeros determine how much of each mode will appear in the response of any given varibale. Consequently knowing the poles of the transfer function gives a good description of the response to be expected, wether it will be stable or unstable.

Since the roots will have complex values it is convenient to display them on the complex plane plotting the imaginary part against the real part. It is then possible to associate certain characteristics with the location of the poles on this diagram. If a pole has a positive real part, the mode is unstable, so that all poles on the right half of the complex plane are unstable while any on the left are stable. Complex roots always appear as conjugates yielding oscillating modes, the imaginary part being the frequency in rad/sec and the real part being the time constant of the exponental envelope determining the rate of decay. To convert the co-ordinates of this plot into more easily visualized physical dimensions, it is a simple matter to substitute period in seconds for the frequency along the imaginary axis, and the time to double or half amplitude for the reciprocal time scale of the real axis. This conversion is illustrated in the plot of the complex plane in Figure 55.

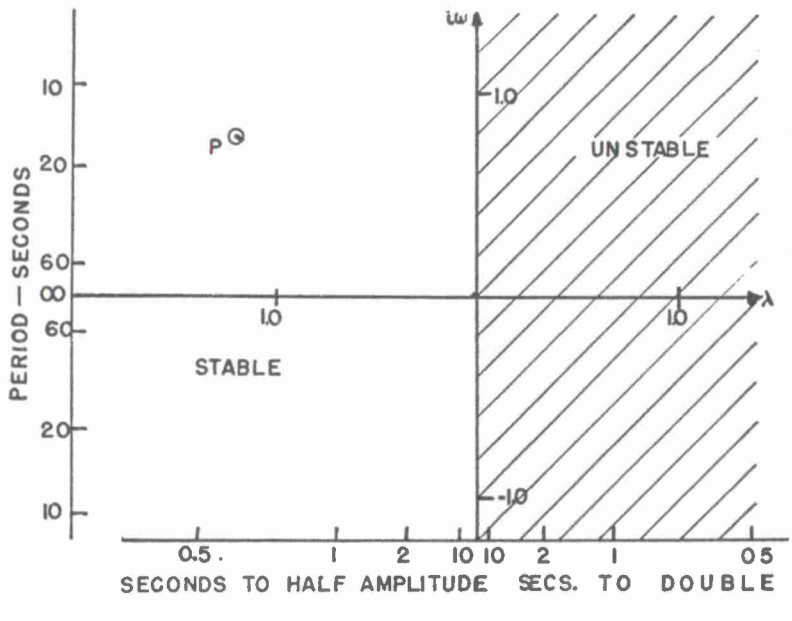


Figure 55 Roots on the complex plane

In the complex plane the loci of the roots for a variation of a parameter easily can be visualized; and the root locus methods are most helpful in the design of automatic stability and control systems.

Helicopter static stability

It is customary to split the six degrees of freedom of a helicopter into two groups of three each. One group is known as the symmetrical and comprises longitudinal (x) and vertical (z) linear motion and rotational motion about the pitching axis (ω_y). The other group is the asymmetrical and embraces the remaining degrees of freedom, namely linear motion in the lateral direction (y) and angular motions about the rolling (ω_x) and the yawing (ω_z) axes. This separation follows airplane practice. For helicopters, the cross-derivatives between the two groups are normally not negligibly small, so that the sepa-

ration is only very approximate; but it seems to be suitable to get an understanding of the fundamentals.

Most important is the symmetrical motion of the helicopter. Inasmuch as the helicopter can be displaced in pitch (angle-of-attack change) or by a change in forward speed or vertical velocity, three aspects of static stability exist because of the three sets of forces and moments produced by these two changes. In the following discussion only the most significant terms will be discussed.

For a rotor mounted on a helicopter, the effect of the translational velocity is to tilt the tip-path in a direction away from the velocity of translation (as shown in Figure 39). This tilting of the rotor plane is a result of blade flapping. The rotor plane will tilt farther backwards with increasing translational speeds, inasmuch as the velocity of the advancing blades becomes increasingly greater than the velocity of the retreating blades. This tilt of the rotor plane due to translational velocity will produce a moment about the helicopter center of gracity. The moment will be nose-up with increasing speed and nose-down with decreasing speed. The variation of moments due to changes in translational velocity is a measure of stability with speed, which can be expressed mathematically as $\Delta M/\Delta V_x$ or M_{V_x}. Inasmuch as nose-up moments are considered positive, M_{V_x} is positive for the helicopter, it tends to reduce the velocity. In addition to the moment a force X_{V_x} with a stabilizing tendency is produced. As was shown in Chapter 2.2 a change in attitude of the hovering helicopter (which is prevented from translating) results in an equal tilt of the rotor plane with the result that no rotor moment or change in thrust occurs. Thus, the hovering helicopter has neutral stability with attitude change. In forward flight, however, a change in longitudinal attitude (fuselage angle of attack) will produce a rotor moment and a thrust change. This moment, which is due to a change in fuselage angle of attack at constant velocity, arises from the change in flapping (tilt of the rotor plane relative to the fuselage) and the combined change in inflow. The contribution is in an unstable sense normally; but it depends to a large extent, as can be shown, on the collective pitch of the rotor causing a different behaviour of the helicopter operating at a high collective pitch and operating at low collective pitch in autorotation. The angle-of-attack or attitude stability has additional contributions from the fuselage in unstable sense and from a stabilizer in a stable sense, as illustrated in Figure 56. The figure shows, that a rigid or hingeless rotor produces a larger destabilizing moment compared to an articulated rotor. To obtain stable moment conditions, a rigid rotor helicopter would need a larger stabilizer than a helicopter with articulated rotor.

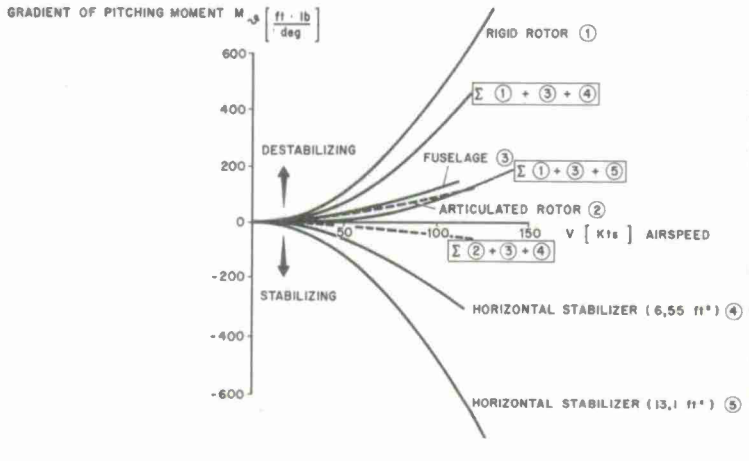


Figure 56 Pitching moment derivative with respect to angle of attack vs. speed

The derivative of the vertical force Z with regard to vertical velocity V_z which is called vertical damping is stable.

Considering the all-round static stability represented by the constant term A_o of the characteristic equation, it can be shown to be proportional to

$$- M_{\theta_L} \cdot Z_{V_x} + M_{V_x} \cdot Z_{V_z} \quad .$$

Without a stabilizer M_{θ_L} normally will be positive resulting in a negative or unstable constribution to A_o for a positive Z_{V_x}. At higher flight speeds Z_{V_x} may change sign resulting in a changed behaviour. M_{V_x} normally is stable, but may change sign at high forward speed, too. These relations may lead to the conclusion that it is very difficult to operate with the different static stabilities which are the derivatives of the forces and moments with respect to the variables of flight, and that a statement about the all-round static stability necessitates a relatively accurate investigation.

For good handling characteristics static stability with respect to the stick position is considered to be essential, meaning that for a higher speed always a larger stick displacement will be necessary. The stick position gradient is strongly influenced by the derivative M_{V_x} (change of moment with respect to speed). In forward flight, at some high enough speed, velocity stability may change sign, and negative values will lead to unstable trim gradients. A more accurate consideration would show that other derivatives are involved, in addition, and that there is a relation between the all-round static stability and the stick position gradient.

A stable stick position gradient is desirable also during maneuvers. As Figure 57 is illustrating, the stick position characteristics are very sensitive and may be influenced by small modifications in the design parameters of the rotor. The figure gives a comparison of the maneuver-characteristics with two different blade airfoil sections. On the rotor with symmetrical 0012-profile section a turn of stick travel over g is reached at a maneuver range of about 1.5 g. By the use of a unsymmetrical profile section the stick in-

stability is postponed to higher maneuver loads.

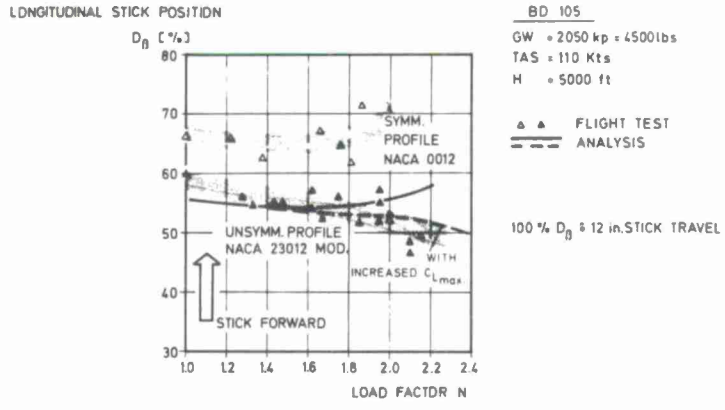


Figure 57 Longitudinal stick position during maneuvers

Helicopter dynamic stability

The simplest analysis of dynamic stability deales with hovering flight. Most of the derivatives of the forces and moments are functions of the speed of flight, and many of them are zero in hovering. In addition, it can be shown that vertical motions and control are independent of translation and pitching motions, and their control. In hovering or at very low speeds the vertical component of motion does not influence the horizontal forces or the moments about horizontal axes, whilst horizontal or tilting motion does not affect the thrust. Therefore, the coupling between these degrees of freedom can be removed. This altogether causes a major simplification for analysis and for piloting.

For the sake of simplicity, separation of longitudinal and lateral motions is assumed. In the single rotor configuration there is no difference in principle between the two - only the moments of inertia, with which each of these groups of motions is associated, are different.

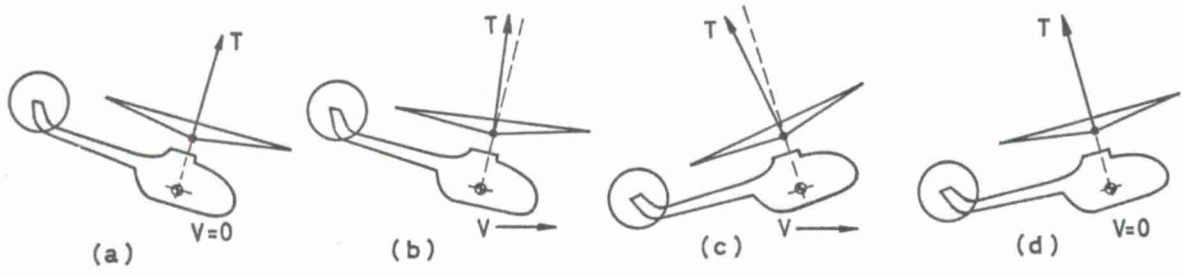


Figure 58 Oscillation of a helicopter following an angular displacement in hovering

First, a brief explanation of the dynamic instability of a helicopter in hovering flight will be given. The motion after an initial angular displacement of a helicopter is as follows (see Figure 58): The inclination of the rotor produces a horizontal force and the helicopter starts to move horizontally. The relative flow at the rotor causes a restoring moment due to the static stability with speed; this moment tends to return the helicopter to its precious position so that its motion is decelerated to zero. However, the restoring moment will turn the helicopter beyond its neutral position, therefore, the helicopter will start to move in the other direction. Due to the rotary motion itself, an additional restoring moment, known as pitch damping, is produced. This pitch damping normally is small compared to the restoring moment of speed stability. Thus it happens that the process of motion, composed of a back-and-forth motion with a rotory motion, is steadily amplified in the form of an unstable oscillation.

In the mathematical evaluation, especially for more rough investigations, the motions of the rotor may be considered in a quasistatic treatment, meaning that there are no further degrees of freedom of the rotor itself and that there are certain relations between the rotor motion and the helicopter motion. The first order flapping in longitudinal and lateral directions, which have to be considered for the forces and moments, are no degrees of freedom in such an approach. The criterion of applicability of the quasistatic treatment is given by the frequency ratio between the free helicopter oscillations and the blade frequency which are in an other order of magnitude, normally.

Using these assumptions, the equations of longitudinal motion of a hovering helicopter render a cubic frequency equation. One of the three solutions represents a heavily damped motion, which is nearly of no practical interest. The other two solutions represent a periodic motion in both degrees of freedom having a period and a damping coefficient. All present-day helicopters with hinged blades or hingeless articulated blades of high elasticity exhibit an unstable free oscillation. But the parameters of the instability

very a great deal.

The most important stability derivatives are those of the moment equation, specifically the speed and angular velocity derivatives. An improvement in the characteristics of the instability could be expected if it would be possible to increase the pitch damping and to decrease the static speed stability. A more detailed calculation reveals that, generally, stable derivatives of the "direct" kind (such as pitch danping, which is a moment derivative relative to angular velocity) reduce dynamic instability, but stable derivatives of the "coupled" type (such as speed stability coupling a moment to a translational motion) increase dynamic instability.

In Chapter 3.1 was deduced, that pitch damping can be influenced strongly by the moment of inertia of the blades expressed by their mass constant γ. In addition and still to a higher amount, pitch damping will be enlarged by the introduction of offset flapping hinges or by a hingeless rotor. Results of a hovering flight stability analysis done with different offset hinge distances are shown in Figure 59. The typical helicopter, used in the calculations, would have a time to double amplitude of about 5 sec; a small hinge offset would increase this value to about 9 sec, whereas a hingeless blade attachment could bring it up to about 27 sec. The period of the motion is not strongly influenced. The improvement in stability is especially distinct in Figure 60. In this diagram, the motion curves are plotted for the four degrees of freedom: pitch, roll, forward speed and lateral speed following an initial pitch displacement. Because of the coupling effects between the individual degrees of freedom, all motion components are unstable. The instability is lowest with a hingeless rotor. It should be mentioned that the helicopter with the hingeless rotor has excellent control characteristics, too, as described in Chapter 3.1. The helicopter of the diagram, with zero hinge offset, would have poor flying qualities because both stability and control characteristics are poor.

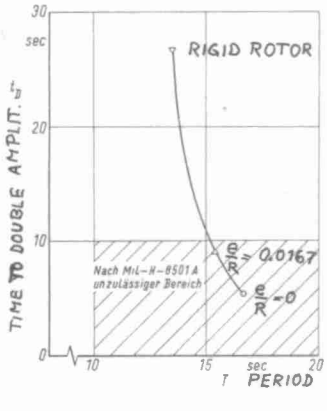


Figure 59 Stability values of a hovering helicopter

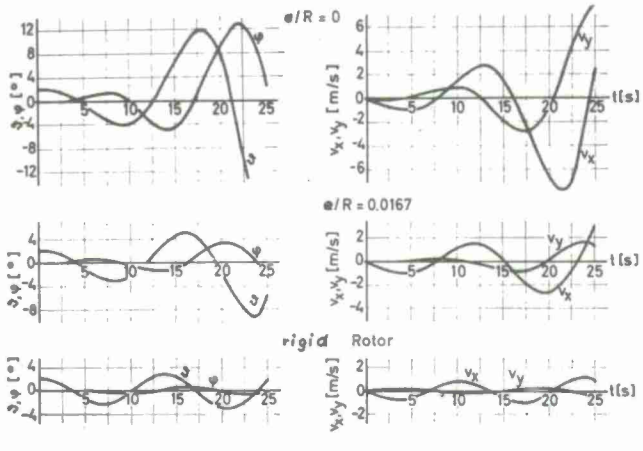


Figure 60 Motion curves following an initial pitch disturbance

In forward flight, the separation of the longitudinal and the vertical motion no longer is possible; and the unstable static stability of the moment with respect to changes of attitude or angle of attack, which is zero in hovering flight, gets more and more important. Figure 61 illustrates results of a forward flight stability analysis for a helicopter with an articulated and with a hingeless rotor. Period and time to half or double amplitude of the most critical roots of the characteristic equation are plotted versus speed. For the helicopter with articulated rotor, the period is increased in forward flight relative to the value of hovering flight, and the instability (characterized by the time to double amplitude) is decreased changing to a stable oscillation at a flight speed of about 85 knots. This behaviour is mainly determined by the influence of the horizontal stabilizer. For the helicopter with a hingeless rotor the period changes only

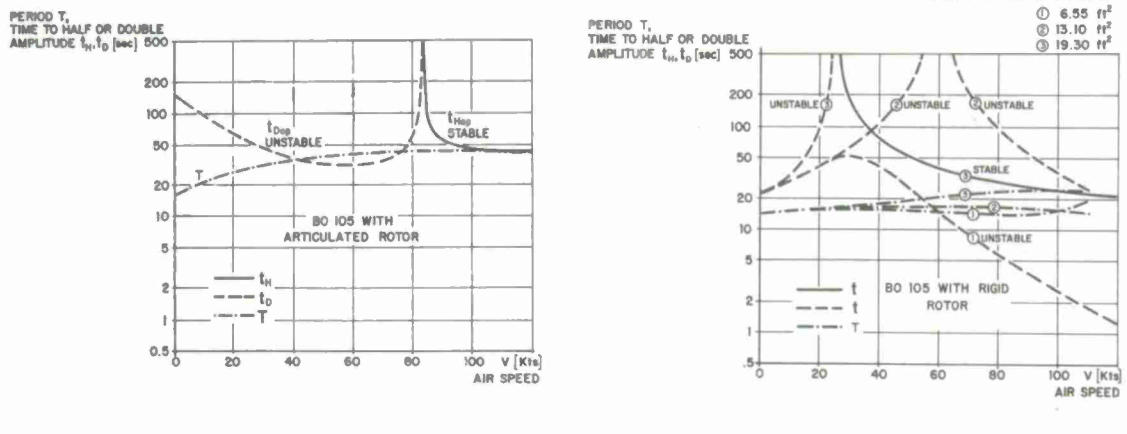


Figure 61 Forward flight dynamic stability characteristics

slightly with speed, but there is a strong tendency to a high instability at high forward speed caused by the very strong moment instability with respect to attitude. The instability at high speed can be reduced by enlarging the stabilizer.

Hingeless rotor helicopters, like the BO 105, are flying with such instabilities at high speeds, and it is quite surprising that the pilots feel them to be good in handling. This can be understood only in such a way, that they do not feel the instability because of the excellent control characteristics of the hingeless rotor helicopter. In the fact, really this happens as can be shown by simulation studies or mathematical evaluation using a mathematical representation of the pilot. Figure 52 illustrates some results of such an investigation plotting the stability values of the closed system helicopter and pilot with the parameters of the pilot, which are lead time constant T_L and gain K_P. The instability without pilot has a time to double amplitude of 2.5 sec; and the figure shows that even for the most simple model of a pilot without lead there is a broad region of stability. The best stability values of the diagram with a time to half amplitude of 2.4 sec is only slightly improved with a lead in the pilot's reaction. Zero lead and the used gain is a normal reaction of a pilot without special skill, thus resulting in good pilot ratings.

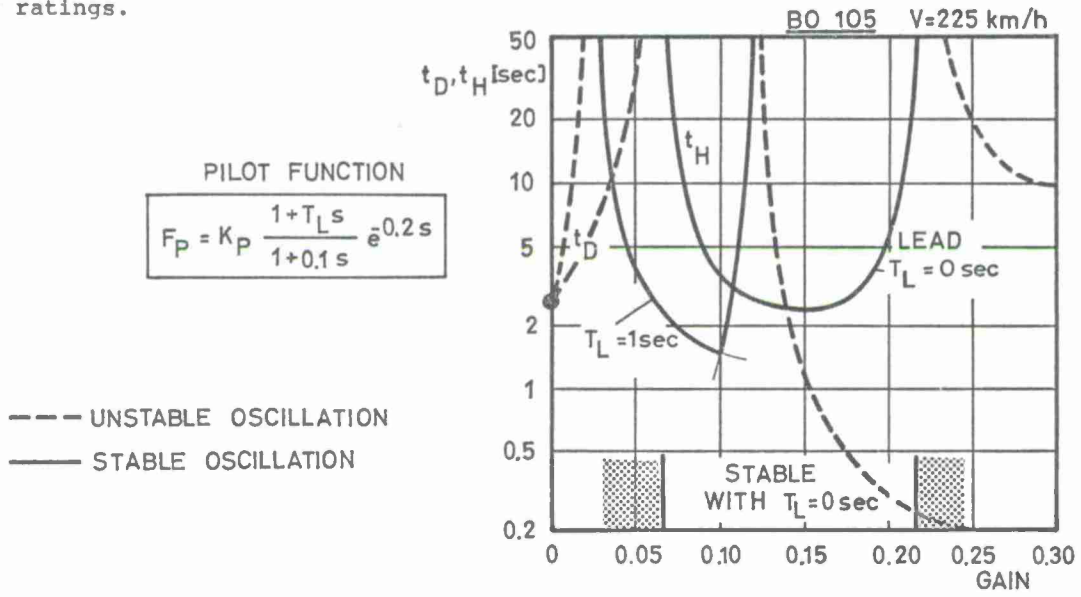


Figure 62 Stability characteristics of the system helicopter-pilot

From this behaviour it must be concluded that separated investigations of control and of stability characteristics are not sufficient and may be misleading sometimes. The control characteristics are the more important, and instability seems to be critical only in combination with poor control characteristics.

Maneuver capability

Whilst for the older helicopters too little consideration was given to handling characteristics, the requirements for good flying qualities are influencing the design parameters of modern helicopters very strongly, and important improvements could be achieved. The application of the helicopter as a military vehicle including missions as a weapons platform will demand still improved qualities.

The older helicopters were given a bad name, and rightfully so, for requiring great pilot skill just to fly them. These characteristics left the pilot little time to perform missions other than flying. These traits limited the overall practical utility of the helicopter to daytime visual missions. Now with increased performance capabilities and increased emphasis on the combat utility of helicopters, handling qualities have to be provided which assist, not just allow, the pilot to perform the assigned mission.

The maneuverability, which seems to be most important for modern utility helicopters, especially for military helicopters, may be defined as the ability to execute a maneuver or to make rapid changes in its flight path and attitude under the precise control of the pilot. Maneuverability is described in terms of achievable attitudes, speeds (angular and linear in all directions) and accelerations (angular and linear in all directions) and combinations of these variables.

Important maneuvers are, for instance:

hovering maneuvers (turns, jump take-offs and qzick discents),
accelerations and decelerations,
target acquisition, weapons delivery and evasive maneuvers (26).

Time histories of load factor during a sharp, decelerating turn and a steady turn at high speed are shown in Figure 63. In the decelerating turn, the design load factor was reached briefly. Load factor varied over a wide range throughout the maneuver. In the high speed turn, since rotor speed and forward speed were not allowed to droop, the load

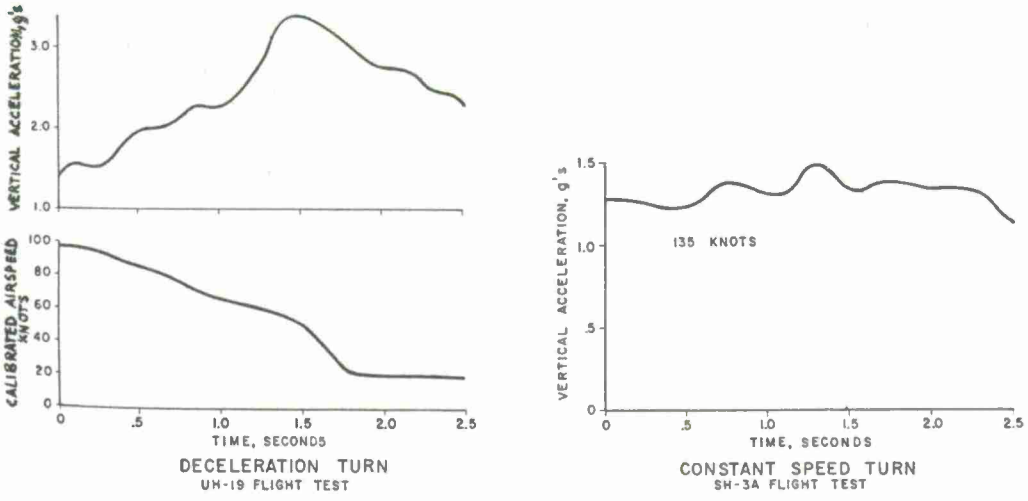


Figure 63 Time history of load factor during turns

factor was lower and more nearly constant. A typical turn maneuver is described at the left side of Figure 64, at the right side the different results in time and distance are shown for different initial velocities. Figure 65 illustrates the envelope of target acquisition maneuvers including the possibility to make the return in minimum time by employing a climbing turn.

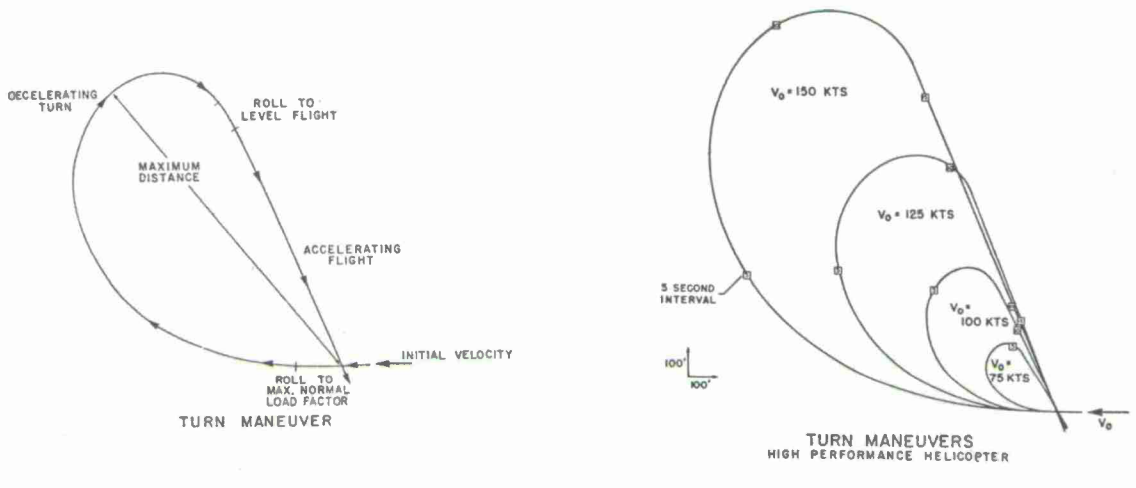


Figure 64 Turn maneuvers

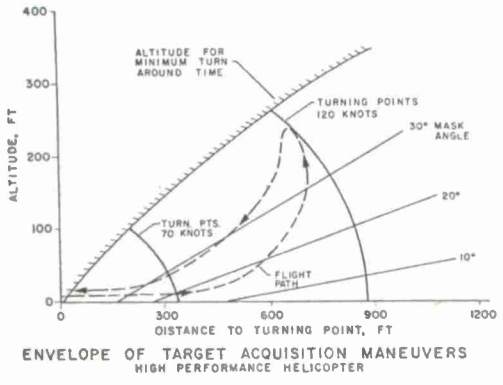


Figure 65 Envelope of target acquisition maneuvers

Considering maneuverability, the load factor capability is most important. For each helicopter design, load factor versus airspeed curves can be prepared as in Figure 66. The limits are power in a steady turn and rotor stall in a deceleration turn. The rotor stall limits can be shifted to higher values of load factor or speed by an additional wing, as shown in Figure 67. Different mission requirements will require different load factors at different speeds indicated in the diagram by (a) to (d), but there is no doubt, that for future helicopters g-levels over 2.0 up to high speeds will be required.

As a typical requirement for a new design, the UTTAS terrain-avoidance maneuver may be considered. It requires pull-up to achieve 1.75 g's at 150 knots within 1.0 second, sustain 1.75 g's for 3.0 seconds, push-over to achieve 0.0 g for 1.0 seconds.

Such maneuvers require, in addition to the load factor capability, excellent control characteristics during the whole maneuver. In this regard, hingeless rotor systems offer good characteristics, their controllability is nearly unchanged versus speed (see Chapter 3.1).

Unloading the rotor by an auxiliary wing improves the load capability at high speeds, but it may cause additional problems considering the control characteristics, e.g. reduced

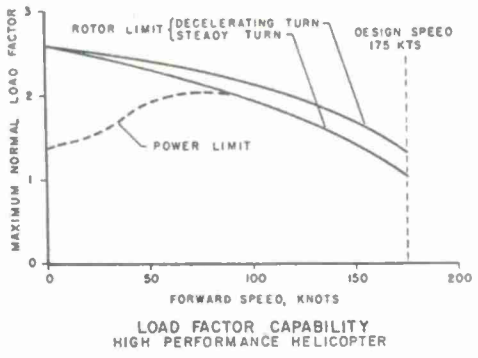


Figure 66 Load factor capability

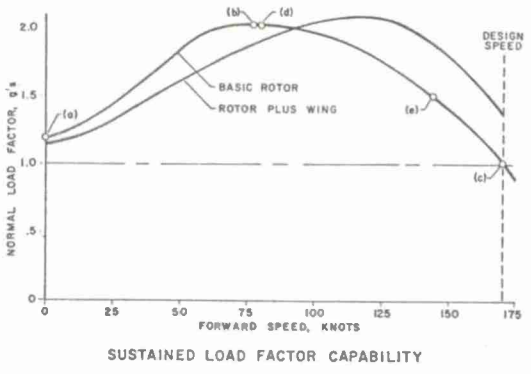


Figure 67 Sustained load factor capability

control power with articulated rotors or difficulties for the high speed autorotation entry (autorotation entry causes a nose-up attitude change by which the wing will be still more loaded). In many cases, an over-bladed rotor design could be more effective than an additional wing (over-bladed means a rotor which is aerodynamically lowly loaded in normal conditions of flight).

The theoretical tools to handle even extreme maneuvers seem to be sufficient. Figure 68 shows a comparison of theoretical and flight test data for one of the most extreme maneuvers, a loop. Some of the modern helicopters offer the potential for acrobatic flight, for loops and rolls or horizontal spirals.

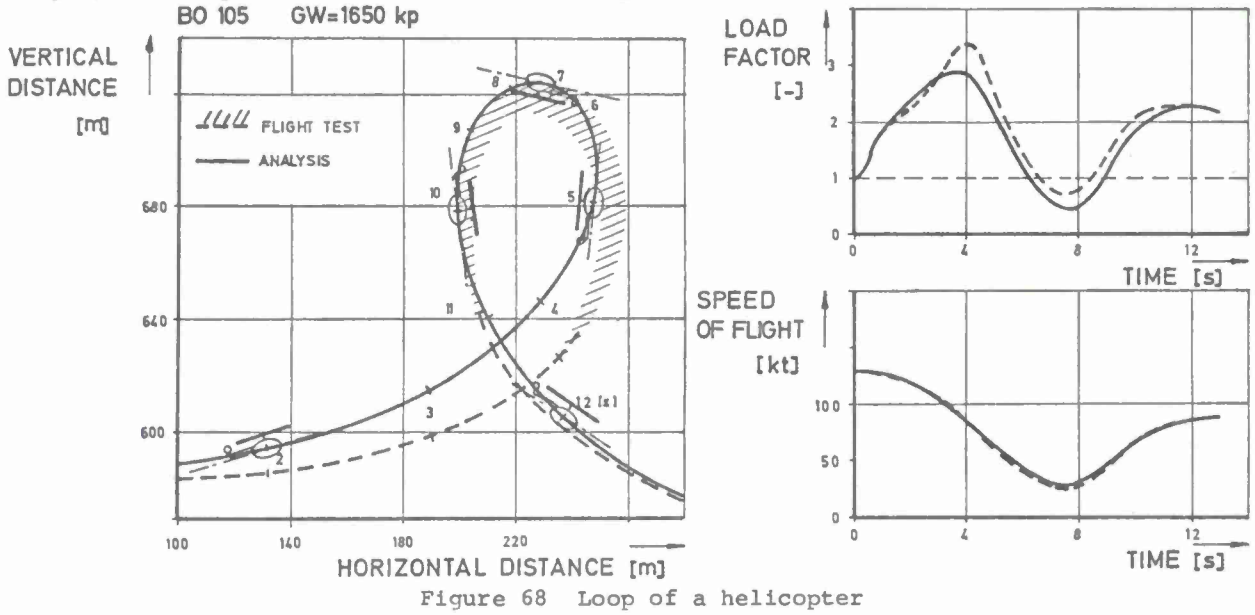


Figure 68 Loop of a helicopter

3.3 STABILITY AND CONTROL AUGMENTATION SYSTEMS

General remarks

The kind of artificial stability, which will be considered here, is where signals proportional to the variables of flight are mixed with the pilot's control displacements to command the final control deflection. By this way, the stability derivatives can be altered, and it is possible to reach stability.

There is considerable difference of opinion among the people feeling to be expert about the merits and utility of artifical stability for helicopters. Most of the discussion is about the necessity of stability devices. If there is a reasonable way to attain good handling qualities without devices, then their cost and complexibility should certainly be avoided. But there is no doubt, that stability and control augmentation systems will assist the pilot in IFR-flight and during extreme maneuvers, expecially for military missions. The latter will necesitate relatively complex systems because they have to be complete control systems for which it is not sufficient to improve only the stability characteristics.

Mechanical devices

A limited degree of artificial stability can be produced by strictly mechanical systems. The Bell stabilizer bar and the Hiller control rotor are of this type - see

Figure 69 and 70. The bar or the servo-rotor behave like gyro generating signals proportional to changes in attitudes and to the rate of this changes. An important parameter is the damping of these systems, which are a mechanical damper for the Bell bar and aerodynamic damping for the Hiller servo-rotor. This damping causes that the rotating devices will follow the oscillation of the helicopter with a certain lag. Such devices really can give stability because the effective control signals are proportional to the attitude and the angular rate. Kinematically the two systems are very different. The Bell stabilizer bar is displaced, the manual control linkage acts as a datum point. The Hiller stabilizer is also used as a servo control. It can be said, that the stabilizer is introduced in series between the manual control and the control of the main rotor blades.

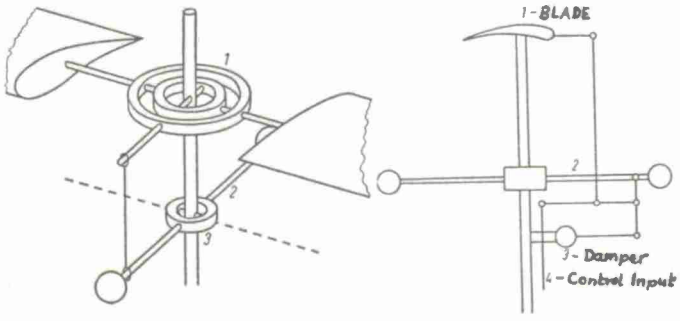


Figure 69 Bell stabilizer bar

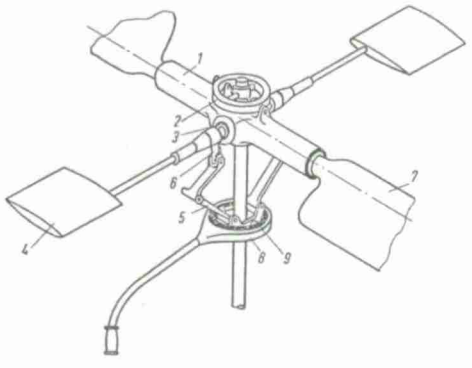


Figure 70 Hiller servo rotor

In modern helicopter designs, such mechanical devices are no longer used because they give additional mechanical complexity and because the improvement in stability is combined to a certain amount by a deterioration of the control characteristics. Modern electronical systems are superior by far. In the more recent era, only for the Lockheed rigid rotor system a control gyro system was developed (see Figure 71), and it is no secret that it caused so many problems, which could not arise with an electronic device.

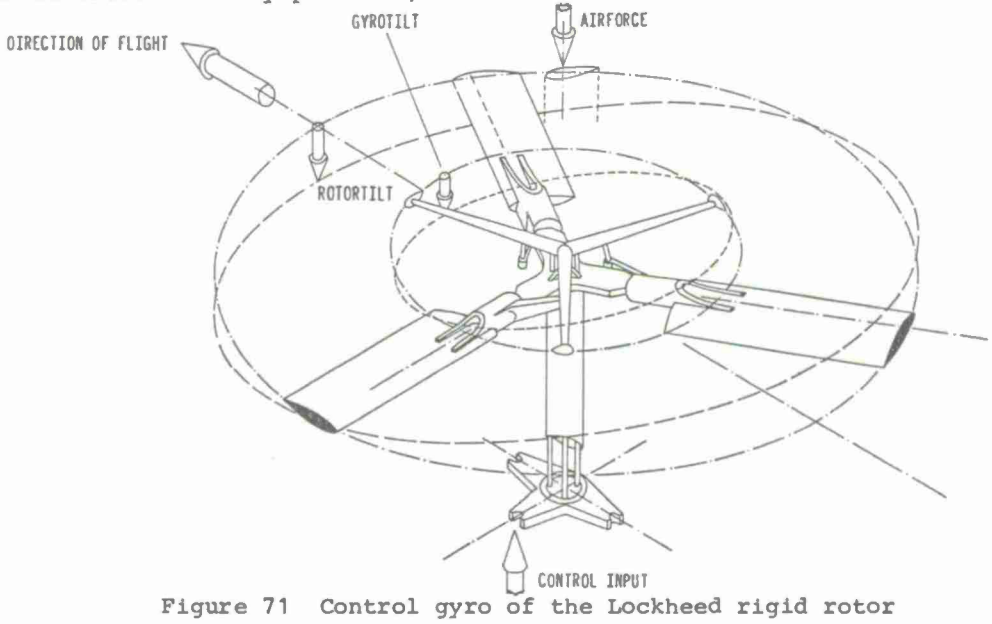


Figure 71 Control gyro of the Lockheed rigid rotor

Modern stability and control augmentation systems

It is to state that the design and utilization of stability and control augmentation systems is highly complex and filled with many aspects going far beyond the scope of this introductory review.

To correct the helicopter instability an autostabilizer must apply control inputs which contributes both a restoring moment and damping as can be seen from Figure 72, (27). In the figure the individual effects of feedings back a control correction proportional to the attitude, to the angular rate, and the angular acceleration for a typical hovering helicopter are considered. Neither rate nor acceleration feedbacks by themselves can stabilize the unstable mode; while the plot does indicate that proportional feedbyck does bearly achieve stability. A combination of both, attitude and rate signals, seems to be optimal, see Figure 73.

In this case, the control equation is

$$B_1 = - k_\theta \cdot \theta_L - k_{\dot\theta} \cdot \dot\theta_L \quad .$$

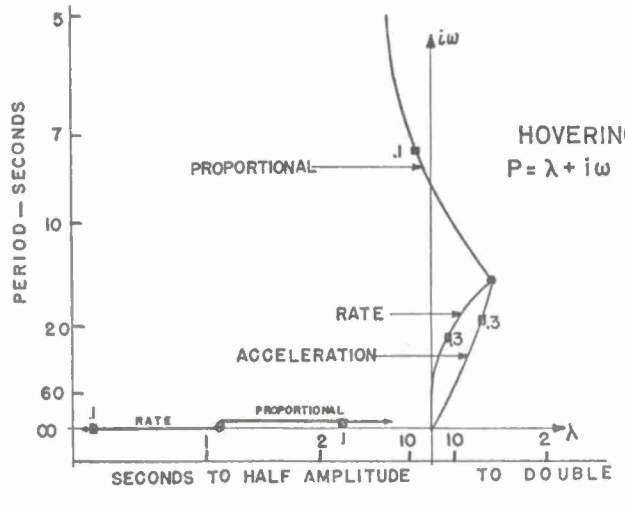


Figure 72 Effect of proportional, rate and acceleration feedback

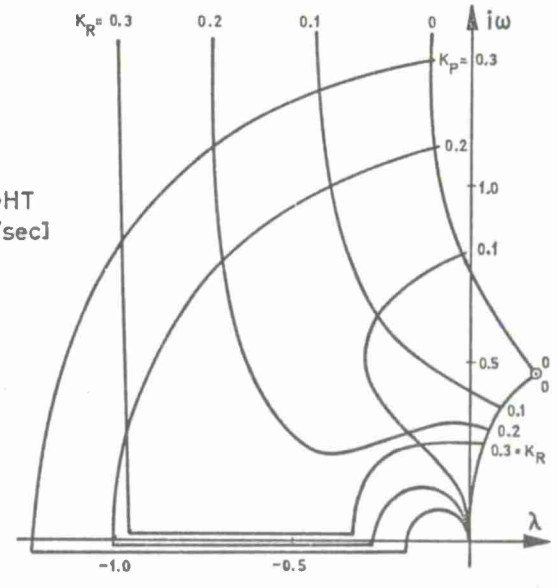


Figure 73 Effect of combined proportional and rate feedback

Based on this control equation, there are two different types of helicopter auto-stabilizer currently in use, and there are some interesting arguments concerning their relative merits (28).

The SAS (Stability Augmentation System) is a typical example of a limited authority series automatic control system in which pilot's control inputs and stabilisation demands are mixed and applied to the controls. A block diagram for the pitch channel is shown in Figure 74.

In the SAS the control is produced by using a rate gyroscope as the basic sensor. This gives a pitch rate signal which is integrated, using what is referred to as a "leaky integrator" technique, to produce something that appears like an attitude error signal. In this case, the control equation becomes

$$B_1 = -\left[K_{\dot{\theta}} + \frac{K_O n}{1+ns}\right] \cdot \dot{\theta}_L$$

n is the time constant of the leaky integrator and the term $K_O \frac{n}{1+ns} \cdot \dot{\theta}_L$ replaces $k_o \cdot \theta$.

In simple terms the use of the leaky integrator produces, in response to a disturbance, a signal which is proportional to the angle through which the helicopter is displaced from the datum existing at the time of the disturbance. Hence, control can be applied to reduce this angular displacement to zero. The presence of the "leak" in the integration means that if the helicopter does not respond to the corrective control application, or is actually held in the new attitude, for example by the pilot, the integrated θ signal would disappear in a short time and the helicopter would regard its new position as its datum.

In practice, this means that the control system will try to maintain any datum to which the helicopter is trimmed and will return the helicopter sensibly to this datum if disturbed, so that it behaves like a stable trimmed aircraft.

The long term attitude holding performance of such a system depends in the main on two factors, the threshold sensitivity of the rate gyro and the time constant of the leaky integrator. The latter is a matter of careful design, the former a function of the gyro chosen. Typically a gyro with the ability to measure a maximum of 30°/second, which is suitable for an auto-stabiliser application, will have a threshold sensitivity better than 2° minute. Thus any practical disturbance likely to be encountered by the helicopter will be detected and corrected and any divergence from a fixed path will occur at a rate slower than the threshold sensitivity of the gyro. This means that, with a correctly designed SAS, hands-off flight for several minutes is possible. The pilot's work load when flying with such a system is reduced to an occasional monitoring of the flight path either by visual or instrument references. The salient features of an SAS type system are:

- It is simple and robust. It is based on a small and inherently reliable rate gyro, independent of the flight instrumentation.
- The system requires no electrical trimming or setting up for varying cg positions or flight conditions since, whatever the attitude of the helicopter, there is zero input to the servo when there is no rate and no displacement from the instantaneous datum.
- The relationship between stick position and speed, or attitude, is not affected by the presence of the SAS servo and the overall response of the controls is not materially affected by the series servo.

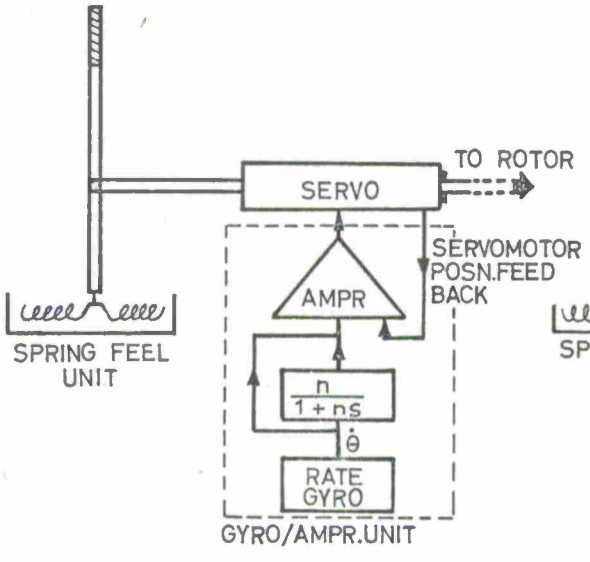


Figure 74 SAS (pitch channel)

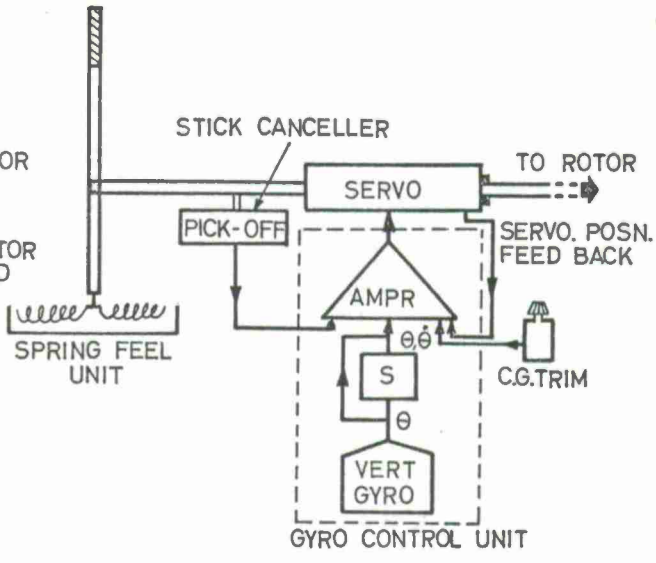


Figure 75 ASE (pitch channel)

In the ASE-type(Automatic Stabilisation Equipment)the control equation is generated in the usual autopilot form. The basic sensor is a gyro vertical producing a θ signal (for the pitch axis) and this is normally differentiated by means of a passive network to produce some $\dot{\theta}$. A typical system is shown in Figure 75.

It will be understood that the use of a genuine θ signal normally implies a real attitude datum,and to be able to fly the helicopter at any attitude or speed it is necessary that this datum should be variable. Similarly, the ability to maneuver depends on the ability to shift the datum since, if this were not possible, the automatic system would tend to oppose any pilot's stick input and try to drive the helicopter back to where it was. This, of course, is similar to the situation when maneuvering with an SAS but, with SAS, any opposing signal dies away immediately a steady state attitude is achieved.

In an ASE system the maneuvering capability is provided through the medium of a device often called a "stick-canceller". The signal from this, which is produced when the pilot displaces the control from the set datum, does two things. First, it tells the equipment that the pilot wishes to maneuver and backs off the vertical gyro signal which is produced as a result of a maneuver. Second, when the stick is trimmed to a new datum position appropriate to the desired flight conditions, it establishes the new reference datum for the gyro vertical. This simple solution gets over, in the main, the basic difficulties of using a vertical gyro as a reference but introduces an interesting result as far as control characteristics are concerned.

In effect it relates aircraft attitude directly to stick position in a linear fashion and produces a response to the flying controls in which attitude change rather than rate of change of attitude is proportional to stick displacement. It should be remarked that unusual characteristic is particularly significant in the roll channel where it requires a technique for turning by holding the stick over to maintain the desired bank angle. This is instead of effectively centralising it once the bank angle has been established.

The fact that the ASE, thus described, defines a particular relationship between stick position and attitude, requires the addition of another control input to the automatic control system. This is a trimmer (usually referred to as a "cg trim"), the purpose of which is to center the series servo for any given flight condition. The trimmer deals with the small differences between the theoretical and actual relationship between stick and attitude and in particular copes with cg shift.

The advantages claimed for the ASE system are: -

- It holds attitude indefinitely, irrespective of time and maneuver.
- In a maneuver, in the event of any emergency or external disturbance, the pilot need only release the stick to roll out of a turn and establish straight and level flight.

To summarise the two systems SAS and ASE perform essentially the same control function, the SAS being a classical auto-stabilizer while the ASE is really a stick steering autopilot. From an equipment point of view the SAS is probably simpler and is independent of the flight instrument system.

There are many possibilities for modification and completion with regard to automatic trim, automatic maneuvers, automatic flight control, changed control characteristics etc. These extensions cannot be discussed here, but there are many special papers about stability and control augmentation system for helicopters, see for instance (29; 30).

Finally, it should be mentioned that most of the helicopters have relatively good

flight characteristics without artificial stability devices. Therefore, a failure of the stability system must not be critical, and in most cases it will be not necessary to use a redundant system. But it has to be proved, that a failure with its induced disturbance cannot bring the helicopter to a critical situation. Most critical are run-away failures of the servo-actuators. To prevent critical situations, stability augmentation systems are used with limited control authority only.

4. AERODYNAMICS AND DYNAMICS OF ADVANCED ROTARY-WING CONFIGURATIONS

There is full agreement that as far as hovering and low speed (up to about 160 knots) regimes of flight are concerned, the helicopter represents the most efficient configuration, both aerodynamically and operationally. However, in forward flight the helicopter rotor will reach its physical limitations. Because of Mach number limitations at the advancing blade and stall effects at the retreating blade it will no longer be possible to produce the thrust necessary to provide the lift and to overcome drag.

All over the years, there was very much research work aligned to improve the forward flight characteristics by advanced rotor systems or by advanced rotary-wing VTOL configurations using the rotor only for low speed flight regimes and providing the lift in forward flight by wings. But still today, the helicopter is the only rotary-wing aircraft which is in production; some of the advanced rotary-wing configurations flew as research vehicles. The enthusiasm for the advanced configuration has been damped remarkably.

In the following, some of the advanced rotor systems and of advanced rotary-wing configurations will be reviewed briefly, and aerodynamic and dynamic aspects of design and operation will be discussed to help in the understanding of the physical aspects.

4.1 ADVANCED ROTOR SYSTEMS

Several possibilities exist for improving the performance of rotors, especially in forward flight, simply by a departure from the common design philosophy, which employs rectangular, linearly twisted blades. The modern possibilities of blade manufacturing allow to obtain the improvements available from non-linear twist, tapered or more exotic planform shapes, and new blade tip geometries. The improvements will be still more pronounced by the use of specially designed rotor blade airfoil sections. The technology, also in its aerodynamic relations, necessary to realize such optimum geometry rotors is now available, and it may be used for the helicopters of the next generation.

In addition to the possible benefits of advanced rotor geometry, variable geometry rotor blades are also being studied. Such features include variable twist, spanwise segmented blades, leading-adge camber changes, and variable diameter rotors.

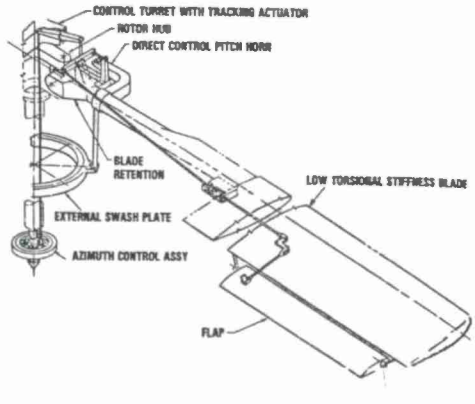


Figure 76 Control arrangements for the Controllable Twist Rotor

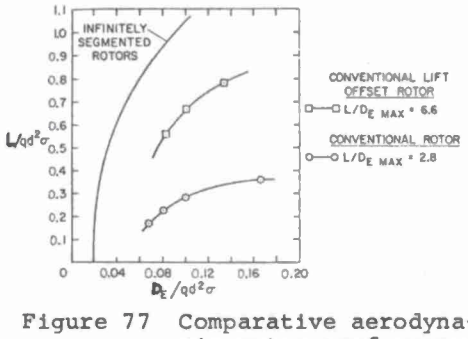


Figure 77 Comparative aerodynamic rotor performance

Figure 76 illustrates the Controllable Twist Rotor (CTR). This rotor system consists of torsionally soft blades with dual controls which are a conventional pitch horn linkage at the inboard end and an aerodynamic control flap at the outboard end. For such a rotor system, an accurate investigation of the aeroelastic behaviour has to be performed because the torsional behaviour of the blades is essential for a good operating of the system. The dual rotor controls offer the possibility to match the rotor control to the optimal control of any special condition of flight in a better way than with single control, resulting in an improved performance and loading situation (31). Similar effects can be achieved with segmented blades using separate control systems for the inboard and the outboard blade sections.

The most severe restriction concerning the lift capability of a rotor in forward flight is the need to maintain rotor lateral balance by cyclic pitch control. The performance potential of a rotor without this restriction is illustrated in Figure 77. This figure is for illustrative purposes only, based on a theoretical study. However, it is seen that a theoretical infinitely segmented rotor whose sections can be set to optimum angle of attack for any given condition establishes an ideal boundary considerable in excess of the conventional rotor. The case shown for the conventional rotor has a twist distribution representative of best current practice and has cyclic pitch applied to maintain lateral balance on the rotor. The third curve of the figure is for the same rotor with the same blade twist, but without cyclic pitch for lateral balance. A significant improvement is indicated, but a single rotor cannot operate in steady flight with this lift offset. For the ideal boundary rotor, the maximum lift which can be carried at any part of the rotor is a function of the advance ratio

μ and the assumed lift coefficient. Figure 78 presents the spanwise distribution of lift which is encountered on such a rotor. There is a large reduction in lift on the retreating side (practically the same as with a conventional rotor) and a large increase in lift on the advancing side. The net result is a large rolling moment, since most of the lift is carried on the advancing side.

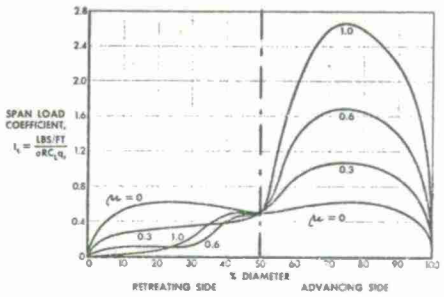


Figure 78 Spanwise lift distribution with all elements working at fixed lift coefficient

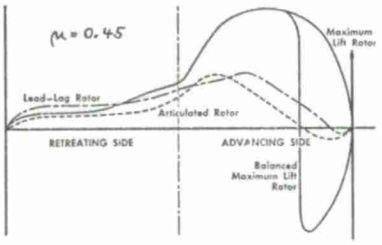


Figure 79 Spanwise lift distribution on different types of rotors

Practical rotors will attain lift along their diameter as shown on Figure 79 for the assumed case of $\mu = 0.45$. A normal articulated rotor operates with the moment of the lift on the blade constant with azimuth angle. The advancing blade operates with some download at the tip and considerable upload on the inner portion. The lift at the center of the rotor is contributed mostly by the fore and aft direction blades; it is less on articulated rotors than is possible on a maximum lift rotor, in order that the lift moments about the articulation hinge will be the same as for the retreating blade, which has the limiting lift moment.

The application of a second harmonic pitch angle variation with azimuth makes it possible to load the fore and aft blades to lift moments that are higher than the lift moment on the retreating blade (32). But it should be mentioned that such a second harmonic control will increase the vibratory loads at the hub. There are investigations to use second and higher harmonic control in the opposite way to reduce vibratory loads (33).

It is possible to increase the lift on the advancing blade by the use of flaps or high twists. This produces a large shear load at the hub which materially assists the lift of such a rotor while still keeping the lift moment of the advancing blade equal to that of the retreating blade. This requires a greater download on the advancing tip. Such a rotor with cyclic pitch change and with additional lift on the advancing blade is the "Balanced Maximum Lift Rotor" of Figure 79. The controllable twist rotor belongs to this type of rotor.

In the so-called lead-lag rotor (34), the velocity of the retreating blade is increased by a first harmonic, forced lead-lag motion of the blades and the velocity of the advancing blade is decreased to provide a more uniform tip velocity with azimuth. This increases the lift available on the retreating side and thereby permits still more lift on the advancing side. But such a rotor is of high mechanical complexity, and the changed loading situation, especially the high dynamic inplane loads cause severe problems for a realization.

The lifting ability of these four types of rotors is shown on Figure 80, which is a plot of the variation in the maximum lift that a rotor can carry as influenced by the maximum section lift coefficient and forward speed at constant rotational speed. It is evident that the lift which a helicopter rotor can carry is materially reduced with increasing forward speed. The lift capability of the rotor will be a maximum in the hover case, it is limited by stall. The considered advanced rotor systems offer good lift capability in forward flight.

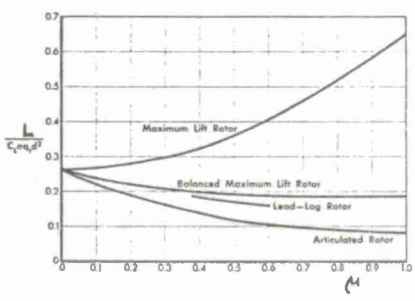


Figure 80 The effect of forward speed on rotor lift

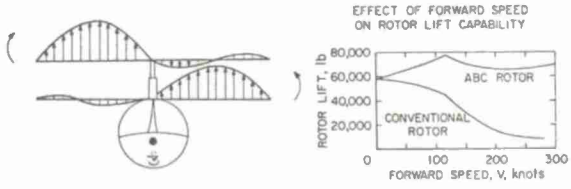


Figure 81 Coaxial rigid rotor - Advancing Blade Concept

The problems withstanding the realization of such advanced rotor systems are mainly dynamical and structural problems. It is possible that means can be discovered to more closely approximate this ideal limit.

The improvement from lift offset has prompted ingenious configurations to take advantage of this factor such as the so-called Advancing Blade Concept, which is illustrated in Figure 81. The ABC design uses coaxial, counter-rotating, rigid rotors. The figure shows the typical advancing and retreating blade loadings. Because of the requirement to substantially zero aircraft rolling moment, the upper rotor advancing blade moment is balanced by the lower rotor advancing blade moment, and there is no requirement for carrying significant moment (or lift) on the retreating blades. Thus, stall onset can be greatly delayed and the lift capacity of the rotor system is set primarily by structural or power considerations, rather than by aerodynamic limitations. The problems of compressible flow on the advancing blade can also be alleviated, if desired, by reducing the loading on the advancing side and carrying the load primarily in the fore and aft quadrants. The problems of blade aeroelastic behaviour for this configuration have been investigated and proved feasible in full-scale rotor tests. The blades and the hub of this rotor concept are very highly loaded, and it seems that a realization will depend on material problems, mainly. The blades are very stiff, and the rotor is a real rigid rotor (35).

Extensive research efforts are being pursued in the utilization of a jet flap on rotor blade sections (36). Analytical and limited experimental investigations have shown a decisive advantage in terms of lift capability for the jet flap rotor over that of the conventional rotor of equivalent size and solidity. This advantage is illustrated in Figure 82. It is seen that both increased static lift capability and increased capability for high-speed flight are realized. The ability to generate very high lift coefficients essentially eliminates the blade stall limit on the retreating blade, and thereby indicates a possibility of minimizing the retreating blade stall problem of conventional rotors. This capability is also beneficial in reducing the problems of vibration which result from blade stall. It is recognized that the basic efficiencies of pneumatic systems are significantly less than of the conventional, mechanically driven rotor. The possibility of utilizing such systems as those for producing near uniform loadings on the rotor is being researched.

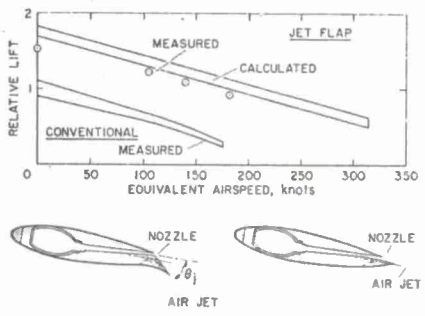


Figure 82 Jet flap rotor performance

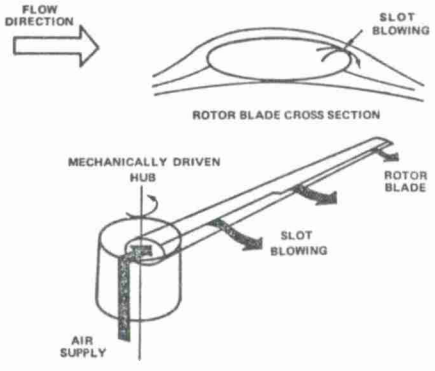


Figure 83 Basic concept of Circulation Control Rotor

There is a special research effort related to "Circulation Control Rotors" using blades with circular or elliptical cross section and blowing slots, the principle of which is illustrated in Figure 83. A special variant of a rotor for speeds higher than about 200 knots is described in Figure 84. The jet flap principle is applied at the trailing and the leading edge of the blade. The slot at the leading edge is only blown in the reversed flow region of the retreating side. In this manner the problems of retreating blade stall are sensibly eliminated. If the rotational speed is kept low by use of the high section lift capability, the rotor is aerodynamically capable of achieving speeds in excess of 400 knots with relatively high efficiencies. Up to now, it seems that the aerodynamic aspects have been considered mainly; several areas require further activities. These include handling qualities as well as blade dynamics and structural design (37; 38).

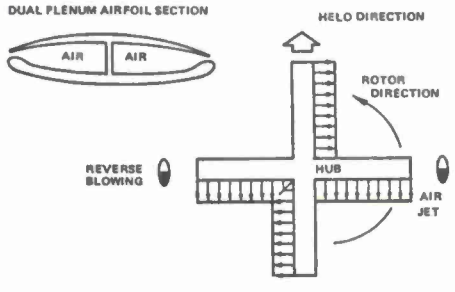


Figure 84 High advance ratio dual blowing concept

Helicopter designers and engineers are rather conservative, and it is hardly to expect that advanced rotor concepts will be realized in helicopter developments of the near future. Probably, the main effort of the next years will be related less to an improvement of the speed capability of the helicopter but more to improvements related to aspects which will influence its overall operational efficiency such as maintenance and reliability, vibration and noise, performance, IFR-capability etc.

Some of the material presented in this section has been extracted from other excellent reviewing presentations (39, 30).

4.2 ADVANCED ROTARY-WING CONFIGURATIONS

The potential improvements in the speed and range capabilities of the pure helicopter gained by the addition of wings and auxiliary propulsion have been recognized for many years. The resultant compound helicopter shifts the basic rotor limitations of retreating blade stall to higher flight speeds and allows flight characteristics comparable in many respects to those of fixed wing aircraft. Despite these advantages, the development of the compound helicopter has been rather slow. Many research vehicles have flown, and there is a relatively good knowledge about the technical problems. Therefore it seems to be not a problem of technology that there are no compounds in operation. May be that there is really no necessity for such an aircraft, or that nobody is willing to pay for an aircraft combining the low speed advantages of the helicopter with a higher speed capability.

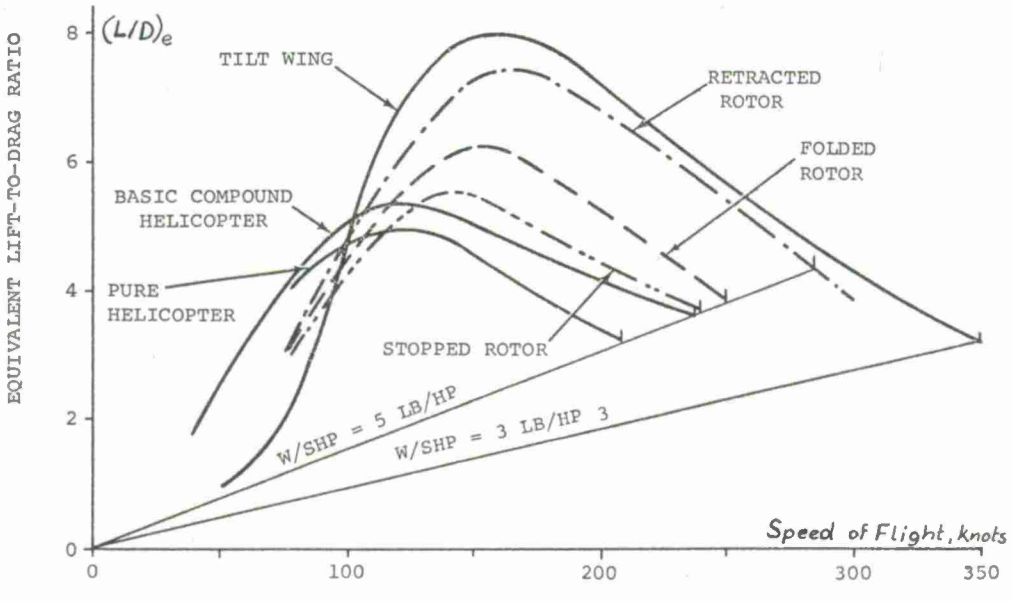


Figure 85 Equivalent lift-to-drag ratios for various configurations

In forward flight, the overall efficiency of the helicopter is poor compared with that of fixed-wing aircraft. This efficiency can be measured by the lift to equivalent drag ratio which is shown in Figure 85 (41). The figure, comparing lift to drag ratios of the rotary-wing type like helicopters and compounds with those of fixed-wing type aircraft like tilt-wing or aircraft with stoppable, foldable or rectractable rotors, explains why there is a continious search for configurations where, in cruise and high speed flight, the weight of the aircraft will be supported by a fixed wing. The compounded helicopter gives some more potential than the pure helicopter, but at higher flight speeds the convertible rotor/propeller aircrafts offer an improved efficiency. They may be defined as configurations where through a conversion process the airscrew or rotor, used for vertical thrust in hover and low-speed regimes, changes its role from a vertical thrust generator to that of a forward propulsor. For still higher speed regimes, in which a propeller will be no longer an efficient propulsor, the rotor or propeller blades have to be folded and retracted and other propulsion means have to be provided. Since long years, research work related to such rotory-wing vehicles as tilt-rotor and tilt-wing aircrafts, stoppable and foldable rotor systems is performed; some research aircraft flew, but there is no real development. The reasons may be that there has been no strong military requirement funding such a development. A pure civilian development seems to be improbable, because people are strongly jet-minded,today. A change of opinion only could occur if there would be good military experience available.

In the following section the basic aerodynamic and dynamic problems of compound helicopters and of convertible rotor/propeller aircraft briefly will be reviewed.

Compound helicopter (partly following (40; 42)).

The lifting capability of a helicopter rotor is lower in forward flight than in hover and decreases steadily with increasing forward speed. The cause of this characteristic is the difference in velocities relative to the blades on the "advancing" and "retreating" halves of the rotor disk. No conventional rotor system is able to support large rolling moments, either because of flapping hinges or limited capacity of the blade structure, head, or shaft to withstand vibratory bending moments. For single rotor helicopters, the rolling moment must be essentially zero in any case due to trim requirements. Consequently the large dynamic pressures on the advancing side of the rotor cannot be utilized, and advancing blade lift must be reduced to the level of the retreating blade lift capability, which decreases rapidly with increasing forward speed.

To illustrate the above elementary considerations, the reduction in size of the operating envelope of a typical helicopter rotor with increasing forward speed is presented in Figure 86. Rotor lift is plotted vertically against propulsive force (or drag on the

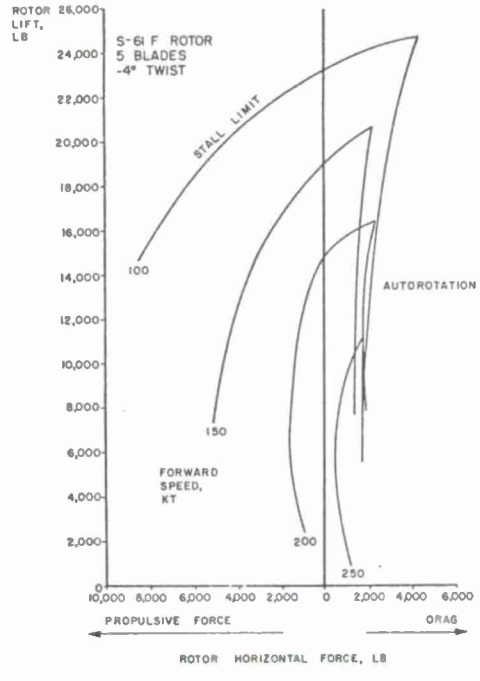


Figure 86 Effect of forward speed on rotor operating envelope

horizontal scale; thus a line from the origin to any point on the graph represents the rotor resultant force vector for that point. The operating limits for given forward speed are retreating blade stall and a line corresponding to autorotation (zero power). The stall line represents a moderate retreating blade stall condition. Operation to the right of the autorotation line is not normally possible because this corresponds to negative rotor power. Within these two basic limits, however, the rotor may operate at any point. As may be seen, the operating envelope shrinks rapidly with increasing forward speed. At 200 knots the maximum rotor lift capability is only about two thirds that at 100 knots, and maximum propulsive force is less than 20 percent that at 100 knots, although the parasite drag that must be overcome has increased by a factor of four. At 250 knots the propulsive force capacity has entirely vanished, with the rotor producing drag at all operating conditions. Thus it is clear that auxiliary propulsion is required for rotorcraft in the speed range above 200 knots; it is also clear that a wing, with inherently good aerodynamic efficiency and a lift capability that increases rapidly with forward speed, is most desirable to supplement rotor lift at high speeds. The compound helicopter is therefore a logical extension of the pure helicopter. With a propeller geared to the main rotor, even this autorotation limit can be exceeded, since it is then possible to operate the rotor at negative power and high drag. This can be a useful procedure in maneuvers demanding maximum aircraft deceleration rates.

It is useful to identify a number of separate categories of helicopters and compounds, according to the degree of complexity and speed potential. Accordingly, a chart of six distinct categories is presented in Figure 87.

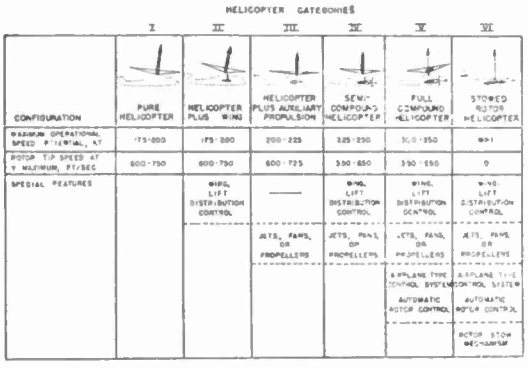


Figure 87 Categories of rotory wing aircraft

The first category is the pure helicopter, with an indicated maximum cruise speed potential of 175 to 200 knots. The second type is the helicopter plus a wing. This category aircraft will probably not have a higher maximum speed potential than the pure helicopter but will be capable of carrying larger payloads at high speed. Once a wing of appreciable size is added to the aircraft, it will be necessary to provide means to control distribution of lift between the wing and and rotor, as indicated by the item opposite "Special Features". This control may be achieved by a wing of variable incidence, a maneuver flap, longitudinal trim control of the fuselage, or some other means, but in any case it represents a feature not required on the pure helicopter.

The third category is the helicopter plus auxiliary propulsion but without a wing. This configuration does have an increased speed potential, but the practical magnitude of this increase is believed to be modest because of the deteriorating rotor lift capability. Special features are auxiliary powerplants or means of transfering power from the rotor drive system to fans or propellers for forward thrust.

The fourth, fifth, and sixth categories of rotary wing aircraft all employ both a wing and propusion, and all may be considered to be compound helicopters. The sixth category is the stowed rotor helicopter, in which the rotor is stopped in flight and stowed in the fuselage or elsewhere, thus permitting very high design flight speeds, including supersonic.

The remaining categories, types IV and V, have been labeled "Semi-Compound" and "Full Compound", respectively. While the external appearance of these two types may be virtually identical, there are important distinctions between them. The distinctions are based on the forward speeds and rotor tip speeds at which the two types operate and the means for achieving longitudinal and lateral control. The category IV compound operates at speeds not exceeding 250 knots and at relatively high rotor tip speeds within the range of conventional helicopter operation. At these high tip speeds, rotor behaviour is quite normal and the control power achieved with cyclic pitch, at least for the offset-hinge rotor system, is adequate in both pitch and roll to serve as the primary flight control means.

If higher forward speeds are desired, it will be necessary to reduce rotor rpm to avoid excessive compressibility losses due to high advancing blade tip Mach numbers. As forward speed is increased and tip speed is reduced, the rotor advance ratio (ratio of

forward speed to tip speed) increases rapidly, and rotor behaviour is altered significantly, with greatly increased sensitivity to control inputs or gusts, and reversal of some control derivatives. Thus in this higher speed range it appears to be necessary to decouple the rotor from the pilot's control, partially or completely, with an automatic rotor control system, and to introduce elevators and possibly ailerons to provide primary flight control. A rudder is also required since a conventional tail rotor is likely to be unsatisfactory at very high speeds. The aircraft now has all of the flight controls of the conventional fixed wing airplane, and the helicopter has become the full compound of category V.

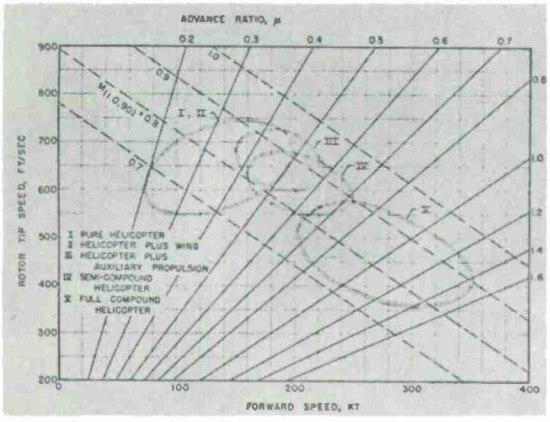


Figure 88 Helicopter operating regimes

The distinctions between the various categories of helicopters may be clarified further by examination of their respective operating regimes. Figure 88 presents the approximate ranges of forward speed and rotor tip speed at which the various types may be expected to operate in cruising flight. Also indicated on this chart are lines of constant advance ratio and advancing tip Mach number, two pertinent parameters in determining rotor characteristics. It should be understood that all category aircraft will utilize tip speeds in the normal helicopter range in hovering and low speed flight.

The operating regimes of categories I and II, pure helicopter and helicopter plus wing, are essentially the same, although use of a wing at low cruise speeds is less attractive than at high speeds. The envelope of this regime is shown with a slight upward slope to the right, since higher tip speeds will be required at the higher forward speeds to provide the necessary lift and/or propulsive force. The remaining categories have design operating boundaries tending to slope downward along the lines of constant advancing tip Mach number in an overlapping pattern. All of the categories are restricted to advancing tip Mach number less than 1.0, since severe performance penalties are encountered at advancing tip Mach numbers exceeding about 0.9. It may be seen from this diagram that the category IV and I compound helicopter occupy distinctly different regions on the chart, with the category V covering a broader range of speed and advance ratio. The dividing line between categories IV and V occurs at roughly 0.7 advance ratio, which corresponds to the point at which rotor characteristics start deviating substantially from lower speed behaviour. The distinctions between the categories IV and V compound helicopters are very important, the latter category having a considerably greater performance potential but at the expense of increased complexity and sophistication required in the overall control system.

The compound helicopter has characteristics substantially different from the conventional pure helicopter. Knowledge is required in many areas, including rotor performance at high speeds; interference between wing, fuselage, and rotor; aerodynamic loads; rotor dynamic behaviour; vibration characteristics; and flying qualities.

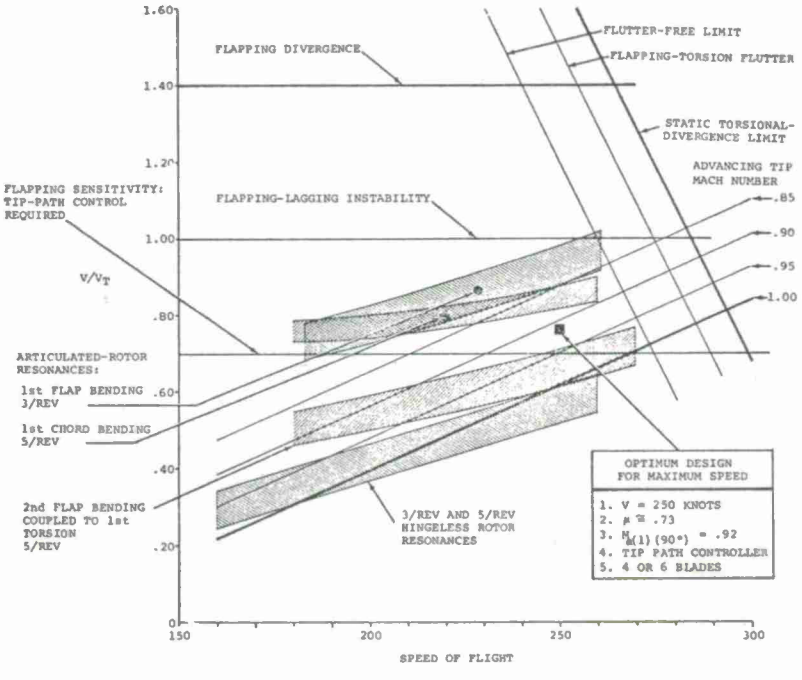


Figure 89 Unloaded rotor operating limits

Most of the properties of these aircrafts can be analyzed by using helicopter theories especially for the investigation of the rotor; the ordinary fixed-wing theory will be used for the aircraft including the wing. Complications are the division of lift between rotor and wing, which is really a design parameter, and the aerodynamic interference of the rotor on the wing and tail due to downwash. As a result of many studies, a reasonably complete understanding of the potential of these aicraft has been obtained. It has been ascertained that only limited gains in performance can be obtained by this method. While these aircraft can obtain an increase in flight speeds, generally limited to approximately 220 to 240 kt, performance at speeds comparable with conventional rotorcraft is usually degraded by increases in weight and complexity of the aircraft. Ultimate speed limitations are imposed by rotor dynamic problems characteristic of conventional rotorcraft which again appear at the higher flight speeds, even though the rotor may be unloaded and slowed. This does not mean that compound aircraft are without merit or application. However, it is intended to point out that these aircraft are definitely limited in their operating capability. An indication of these limits is given in Figure 89. It is seen that the various resonances, instabilities, and divergences experienced in rotary wing systems, which will be discussed in Session 4, provide only a narrow corridor of possible operation. This corridor is limited in both advance ratio and forward speed by the rotor dynamic considerations. The figure gives no absolute limitations, because most of them can be influenced by design modifications. The dynamic problems will increase with increasing advance ratio. The "Full Compound" will be most critical, and the knowledge about its problems is not complete, today.

Nevertheless, certain utilisations of the compound device can prove to be useful. The possibilities of an application of this technique have been demonstrated by the Lockheed Cheyenn AH-56, which was developed as an armed compound helicopter. Unfortunately, this program is cancelled, now.

The final configuration to be discussed in this section is that which eliminates the problems of the rotorcraft discussed earlier by discretly folding it away. A typical configuration is illustrated in Figure 90. A significant amount of research has been devoted to this aircraft concept and wind tunnel experiments at large scale have demonstrated the capability of stopping and folding the rotor. It is obvious that such a concept involves the weight penalties and volume requirements of a system which is utilised during only a portion of the flight mission. However, the flight benefits which will accrue from the vertical flight capability, and particularly for those missions which couple extensive hovering time necessitating good hovering economy with high cruise speed requirements, make this concept attractive. Current research efforts are directed primarily toward establishing satisfactory control to meet the requirements of the starting and stopping cycle. It is obvious that to preclude excessive blade flapping and bending moments during these phases, and also to prevent blade divergence, it will be necessary to assure adequate blade pitch control.

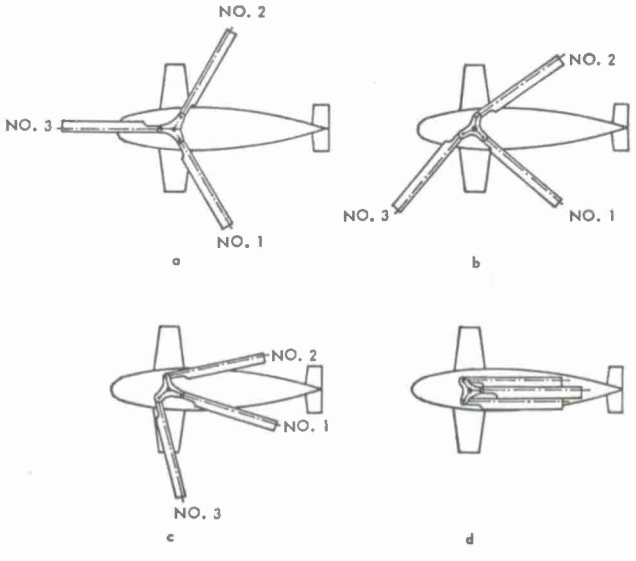


Figure 90 Folding sequence, stowed rotor

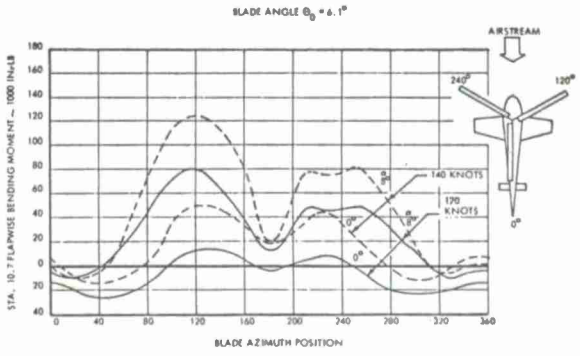


Figure 91 Measured flapwise bending moment vs. azimuth position

This requirement is further emphasised by the requirement for the rotor to withstand thrust and maneuvering loads during the stopping and starting cycle. Static aeroelastic divergence must not occur at any blade azimuth position. These requirements are illustrated on Figure 91. The azimuth varation of flapwise bending moment for the rotor stopped at two aircraft forward airspeeds and two aircraft angles of attack give an indication of the problems which would be encountered in withstanding atmosperic gusts. Considerable experimental research has been performed, and additional research is contemplated to investigate the requirements for avoiding these problems and to provide adequate control in the start/stop cycles (43; 44).

The possibility of applying circulation control rotors to the stopped/stowed rotor concept is being considered and research will be implemented to further evaluate this technique. Advantages of such a move are obvious since the rotor can be of considerably smaller size and weight and thereby occupy less volume when it is stowed. Several other potentials such as the elimination of the transmission and the conventional mechanical blade pitch control system also accrue which may make this a desirable concept to be pursued (45).

A stoppable rotor is used for the rotor/wing composite-lift aircraft (see Figure 92), also. For hovering and low speed flight, the lifting surface rotates, while for aircraft flight the rotor is stopped with one blade forward in the direction of flight. Such an aircraft will experience strong attitude disturbances during attempts to either start or stop the rotor if all lift is maintained by the rotor, caused by the center-of-pressure movement as indicated in Figure 93. It will be very difficult to overcome the related problems (46).

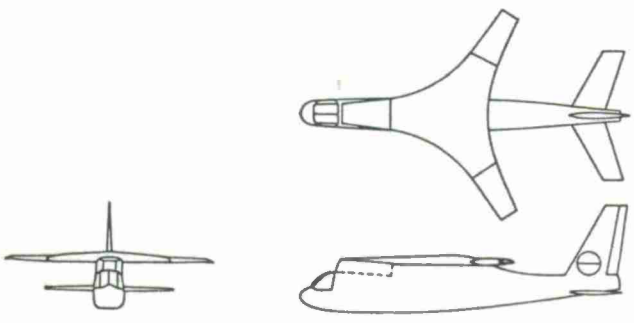


Figure 92 Typical rotor/wing design

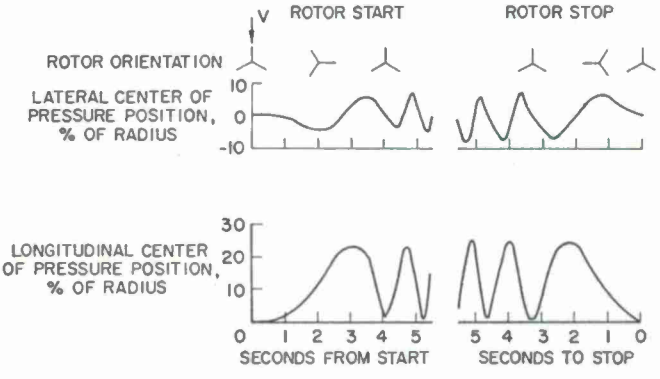


Figure 93 Center of pressure movement during rotor starting and stopping

Advanced convertible configurations

The prop/rotor and the tilt wing are two generic design concepts which are of special interest in application to V/STOL aircraft. Each of these design concepts is capable of efficient hover and cruise speeds which approach 400 knots. Transition from hover to cruise is accomplished in the first case by tilting the rotor/nacelle forward to the propeller mode, and in the second case by tilting the wing together with the lifting propellers forward to a horizontal cruise position. Of course, transition must occur at speeds sufficiently high to provide an adequate aerodynamic lift to sustain flight. Figure 94 illustrates both, a typical tilt rotor aircraft and a typical tilt wing aircraft.

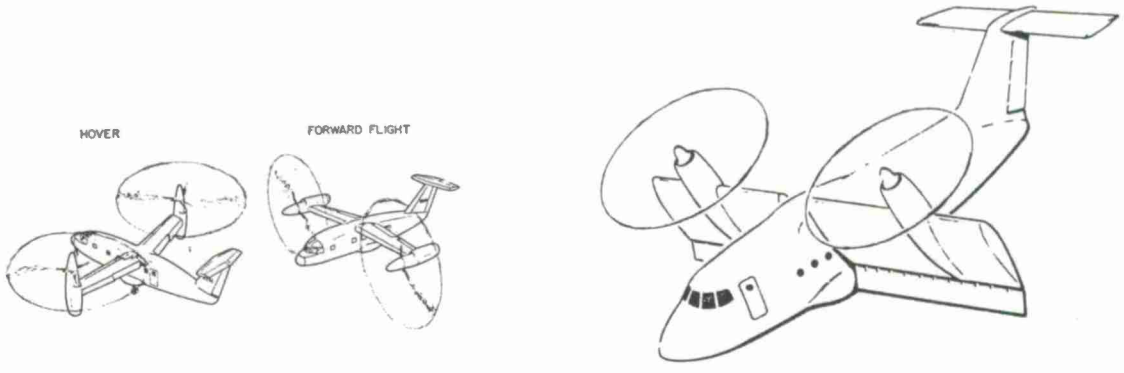


Figure 94 Typical rilt rotor and typical tilt wing aircraft

The tilting propeller-rotor aircraft concept holds considerable interest since it can provide the hovering economies of a conventional rotorcraft as well as a smooth and highly controllable transition to conventional fixed-wing flight.

However, consideration of this concept must include the rather basic aeroelastic and dynamic problems which are associated with it. There are differences between the two concepts; whereas the tilt rotor uses relatively large flexible rotors (similar to helicopter rotors, are the propellers of a tilt wing aircraft relatively smaller and of a larger stiffness. In general, the aeroelastic aspects of helicopters and of fixed-wing aircraft have to be considered, and there are additional effects resulting from the inter-

actions between the flexible rotors and the flexible wings carrying the rotors. Analytical methods have been developed for these dynamic and aerodynamic characteristics of the nacelle combination. The effects will be discussed in detail in Session 3.

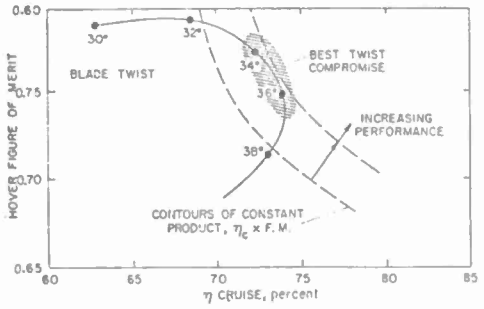


Figure 95 Effect of blade twist on hover-cruise efficiency

The penalties of mismatch in propeller area between hover and forward flight make it difficult to maintain a high hover fig.of merit and a high propulsive efficiency in forward flight. An illustration of this trade-off is given in Figure 95. The application of a variable diameter rotor could minimize those problems.

Some attention should be given to the conversion corridor, as illustrated in Figure 96. Normally, the corridor is limited by the stall boundaries of the wing and by structural rotor limitations as indicated in Figure 97. In addition, trim in any flight condition must be possible, allowing a margin for countering disturbances or for maneuvering. Of course, there are differences for the tilt prop and the tilt wing concept because of the different wing situation. An interesting facet of control position versus speed, during transitions, may be pointed out.

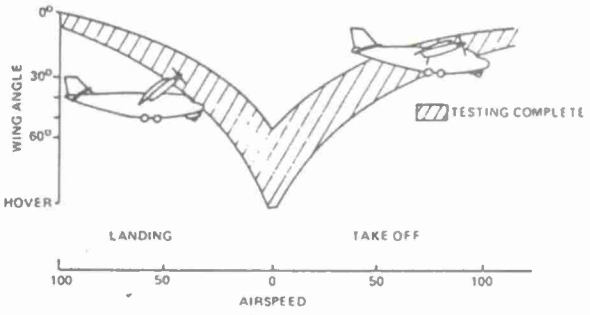


Figure 96 Conversion of a tilt wing aircraft

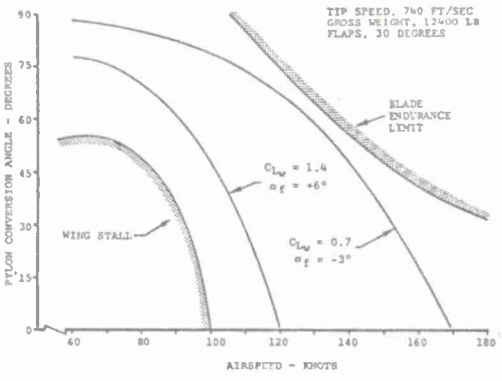


Figure 97 Typical conversion corridor of a tilt rotor aircraft

If the vehicle is like a helicopter in hovering, its velocity stability will require a locally stable trim gradient, i.e., forward stick for forward velocity, as shown in Figure 98. For cruising and high speed flight, if the characteristics are those of conventional airplane, the trim curve would be like the one shown. The transition must join the two curves in some way like the dotted line. An adverse control position gradient seems almost inevitable during the transition. Of course, the exact shape and position of the connecting curve depends on pilot programming of thrust-tilt and power versus speed. There are some possibilities to eliminate the bump in the trim curve. The airplane part could be moved up, by changing tail incidence; and the helicopter part could be moved down, by rigging the controls off-center, but a number of compromises will be necessary.

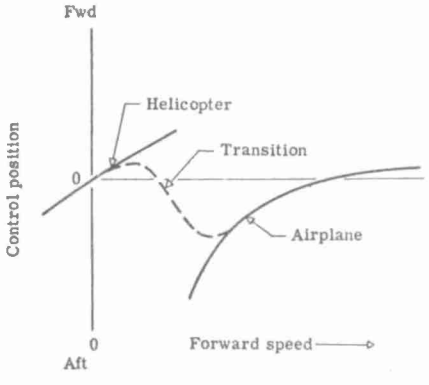


Figure 98 Tilt prop/rotor aircraft trim position versus speed

The convertible concepts all present challanging and novel stability and control problems. In high speed flight the characteristics are similar to those of fixed wing aircraft; the behaviour in hovering and low speed flight is determined by the rotor characteristics. The tilt rotor will behave similar as a dual rotor (side-by-side) helicopter; the hovering characteristics of the tilt wing concept using highly loaded, stiff propellers are those of a multirotor helicopter with very high disc loading. The angular damping will be too low and the velocity stability undesirably high, resulting in poor handling characteristics without a stability and control augmentation system.

Problems can arise from the gust sensitivity. The blades of a tilt prop/rotor aircraft in forward flight are lightly loaded and operate at very low section angles of attack; therefore a given change in axial velocity will result in high precentage changes in thrust. As well as to the axial gusts, there will be sensitivity to longitudinal gusts. An improvement in airplane response can be obtained by use of a feedback control system into

collective and cyclic pitch of the rotors.

The knowledge of today, resulting from extensive experimental and theoretical research work, seems to be sufficient to predict all the essential features which are performance, aeroelastic behaviour, flying qualities etc, and it can be concluded that tilt prop/rotor technology has been developed to the state where industry could go ahead with an operational aircraft with high confidence. Therefore, it is most probable that the demonstrator aircraft, which will be developed in USA, will prove successfully.

A more advanced version of the tilt prop/rotor aircraft is the tilt-fold-proprotor aircraft. Following the helicopter, conversion, and proprotor aircraft flight modes, the rotor will be stopped; folded and eventually stowed away, as illustrated in Figure 97. The stopping and folding operates in a situation with axial flow. The main parameters, which have to be controlled during stopping, are rotor speed and flapping. During slowdown, rotor flapping sensitivity to external disturbances increases and flapping must be restrained at low rpm. With the stopped and folded rotor, the aircraft is operating as a normal fixed-wing aircraft which has independent propulsion.

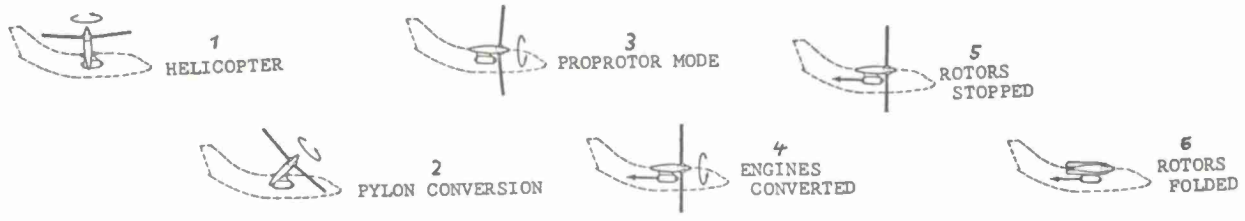


Figure 97 Transition sequence of a tilt-fold-proprotor aircraft

This section uses extractions and data from the references (20; 40; 41; 47 ÷ 51).

5. CONCLUDING REMARKS

It was intendet to select and present the subjects of the foregoing discussions in such a way as to help the reader to better understand the basic aspects of the dynamics of rotor and helicopter and to give a feeling for possible improvements in technology and advanced configurations.

The physical aspects of the discussed phenomena were strongly underlined, the basic assumptions were reviewed, and the methods for analysis were briefly discussed, but mathematical presentation was kept to a minimum. Most important in the sense of an introductory survey, the basic dynamic phenomena of the rotor were considered, because they are the key for the rotary-wing physics at all. Therefore, a broad discussion was given to the dynamic behaviour of articulated and hingeless rotors, such as flapping, lagging and control motions of the blades. Only a limited selection of literature was presented, because it was considered to be beyond the scope of this presentation to give a full literature survey.

These lecture notes were prepared using experience available at the Messerschmitt-Bölkow-Blohm GmbH, from material existing in the form of various already existing scripts and to a large extent, by extracting material from excellent textbooks and special papers dealing with the subject of the lecture. It is hoped that the resulting presentation is balanced as a whole,inspite of the race against the deadline for the manuscript. If there are too many strange idioms, resulting from the German language of the lecturer, the reader hopefully will pardon him.

6. REFERENCES

1. Bennett, J.A.J.: "The Era of the Autogiro", J. Royal Aeronautical Soc., Vol. 65, October 1961

2. Mosinskis, V.S.; Schneider, E.: "Design and Development of an Elastomeric-Bearing Rotor Hub", American Helicopter Soc., Proceedings 24th Annual National Forum, May 1968

3. Stewart, W.: "Research and Development of Rotating Wing Aircraft", J. Royal Aeronautical Sov., Vol. 66, November 1962

4. Nikolsky, A.A.: "Helicopter Analysis", John Wiley & Sons, Inc., New York, Chapman & Hall, Ltd., London, 1951

5. Gessow, A.; Myers, G.C., Jr.: "Aerodynamics of the Helicopter", The Macmillan Comp., New York, 1952, unrevised republished by Frederick Ungar Publishing Co, New York, 1967

6. Shapiro, J.: "Principles of Helicopter Engineering", Temple Press, London, 1955

7. Payne, P.R.: "Helicopter Dynamics and Aerodynamics", Pitman, London, 1959

8. Just, W.: "Hubschrauber und Vertikalstartflugzeuge", Verlag Flugtechnik, Stuttgart, 1963

9. Just, W.; Jaeckel, K.: "Aerodynamik der Hub- und Tragschrauber Teil 2, Berechnung des Rotors", Verlag Flugtechnik, Stuttgart, 1954

10. Allen, R.W.: "Flapping Characteristics of Rigid Rotor Blades", J. Aeronautical Sciences, Vol. 13, April 1946

11. Young, M.I.: "A Simplified Theory of Hingeless Rotors with Application to Tandem Helicopters". American Helicopter Soc., Proceedings 18th Annual National Forum, May 1962

12. Reichert, G.: "Flugeigenschaften bei Hubschraubern mit elastisch angeschlossenen Rotorblättern", Wissensch. Ges. Luft- und Raumfahrt, Jahrbuch 1963; or translated: "Handling Qualities of Helicopters with Elastically Attached Rotor Blades", NASA-TTF-11374, July 1968

13. Reichert, G.: "Flugmechanische Besonderheiten des gelenklosen Hubschrauberrotors", Wissensch. Ges. Luft- und Raumfahrt, Jahrbuch 1965; or translated: "Flight-Mechanical Properties of the Hingeless Helicopter Rotor", NASA-TTF-11373, December 1967

14. Shupe, N.K.: "A Study of the Dynamic Motions of Hingeless Rotored Helicopters", US Army Electronics Command ECOM-3323, AD 713 402, August 1970

15. Bramwell, A.R.S.: "A Method for Calculating the Stability and Control Derivatives of Helicopters with Hingeless Rotors", The City University London, Research Memo Aero 69/4

16. Reichert, G.; Huber, H.: "Influence of Elastic Coupling Effects on the Handling Qualities of a Hingeless Rotor Helicopter", 39th AGARD Flight Mechanics Panel Meeting, Hampton, Virginia, September 1971

17. Huber, H.: "Some Objectives in Applying Hingeless Rotors to Helicopters and V/STOL Aircrafts", AGARD-CPP 111, September 1972

18. Ormiston, R.A.; Hodges, D.H.: "Linear Flap-Lag Dynamics of Hingeless Helicopter Rotor Blades in Hover", J. American Helicopter Soc., Vol. 17, No. 2, April 1972

19. Kisielowski, E.; Permutter, A.; Tang, J.: "Stability and Control Handbook for Helicopters", AD 662 259, Dynasciences Corp., Blue Bell, Pennsylvania, August 1967

20. Seckel, E.: "Stability and Control of Airplanes and Helicopters", Academic Press, New York, London, 1964

21. Salmires, S.; Tapscott, R.J.: "The Effects of Various Combinations of Damping and Control Power on Helicopter Handling Qualities During Both Instrument and Visual Flight", NASA TN D-58, 1959

22. Anon.: "Helicopter Flying and Ground Handling Qualities; General Requirements for", Milit. Specification MIL-H-8501A, 1961

23. Edenborough, H.K.; Wernicke, K.G.: "Control and Maneuver Requirements for Armed Helicopters", American Helicopter Soc., 20th Annual National Forum, May 1964

24. Reichert, G.; Oelker, P.: "Handling Qualities with the Bölkow Rigid Rotor System", American Helicopter Soc., 24th Annual National Forum, Preprint No. 218, May 1968

25. Just, W.: "Steuerung und Stabilitiät von Drehflügelflugzeugen", Verlag Flugtechnik, Stuttgart, 1957

26. Jenny, D.S.; Decker, R.; Stutz, R.G.: "Maneuverability Criteria for Weapons Helicopters", American Helicopter Soc., Proceedings 20th Annual National Forum, May 1964

27. Carter, E.S.: "An Analysis of the Helicopter Transfer Function to Predict Achievable Handling Characteristics of the Stabilized Helicopter", American Helicopter Soc. Proceedings 8th Annual National Forum, May 1952

28. Curties, M.C.: "Helicopter All-Weather Operation - Equipment for the Transport Role", Aeronautical J. Royal Aeronautical Soc., Vol. 72, March 1968

29. König, H.; Schmitt, H.: "Optimization of Automatic Flight Control Concepts for Light Helicopters with All-Weather Capability", AGARD-CP-86-71, June 1971

30. Murray, J.B.; Phillips, D.E; Ekstrom, P.J.; Laughlen, D.C.: "AH-56 Cheyenne Control Augmentation System Study", US Electronics Command Report, July 1970

31. Lemnios, A.Z.; Smith, A.F.; Nettles, W.E.: "The Controllable Twist Rotor, Performance and Blade Dynamics", American Helicopter Soc., 28th Annual National Forum, Preprint No. 614, May 1972

32. Stewart, W.: "Second Harmonic Control on the Helicopter Rotor", Reports and Memoranda No. 2997, August 1952

33. Daughaday, H.: "Suppression of Transmitted Harmonic Rotor Loads by Blade Pitch Control J. American Helicopter Soc., Vol. 13, No. 2, April 1968

34. Derschmidt, H.: "High-Speed Rotor with Blade-Lag Motion Control", IAS-Preprint 63-74, 1963

35. Paglino, V.M.: "Forward Flight Performance of a Coaxial Rigid Rotor", American Helicopter Soc., 27th Annual National Forum, Preprint No. 524, May 1971

36. Kretz, M.: "Fields of Application of Jet Flapped Rotors", 39th AGARD Flight Mechanics Panel Meeting, Hampton, Virginia, September 1971

37. Cheeseman, J.C.; Seed, A.R.: "The Application of Circulation Control by Blowing to Helicopter Rotors", J. Royal Aeronautical Soc., Vol. 71, July 1967

38. Williams, R.M.; Rogers, E.O.: " Design Considerations of Circulation Control Rotors", American Helicopter Soc., 28th Annual National Forum, Preprint No. 603, May 1972

39. Schairer, G.S.: "Some Opportunities for Progress in Aircraft Performance", J. Aircraft, Vol. 1, No. 2, March-April 1964

40. Yaggy, P.F.: "Future Rotorcraft Research in the USA", Aeronautical J. Royal Aeronautical Soc., Vol. 73, September 1969

41. Stepniewski, W.Z.; Young, M.I.: "Helciopters and Propeller-Type VTOL Aircraft in the Light of Technologies", SAE-Preprint No. 650193, April 1965

42. Fradenburgh, E.A.; Segel, R.M.: "Model and Full Scale Compound Helicopter Research", American Helicopter Soc., Proceedings 21st Annual National Forum, May 1965

43. Watts, A.G.: "Horizontal Stoppable Rotor Conversion", American Halicopter Society, 27th Annual National Forum, Preprint No. 502, May 1971

44. Donham, R.E.: "Analyses of Stowed Rotor Aerodynamic/Aeroelastic Characteristics", AGARD CP-22, September 1967

45. Taylor, J.: "Stopped Rotor Aircraft Using Circulation Controlled Rotors", 39th AGARD Flight Mechanics Panel Meeting, Hampton, Virginia, September 1971

46. Huston, R.J.; Shrivers, J.P.: "The Conversion of the Rotor/Wing Aircraft", AGARD CP 22, September 1967

47. Wernicke, K.G.; Edenborough, H.K.: "Full-Scale Proprotor Development", American Helicopter Soc., 37th Annual National Forum, Preprint No. 501, May 1971

48. Gillmore, K.B.: "Survey of Tilt Rotor Technology Development", 39th AGARD Flight Mechanics Panel Meeting, Hampton, Virginia, September 1971

49. Jackson, A.: "Meeting Propulsion Needs of Future High Performance V/STOL", in: Entwurfsprobleme von V/STOL-Propellern und Rotoren", Deutsche Luft- und Raumfahrt Mitt. 71-18, DGLR, Köln, Dezember 1971

50. Fraga, D.E., Liiva, J.: "Design Studies and Model Tests of the Stowed Tilt-Rotor Concept", AIAA Paper No. 72-804, August 1972

51. Engle, F.V.; Sambell, K.W.: "Performance Aspects of Folding Proprotor V/STOL Aircraft", American Helicopter Soc., 25th Annual National Forum, Preprint No. 302, May 1969

AEROELASTICITY OF ROTARY WING AIRCRAFT

by

Rolland Dat
Office National d'Etudes et de Recherches Aérospatiales (O.N.E.R.A.)
29, avenue de la Division Leclerc
92320 Châtillon
France

SUMMARY

In the first part the flutter instability is illustrated by the case of an aerofoil and the theoretical tools used to investigate the flutter of a flexible wing are presented.

The second part is devoted to the basic tools used for the prediction of the aerodynamic forces on blades.

In the third part a formulation of the problem of forced vibration in forward flight is given.

INTRODUCTION

The aeroelastic phenomena encountered on aircraft are due to a coupling between aerodynamic, elastic and inertial force. They can be related to the fluctuations of lift distribution which occur on the lifting surfaces when the structure deforms or when the aircraft is flying in turbulent atmosphere. The aerodynamic forces provide the energy necessary to maintain a forced oscillation or to produce an instability.

The flutter instability is particularly dangerous and a great effort has been devoted to the development of the aerodynamic and structural tools necessary for its analysis and prediction.

The aeroelastic phenomena occurring on helicopters are not fundamentally different from those which are observed on fixed wing aircraft, but they occur in a much more complicated aerodynamic environment, since the lifting surfaces are both advancing and rotating.

Then, in order to understand what happens on helicopters, it is necessary to have a clear understanding of what happens in the simpler case of fixed wing aircraft.

The lecture is divided into three parts.

In the first part, the theoretical tools used for the representation of the aircraft structures are briefly described ; a physical analysis of the flutter instability is given on a simple example, and a list of the most important aeroelastic problems encountered on helicopters is given.

In the second part the basic tools used for the prediction of the blade aerodynamic loads are described.

In the third, a formulation of the problem of forced vibration in forward flight is presented.



First part - THE AEROELASTIC VIBRATIONS

In this first part, the properties of the natural modes of vibration of a flexible structure are analyzed, and it is shown that the mode shapes are particularly convenient for the representation of the motion when the structure is excited by a source of energy.

Then the mechanism of bending-torsion flutter is shown on the simple example of a rigid aerofoil, with simplified aerodynamic forces.

Lastly, the most important aeroelastic phenomena encountered on rotary wing aircraft are listed.

I,1. METHODS USED FOR THE REPRESENTATION OF AN AIRCRAFT STRUCTURE

1,1.1. Discretization

The simple example of a cantilever beam will be used to illustrate the techniques used for the representation of a structure ; these can easily be extended to more complicated structures.

The beam is a continuous system (fig. 1). Its motion is defined by a function of time and of the spatial coordinate, the deflexion law.

The equilibrium of an elementary section of the beam is governed by a partial differential equation, and a boundary value problem can be defined. The solutions are easily obtained with the technique of variable separation when the beam has a uniform section. But the extension of the technique of variable separation to a more complex structure, such as an aircraft structure, would be almost impossible.



Fig. 1 - Case of a simple beam.

A more general technique based on a discretization procedure will be presented here.

A set of n spatial functions $Z_i(x)$ is chosen and the deflexion is approximated by a linear combination :

(1) $$z(x,t) = \sum_{i=1}^{n} Z_i(x)\, q_i(t)$$

The basis functions $Z_i(x)$ must satisfy the geometrical conditions at the section $x = 0$. For example, they could be defined as :

$$Z_i(x) = x^2 P_i(x)$$

$P_i(x)$ being a set of independant polynomials of degree $i-1$. Then, $Z_i(x)$ are such that $Z_i = Z_i' = 0$ for $x = 0$.

In this case, the deflexion would be a polynomial of degree $n-1$.

Obviously, the validity of the approximation (1) depends on the number and nature of the functions $Z_i(x)$. The basis of polynomial which is suggested here would be a poor choice for many practical applications.

With the approximation (1), the actual continuous system has been assimilated to a discrete system since its position is defined by a finite number of functions of time $q_i(t)$. These last functions are the generalized coordinates.

A matrix notation can be used if the sets of basis functions and of generalized coordinates are defined respectively as a line and a column matrix.

$$\mathbf{Z}(x) = \left[Z_1(x) \ldots Z_i(x) \ldots Z_n(x) \right]$$

$$\mathbf{q}(t) = \begin{pmatrix} q_1(t) \\ q_i(t) \\ q_n(t) \end{pmatrix}$$

The equation (1) can be written as

(2) $$z(x,t) = \mathbf{Z}(x)\mathbf{q}(t)$$

The kinetic and potential energy can be given in terms of the column $\mathbf{q}(t)$:

kinetic energy :

$$T = \frac{1}{2}\int_0^L \sigma(x)\, \dot{\bar{z}}(x,t)\, \dot{z}(x,t)\, dx \qquad (\sigma = \text{mass per unit length}),$$

$$= \frac{1}{2}\dot{\bar{\mathbf{q}}}\int_0^L \sigma(x)\, \bar{\mathbf{Z}}(x)\, \mathbf{Z}(x)\, dx\, \dot{\mathbf{q}} \qquad \text{(according to (2))}.$$

The integral is a positive definite matrix, the matrix of generalized masses. Let us denote it by $\mathbf{M}$. Then

(3a) $$T = \frac{1}{2}\dot{\bar{\mathbf{q}}}\,\mathbf{M}\,\dot{\mathbf{q}}$$

with

(3b) $$\mathbf{M} = \int_0^L \sigma\, \bar{\mathbf{Z}}\mathbf{Z}\, dx \quad , \quad \text{or} \quad , \quad M_{ij} = \int_0^L \sigma(x)\, Z_i(x)\, Z_j(x)\, dx$$

potential energy :

$$U = \frac{1}{2}\int_0^L EI\, \frac{\partial^2 \bar{z}}{\partial x^2}\, \frac{\partial^2 z}{\partial x^2}\, dx \qquad \text{with} \begin{cases} E = \text{Young modulus} \\ I = \text{bending moment of inertia} \end{cases}$$

$$= \frac{1}{2}\bar{\mathbf{q}}\int_0^L EI\, \bar{\mathbf{Z}}''(x)\, \mathbf{Z}''(x)\, dx\, \mathbf{q} \qquad \text{(according to (2))}$$

The integral is a positive definite matrix, the matrix of generalized stiffnesses. Let us denote it by $\mathbf{K}$. Then

(4a) $$U = \frac{1}{2}\bar{\mathbf{q}}\,\mathbf{K}\,\mathbf{q}$$

with

(4b) $$\mathbf{K} = \int_0^L EI\, \bar{\mathbf{Z}}''\mathbf{Z}''\, dx \quad , \quad \text{or} \quad , \quad K_{ij} = \int_0^L EI\, Z_i''(x)\, Z_j''(x)\, dx$$

Lagrangian equations

Since the only forces are the elastic and inertia forces, the Lagrangian equations can be written :

$$\frac{d}{dt}\left(\frac{\partial \bar{T}}{\partial \dot{\mathbf{q}}}\right) - \frac{\partial \bar{T}}{\partial \mathbf{q}} + \frac{\partial \bar{U}}{\partial \mathbf{q}} = 0$$

Equations (3a) and (3b) show that T is independent from $\mathbf{q}$. Consequently, $\frac{\partial T}{\partial \mathbf{q}} = 0$.

The remaining terms can be derived from (3a) and (4a) :

(5) $$\mathbf{M}\ddot{\mathbf{q}} + \mathbf{K}\mathbf{q} = 0$$

This matrix equation is verified with fundamental solutions of the form :

(6a) $$q_r(t) = X_r e^{i\omega_r t}$$

substituting (6a) into (5) and using the notation

(6b) $$\lambda_r = \omega_r^2$$

an eigen value formulation is arrived at :

(7) $$-\lambda_r M X_r + K X_r = 0$$

or

$$[\lambda_r - M^{-1}K] X_r = 0$$

I,1.2. Natural modes and modal representation

The motion corresponding to a fundamental solution is obtained if (6a) is substituted into (2). The resulting motion is a natural mode of vibration :

$$z_r(x,t) = Z(x) X_r e^{i\omega_r t}$$

let us use the notations

(8) $$Z_r^*(x) = Z(x) X_r = \sum_i Z_i(x) X_r^{(i)}$$

We get

(9) $$z_r(x,t) = Z_r^*(x) e^{i\omega_r t}$$

$Z^*(x)$ is the mode shape, ω_r is the natural circular frequency.

As the matrices M and K are Hermitian and positive definite, it can be shown that :

- the eigen values λ_r are real and positive and, consequently, ω_r is a real number according to (6.2),
- the coefficients $X_r^{(i)}$ of the vector column X_r have the same argument and X_r can be made a real column by normalization (i.e., by multiplying by a constant coefficient).

Consequently the mode shape $Z_r^*(x)$ defined by (8) is a real function of x and the natural mode defined by equation (9) is a harmonic vibration in which all the points vibrate at the same frequency ω_r, with the same phase. In this motion the total energy (kinetic energy + potential energy) remains constant. Then we say that the structure which is analyzed is a conservative system.

Orthogonality

The natural modes are often named normal modes because they verify orthogonality relations which will be shown here.

Let us consider equation (7) and premultiply it by the transpose of an eigen vector X_s .

(10a) $$\lambda_r \bar{X}_s M X_r = \bar{X}_s K X_r$$

a permutation of the suffixes r and s gives :

(10b) $$\lambda_s \bar{X}_r M X_s = \bar{X}_r K X_s$$

Let us transpose this equation, taking account of the property $\bar{M}=M$ sent $\bar{K}=K$

(10c) $$\lambda_s \bar{X}_s M X_r = \bar{X}_s K X_r$$

The difference (10a) – (10c) gives :

$$\bar{X}_s M X_r [\lambda_r - \lambda_s] = 0$$

Consequently :

(11a) $\bar{X}_s M X_r = 0$ if λ_r and λ_s are different ;

Substituting into (10a) we get :

(11b) $\bar{X}_s K X_r = 0$ if λ_r and λ_s are different.

Then, assuming that all the eigen values are distinct, two diagonal matrices μ and γ can be defined :

(12a) $$\mu_r^{(s)} = \bar{X}_s M X_r = 0 \quad \text{if } r \neq s$$

(12b) $$\gamma_r^{(s)} = \bar{X}_s K X_r = 0 \quad \text{if } r \neq s$$

and we have a relation between the diagonal terms :

$$\gamma_r^{(r)} = \lambda_r \mu_r^{(r)} \quad \text{(according to (10a)),}$$

$$= \omega_r^2 \mu_r^{(r)} \quad \text{(according to (6b)).}$$

Equations (11a) and (11b) define a propertie of orthogonality of the eigen vector X_r , X_s with respect to the matrices of generalized masses and stiffnesses. This properties can be related to an orthogonality of the mode shapes $Z_r^*(x)$ with respect to the

mass and stiffness distribution as will be shown.

Let us consider the equation (12a) and substitute (3b) for M

$$\mu_s^{(r)} = \bar{X}_r \int_0^L \sigma \bar{Z} Z \, dx \, X_s = 0 \quad \text{if} \quad s \neq r$$

but

$$Z(x) X_s = Z_s^*(x) \qquad \text{(according to (8))}$$

and in the same way,

$$\bar{X}_r Z = \overline{Z X_r}$$
$$= \bar{Z}_r^*$$
$$= Z_r^* \text{ (because } Z_r^* \text{ is a real function)};$$

then :

(13a)
$$\mu_s^{(r)} = \int_0^L \sigma(x) Z_r^*(x) Z_s^*(x) \, dx = 0 \quad \text{if} \quad s \neq r$$

This equation shows that the mode shapes Z_r^*, Z_s^* are orthogonal with respect to the mass distribution.

In the same way, (4b) can be substituted into (12b) :

$$\gamma_s^{(r)} = \bar{X}_r \int_0^L EI \bar{Z}'' Z'' \, dx \, X_s = 0 \quad \text{if} \quad s \neq r$$

but
$$Z'' X_s = Z_s^{*\prime\prime}$$
$$\bar{X}_r Z'' = Z_r^{*\prime\prime}$$

and

(13b)
$$\gamma_s^{(r)} = \int_0^L EI Z_r^{*\prime\prime} Z_s^{*\prime\prime} \, dx = 0 \quad \text{if} \quad s \neq r$$

This equation shows that the mode shapes are orthogonal with respect to the stiffness distribution.

REMARK : The normal modes (9) have not been determined on the actual continuous structure but on an approximate discrete system. The nomber of normal modes obtained in solving equation (7) is equal to the number of degrees of freedom of the discrete system while the number of modes of the actual beam is infinite.

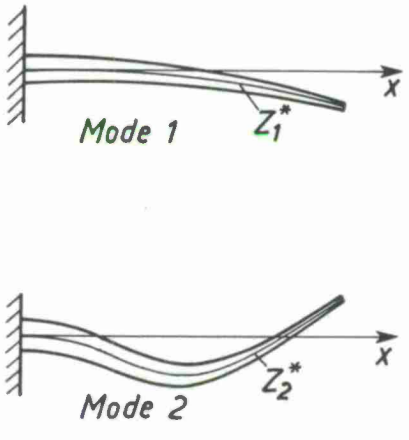


Fig. 2 - Simple beom - First two bending modes.

The difference between a natural mode of the discrete system and the corresponding mode of the continuous beam depends on the capacity of the set of functions $Z_i(x)$ to represent the mode shape of the actual beam. For example, the first mode, or fundamental bending shown in figure 2, can be represented with a good approximation with a polynomial of degree 4 or 5, and the use of the basis of polynomials suggested in paragraph I,1.1 would be accurate enough with a number of generalized coordinates equal to 3 or 4. But a higher number would be necessary if a good accuracy were also needed for mode 2 and even more if modes of higher order were considered.

Generally, if m is the number of modes for which a good accuracy is needed, the number of generalized coordinates, n, must be much larger than m :

$$n \gg m$$

This remains valid whatever the method used for the calculation of the normal modes of a structure. For example, when the designers use the finite element method, what they generally do for aircraft structures, they use several thousands of coordinates to obtain significant results for about 20 or 30 normal modes.

I,1.3. Modal representation and ground vibration test

Modal representation

Let us assume that the natural modes of the beam are known. Then the mode shapes $Z_i^*(x)$ can be used instead of the arbitrary functions $Z_i(x)$.

Equation (1) will be replaced by :

(14)
$$\zeta(x,t) = \sum_i Z_i^*(x) q_i(t)$$
$$= Z^*(x) q(t)$$

$Z^*(x)$ being the line matrix of basis functions.

The matrix of generalized mass is given, after (3b), by :

$$M_{ij}^{*(i)} = \int_0^L \sigma Z_i^* Z_j^* \, dx$$
$$= \mu_j^{(i)} \qquad \text{(according to (13a))},$$

and, similarly, the matrix of generalized stiffness is given, after (4b), by :

$$K_{ij}^{*(e)} = \int_0^L E I Z_i^{*''} Z_j^{*''} dx$$

$$= \gamma_{ij}^{(e)} \qquad \text{(according to (13b).}$$

Then the Lagrangian equation (5) is valid if M and K are replaced respectively by μ and γ :

(15) $$\mu \ddot{q} + \gamma q = 0$$

The diagonal matrices μ and γ are the matrices of generalized masses and stiffnesses for the modal representation.

This representation, which can be used only when the normal modes have been determined (either computed or measured) is generally interesting to analyze the vibrations induced by any source of energy.

The dissipotive structure with external forces

The actual structures are always dissipative. The system obtained from the actual structure, if the dissipative forces are neglected, is conservative and will be designated by "associated conservative system".

The mode shapes of the associated conservative system can be used to represent the motion of the actual dissipative structure when it is subjected to external forces.

In this case, equation (15) must be complemented by a matrix of generalized viscosity β and by a column of generalized forces :

(16) $$\mu \ddot{q} + \beta \dot{q} + \gamma q = Q$$

The structural damping forces are assimilated to viscous forces, $\beta \dot{q}$, and for many applications to stightly dissipative structure the non-diagonal terms of the matrix β are neglected.

The column of generalized forces is obtained from the virtual work.

For exemple, if forces $f_r(t)$ are applied at points located at x_r, the virtual work is given by :

$$\delta \mathcal{A} = \sum_r \delta z(x_r) f_r(t)$$

$$= \sum_{r,s} \delta q_s Z_s^*(x_r) f_r(t) \qquad \text{(according to (4)),}$$

And the generalized forces are the coefficients of the δq_s :

$$Q_s = \sum_r Z_s^*(x_r) f_r(t)$$

or, in matrix notation :

(17) $$Q = \bar{Z} f$$

where Z is the matrix of mode shapes at the points of application of the forces.

$$Z_{sr}^{(e)} = Z_s^*(x_r)$$

f is the column of forces f_r

After substitution of (17) into (16) we have :

(18) $$\mu \ddot{q} + \beta \dot{q} + \gamma q = \bar{Z} f$$

Ground vibration test

The normal modes which are necessary for the modal representation can be computed or determined experimentally with a harmonic ground vibration test.

Equation (18) determines the response to external forces. The forces f_r can be applied by means of shakers. Suppose that they are sinusoïdal with the same frequency and the same phase. Then the column f can be written :

$$f(t) = F e^{i\omega t}$$

and the solution takes the same force :

$$q(t) = \tilde{q} e^{i\omega t}$$

After substitution into equation (18) we obtain :

(19a) $$[-\omega^2 \mu + i\omega \beta + \gamma] \tilde{q} = \bar{Z} F$$

In order to determine the characteristics of a normal mode of the associated conservative system, it is necessary to isolate this mode of vibration by an "appropriation" of the excitation. The "phase criterium" permits the experimenters to check that this appropriation is performed satisfactorily.

The excitation forces having a commun phase, the phase criterium states that if all the points of the structure vibrate with a phase difference of 90° with respect to the excitation, then its motion is a natural mode of the associated conservative system.

To show it, we take the phase of the response as a phase reference (this can be done since we assume that all the points vibrate with the same phase). Then $\tilde{q}$ is a real column and F an imaginary column since there is a phase difference of 90° between f and q.

In equation (18), the real and imaginary parts can be separated. We get

(19b) $$(-\omega^2 \mu + \gamma)\,\tilde{q} = 0$$

(19c) $$i\omega\beta\,\tilde{q} = \tilde{Z} F$$

Equation (19b) governs the motion of the associated conservative system so that ω is one of the natural frequencies, ω_r, and $\tilde{q}$ is one of the eigen vectors $\tilde{q}_r$, and the resulting motion is one of the normal modes.

Equation (19c) determines the force distribution which permits the criterium to be verified. It shows that the excitation compensates the dissipative forces.

When the phase criterium is verified we say that the approximation of the excitation has been obtained. Then the natural frequency ω_r and the mode shape $Z_r^*(x)$ an recorded.

Several complementary manipulation are performed to determine the value of the generalized mass μ_r and generalized viscosity β_r.

The appropriation of the excitation is one of the major difficulties of the harmonic ground vibration test. The adjustment of the frequency and of the forces are performed either manually or automatically and the phase criterium is verified after several iterations. In principle it is necessary to distribute the forces according to equations (19c), but the matrix β is not known when the test is performed.

Fortunately, the aeronautical structures are only slightly dissipative and in this case it can be shown that the isolation of a normal mode can be performed satisfactorily even if the excitation is not distributed rigorously according to equation (19c) because the mode is selected with the frequency of excitation.

To show it, let us consider the matrix equation (19a). Using the notation $\tilde{Q} = \tilde{Z} F$ for the generalized forces, we have :

$$[-\omega^2 \mu + i\omega\beta + \gamma]\,\tilde{q} = \tilde{Q}$$

and the r^{th} equation can be written as :

$$-\omega^2 \mu_{rr} \tilde{q}_r + i\omega \sum_s \beta_{rs} \tilde{q}_s + \gamma_{rr} \tilde{q}_r = \tilde{Q}_r$$

if the non diagonal terms of the matrix β an neglected we get :

$$(-\omega^2 \mu_{rr} + i\omega \beta_{rr} + \gamma_{rr})\,\tilde{q}_r = \tilde{Q}_r$$

Generally a dimensionless damping coefficient α_r is defined by writting :

$$\beta_{rr} = 2\alpha_r \omega_r \mu_{rr}$$

Then, with the relation $\gamma_{rr} = \omega_r^2 \mu_{rr}$, we have :

$$\tilde{q}_r = \frac{\tilde{Q}_r}{\mu_{rr}\left[(\omega_r^2 - \omega^2) + 2i\omega\omega_r\alpha_r\right]}$$

The numerical value of α_r is normally of the order of 10^{-2}.

This equation shows that if a generalized coordinate q_r is excited at its resonance frequency, $\omega = \omega_r$, the value of $\tilde{q}_r$, which is inversely proportional to α_r, is very high. On the contrary, if the frequency of excitation is such that $\omega - \omega_r$ is not small compared to ω_r, then the response is governed by the inertial and elastic forces and it is much smaller :

The ground vibration tests give the experimental values of the coefficients entering into equations (18) (matrices μ, β and γ) and the mode shapes necessary to evaluate the generalized forces (matrix $\tilde{Z}$). Equation (18) may be used to investigate a forced excitation or an instability. In the last case, the forces f_r are determined by the response (column q and its derivatives).

The number of modes which must be measured in a ground vibration test depends on the nature of the problem which is to be treated later. Generally, the rate of convergence of the modal representation is better than for other representations : relatively few modes are necessary when the damping is small. For example suppose that the time variation of the excitation is defined by its frequency spectrum and that the frequency spectrum of the response is needed. Then, for each value of the frequency ω it will be necessary to consider only the normal modes whose resonance frequency is close to ω .

1,2,2. The flutter instability and the response to turbulence illustrated with a simple example.

Let us consider a rigid aerofoil mounted on two springs of stiffness k_1 and k_2 in a flow of velocity V . The flow may be turbulent.

The two degrees of freedom are the translation, $h(t)$, measured at the forward quarter chord point (conventionally) and the pitch angle, $\theta(t)$.

The flow turbulence would be characterized in the absence of the aerofoil by a velocity field $\vec{v}_T(x, z, t)$. The presence of the aerofoil creates another velocity field $\vec{v}(x, z, t)$ and the resulting field satisfies the condition of tangency on the aerofoil, i.e., the resulting velocity is tangent to the aerofoil for the particles in contact with the aerofoil surface (the flow can neither separate from nor cross the aerofoil).

The aerofoil is assimilated to a thin plate and its deflexion is given by :

$$z = c\,h(t) + x\,\theta(t)$$

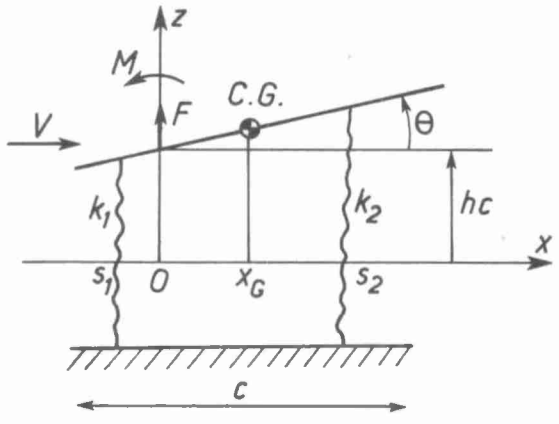


Fig. 3 - Representation of an aerofoil

Denoting by $\vec{i}$ and $\vec{k}$ the unit vectors along the axes ox and oz respectively, the velocity of a point of the aerofoil is given by : $\vec{k}\,\dot{z} = \vec{k}\,(c\dot{h} + x\dot{\theta})$ and the resulting relative velocity is :

$$\vec{V}_R = \vec{i}\,V + \vec{v}_T + \vec{v} - \vec{k}\,\dot{z}$$

The unit vector normal to the aerofoil is given by :

$$\vec{n} = \vec{k} - \vec{i}\,\theta$$

The condition of tangency is satisfied if the scalar product $\vec{V}_R \cdot \vec{n}$ is null ;

thence :

$$[\vec{i}\,V + \vec{v}_T + \vec{v} - \vec{k}\,\dot{z}][\vec{k} - \vec{i}\,\theta] = 0$$

Assuming that $\vec{v}_T$, $\vec{v}$, z and θ are small and neglecting second order terms, we get :

$$\vec{k}\,\vec{v} + \vec{k}\,\vec{v}_T - \dot{z} - V\theta = 0$$

or

$$\vec{k}\,\vec{v} = V\theta + \dot{z} - \vec{k}\,\vec{v}_T$$

$\vec{k}\,\vec{v}$ and $\vec{k}\,\vec{v}_T$ are the vertical components of $\vec{v}$ and $\vec{v}_T$ respectively. Denoting these components by w and w_T, we get :

$$w = V\theta + \dot{z} - w_T$$

Since w is the douwnwash created by the aerofoil, it determines the pressure field, the lift and the moment.

Usually a nondimensional quantity, the local angle of attack, is used instead of the downwash :

$$\alpha(x,t) = \theta + \frac{\dot{z}}{V} - \frac{w_T}{V}$$

and, with $z = ch + x\theta$

$$\alpha = \theta + \frac{c\dot{h}}{V} + \frac{x\dot{\theta}}{V} - \frac{w_T}{V} \tag{20}$$

The aerodynamic force acting on the aerofoil depends on the angle of attack, on the uniform velocity V and on the fluid density ρ.

An oversimplifying assumption which is valid only for a qualitative analysis will be made for the evaluation of this force. We assume that there is a lift acting on the forward quarter chord point ($x = 0$) proportional to the local angle of attack, and a pitch damping moment proportional to $\dot{\theta}$.

The lift is given by

$$F = -\tfrac{1}{2}\rho V^2 c\,\ell\,C_{z\alpha}\left(\theta + \frac{c\dot{h}}{V} - \frac{w_T}{V}\right) \tag{21a}$$

where ℓ is the width of the aerofoil, c the chord length and $C_{z\alpha}$ the lift derivative.

The pitch damping moment is given by :

$$M = -\tfrac{1}{2}\rho V c^3 \ell\,C_{m\dot{\theta}}\,\dot{\theta} \tag{21b}$$

where $C_{m\dot{\theta}}$ is the pitch damping derivative.

Equations (21a) and (21b) can be written in a matrix force :

$$\begin{pmatrix} Fc \\ M \end{pmatrix} = -\tfrac{1}{2}\rho V^2 c\,\ell \begin{bmatrix} \cdot & C_{z\alpha} \\ \cdot & \cdot \end{bmatrix} \begin{pmatrix} h \\ \theta \end{pmatrix} - \tfrac{1}{2}\rho V c^3 \ell \begin{bmatrix} C_{z\alpha} & \cdot \\ \cdot & C_{m\dot{\theta}} \end{bmatrix} \begin{pmatrix} \dot{h} \\ \dot{\theta} \end{pmatrix} + \tfrac{1}{2}\rho V w_T c^2 \ell\, C_{z\alpha} \begin{pmatrix} 1 \\ \cdot \end{pmatrix} \tag{22}$$

The equations show that the aerodynamic forces can be divided into two parts : a term independant of the oscillations of the aerofoil, and proportional to w_T, and the other terms which have a linear dependency on the oscillations.

Then the system can be represented in a block diagram like that of figure 4.

One of the blocks represents the structural dynamics. The input is the aerodynamic forces and the output is the response oscillation. The other block represents the aerodynamics of the aerofoil : the input is the angle of attack and the output the aerodynamic forces.

As the angle of attack is determined by the motion of the structure and by the velocity of turbulence, the block diagram shows that there is a closed loop and an independant input. The instabilities will be due to the closed loop and the forced excitations will be produced by the turbulence

The equilibrium equations can be derived from the kinetic and potential energies and from the virtual work, through the Lagrangian equations.

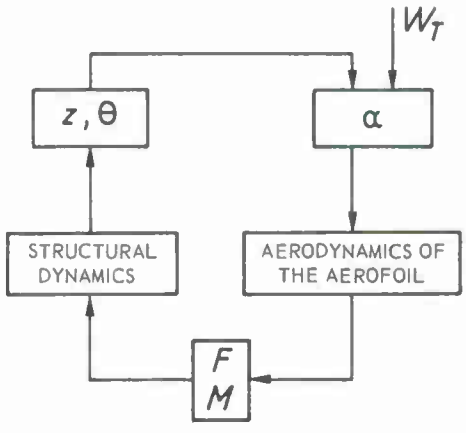


Fig. 4 - Block diagram of aerofoil response

Denoting by m the mass of the aerofoil and by I_θ its moment of inertia, the kinetic energy is given by :

$$T = \frac{1}{2} m (c\dot{h} + \dot{\theta} x_G)^2 + \frac{1}{2} I_G \dot{\theta}^2$$

Or,

$$2T = [\dot{h} \;\; \dot{\theta}] \begin{bmatrix} mc^2 & mcx_G \\ mcx_G & mx_G^2 + I_G \end{bmatrix} \begin{pmatrix} \dot{h} \\ \dot{\theta} \end{pmatrix} \tag{23a}$$

The potential energy is given by :

$$2U = [h \;\; \theta] \begin{bmatrix} c^2(k_1 + k_2) & c(k_1 s_1 + k_2 s_2) \\ c(k_1 s_1 + k_2 s_2) & k_1 s_1^2 + k_2 s_2^2 \end{bmatrix} \begin{pmatrix} h \\ \theta \end{pmatrix} \tag{23b}$$

and the virtual work of the aerodynamic forces :

$$\delta a = c\,\delta h\, F + \delta\theta\, M = [\delta h \;\; \delta\theta] \begin{pmatrix} cF \\ M \end{pmatrix}$$

The column $\begin{pmatrix} cF \\ M \end{pmatrix}$ can be identified with the column of generatized forces and we can write the Lagrangian equations using (22), (23a) and (23b)

$$\begin{bmatrix} mc^2 & mcx_G \\ mcx_G & mx_G^2 + I_G \end{bmatrix} \begin{pmatrix} \ddot{h} \\ \ddot{\theta} \end{pmatrix} + \begin{bmatrix} c^2(k_1 + k_2) & c(k_1 s_1 + k_2 s_2) \\ c(k_1 s_1 + k_2 s_2) & k_1 s_1^2 + k_2 s_2^2 \end{bmatrix} \begin{pmatrix} h \\ \theta \end{pmatrix} + \cdots \tag{24}$$

$$\cdots + \frac{1}{2} \rho V^2 c^2 \ell \begin{bmatrix} \cdot & C_{3\alpha} \\ \cdot & \cdot \end{bmatrix} \begin{pmatrix} h \\ \theta \end{pmatrix} + \frac{1}{2} \rho V c^3 \ell \begin{bmatrix} C_{3\alpha} & \cdot \\ \cdot & C_{m\dot{\theta}} \end{bmatrix} \begin{pmatrix} \dot{h} \\ \dot{\theta} \end{pmatrix} = \frac{1}{2} \rho V w_T c^2 \ell C_{3\alpha} \begin{pmatrix} 1 \\ 0 \end{pmatrix}$$

Using the notation :

$$q = \begin{pmatrix} h \\ \theta \end{pmatrix} \qquad [M] = \begin{bmatrix} mc^2 & mcx_G \\ mcx_G & mx_G^2 + I_G \end{bmatrix}$$

$$[K] = \begin{bmatrix} c^2(k_1 + k_2) & c(k_1 s_1 + k_2 s_2) \\ c(k_1 s_1 + k_2 s_2) & k_1 s_1^2 + k_2 s_2^2 \end{bmatrix}$$

$$[B] = \frac{1}{2} c^3 \ell \begin{bmatrix} C_{3\alpha} & \cdot \\ \cdot & C_{m\dot{\theta}} \end{bmatrix} \qquad [C] = \frac{1}{2} c^2 \ell \begin{bmatrix} \cdot & C_{3\alpha} \\ \cdot & \cdot \end{bmatrix} \qquad (S) = \frac{1}{2} c^2 \ell C_{3\alpha} \begin{pmatrix} 1 \\ 0 \end{pmatrix}$$

we get :

$$M\ddot{q} + \rho V B \dot{q} + (K + \rho V^2 C) q = \rho V w_T S \tag{25a}$$

it can be seen that the mass and stiffness matrices, M and K, are Hermitian, i.e., $\bar{M} = M$ and $\bar{K} = K$ (the symbol ($\bar{}$) denoting the transpose.

As they determine the kinetic and potential energies, according to (23a) and (23b), these matrices are positive definite, i.e. they are such that for any column X, real or complex, the products $\bar{X} M X$ and $\bar{X} K X$ are real and positive numbers. To verify this condition, the eigen values of M and K must be positive (these eigen values are real since the matrices are Hermitian).

The property of Hermiticity of the matrices M and K is a consequence of a symmetry of the structural forces. For example, $\bar{K} = K$ is a consequence of the principle of reciprocity of Maxwell.

There is no reason for the aerodynamic matrices B and C to have the same property. In fact, we can check that C is not Hermitian ($\bar{C} \neq C$). The matrix B is Hermitian and positive definite, but this particular feature results from the simplification used in the derivations of the aerodynamic forces.

Equations (25a) is a set of ordinary differential equations with a right hand side. The response of the system to turbulence is

determined by a particular solution of the complete equations and its stability is governed by the equations without right hand side. This last problem only will be considered.

The matrix equation is :

(25b) $$M\ddot{q} + \rho V B\dot{q} + (K + \rho V^2 C)q = 0$$

The fundamental solutions are exponential terms of the form :

$$q(t) = \begin{pmatrix} h(t) \\ \theta(t) \end{pmatrix} = \begin{pmatrix} Z \\ \Theta \end{pmatrix} e^{pt}$$

(26a) $$q(t) = X e^{pt} \qquad \text{(with the notation } X = \begin{pmatrix} Z \\ \Theta \end{pmatrix}\text{)}.$$

If the number p and the vector column X are complex, it is implicit that the real part of $q(t)$ must be taken to obtain a physical solution. Then, the real part of p determines the damping, and the imaginary part is the circular frequency.

Substituting (26a) into (25b) we get :

(26b) $$[p^2 M + p\rho V B + K + \rho V^2 C]X = 0$$

Solutions $X \neq 0$ are obtained only for values of p which make the matrix inside the brackets singular. Hence the values of p which must be considered are the roots of the equation :

$$\det(p^2 M + p\rho V B + K + \rho V^2 C) = 0$$

(characteristic determinant).

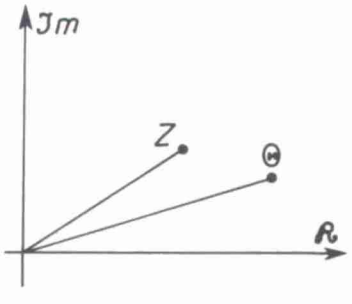


Fig. 5 - Representation of the roots in the complex plane.

To each root p_r corresponds an eigen vector X_r. If p_r is complex, the vector X_r is generally complex and its coefficients can be represented in the complex plane (fig. 5). Then the modulus of each term is the amplitude of the corresponding variable at the time $t = 0$ and the argument is the phase difference with respect to a given phase reference.

When Z and Θ have the same argument, i.e., when they are on the same axis in the complex plane, all the points of the system vibrate with the same phase.

The stability of the system is determined by the roots p_r : the flutter instability is obtained for p_r complex with a positive real part.

For each value of ρ and V a set of roots is obtained. For small values, all the p_r have their real part negative and the aerofoil is stable, but there is a range of values of ρ and V for which there are roots with a positive real part (region of instability).

If ρ and/or V is increased from zero to the region of instability, the dampings and frequencies, given respectively by the real parts and imaginary parts of the p_r, varies as shown in figure 6.

The description of the mechanism which permits the flutter instability can be made clearer if we imagine that a harmonic excitation is applied to the aerofoil by an external source of energy by means, for instance, of electrodynamic shakers.

Then equation (25b) must be complemented by a column of generalized forces, at the right hand side, which will take the form :

$$Q(t) = F e^{i\omega t}$$

ω being the circular frequency of the excitation.

The solution determining the forced response takes a similar form :

$$q(t) = X e^{i\omega t}$$

After substitution into (25b) we obtain :

(27) $$-\omega^2 MX + i\omega\rho V B X + (K + \rho V^2 C)X = F$$

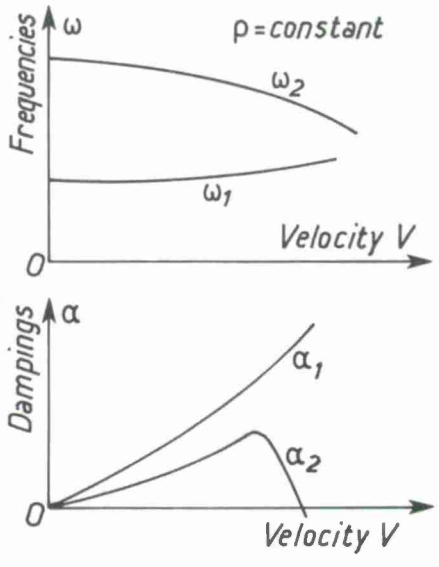


Fig. 6 - Variations of the real and imaginary of the roots.

The vector X is the complex representation of the displacement. Similarly, $V = i\omega X$ is the complex representation of the velocity of oscillation. The transpose $\bar{V}$ is a line matrix (the symbol $(^-)$ denotes the change of columns into lines and of complex elements into their conjugates) and the product $w = \bar{V}F$ in the complex power. Separating real and imaginary parts, we get :

(28) $$w = -i\omega \bar{X} F$$
$$= w_A + i w_R$$

The real part, w_A is the active power and the imaginary part, w_R is the reactive power.

Substituting 8 into 9 we obtain :

$$w = -\iota\omega^3 \bar{X} M X + \omega^2 \rho V \bar{X} B X - \iota\omega \bar{X} K X - \iota\omega\rho V^2 \bar{X} C X = w_A + \iota w_R \tag{29a}$$

The conjugate of w is given by

$$\bar{w} = \iota\omega^3 \bar{X} M X + \omega^2 \rho V \bar{X} \bar{B} X + \iota\omega \bar{X} K X + \iota\omega\rho V^2 \bar{X} \bar{C} X = w_A - \iota w_R \tag{29b}$$

The active and reactive powers are given by $w_A = \frac{1}{2}(w + \bar{w})$ and $w_R = \frac{1}{2}(w - \bar{w})$.

We obtain :

$$w_A = \omega^2 \rho V \bar{X} \frac{B+\bar{B}}{2} X - \iota\omega\rho V^2 \bar{X} \frac{C-\bar{C}}{2} X \tag{30a}$$

$$\iota w_R = \iota\omega^3 \bar{X} M X + \omega^2 \rho V X \frac{B-\bar{B}}{2} X - \iota\omega \bar{X} K X - \iota\omega\rho V^2 X \frac{C+\bar{C}}{2} X \tag{30b}$$

If w_A is positive, an active power is furnished to the aerofoil by the shakers and if w_A is negative, the power is taken from it. Now if w_A is negative and if at the same time the reactive power is null $w_R = 0$ we can infer that the aerofoil would be naturally unstable.

Consequently, the condition $w_A < 0$ is necessary for an instability to occur. It is written as :

$$\omega^2 \rho V \bar{X} \frac{B+\bar{B}}{2} X - \iota\omega\rho V^2 X \frac{C-\bar{C}}{2} X < 0 \tag{31}$$

In the simple example which is considered here, the matrix B is given by :

$$[B] = \frac{1}{2} c^3 \ell \begin{bmatrix} C_{z\alpha} & \circ \\ \circ & C_{m\dot{\theta}} \end{bmatrix}$$

As it is diagonal, its eigen values are the diagonal terms $C_{z\alpha}$ and $C_{m\dot{\theta}}$, and these terms are normally positive. Thus B is a positive definite matrix. As it is Hermitian, we have : $\frac{B+\bar{B}}{2} = B$ and

$$X \frac{B+\bar{B}}{2} X = \bar{X} B X$$

is a real and positive number.

Then the instability can occur only if the term $\iota\omega\rho V^2 X \frac{C-\bar{C}}{2} X$ is large enough. X is generally a complex column which can be separated into real and imaginary parts, $X = X' + \iota X''$

We get :

$$X \frac{C-\bar{C}}{2} X = (\bar{X}' - \iota \bar{X}'') \left[\frac{C-\bar{C}}{2}\right] (X' + \iota X'')$$

$$= \bar{X}' \frac{C-\bar{C}}{2} X' + \bar{X}'' \frac{C-\bar{C}}{2} X'' + \iota \left[\bar{X}' \frac{C-\bar{C}}{2} X'' - \bar{X}'' \frac{C-\bar{C}}{2} X'\right]$$

X', X'', C and $\bar{C}$ being real, $\bar{X}'(C-\bar{C})X', \ldots, \bar{X}''(C-\bar{C})X'$ are real numbers and equal to their conjugates. Consequently :

$$\bar{X} \frac{(C-\bar{C})}{2} X = \iota \bar{X}'(C-\bar{C})X''$$

and

$$\iota\omega\rho V^2 \bar{X} \frac{C-\bar{C}}{2} X = \omega\rho V^2 \bar{X}'(C-\bar{C})X'' \tag{32}$$

$C - \bar{C}$ is the anti-Hermitian component of the matrix C, in the example which has been treated, we have :

$$[C] = \frac{1}{2} c^2 \ell \begin{bmatrix} \circ & C_{z\alpha} \\ \circ & \circ \end{bmatrix}$$

and

$$\frac{C-\bar{C}}{2} = \frac{1}{4} c^2 \ell \begin{bmatrix} \circ & C_{z\alpha} \\ -C_{z\alpha} & \circ \end{bmatrix}$$

The presence of this anti-Hermitian component is necessary for the instability to take place. Its presence stems from the fact that the aerodynamic forces have not the same properties of symmetry as the structural forces. In this example $C_{z\alpha}$ denotes a lift induced by the pitching deflexion which is not reciprocated by a pitching moment induced by the translational deflexion.

Now let us consider equation (32) and assume that all the complex numbers in the column X have the same argument. This would indicate that all the points of the aerofoil oscillate with the same phase. Then X'' would be proportional to X', i.e. $X'' = \delta X'$, δ being a real number. After substitution into (32) we have :

$$\iota\omega\rho V^2 \bar{X} \frac{C-\bar{C}}{2} X = \delta\omega\rho V^2 \bar{X}'(C-\bar{C})X'$$

$$= 0 \quad \text{since} \quad \bar{X}'\bar{C}X' = \bar{X}'CX'$$

This shows that in order to make the term (32) different from zero it is necessary that the column vectors X' and X'' be independent. This independency is obtained only if the coefficients of the column X have different arguments and in that case the different points of the aerofoil vibrate with different phases.

This phase difference is fundamental for the energy transfer from the flow to the structure as illustrated in figure 7. In this figure, the aerofoil is moving from right to left and oscillating in pitch and translation. The vertical displacements have been amplified. If the phase difference between translation and pitch is 90° as shown in the figure, it can be seen that the lift acts upward when the aerofoil is moving upward and downward when it is moving downward. In other words, it is always acting in the direction of the motion and performing a positive work which may increase the amount of energy of the structure.

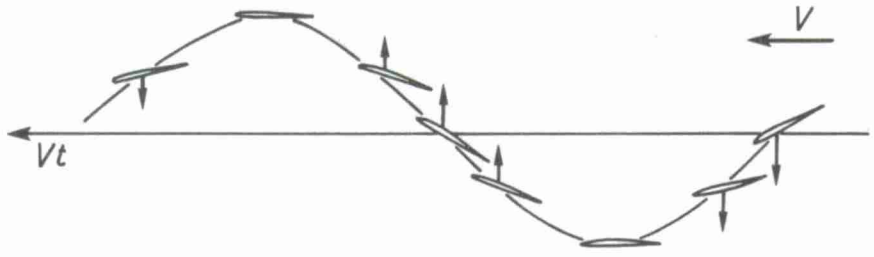


Fig. 7 - Energy transfer from the flow to the structure.

The phase difference between pitch and translation is not equal to 90° in actual flutter instabilities because a smaller phase difference may be sufficient for the aerodynamic forces to provide the amount of energy necessary to compensate the energy dissipated in the structure and the aerodynamic damping (matrix B). But the presence of a phase difference is a fundamental feature of this type of instability.

The conditions which permit such a phase difference to occur depends on the elastic and inertia characteristics of the structure, i.e. of the mass and stiffness distribution. For example, if the centre of gravity of the aerofoil and the elastic axis resulting from the two springs were located at the quarter chord point ($x = 0$) the flutter instability coud not be met. Also, if the spring stiffnesses k_1 and k_2 were very high, the instability could be met only for high values of the dynamic pressure.

This example is an illustration of the bending-torsion flutter which could occur on wings or helicopter blades with a poor design.

The necessary condition (31) has been fulfilled with the anti-Hermitian component of the matrix C because B is a positive definite matrix. But there are situations in which $B + \bar{B}$ is not positive definite. Then $\bar{X}(B+\bar{B})X$ can be negative and the presence of the anti-Hermitian component $C - \bar{C}$ is not necessary for the condition (31) to be fulfilled. Furthermore, in this case, there is no need for the vector column X to be complex. If it is real, it defines a simple oscillation of the aerofoil, with the same phase at all points, which could be obtained with only one degree of freedom. This type of instability is named «single degree of freedom flutter». The term $\bar{X}\frac{B+\bar{B}}{2}X$ can be assimilated to the power dissipated by a damper. When it is negative, we say that the aerodynamic forces provide a negative damping. This situation may be encountered when there is an important delay between the variation of angle of attack and the variation of the pressure distribution over the aerofoil. It can be observed in low supersonic and in transonic flow- when the perturbations due to the aerofoil motion are travelling at small velocity with the receding acoustic wave front. The phenomenon may be complicated by the presence of a shock wave interacting with the boundary layer.

At lower speed an effect of negative damping may be observed on aerofoils oscillating at a high mean angle of attack, near stall (stall flutter). Then the unsteady forces are provided by the flow separation and reattachment associated with the oscillation.

1,3. AEROELASTIC PHENOMENA OF ROTARY WING AIRCRAFT

Phenomena of forced or self excited vibrations such as those which have been illustrated with an aerofoil mounted on a flexible support (section 1.1) may occur when a flexible structure is associated with a source of energy. As was shown, the instability may be due to a coupling effect between the structural degrees of freedom or to a negative damping.

As the structures of the rotary wing aircraft have many degrees of freedom there are many ways for the aerodynamic forces, and even for the engine, to provide a vibratory energy, and many types of instabilities can be observed if the design of the structure is inadequate.

The conditions in which the vibrations are generated are particularly complex in a helicopter in forward flight, when the advancing velocity combines with the rotation.

More and more attention is given to the vibration problems of rotary wing aircraft and there is a need for analytical and experimental methods for the design and development of new aircraft.

As this lecture is devoted mainly to the fundamental methods, the different types of instabilities which can be met will only be mentioned. A more detailed description can be found in the references.

A distinction will be made between phenomena which can occur with only an axial flow and those which result from the combination of the advancing and rotational velocity.

1,3.1. Vibrations observed with axial flow

The flow field around a blade is much simpler when the velocity component in the rotor plane is equal to zero. This is the case for a helicopter in hovering or for a propeller.

Then it is interesting to consider a system of Cartésian coordinates rotating at constant speed with the rotor. When they vibrate, the blades assume small displacement with respect to these axes, and the flow field is a combination of a steady field due to the uniform rotation and of a small perturbation unsteady field due to the vibration.

Those vibrations, can be separated into :

- flapping, or normal vibrations,
- lagging, or coplanar vibrations,
- oscillations of the rotor disc due to the flexibility of the fuselage and hub support.

The instabilities which are most frequently observed in this condition are : the ground resonance, the whirl flutter, the flap-lag instabilities, and the blade interference.

Ground resonance : The ground resonance denotes a vibration which can often be observed during the ground test of a helicopter. It is due to the coupling between the fuselage and rotor in-plane degrees of freedom, the engine providing the energy. This instability is sensitive to the landing gear characteristics and to the damping of the lead-lag blade vibrations.

Whirl flutter : The whirl flutter may be observed whenever a rotor is mounted on a flexible support. If we consider a helicopter rotor, for example, the pitching and rolling oscillations of the rotor are coupled by the gyroscopic and aerodynamic forces, the pitching oscillation inducing a rolling moment, and the rolling oscillations inducing a pitching moment. This instability, which was previously observed on propellers of turbo-prop aircraft is an important difficulty for the development of new solutions to the problem of vertical take-off (such as tilt-rotor).

Flap-lag instability: The flap-lag instability is experienced with hingeless rotors. The relevant degrees of freedom are the blade flap, lead-lag and torsional deflexion with respect to the coordinate system rotating with the rotor shaft. The instability is influenced by the location of the pitch bearing or by the relative flexibility occuring inboard and outboard of the pitch bearing.

Blade interference :

Aerodynamic interferences are transmitted from one blade to another through the wakes.

The geometry of these wakes is determined by the trajectory of the blades. If the contraction of the flow is neglected, each wake can be assimilated to a helicoidal sheet of vortices. The strength of the vortices is determined by the variations of lift (span wise variation and time rate of variation) at the instant of their formation.

The wake interference is particularly important when the inflow through the rotor is small because then each blade is at a short distance from the wake of the preceding one.

In that situation, the blade is strongly influenced by the «memory» of the lift variation on the preceding blade.

Obviously, this interaction has not the same properties of reciprocity as the structural forces and consequently it may give an instability in certain conditions.

I,3.2. Vibrations in forward flight

With the combination of the advancing and rotational speeds which occur in forward flight, very severe forced or self-excited vibrations may be observed on helicopters.

The variation of blade velocity which occurs periodically depends on the advancing ratio, $\mu = V/\omega R$, where V is the advancing velocity and ωR the blade tip velocity due to rotation. The resulting tip blade velocity varies between $\omega R - V$ on the retreating blade and $\omega R + V$ on the advancing blade (fig. 8).

For a blade section of radial coordinate r , the velocity component normal to the leading edge is given by :

$$U = \omega r + V \sin\theta$$

This velocity component determines the dynamic pressure acting on each blade section.

On the retreating side of the rotor disc, U may take negative values. The locus of the points for which $U = 0$ is defined by the equation

$$\omega r + V \sin\theta = 0 \qquad \text{or} \qquad \frac{r}{\sin\theta} = \mu R$$

This equation shows that the points for which $U = 0$ are located on a circle of diameter μR, the "reverse circle". Inside this circle, U is negative, i.e. the flow is going from trailing to leading edge.

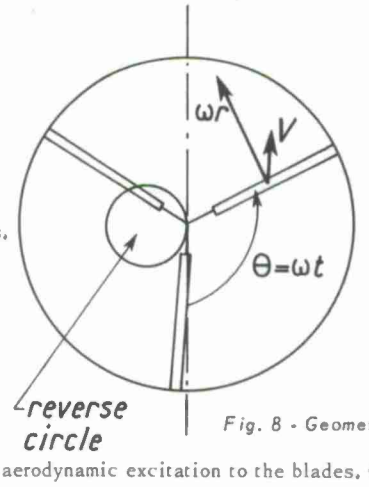


Fig. 8 - Geometry of advancing flight.

The cyclic variations of velocity and of pitch angle provide a forced aerodynamic excitation to the blades. Furthermore, several aeroelastic phenomena may occur as a consequence of the high speed on the side of the advancing blade, and of the large angle of attack on the side of the retreating blade.

The bending-torsion flutter may occur on the advancing blade if the torsion stiffness and the location of the elastic axis and of the section center of gravity are inadequate.

The buzz is a transonic instability which may be observed on the advancing blade tip.

The stoll-flutter is a self excited vibration associated to the high angle of attack on the retreating blade.

The periodic vibrations can always be observed in forward flight.

I,3.3. The predictions of aeroelastic vibrations

The analysis and the prediction of the aeroelastic phenomena is much more difficult for a rotary wing aircraft than it is for an aircraft wing.

Some of the calculation methods in current use are described in the references. Several authors have developed sophisticated methods for the determination of the aerodynamic forces, taking account of the wakes. Others have developed calculation methods

adapted to the prediction of a particular instability.

The form of the equations governing the response of the complete structure with the flexible fuselage and blades depends on the formulation used for representating the aerodynamic forces. If a simplified quasi-steady strip theory is used, for example, a system of differential equations with periodic coefficients is obtained.

When the analysis is restricted to a particular instability some simplifications can be done. For example, for an investigation on the bending-torsion flutter of the advancing blade, the degrees of freedom of the fuselage are generally neglected.

The problems which are particularly difficult to analyse theoretically can be investigated with wind tunnel tests of aeroelastic similar models.

The problem of response to the cyclic excitation in forward flight can be solved with numerical procedures based on a linear theory. In this lecture we shall concentrate on this problem to illustrate an application of the fundamental methods.



Second part - THE UNSTEADY AERODYNAMIC FORCES

This second part is devoted to the basic tools used for the prediction of the aerodynamic loads on the blades.

The theory of the lifting surface moving at constant speed and vibrating at small amplitudes is currently applied for aircraft flutter investigations.

But the motion of the helicopter blades is so complex that the prediction of the aerodynamic forces acting on them must be based on a more general theory, valid for a lifting surface moving arbitrarily.

Numerical procedures have been developed by several authors to perform calculations based on a discrete representation of the wakes.

The method which will be used in the third part of the lecture, for the prediction of the periodic excitations in forward flight, is based on a general linearized theory. The basic formulation is an integral equation relating the velocity potential to the time history of the motion and lift of a lifting surface moving arbitrarily.

The basic assumptions are : the fluid is inviscid, the transformations are isotropic, the perturbations due to the motion of the lifting surface are small -which permits to linearize the problem-, and the flow remains attached.

With the first assumption, a velocity potential can be defined and the last assumption provides the values of the normal derivative on the lifting surface (boundary condition).

The derivation of the integral equation is given in the following paragraphs.

II,1. GENERAL EQUATIONS

Since a lifting surface is assumed to move arbitrarily, the velocity field will be related to a fixed origine O. Then a point P will be defined by a vector $\overrightarrow{OP}$, noted $\vec{P}$.

A velocity potential φ can be defined as well as an acceleration potential ψ, and the substantial derivative d/dt is equal to the partial derivative $\partial/\partial t$.

The velocity potential verifies the wave equation :

$$\nabla^2\varphi - \frac{1}{a^2}\frac{\partial^2\varphi}{\partial t^2} = 0$$

where a is the sound velocity.

The velocity of the fluid at a point P is given by :

$$\vec{v}(P,t) = \overrightarrow{grad}\,\varphi$$

and the acceleration :

$$\frac{d\vec{v}}{dt} = \overrightarrow{grad}\,\frac{\partial\varphi}{\partial t}$$

The acceleration potential is defined by :

$$\psi = \frac{\partial\varphi}{\partial t} \tag{33}$$

and the reciprocal relation can be written :

$$\varphi(P,t) = \int_{-\infty}^{t} \psi(P,t_0)\,dt_0 \tag{34}$$

ψ verifies the wave equation as well as φ :

$$\nabla^2\psi - \frac{1}{a^2}\frac{\partial^2\psi}{\partial t^2} = 0$$

φ, ψ, $\vec{v}$ are small quantities.

Let p and ρ be respectively the fluid pressure and the density ; p_∞ and ρ_∞ are the values at infinity.

$p - p_\infty$ is a small quantity, the pressure perturbation, and similarly $\rho - \rho_\infty$ is a small quantity.

Neglecting second order terms, the equation of equilibrium of pressure and inertia forces can be written :

$$\begin{aligned} \overrightarrow{grad}\, p &= -\rho_\infty \frac{d\vec{V}}{dt} \\ &= -\rho_\infty \frac{d}{dt} \overrightarrow{grad}\, \varphi \\ &= -\rho_\infty \overrightarrow{grad}\, \frac{d\varphi}{dt} \\ &= -\rho_\infty \overrightarrow{grad}\, \psi \qquad \text{(according to (33))} \end{aligned}$$

And, after integration : $p - p_\infty = -\rho_\infty \psi$ (according to (33))

(35)

II,2. THE BOUNDARY CONDITIONS ON THE LIFTING SURFACE

The lifting surface is assimilated to an infinitely thin plate. The pressure is different on the two faces and the pressure difference, or pressure discontinuity creates the lift.

Let us consider a lifting surface element, of area $d\sigma$, centered on a point P (fig. 9). At an instant t, its position is defined by a vector $\vec{P}$, its velocity by a vector $d\vec{P}/dt = \dot{\vec{P}} = \vec{V}$ and its orientation by the unit normal vector $\vec{n}$.

If we consider a fluid particle in contact with the point P, the relative velocity (i.e., velocity of P - velocity of the particle) is $\dot{\vec{P}} - \overrightarrow{grad}\, \varphi$

Then, if we assume that there is no flow separation, the velocity is tangent to the lifting surface, or normal to $\vec{n}$, and we have the condition :

$$(\dot{\vec{P}} - \overrightarrow{grad}\, \varphi).\vec{n} = 0$$

or

(36) $$\overrightarrow{grad}\, \varphi . \vec{n} = \dot{\vec{P}}.\vec{n}$$

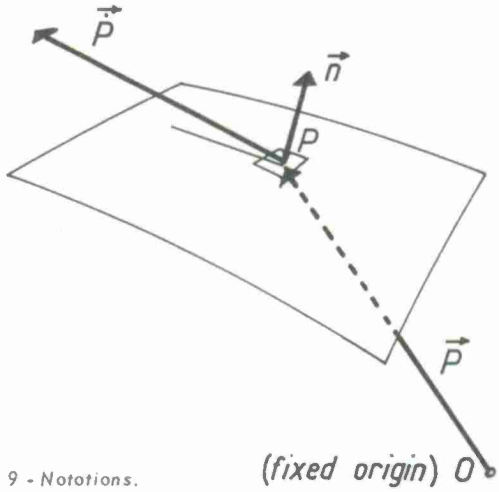


Fig. 9 - Notations.

$\dot{\vec{P}}\vec{n}$, the normal component of the velocity $\dot{\vec{P}}$, is defined when the motion of the lifting surface is given.

Equation (36) is the boundary condition on the lifting surface.

The linearization of the boundary value problem is valid only if the normal component of velocity $\dot{\vec{P}}\vec{n}$ (which produces the perturbation into the fluid according to (36)) is small.

The scalar product $\overrightarrow{grad}\, \varphi . \vec{n}$ is the normal derivative of φ. Its value at point P is given by :

$$\overrightarrow{grad}\, \varphi . \vec{n} = \lim_{\varepsilon = 0} \frac{1}{\varepsilon} \left[\varphi(\vec{P} + \varepsilon \vec{n}) - \varphi(\vec{P}) \right]$$

In the applications described in the third part of this lecture, this quantity will be determined numerically by a finite difference procedure.

II,3. THE ACCELERATION DOUBLET IN AN INCOMPRESSIBLE FLUID

The solution of the boundary value problem will be built with a combination of fundamental singular solutions of the wave equation. The acceleration doublet will be particularly convenient because it is equivalent to an element of lifting surface. It will be derived from the acceleration source.

An incompressible fluid will be considered first for the sake of simplicity. Then the sound velocity, a, is infinite and the wave equation is replaced by the simpler Laplace equation.

Let us consider an acceleration source of strength $q(t)$ moving along a path defined by a vector $\vec{OP_o}(t)$, or, more briefly, $\vec{P_o}(t)$. If the fluid is incompressible, the acceleration potential induced by the source at a point P is inversely proportional to the distance :

$$\psi_s(P,t) = -\frac{q(t)}{4\pi |\vec{P} - \vec{P_o}|}$$

The acceleration doublet can be built with two sources of opposite strength located at an infinitely small distance along the axis of the doublet, which is defined by a unit vector $\vec{n_o}(t)$ (fig. 10).

Hence, the acceleration potential ψ_D is given by :

$$\psi_D(P,t) = \lim_{\varepsilon = 0} \frac{1}{\varepsilon} \left[\psi_s(\vec{P} - \vec{P_o}) - \psi_s(\vec{P} - [\vec{P_o} + \varepsilon \vec{n_o}]) \right]$$

or

$$\varphi_D(P,t) = \overrightarrow{grad}\,\varphi_S \cdot \vec{n}_0$$

(37)
$$= \frac{q(t)\,[\vec{P}-\vec{P}_0]\,\vec{n}_0}{4\pi\,|\vec{P}-\vec{P}_0|^3}$$

The pressure field is given by substitution of φ_D into (35) :

(38)
$$p-p_\infty = -\rho_\infty \frac{q(t)\,[\vec{P}-\vec{P}_0]\,\vec{n}_0}{4\pi\,|\vec{P}-\vec{P}_0|^3}$$

From this equation, it is possible to show that the acceleration doublet is equivalent to an element of lifting surface.

Let us denote by $\vec{r}$ the vector distance $\vec{P}-\vec{P}_0$. The pressure perturbation is :

$$p-p_\infty = -\rho_\infty\, q\, \frac{\vec{r}\,\vec{n}_0}{4\pi\,|\vec{r}|^3}$$

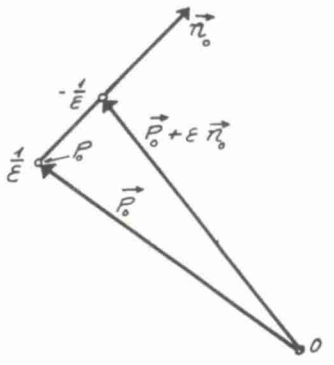


Fig. 10 - The acceleration doublet.

Let us consider a plane π normal to the doublet axis $\vec{n}_0$, located as shown in figure 11, and a surface Σ .

The force due to the pressure perturbation on Σ , on the upper side of the plane π , is :

$$\vec{F}_1 = -\vec{n}_0 \iint_{(\Sigma)} (p-p_\infty)\,d\sigma$$

$$= \vec{n}_0\,\rho_\infty \frac{q(t)}{4\pi} \iint_{(\Sigma)} \frac{\vec{r}\,\vec{n}_0}{|\vec{r}|^3}\,d\sigma$$

But $\vec{r}\,\vec{n}_0/|\vec{r}|^3$ is the elementary solid angle $d\Omega$ under which $d\sigma$ is seen from P_0 .

Then

$$\vec{F}_1 = \vec{n}_0\,\rho_\infty\, q(t)\,\frac{\Omega}{4\pi}$$

Ω being the solid angle corresponding to Σ .

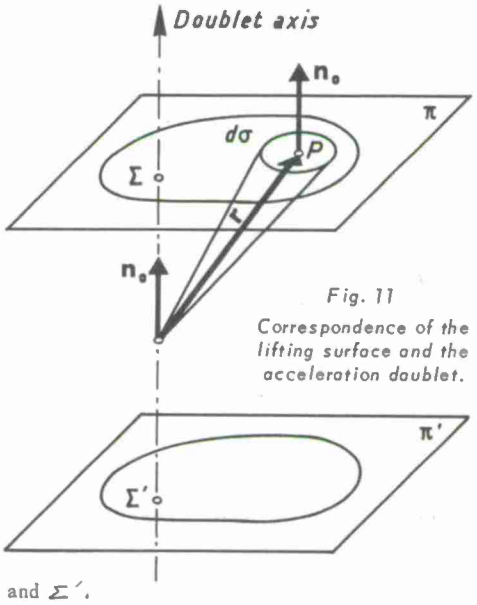


Fig. 11
Correspondence of the lifting surface and the acceleration doublet.

Let us consider now the plane π' symmetric of π with respect to P_0 and the surface Σ' symmetric of Σ . The force acting on Σ', on the lower side of π', is given by :

$$\vec{F}_2 = \vec{n}_0 \iint_{(\Sigma')} (p-p_\infty)\,d\sigma$$

$$= \vec{n}_0\,\rho_\infty\, q(t)\,\frac{\Omega}{4\pi}$$

When the distance between the two planes tends to zero, Ω tends to 2π if Σ and Σ' are cut by the doublet axis, and to 0 when this axis is outside of Σ and Σ'.

When the distance between the two planes is made infinitely small, the two surfaces can be assimilated to the upper and lower surface of an element of lifting surface.

The lift acting on this surfaces is given by :

$$\vec{F}_1 + \vec{F}_2 = \vec{n}_0\,\rho_\infty\, q(t)$$

So that the doublet is equivalent to an element of lifting surface of normal vector $\vec{n}_0$ and lift $\rho_\infty\, q(t)$. Reciprocally, a lifting surface element of area $d\sigma$, with a pressure discontinuity Δp , and a normal vector $\vec{n}_0$ is equivalent to an acceleration doublet of axis $\vec{n}_0$ and strength

(39)
$$q(t) = \frac{\Delta p(t)\,d\sigma}{\rho_\infty}$$

II,4. INTEGRAL EQUATION

The velocity potential of the acceleration doublet, φ_D , is obtained after substitution of (37) into (34) :

(40)
$$\varphi_D(P,t) = \frac{1}{4\pi} \int_{-\infty}^{t} \frac{q(t_0)\,[\vec{P}-\vec{P}_0(t_0)]\,\vec{n}_0(t_0)}{|\vec{P}-\vec{P}_0(t_0)|^3}\,dt_0$$

Since a lifting surface element is equivalent to an acceleration doublet, the complete lifting surface will be equivalent to a distribution of doublets of strength $\Delta p\,d\sigma/\rho_\infty$, according to (39). The velocity potential due to this distribution will be obtained from (40) after an integration over the lifting surface :

(41)
$$\varphi(P,t) = \frac{1}{4\pi\rho_\infty} \iint_{(A)} \int_{-\infty}^{t} \frac{\Delta p(P_0(t_0),t_0)\,[\vec{P}-\vec{P}_0(t_0)]\,\vec{n}_0(\vec{P}_0(t_0))\,dt_0\,d\sigma}{|\vec{P}(t)-\vec{P}_0(t_0)|^3}$$

In this integral, $\vec{P}_0(t_0)$, $\vec{n}_0(t_0)$, and $\Delta p(P_0,t_0)$ denote respectively the time history of the position, orientation and lift of the lifting surface element.

This time integration (dummy variable t_0) is performed along the path of each lifting surface element. This path constitutes the undistorted wake of the lifting surface (fig. 12).

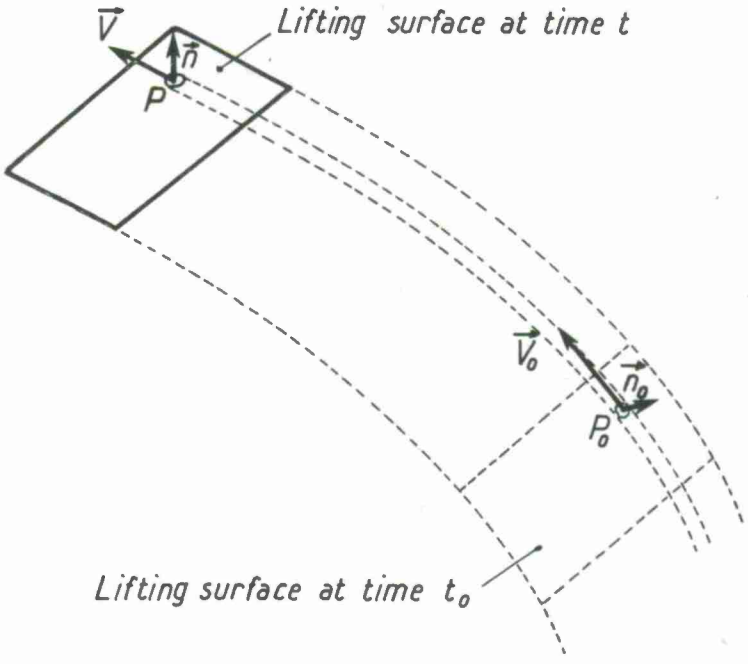


Fig. 12 - Time integration

II,5. COMPRESSIBLE FLUID

With a compressible fluid, the fundamental solutions contain the time delay resulting from the fact that the perturbations are transmitted at finite velocity with acoustic waves.

For a fixed acceleration source, the acceleration potential is given by :

$$\psi_s(P,t) = -\frac{q(\tau)}{4\pi\,|\vec{P}-\vec{P}_0|}$$

with

$$t-\tau = \frac{|\vec{P}-\vec{P}_0|}{a}$$

τ is the emission time of the perturbation which is felt at P at time t .

When the source is moving, its velocity modifies the potential and we have (see Morse and Feshbach [36]) :

(42)
$$\psi_s(P,t) = -\frac{q(\tau)}{4\pi\,|\vec{P}-\vec{P}_0(\tau)|\left|1-\dfrac{\vec{V}_0(\tau)\,[\vec{P}-\vec{P}_0(\tau)]}{a\,|\vec{P}-\vec{P}_0(\tau)|}\right|}$$

with

$$t-\tau = \frac{|\vec{P}-\vec{P}_0(\tau)|}{a}$$

$$\vec{V}_0 = \left(\frac{d\vec{P}_0}{dt}\right)_{t-\tau}$$

With a view to the application to helicopter blades, we assume that the flow remains subsonic everywhere, so that $|\vec{V}| < a$

Then,

$$\left|1-\frac{\vec{V}_0\,[\vec{P}-\vec{P}_0]}{a\,|\vec{P}-\vec{P}_0|}\right| = \left[1-\frac{\vec{V}_0\,[\vec{P}-\vec{P}_0]}{a\,|\vec{P}-\vec{P}_0|}\right]$$

To obtain the potential of a doublet moving along a path defined by the vector $\vec{P}_0(\tau)$, with an orientation $\vec{n}_0(\tau)$, it is convenient to introduce a parameter ξ and to consider the potential ψ_s of a source moving along a path $\vec{P}_0(\tau) + \xi\,\vec{n}_0(\tau)$. Then, the doublet potential is the derivative of $-\psi_s$ with respect to ξ , for $\xi = 0$.

Let $\vec{D}$ be the vector

(43a)
$$\vec{D} = \vec{P}-\vec{P}_0-\xi\,\vec{n}_0$$

From equation (42) we have :

(43b)
$$-\psi_s(P,\xi,t) = \frac{q(\tau)}{4\pi|\vec{D}|\left|1-\dfrac{\vec{V}_0\,\vec{D}}{a\,|\vec{D}|}\right|}$$

(43c)
$$t-\tau = \frac{|\vec{D}|}{a}$$

The potential of the doublet is given by :

(44) $$\Psi_D = -\left(\frac{d\psi_1}{d\xi}\right)_{\xi=0}$$

$$= \frac{dq/d\tau}{4\pi|\vec{D}|\left[1-\frac{\vec{V}_o\vec{D}}{a|\vec{D}|}\right]}\frac{d\tau}{d\xi} + \frac{q\vec{D}}{4\pi a|\vec{D}|^2\left[1-\frac{\vec{V}_o\vec{D}}{a|\vec{D}|}\right]^2}\frac{d\vec{V}_o}{d\xi} - \frac{q[a\vec{D}-|\vec{D}|\vec{V}_o]}{4\pi a|\vec{D}|^3\left[1-\frac{\vec{V}_o\vec{D}}{a|\vec{D}|}\right]^2}\frac{d\vec{D}}{d\xi}$$

The derivatives $d\tau/d\xi$ and $d\vec{D}/d\xi$, can be obtained from the differentiation of (43a) and (43c) :

$$\frac{d\vec{D}}{d\xi} = -\left(\vec{V}_o\frac{d\tau}{d\xi} + \vec{n}_o\right) \qquad \text{for } \xi = o$$

$$\frac{d\tau}{d\xi} = -\frac{\vec{D}}{a|\vec{D}|}\frac{d\vec{D}}{d\xi}$$

and we get :

(45a) $$\frac{d\tau}{d\xi} = \frac{\vec{D}\vec{n}_o}{a|\vec{D}|\left[1-\frac{\vec{V}_o\vec{D}}{a|\vec{D}|}\right]}$$

(45b) $$\frac{d\vec{D}}{d\xi} = \left[\vec{n}_o + \frac{(\vec{D}\vec{n}_o)\vec{V}_o}{a|\vec{D}|\left[1-\frac{\vec{V}_o\vec{D}}{a|\vec{D}|}\right]}\right]$$

To obtain the derivative $d\vec{V}_o/d\xi$, we consider the path $\vec{P}_o(\tau) + \xi\,\vec{n}_o(\tau)$, and write :

$$\vec{V}_o = \frac{d\vec{P}_o}{d\tau} + \xi\frac{d\vec{n}_o}{d\tau}$$

and

$$\frac{d\vec{V}_o}{d\xi} = \frac{d^2\vec{P}_o}{d\tau^2}\frac{d\tau}{d\xi} + \frac{d\vec{n}_o}{d\tau}$$

or

(45c) $$\frac{d\vec{V}_o}{d\xi} = \frac{\vec{\gamma}_o(\vec{D}\vec{n}_o)}{a|\vec{D}|\left[1-\frac{\vec{V}_o\vec{D}}{a|\vec{D}|}\right]} + \frac{d\vec{n}_o}{d\tau}$$

where $\vec{\gamma}_o$ is the acceleration $d^2\vec{P}_o/d\tau^2$.

One remark is essential before doing the substitution of the derivatives into equation (44). Since the acceleration doublet is to be used to represent a lifting surface element with a small angle of attack, the velocity component along the axis $\vec{n}_o$, which is perpendicular to the lifting surface, remains small. Then the scalar product $\vec{V}_o\vec{n}_o$ is a first order term. In order to be consistant with the assumption of small perturbations, we must also assume the doublet strength, $q(t)$, is a first order term.

Then we can make the substitution of (45a), (45b), (45c) into (44), and neglect the second order terms. We get :

(46) $$\Psi_D(P,t) = \frac{q'\vec{D}\vec{n}_o}{4\pi a|\vec{D}|^2\left[1-\frac{\vec{V}_o\vec{D}}{a|\vec{D}|}\right]^2} + \frac{q(\vec{D}\vec{\gamma}_o)(\vec{D}\vec{n}_o)}{4\pi a^2|\vec{D}|^3\left[1-\frac{\vec{V}_o\vec{D}}{a|\vec{D}|}\right]^3} + \frac{q\vec{D}\frac{d\vec{n}_o}{d\tau}}{4\pi a|\vec{D}|^2\left[1-\frac{\vec{V}_o\vec{D}}{a|\vec{D}|}\right]^2} + \frac{q[a^2-|\vec{V}_o|^2]\vec{D}\vec{n}_o}{4\pi a^2|\vec{D}|^3\left[1-\frac{\vec{V}_o\vec{D}}{a|\vec{D}|}\right]^3}$$

with

$$\vec{D} = \vec{P} - \vec{P}_o(\tau) \quad , \quad \vec{V}_o = \frac{d\vec{P}_o}{d\tau} \quad , \quad \vec{\gamma}_o = \frac{d^2\vec{P}_o}{d\tau} \quad , \quad \tau = t - \frac{|\vec{D}(\tau)|}{a}$$

The velocity potential is given by an integration with respect to time according to (34) :

$$\varphi_D(P,t) = \int_{-\infty}^{t}\Psi_D(P,t_o)\,dt_o$$

But Ψ_D is given explicitly as a function of the time of emission, τ, in equation (46). Then it will be convenient to use this emission time as a dummy variable.

The change of variable is defined by :

$$t_o = \tau_o + \frac{|\vec{D}(\tau_o)|}{a}$$

we get :

$$dt_o = \left[1-\frac{\vec{V}_o\vec{D}}{a|\vec{D}|}\right]d\tau_o$$

and

(47a) $$\varphi_D(P,t) = \int_{-\infty}^{\tau}\Psi_D\left(P,\ \tau_o + \frac{|\vec{D}(\tau_o)|}{a|\vec{D}|}\right)\left[1-\frac{\vec{V}_o\vec{D}}{a|\vec{D}|}\right]d\tau_o$$

The upper limit of integration is given by the equation :

(47b) $$t-\tau = \frac{|\vec{D}(\tau)|}{a}$$

As for the incompressible fluide, the lifting surface will be assimilated to a distribution of acceleration doublet of strength $\Delta p\, d\sigma / \rho_\infty$ according to (39). Then the acceleration potential due to an element of lifting surface is obtained after substitution of $q = \Delta p(t_0) d\sigma / \rho_\infty$ into (46). The result of this substitution is substituted again to ψ into equation (47a) to obtain the velocity potential and, lastly, an integration over the lifting surface is performed to obtain the resulting potential.

The resulting equation can be written :

$$(48) \qquad \varphi(P,t) = \iint_{(A)} \int_{-\infty}^{\tau} \left[K\left(\vec{P}-\vec{P}_0(\tau_0), \vec{V}(\tau_0), \vec{\gamma}_0(\tau_0), \vec{n}_0(\tau_0), \frac{d\vec{n}_0}{d\tau_0}\right) \Delta p(\vec{P}_0(\tau_0)) + H\left(\vec{P}-\vec{P}_0(\tau_0), \vec{V}_0(\tau_0), \vec{n}_0(\tau_0)\right) \frac{d\left(\Delta p(\vec{P}_0(\tau_0))\right)}{d\tau_0} \right] d\tau_0\, d\sigma_0$$

with $$t-\tau = \frac{|\vec{P}-\vec{P}_0(\tau_0)|}{a}$$

A is the lifting surface.

The kernel functions K and H are given by :

$$K = \frac{(\vec{D}\vec{\gamma}_0)(\vec{D}\vec{n}_0) + (a^2 - |V_0|^2)\vec{D}\vec{n}_0}{4\pi a^2 |\vec{D}|^3 \left[1 - \frac{\vec{V}_0\vec{D}}{a|\vec{D}|}\right]^2} + \frac{\vec{D}\,\frac{d\vec{n}_0}{d\tau_0}}{4\pi a |\vec{D}|^2 \left[1 - \frac{\vec{V}_0\vec{D}}{a|\vec{D}|}\right]} \qquad H = \frac{\vec{D}\vec{n}_0}{4\pi a |\vec{D}|^2 \left[1 - \frac{\vec{V}_0\vec{D}}{a|\vec{D}|}\right]}$$

The application of this equation will be illustrated in the third part of the lecture.

II,6. SIMPLIFIED AERODYNAMICS

The integral equation (48) is particularly convenient for the prediction of the periodic excitations occurring in forward flight, as will be shown in the third part. But the basic assumptions of small perturbations and of absence of separation may be invalidated locally at high advancing velocity by the high angle of attack, on the side of the retreating blade, and by the transonic effects, on the advancing blade tip. Then it will be necessary to complement the theoretical formulation, which takes account of the three-dimensional and wake effects, by empirical corrections based on wind tunnel data. The methods necessary to make these corrections in a consistent manner have not yet been developed.

Furthermore, the use of a simple formulation, such as that used for the aerofoil, in paragraphe I,1, may be sufficient to analyse a certain number of instabilities in which the wake interference has negligible effect.

Then, we can assume, as we did for the aerofoil, that at each blade spanwise location there is a lift and a pitch moment given by

$$(49a) \qquad F = -\tfrac{1}{2}\rho c\, C_{z_c}\, U w$$

$$(49b) \qquad M = -\tfrac{1}{2}\rho c^3 C_{m\dot{\theta}}\, U\dot{\theta}$$

where U is the component of the blade local velocity normal to the leading edge (chordwise component)

w is the component normal to the blade mean surface at a significant chordwise station

θ is the pitch angle

c the chord length

C_{z_c} and $C_{m\dot{\theta}}$ are empirical coefficients resulting from aerofoil wind tunnel tests.

Apart from the fact that the wake and the spanwise three-dimensional effects are neglected, equations (49) must be considered as a quasi-steady formulation valid only if the flow field varies relatively slowly. The rate of variation may be appreciated if we define a local reduced frequency $\nu = \omega c / U$ where ω may be the fundamental circular frequency of the lift variation and U the chordwise velocity component. Then equations (49) may be used only when ν is small compared to unity. Fortunately this is normally the case.

The formulation of the two-dimensional unsteady flow theory given by Kussner and Theodorsen have also been used.

An empirical formulation may also be used for the analysis of the drag effects. The local drag is a chordwise force supposedly proportional to U^2 : $\qquad D = \tfrac{1}{2}\rho c\, C_x\, U^2$

where C_x is an empirical coefficient.

In many applications, the angle of attack of the blade remains small and the dependency of C_x on the angle of attack may be neglected.

Third part - FORCED VIBRATION IN FORWARD FLIGHT *

In this third part, a formulation of the problem of forced vibration in forward flight is given.

The amplitude of these vibrations is determined by the flight configuration, the blade profile and plan form, and the blade and fuselage structure. The noise, the risk of fatigue failure and the lack of comfort which result from these vibrations often limit the performance of the helicopters.

---

* *This port, unpublished yet, wos presented ot the I.U.T.A.M. (Internotionol Union Theoreticol ond Applied Mechonics) Congress - Moscow, 21-26 August 1972.*

Generally the designers try to improve the structure in order to reduce the amplitude of the vibrations, but they cannot do it efficiently because the prediction methods which they use are insufficient.

A considerable effort is being done now in several countries in order to develop new methods.

An analytical formulation of the problem of forced vibrations in forward flight, which is being developed in France, will be presented here.

The modal representation described in the first part of the lecture will be used separately for the rotating blades and for the fuselage, and the integral equation derived in the second part will be used for the determination of the aerodynamic forces.

A simplification will result from the assumption of periodicity of the motion and loads.

The structural damping, the cyclic pitch and the blade drag will be neglected for the sake of simplificity, but they could be introduced in a straightforward manner by means of the Lagrangian equations.

The structural and aerodynamic forces are linearized.

III,1. THE HELICOPTER IN ABSENCE OF AERODYNAMIC FORCES

A three blade helicopter is considered. The rotor shaft hub is fixed on the upper part of the fuselage and moving with it. Its motion is a combination of a translation at a finite constant velocity V and small angular and translational oscillations.

We assume that the three blades are similar and symmetrically positioned on the rotor disc. Their motion can be separated into a rotation at constant finite velocity ω, and small vibrations resulting from the oscillations of the hub and from the deflexion relative to a coordinate system rotating with the rotor.

III,1.1. Velocity of a blade point

Let $\mathcal{S} = [\vec{\imath}\ \vec{\jmath}\ \vec{k}]$ be a unitary vector basis (fig. 13).

A basis $\mathcal{S}_1 = [\vec{\imath}_1\ \vec{\jmath}_1\ \vec{k}_1]$ is obtained from $\mathcal{S}$ with a small rotation φ around $\vec{\imath}$.

A basis $\mathcal{S}_2 = [\vec{\imath}_2\ \vec{\jmath}_2\ \vec{k}_2]$ is obtained from $\mathcal{S}_1$ with a small rotation ψ around $\vec{\jmath}_1$.

A basis $\mathcal{S}_3 = [\vec{\imath}_3\ \vec{\jmath}_3\ \vec{k}_3]$ is obtained from $\mathcal{S}_2$ with a rotation of a finite angle $\theta - \pi/2$ around $\vec{k}_2$ (fig. 13a).

The angles φ and ψ define the small angular oscillations of the hub.

The small translational oscillation are defined by their components ξ, η, ζ in the basis $\mathcal{S}$ (vector $\vec{\imath}\xi + \vec{\jmath}\eta + \vec{k}\zeta$).

Similarly, the translational advancing velocity is defined by the vector $-\vec{\imath} V\sin\Lambda + \vec{k} V\cos\Lambda$ (fig. 13b).

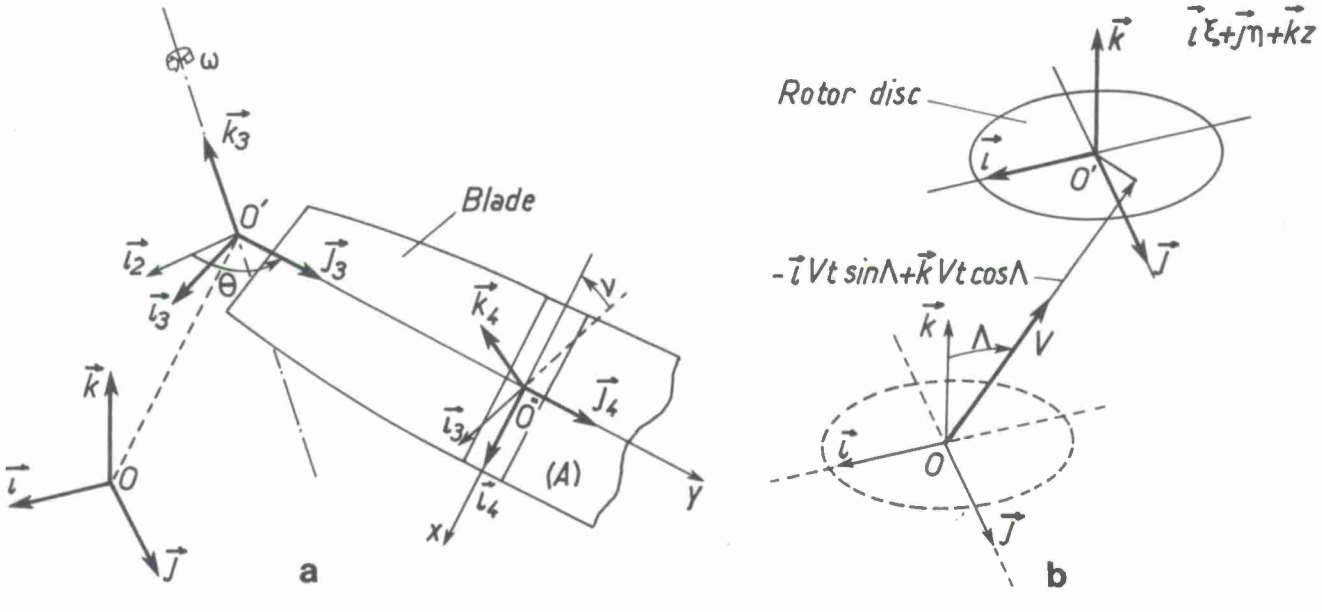


Fig. 13 - Notations - a) Rotation movement ; b) Translation movement

The basis $\mathcal{S}_3 = [\vec{\imath}_3\ \vec{\jmath}_3\ \vec{k}_3]$ is attached to the rotor. The vector $\vec{k}_3$ defines the shaft hub and $\vec{\imath}_3\ \vec{\jmath}_3$ the plane of the rotor disc.

The axis $o'y$ defined by the vector $\vec{\jmath}_3$ will be the reference axis for one of the blades, blade 1 for example. Since the angle θ in the azimuth of blade 1, the notation θ_1 will be used.

As the rotation velocity may have small variations, we have :

$$\theta_1 = \omega t + \Delta\theta$$

where ω is finite and constant and $\Delta\theta$ is a small quantity varying with time.

Similarly, an azimuth θ_k can be associated to each blade k.

We have : $\theta_2 = \theta_1 + 2\pi/3$ and $\theta_3 = \theta_1 - 2\pi/3$ and the velocity of rotation is the same for the three blades, $\dot{\theta}_1 = \dot{\theta}_2 = \dot{\theta}_3 = \omega + \Delta\dot{\theta}$.

The blades thickness, which is small compared to the span and chordlength, will be neglected in the determination of the aerodynamic forces and the kinetic energy. Then the blades will be assimilated to infinitely thin plates and the mass distribution will be defined by the mass per unit area, σ . The spanwise location of each blade section is determined by the radial coordinate $O'O'' = y$. The angle $\nu(y)$ is the local twist angle of the blade. We assume that the chordwise section remains rectilinear.

A local basis $S_4 = [\vec{i}_4\ \vec{j}_4\ \vec{k}_4]$ is obtained from S_3 with a rotation of an angle $\nu(y)$ around $\vec{j}_3$. The twist angle ν may be finite.

Then the points of the blade are defined by the radial coordinate y in the basis S_3 , and by the chordwise coordinate x in the basis S_4 , $(\vec{j}_3 y + \vec{i}_4 x)$.

For a blade k the small deflexion relative to the rotating basis S_4 can be separated into a flapping or normal deflexion $w_k(x,y,t)$ along $\vec{k}_4$ and a lagging, or coplanar deflexion $u_k(y,t)$ along $\vec{i}_4$. If the assumption of constant blade length is made, a second order deflexion along $\vec{j}_4$ must be associated to u_k and w_k . This deflexion is given by :

$$v_k = -\frac{1}{2}\int_0^y \left[\left(\frac{\partial u_k}{\partial y_0}\right)^2 + \left(\frac{\partial w_k}{\partial y_0}\right)^2_{x=x_t} \right] dy_0$$

x_t is the abscissa of the neutral axis.

The position of a point P of the deformed blade is defined by a vector $\vec{OP}$, O being a fixed origin. The notation $\vec{P}$ will be used instead of $\vec{OP}$. We get :

$$\vec{P} = S \begin{pmatrix} -Vt\sin\Lambda + \xi \\ \eta \\ Vt\cos\Lambda + \zeta \end{pmatrix} + S_4 \begin{pmatrix} x + u_k \\ y + v_k \\ w_k \end{pmatrix} \tag{50}$$

The basis transformation formulas are :

$$S_1 = S K_1 \qquad S_2 = S_1 K_2 \qquad S_3 = S_2 K_3 \qquad S_4 = S_3 K_4$$

with

$$K_1 = \begin{pmatrix} 1 & \cdot & \cdot \\ \cdot & \cos\varphi & -\sin\varphi \\ \cdot & \sin\varphi & \cos\varphi \end{pmatrix} \qquad K_2 = \begin{pmatrix} \cos\psi & \cdot & \sin\psi \\ \cdot & 1 & \cdot \\ -\sin\psi & \cdot & \cos\psi \end{pmatrix} \qquad K_3 = \begin{pmatrix} \sin\vartheta_k & \cos\vartheta_k & \cdot \\ -\cos\vartheta_k & \sin\vartheta_k & \cdot \\ \cdot & \cdot & 1 \end{pmatrix} \qquad K_4 = \begin{pmatrix} \cos\nu & \cdot & \sin\nu \\ \cdot & 1 & \cdot \\ -\sin\nu & \cdot & \cos\nu \end{pmatrix}$$

From (50) we can derive the velocity vector. The second order terms must be kept in view of the calculation of the kinetic energy. We get :

$$\vec{V} = \dot{\vec{P}} = S_3 \begin{pmatrix} -V\sin\Lambda\sin\vartheta_k - \dot{\vartheta}y \\ -V\sin\Lambda\cos\vartheta_k + \dot{\vartheta}x\cos\nu \\ V\cos\Lambda \end{pmatrix} + S_3 \left(\begin{array}{ccc|ccc} Z_k\cos\vartheta_k & Z_k\sin\vartheta_k & \sin\vartheta_k & -\cos\vartheta_k & \cdot & \cdot \\ -Z_k\sin\vartheta_k & Z_k\cos\vartheta_k & \cos\vartheta_k & \sin\vartheta_k & \cdot & \cdot \\ Y_k & -X_k & \cdot & \cdot & 1 & \cdot \end{array} \right) \begin{pmatrix} \dot{\varphi} \\ \dot{\psi} \\ \dot{\xi} \\ \dot{\eta} \\ \dot{\zeta} \\ \dot{x} \end{pmatrix} + \ldots$$

$$\ldots + S_3 \begin{pmatrix} \dot{u}_k^* \\ \cdot \\ \dot{w}_k^* \end{pmatrix} + S_3 \begin{pmatrix} \cdot \\ \dot{\vartheta} u_k^* \\ \cdot \end{pmatrix} + S_3 \left(\begin{array}{cc} -V\cos\Lambda\cos\vartheta_k & -V\cos\Lambda\sin\vartheta_k \\ V\cos\Lambda\sin\vartheta_k & -V\cos\Lambda\cos\vartheta_k \\ \cdot & -V\sin\Lambda \end{array} \right) \begin{pmatrix} \varphi \\ \psi \end{pmatrix} + \ldots$$

$$\ldots + S_3 \begin{pmatrix} -\dot{\varphi}\psi Y_k - \dot{\vartheta} v_k \\ \dot{\varphi}\psi X_k + \dot{v}_k \\ \cdot \end{pmatrix} + S_3 \left(\begin{array}{cc} w_k^*\cos\vartheta_k & w_k^*\sin\vartheta_k \\ -w_k^*\sin\vartheta_k & w_k^*\cos\vartheta_k \\ -u_k^*\cos\vartheta_k & -u_k^*\sin\vartheta_k \end{array} \right) \begin{pmatrix} \dot{\varphi} \\ \dot{\psi} \end{pmatrix} + \ldots$$

$$\ldots + S_3 \begin{pmatrix} \cdot & \cdot & -\varphi\cos\vartheta_k - \psi\sin\vartheta_k \\ \cdot & \cdot & \varphi\sin\vartheta_k - \psi\cos\vartheta_k \\ \psi & \varphi & \cdot \end{pmatrix} \begin{pmatrix} \dot{\xi} \\ \dot{\eta} \\ \dot{\zeta} \end{pmatrix} \tag{51}$$

with

$$X_k = x\cos\nu\sin\vartheta_k + y\cos\vartheta_k \qquad Y_k = -x\cos\nu\cos\vartheta_k + y\sin\vartheta_k \qquad Z_k = -x\sin\nu$$

$$u_k^* = u_k\cos\nu + w_k\sin\nu \qquad w_k^* = -u_k\sin\nu + w_k\cos\nu$$

III,1.2. Modal representation - Fuselage and blade generalized coordinates

The modal representation can be used separately for the fuselage and the blades.

Let $\vec{U}(P,t)$ be the vector defining the motion of a point P of the fuselage. We write :

$$\vec{U}(P,t) = \sum_{i=1}^{n} \vec{U}_i(P)\, q_i(t)$$

The spatial vector functions $\vec{U}_i(P)$ may be the mode shapes of the fuselage separated from its rotor. $q_i(t)$ are the fuselage generalized coordinates.

The small oscillations of the rotor hub can also be written in terms of the fuselage generalized coordinates :

$$\varphi = \sum_i \varphi_i q_i(t) \qquad \psi = \sum_i \psi_i q_i(t) \qquad \xi = \sum_i \xi_i q_i(t)$$

$$\eta = \sum_i \eta_i q_i(t) \qquad \zeta = \sum_i \zeta_i q_i(t)$$

where φ_i , ψ_i , ξ_i , η_i , ζ_i are the components of displacements of the rotor hub in the fuselage mode shapes.

Similarly, for a blade k , the flapping and lagging deflexions can be written as :

$$w_k(x,y,t) = \sum_{i=1}^{m} w_i(x,y)\, \beta_{ik}(t)$$

$$u_k(y,t) = \sum_{i=1}^{m} u_i(y)\, \beta_{ik}(t)$$

The spatial functions $w_i(x,y)$ and $u_i(y)$ may be derived from the mode shape of the blades separated from the fuselage and fixed on a wall.

$\beta_{ik}(t)$ are the blade k generalized coordinates.

The mode shapes $w_i(x,y)$, $u_i(y)$ are the same for the three blades.

The matrix notation $\boldsymbol{q}(t)$ and $\boldsymbol{\beta}_k(t)$ will be used for the column of generalized coordinates $q_i(t)$ and $\beta_{ik}(t)$.

With the property or orthogonality of the mode shapes, some simplifications will arise in the kinetic and potential energy.

III,1.3. Kinetic and potential energy

The kinetic energy of the blades is derived from equation (51). After some laborious calculation, the kinetic energy of the complete structure can be written in the form :

(52)
$$2T = \dot\theta^2 I_z + 2\dot\theta \sum_k \boldsymbol{\Lambda}\dot{\boldsymbol{\beta}}_k + 2\dot\theta^2 \sum_k \boldsymbol{\Gamma}\boldsymbol{\beta}_k + 2\dot\theta\, \bar{\boldsymbol{q}}\boldsymbol{A}\boldsymbol{q} - \dot\theta^2 \sum_k \bar{\boldsymbol{\beta}}_k \boldsymbol{\Phi} \boldsymbol{\beta}_k - 2\dot\theta \sum_k \bar{\dot{\boldsymbol{\beta}}}_k \boldsymbol{H} \boldsymbol{\beta}_k + \cdots$$

$$\cdots + \bar{\dot{\boldsymbol{q}}} \boldsymbol{M} \dot{\boldsymbol{q}} + \sum_k \bar{\dot{\boldsymbol{\beta}}}_k \boldsymbol{\mu} \dot{\boldsymbol{\beta}}_k + 2 \sum_k \bar{\dot{\boldsymbol{q}}} [\boldsymbol{F} + \cos\vartheta_k \boldsymbol{G} + \sin\vartheta_k \boldsymbol{J}] \dot{\boldsymbol{\beta}}_k + 2\dot\theta \sum_k [\cos\vartheta_k \boldsymbol{S} + \sin\vartheta_k \boldsymbol{T}] \boldsymbol{\beta}_k$$

where I_z is the axial moment of inertia of the rotating parts,

$\boldsymbol{\Lambda}$ and $\boldsymbol{\Gamma}$ are line matrices resulting from an integration over one blade (A),

$\boldsymbol{A}$, $\boldsymbol{\Phi}$, $\boldsymbol{H}$, $\boldsymbol{M}$, $\boldsymbol{\mu}$, $\boldsymbol{F}$, $\boldsymbol{G}$, $\boldsymbol{J}$, $\boldsymbol{S}$, and $\boldsymbol{T}$ are matrices resulting from integration over one blade (A) and over the structure separated from the blades (F).

$$\Lambda^{(i)} = -\iint_{(A)} y\,(u_i \cos\nu + w_i \sin\nu)\,\sigma\, dx\, dy$$

$$\Gamma^{(i)} = \iint_{(A)} x \cos\nu\,[u_i \cos\nu + w_i \sin\nu]\,\sigma\, dx\, dy$$

$$A_j^{(i)} = I_z \varphi_i \psi_j$$

$$\Phi_j^{(i)} = \iint_{(A)} y \int_0^y \left(\frac{\partial u_i}{\partial y_0}\frac{\partial u_j}{\partial y_0} + \frac{\partial w_i}{\partial y_0}\frac{\partial w_j}{\partial y_0} \right) dy_0\, \sigma\, dx\, dy - \iint_{(A)} [u_i u_j \cos^2\nu + (u_i w_j + u_j w_i)\sin\nu\cos\nu + w_i w_j \sin^2\nu]\,\sigma\, dx\, dy$$

$$H_j^{(i)} = \iint_{(A)} x\cos\nu \int_0^y \left(\frac{\partial u_i}{\partial y_0}\frac{\partial u_j}{\partial y_0} + \frac{\partial w_i}{\partial y_0}\frac{\partial w_j}{\partial y_0} \right) dy_0\, \sigma\, dx\, dy$$

$$\mu_j^{(i)} = \iint_{(A)} (u_i u_j + w_i w_j)\,\sigma\, dx\, dy$$

$$M_j^{(i)} = I_{px}[\varphi_i \varphi_j + \psi_i \psi_j] + S_{pz}[\psi_i \xi_j + \xi_i \psi_j - \varphi_i \eta_j - \varphi_j \eta_i] + M_p(\xi_i \xi_j + \eta_i \eta_j + \zeta_i \zeta_j) + \iiint_{(F)} \rho(P)\, \vec{U}_i(P)\, \vec{U}_j(P)\, d\Omega$$

$$F_j^{(i)} = \zeta_i \iint_{(A)} (-u_j \sin\nu + w_j \cos\nu)\,\sigma\, dx\, dy$$

$$G_j^{(i)} = -\varphi_i \iint_{(A)} x w_j\, \sigma\, dx\, dy + \psi_i \iint_{(A)} y(u_j \sin\nu - w_j \cos\nu)\,\sigma\, dx\, dy - \eta_i \iint_{(A)} (u_j \cos\nu + w_j \sin\nu)\,\sigma\, dx\, dy$$

$$J_j^{(\ell)} = -\varphi_\ell \iint_{(A)} y(u_j \sin\nu - w_j \cos\nu)\sigma\,dx\,dy - \psi_\ell \iint_{(A)} x\, w_j \sigma\,dx\,dy + \xi_\ell \iint_{(A)} (u_j \cos\nu + w_j \sin\nu)\sigma\,dx\,dy$$

$$S_j^{(\ell)} = \varphi_\ell \iint_{(A)} y(u_j \sin\nu - w_j \cos\nu)\,\sigma\,dx\,dy + \psi_\ell \iint_{(A)} x[w_j(\cos^2\nu - \sin^2\nu) - 2u_j \sin\nu\cos\nu]\sigma\,dx\,dy + \xi_\ell \iint_{(A)} (u_j \cos\nu + w_j \sin\nu)\sigma\,dx\,dy$$

$$T_j^{(\ell)} = -\varphi_\ell \iint_{(A)} x[w_j(\cos^2\nu - \sin^2\nu) - 2u_j \sin\nu\cos\nu]\sigma\,dx\,dy + \psi_\ell \iint_{(A)} y[u_j \sin\nu - w_j \cos\nu]\sigma\,dx\,dy + \eta_\ell \iint_{(A)} (u_j \cos\nu + w_j \sin\nu)\sigma\,dx\,dy$$

The coefficients I_{px}, S_{px}, M_p are respectively the moment of inertia with respect to the axis $\vec{x}_2$ or $\vec{y}_2$, the static moment $\int z\,dm$ and the mass of the tree blades.

I_z is the axial moment of inertia of the blades and all the rotating parts.

As $u_\ell(y)$ and $w_\ell(x,y)$ are mode shapes, $\mu_j^{(\ell)}$ is a coefficient of the matrix of generalized masses. With the property of orthogonality we have $\mu_j^{(\ell)} = 0$ if $j \neq \ell$.

Similarly, the integral $\iiint_F \rho(P)\vec{U}_\ell(P)\vec{U}_j(P)\,d\Omega$ is a coefficient of the matrix of generalized masses of the fuselage and is equal to zero for $j \neq \ell$.

The matrices M, μ, Φ and H are Hermitian.

The rotational velocity $\dot\theta$ which appears in (52) will be replaced by $\omega + \Delta\dot\theta$ and the quantities of order higher than two will be neglected (q and Δ_k and $\Delta\dot\theta$ are small quantities of first order).

The structure potential energy can be written directly in terms of the generalized coordinates with the generalized stiffnesses of fuselage and blades :

(53) $$2U = \bar q \gamma' q + \sum_k \bar\Delta_k \gamma \Delta_k$$

γ' is the diagonal matrix of generalized stiffnesses of the fuselage separated from the blades,
γ is the diagonal matrix of generalized stiffnesses of one blade separated from the fuselage.

From (52) and (53) the Lagrangian equations can be derived.

A set of differential equations with periodic coefficients are obtained. The periodic coefficients proceed from the terms $\cos\theta_k$ and $\sin\theta_k$ which are apparent in equation (52).

The matrices of generalized masses and generalized stiffnesses, and the mode shapes necessary to build the matrices arising in (52) and (53) can be determined either by computation or by ground vibration tests.

III,1.4. Overall rotor generalized coordinates

With the periodic coefficients which arise in the differential equations the solutions cannot be written explicitly.

But it is possible to get rid of these terms if a set of variables taking account of the rotor symmetries is used instead of the individual blade coordinates

The new rotor generalized coordinates are related to the old ones by the equations :

$$r_{\ell 1}(t) = \frac{1}{3}\sum_k \Delta_{\ell k}(t) \qquad (k \text{ is the blade index})$$

$$r_{\ell 2}(t) = \frac{2}{3}\sum_k \cos\theta_k\, \Delta_{\ell k}(t)$$

$$r_{\ell 3}(t) = \frac{2}{3}\sum_k \sin\theta_k\, \Delta_{\ell k}(t)$$

Reciprocally :

(54) $$\Delta_{\ell k}(t) = r_{\ell 1}(t) + \cos\theta_k\, r_{\ell 2}(t) + \sin\theta_k\, r_{\ell 3}(t)$$

When (54) is substituted into the kinetic energy (52) and potential energy (53), we obtain equations in which $\cos\theta_k$ and $\sin\theta_k$ are no longer apparent :

(55) $$2T = \dot\theta^2 I_z + 6\dot\theta \Lambda \dot r_1 + 6\dot\theta^2 \Gamma r_1 + 2\dot\theta \bar q A q - \dot\theta^2\left[3\bar r_1 \Phi r_1 + \frac{3}{2}\bar r_2 \Phi r_2 + \frac{3}{2}\bar r_3 \Phi r_3\right] + \cdots$$

$$\cdots + \bar{\dot q} M \dot q + 3\bar{\dot r}_1 \mu \dot r_1 + \frac{3}{2}\bar{\dot r}_2 \mu \dot r_2 + \frac{3}{2}\bar{\dot r}_3 \mu \dot r_3 + 3\dot\theta\left[\bar r_2 \mu \dot r_3 - \bar r_3 \mu \dot r_2\right] + \cdots$$

$$\cdots + \frac{3}{2}\dot\theta^2\left[\bar r_2 \mu r_2 + \bar r_3 \mu r_3\right] + 3\bar r_1 H \dot r_1 + \frac{3}{2}\bar r_2 H \dot r_2 + \frac{3}{2}\bar r_3 H \dot r_3 + 2\bar{\dot q}\left[3F\dot r_1 + \frac{3}{2}G\dot r_2 + \frac{3}{2}J\dot r_3\right] + \cdots$$

$$\cdots + 2\dot\theta \bar q [S - J] r_2 + 2\dot\theta [T + G] r_3$$

(56) $$2U = \bar{q}\gamma' q + 3\bar{\Gamma}_1\gamma' r_1 + \tfrac{3}{2}\bar{\Gamma}_2\gamma' r_2 + \tfrac{3}{2}\bar{\Gamma}_3\gamma' r_3$$

The Lagragian equations can be derived from (55) and (56) and a set of differential equations with constant coefficients is obtained. It can be written in the

(57) $$\mathcal{M}\ddot{Y}(t) + \mathcal{B}\dot{Y}(t) + \mathcal{K}Y(t) = C$$

where $Y(t)$ is the column of generalized coordinates :

(58) $$Y(t) = \begin{pmatrix} \Delta\theta \\ q \\ r_1 \\ r_2 \\ r_3 \end{pmatrix}$$

C is a constant column

$$C = \begin{pmatrix} \vdots \\ 3\omega^2\bar{\Gamma} \\ \vdots \end{pmatrix}$$

The coefficients of the matrices $\mathcal{M}$, $\mathcal{B}$ and $\mathcal{K}$ are constant.

In the analysis of the dynamic responses, the constant column C, in the right hand side of (57), will be neglected.

It can be seen that the matrices $\mathcal{M}$, $\mathcal{B}$ and $\mathcal{K}$ have the properties of symmetry characteristic of a conservative system with gyroscopic coupling. From this remark we can infer that the helicopter and his rotating blades have natural modes of vibration in which the coordinates $\Delta\theta$, q and r_i are harmonic functions of time, with the same frequency but different phases. The property of orthogonality of the mode shapes is not valid in this case.

The motion of the actual structures would be damped by the structural damping.

$\mathcal{M} =$

I_z		3Λ		
	M	$3F$	$\frac{3}{2}G$	$\frac{3}{2}J$
$3\bar{\Lambda}$	$3\bar{F}$	3μ		
	$\frac{3}{2}\bar{G}$		$\frac{3}{2}\mu$	
	$\frac{3}{2}\bar{J}$			$\frac{3}{2}\mu$

$\mathcal{B} =$

		$6\omega\Gamma$		
	$\omega(A-\bar{A})$		$\frac{3}{2}\omega(S-J)$	$\frac{3}{2}\omega(T+G)$
$-6\omega\bar{\Gamma}$				
	$-\frac{3}{2}\omega(\bar{S}-\bar{J})$			$3\omega\mu$
	$-\frac{3}{2}\omega(\bar{T}+\bar{G})$		$-3\omega\mu$	

$\mathcal{K} =$

	γ'			
		$3\gamma + 3\omega^2\phi$		
			$\frac{3}{2}[\gamma + \omega^2(\phi-\mu)]$	
				$\frac{3}{2}[\gamma + \omega^2(\phi-\mu)]$

REMARK

The mode shapes of a blade rotating at constant speed around a fixed axis can be used instead of the mode shapes of the fixed blades for the modal representation. Then the derivation of the kinetic and potential energy is performed in the same manner, and the formulas (55) and (56) can be used, except for the terms depending on the matrix ϕ which results from the centrifugal force, and which are already included in the natural modes of the rotating blades.

An improvement of convergence must normally result from the use of the rotating blade characteristics, resulting in a smaller number of blade generalized coordinates.

The determination of the natural modes of a rotating blade can be done separately.

III,2. BLADE AERODYNAMICS

III,2.1. Integral equation

The determination of the aerodynamic forces is based on the following assumptions : the fluid is inviscid, the perturbations due to the blade motion remain small (first order) and there is no flow separation. In addition to these assumption the Kutta-Joukowsky condition, at the trailing edge, is necessary to obtain a unique solution.

The blades are assimilated to thin lifting surfaces and the difference Δp between the pressure on both faces provides the lift. Due to the absence of flow separation, the velocity component normal to the lifting surfaces is the same for points belonging to a lifting surface and for fluid particles in contact with these points.

The velocity of the fluid particles relative to a fixed origin is defined by a vector field $\vec{v}(P,t)$ deriving from a velocity potential

$|\vec{v}|$ is a small quantity.

In the second part of this lecture it is shown that the velocity potential can be related to the time history of the motion and lift of the lifting surface :

$$(59)\quad \varphi(P,t) = \iint_{(A)} \int_{-\infty}^{\tau} [K(\vec{P}-\vec{P}_0(\tau_0), \vec{V}_0(\tau_0), \vec{\gamma}_0(\tau_0), \vec{n}_0(\tau_0), \frac{d\vec{n}_0}{d\tau_0}) \Delta p(\vec{P}_0(\tau_0)) + \dots$$

$$\dots + H(\vec{P}-\vec{P}_0(\tau_0), \vec{V}_0(\tau_0), \vec{n}_0(\tau_0)) \frac{d\Delta p}{d\tau_0}]\, d\tau_0\, d\sigma_0$$

with $$t-\tau = \frac{|\vec{P}-\vec{P}_0(\tau)|}{a}$$

$\vec{P}_0(\tau_0)$ defines the path of a point P_0 of the lifting surface (fig. 14) ; $\vec{V}_0$ is the velocity ($\vec{V}_0 = d\vec{P}_0/d\tau_0$) and $\vec{\gamma}_0$ the acceleration ($\vec{\gamma}_0 = d^2\vec{P}_0/d\tau_0^2$) ; $\vec{n}_0$ is the unit vector normal to the lifting surface at the point P_0 ; $d\sigma_0$ is the area of an element of lifting surface and a is the sound velocity.

We assume that the pressure jump Δp is a first order quantity. Then finite terms only will be considered in the kernel functions K and H , which are given in the second part of the lecture.

Equation (59) is valid even if there are several lifting surfaces. In the application to the three blade rotor, the observation point P will be located in the vicinity of one blade. Let us assume that it is blade 1. The integration will be performed over the three blades.

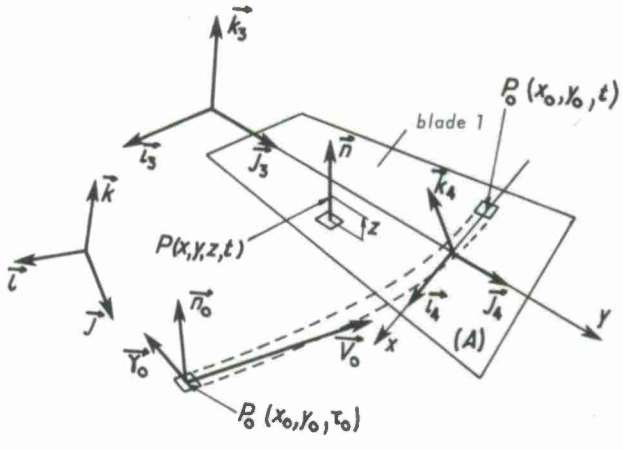


Fig. 14 - Forword flight. - Nototions.

For a point P located at a distance z from blade 1, we have, with the notation of paragraph III,1.1. :

$$(60a)\quad \vec{P} = S\left[\begin{pmatrix} -Vt\sin\Lambda \\ \cdot \\ Vt\cos\Lambda \end{pmatrix} + \begin{pmatrix} \sin\vartheta_1(t) & \cos\vartheta_1(t) & \cdot \\ -\cos\vartheta_1(t) & \sin\vartheta_1(t) & \cdot \\ \cdot & \cdot & 1 \end{pmatrix} \begin{pmatrix} \cos\nu(y) & \cdot & \sin\nu(y) \\ \cdot & 1 & \cdot \\ -\sin\nu(y) & \cdot & \cos\nu(y) \end{pmatrix} \begin{pmatrix} x \\ y \\ z \end{pmatrix}\right]$$

$$(60b)\quad \vec{P}_0 = S\left[\begin{pmatrix} -V\tau_0\sin\Lambda \\ \cdot \\ V\tau_0\cos\Lambda \end{pmatrix} + \begin{pmatrix} \sin\vartheta_k(\tau_0) & \cos\vartheta_k(\tau_0) & \cdot \\ -\cos\vartheta_k(\tau_0) & \sin\vartheta_k(\tau_0) & \cdot \\ \cdot & \cdot & 1 \end{pmatrix} \begin{pmatrix} \cos\nu(y_0) & \cdot & \sin\nu(y_0) \\ \cdot & 1 & \cdot \\ -\sin\nu(y_0) & \cdot & \cos\nu(y_0) \end{pmatrix} \begin{pmatrix} x_0 \\ y_0 \\ \cdot \end{pmatrix}\right]$$

$\vec{V}_0$ and $\vec{\gamma}_0$ are obtained with a differentiation with respect to τ_0 .

The unit normal vector $\vec{n}_0$ is given by :

$$(60c)\quad \vec{n}_0 = S\begin{pmatrix} \sin\vartheta_k(\tau_0) & \cos\vartheta_k(\tau_0) & \cdot \\ -\cos\vartheta_k(\tau_0) & \sin\vartheta_k(\tau_0) & \cdot \\ \cdot & \cdot & 1 \end{pmatrix} \begin{pmatrix} \sin\nu(y_0) \\ \cdot \\ \cos\nu(y_0) \end{pmatrix}$$

$$(60d)\quad \begin{cases} \vartheta_1(t) = \omega t \\ \vartheta_k(\tau_0) = \begin{cases} \omega\tau_0 & \text{for } k=1 \\ \omega\tau_0 + \frac{2\pi}{3} & \text{for } k=2 \\ \omega\tau_0 - \frac{2\pi}{3} & \text{for } k=3 \end{cases} \end{cases}$$

These equations show that the vector $\vec{P}$ is a function of x , y , z , t and, similarly, $\vec{P}_0$ is a function of x_0 , y_0 and τ_0 .

Then equation (59) can be written in the form :

$$(61)\quad \varphi_1(x,y,z,t) = \sum_k \iint_{(A)} \int_{-\infty}^{\tau} [K_k(x,y,z,t,x_0,y_0,\tau_0)\, \Delta p_k(x_0,y_0,\tau_0) + \dots$$

$$\dots + H_k(x,y,z,t,x_0,y_0,\tau_0)\, \Delta\dot{p}_k(x_0,y_0,\tau_0)]\, d\tau\, dx_0\, dy_0$$

where Δp_k is the pressure jump through blade k .

III,2.2. Wake correction

The time integration (dummy variable τ_0) is performed along the paths $\vec{P}_0(\tau_0)$ of the elements of the lifting surfaces. The locus of these paths define the undeformed wakes.

But the vortices which make the actual wakes are displaced at low velocity by the inflow through the rotor.

This displacement may result in a significant modification of the distance between each blade and the wake of the preceding one, resulting in its turn in a modification of the blade interferences.

This effect may be relatively important when the velocity component along the rotor shaft is small, because, in this case, the wakes remain in the vicinity of the rotor plane. Then it is advisable to consider a modified path for the calculations of the integral (61).

The modification consists in replacing the actual axial velocity component $V\cos\Lambda$ by $V\cos\Lambda + v$ in formula (60), v being a small velocity (first order quantity) which is determined by the rotor lift.

III,2.3. Lift

The forward flight is considered and we assume that the structure motion and the aerodynamic forces are periodic functions of time, of period $T = \frac{2\pi}{\omega}$.

Then the pressure jump can be expanded in a Fourier series. A finite number of terms will be considered. Considering the pressure jump Δp_1 through blade 1, we write :

$$(62)\qquad \Delta p_1(x,y,t) = \sqrt{\frac{1-x^*}{1+x^*}}\sqrt{1-y^{*2}}\left[\sum_{i=1}^{M}\sum_{j=1}^{N}\sum_{p=0}^{R}\cos p\omega t\; P_i(x^*)\,Q_j(y^*)\,X'_{ijp} + \cdots + \sum_{i=1}^{M}\sum_{j=1}^{N}\sum_{p=1}^{R}\sin p\omega t\; P_i(x^*)\,Q_j(y^*)\,X''_{ijp}\right]$$

$x^*(x)$ is a dimensionless chordwise coordinate taking the values + 1 at the trailing edge and −1 at the leading edge and given by : $x = \frac{1}{2}\left[(x_{TE}-x_{LE})x^* + x_{TE}+x_{LE}\right]$; $y^*(y)$ is a dimensionless coordinate taking the values +1 at the outboard side edge and −1 at the inboard side edge and given by $y = \frac{1}{2}\left[(R-R_0)y^* + R + R_0\right]$, R being the outboard radius and R_0 the inboard radius.

The function $\sqrt{\frac{1-x^*}{1+x^*}}\sqrt{1-y^{*2}}$ is a weight function giving to Δp_1 a prescribed behaviour on the side edges $(x^* = \pm 1, y^* = \pm 1)$. The Kutta-Jokowsky condition at the trailing edge $(x^* = 1)$ results from this weight function (see figure 15).

The $P_i(x^*)$ and $Q_j(y^*)$ may be limited series of polynomials ; X'_{ijp} and X''_{ijp} are a set of $M \times N \times (2R+1)$ unknown coefficients.

Equation (62) can be written in the form :

$$(63a)\qquad \Delta p_1(x,y,t) = \sum_{i=1}^{M}\sum_{j=1}^{N}\left[\sum_{p=0}^{R} f'_{ijp}(x,y,t)\,X'_{ijp} + \cdots + \sum_{p=1}^{R} f''_{ijp}(x,y,t)\,X''_{ijp}\right]$$

Assuming that the dependency of the aerodynamic forces on the azimuth is the same for all the blades, the pressure jump through blades 2 and 3 can be derived from (63a) with a time lag of $\pm \frac{2\pi}{3}$

$$(63b)\qquad \Delta p_2(x,y,t) = \Delta p_1\left(x,y,t+\frac{2\pi}{3\omega}\right)$$
$$\Delta p_3(x,y,t) = \Delta p_1\left(x,y,t-\frac{2\pi}{3\omega}\right)$$

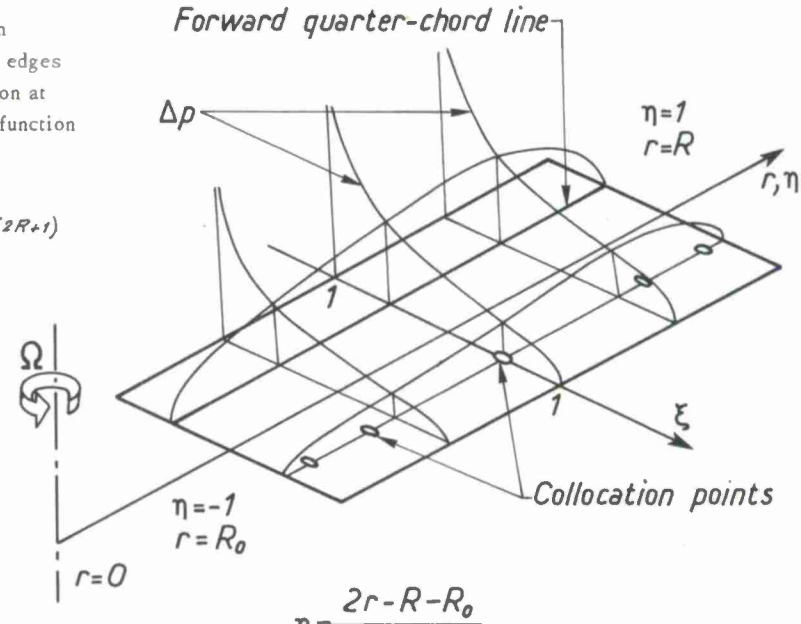


Fig. 15 - Weight function.

III,2.4. Determination of the velocity potential and the downwash

After substitution of (63a) and (63b) into (61), the potential is given in terms of the unknown coefficients X'_{ijp} and X''_{ijp}

$$(64)\qquad \varphi_1(x,y,z,t) = \sum_{i=1}^{M}\sum_{j=1}^{N}\left[\sum_{p=0}^{R} F'_{ijp}(x,y,z,t)X'_{ijp} + \sum_{p=1}^{R} F''_{ijp}(x,y,z,t)\,X''_{ijp}\right]$$

F'_{ijp} is obtained if $f'_{ijp}(x_0,y_0,\tau_0)$, $f'_{ijp}(x_0,y_0,\tau_0+\frac{2\pi}{3\omega})$ and $f'_{ijp}(x_0,y_0,\tau_0-\frac{2\pi}{3\omega})$ are substituted respectively to Δp_1, Δp_2 and Δp_3 and similarly for F''_{ijp} an f''_{ijp}.

The integrals giving the numerical values of F'_{ijp} and F''_{ijp} are regular if the point x, y, z, t is located outside the wakes, and the numerical integrations can be performed systematically with the generalized Gaussian method (see annex and ref. [35]).

If two points located respectively at a distance $z = \varepsilon$ and $z = 2\varepsilon$ of the lifting surface are considered, the downwash or velocity normal to the lifting surface at point x, y can be obtained with a finite difference procedure.

Let v_n be this downwash. Then for a small value of ε we have :

$$(65)\qquad v_n(x,y,t) \cong \sum_{i=1}^{M}\sum_{j=1}^{N}\left[\sum_{p=0}^{R} a'_{ijp}(x,y,t)\,X'_{ijp} + \sum_{p=1}^{R} a''_{ijp}(x,y,t)\,X''_{ijp}\right]$$

with

$$a'_{ijp}(x,y,t) = \frac{1}{\varepsilon}\left[F'_{ijp}(x,y,2\varepsilon,t) - F'_{ijp}(x,y,\varepsilon,t)\right]$$

$$a''_{ijp}(x,y,t) = \frac{1}{\varepsilon}\left[F''_{ijp}(x,y,2\varepsilon,t) - F''_{ijp}(x,y,\varepsilon,t)\right]$$

This finite difference procedure can be used with values of ε ranging to 2 % or 3 % of the chord length without appreciable error.

But it is valid only if the points $x, y, \mathcal{E}$ and $x, y, 2\mathcal{E}$ are not separated by a surface of potential discontinuity, i.e. by a wake. Account must be taken of this remark in the choice of $\mathcal{E}$.

III,2.5. Collocation points

In order to define the aerodynamic characteristics of the rotor by a matrix relation, a set of $M \times N$ points, named collocation points, are defined on blade 1. This choice is made according to the rules already used for the wings (see annex and ref. [35]).

The dimensionless coordinates of these collocation points are x_r^*, y_s^*, with $r = 1, \ldots, M$ and $s = 1, \ldots, N$.

Then $2R+1$ values of the time, t_q, are considered in one period :

$$t_q = t_0 + \frac{2\pi q}{2R+1}$$

where t_0 is an arbitrary time origin.

With the x_r^*, y_s^* and t_q a set of $M \times N \times (2R+1)$ collocation stations is defined on the rotor disc.

The downwash at these collocation stations is given, according to (65) :

$$v_n(x_r^*, y_s^*, t_q) = \sum_{i=1}^{M} \sum_{j=1}^{N} \left[\sum_{p=0}^{R} a'_{ij,p}(x_r^*, y_s^*, t_q) X'_{ij,p} + \sum_{p=1}^{R} a''_{ij,p}(x_r^*, y_s^*, t_q) X''_{ij,p} \right]$$

This equation can be written in a matrix form :

(66) $$v_n = aX$$

where

v_n is the column of values of downwash at the $M \times N \times (2R+1)$ collocation stations,

X is the column of the $M \times N \times (2R+1)$ unknown coefficients $X'_{ij,p}$ and $X''_{ij,p}$

and a is the matrix of coefficients $a'_{ij,p}(x_r^*, y_s^*, t_q)$ and $a''_{ij,p}(x_r^*, y_s^*, t_q)$.

Equations (66) defines the rotor aerodynamic characteristics. The downwash v_n and the coefficients $X_{ij,p}$ are small quantities of first order and the matrix contains only finite terms independent of the small displacements of the blades. But it is depending on the blade planform, advancing and rotational velocities, and on the inflow through the rotor ($V \sin \Lambda$, $V \cos \Lambda + v$, ω).

III,2.6. Comparison with experiment

The comparison of the theoretical and experimental blade lift is illustrated in figure 16. The local lift is plotted against the azimuth angle for several radial stations on one blade.

The experimental curves have been obtained from a wind tunnel test performed at the S1 wind tunnel of Modane on an experimental rotor built by the Société Nationale Industrielle Aérospatiale (S.N.I.A.S.). The blades were rigid and the normal velocities at the collocation stations were derived from the measurements of the flapping and lagging rotations.

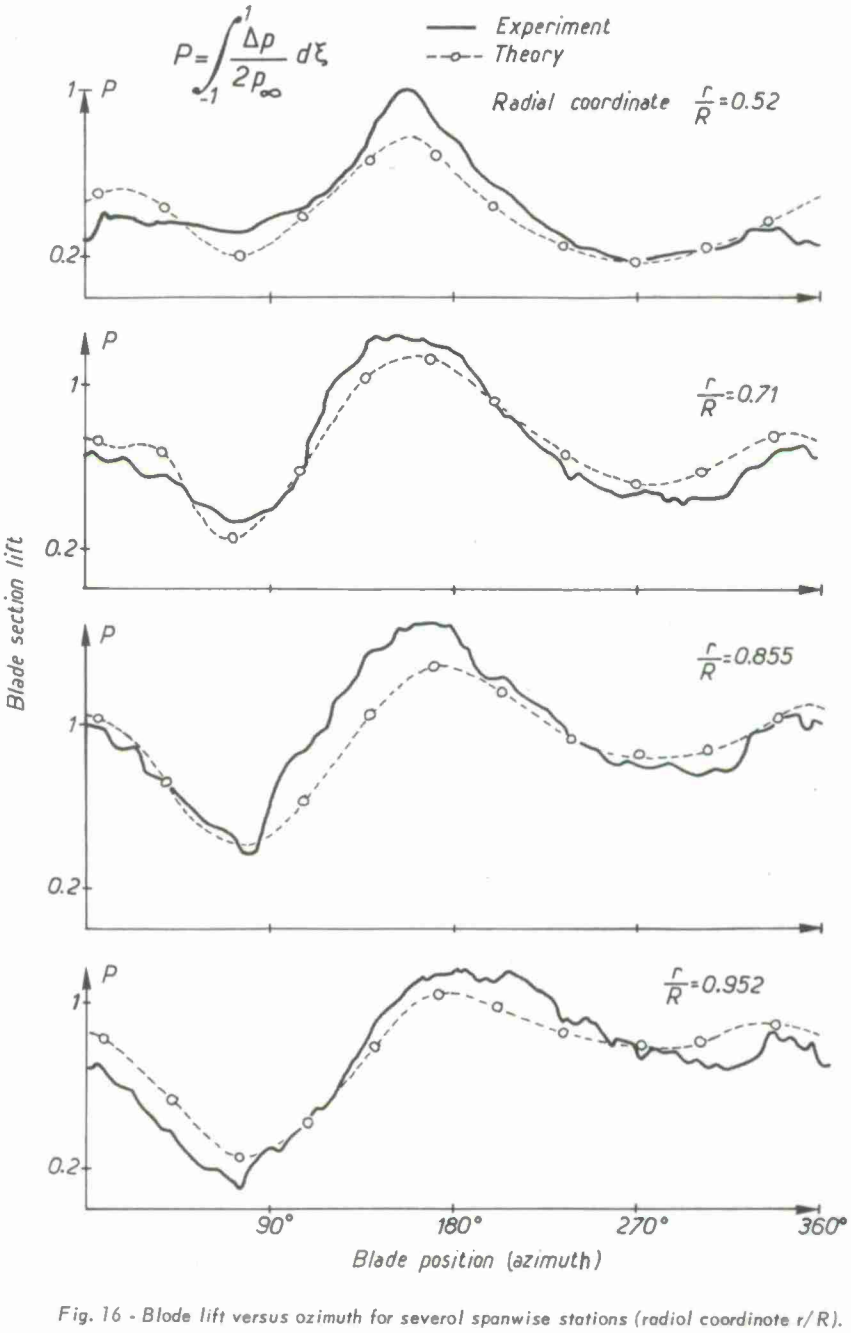


Fig. 16 - Blade lift versus azimuth for several spanwise stations (radial coordinate r/R).

III,3. NORMAL VELOCITY OF THE BLADES

Since the absence of flow separation is assumed, the downwash $v_n(x^*,y^*,t_q)$ given by (65) is equal to the normal velocity of the point (x,y) of the blade (see equation (36)). But this normal velocity can be given in tetms of the generalized coordinates $\gamma_\mu(t)$ defined by (58), with kinematic relations.

The unit vector normal to the blade I is given by

$$\vec{n} = S_3 \left[\begin{pmatrix} \sin\nu \\ \cdot \\ \cos\nu \end{pmatrix} + \begin{pmatrix} -(\partial w_1/\partial x)\cos\nu \\ -\partial w_1/\partial y \\ (\partial w_1/\partial x)\sin\nu \end{pmatrix} \right] \tag{67}$$

The velocity $\vec{P}=\vec{V}$ is given by (51). The desired normal component is the scalar product $v_n = \vec{V}\vec{n}$

Neglecting the second odet terms, we have :

$$v_n(x,y,t) = -V\sin\Lambda\sin\nu\sin(\omega t+\Delta\theta) + V\cos\Lambda\cos\nu - (\omega+\Delta\dot{\theta})\,y\sin\nu + \dot{\varphi}(-x\cos\omega t + y\cos\nu\sin\omega t) + \cdots$$

$$\cdots + \dot{\psi}(-x\sin\omega t + y\cos\nu\cos\omega t) + \dot{\xi}\sin\nu\sin\omega t - \dot{\eta}\sin\nu\cos\omega t + \dot{z}\cos\nu + \dot{w}_1 + \cdots \tag{68}$$

$$\cdots + \frac{\partial w_1}{\partial x}(V\sin\Lambda\cos\nu\sin\omega t + V\cos\Lambda\sin\nu + \omega y\cos\nu) + \frac{\partial w_1}{\partial y}(V\sin\Lambda\cos\omega t - \omega x\cos\nu) - \varphi V\cos\Lambda\cos\omega t - \psi(V\cos\Lambda\sin\nu\sin\omega t + V\sin\Lambda\cos\nu).$$

where $w_1(x,y,t)$ is the normal deflexion of blade 1.

Let us use the modal representation $\varphi = \sum_\iota \varphi_\iota q_\iota(t), \ldots, z = \sum_\iota z_\iota q_\iota(t)$, $w_1(x,y,t) = \sum_\iota w_\iota(x,y)\Lambda_{\iota 1}(t), \ldots$ and the rotor generalized coordinates $r(t)$ defined in III,1.4. :

$$\Lambda_{\iota 1}(t) = r_{\iota 1}(t) + \cos\omega t\, r_{\iota 2}(t) + \sin\omega t\, r_{\iota 3}(t) :$$

Then equation (68) can be written in the form :

$$v_n(x^*,y^*,t) = v_{no}(y^*,t) + \sum_\mu \mathcal{C}_\mu(x^*,y^*,t)\,\gamma_\mu(t) + \sum_\mu \mathcal{C}'_\mu(x^*,y^*,t)\,\dot{\gamma}_\mu(t) \tag{69}$$

where $\mathcal{C}_\mu$ and $\mathcal{C}'_\mu$ are functions of x,y,t and v_{no} a function of y,t given by :

$$v_{no}(y^*,t) = V\cos\Lambda\cos\nu(y) - \omega y\sin\nu(y) - V\sin\Lambda\sin\nu(y)\sin\omega t$$

v_{no} is independent of the generalized coordinates $\gamma_\mu(t)$ (i.e. independent of the small vibrations of the blades), but it contains a time depending tetm $V\sin\Lambda\sin\nu(y)\sin\omega t$ which will cause the forced aerodynamic excitations. For the linearization to be valid, the values of $\nu(y)$, V, Λ and ω must be such that v_{no} remains a small quantity. This condition is normally satisfied on the major part of the rotor disc except in a region of more or less extent on the side of the retreating blade.

The velocity at the collocation stations is obtained if we consider the coordinates x_r^*, y_s^* and the instants t_q :

$$v_n(x_r^*,y_s^*,t_q) = v_{no}(y_s^*,t_q) + \sum_\mu \mathcal{C}_\mu(x_r^*,y_s^*,t_q)\,\gamma_\mu(t_q) + \sum_\mu \mathcal{C}'_\mu(x_r^*,y_s^*,t_q)\,\dot{\gamma}_\mu(t_q)$$

This equation can be written in a matrix form:

$$v_n = v_{no} + \mathcal{C}\gamma + \mathcal{C}'\gamma'$$

v_n is the column of normal velocity at the collocation stations, equal to the downwash column of equation (66).

v_{no}, γ, γ', $\mathcal{C}$ and $\mathcal{C}'$ are columns and matrices defined by

$$v_{no}^{(rsq)} = v_{no}(y_s^*,t_q)$$

$$\gamma^{(\mu q)} = \gamma_\mu(t_q)$$

$$\gamma'^{(\mu q)} = \dot{\gamma}_\mu(t_q)$$

$$\mathcal{C}_{\mu p}^{(rsq)} = \mathcal{C}_\mu(x_r^*,y_s^*,t_q)\,\delta_{pq} \qquad (\delta_{pq} = \text{Kronecker symbol})$$

$$\mathcal{C}'^{(rsq)}_{\mu p} = \mathcal{C}'_\mu(x_r^*,y_s^*,t_q)\,\delta_{pq}$$

III,4. AERODYNAMIC FORCED EXCITATION

III,4.1. Generalized aerodynamic forces

The pressure jump through blade 1, $\Delta p_1(x,y,t)$ acts in the direction of the normal vector $\vec{n}(x,y,t)$, and the virtual work is given by the integral :

$$\delta a = \iint_{(A)} \delta\vec{P}\,\vec{n}\,\Delta p_1\,dx\,dy$$

The vector $\delta\vec{P}$ is the virtual displacement of the point P, of coordinates x,y. We have : $\delta\vec{P} = \sum_\mu \frac{\partial\vec{P}}{\partial\gamma_\mu}\delta\gamma_\mu = \sum_\mu \frac{\partial\vec{V}}{\partial\dot{\gamma}_\mu}\delta\gamma_\mu$ and :

$$\delta a = \sum_\mu \delta\gamma_\mu \iint_{(A)} \frac{\partial\vec{V}}{\partial\dot{\gamma}_\mu}\vec{n}\,\Delta p_1\,dx\,dy$$

But the vector $\vec{n}$ is independant of the time derivatives of the generalized coordinates, $\dot{y}_u$, so that $\frac{\partial \vec{V}}{\partial \dot{y}_u}\vec{n} = \frac{\partial (\vec{V}\vec{n})}{\partial \dot{y}_u} = \frac{\partial v_n}{\partial \dot{y}_u}$

and

$$\delta a = \sum_u \delta y_u \iint_{(A)} \frac{\partial v_n}{\partial \dot{y}_u} \Delta p_1 \, dx\, dy$$

This equation is in the form :

$$\delta a = \sum_u \delta y_u \, Q_{u1}$$

and we can identify

$$Q_{u1} = \iint_{(A)} \frac{\partial v_n(x,y,t)}{\partial \dot{y}_u} \Delta p_1(x,y,t)\, dx\, dy$$

Q_{u1} is the contribution of blade 1 to the generalized force corresponding to the generalized coordinate y_u.

v_n is given by equation (69) and we have :

$$\frac{\partial v_n}{\partial \dot{y}_u} = \mathcal{C}'_u(x^*, y^*, t)$$

Hence,

$$Q_{u1} = \iint_{(A)} \mathcal{C}'_u(x^*, y^*, t)\, \Delta p_1(x,y,t)\, dx\, dy$$

After substitution of equation (62) for Δp_1, the generalized force Q_{u1} is given in terms of the coefficients $X'_{\ell jp}$ and $X''_{\ell jp}$.

Then we notice that Q_{u2} and Q_{u3} can be derived from Q_{u1} through the relations

$$Q_{u2}(t) = Q_{u1}(t + 2\pi/3)$$

$$Q_{u3}(t) = Q_{u1}(t - 2\pi/3)$$

and we perform the summation :

$$Q_u = Q_{u1} + Q_{u2} + Q_{u3}$$

With the symmetries the only terms which remain in the summation are constant terms and harmonics $3n\omega$, n being an integer.

The resulting column of generalized forces can be written in the form :

(71) $$Q(t) = \left[G_o + \sum_n \mathcal{R}\left(e^{3\imath n\omega t} G_n\right) \right] X$$

where

X is the column of coefficients $X'_{\ell jp}$ and $X''_{\ell jp}$.

G_o and G_n are constant matrices.

III,4.2. Dynamic response of the structure

The response of the structure is defined by the column of generalized coordinates $Y(t)$.

In order to take account of the aerodynamic forces, the generalized forces $Q(t)$, given by (71), will complement, in the right hand side, the equations (57). We get :

(72) $$\mathcal{M}\ddot{Y} + \mathcal{B}\dot{Y} + \mathcal{K}Y = \left[G_o + \sum_n \mathcal{R}\left(e^{3\imath n\omega t} G_n\right) \right] X$$

The admittance matrix can be used to characterize the dynamic properties of the structure. This admittance is defined for an arbitrary frequency :

$$\mathcal{A}(\imath\Omega) = \left(-\Omega^2 \mathcal{M} + \imath\Omega \mathcal{B} + \mathcal{K}\right)^{-1}$$

Then the response can be written as :

(73a) $$Y(t) = R(t) X$$

(73b) $$\dot{Y}(t) = R'(t) X$$

where the matrices R and R' are given by :

$$R(t) = \mathcal{A}(0) G_o + \sum_n \mathcal{R}\left(\mathcal{A}(3\imath n\omega)\, G_n\, e^{3\imath n\omega t}\right)$$

$$R'(t) = \sum_n \mathcal{R}\left(3\imath n\omega\, \mathcal{A}(3\imath n\omega)\, G_n\, e^{3\imath n\omega t}\right)$$

The columns y and y' defined in section III.3 and giving the values of the generalized coordinates at the instant of collocation, t_q, are given by

$$\left(y\right) = \begin{pmatrix} Y(t_1) \\ \vdots \\ Y(t_q) \\ \vdots \end{pmatrix} = \begin{bmatrix} R(t_1) \\ \vdots \\ R(t_q) \\ \vdots \end{bmatrix} \left(X\right)$$

$$\left(y'\right) = \begin{pmatrix} \dot{Y}(t_1) \\ \vdots \\ \dot{Y}(t_q) \\ \vdots \end{pmatrix} = \begin{bmatrix} R'(t_1) \\ \vdots \\ R'(t_q) \\ \vdots \end{bmatrix} \left(X\right)$$

These equations can be written in the form :

(74a) $$y = \mathcal{S} X$$

(74b) $$y' = \mathcal{S}' X$$

where $\mathcal{S}$ and $\mathcal{S}'$ are the matrices :

$$\mathcal{S} = \begin{bmatrix} \\ R(t_1) \\ \vdots \\ R(t_q) \\ \vdots \end{bmatrix}$$

$$\mathcal{S}' = \begin{bmatrix} \\ R'(t_1) \\ \vdots \\ R'(t_q) \\ \vdots \end{bmatrix}$$

III,5. SOLUTION

The solution of the problem of forced vibrations in forward flight is obtained from the matrix equations (66), (70) and (74).

(66) $$v_n = a X$$

(70) $$v_n = v_{no} + \mathcal{C} y + \mathcal{C}' y'$$

(74a) $$y = \mathcal{S} X$$

(74b) $$y' = \mathcal{S}' X$$

Equation (66) relates the normal velocities to the aerodynamic forces and characterises the rotor aerodynamics ; equation (70) relates the normal velocity to the response of the structure through kinematic relations ; finally equations (74) relate the response of the structure to the aerodynamic forces and characterises the structural dynamics.

After substitution of (66) and (74) into (70) we get :

$$[a - (\mathcal{C}\mathcal{S} + \mathcal{C}'\mathcal{S}')] X = v_{no}$$

Hence the column of aerodynamic coefficients :

(75) $$X = [a - (\mathcal{C}\mathcal{S} + \mathcal{C}'\mathcal{S}')]^{-1} v_{no}$$

The vibratory response is obtained after substitution of X into (74) or (73).

III,6. REVERSE CIRCLE

As already mentioned, the basic assumption of small perturbations is invalidated locally on the side of the retreating blade, in the vicinity and inside the reverse circle. Furthermore, if formulas (62), (66) and (70) are used for the determination of the aerodynamic forces, the Kutta-Joukowsky condition is applied in a wrong manner inside the circle since account has not been taken of the fact that the flow is travelling from trailing to leading edge.

Large discrepancies may result, between experiment and theory, from these inconsistencies.

A significant improvement is obtained if we take account of the fact that the lift is generally small in the vicinity of the reverse circle (because the dynamic pressure is small) and write a condition of zero lift, for the points which are concerned, instead of introducing the actual blade normal velocity.

In doing that, we assume implicitly that the blade is distorded, when it passes through the reverse circle, in a manner which makes the lift equal to zero. With this fictitious deflexion, the calculations are consistent with the basic assumptions.

This condition of zero lift has been omitted here for the sake of simplicity but it was introduced in the calculations giving the results of figure 15.

III,7. CONCLUDING REMARKS

The fundamental methods which have been used in the formulation of the problem of forced vibrations in forward flight can be considered as extensions to helicopters of the methods currently applied to fixed wing aircraft for flutter investigations.

The assumption of small vibrations is justified for the helicopters as well as for aircraft, and the modal representation is also convenient for the determination of the structural dynamics.

For the actual helicopters, the formulation should be complemented with the introduction of the cyclic pitch, the drag and the

viscous forces simulating the structural damping. The introduction of the cyclic pitch would result in a cyclic variation of the normal velocity and, consequently, in a new cyclic excitation.

In spite of the difficulties, arising on the retreating blade, the correlation between theoretical and experimental results illustrated in figure 16 is rather satisfactory. The value of the advancing ratio $\mu = 0.3$ which was considered in this application is a significant figure for a modern helicopter.

But we must not forget that the increase of the cruise velocity, which is aimed at in the new designs, will be paid by an increase of the advancing ratio, i.e. by a larger extension of the reverse circle.

On the other hand, the linear methods seem to be particularly convenient for new types of rotary wing aircraft, such as the tilt rotor aircraft, because in that case the configuration of the blades can be adjusted to every flight condition, in order to improve the flow.

☆ ☆ ☆

ANNEX

METHODS OF INTEGRATION AND CHOICE OF COLLOCATION POINTS (see also ref. [35])

A-1 - Gaussian integration

We wish to find an integration formula for the integral :

$$\int_a^b W(x)\, f(x)\, dx$$

where $W(x)$ is a weight function containing, eventually, an integrable singularity.

The formula will be in the form :

$$\int_a^b W(x)\, f(x)\, dx = \sum_{\alpha=1}^{n} H_\alpha\, f(x_\alpha) \tag{A.1}$$

The x_α are the integration points and the H_α the weights.

Since there are 2 n parameters ($x_1 \dots x_n$, $H_1 \dots H_n$), their values can be optimized in such a way that equation (A.1) will be exact when $f(x)$ is any polynomial of degree $2n-1$.

With the n integration points x_α , we can define a polynomial of degree n :

$$G_n(x) = \prod_{\alpha=1}^{n} (x - x_\alpha) \tag{A.2}$$

From $G_n(x)$ a set of Lagrangian interpolation polynomials of degree $n-1$ can be obtained :

$$g_\alpha(x) = \frac{G_n(x)}{(x - x_\alpha)\, G_n'(x)} \tag{A.3}$$

These polynomials have the property of being equal to zero or to unity at the integration points :

$$g_\alpha(x_\beta) = \delta_{\alpha\beta} \tag{A.4}$$

They can be used to define an interpolated approximate function $f^*(x)$:

$$f^*(x) = \sum_{\alpha=1}^{n} g_\alpha(x)\, f(x_\alpha) \tag{A.5}$$

$f^*(x)$ is equal to $f(x)$ at the integration points :

$$f^*(x_\beta) = f(x_\beta) \tag{A.6}$$

Then an approximate integration formula of the desired form can be obtained if we use the function f^* instead of f into (A.1) :

$$\int_a^b W(x)\, f^*(x)\, dx = \sum_{\alpha=1}^{n} \int_a^b W(x)\, g_\alpha(x)\, dx\, f(x_\alpha) \tag{A.7a}$$

The identification with formula (A.1) gives :

$$H_\alpha = \int_a^b W(x)\, g_\alpha(x)\, dx \tag{A.7b}$$

The optimization of the integration points is realized if the approximate integral is equal to the exact integral when $f(x)$ is a polynomial of degree $2n-1$. In other words, the condition is :

$$\int_a^b W(x)\, [\, f(x) - f^*(x)\,]\, dx = 0 \tag{A.8}$$

if $f(x)$ is a polynomial of degree $2n-1$.

But $f(x) - f^*(x)$ is equal to zero at the integration points $x = x_\alpha$. It means that $f(x) - f^*(x)$ can be written in the form :

$$f(x) - f^*(x) = \prod_{\alpha=1}^{n} (x - x_\alpha)\, P_{n-1}(x)$$

where $P_{n-1}(x)$ is some polynomial of degree $n-1$.

Then we have :

$$\int_a^b W(x)\,[f(x) - f^*(x)]\,dx = \int_a^b W(x) \prod_{\alpha=1}^{n} (x - x_\alpha)\, P_{n-1}(x)\,dx$$

$$= \int_a^b W(x)\, G_n(x)\, P_{n-1}(x)\,dx \qquad \text{(according to (A.2).}$$

Let us assume that $G_n(x)$ in the polynomial of degree n of a set of polynomials $G_r(x)$ orthogonal with respect to $W(x)$, i.e, verifying the orthogonality relation :

$$\int_a^b W(x)\, G_r(x)\, G_s(x)\,dx = 0 \qquad s \neq r$$

Then, $P_{n-1}(x)$ is a combination of the first $n-1$ polynomials of the same set and the integral $\int_a^b W(x)\, G_n(x)\, P_{n-1}(x)\,dx$ is equal to zero, so that the desired conditions (A.8) is satisfied.

This shows that the integration points must be the zeros of the polynomial of degree n belonging to a set of polynomials orthogonal with respect to the weight function $W(x)$. The weights are given by equation (A.7b).

Particular weight functions

We shall transfer our coordinates so that the range of integration is (-1, 1). The particular weight functions which are used in the integrals giving the aerodynamic forces in the third part of the lecture are $\sqrt{1-y^2}$ for the spanwise integration and $\sqrt{\frac{1-x}{1+x}}$ for the chordwise integration.

For these particular functions the results can be summarized :

$$W(y) = \sqrt{1-y^2} \;\Rightarrow\; H_\alpha = \frac{\pi}{n+1}(1 - x_\alpha^2) \quad , \quad x_\alpha = \cos\theta_\alpha \quad \text{with} \quad \theta_\alpha = \frac{\alpha\pi}{n+1}$$

$$W(x) = \sqrt{\frac{1-x}{1+x}} \;\Rightarrow\; H_\alpha = \frac{2}{2n+1}(1 - x_\alpha) \quad , \quad x_\alpha = -\cos\theta_\alpha \quad \text{with} \quad \theta_\alpha = \frac{2\alpha+1}{2n+1}\pi$$

When $W(x) = 1$, the orthogonal polynomials to consider are the legendre polynomials.

A-2 - The choice of the collocation points

The choice of the collocation points is derived from the consideration of simple aerodynamic problems for which the analytical solution is known. The same choice is convenient for more complex problems because it takes account of the main singularities of the lifting surface theory.

A-2.1. Chordwise distribution

The two-dimensional steady incompressible flow is considered. The integral equation which connects the chordwise pressure $\Gamma(x)$ and the downwash $w(x)$ is given by

$$2\pi\, w(x) = \int_{-1}^{1} \frac{\Gamma(\xi)}{x - \xi}\, d\xi$$

The solution is given by

$$\Gamma(x) = \frac{\pi}{2}\sqrt{\frac{1-x}{1+x}} \int_{-1}^{1} \sqrt{\frac{1+\xi}{1-\xi}}\; \frac{w(\xi)}{\xi - x}\, d\xi$$

$w(\xi)$ will be approximated by an interpolated polynomial $w^*(\xi)$.

Let $\Gamma^*(x)$ be the corresponding approximate lift.

We have :

$$\Gamma(x) - \Gamma^*(x) = \frac{\pi}{2}\sqrt{\frac{1-x}{1+x}} \int_{-1}^{1} \sqrt{\frac{1+\xi}{1-\xi}}\; \frac{w(\xi) - w^*(\xi)}{\xi - x}\, d\xi \quad ;$$

$w^*(x)$ is equal to $w(x)$ at the n interpolation points ξ_α.

If $w(x)$ is a polynomial of degree $2n-1$ we have :

$$w(x) - w^*(x) = \prod_{\alpha=1}^{n} (x - x_\alpha)\, P_{n-1}(x)$$

P_{n-1} being some polynomial of degree $n-1$

Let us denote by G_n the polynomial of degree n :

$$G_n(x) = \prod_{\alpha=1}^{n} (x - x_\alpha)$$

Then,

$$w(x) - w^*(x) = G_n(x)\, P_{n-1}(x)$$

We shall try to choose the points x_α so that

$$\int_a^b [\Gamma(x) - \Gamma^*(x)]\,dx = 0$$

or,

$$\int_{-1}^{1}\sqrt{\frac{1-x}{1+x}}\int_{-1}^{1}\sqrt{\frac{1+\xi}{1-\xi}}\;\frac{G_n(\xi)\,P_{n-1}(\xi)}{\xi-x}\,d\xi\,dx=0$$

or

$$\int_{-1}^{1}\sqrt{\frac{1+\xi}{1-\xi}}\;G_n(\xi)P_{n-1}(\xi)\left[\int_{-1}^{1}\sqrt{\frac{1-x}{1+x}}\;\frac{dx}{\xi-x}\right]d\xi$$

The inner integral is equal to π and the condition is :

$$\int_{-1}^{1}\sqrt{\frac{1+\xi}{1-\xi}}\;G_n(\xi)P_{n-1}(\xi)\,d\xi=0$$

This condition is satisfied if $G_n(\xi)$ is the polynomial of degree n of the set of polynomials orthogonal with respect to the weight function $\sqrt{\frac{1+\xi}{1-\xi}}$. Then the interpolation points to be considered are the zeros of $G_n(\xi)$. These points are the more significant for the downwash and they are used as collocation points. They are integration points for the weighting function $\sqrt{\frac{1+\xi}{1-\xi}}$. Since this function is symmetric to the weight function $\sqrt{\frac{1-x}{1+x}}$, the collocation points are symmetric of the integration points given in section A.1.

A-2.1. Spanwise distribution

The best spanwise collocation points are formed in the same manner. The integral equation which connects the two-dimensional steady incompressible spanwise downwash with the pressure is :

$$2\pi w(y)=\int_{-1}^{1}\frac{\Gamma(\eta)}{(y-\eta)^2}\,d\eta$$

The solution is :

$$2\pi\Gamma(y)=\sqrt{1-y^2}\int_{-1}^{1}\frac{\sqrt{1-\eta^2}}{(y-\eta)^2}\;w(\eta)\,d\eta$$

As before we define an interpolated polynomial $w^*(\eta)$ such that the resulting $\Gamma^*(y)$ satisfies the conditions :

$$\int_{-1}^{1}\left(\Gamma(y)-\Gamma^*(y)\right)dy=0$$

We have :

$$\int_{-1}^{1}\left(\Gamma(y)-\Gamma^*(y)\right)dy=\int_{-1}^{1}\sqrt{1-y^2}\int_{-1}^{1}\frac{\sqrt{1-\eta^2}}{(y-\eta)^2}\left[w(\eta)-w^*(\eta)\right]d\eta\,dy$$

$$=\int_{-1}^{1}\sqrt{1-\eta^2}\left[w(\eta)-w^*(\eta)\right]\left[\int_{-1}^{1}\frac{\sqrt{1-y^2}}{(y-\eta)^2}\,dy\right]d\eta$$

The inner integral is equal to π and we have :

$$\int_{-1}^{1}\sqrt{1-\eta^2}\left[w(\eta)-w^*(\eta)\right]d\eta=0$$

If η_α are the interpolation points the difference $w(\eta)-w^*(\eta)$ can be written :

$$w(\eta)-w^*(\eta)=\prod_{\alpha=1}^{n}(\eta-\eta_\alpha)\;P_{n-1}(\eta)$$

and the condition to be fulfilled is :

$$\int_{-1}^{1}\sqrt{1-\eta^2}\prod_{\alpha=1}^{n}(\eta-\eta_\alpha)\;P_{n-1}(\eta)\,d\eta=0$$

It is verified if the η_α are the zeros of the polynomial of degree n belonging to the set of polynomials orthogonal with respect to the weight function $\sqrt{1-\eta^2}$.

Then, the collocation points are the integration points corresponding to the weight function $\sqrt{1-\eta^2}$.

REFERENCES

[1] HAMMOND G.E. – *A parametric study of helicopter rotor blade flutter under low inflow conditions, using incompressible aerodynamics.* Georgia Institute of Technology, A.E. 604, June 1968.

[2] HAMMOND G.E. – *Compressibility effects in helicopter rotor blade flutter.* GITAER Report N° 69-4, Georgia Institute of Technology.

[3] HAM N.D. – *Helicopter blade flutter.* AGARD Manual of Aeroelasticity, Vol. 3, Chapter 10, Dec. 1967.

[4] HAM N.D. and YOUNG M.I. – *Torsional oscillation of helicopter blades due to stall.* Journal of Aircraft, Vol. 3, N° 3, May-June 1966.

[5] HAM N.D. – *Stall flutter of helicopter rotor blades : a special case of the dynamic stall phenomenon.* Journal of the American Helicopter Society, vol. 12, N° 4, October 1967, p. 19-21.

[6] HAM N.D. and GARELICK M.S. – *Dynamic stall considerations in helicopter rotors.* Joutnal of the American Helicoptet Society, vol. 13, nº 2, April 1968, p. 49-55.

[7] LIIVA J. and DAVENPORT F.J. – *Dynamic stall of airfoil sections for high-speed rotors.* Journal of the American Helicopter Society, vol. 14, nº 2, April 1969, p. 26-33 ; also U.S. Army Aviation Material Laboratories Report TR 68-13, 1968.

[8] CARTA F.O. – *An analysis of the stall flutter instability of Helicopters rotor blades.* Journal of the American Helicopter Society, vol. 12, nº 4, October 1967, p. 1-18.

[9] U.S. Army Aviation Materiel Laboratories (AAVLABS) – *Soft in-plane matched-stiffness/flexure-root-blade rotor system summary report.* USAAVLABS Technical Report 68-72 (not yet published).

[10] COLEMAN R.P., FEINGOLD A.M. – *Theory of self-excited mechanical oscillations of helicopter rotors with hinged blades.* National Advisory Committee for Aero, Report 1351, 1958.

[11] BROOKS G.W. – *The mechanical instability and forced response of rotors on multiple-degree-of-freedom supports.* Princeton University, Doctoral dissertation, New Jersey, 1961.

[12] BIELAWA R.L. – *An experimental and analytical study of the mechanical instability of rotors on multiple-degree-of-freedom supports.* Princeton University, Department of Aeronautical Engineering, report Nº 612, New Jersey, 1962.

[13] SISSINGH, Dr. G.J. – *Response characteristics of the gyro-controlled Lockheed rotor system.* Journal of the American Helicopter Society, vol. 12, Nº 14, October 1967.

[14] SISSINGH, Dr. G.J. – *Dynamics of rotors operating at high advance ratios.* Journal of the American Helicopter Society, July 1968.

[15] KUCZYNSKI W.A. and SISSINGH G.J. – *Research program to determine rotor response characteristics at high advance ratios.* NASA CR 114290, February 1971.

[16] KUCZYNSKI W.A. and SISSINGH G.J. – *Theoretical and experimental investigation of rotors with hub moment feedback controls.* Draft final report, phase II, contract NAS 2-5419, Research program to determine rotor response characteristics at high advance ratios, October 1971.

[17] WAATS G.A., LONDON R.J. and SNODDY R.J. – *Trim, control and stability of a gyro-stabilized hingeless rotor at high advance ratio and low rotor speed.* NASA CR-114362, May 1971.

[18] SHUPE N.K. – *A study of the dynamic motions of hingeless rotored helicopters.* Ph. D. Thesis, Princeton University, 1970.

[19] DONHAM R.E., CARDINALE S.V. and SACHS I.B. – *Ground and air resonance characteristics of a soft in-plane rigid rotor system.* Journal of the American Helicopter Society, Volume 14, Nº 4, October 1969.

[20] WOITSCH W. and WEISS H. – *Dynamic behavior of a hingeless fiberglass rotor.* AIAA/AHS VTOL Research, Design, and operations Meeting, Georgia Institute of Technology, Atlanta, Georgia, February 1969.

[21] ORMISTON R.A. and HODGES D.H. – *Linear flap-lag dynamics of hingeless rotor blades in hover.* Journal of the American Helicopter Society, vol. 17, Nº 2, April 1972.

[22] ORMISTON R.A. and PETERS D.A. – *Hingeless rotor response with non uniform inflow and elastic blade bending. Theory and Experiment.* A.I.A.A. Paper Nº 72-65.

[23] ORMISTON R.A. and BOUSMAN W.G. – *A theoretical and experimental investigation of flap-lag stability of hingeless rotor blades.* NASA TM X 62-179, August 1972.

[24] JONES W.P., Mc CROSKEY W.J. and COSTES J.J. – *Unsteady aerodynamics of helicopter rotors.* AGARD report nº 595.

[25] MILLER R.H. – *Rotor blade harmonic air loading.* A.I.A.A. Journal, vol. 2, nº 7, July 1964.

[26] PIZIALI R.M. – *Method for solution of the aeroelastic response problem for rotating wings.* Symposium on the noise and loading actions on helicopter V/STOL Aircraft (Aug. Sept. 1965). Institute of Sound and Vibration Research, University of Southampton, England.

[27] GESSOW A. and MYERS G.D. Jr. – *Aerodynamics of the helicopter,* Frederik Ungar Publishing Co, New York, 1967.

[28] LOEWY R.G. – *A two-dimensional approximation to the unsteady aerodynamics of rotary wings.* Journal of the Aerospace Sciences, vol. 24, Nº 2, February, 1957.

[29] JONES J.P. – *The influence of the wake on the flutter and vibration of rotor blades.* British Aeronautical Research Council Report 18, 173, January 1956 and The Aeronautical Quarterly, vol. IX, 1958.

[30] JONES W.P. and RAO B.M. – *Compressibility effects on oscillation rotor blades in hovering flight.* A.I.A.A. Journal, Vol. 8, Nº 2, February 1970.

[31] KUSSNER H.G. – *Schwingungen von Flugzeugflügeln.* Luftfahr forschung, vol. 4, June 1924.

[32] THEODORSEN T. – *General theory of aerodynamic instability and the mechanism of flutter.* NACA Report 496, 1935.

[33] BAILEY F.J. Jr. – *A simplified theoretical method of determining the characteristics of a lifting rotor in forward flight.* NACA Report 716, 1941.

[34] JENNEY D.S., ARCIDIACANO P.J. and SMITH A.F. – *A linearized theory for the estimation of helicopter rotor characteristics at advance ratios above 1.0.* Proc. 19th Annual National Forum of the American Helicopter Society, Washington, D.C., May 1963.

[35] WILLIAM D.E. – *Three-dimensional subsonic theory.* AGARD Manual of Aeroelasticity, vol. II, chapter 3.

[36] MORSE and FESHBACH – *Methods of theoretical physics. Part I, p. 841.* International Student Edition Mc. Graw Hill Book Company, (1953).



HELICOPTER NOISE: ANALYSIS - PREDICTION AND METHODS OF REDUCTION

by

Martin V. Lowson,
Loughborough University of Technology,
Leicestershire, England.

SUMMARY

The fundamentals of helicopter noise radiation phenomena are presented, including a review of the leading features of subjective response. Emphasis is placed on the underlying mechanisms of rotor noise generation, both for discrete frequency and broad band noise components. The implications for helicopter noise control are discussed, including a brief review of possible propagation effects and the potential costs of helicopter noise reduction.

1. Introduction 1

2. Some Fundamentals of Acoustics 3
   2.1 Decibel Scales 3
   2.2 Subjective Response to Noise 4

3. Mechanisms of Rotor Noise Generation 7
   3.1 The first studies 7
   3.2 Discrete frequencies 9
      3.2.1 Theory 9
      3.2.2 Aerodynamics 13
      3.2.3 Prediction and Comparison with Experiment 15
   3.3 Broad Band Noise 17
      3.3.1 Theory 17
      3.3.2 Experimental Results and Predictions 20
   3.4 Other Source Mechanisms 24
   3.5 Some Recent Experiments 24

4. Application to Noise Control 27
   4.1 The Effects of Design Parameters 27
   4.2 Detail Improvements 27
   4.3 Propagation Effects 29
   4.4 The Cost of Noise Control 31

5. Conclusions 32

6. References 33

1. INTRODUCTION

The noise radiated by a helicopter has become a limiting feature in many of its operations. Helicopters could play a vital role in urban transportation systems, but their use has been considerably restricted, often to the point of outright banishment, because of their noise radiation. Reduction of community noise annoyance resulting from helicopter operations is clearly a prerequisite for their downtown use. Equally, in military operations, the easily recognised noise signature of a helicopter has severely predjudiced their military effectiveness, not only in attack, but also in casualty evacuation, and similar situations. Helicopter noise reduction has therefore become a prime military as well as civil goal.

Internal noise problems also demonstrate serious inadequacies in present day design methods. Noise and vibration levels inside virtually all helicopters are high - approaching the intolerable in some cases. Such levels are a major deterrent for many passengers. In military use noise levels considerably exceed deafness risk criteria in many cases and seriously hamper communication. Thus internal noise jeopardises the effectiveness of the helicopter in both civilian and military roles. Unfortunately it will not be possible to cover internal noise problems in any detail in these notes.

The main features of radiated helicopter noise are well known. The noise can be divided into two groups: that arising mechanically, and that arising aerodynamically. Mechanically generated noise includes that due to a piston engine (now obsolescent), and to the gear box, transmission and other vibrating components of the aircraft system. In general, the mechanical sources are only of dominant interest for internal noise, or very close to the helicopter. In the radiated far field the aerodynamically generated sources are dominant. The latter includes various types of noise commonly categorised as rotational noise, vortex noise and blade slap. Which of these is most significant depends

on several factors, the more important of which are the relative location of the observer, and the flight configuration of the helicopter. At moderate distances from the helicopter the various sources, listed in their order of importance in a subjective loudness rating scheme, are

- blade slap (when it occurs)
- tail rotor rotational noise
- main rotor vortex noise
- main rotor rotational noise
- gearbox noise
- turbine engine noise
- other sources

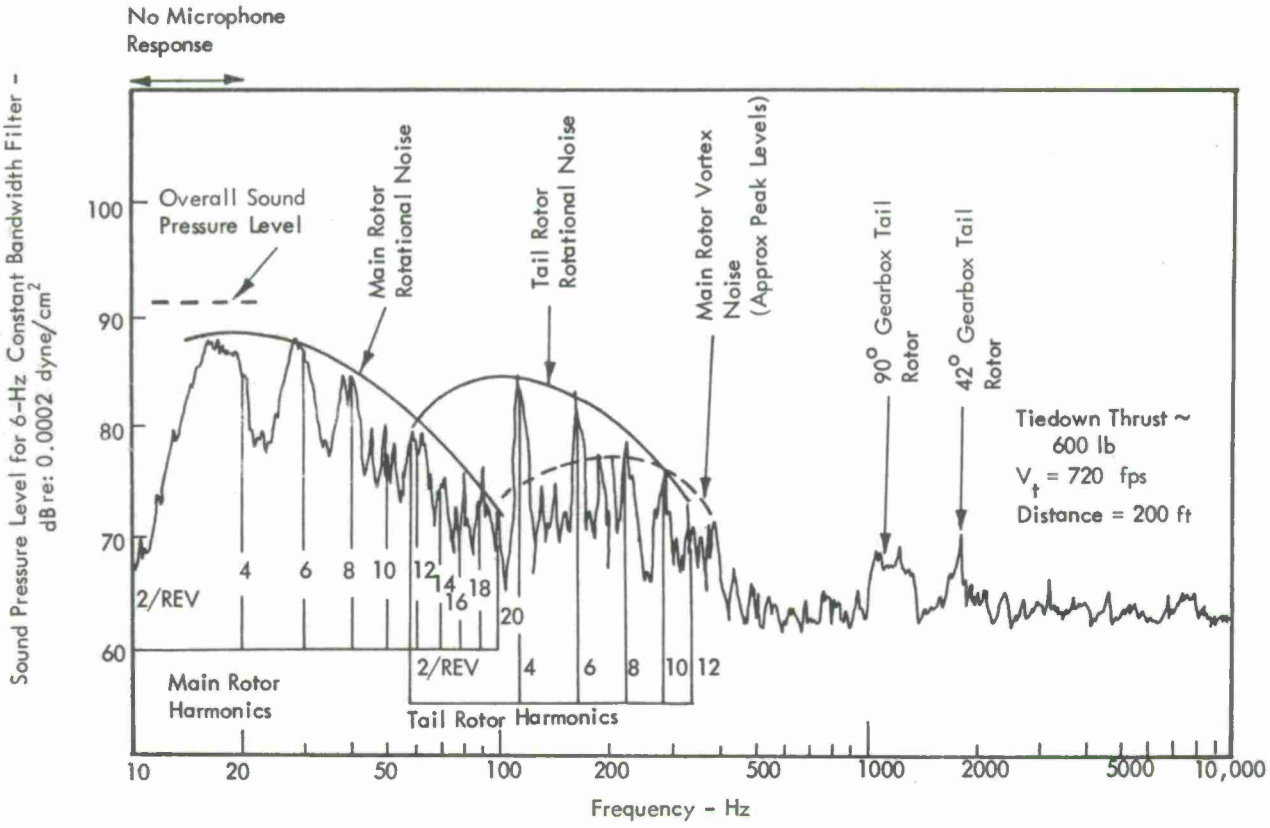


Figure 1.1: UH-1A external noise spectrum. Derived from Reference 1.

Some of these sources are identified in the UH-1 helicopter noise spectrum shown in Figure 1.1 which is derived from the results of Cox and Lynn[1]. The four major noise sources are aerodynamic in origin and it is with such sources that this paper is concerned.

In order to understand the cause of these aerodynamic sound sources, it is necessary, first of all, to understand the nature of the rotor aerodynamics. The most important feature of the helicopter aerodynamics from the standpoint of noise and vibration is the rotor wake. As has been discussed in other sections of these notes, each blade acts in the same way as a wing in flight, and the lift on it generates a vortex wake behind it. This vortex wake has a strong tendency to roll up into concentrated vortices. Each blade must therefore pass over the concentrated vortex wake left by its predecessor. Depending on the exact value of aerodynamic parameters such as advance ratio, net lift force, and so on, this vortex may pass either extremely close to, or far away from, the following blade. If the vortex passes close to the blade then a substantial local increase in lift will occur temporarily. The magnitude of the increase is dependent on such features as vortex strength, inclination, distance from the blade, and blade chord. These comparatively rapid increments in lift, caused by vortex interaction, are very efficient noise radiators. It appears that a very large part of the observed noise from a helicopter can be attributed to these vortex effects.

A particularly severe case of this is well known in helicopter operations under the name "blade slap". It is found that under various conditions, for instance during low power descent, the helicopter produces a particularly loud slapping or banging noise, which occurs at the blade passage frequency. Narrow band analysis of blade slap noise reveals it to be harmonic in nature with the fundamental equal to the blade passage frequency and a large number of significant harmonic components. Blade slap occurs at precisely those conditions where the vortex wake can be expected to pass very close to the rotor, and can be particularly severe on a tandem rotor aircraft where the wake from the first rotor can pass through the second. In fact, the sharpest banging case will occur when the vortex wake interactions cause the flow over a rotor blade to go locally supersonic, and blade

slap is thus most severe for high speed rotors. A second form of blade slap can occur on high speed rotors, which correlates with the appearance of supersonic flow on the blades. It may be noted that the description of both these blade slap phenomena is fairly straightforward acoustically and the effects mentioned above can be readily predicted from the theory presented later. Reference can also be made to the interesting studies by Leverton and Taylor[2], and to recent work by Leverton[3], Widnall[4] and Lyon[5]. Blade slap conditions must always be avoided in a quiet helicopter, and the phenomenon is not therefore considered in any detail in this paper.

However, even in the absence of blade slap the rotor is always undergoing some form of wake interaction, which is generally less severe. The resulting "rotational noise" is still attributable to fluctuating forces acting on the blades and exhibits the same discrete frequency characteristics. But in this case the acoustic harmonic amplitudes decrease more rapidly with increasing frequency (as is shown in Figure 1.1). The same mechanisms also apply at the tail rotor, which operates in an extremely non-symmetric flow field. It will be observed that the harmonic spectrum shape of the tail rotor noise in Figure 1.1 is not very different from that of the main rotor, thus suggesting that basically similar mechanisms are at work.

The third aerodynamic noise source which has been generally associated with the main rotor is its "vortex noise". This is a rather misleading name generally given to the underlying broad band noise component. As will be shown in Section 3.3, precise definition of this component is rather difficult, since it is very hard to separate from the higher harmonics of the rotational noise. Indeed rigid classification of any noise source is always difficult. Helicopter noise is a composite phenomenon and must be dealt with via a composite approach. In these notes emphasis will be placed on the mechanisms underlying observed noise radiation phenomena and their implications for noise control. Nevertheless, the whole approach to helicopter noise problems is founded on phenomena associated with subjective response. It is therefore appropriate, first of all, to discuss the fundamentals of human response to noise, and the scales of measurement used for the quantification of noise levels.

2. SOME FUNDAMENTALS OF ACOUSTICS

2.1 Decibel Scales

The unit used for measuring noise is the decibel or dB. This is simply a ratio expressed on a logarithmic scale. In fact there are two possible methods for quantifying the sound radiation from any source on a dB scale. These correspond to describing the acoustic source either by the local pressure measure at a particular point some distance from the source, or by the total acoustic power radiation of the source.

The sound pressure level is defined by

$$SPL = 10 \log_{10} \frac{p^2}{p_{ref}^2} \qquad \ldots\ldots\ldots\ldots (2.1)$$

where p^2 is the mean square pressure at the point in question, and p_{ref} is a reference pressure. The reference pressure is usually taken as 2×10^{-5} N/m^2, but this should always be quoted.

The sound power level (PWL) is defined by

$$PWL = 10 \log_{10} \frac{W}{W_{ref}} \qquad \ldots\ldots\ldots\ldots (2.2)$$

where W is the mean acoustic power radiated and W_{ref} is a reference power. W_{ref} is conveniently taken as 10^{-12} Watts when working in metric units, but a reference of 10^{-13} Watts is very common for convenience in Imperial or U.S. customary units. Thus it is essential to quote a reference level for a PWL figure.

Naturally, the two descriptions of the sound from a source are related, and for a point omnidirectional source of sound the relation for the reference levels given as above is

$$SPL = PWL - 10 \log_{10} A + 0{\cdot}16 \qquad \ldots\ldots\ldots\ldots (2.3)$$

where A is the area in metres^2 over which the sound has spread, and the levels as given.

For a point source in free air $A = 4\pi r^2$ where r is the distance from the source to the point of pressure measurement.

Decibel scales are of use in acoustics for two reasons. The first is that absolute levels of acoustic pressure and power can vary by very many orders of magnitude. For instance, the difference in intensity between the level of sound which is just detectable by a human observer, and that which is at the threshold of pain represents a factor of 10^{14}. Decibel scales allow this difference to be represented as a 140dB variation, thus bringing the numbers into a more comprehensible range. The logarithmic scales have another

benefit, in that they mimic the response of the human observer to the variations in noise level. Indeed there is a general psycho-physical law due to Weber and Fechner that for a wide range of stimuli the absolute change in response is equal to the proportional change in the stimulus. This corresponds to a logarithmic response curve. Sound can be regarded simply as a pressure fluctuation. It satisfies a well defined mathematical equation, and is similar to other fluctuating mechanical phenomena such as vibration or turbulence. However, for the reasons mentioned above, decibel scales have achieved wide acceptance for describing noise levels and their use now seems an essential feature of the basic understanding.

As has been emphasised it is subjective response to sound that dominates the choice of approach. There are two major points relating to this that must be appreciated, and have far-reaching consequences. The first is that the ear is a wonderfully sensitive instrument which is able to detect fluctuating pressure phenomena beyond the range of any but the most sensitive instruments. Thus miniscule amounts of acoustic energy can give rise to large subjective response. For example, internal noise levels approaching the threshold of pain correspond to fluctuations in pressure of about one thousandth of an atmosphere. At detection threshold it is estimated that the motion of the ear drum has an amplitude of one tenth of the diameter of a hydrogen molecule (10^{-11}m). Thus minute fluctuations at the helicopter, entirely insignificant from the point of view of performance, can have dominant effects on the noise field.

Factor change in intensity	*dB value*	*Subjective effect*
2	3	Barely distinguishable
4	6	Noticeable
16	12	Pronounced

Table 1: Effect of changes in acoustic intensity

The second significant feature of subjective response is the comparative insensitivity of the ear to changes in level. This necessitates fundamental reconsideration of the optimum approach to noise control. The problem is illustrated by Table 1. It can be observed that a factor of 2 (i.e. 100%) change in intensity at 3dB is barely distinguishable subjectively. Successful noise control measures will require reductions by a factor of perhaps 10. It therefore becomes clear that a conventional design optimisation approach in which parameters are varied by perhaps 25% has little possibility of achieving the desired noise reduction goals. Indeed, in my opinion, once design layout is complete the acoustic output is largely determined, and noise reductions after that point in time will not generally be possible unless there was a fundamental acoustic problem in the original design. An alternative way of looking at the problem is to consider that a typical helicopter uses around 1 MW of power, and only emits around 1 kW as sound. Thus it is already 99·9% efficient at being quiet and will be difficult to improve to the 99·99% quietness necessary to make a useful noise reduction. In fact helicopter rotors, in their present state of development, seem to be unusually noise sensitive to detail modifications. Nevertheless, the general ideas above still have considerable force, and it is vital to consider overall acoustic goals from the outset of the design process.

2.2 Subjective Response to Noise

Subjective response to any noise depends not only on the level of the sound but also its frequency. The typical response curves for the human ear are shown in Figure 2.1. These correspond to the A and D frequency weighting scales, which are based on extensive laboratory testing. Each curve predicts a maximum sensitivity to frequency components around 2000Hz. If a noise signal is passed through a filter network with the A or D frequency characteristics shown in the figure, then the output level is described as 'A' or 'D' weighted and bears a close relation to the subjectively judged loudness of the original noise. The 'A' scale is perhaps the more widely used while the 'D' scale represents current estimates of response more closely. Each scale very roughly follows a frequency squared law at low frequencies, as shown in Figure 2.1, and this fact is used later.

It will be noted that there are quite large differences between the curves, and although the D scale is now widely accepted these differences mainly represent genuine differences in experimental results under varying test conditions. Human response to any stimulus is a very variable factor.

For this reason, no single curve is ever likely to be found to give "accurate" results. The commercial pressure for more closely defined subjective criteria is intense, because of the engineering significance of a single dB (it is a 25% change of intensity). The result of this pressure has been a surfeit of subjective scales in recent years, few of which show any major improvement. A form of uncertainty principle seems to apply in that criteria which can be defined more and more closely for a particular class of sounds seem less and less likely to apply to other noises[6]. The present aircraft standards, based on the PNdB[7], have been developed to describe community annoyance around airports during aircraft take-off and landing operations. The standards are moderately successful at this, but there is growing evidence that the methods used may be rather inadequate for helicopters. Leverton[8] argues that the terms of clear subjective importance when listening

to a helicopter do not seem to carry any weight in its PNdB estimate, and that the result is a strong bias against helicopter noises using present rating scales.

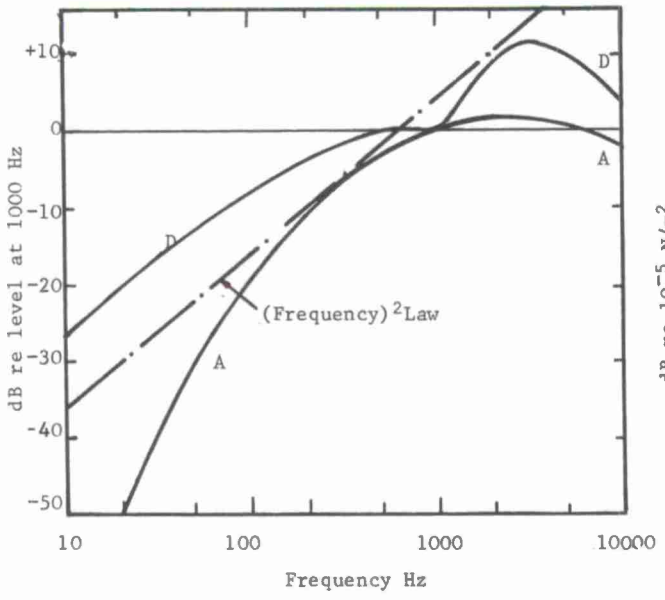


Figure 2.1: Frequency weighting curves for subjective response

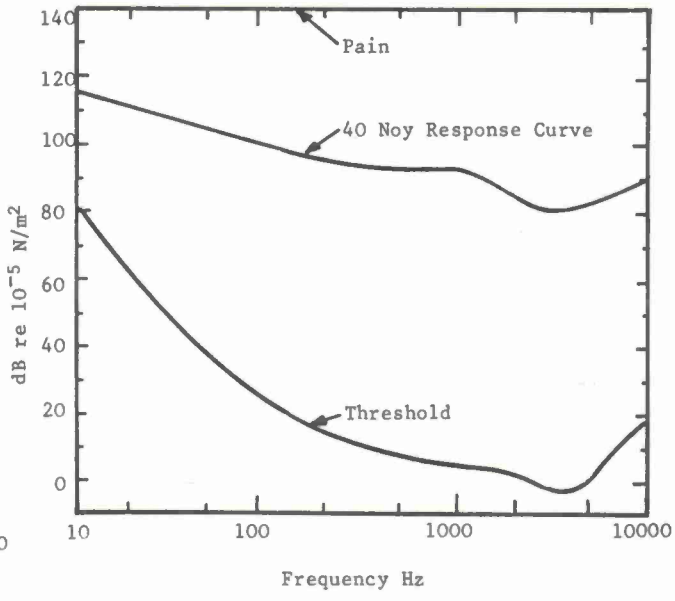


Figure 2.2: Equal response curves

Details of current rating scales will not be discussed herein. Reference may be made to the official standards on this[7]. For practical purposes the PNdB scales closely match the linear weighting scales shown on Figure 2.1, and comparison has shown that for a wide range of sounds

$$\left.\begin{aligned} L_{PN} &= L_A + 13 \\ \text{or } L_{PN} &= L_D + 7 \end{aligned}\right\} \qquad \ldots\ldots\ldots\ldots (2.4)$$

where L_{PN} is the sound level in PNdB,
L_A is the sound level measured on the 'A' weighting scale,
and L_D is the sound level measured on the 'D' weighting scale.

For practical purposes the vital feature of any subjected response scale is the high weighting it puts on the intermediate frequencies (1000 - 4000Hz) compared to either low or high frequency content. This is of considerable importance in interpreting helicopter noise spectra.

In military applications (and, in effect, in civilian applications too, as will be shown), the acoustic criterion of dominant significance is detection. This aspect of aircraft noise has received comparatively little study. A paper by Loewy[9] gave the first systematic analysis, but fortunately the subject has now been comprehensively investigated by Ollerhead[10]. Again it is not intended here to present the results of this psychophysical investigation in any detail here, but the principal conclusions may be summarised straightforwardly.

The fundamental threshold curves for human response are shown in Figure 2.2. This also gives curves for the threshold of pain, and a typical equal response curve at the intermediate noise level. It will be observed that this equal response curve is the inverse of the 'D' weighting scale (Figure 2.1) and this was, in fact, how the 'D' weighting was derived. However detection of a signal in the presence of background noise is a function of more than just the absolute threshold level. The laws governing detection may be stated as follows.

A signal will not be detected if all "critical bands" of its spectrum are more than 5dB below the ambient noise level. The critical band is a function of frequency but corresponds fairly closely to one third octave sections. Also any critical band of the noise spectrum will not be detected if it is below the threshold of hearing for that band.

The effect of two laws in combination is as follows. The background level in each critical bandwidth can be determined. The threshold level can be defined as a function of critical band. A combined threshold curve can be drawn by decibel addition of the threshold curve and a masking curve 5dB below the background level. The noise will be detected if any critical band of its spectrum exceeds this combined threshold curve.

These laws may have considerable relevance to the civil case. For urban environments fairly high levels of background noise exist, and it is clear that an undetected helicopter

recording. From this, Fourier analysis was in principle possible, but little spectral data was published. However, these shortcomings necessitated more active reliance on intelligent subjective observation and reported results of tests[16] correctly define features which were still a matter of controversy fifty years later. Perhaps there is an important moral here.

Two of these features were the minimum of propeller noise observed on axis, and the major difference between ground and flight tests at nominally equivalent conditions. This latter point is often overlooked even today. Much reported data on propeller noise taken on ground rigs is irrelevant to noise in flight. For helicopter rotors the problem is less acute, and ground data is probably more representative, but considerable care in extrapolation will always be necessary.

Theoretical work on the propeller noise problem was also undertaken. Lynam and Webb[17] considered the propeller as a ring of sources and sinks, and properly evaluated the retarded time integral to give a solution in terms of Bessel functions. However, their basic model of the propeller was equivalent to an axial dipole and necessarily led to the prediction of zero sound in the rotor disc plane, completely contrary to experiemental findings. They therefore removed the sinks to infinity, and the rotating source results, although physically rather meaningless, at least resembled experimental trends. Bryan's[18] approach was more fundamental, and he did indicate the solutions for dipoles oriented in each of the three major directions, but he avoided explicitly modelling the propeller.

In the inter-war years interest in propeller noise reduced. The official attitude appears to have been that, quoting from Reference 16, "The problem of silencing an aircraft in flight was one of such difficulty that substantial progress was unlikely". The author went on to make a plea for improved instrumentation, and indeed it appears that only now do we at last have sufficiently good instruments and analysis methods to permit a full understanding of rotor noise sources.

British work concentrated on internal noise problems in aircraft, for, to quote from Davis[19] in 1932, "It is common knowledge that until comparatively recently the noise in the cabins of aircraft was so extreme that for many persons it constituted the chief deterrent to air travel. Conversation was wholly impossible, and often wads of cotton wool were issued to passengers to enable them to obtain some slight - but welcome - relief from the pandemonium of sounds, and to protect them in some measure from the period of perceptible deafness which followed an excursion by air". Possibly the same remarks apply to certain rotor powered craft today, but, in general, the achievement of acoustic science so far has been to remove the noise problem from the interior of aircraft and to impose it instead on the community at large.

Some valuable experimental work in propeller noise was reported by Kemp[20] and Paris[21]. They both found that the sound showed a marked peak just behind the rotor disc. Paris attempted to explain this by combining the single and double source hypotheses from Lynam and Webb's work. This arbitrary assumption was quite close to the truth, but the problem of modelling the boundary conditions for the propeller was still not solved correctly. This remained the case until 1936, when Gutin[22] produced his now classic paper, identifying the forces on the rotor as dipole acoustic sources. The result used was based on a formula in Lamb's Hydrodynamics[23], a book which must have been familiar to the earlier workers. By combining terms proportional to both thrust and drag (torque), Gutin predicted sound with a maximum behind the disc and a non-zero level in the disc plane, in agreement with experimental trends. Furthermore the theoretical value for the overall level of noise radiation was encouragingly close to experiment. Thus Gutin's model of noise radiation by the action of rotating steady forces on the propeller became widely accepted, and the discrete frequency noise due to the steady forces alone acting on a rotor is now often known as 'Gutin' noise.

The second major component of noise from a rotor is broad band in nature. The first experiments relevant to this source were performed by Stowell and Deming[24], who measured the noise from rotating cylindrical rods. Cylinders in a uniform flow radiate Aeolian tone noise due to the action of their Karman vortex street, and Stowell and Deming found that the noise radiation from the rotating cylinders was within a frequency range compatible with the expected variation of Strouhal frequency over the road. Fuller experiments were reported by Yudin[25]. He analysed the noise from several rotating shapes, and also presented a theoretical analysis. This followed Gutin in modelling the fluctuating forces on the rods as dipoles. Yudin found that the sound power was given by an equation of the form $W \sim S V_T^6$ where S is area and V_T the tip speed. Yudin found that a wide variety of profiles, including both aerofoils and circular cylinders, obeyed this general law, differing only in their value of the constant of proportionality. Essentially equivalent formulae are in use today for prediction, as will be discussed later. Further experiments along similar lines were later reported by Von Wittern[26]. These are of interest because they are the first to demonstrate the Doppler broadening of the broad band noise spectrum at the higher rotational speeds on a rotor. This is as expected after the first experiments of Mach[14].

Thus, at the end of the second war work, principally in Russia and England, had laid a foundation for the understanding of the noise from rotating sources. In addition a substantial amount of information was available from abortive German work aimed at acoustic location of aircraft[27]. But comparatively little experimental work had been performed on noise from full scale propellers. This deficiency was soon remedied in America, when a series of systematic acoustic experiments on far field sound radiation commenced at NACA Langley. This data provided the basis of our knowledge of rotor noise today. A series of reports were produced, for example References 27-32. Much of the presented data suffer

cannot be annoying. Furthermore, there is growing evidence that annoyance is related to audibility, that is, the level about the combined threshold curve in each band. Thus threshold and audibility calculations may have considerable relevance to the urban community noise situation.

There are, however, two problems here. Hostile community reaction to proposed VTOL ports cannot necessarily be countered by scientific appraisal. The recently proposed Harlem STOL port was defeated, predominantly on noise grounds, in spite of fairly convincing evidence that operations would be largely inaudible because of the high ambient noise levels already existing. The second problem is that urban areas are somewhat quieter than commonly thought. Figure 2.3 below, taken from Reference 11, and based on data given in the Wilson Report[12] shows typical noise levels at various non-industrial locations in London: 10% - 90% noise limits by day (open block) and by night (dark blocks) are given. Also shown is a 90 PNdB at 500ft limit often suggested for urban VTOL operations. This is several dB below the best current helicopter designs. It is clear that this level of noise would substantially degrade the noise climate except at a very small proportion of locations.

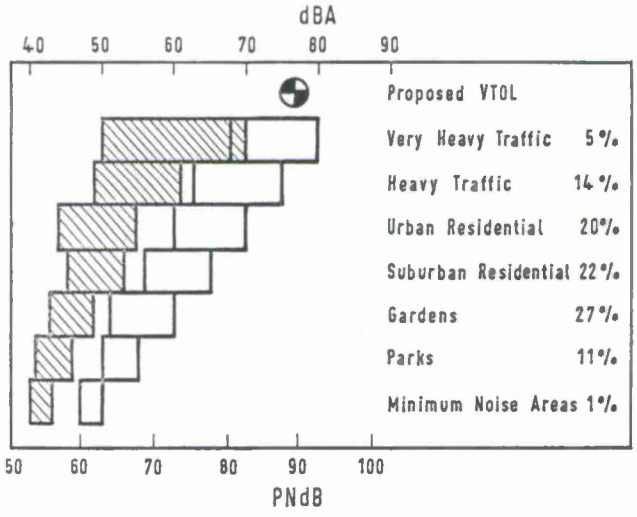


Figure 2.3: Typical urban noise levels, based on data from Reference 12.

3. MECHANISMS OF ROTOR NOISE GENERATION

Having now defined the fundamental features of subjective response to noise, the mechanical features of the noise generation and control can be investigated in more detail. It is convenient to approach these from a historical viewpoint, and the discussion below is largely taken from Reference 13.

3.1 The first studies

The earliest demonstration of sound from a rotating source appears to have been performed by Mach[14]. The apparatus is described by Rayleigh[15], with his customary lucidity, as follows: "It consists of a tube six feet (183cm) in length, capable of turning about an axis at its centre. At one end is placed a small whistle or reed which is blown by wind forced along the axis of the tube. An observer situated in the plane of rotation hears a note of fluctuating pitch, but if he places himself in the prolongation of the axis of rotation the sound becomes steady". The effect is due to the modulated Doppler shift in observed frequency at off-axis positions. Frequency modulation of a rotating source is a fundamental property, and has many significant implications for rotor noise as will be shown.

Sound radiation from rotating sources was solely a laboratory curiosity for many years, until the advent of propeller powered aircraft. It then became apparent that a rotating propeller was a source of significant noise radiation. This had immediate military relevance because of the possibility of acoustic detection and location of aircarft, and in Britain a special experimental station was set up at Butley, Suffolk, for noise studies[16]. Acoustic measuring apparatus available in 1917 was crude. The most advanced form of analysis was made via measurements of groove depth on a phonograph

from one obvious drawback. They were taken on a stationary propeller. However, the propellers were mounted in a clear area and acoustic data were only taken during calm air conditions. Wind can have a major effect. Hicks and Hubbard[28] record that "measurements taken on a day when gusts were approximately 20m.p.h. showed sound pressure variations of approximately 15 decibels". Other experimenters have not been so careful either in their choice of rig location, or of test conditions.

Data from the early tests were presented principally in terms of overall sound pressure level at the position of maximum noise. The Gutin theory gives fairly acceptable results for such points, at least for tip Mach numbers greater than about 0·6. But at lower tip Mach numbers the Gutin theory systematically underestimates even the overall noise level, especially for rotors with high blade numbers. This discrepancy was explained as "the contribution from the oscillating disturbances in the flow around the propeller blade"[28]. The concept that turbulence interacting with the blade can give rise to a significant broad band noise spectrum is undoubtedly correct. Unfortunately, the physical model taken for this noise was based on the earlier experiments on rotating rods, discussed above. Consequently, this original rather general concept of vortex noise was re-interpreted as a noise specifically due to trailing edge vortex shedding. This is rather misleading.

The original experiments involved rotating cylinders in their own wake, forcing a response at the wake frequency. It is noteworthy that Yudin's results show how the noise radiated by a flat plate actually reduces compared to the zero incidence case when the plate is at 10^0 incidence. In the latter case, the blades would not pass through their own wake. The importance of this was demonstrated as early as 1924 in a paper by G.I. Taylor[34] based on observations on a toasting fork. The fork was observed to radiate far more noise when moved rapidly through the air with the prong plane held parallel to the motion than with the prong plane at right angles to the motion. In the first case each prong is bathed in the wake of its leader, while in the latter case each prong can react independently. This clearly shows the relative significance of self-induced and external turbulence.

The first paper specifically oriented towards helicopter rotor noise was also the result of work of the NACA Langley group. Hubbard and Maglieri's paper[33] contains much significant information, and their principal results are shown here as Figure 3.1. This shows several important features of rotor noise. Firstly, the noise increases rapidly with tip speed. Secondly, it can increase markedly as the blade approaches stall, (solid symbols on Figure 3.1). Thirdly, the noise levels can also increase at low rotor incidences. Thus a minimum in rotor noise occurs in the intermediate operating range of the rotor. This is of obvious interest to the designer. Hubbard and Maglieri found the sound at high speeds for low rotor incidences to be particularly intense. Today this would be known as blade slap. It is obviously directly related to the wake interaction effects demonstrated by the experiments of Yudin and Taylor.

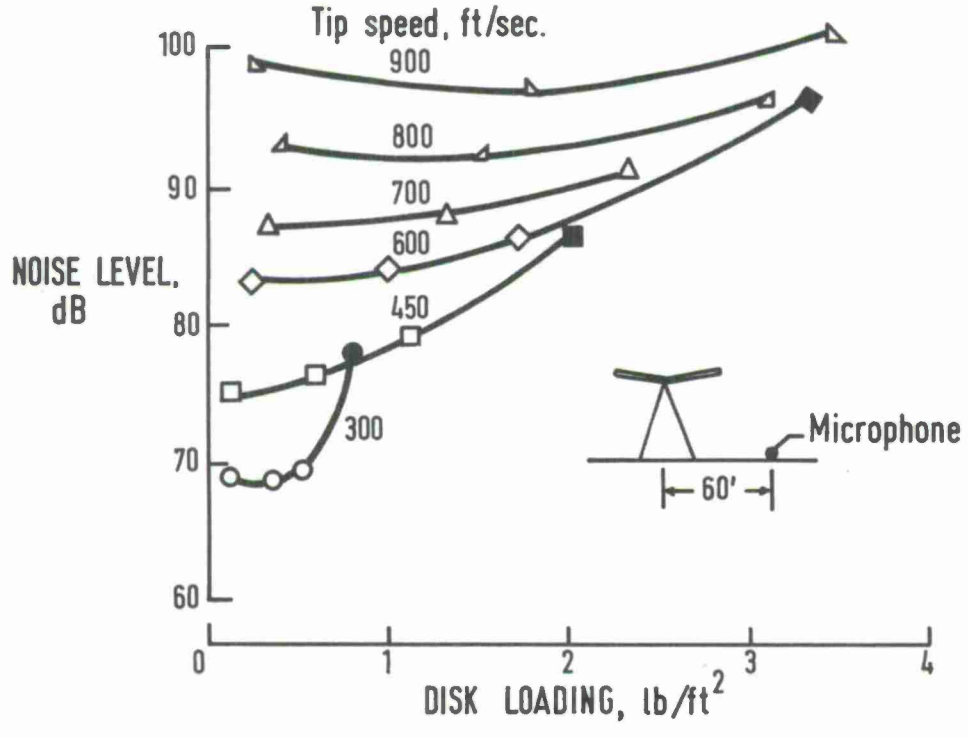


Figure 3.1: Rotor noise levels after Hubbard and Maglieri[33]

Comparison of the then existing theory with the helicopter noise data gives mixed results. For prediction of overall levels near the plane of the rotor disc the Gutin theory for the rotational noise, supported by a vortex noise formula at the lower rotational speeds is generally acceptable. Unfortunately, more detailed predictions are required for subjective ratings, including definition of the frequency spectrum. In the early experimental work on propellers spectral measurements were tedious, and only limited results from the wave analyser were usually presented. These showed that the Gutin formula systematically underestimated the noise level at the higher frequencies, especially for low tip speeds or many bladed propellers. One further discrepancy was also clear. The Gutin theory predicts zero discrete frequency noise on the rotor axis. However, significant discrete frequency levels are inevitably measured on the axis.

All these problems became especially acute for helicopter noise. The fundamental frequency for a helicopter rotor is normally below the range of hearing so that it is only the higher harmonics which are important. The rotors normally operate at moderate tip speeds, and near axis locations have far more practical significance. Vortex noise concepts cannot explain all these problems, and it became clear that, in some important respect the theory was incomplete. A significant improvement was necessary to allow understanding of helicopter noise predictions. A vital clue could have been found from the work of Kemp[20] in 1932. He found that sound just behind the propeller disc (where the Gutin noise is at its maximum) was comparatively steady in level. But he also found substantial fluctuations in level near the axis and for the higher harmonics; that is, for just those conditions where the Gutin theory is inadequate. Gutin considered the noise resulting from steady loads only. This suggests that the key to all the problems is the action of the fluctuating loads.

The possible significance of unsteady load components was recognised by many workers and was, indeed, the motivation behind the original vortex noise concepts. But their explicit inclusion in a rotating source theory has only occurred recently[35-38]. The first work applying these ideas to rotor noise was that of Schlegel, King and Mull[35] who numerically evaluated the retarded time integrals of the unsteady source functions. Computer time and accuracy were their main problems. Shortly thereafter Lowson and Ollerhead[36] and Wright[37] gave analytic solutions for the noise as the summation of an infinite series of Bessel functions. The analysis given here is taken directly from the Lowson-Ollerhead paper[36], further details may be found in the USA AVLABS Report[36].

3.2 Discrete Frequencies

3.2.1 Theory

The theory is based on the Lighthill[39] formulation of the wave equation, which can be written

$$\frac{\partial^2 \rho}{\partial t^2} - a_0^2 \frac{\partial^2 \rho}{\partial x_i^2} = \frac{\partial Q}{\partial t} - \frac{\partial F_i}{\partial x_i} + \frac{\partial^2 T_{ij}}{\partial x_i \partial x_j} \qquad \ldots\ldots\ldots\ldots (3.1)$$

where $T_{ij} = \rho v_i v_j + p_{ij} - a_0^2 \rho \delta_{ij}$ (the acoustic stress),

$\delta_{ij} = 1$, $i = j$; $= 0$, $i \neq j$ (the Kronecker δ),

F_i is the force per unit volume acting on the fluid,

Q is the mass source strength per unit volume, and

$x_i (i = 1,2,3)$ are Cartesian co-ordinates.

The usual tensor notation and summation convention are assumed. The right-hand side of equation (3.1) gives the various possible sources of sound present. In our case, we are interested in the effect of fluctuating forces F_i. Now the solution to the wave equation is well known. If the right-hand side of equation (3.1) is written as $g(\mathbf{y})$, the solution to equation (3.1) is

$$\rho = \frac{1}{4\pi a_0^2} \int \left[\frac{g}{r}\right] d\mathbf{y} \qquad \ldots\ldots\ldots\ldots (3.2)$$

where ρ = a fluctuating density, r = the distance from source to observer, and $\mathbf{y}$ = the co-ordinate of the source position; $\mathbf{y}$ is bold face implying it is a vector quantity. The square brackets around the g/r term are of extreme importance, since they imply evaluation of their contents at retarded time $\tau = t - r/a_0$. Also, the solution for the case of the force distribution F_i can be written as

$$\rho = \frac{-1}{4\pi a_0^2} \frac{\partial}{\partial x_i} \int \left[\frac{F_i}{r}\right] d\mathbf{y} \qquad \ldots\ldots\ldots\ldots (3.3)$$

Comparing equations (3.2) and (3.3) we see that the solution for the force case may be found from the solution to the simple source case (equation (3.2)) by differentiation after an integration of a simple source strength F_i over the appropriate retarded co-ordinates. This approach is particularly convenient in the present case.

Consider now the case of radiation from a point force rotating at angular velocity Ω, radius R, as defined by the co-ordinate system in Figure 3.2. We use Cartesian co-

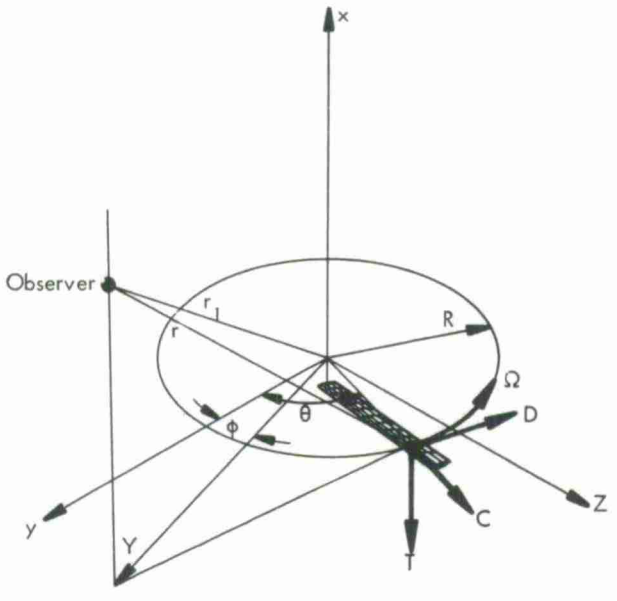


Figure 3.2: Co-ordinate system for helicopter acoustic calculations.

ordinates x,y,z, with x along the rotor axis. The observer is located a distance Y from the x axis, so that the reference angle between the observer (Y axis) and the y axis is ϕ (see also Figure 3.2). We wish first of all to define the Fourier coefficients of the sound radiation due to a rotating simple source, which requires multiplication by exp(in Ωt) and integration at the observer's time t. Since the source is moving we can transform to appropriate source co-ordinates η using, as first shown by Lighthill[39], $\eta = y + Mr$, $d\eta = (1 - M_r)dy$ where M_r is the component of convection Mach number in the direction of the observer. We also transform to source time r by $r = t - r/a_0$ and $dt = \partial r(1 - M_r)$. These two co-ordinate transformations have cancelling effects so that the final result for the complex magnitude of the n^{th} sound harmonic is

$$c_n = \frac{1}{4\pi^2} \int_0^{2\pi} \left[\frac{g}{r}\right] \exp\, in(\theta + \Omega r/a_0) d\theta \qquad \ldots\ldots\ldots\ldots (3.4)$$

where Ωr has been replaced by θ.

Then defining the source term g by a complex Fourier series

$$g(\theta) = \sum_{\lambda=-\infty}^{+\infty} A_\lambda \exp(-i\lambda\theta) \qquad \ldots\ldots\ldots\ldots (3.5)$$

and using the standard far-field approximation for propeller noise theory[22,40] $r = r_1 - yR\cos(\theta - \phi)/r_1$, where r_1 is distance from the hub, equations (3.4) and (3.5) give, after rearrangement,

$$c_n = \frac{1}{4\pi^2} \int_0^{2\pi} \sum_{\lambda=-\infty}^{+\infty} \frac{A_\lambda}{r_1} \exp\, i\left\{(n - \lambda)(\theta - \phi) - \frac{n\Omega YR}{a_0 r_1} \cos(\theta - \phi)\right\} d(\theta - \phi) \qquad \ldots\ldots\ldots\ldots (3.6)$$

$$\times \exp\, i\left\{\frac{n\Omega r_1}{a_0} + (n - \lambda)\phi\right\}$$

Since the integral applies over any interval 2π it can be expressed in Bessel function form, using formula 42 in McLachlan[89], so that

$$c_n = \frac{1}{2\pi} \sum_{\lambda=-\infty}^{+\infty} i^{-(n-\lambda)} \frac{A_\lambda}{r_1} J_{n-\lambda}\left(\frac{n\Omega Y R}{a_0 r_1}\right) \exp i\left\{\frac{n\Omega r_1}{a_o} + (n-\lambda)\phi\right\} \quad \ldots\ldots\ldots\ldots (3.7)$$

Equation (3.7) gives, in complex form, the sound harmonics from a point simple source describing a circular path. The equation could be applied directly to the calculation of rotating mass sources providing the time differential is observed (see equation (3.1)) and proper account is taken of momentum output (see References 40 and 41). However, we are interested in deriving the results for the force cases. Using equation (3.3) these are

$$\left.\begin{aligned}
&\text{Axial:} && \frac{-\partial c_n}{\partial x'} = -\sum_{\lambda=-\infty}^{+\infty} i^{-(n-\lambda)} \frac{in\Omega x}{2\pi a_0 r_1^2} A_\lambda J_{n-\lambda}\left(\frac{nMy}{r_1}\right) \\
&\text{Circumferential:} && \frac{-1}{R}\frac{\partial c_n}{\partial \phi} = -\sum_{\lambda=-\infty}^{+\infty} i^{-(n-\lambda)} \frac{i(n-\lambda)}{2\pi r_1} \frac{A_\lambda}{R} J_{n-\lambda}\left(\frac{nMy}{r_1}\right) \\
&\text{Radial:} && \frac{+\partial c_n}{\partial R} = +\sum_{\lambda=-\infty}^{+\infty} i^{-(n-\lambda)} \frac{n\Omega Y}{2\pi a_0 r_1^2} A_\lambda J'_{n-\lambda}\left(\frac{nMy}{r_1}\right)
\end{aligned}\right\} \quad \ldots\ldots\ldots\ldots (3.8)$$

Only the far-field terms have been retained in Equation (3.8).

The prime on the Bessel function in the radial expression denotes differentiation, $M = \Omega R/a_0$ is the rotational Mach number of the point force. Negative signs must be applied in the first two equations because differentials are based on observer co-ordinates whereas the differential on the last equation is on a source co-ordinate.

Notation in Equations (3.8) must now be changed to specify the forces acting. Defining the three components by simple Fourier series

$$\left.\begin{aligned}
&\text{Thrust:} && T(\theta) = a_{0T} + \sum_{\lambda=1}^{\infty} a_{\lambda T} \cos\lambda\theta + b_{\lambda T} \sin\lambda\theta, \\
&\text{Drag:} && D(\theta) = a_{0D} + \sum_{\lambda=1}^{\infty} a_{\lambda D} \cos\lambda\theta + b_{\lambda D} \sin\lambda\theta, \\
&\text{Outward components:} && C(\theta) = a_{0C} + \sum_{=1}^{\infty} a_{\lambda C} \cos\lambda\theta + b_{\lambda C} \sin\lambda\theta.
\end{aligned}\right\} \quad \ldots\ldots\ldots\ldots (3.9)$$

The thrust, drag, and outward components of force are assumed to act in the axial, circumferential, and radial directions, respectively. In conversion to thrust, a minus sign must be incorporated because the force on the air is in the negative x direction.

Equations (3.8) are converted to the required form using Equation (3.9). Note that terms for both plus and minus λ in the summations in Equations (3.8) contribute to the result for any given loading harmonic. Thus, the final result for the complex magnitude of the sound harmonic is

$$\begin{aligned}
c_n &= a_n + ib_n \\
&= \sum_{\lambda=0}^{+\infty} \frac{i^{-(n-\lambda)}}{4\pi}\left\{\frac{n\Omega x}{a_0 r_1^2}\left\{+ia_{\lambda T}\left(J_{n-\lambda} + (-1)^\lambda J_{n+\lambda}\right) - b_{\lambda T}\left(J_{n-\lambda} - (-1)^\lambda J_{n+\lambda}\right)\right\}\right. \\
&\quad - \left\{\frac{ia_{\lambda D}}{Rr_1}\left((n-\lambda)J_{n-\lambda} + (-1)^\lambda (n+\lambda) J_{n+\lambda}\right) - \frac{b_{\lambda D}}{Rr_1}\left((n-\lambda)J_{n-\lambda} - (-1)^\lambda (n+\lambda) J_{n+\lambda}\right)\right\} \\
&\quad \left. + \frac{n\Omega Y}{a_0 r_1^2}\left\{a_{\lambda C}\left(J'_{n-\lambda} + (-1)^\lambda J'_{n+\lambda}\right) + ib_{\lambda C}\left(J'_{n-\lambda} - (-1)^\lambda J'_{n+\lambda}\right)\right\}\right\} \quad \ldots\ldots\ldots\ldots (3.10)
\end{aligned}$$

The argument of all the Bessel functions is nMy/r_1.

Equation (3.10) gives the desired result for the sound radiation by a rotating three component fluctuating point force. Putting $\lambda = 0$ in the above equation gives the result for the steady loading only as

$$c_n = \frac{(i)^{-n+1} n\Omega}{2\pi a_0 r_1}\left\{\frac{xT_0}{r_1} - \frac{D_0}{M}\right\} J_n\left(\frac{nMy}{r_1}\right) - \frac{i^{-n} n\Omega}{2\pi a_0 r_1} \cdot \frac{YC_0}{2r_1}\left\{J_{n-1}\left(\frac{nMy}{r_1}\right)\right\} \quad \ldots\ldots\ldots\ldots (3.11)$$

The first term in the above equation is identical with the classical propeller noise solution due to Gutin[22] while the second, radial component term, is the same as that derived in reference[41]. One important effect not explicitly given in Equation (3.11) is the effect of blade number. If B blades are present, harmonics which are not integral multiples of B will cancel out. Those harmonics which are multiples of B will add. Thus the effect of blade number may be included in Equations (3.10) and (3.11) by replacing n by mB. In this case the coefficients of the force harmonics must be taken as the values for the complete rotor, which are B times the values for the individual blades.

The effect of forward velocity is also of considerable interest. In Reference 40 it was pointed out how the equations for constant velocity convection of the hub could be obtained from those for the stationary case by replacing the term r_1 in the stationary case by $r_1(1 - M_{0r})$ where M_{0r} is the component of the hub convection Mach number in the direction of the observer. In utilising this transformation it is important to note that it applies to the retarded position of the helicopter. In other words the dimension r_1 used must be taken as the distance from the observer to the position of the helicopter when it emitted the sound. Relation of the results to the instantaneous position of the helicopter requires another transformation, discussed in Reference 1 and 2. Also, in Reference 37 it was shown that the above $(1 - M_{0r})$ correction term gave the Garrick and Watkins[42] moving propeller result directly from that of Gutin[22] for the stationary case.

On the rotor axis there is a one to one relation between input modes and output harmonics. Equation (3.10) takes a particularly simple form for this case reducing to

$$c_n = \frac{in\Omega}{2\pi a_0 r_1} a_{nT} \qquad \ldots\ldots\ldots\ldots (3.12)$$

Equation (3.12) has important implications in experiment, for measurements of the on-axis sound radiation will be directly related to fluctuating forces on the rotor disc. Thus the levels of these forces can be inferred from the on-axis acoustics. It seems that on-axis measurements can be used to some extent as acoustic diagnosis of the rotor unsteady aerodynamics. Once the fluctuating force field is known the whole rotor noise field can be calculated by Equation (3.10) as shown for instance by Barry and Moore[61]. Thus, the on-axis point becomes theprime location for acoustic measuring instruments for any test.

The effect of the analysis can be summarised as follows. The non-uniform inflow into the disc is Fourier analysed into a series of "modes". Each mode is a steady sinusoidal distortion pattern around the disc, which causes a sinusoidal force fluctuation at the rotor. Thus each mode causes a fluctuating force of different frequency on the rotor disc. On the axis of the rotor each frequency is heard directly, but off the axis the modulated Doppler frequency shift reported by Mach causes a large number of acoustic frequencies to result from each single mode input. Thus it is found that away from this axis each mode is an effective sound generator over a range of harmonic frequencies. Inverting this argument it is seen that each sound harmonic results from contributions from a limited number of modes. Figure 3.3, taken from Reference 36, shows the effect for a particular sound harmonic mB = 16 where m is the harmonic order and B is the blade number. It will be observed that the contribution to this harmonic drops away very rapidly outside a central range over which the efficiency is essentially constant. The range of distortion modes which are important for each sound harmonic is shown in Figure 3.4, also from Reference 36.

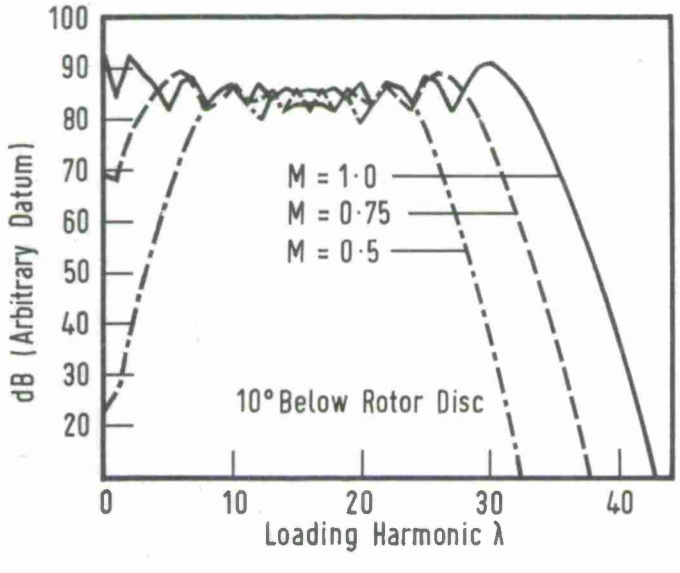


Figure 3.3: Contribution of higher harmonics to rotor noise[36]

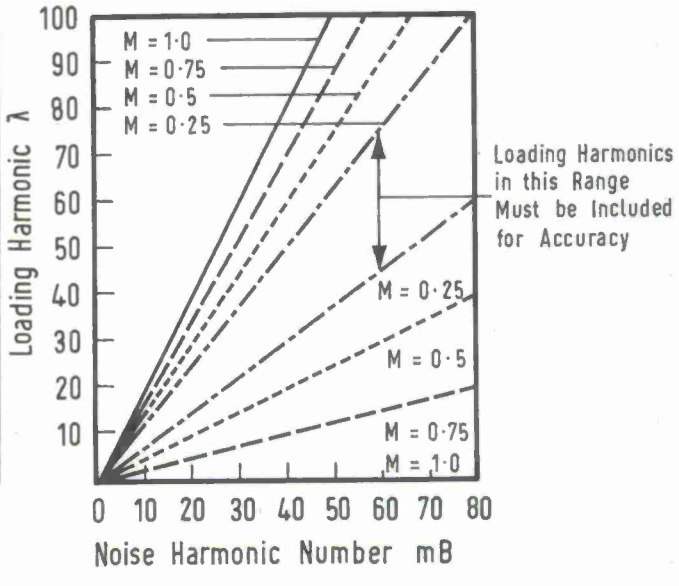


Figure 3.4: Range of effective contribution of loading harmonics to sound radiation[36]

In fact, analysis of the nature of the Bessel function results shows that the range of interest is given by roughly

$$mB(1 - My/r) < \lambda < mB(1 + My/r) \qquad \ldots\ldots\ldots\ldots (3.13)$$

so that there is an effect of position on the harmonic contribution, fewer harmonics contributing closer to the axis. This has already been foreshadowed by Equation (3.12) which demonstrated that only a single harmonic contributed to the noise exactly on axis.

Now the steady loads correspond to the zeroth order mode. Going back to Figure 3.3 this can be seen to have very minimal contribution to the higher harmonic case given here. Indeed the steady load contribution at M = 0·5 is seen to be about 60dB down on the contribution in the central range. Thus the direct contribution of Gutin noise, or of any steady rotating acoustic source, to subjective levels of a low speed rotor is very small. For the case shown a high order mode with intensity of only one millionth of the steady (that is, an amplitude of one thousandth of the steady) will have an equal acoustic effect. Thus the enormous acoustic efficiency of the higher order modes more than compensates for their small source strength. It can be seen that very minor levels of fluctuation in the aerodynamic input to the rotor can give rise to very large levels of high harmonic acoustic output from the rotor. The increase of noise level by 15dB due to a 20m.p.h. wind reported by Hicks and Hubbard[28] is immediately explained by these arguments.

The theory successfully explains the source of rotor noise observed at both high frequencies and low tip speeds. Furthermore, the unsteady sources can be seen to radiate on the rotor axis. Thus, virtually all the disagreements between Gutin's steady force theory and experiment are resolved simultaneously. In addition, theory demonstrates unequivocally that the rotor noise subjective levels can be controlled directly by minimisation of all unsteady inflow into the rotor.

Unfortunately, the theory does not allow immediate prediction of the rotor noise. The input loading data for the Gutin theory was simply thrust and torque, which will be known for any rotor. But predictions using the unsteady theory require a knowledge of the miniscule levels of loadings in all the higher modes. On-axis acoustic measurements are a direct source of this information. However, this knowledge is unlikely to be available at the design stage except in special cases. Alternative methods for predicting these higher order modal levels must therefore be sought, and for this reason it is necessary to study the unsteady aerodynamics of the rotor in more detail.

3.2.2 Aerodynamics

These fluctuating loads which act on the rotor blade are dominated by the effects of the vortex wake interactions. Unfortunately, it is extremely difficult to make any realistic estimate of the wake dynamics,aand consequently almost impossible to predict the resulting fluctuating forces on the blades. In Reference 1 a detailed study of the basic performance equations was made, and it was shown that even predictions of the second harmonic airloads were seriously in error when compared to experiment. Several workers have attempted to construct detailed computer solutions of the blade/wake system. Although such approaches have given some of the same trends as experiment, it is certainly true to say that no sufficiently detailed prediction of the airloads is yet possible via the computer. Furthermore, such approaches are found to require excessive computer time. A discussion of some of theproblems associated with this approach has been given by White[43] and more recently by Cheney and Landgrebe[44].

Thus a simpler method must be sought. Experimental data on the first ten harmonics of the fluctuating airloads are available in reports by Schieman[45] and Burpo and Lynn[46]. Some of these data are shown here in Figure 3.5. Figure 3.5 shows harmonic sectional lift as a function of harmonic number, based on Scheiman's data. The data are shown on a log-log plot, and the mean (steady) sectional lift is also shown plotted at $\lambda = 1$. The remarkable thing about the data is that advance ratio μ (the forward speed divided by the tip speed) makes so little difference. The general trend in each plot is the same. Simple arguments based on basic rotor aerodynamic theory suggest that harmonic levels should increase with advance ratio. It is clear that this does not occur to any marked degree although there is some evidence of increased higher harmonic loadings for small advance ratios ($\mu \sim 0{\cdot}05$). Thus, even in hover, the helicopter rotor is very far from acting like a propeller. One possible reason for this is the predicted instability of the helical vortex wake for axial advance ratios below 0·3 [47]. From the present viewpoint the data offer a useful simplification, in that effects of forward velocity may apparently be ignored in estimating the harmonic airloads.

Available data include harmonic amplitudes up to the tenth. In order to extrapolate these results to higher frequencies, "power laws" based on some harmonic are very helpful. That is, a relationship is assumed for the harmonic amplitude L_λ of the λ^{th} harmonic of the form $L_\lambda = L_\Lambda(\lambda - \Lambda)^{-k}$ where L_Λ is the amplitude of the Λ^{th} harmonic ($\Lambda \leq \lambda$). Two possible laws are shown in Figure 3.5. The dashed line gives a power law based on the second harmonic loading ($\Lambda = 2$), and the solid line one based on the steady loading, plotted at the $\lambda = 1$ point. It will be observed that the second harmonic power law gives some variation in slope, while the law based on the steady loading gives a fairly constant result, close to a "6 dB per octave" fall off. Thus an inverse square power law based on the steady loading has been chosen in the present paper to give the predicted noise levels. Figure 3.5 shows that such a law is in reasonable agreement with the data for clean flow cases, except for the $\lambda = 1$ case which is consistently overestimated. Since the $\lambda = 1$ loading does not contribute significantly to the more important higher

harmonic levels, no modification to the simple basic power law was thought to be justified at this time.

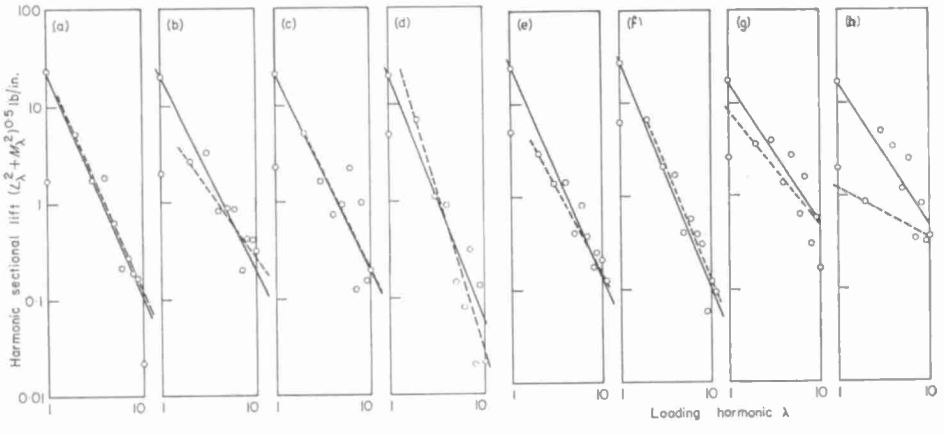


Figure 3.5: Rotor loading harmonic laws at various advance ratios. Data from Schieman[45] and Burpo and Lynn[46].

(a) hover V = 0, μ = 0
(b) V = 42kt, μ = 0·112
(c) V = 66kt, μ = 0·20
(d) V = 112kt, μ = 0·3
(e) V = 92kt, μ = 0·216
(f) V = 111kt, μ = 0·260
(g) level flight in ground effect V = 27kt
(h) partial power descent V_D = 80ft/min.

Figure 3.5(a-d) gives results for a four bladed CH-34 helicopter, from Scheiman[45]. Figure 3.5(e,f) gives results for a two-bladed UH-1A helicopter from Burpo and Lynn[46]. It will be noted that the basic power law trends noted in Scheiman's data are repeated here. This enables a little more confidence to be placed in the power law as a general prediction method for all helicopters. Figure 3.5(g,h) show some rough running cases, again from Scheiman. It will be observed that the levels of the higher loading harmonics have definitely increased here compared with the steady cases described above. Thus, the power laws based on the second harmonic substantially increase in order. Possibly an inverse first power based on the steady would be an adequate description, although it is clear that no accurate general prediction method is feasible at the present time. Even for the steady cases in Figure 3.5 it will be observed how, for instance, the third harmonic in Figure 3.5(b) and the sixth in Figure 3.5(c) are much higher than expected. These small differences in loading harmonics must be reflected in small differences in the sound field in a real case.

In fact, it is very probable that these instantaneous loadings vary considerably along the blade span. Peak loads are basically due to the close proximity of a wake vortex. As the blade passes over a vortex the intersection point will also move along the span. This is discussed in more detail in Reference 36. One possibility of particular interest is that the intersection point velocity, and thus the velocity of the major pressure disturbance on the blade, can move across the span at supersonic speeds, and could thus be a particularly efficient radiator of sound. Such an effect is not included in the present work but has been discussed recently by Widnall[4] as a mechanism for blade slap. In Reference 36 the harmonic levels along the span were studied, and it was found that levels of the higher loading harmonics were greater at the tip than at the root. However, it seems that the inverse square law for loading harmonics still gives the best single approximation for this overall blade.

A further important effect is that of phase. Consider first the effect of thephase between the loading harmonics. Referring back to Equation (3.10) note that the phase is dependent on the parameter

$$i^{-(n-\lambda)}.$$

Thus the same phase input (i.e. ratio of a_λ to b_λ) of the load coefficients will result in acoustic outputs which are 180° shifted for every two loading harmonics. Now at the high values of λ there will be little difference in magnitude between successive odd or even harmonics, and their acoustic effect would therefore cancel if they had the same phase. Unfortunately available data do not give any useful information in the loading phase. Clearly the effect described above is unrealistic, and it is more appropriate to assume a random phase angle between harmonics. If this is done then the sums of the squares for each loading harmonic input may be added directly to give the observed intensity.

An equivalent effect occurs with respect to the loading along the span, again discussed in more detail in Reference 36. In view of the vortex intersection effects discussed above, it would not be correct to assume that the higher harmonic loads were in phase across the whole blade span. Thus, it becomes necessary to incorporate a correlation length in the loading specification to enable the acoustic predictions to be made. It seems probable that correlation length will be inversely proportional to loading harmonic order (λ). It will be assumed that the non-dimensional spanwise correlation

length is numerically equal to λ^{-1}. Recalling that the acoustic intensity is proportional to the pressure squared, and thus to the force input squared, it will be seen that this correlation assumption amounts to an additional -0·5 power in the harmonic loading law. Thus if the local loadings are falling in magnitude as λ^{-2}, then the effective loading law including random effects is $\lambda^{-2.5}$.

These results can now be used in the acoustic equations to give results for helicopter noise output.

3.2.3 Prediction and Comparison with Experiment

Given the theoretical expression of Equation (3.10) and empirical information on the magnitudes of the higher harmonics of loading then the rotor sound output can be predicted. In the work discussed here attention has been confined to power law extrapolations to the higher harmonics as suggested by Figure 3.5 and also to point rotating force representations of the blade. Clearly improved results should be attainable by using better information on higher harmonic loading levels and by an integration over the whole blade, thus taking account of the variation of loading over it. These improvements can lead to considerable complexity, and rarely seem to give much enhancement in the accuracy of the results. They are not recommended except for special purposes.

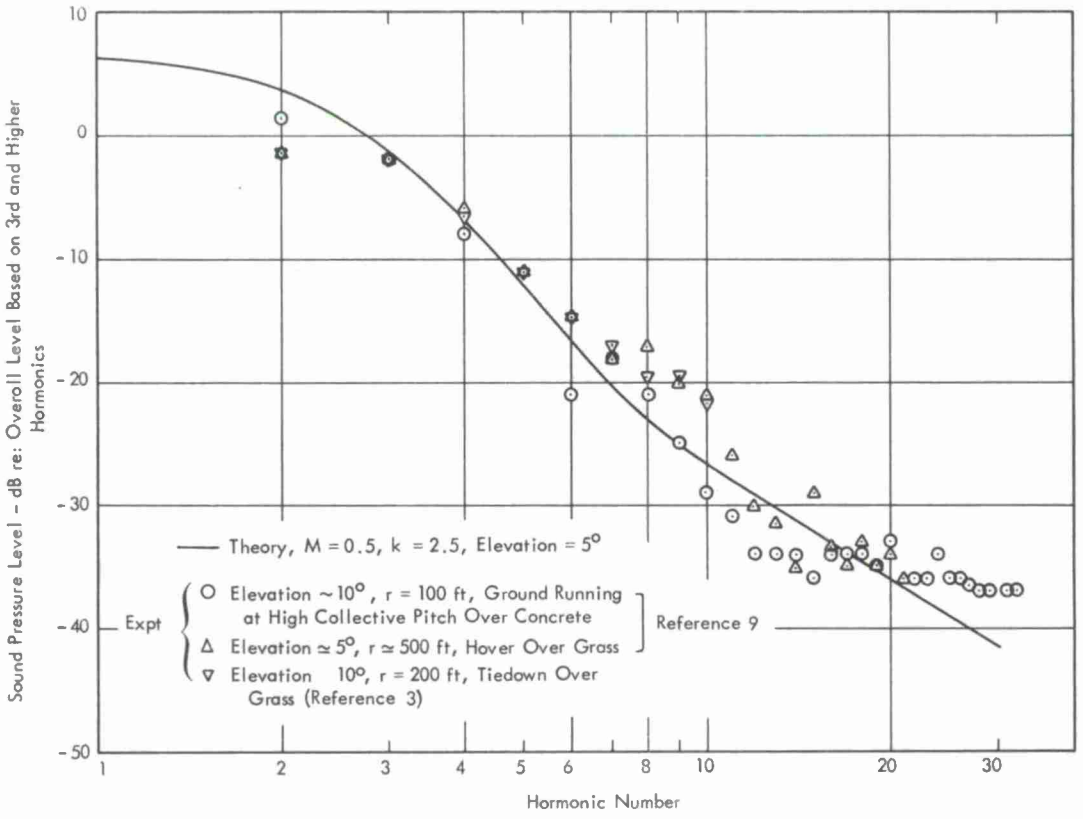


Figure 3.6: Noise Spectrum - Comparison of Theory and Experiment for two-blade Rotor (UH-1A and UH-1B)[36]

The power law prediction method has been applied to several cases. Figure 3.6 gives a comparison of theoretical prediction with noise spectra from UH-1 helicopters[36]. It will be observed that acceptable agreement is found beyond the thirtieth harmonic. This agreement is for spectral shape only, since the data has been non-dimensionalised about the level of the third harmonic. But comparisons for actual level have been made and are drawn in Figure 3.7.

A further explicit assumption in this prediction was that of random phase for the input modes. This assumption appears to be in fair agreement with experiment, and allows the theory to adopt a simpler, phase independent form giving an axisymmetric sound field around the rotor. The noise output of systematic azimuthal events such as vortex intersection would not be satisfactorily predicted by this form of the theory, but for most cases the random phase assumption gives a significant improvement in computational time and ease of interpretation. In general terms, basic understanding of the discrete frequency radiation from a rotor is now fairly complete.

Having established that the theory is in reasonable agreement with experiment it may be used with some confidence for prediction purposes. For example, the directionality of the sound harmonics beneath the rotor may be calculated. This is shown in Figure 3.8.

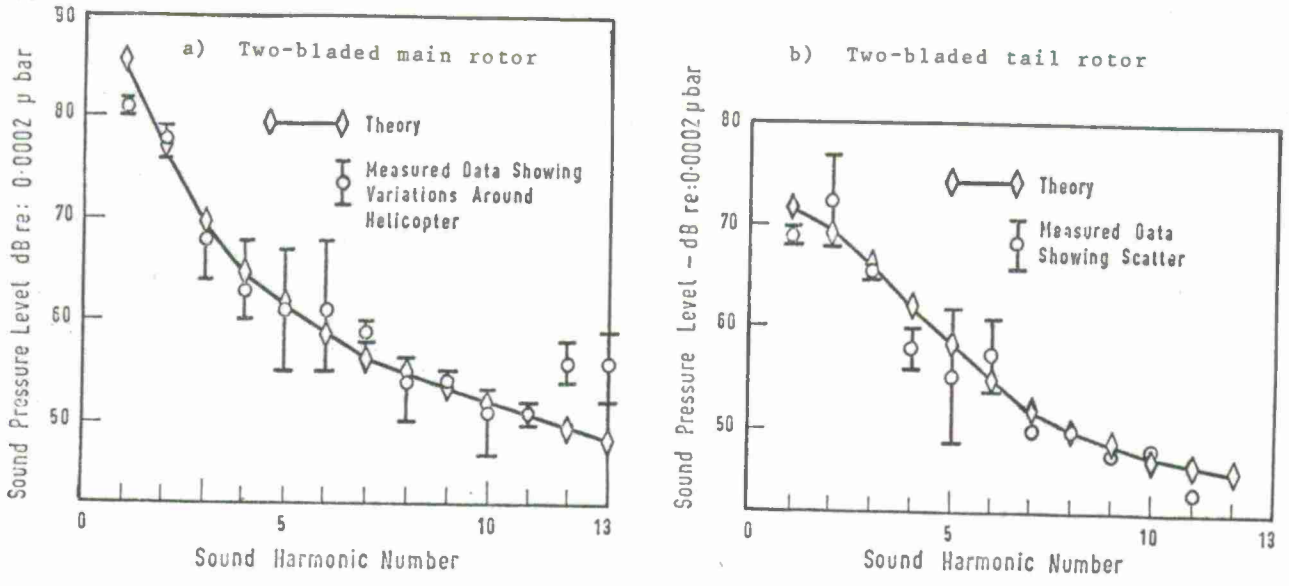


Figure 3.7: Theory and experiment for noise from a light helicopter[48].

Little data has been available of a directionality pattern but recent balloon measurements by Leverton[49] have given patterns in fair agreement with these theoretical predictions.

The effect of forward motion may also be established. Figures 3.5 suggest that forward motion has comparatively little effect on the loading harmonic laws, so that the same -2 law may again be chosen. In Reference 36 it was shown that the effect of forward motion can be approximated by adding the component of velocity in the direction of the observer to the rotational speed. The effect of this on directionality and level is also shown in Figure 3.8. It can be seen that sound is thrown forward by helicopter motion, with as much as 20dB more noise forward compared to aft at M = 0·25 for the second and third harmonics.

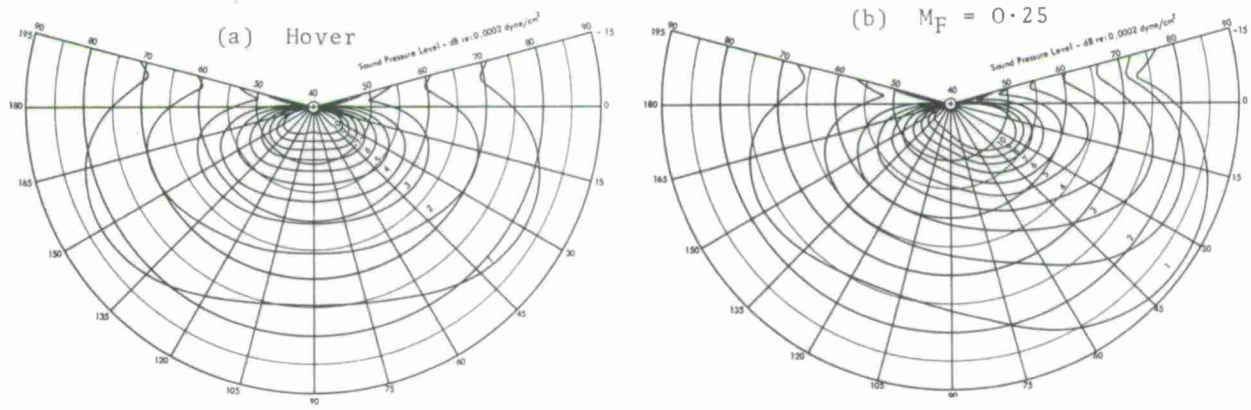


Figure 3.8: Overall Sound Patterns beneath Rotor for Various Harmonics[36]
Calculated for 10,000-lb thrust rotor, 40-ft diameter, 4 blades
Rotational Mach number M = 0·5, Range - 1000 ft

Practical prediction of rotational noise is a complicated process. Firstly the equations (3.10) are themselves complex. Secondly the actual levels of harmonic loads on the blades are rarely known. A hand calculation method based on power laws extrapolations was presented in References 36 and 48 and has been widely used. But although good agreement has been demonstrated for this method in Figures 3.5 and 3.6, equivalent accuracy is certainly not always obtained. It appears that different families of rotor designs obey different loading laws. The most credible method for prediction is to find the loading power laws obeyed by a particular helicopter - perhaps by on-axis acoustic measurements - and then to apply these empirically derived laws for predictions of the same rotor family. Note, however, that the loading laws are liable to change substantially if quite different rotor types are considered. A rough guide to levels can be found by the hand calculation method mentioned above, but there is evidence that this often gives

results which are too low for the higher harmonics.

3.3 Broad Band Noise

3.3.1 Theory

The general concept underlying the discrete frequency radiation by rotor apply equally well to the broad band case. Random source fluctuations on the blade will generate broad band noise, with a Doppler broadened spectrum due to the rotation. Theoretical calculations can be made following this idea (see References 36,50,51). However, here we shall follow a more elementary approach and consider the radiation resulting from pressure fluctuations on the rotor surface, essentially following Sharland[52]. If the speed is subsonic the acoustic wavelength will be larger than the turbulence scale so that sound radiated by aerofoils with chords of, perhaps, up to several times the turbulent scale should be calculable simply from the fluctuating pressures.

The expression (3.3) for the fluctuating pressure from a distribution of fluctuating sources can be reduced to (e.g. References 38,39)

$$p = \frac{x_i - y_i}{4\pi a_0 r^2} \int \left[\frac{\partial p_i}{\partial t}\right] dS \qquad \ldots\ldots\ldots\ldots (3.14)$$

The power is the integral of $p^2/\rho_0 a_0$ over the field which is

$$W = \frac{1}{12\pi\rho_0 a_0^3} \int_S \int_{S'} \left[\frac{\partial p(x)}{\partial t}\right] \left[\frac{\partial p(x')}{\partial t}\right] dS\, dS' \qquad \ldots\ldots\ldots\ldots (3.15)$$

Thus we should evaluate the retarded time correlation of the rate of change of pressure on the plate. Now to use this expression we have already had to assume the plate dimension was of the order of the acoustic wavelength. If we now assume it is small compared to the wavelength then the "compact" source assumption can be utilised and the retarded time effects dropped. Next, one of the integrations over the surface is simply a correlation integral and we can write

$$\int_{S'} \overline{\frac{\partial p(x)}{\partial t} \frac{p(x')}{\partial t}}\, dS = \overline{\left(\frac{\partial p}{\partial t}\right)^2} S_c \qquad \ldots\ldots\ldots\ldots (3.16)$$

where S_c is the correlation area of the pressures. This gives

$$W = \frac{1}{12\pi\rho_0 a_0^3} \int_S \overline{\left(\frac{\partial p}{\partial t}\right)^2} S_c\, dS \qquad \ldots\ldots\ldots\ldots (3.17)$$

If the blade is in a homogeneous patch of turbulence then the integral simply becomes a multiple by the blade area S. The effects of variation of conditions over the blade span will be discussed later.

To evaluate Equation (3.17) for the case of impinging turbulence we may take advantage of the result obtained by Sears[53] for the fluctuating lift L on a two-dimensional aerofoil. This is[38]

$$L = \frac{\pi\rho_0 b U u}{(\pi\omega b/U)^{\frac{1}{2}}} \qquad \ldots\ldots\ldots\ldots (3.18)$$

where b is blade chord
U is the mean velocity over the blade
u is the fluctuating velocity magnitude
and ω is the radian frequency of the variation

To extend this to three-dimensional conditions we note that the mean lift in terms of pressure fluctuations is

$$L = p_{rms} \sqrt{l_b b} \,/ \text{unit span}$$

where l_b is the correlation length in the chordwise direction,
and p_{rms} is the root mean square pressure fluctuation.

If we also put

$$\overline{\left(\frac{\partial p}{\partial t}\right)^2} = \omega^2 p_{rms}^2$$

where ω is a typical frequency, then Equation (3.17) becomes, using the results above

$$W = \frac{1}{12\pi\rho_0 a_0^3} S_c(2S) \frac{\omega^2}{b\, l_b} \frac{\pi\, \rho_0^2\, b\, U^3 u^2}{\omega}$$

The 2S arises because both sides of the plate radiate. If we finally put $\omega = U/l$ where l is a typical length and let $S_c = l^2$, $l_b = l$, the final result for the sound power radiated is

$$W = \frac{1}{6} \frac{\rho_0 U^4 u^2 S}{a_0^3} \qquad \ldots\ldots\ldots\ldots (3.19)$$

This result differs from that of Sharland[52] for the same case, by a factor of $3\pi/10$. Somewhat less restrictive assumptions have been made in the present analysis.

The same formula can be applied to radiation from the boundary layer pressure fluctuations acting on the plate.

Equation (3.19) gives

$$W = \frac{1}{12\pi\rho_0 a_0^3} \int \overline{p^2}\, \omega^2\, S_c\, dS \qquad \ldots\ldots\ldots\ldots (3.20)$$

Experiments agree that the level of the pressure fluctuations in an equilibrium boundary layer is given by $p^2 = 36 \times 10^{-6} q^2$ where q is the dynamic head $\frac{1}{2}\rho_0 U^2$. However there is rather less agreement over the correlation area magnitude[54]. Most recent studies of boundary layer pressure fluctuations have broadly agreed with Bull's data[60]

$$S_c = 15\delta^{*2} \qquad \delta^* = 0{\cdot}3\, U/\omega$$

Thus the correlation area can be expressed as

$$\omega^2 S_c = KU^2$$

where the constant K is in the range $0{\cdot}1 < K < 1{\cdot}0$, and equals 0·135 for the figures above.

Substituting into Equation (3.20) gives the approximate result

$$W \approx \frac{10^{-7}\rho_0 U^6 S}{a_0^3} \qquad \ldots\ldots\ldots\ldots (3.21)$$

in agreement with Sharland[52].

Comparing Equation (3.21) with Equation (3.19) shows that an input turbulence level of as little as 0·001 is sufficient to outweigh the direct radiation of the boundary layer pressure fluctuations. Two assumptions were made in the derivation of Equation (3.21), that the blade was small, and the sources compact. The compact source assumption is probably reasonable because the eddy scale is small, but the small blade assumption is not necessarily correct, and it could be more appropriate in this case to calculate the sound as a turbulence reflection. If we crudely assume that the turbulence is similar to that in a jet we can use an empirical model for the radiated jet noise[56].

$$\frac{W}{W_j} = 3 \times 10^{-5} M^5$$

relating the mechanical and acoustic powers of the jet. The mechanical power absorbed by the plate is roughly $0{\cdot}05U^3S$ and the acoustic output must be quadrupled to allow for reflection. Thus it appears that

$$W = \frac{6 \times 10^{-6} U^8 S}{a_0^5} \qquad \ldots\ldots\ldots\ldots (3.22)$$

could be an order of magnitude estimate for the turbulence noise output. Equation (3.22) shows that the sound due to direct turbulent radiation will be higher than that due to pressure fluctuations for speeds greater than $M = 0{\cdot}1$. This offers some confirmation of the small power output of the pressure terms on a large plate. The estimate (3.22) does not include the effect of plate edges on the sound. The trailing edge turbulence radiation should be enhanced by this effect. On the other hand, the turbulence in the boundary layer has an increased decay time scale compared with a jet, and this would result in a noise radiation somewhat less than the above estimate.

The broad band noise generation models discussed above all apply to the uniform flow

such as found over an aerofoil section. On rotating blading the velocity varies substantially over the blade radius, and the theoretical formulae must be modified to take account of this, and to derive an effective velocity for the equivalent point source. This is the velocity at which the whole blade would move uniformly to produce the same noise output. One point on the blade must be moving at this velocity and this is taken as the effective radius.

The velocity over a rotating blade increases directly as blade radius

$$U = \frac{RU_T}{R_T}$$

where U is the velocity at blade radius R, and U_T is the velocity at blade tip R_T.

Thus if the sound output from the blading varies as a simple power law U^n, the overall sound from the blade will be proportional to

$$\int_0^{R_T} U^n \, dR = \frac{R_T \, U_T^{\,n}}{n+1} \qquad \ldots\ldots\ldots\ldots (3.23)$$

so that the effective velocity of the blade is $U_T^{\,n/(n+1)}$. Thus, for instance, if the blade is taken to radiate locally according to the 8th power law its effective velocity is $\sqrt[8]{1/9}$ or 0·76. For a 6th power law the factor is $\sqrt[6]{1/7}$ = 0·723. Note, however, that the input of external turbulence of magnitude u gives rise to a fluctuating force which varies at Uu, and if the external turbulence may be assumed to be unaffected by blade velocity, the basic U^6 law of the blade reduces to a U^4u^2, with effective velocity factor $\sqrt[4]{1/5}$ = 0·67. In practice, of course, no simple velocity exponent expression would be exact. But in view of the rather inexact nature of the whole acoustic prediction process, a rough approximation to the radial distribution of source will probably be quite acceptable.

The calculations above indicate that the radiated field of a boundary layer in a region of uniform pressure is small. In fact a typical rotor aerofoil will have substantial pressure gradient over it, particularly when it is at angle of attack. Under such conditions it is clearly irrelevant to calculate the radiation from a uniform flow model.

Data on pressure fluctuations in non-uniform boundary layers are given by Schloemer[57]. He found that a quite small adverse pressure gradient caused increases in p_{rms}/q of around 50%. The shape factor H was about 1·58 compared with 1·4 for a uniform boundary layer, while separation implies shape factors certainly over 2 and, according to some investigators, over 3. In fully separated flow, typical levels appear to be of the order of p_{rms}/q = 0·05, i.e. a factor of ten up on the uniform boundary layer case.

Schloemer found comparatively little change in correlation area in his experiments, so that the effect of pressure gradient for a non-separated flow appears to be primarily in the change of fluctuating pressure level. Changes by a factor of 2 or 3, i.e. 6-9dB do not seem unreasonable.

Mugridge[58] measured the fluctuating pressures on an aerofoil and found an increase of order ten over the boundary layer case. How much of this is a real effect cannot be fully determined at this time. Mugridge's aerofoil was most unusual, with no well-defined trailing edge, and must therefore be expected to develop substantial areas of unsteady separated flow. It is also possible tunnel turbulence could be an important source of error in this case[54].

An associated problem is that of fluctuating transition and/or laminar separation. This could be the explanation of tne anomalous 'owl wing' results of Soderman. He found a reduction of around 6dB in rotor noise radiation after attaching a series of multiple miniature strakes along the leading edge of thepropeller section (see Reference 59). Blackman[55] found values of $p_{rms}/q \approx 0{\cdot}014$ close to transition but attributed this to a Reynolds number effect. To define this problem further measurements beneath the transition region are required. Recent comparative measurements at Loughborough University of Technology with transition fixed at the leading edge do suggest that the effects discussed above could be important in the transitional Reynolds number range. This would apply primarily to model rotors.

Noise radiated by the tip vortex self-interaction with the blade is also a potential noise source. The flow at the tip of a surface at angle of attack is generally in the form of a concentrated vortex which springs from the forward part of the tip and passes back over the top surface. Although detailed studies of the tip flow are not available extensive data from the equivalent slender wing cases can probably be applied to the present case. At moderate speeds, the scale of the phenomenon is large enough for it to contribute to dipole radiation. We may again use Equation (3.20) to calculate the sound radiated. Pressure fluctuations beneath a vortex core on a delta wing have been studied by several investigators, and data are reviewed by Richards and Fahy[60]. Characteristically the overall pressure fluctuation levels are around 10dB higher than in the boundary layer for moderate incidences (2° and up) and around 20dB higher for the vortex breakdown condition. Correlation lengths are found to be around 1/7 of the semi-span, i.e. 0·05 of the chord for the 20° delta wing studied, and peak frequencies are around $\omega c/U \approx 40$

(before breakdown).

Thus for this case $\omega^2 S_c = 4U^2$, that is somewhat larger than the attached boundary layer case. Taking both the increase in pressure fluctuation level and the correlation area into account indicates that radiated sound levels due to the tip vortex self-interaction could be up to 15dB higher than the equivalent boundary layer case and possibly more under vortex breakdown conditions. The effective area of action of the boundary layer due to the U^6 increase in effectiveness towards the tips is 1/7 of the blade area. It is probably reasonable to assume that vortex action would occur over the outer 5% of the blade surface, so with this area correction self-induced tip vortex noise levels could still be 10dB above the boundary layer radiation figures. This appears to explain much existing data, as will be discussed below.

Clearly one should avoid cases which might cause vortex breakdown at the tips, which implied avoiding tip sweeps of 60°. Alternatively if the vortex can be persuaded to go elsewhere noise could be reduced. Possible methods include wash-out and bent up tips. Possibly the best would be tip cut back, but this may need to be severe to avoid the normal radial inflow that occurs. (Note that the 60° figure above is relative to tip flow direction.)

Thus finally we may summarise the noise levels from the principal possible broad band sources as follows. It is worthy of note that all correspond to the dimensional dependence originally found by Yudin[25].

Source	*Typical level*	*Typical Frequency*
1. Turbulent Input	$p^2 \simeq 2{\cdot}5 \times 10^{-3}\ \rho_0^2 a_0^4 M_T^6 \left(\frac{u_{rms}}{V_T}\right)^2 \frac{S}{r^2}$	as turbulence
2. Attached Boundary Layer	$p^2 \simeq 1{\cdot}5 \times 10^{-9}\ \rho_0^2 a_0^4 M_T^6 \frac{S}{r^2}$	$f \simeq 20V_T/c$
3. Tip Radiation	$p^2 \simeq 4 \times 10^{-8}\ \rho_0^2 a_0^4 M_T^6 \frac{S}{r^2}$	$f \simeq 6V_T/c$

Table 2: Parameters of Broad Band Noise Sources

3.3.2 Experimental Results and Predictions

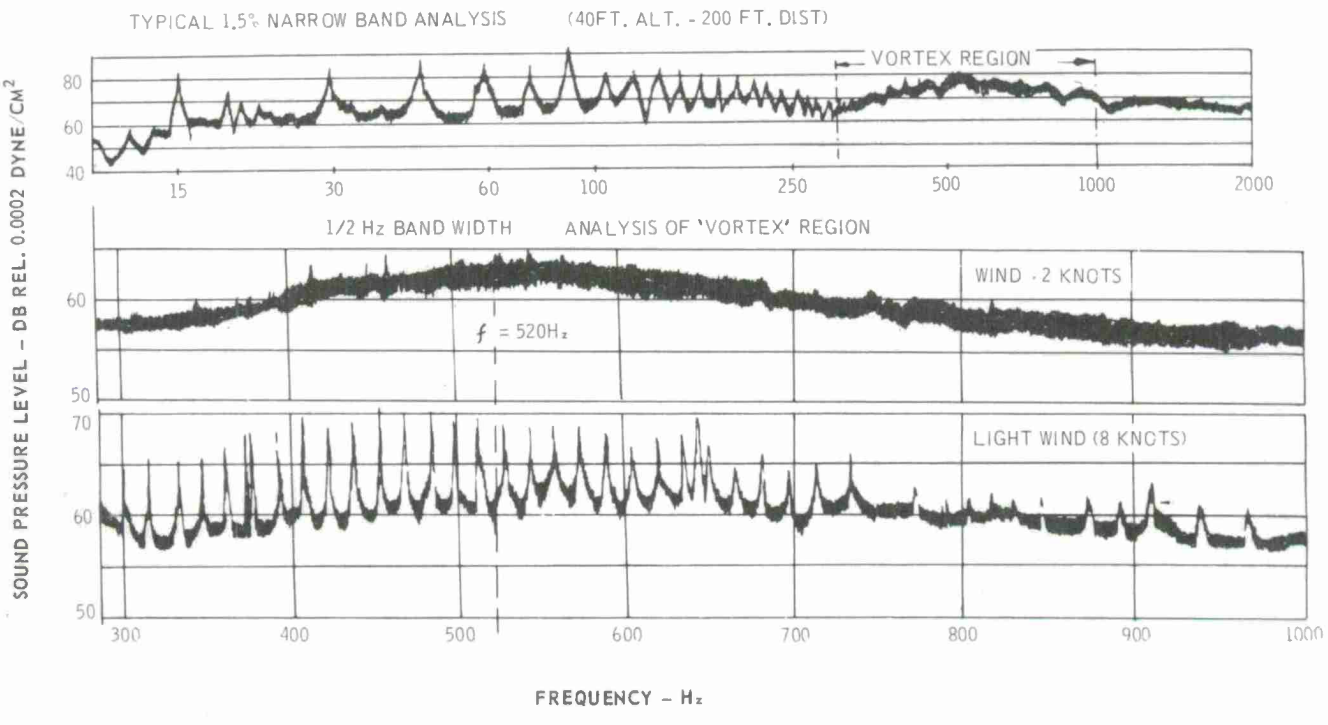


Figure 3.9: Narrow band analysis of helicopter noise - Hovering Wessex - from Leverton[62]

In practice it is very difficult to draw a clear distinction between discrete frequency and broad band noise. Several workers (e.g. References 36,62) showed how much of the region of the rotor noise spectrum which appeared tobe broad band in nature from early tests in fact contained substantial contributions from the higher harmonics of the blade passing frequency. Categorising sound in this region as either broad band or discrete frequency is difficult. An experiment which does show the classes clearly was reported by Leverton[62], and his results are reproduced here as Figure 3.9. This shows analysis of measurements taken on a rotor under conditions of calm, and slight wind. It can be seen that for calm conditions no harmonics are observable, whereas a slight wind immediately results in the presence of discrete frequencies. Furthermore, the underlying broad band level in the slight wind case is unchanged. These experiments therefore demonstrate the existence of a genuine broad band background noise radiation from a rotor. However, the fundamental question is the source of the random fluctuations. As has been discussed, early work was oriented towards a trailing edge vortex mechanism as a fundamental source. The first paper to explicitly contradict this concept was produced by Kramer[63] in 1953. He applied both trailing edge suction and blowing to a propeller, and was unable to detect any change in level. This is a powerful argument against any possible trailing edge effects. Kramer proposed that inflow turbulence to a rotor was the dominant source.

Thus, first of all the effect of external turbulence will be examined. The key experiment in this area was performed by Sharland[52], who measured the noise radiated by a small plate in the turbulent air stream of a jet. The results are shown in Figure (3.10). Sharland also estimated the noise using a formula almost identical to Equation 1 in Table 2, and obtained good agreement, as shown in Figure 3.10. Sharland used established measurements of the turbulent flow parameters in a jet, which should be acceptably accurate for this case. He also measured the noise radiated by a plate in the laminar flow portion of the jet. The results show almost 20dB less sound radiation, thus confirming the significance of external compared to self-generated turbulence.

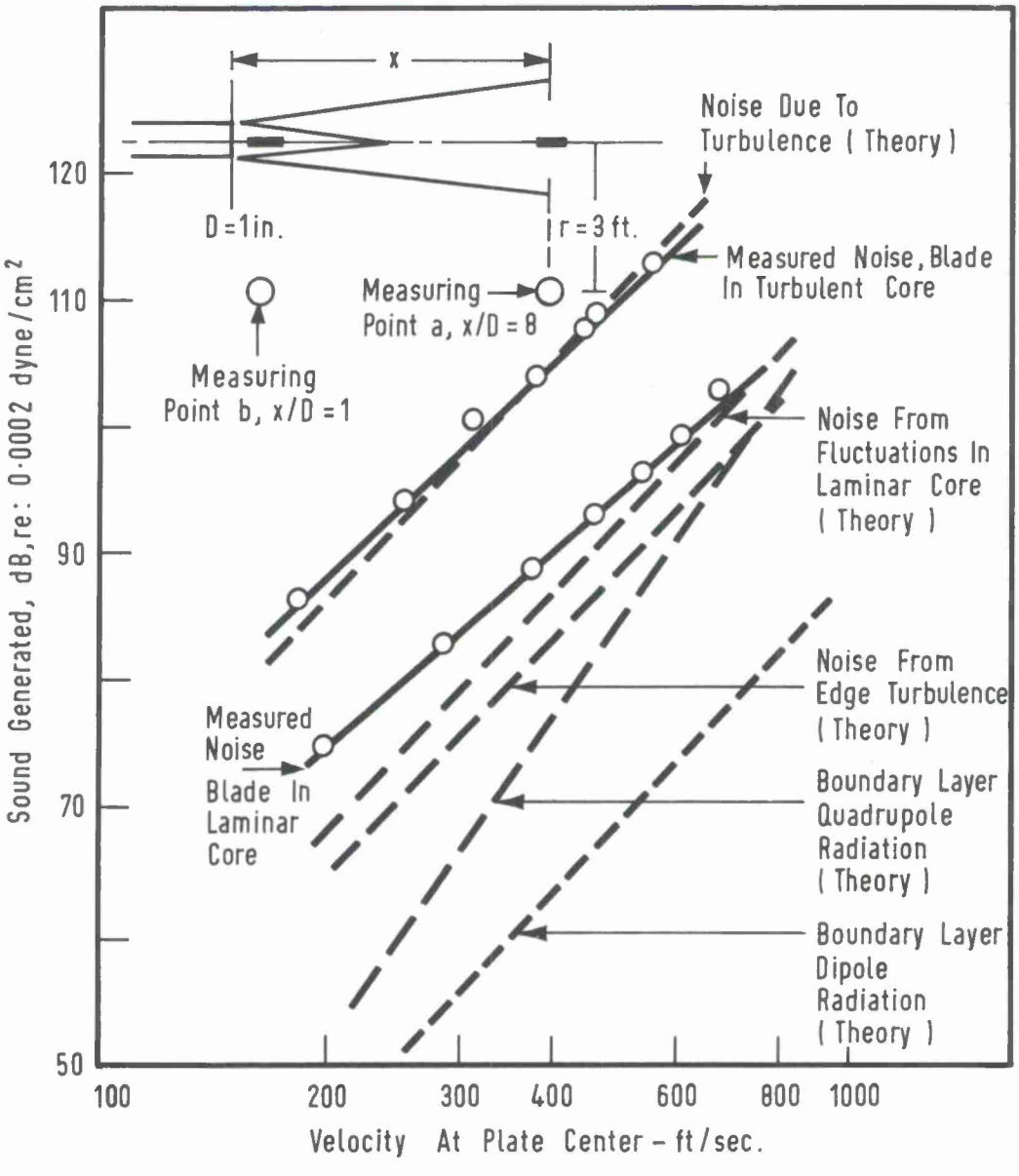


Figure 3.10: Noise radiation from a plate in an airstream - after Sharland[52].

However, detailed interpretation of these "laminar" results is far more difficult. Sharland did estimate the effect of the shear layer turbulence over the part of the plate projecting outside the laminar core, as shown in Figure 3.10. However, he did not consider the possibility of fluctuations within the core itself. Even if the jet exit flow was entirely turbulence-free, recent research has shown how a distinct fluctuating field exists in the core even quite close to the exit. Data taken by Tu[64] and others has shown that the cross-stream component of turbulence will be of order 0·1U at the downstream location used by Sharland, but as high as 0·012U at the core location. These latter levels are quite sufficient to explain Sharland's acoustic radiation in the "laminar" case as shown in Figure 3.10. Thus it seems probable that Sharland's "laminar flow" data is also effectively for an external turbulence case.

In addition to externally induced sources on the blade, typically inflow turbulence, there is the possibility of self-induced sources, for instance the trailing edge effects discussed above. Kramer's experiments are a powerful experimental argument against the reality of trailing edge vortex noise mechanisms. The results of two further relevant studies, unfortunately as yet unpublished, have been kindly communicated to the author by Davis, and by Foley. Both these workers attempted to repeat Sharland's experiments, with a plate in a two-dimensional channel, but with the precaution of removing the turbulent shear layer which passes over the parts of the plate nearest the wall. Davis removed the boundary layers by suction, and Foley mounted his plate just after a substantial contraction, so that the boundary layer was very thin. Both workers were unable to detect any effect of the presence or absence of the plate on the broad band noise radiation, and inferred that actual levels of noise radiated by a plate in an undisturbed flow must be an order of magnitude below those found by Sharland for the laminar case. Thus it must be concluded that the trailing edge vortex mechanism is not of practical significance for aerofoils with attached flow.

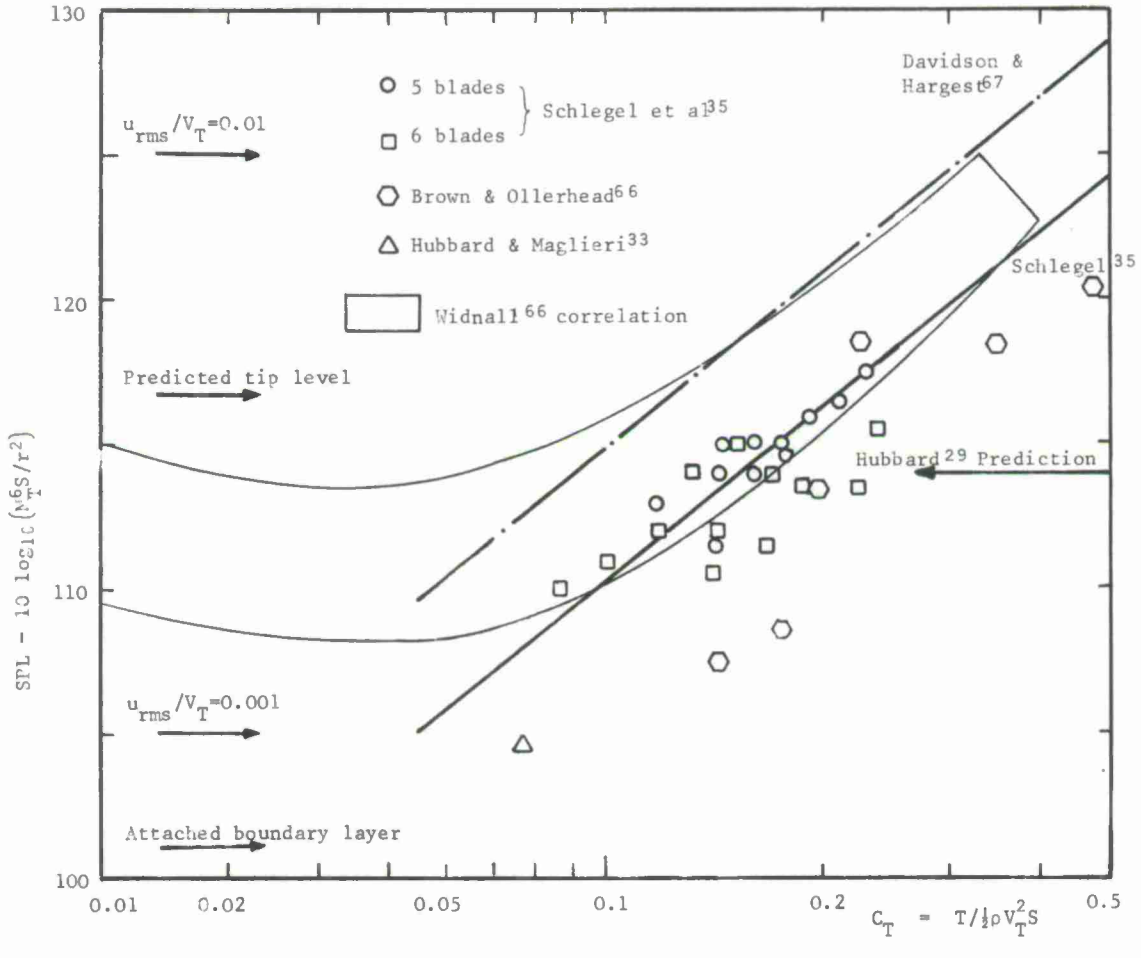


Figure 3.11: A correlation of broad band noise.

It is clearly of interest to be able to predict both the discrete and the broad band components of the rotor noise. As shown by Figure 3.9, the distinction between the two is difficult, and discrete frequency components, at least, are affected by the wind. It

is clear that the discrete frequency noise does result from the non-uniform inflow to the rotor and this in turn appears to be a function of detail rotor geometry. Broad band noise, where turbulence is the cause, is possibly a little less affected by details. It has been examined by an empirical correlation of data along lines very similar to those suggested by Widnall[66]. Her correlation included results from a wide range of helicopter tests, but the data frequently included the full noise radiation and not simply the broad band noise component alone. The correlation shown here in Figure 3.11 features data which includes some attempt to remove the discrete frequency contribution. It is therefore intended to give broad band rotor noise only. It also has the advantage of being non-dimensional. Most of the data points shown are from Schlegel's work[35], which only included contributions above 150Hz. This was helicopter test tower data. Also shown are some recent data from the work of Brown and Ollerhead[66] on noise from a propeller at a stand. Their levels were found by subtracting all observed frequency peaks from the signal. One point from Hubbard and Maglieri's work is shown, this is based on the spectrum given in their paper together with comments received personally from H.H. Hubbard. Only the integrated contribution of the noise above 160Hz is shown for this.

Also shown are prediction formulae due to Hubbard, and to Schlegel. Not surprisingly, Schlegel's empirical formula matches his own data well. But it is also in acceptable agreement with the other data plotted. Thus it appears that this formula does give a reasonable prediction of broad band levels. Further work along equivalent lines has been reported by Davidson and Hargest[67]. Their prediction curve is based on sound analysis of noise from a helicopter in free flight, but the number of data points apparently used is rather small. It is supported by test results on a rotor tower which was almost certainly atypical, with large levels of recirculation. Davidson and Hargest's formula contains a large directional term, and their numerical values must be reduced by 10dB to allow direct comparison with Schlegel. A further 3dB reduction is allowed to account for their "mean peak" level prediction. Even so, their prediction curve is 4·5dB up on Schlegel's, as shown in Figure 3.11. The Davidson and Hargest prediction for broad band noise alone is sometimes higher than than measurements for the full helicopter. Thus it is thought to be somewhat overconservative. On the other hand, it should be noted that the data on Figure 3.11 comes entirely from rig tests and could therefore be suspect. Further systematic tests on full scale helicopters, allowing systematic analysis of broad band noise, are clearly highly desirable.

Also shown on Figure 3.11 are theoretical predictions based on the formulae of Table 2. It is noteworthy that a turbulence level of as little as 0·1% is sufficient to produce broad band noise levels of the order of those measured. Figure 3.11 also shows how predicted levels due to direct blade boundary layer radiation are inadequate to explain observed noise levels. In any case the radiation frequencies would be beyond the range of interest. But the tip noise radiation formula given does indicate levels of the same order as those observed in practice. This empirical evidence is, at least, not in disagreement with the idea that inflow turbulence and tip radiation are the principal sources of broad band noise radiation by rotors.

In order to make full predictions of rotor broad band noise it is necessary to have some knowledge of both its frequency spectrum and its directionality. This is somewhat difficult because of the paucity of evidence. It may be assumed that rotor broad band noise is symmetrical about the rotor axis, however, its directionality in elevation is a matter of conjecture. Full data from a real helicopter flyover does not exist and extrapolations[67] seem to be misleading. The following empirical formula has been suggested[48]

$$DI = 10 \log_{10} \left\{ \frac{\cos^2\phi + 0{\cdot}1}{\cos^2 70^\circ + 0{\cdot}1} \right\} \qquad \ldots\ldots\ldots\ldots (3.24)$$

where ϕ is the angle from the rotor axis.

This correction term can be added directly to the results of Figure 3.11, since the typical measurement location is near 70°. Recently measurements have been made on a rotor tower by Leverton[49] using a balloon microphone system. His data seem to agree reasonably well with the above formula.

Definition of spectral results is far more difficult. The exact mechanisms by which broad band noise is generated are far from clear, so that the governing parameters cannot be specified. The broad band noise is rather obscured by higher rotational harmonics so that it is difficult to define in any exact manner. Furthermore, initially all results have taken on existing rotors which tend to be of very similar size and operating conditions, so that extrapolation is difficult. For instance, there is no evidence on the effect of chord. Thus detailed knowledge of the spectrum does not exist. For prediction purposes it seems natural to put faith in a Strouhal scaling relation based on rotor size and tip velocity. In fact, results taken by Leverton[49] show little indication of a Strouhal scaling law, but no alternative assumption seems tenable. An approximate spectral shape has been defined[48] as

$$p_0^2(f) = \frac{f}{(f_0^2 + f^2)^2} \qquad \ldots\ldots\ldots\ldots (3.25)$$

where $f_0 = V_T/KR_0$

V_T = tip velocity

R_0 = rotor radius
K = 0.035

The original definition of this[48] included a term to allow for the Doppler broadening due to rotation. Although this does occur, the effect is rather small for low Mach numbers. Since low rotor tip Mach numbers are essential for low noise it seems acceptable to ignore the effect.

3.4 Other source mechanisms

To this point the paper has concentrated on sound radiation by fluctuating force (dipole) mechanisms on the blades. As early as 1938 Deming[68] showed the possible effects of blade thickness in producing noise. Although the existence of thickness noise sources is now universally recognised, in most work on rotor noise they are conveniently neglected. Little basis has been given for this, but, in fact, the comparative level of the thickness noise source can be calculated directly. As first stated explicitly by Lighthill[56], for "compact" sources when the acoustic wavelengthis greater than the blade chord, the thickness noise source reduces to an equivalent dipole of strength $\rho V\dot{v}$ where V is the blade volume and $\dot{v}$ the local acceleration. This is very similar to the model proposed by Lynam and Webb in 1919.

Now the force terms have dipole strengths equal to the magnitude of the forces acting. In the rotor case acceleration is U^2/R and the force in the chord direction is the drag $\frac{1}{2}\rho U^2 S C_D$, so that the ratio of thickness to torque noise is $2t/RC_D$, where t is the mean blade thickness and C_D includes any backward orientation of the thrust. The ratio will normally be very small. Thus, theory suggests that thickness noise can be neglected at moderate rotor speeds and radiation frequencies. For high frequencies or at speeds approaching sonic the compactness condition breaks down so that possible noise effects of thickness must again be taken into consideration. Hawkings and Lowson[69] have recently considered this in some detail.

A further source of possible radiation from the blade is the stress system around it. Lighthill's general theory of aerodynamic noise[39] demonstrated the possible significance of fluctuating stresses as quadrupole sources of sound in 1952, but it was not until 1969 that Ffowcs Williams and Hawkings[51] pointed out that the fluctuating stress system on a rotating blade must also radiate. The key features of sound radiation from any rotating source are governed by Mach's modulated Doppler frequency shift, and Figure 3.4 will therefore apply to all sources equally. Thus distinction between the various forms of source is not easy. Any simple theoretical model suggests that a feature of stress (quadrupole) radiation would be a U^8 dependence. There is some evidence of this (see Reference 54) but not enough to be convincing. Direct estimation of quadrupole source strength is difficult. Most simple models tried by the writer seem to result in logarithmically singular integrals, and further theoretical study is required. On the other hand, the fluctuating force (dipole) source strengths can be calculated straightforwardly, and predicted results agree with virtually all the experimental information available. Thus, at the present time, any real significance of fluctuating stress sources is not demonstrated, but the difficulty of early workers in properly modelling the blade boundary conditions is far from being fully clarified.

Ffowcs Williams and Hall[70] and others have extended the basic quadrupole source concept to include the possible effects of blade trailing edges. They find that diffraction around the trailing edge can give large increments in acoustic efficiency so that the U^8 law goes over to a U^5 law. Several objections can be made to their theoretical model - notably, no account of boundary layer velocity gradient at the trailing edge and non-inclusion of the Kutta condition. Equally, no experimental evidence supporting the theory exists. Nevertheless, the possible significance of trailing edge actions on blade noise radiation remains a question of considerable theoretical and experimental interest. The effects of blade motion are also a possible source of noise, but the effects can be shown to be comparatively small. A general theory for point forces in motion[40] shows that the dominant thrust term only radiates as a result of the acceleration of the rotor, proportional to $\Omega^2 R$. Blade motion effects will therefore only be significant overall if the acceleration in question is larger than $\Omega^2 R$, which is extremely unlikely for a helicopter rotor. It is the rotor force fluctuations associated with any blade motion that will be the dominant source in any practical situation. The insignificance of blade motion effects was also shown by direct computation in the report of Lowson and Ollerhead[36].

Finally, it must be emphasised that any unsteady source on the rotor is only important if tip Mach numbers are low (roughly < 0·7). For high tip Mach numbers the direct radiation by the steady rotating sources becomes very efficient, as shown by Figure 2. In this context steady sources would include steady thickness or stress contributions in addition to the steady force (Gutin) terms previously discussed. However, when rotor noise is a problem, low tip Mach numbers must be chosen, so that the unsteady sources will usually dominate practical rotor noise control considerations.

3.5 Some recent experiments

The key to the theoretical studies has been the concept that the unsteady aerodynamic input to the rotor causes its acoustic output. Thus a low speed rotor may be regarded simply as a machine for converting inflow variations into noise. From this viewpoint each rotor will have a unique aero-acoustic transfer function which defines its effectiveness

as a noise generator. Recent experiments[54] at Loughborough University of Technology have attempted to measure this. Experimental definition of the aero-acoustic transfer function requires simultaneous measurement of source strengths and noise. As has been discussed, the immediate source of noise is the fluctuating force system on the rotor. Measurement of this is difficult, and was not attempted in the tests, although some success has been reported in recent work by Heller and Widnall[71]. The fluctuating forces are, in turn, caused by the unsteady inflow. This can be measured straightforwardly and this approach was chosen in the present tests. The disadvantage of the technique is that the fluctuating forces on the blades must be evaluated theoretically, but this is outweighed by the advantages of experimental convenience. Furthermore, the results may be of direct practical value for noise prediction since estimates of unsteady inflow levels to a rotor may be available at the design stage.

The experiments were performed on a small (0·66m dia.) open fan, leading details of which are given in Table 3. The inflow variation was measured using a rotating hot wire, mounted on the hub of the rotor. Circumferential variations of the inflow were thus recorded as time variations at the rotating hot wire, and spectral analysis of the signal gave the levels of the aerodynamic input modes directly. Acoustic output was measured on axis where the one to one relation of output to input applied (equation 3.12). Subtraction of the relevant aerodynamic input levels from the acoustic output levels thus gave a direct estimate of the aero-acoustic transfer function. This is shown in Figure 3.12.

Number of blades	= 2, 7 or 14
Hub diameter	= 0·24m
Rotor disc diameter	= 0·66m
Blade chord at tip	= 0·064m
Blade chord at root	= 0·085m
Maximum blade thickness at tip	= 0·003m
Blade tip angles	= 5^o, 10^o, 15^o, 20^o
Blade root angles	= 25^o, 30^o, 35^o, 40^o
Speed range between 0 and 3000rpm approximately	
D.C. motor of 7·5kW	
½" B & K microphone position - variable on 2·14 radius from fan centre	
Hot wire location - 0·26m from axis, 0·02m from blade leading edge	

Table 3: Rig Parameters

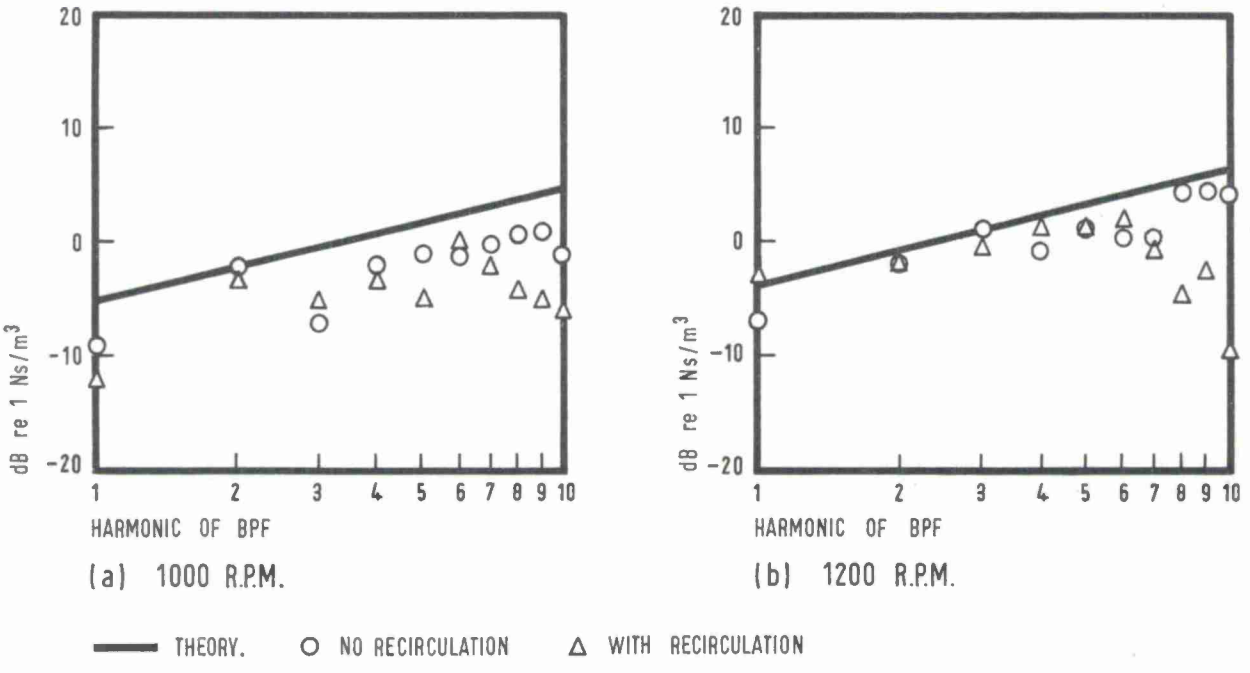


Figure 3.12: Aero-acoustic transfer function[54]

Two different inflow conditions are shown. The fan was mounted in an anechoic chamber, and normally operated in a recirculating condition, giving one set of data points. However, the recirculation took some time (3 - 5 secs) to build up to its full value. Thus at the start of each run different flow conditions prevailed, and data for this initial case are also shown. Both the acoustics and aerodynamics of these two cases are very different. But if the basic concept is correct, the aeroacoustic transfer function should be the same. This is verified by Figure 3.12 within experimental accuracy, at least for the low harmonics of the noise. A theoretical curve is also shown. This is based on equation (3.12), with the relation of unsteady aerodynamics to the unsteady forces being estimated from the theory of Sears[53]. Agreement between theory and experiment is also good, both for trends and for absolute levels.

At the highest harmonics some discrepancies appear for the recirculating case. This is thought to be the result of increased levels of turbulent inflow and is currently the subject of further study. A comparison of broad band noise with turbulent inflow was also made for the 1200rpm case with clipped blades (see also below). Both aerodynamic and acoustic broad band levels were estimated from integrations of the measured spectra with discrete frequency peaks removed. The root mean square turbulent input level measured by the rotating hot wire was 0·556m/sec. The broad band acoustic level may then be predicted to be 70dB via equation 1 of Table 2. The measured level for this one case so far studied was also 70dB. Thus theory gives vary acceptable predictions of level for both the discrete frequency and broad band parts of the rotor noise radiation, showing a dominant effect of rotor inflow on noise.

Further experiments showed that the high frequency component of the noise was strongly affected by tip condition. The measured effect of tip shape is shown on Figure 3.13. It can be seen that clipping the trailing edge of the blade reduced noise at the higher frequencies by over 10dB. The reduction observed is consistent with the idea advanced earlier that separated vortex flow over the tips is a significant source of noise.

Thus from these experiments it may be concluded that there were three principal sources of noise from the rotor tested

1. Discrete frequency noise, governed by inflow distortion
2. Low frequency broad band noise governed by inflow turbulence
3. High frequency broad band noise governed by the blade tips.

This has interesting consequences for rotor noise control.

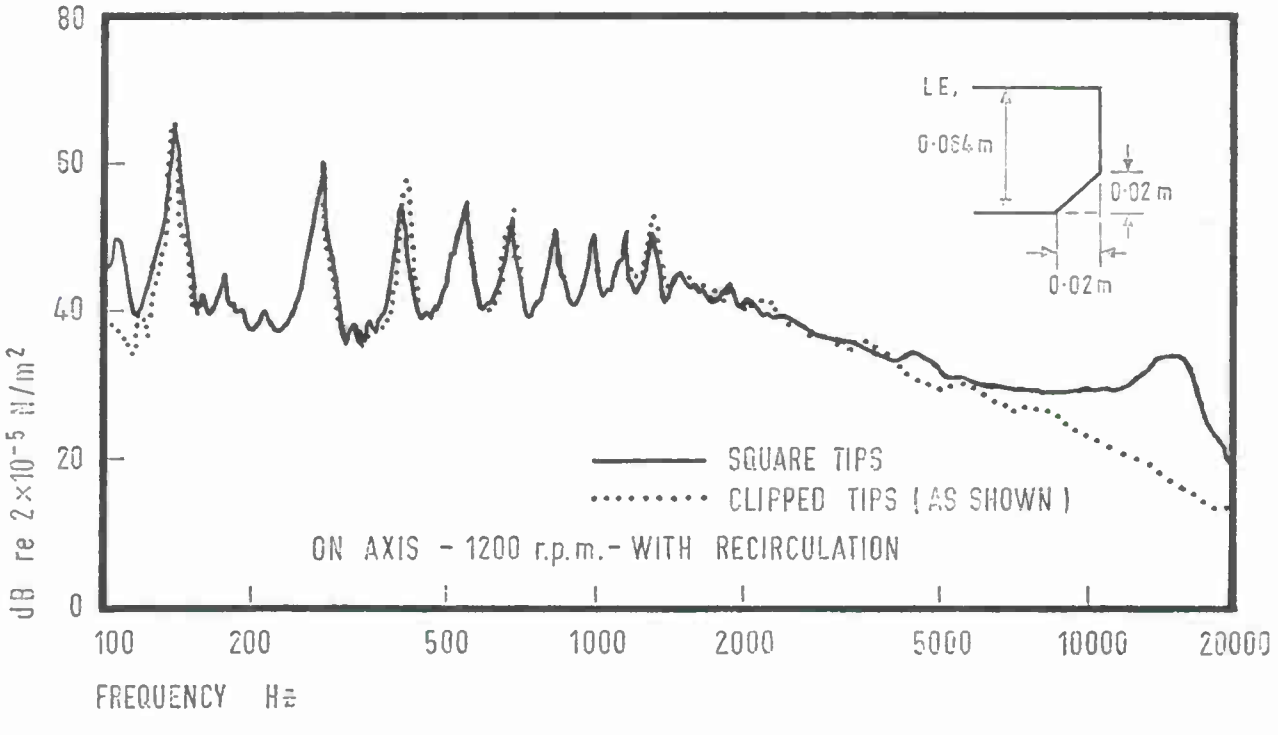


Figure 3.13: Effect of tip shape on fan noise spectra[54]

4. APPLICATION TO NOISE CONTROL

4.1 The Effect of Design Parameters

Integrating all of the effects discussed so far to give practical methods for helicopter noise control is very difficult. A dominating effect is the insensitivity of the ear to detail changes as emphasised by Table 1. It therefore becomes extremely important to choose fundamental design parameters of the helicopter, such as rotor speed and size, very carefully. In making this choice some account must be taken of the frequency response of the ear. Here a frequency squared law will be used, as suggested by Figure 2.1

Now equation 2 shows that the discrete frequency radiation is governed by disc loading, while equation 1 and Table 1 suggest that the broad band noise is governed by blade loading. Thus at the low blade loadings characteristic of a helicopter rotor broad band noise would be more important. This concept is discussed in more detail in Reference 11. For design purposes, an idea of trends of noise with the principal design parameters is of interest, and some general arguments may be put forward for this.

As shown by Figure 3.11, for a helicopter rotor the physical levels of sound intensity vary roughly as

$$p^2 \sim U^2T^2/S \sim T^3/S^2 \qquad \ldots\ldots\ldots\ldots(4.1)$$

where U is velocity, T thrust and S blade area.

The typical frequency squared varies as

$$f^2 \sim U^2/\ell^2 \sim T/\ell^2 S \qquad \ldots\ldots\ldots\ldots(4.2)$$

where ℓ is a typical length (say equal to $S^{0.5}$).

In each case the velocity has been eliminated by using the relation $T \sim U^2S$. Thus the perceived noise levels measured in any unit will typically vary as

$$L_{PN} \sim f^2p^2 \sim \frac{T^4}{S^4} \sim \frac{T^4}{\ell^8} \sim U^8 \qquad \ldots\ldots\ldots\ldots(4.3)$$

Thus the perceived sound levels are a strong function of disc loading. Although demonstrated here for the broad band case, the general features of the results apply equally to the discrete frequency components[11]. The arguments have interesting consequences. Firstly, it will be seen that rotors of any scale are predicted to sound as loud as each other provided disc loading (or velocity) is the same. It therefore appears that some empirical design predictions of noise from large rotors may have been overconservative, and also that a scale model rotor will sound as loud as the real thing. Secondly, it will be seen that increase of scale at constant thrust has a major benefit on noise. This is equivalent to a reduction in velocity. For either parameter the variation is as the (±) eighth power.

These arguments are based on very rough power law approximations both to the sound intensity laws and to the subjective response. More detailed examination has therefore been carried out on a general rotor noise prediction programme at Loughborough University of Technology. The programme includes both a full discrete frequency calculation based on equation 3.10 and a broad band noise calculation based on the empirical results of Figure 3.11, and includes many additional detail features which will not be discussed here. This programme will be described in a later document. Results shown here are given in PNdB, the more elaborate subjective response scale essentially equivalent to the frequency weighting curves of Figure 2.1.

Two results are shown here. Figure 4.1 gives the effect of variation of scale for a two-bladed rotor at a constant disc loading of 4lb/ft^2 (191N/m^2). Non-uniformities in the curve are caused by non-linearities in the PNdB function[7], especially the low frequency cut-off. Nevertheless, over a scale range of 20:1 PNdB levels vary by less than ±3dB from the mean value. Note that thrust would vary by 400:1 over this range.

Figure 4.2 demonstrates the effect of variation of scale at a constant thrust of 10,000 lb (4550 kg). A dramatic reduction in noise ensues as scale is increased or tip velocities reduced; roughly as the eighth power predicted. At higher Mach numbers the reduction is even more pronounced. Choice of large size low tip speed rotors must impose many problems on the designer, but it is hoped that this curve will suggest that these problems justify study in order to minimise rotor noise output.

4.2 Detail Improvements

For helicopter rotors there appears to be some genuine hope that detail variations can have useful effects on noise. As has been discussed, there appear to be three main sources of noise from a rotor: inflow distortion, inflow turbulence and tip effects. On a rotor each of these is fundamentally controlled by the rotor vortex system. This may well be sensitive to detail modifications.

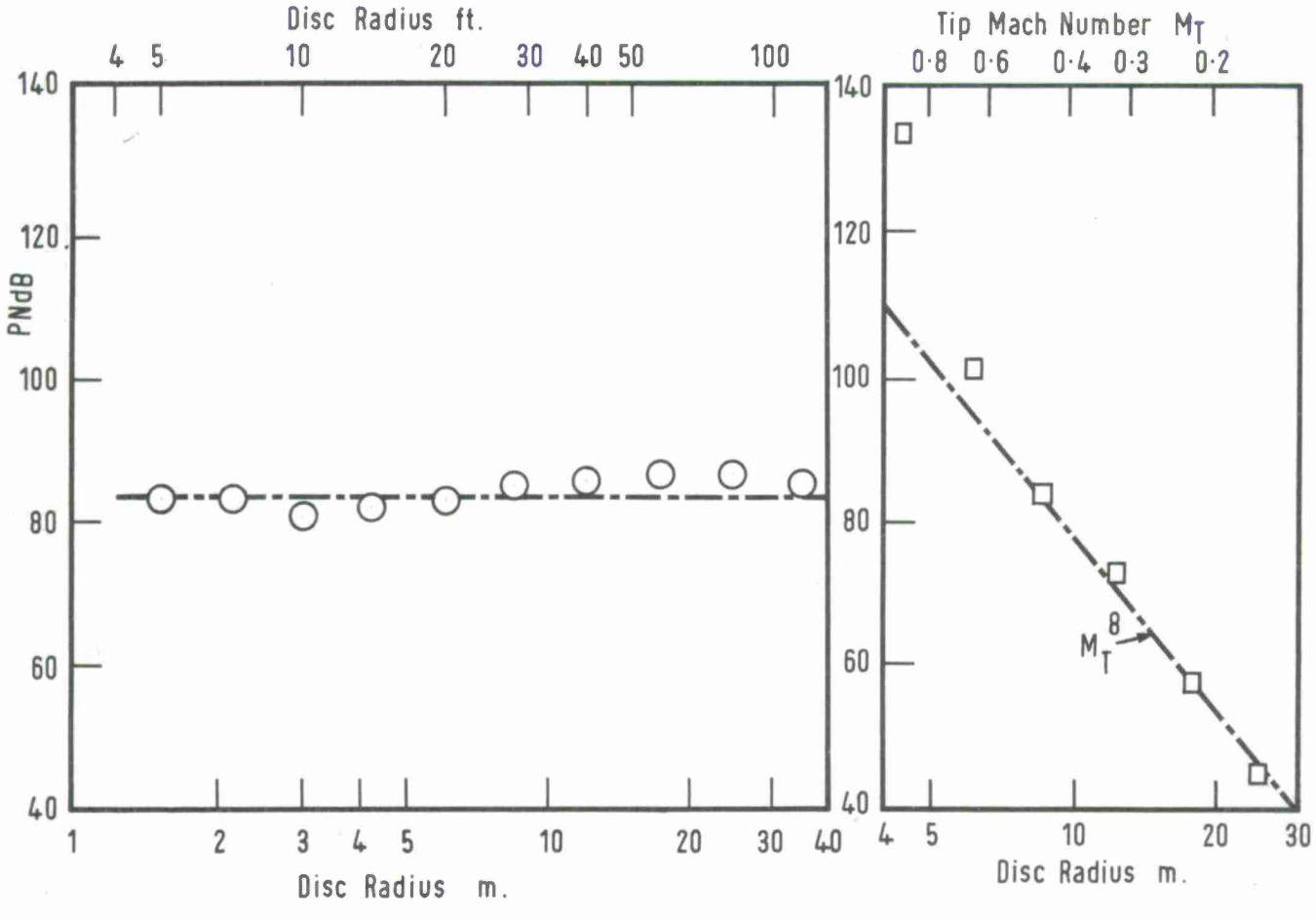


Figure 4.1: PNdB vs Scale for constant disc loading

Figure 4.2: PNdB vs Scale for constant thrust

Jones[72] and others have demonstrated how the tip vortex from a helicopter rotor can actually move upwards as it moves away from the blade, and frequently passes above the following blade. Direct interaction of a blade with a vortex is a known cause of blade slap as discussed by Leverton[2] and, more recently, by Widnall[4]. Blade slap will not be considered in any detail here since it is an excessive noise, unlikely to be tolerated when noise is a problem. Also it appears that it can be substantially controlled by operating procedures. However, there can be little doubt that more moderate blade vortex interactions are a prime cause of noise problems, so that the rotor noise problem can perhaps be regarded as a problem in mild blade slap.

The noise radiation is reduced by reducing the aerodynamic fluctuations. This involves minimising vortex strength and maximising its distance from the following blade. Several workers have reported attempts to reduce vortex strength[73,74], normally via tip modifications. Notable recent suggestions are tip blowing and the 'ogee' plan form. Unfortunately, tip modifications have had mixed success when applied to flight hardware. On the other hand, there has been comparatively little attempt to reduce noise by increasing blade-vortex separation. Calculation of shed vortex paths should, in principle, be possible, and some success has been reported[72]. Close to the blade the vortex paths must be a strong function of the loading distribution, and it should be possible to find loading distributions which maximise separation from the following blade, particularly for multi-bladed rotors. Equally the rate of roll-up of the vortex must also be a function of blade loading. Thus renewed attack on the rotor vortex wake problem from the noise viewpoint appears to have useful potential.

When considering vortex wakes it is important also to consider non-ideal conditions such as that of wind and unfavourable manoeuvres. The increase in noise level due to wind is well documented but comparatively little substantive data is available. Most useful existing rotor noise data have been carefully taken under calm conditions. However it is clear that reduction of rotor noise under ideal conditions may result in comparatively little benefit for practical rotorcraft operating in a real atmosphere. Reduction of the wind induced rotor noise level is a major problem facing the designer, and fuller data on this is certainly desirable.

Much of the existing work on rotor noise control has concentrated on tip modifications [35,72,73], and benefits of over 6dB are often reported. On the other hand, these benefits

are not always found in flight, or in repeat tests at other centres. Leverton[76], for instance, found an increase in noise for most tip modifications tested. It has been argued here, via Figure 3.13, that the tip does have a specific effect on the high frequencies. Strouhal scaling these results up to a helicopter suggests that the effect will be centred around 2000Hz.

From tower tests on a rotor, Leverton[49,77] has defined a second broad band hump in this region. In the author's opinion, this hump is due to tip effects, and represents the modulated swishing sound observed on helicopters. In this context it is noteworthy that experiments by Schlegel[35] on trapezoidal tips reduced the depth of modulation of the broad band noise as well as the absolute levels. Maximum modulation might be expected from tip sources when Doppler changes in frequency, and in near field amplitude, would be at a maximum. Further experiments on a wide range of tips have recently been reported by Pollard and Leverton[78]. Variations of level of up to 15dB due to tip modifications are found, but the optimum tip is a function of rotor rpm, and a strong function of blade pitch. Noise benefit was also found to be a strong function of pitch in the recent tests at Loughborough[54]. Leverton's recent results show little benefit of a clipped trailing edge, in contradistinction to that shown in Figure 3.13. This may be due to the relatively thick (12%) sections used in his tests compared to the thinner (5%) sections of Figure 3.13.

The one clear conclusion from all these studies is that tip shape does have a major effect on rotor noise. The reasons for the effect must lie in the varying structures of the shed vortex from each tip. Systematic understanding of this does not exist, and represents an obvious area of profitable research. Meanwhile it is clear that rotor noise control programmes must include empirical evaluation of various tip shapes, perferably at full scale.

A major source of subjective annoyance from helicopters is the tail rotor. The general considerations for rotor noise radiation apply equally to tail rotor noise. The tail rotor typically operates in inflow which is badly distorted by the proximity of the tail boom and pylon, and by the action of the main rotor. This must result in severe increases of noise level, and the design modifications necessary to improve the situation are apparent. A longer tail boom should add little to helicopter weight, and give a useful noise benefit. From the noise point of view alone a canted front anti-torque rotor would be preferable, but presumably this would not be acceptable on operational grounds. Note that the asymmetry caused by forward flight of the rotor would not directly generate significant noise levels. This is because the asymmetry causes a first order input mode at the rotor which is of extreme inefficiency, as shown by Figure 3.3.

4.3 Propagation Effects

In any real noise situation the sound must propagate over a substantial distance before reaching the observer, and during propagation the noise can be substantially altered in character and level. The most recent systematic discussion may be found in a report by Ollerhead[10]. It is only proposed to give a summary of the effects here. Propagation of the noise is affected by three main parameters

(a) atmospheric conditions,
(b) the position of the source relative to the ground, and
(c) the propagation path.

Possible effects may be classified either as spreading, involving no loss in total acoustic energy, or as absorption, which includes some acoustic energy loss as well as possible redirection of the sound. The principal phenomena in each category may be listed as follows

Spreading:

- Uniform spherical spreading - inverse square law reduction
- Reflection and diffraction by solid boundaries
- Refraction by a non-uniform atmosphere
- Scattering by atmospheric turbulence

Absorption:

- Atmospheric attenuation
- Absorption by ground

Spherical spreading corresponds simply to the normal inverse square law reduction in sound pressure level as distance from the source is increased. Thus sound pressure levels at all frequencies reduce by 6dB for each doubling of distance. Very close to the source, within about two rotor diameters[36], the levels drop off somewhat more rapidly with distance. This near field effect is not of importance for subjective effects, but sound measurement locations for helicopters should not be less than two diameters from the rotor, if possible.

Reflection and diffraction by boundaries can often be important. The sound field above a solid boundary consists of a combination of the direct and reflected sound fields which will alternately reinforce and cancel. The cancellations often lead to specious spectral dips in the measured noise signal and possible effects should be considered for

all measurements. A vertical surface is sometimes used as a noise barrier, and may be a feature which can be used to minimise community noise from heliports. Some simple formulae for the effects of a barrier have been given by Maekawa[79]. Urban noise propagation is strongly affected by the channelling of sound between buildings. Experiments[80] have shown that increased peak noise levels do occur with helicopter overflights. Such increases will undoubtedly affect urban community reaction to helicopter noise.

Noise levels are also significantly affected by atmospheric refraction. Both wind and temperature gradients can cause substantial redirectionning of the radiated sound. The effects can be calculated quite straightforwardly[10] by methods of geometrical acoustics, providing the wind and temperature gradients are known. Unfortunately, of course, in any practical situation the wind and temperature gradients cannot be predicted accurately in advance, so that the direct value of these calculation schemes is small. However, some general features can be defined. Most of the velocity, or temperature stratification is in planes parallel to the ground, and sound paths which are nearly parallel to the ground will be the most affected by refractive effects. In practice this means that noise from near ground operations of the helicopter will be affected, whereas overflight noise will not. The effect of wind (through its typical boundary layer gradient) is to refract the noise towards the ground downwind, and away from the ground upwind. The effect of a thermal gradient is to refract sound towards the ground for positive temperature gradient, and away from the ground for a negative gradient. This effect can have considerable significance, particularly in locations with large diurnal temperature variations. This will cause strong ground propagation of noise during the early morning, and conversely strong upward refraction of noise during the later hours of daylight. These features can undoubtedly have major effects on both community response and detection, and will require consideration during operational planning.

Scattering by atmospheric turbulence is only partially understood. However, the possible redirectioning of helicopter noise by turbulent scattering is clear, and the overall effect is to reduce the directional features of the noise pattern. It is known that even highly directional sound fields reduce to uniform spherical fields at sufficiently large distances[81]. Mani[82] has calculated that a moderate wind would produce the same effect in about 100m for aircraft noise, but the development of the effect for helicopter has not been analysed. Some writers have suggested that turbulence can cause attenuation of acoustic energy as well as simple scattering. Theory indicates that pure scattering effects are dominant. In practice, scattering over the ground could lead to additional ground absorption, so that the overall picture becomes somewhat confused. However, it seems more logical at present to consider ground attenuation separately, and this will be done below.

Atmospheric attenuation of sound is a very complicated phenomenon, which has received considerable attention from physicists. Only now are all the elements of the process becoming clear. There are several possible physical mechanisms which can attenuate sound during its propagation through a real gas, but the principal mechanism is the conversion of acoustic energy into vibrational energy of the air molecules.

Vibrational relaxation of the oxygen molecules is significant for the higher frequency ranges, but the effect is substantially enhanced by the presence of water, so that atmospheric humidity plays a dominant role in determining the rate of absorption of the sound. Peak absorption occurs at around 5% humidity. Recent work has shown that lower frequencies (below 1000Hz) of the sound are affected by a nitrogen/water process and combined predictions using theory for multicomponent gas mixtures seem to be in good agreement with experiment[83]. Approximate values of attenuation in dB/km are given in Table 4 below. This corresponds to 50% relative humidity. Note particularly the very large attenuations occurring at high frequencies. It is for this reason that source radiation above about 2000Hz is rarely important for annoyance or detection. More detailed information can be found in References: 10,83,84.

Octave Band	1	2	3	4	5	6	7	8
Frequency Range (Hz)	20 - 75	- 150	- 300	- 600	- 1200	- 2400	- 4800	- 10000
Atmospheric attenuation - 50% humidity	-	14	3	5	8	11	20	65
Grass 0·5m high	-	6.5	18	25	23	15	6.5	1.6
Sparse jungle	1.3	22	36	44	59	89	148	213

Table 4: Attenuation of Sound in dB/km - Based on data in Reference 10.

Attenuation of sound by ground cover is a further important area which is not clearly defined. Data does exist on typical attenuation rates for sound propagating parallel to the ground surface, and two examples are given in Table 4. Theory also exists, but this required definition of the acoustic impedance of the ground cover - a very difficult task to accomplish meaningfully. Thus again one is forced to use empirical generalisations. Theory[85] and experiment[86] clearly demonstrate the significance of source height on the

attenuation. Maximum absorption occurs when the sound propagates very nearly parallel to the ground. This fact is well known to military pilots who fly close to the ground to minimise aural detection. An approximate formula for quantifying the effect is to multiply the parallel ground attenuation rate (Table 4) by a factor $1/(1 + \gamma)$ where γ is the angle of propagation to the ground in degrees. This does slightly overestimate the attenuation resulting at larger propagation angles, but this is perhaps compensated by the turbulent scattering/ground absorption effects mentioned earlier. Further details of the ground absorption effects can be found in References 10,85,86.

4.4 The Cost of Noise Control

Very little real data exists on the costs of noise control for helicopter design and operation. This is because few present helicopter design methods evaluate noise control possibilities during design in a realistic manner. As has been emphasised by Table 1, effective control of noise is a configurational, rather than a parametric problem, and it therefore needs to be tackled at a very early stage in the design process. The costs of such possibilities as lengthened tail booms, and increased tail rotor/pylon separation have not been evaluated. Clearly the cost of an optimum tip would be virtually negligible if the optimum shape for noise were in fact known.

The gross parametric dependencies of noise are, however, known, and the possible benefits of scale were presented in Figure 4.2. Using essentially equivalent formulae Faulkner[87] has evaluated costs of noise reduction in helicopters using a helicopter design programme existing at M.I.T. Such design programmes are forced to rely very substantially on simple formulae and semi-empirical trends but clearly Faulkner's results justify

	Existing	*Uncon-strained*	*Medium*	*Quiet*	*Silent*
L_{PN} take off at 500ft	95.0	93.6	85.2	79.2	74.9
L_{PN} cruise at 5000ft	84.1	82.5	77.6	73.2	69.4
D.O.C. at 100 mile seat trip	4.36	3.36	3.65	4.25	5.25
Gross weight lb	46,186	36,774	38,637	42,739	47,855
Rated power H.P.	7133	6280	5964	6593	6570
Cruise speed mph	189	237	219	196	168
Advancing Tip Mach No.	0.883	0.95	0.825	0.7	0.575
Tip speed hover f.p.s.	692	680	437	330	270
Number of blades	4	4	4	6	8
Chord, ft.	1.92	2.13	3.03	3.72	4.30
Rotor diameter ft.	59.5	62.4	70.2	73.8	87.2
Solidity	0.089	0.087	0.110	0.193	0.251

Table 5: Effect of Noise Constraints on Helicopter Design[87].

discussion, if onlybecause they are all that is available.

Some leading results are given in Table 5. These are for an approximation to an existing helicopter (Boeing-Vertol 347), and for four helicopters designed according to projected 1975 technology for a fifty passenger payload. Results are given for four levels of noise constraint on design as shown by the first entry in the Table. Two rather minor objections can be raised to the results. Firstly, the unconstrained helicopter at an advancing blade Mach number of 0.95 would almost certainly have very high levels of rotational noise (advancing blade slap) - see Figure 4.2. This was ignored in Faulkner's calculations. Secondly, all the calculations are for tandem rotors, which seem likely to be inherently noisy due to blade-wake interactions. On the other hand, the tail rotor is an important additional noise source for single rotor helicopters.

There does appear to be one major objection to the results. Although the results are given as L_{PN} there is no discussion in Faulkner's report of the PNdB method used, or indeed for defining the spectrum, which would be vital in these calculations. It appears that overall noise level has been simply equated with L_{PN}. Indeed this is approximately true for existing helicopters. However, this would mean that the subjective benefits of increased scale and reduced velocity (discussed in Section 4.1 here) would not appear in Faulkner's results. The results of Figure 4.2 suggest that subjective noise levels from the silent configuration may be overestimated by as much as 10 PNdB. Nevertheless the

major trends suggested by the results would still apply.

The calculations show that, as expected, larger, higher solidity rotors operating at lower tip speed are required to meet more rigourous noise constraints. Performance degrades and D.O.C. increases monotonically as noise constraints are introduced. Possibly the most encouraging result is that D.O.C. is not unduly sensitive. Compared to existing helicopters a 20dB benefit can be obtained by only a 25% increase in D.O.C., and this in spite of a reduction in tip velocity by a factor of over 2·5. If the objection raised above is correct then this can be re-interpreted as a 30PNdB benefit for a 25% increase in D.O.C. Faulkner also investigated the effects of larger helicopters, and of the benefits of future improvements in helicopter technology. His results suggested that an increase in size to an eighty passenger helicopter would show some benefit, but the benefit of further increases in size was marginal. Further benefit from size probably would have resulted if a PNdB calculation had been used, as discussed above. Furthermore, community annoyance is a function of number of movements as well as level[88]. Thus for a fixed number of passenger movements a fleet of larger helicopters would generate less annoyance than the smaller types.

The projected benefits of helicopter technology improvements are also encouraging, since they suggest that the D.O.C. penalty associated with noise control will reduce both absolutely, and relative to the non-constrained design. Faulkner's results indicate that 1985 technology could produce 75dB at 500ft for a D.O.C. of around $4 per 100 mile seat trip, i.e. virtually the same as present day helicopter trip costs. Thus future prospects for the implementation of the quiet helicopter for certain operations seem promising.

A final possibility for noise control is by choice of flight path. This is virtually free. Clearly paths over unpopulated areas should be chosen wherever feasible, although the actual benefits in terms of total community annoyance may be small[88]. Two possibilities seem to exist for noise control. The helicopter can operate close to the ground in order to benefit from increased ground absorption and physical barriers to the noise. However this may be rejected on grounds of safety or passenger psychology. The alternative is to climb rapidly away from the ground. This has geometric benefits in terms of maximum range. But a further possible benefit arises from the aerodynamics. Rotor/wake interactions appear to be the dominant source of noise. Rapid climb should minimise the interaction and give resulting noise benefit. Unfortunately this possibility has not been investigated via real operations.

Minimisation of noise during approach by this method is not possible since interactions are increased during descent. Indeed, blade slap during the landing phase is a common occurrence. Several authors have investigated optimum flight paths via a computational approach. Unfortunately, as has been made clear, present formulae for noise calculation are not sufficiently reliable to enable any firm conclusions to be drawn from such calculations.

Empirical investigation of optimum helicopter operational paths from the noise viewpoint has not been carried out, but would seem to be likely to generate very significant features for operational noise control.

CONCLUSIONS

The fundamental mechanisms of noise radiation by helicopters are now clear, both for the discrete frequency and broad band noise components. This knowledge is reflected in acceptable theories for the acoustic radiation process. However, application of these theories in noise prediction depends on a prior specification of fluctuating aerodynamic source strengths, and it is this area of knowledge which is sadly inadequate at the present time. Empirical knowledge gained by aerodynamic and acoustic testing is of some value, but there is clear evidence that important features of the fluctuating aerodynamic field can be significantly affected by details of helicopter design and operation. Examples are the major effect of tip shape, tail rotor interaction phenomena, and the potential benefits of flight path control.

When helicopter noise control is a primary design goal, existing knowledge suggests that major reductions in tip velocity, with associated increases in rotor size, can reduce radiated noise significantly with only moderate penalties in operating costs. However, if such penalties are unacceptable, noise control becomes a function of design details, the effects of which are inadequately understood at present.

The key to future helicopter noise control appears to lie in the understanding gained by careful experiments. There are several areas of uncertainty at present which justify study. Detailed correlation of ground and flight tests does not yet seem to have been performed. The noise effects of characteristic manoeuvres and of typical wind levels are not fully known, and may provide a practical limit for rotor noise reduction on real aircraft. Possibilities for main rotor noise control seem to centre around a full understanding of the shed vortex wake. Both experimental and theoretical approaches to this problem would be valuable. The most obvious area for study is the effect of tip shape, and blade loading distribution, on the wakes and noise of a rotor. Detailed parametric studies of tail rotor noise are clearly necessary.

Operational studies would also be useful. In the long term it is to be hoped that efforts in these areas will lead to a full understanding of the aerodynamic interaction processes. In the short term such studies should lead to empirical solutions which would be valuable contributions to a quiet helicopter design.

REFERENCES

1. Cox C.R. and Lynn R.R. "A Study of the origin and means of reducing Helicopter Noise", Bell Helicopter Company, TCREC Technical Report 62-73, U.S. Army Transportation Research Command, Fort Eustis, Virginia, November 1962.

2. Leverton J.W. and Taylor F.W. "Helicopter blade slap", J. Sound Vib., Vol 5, pp 50-80, January 1967.

3. Leverton J.W. "Helicopter Noise - Blade Slap", National Aeronautics and Space Administration Contractor Report, NASA CR-12 1, October 1968.

4. Widnall S.E. "Helicopter noise due to blade-vortex interaction", J. Acoust. Soc. Amer., Vol 50, p 354, July 1971.

5. Lyon R.H. "Radiation of noise by aerofoils that accelerate near the speed of sound", J. Acoust. Soc. Amer., Vol 49, pp 894-905, March 1971.

6. Ollerhead J.B. "An evaluation of methods for scaling aircraft noise perception", NASA CR-1883, November 1971.

7. I.S.O. Recommendation R507 "Procedure for describing aircraft noise around an airport", 2nd Ed. 1970.

8. Leverton J.W. "Helicopter noise - can its annoyance or loudness be rated using existing methods", Paper at Brit.Acoust.Soc. Meeting, Chelsea, April 1973.

9. Loewy R.G. "Aural detectability of Helicopters in tactical situations", Journal of the American Helicopter Society, October 1963.

10. Ollerhead J.B. "Helicopter aural detectability", USAAMRDL TR 71-33, July 1971.

11. Lowson M.V. "Noise radiation from V/STOL aircraft", Paper 72-22, ICAS Meeting, Amsterdam, 1972.

12. Wilson A. (Chairman) "Noise", Final Report Cmnd. 2056 HMSO, London, July 1963.

13. Lowson M.V. "Fundamental considerations of noise radiation by rotary wings", Paper 22 in AGARD CPP111 "Aerodynamics of Rotary Wings", September 1972.

14. Mach E. Pogg Ann, Vol 112, p 66, 1861, and Vol 116, p 333, 1868.

15. Rayleigh, Lord "The theory of Sound", 2nd Ed., Dover, N.Y., 1945.

16. Director of Research "The sounds of aeroplanes", A.R.C., R & M 694, October 1920.

17. Lynam E.J.H. and Webb H.A. "The emission of sound by airscrews" A.R.C. R & M 624, March 1919.

18. Bryan G.H. "The acoustics of moving sources with application to airscrews" A.R.C. R & M 684, March 1919.

19. Davis A.H. "Silencing aircraft", A.R.C. R & M 1542, September 1932.

20. Kemp C.F.B. "Some properties of the sound emitted by air screws", Proc. Phys. Soc. Vol 44, pp 151-165, 1932.

21. Paris E.T. "A note on the sound generated by a rotating airscrew", Phil.Mag. Vol 13, No. 82, pp 99-111, 1932 (see also Phil.Mag. Vol 16, p 60, 1933).

22. Gutin L. Ya "On the sound field of a rotating propeller", from Phys.Zeit Sowjet Band A, heft 1, pp 57-71, 1936, Translated as NACA TM-1195, October 1948 (see also J.Applied Physics, Leningrad, Vol 6, pp 899-909, 1936, in A.R.C. Rep 3115, 1946).

23. Lamb H. "Hydrodynamics", 6th Edn. Dover, N.Y., 1945.

24. Stowell E.Z. and Deming A.F. "Vortex noise from rotating cylindrical rods", NACA, TN 519, 1936.

25. Yudin E.Y. "On the vortex sound from rotating rods", Zh. Tekh. Fiz. Vol 14, No. 9, p 561, 1944, translated as NACA TM 1139, March 1947.

26. Von Wittern W.W. "The relation between vortex noise and wind resistance", CADO Tech. Data Digest, Vol 16, pp 20-23, September 1951.

27. Billing H. Modern aeronautical acoustics, A.V.A. Monographs R 1-3, Reports and Translations, 960, 1947.

28. Hicks C.W. and Hubbard H.H. "Comparison of sound emission for two-blade, four-blade and seven-blade propellers", NACA TN 1354, July 1947.

29. Hubbard H.H. and Regier A.A. "Propeller-loudness charts for light aeroplanes", MACH TN 1358, 1947.

30. Hubbard H.H. "Sound from dual-rotating and multiple single rotating propellers", NACA TN 1654, 1948.

31. Hubbard H.H. and Regier A.A. "Free-space oscillating pressures near the tip of rotating propellers, NACA Report 996, 1950.

32. Hubbard H.H. "Propeller-noise charts for transport airplanes", NACA TN 2968, June 1953.

33. Hubbard H.H. and Maglieri D.J. "Noise characteristics of helicopter rotors at tip speeds up to 900 feet per second", J.Acoust. Soc. Amer. Vol 32, pp 1105-1107, September 1960.

34. Taylor G.I. "The singing of wires in a wind", Nature, Vol 63, p 536, 1924.

35. Schlegel R.G., King R.J. and Mull H.R., "Helicopter rotor noise generation and propagation", USA AVLABS Tech. Rep. 66-4, October 1966.

36. Lowson M.V. and Ollerhead J.B. "A theoretical study of helicopter rotor noise", J. Sound Vib., Vol 9, pp 197-222, March 1969 (see also USA AVLABS TR 68-60).

37. Wright S.E. "Sound radiation from a lifting rotor generated by asymmetric disc loading", J. Sound Vib., Vol 9, pp 223-240, 1969.

38. Lowson M.V. "Theoretical analysis of compressor noise", J. Acoust. Soc. Amer., Vol 47, No. 1 (Pt 2), pp 371-385, (see also NASA CR 1287).

39. Lighthill M.J. "On sound generated aerodynamically - I: General Theory", Proc. Roy. Soc., A, Vol 211, pp 564-587, 1952.

40. Lowson M.V. "The sound field for singularities in motion", Proc. Roy. Soc., A, Vol 286, pp 559, 1965.

41. Lowson M.V. "Basic mechanisms of noise generation by helicopters, V/Stol aircraft, and ground effect machines", J. Sound Vib., Vol 3, 1966, pp 454-466.

42. Garrick I.E. and Watkins C.E. A theoretical study of the effect of forward speed on the free-space sound pressure field around propellers, NACA TN 3018, October 1953.

43. White R.P., VTOL periodic aerodynamic loadings: The problems, what is being done and what needs to be done, J. Sound Vib., Vol 4, November 1966, pp 305-344.

44. Cheney M.C. and Landgrebe A.J. "Rotor wakes, the key to performance prediction", Paper 1 in AGARD CPP 111 "Aerodynamics of rotary wings" September 1972.

45. Scheiman J. "A tabulation of helicopter rotor-blade differential pressures, stresses, and motions, as measured in flight", NASA TM-X-952, March 1964.

46. Burpo F.B. and Lynn R.R. "Measurement of dynamic airloads on a full scale semi-rigid rotor", Bell Helicopter Company, TCREC Technical Report 62-42, U.S. Army Transportation Research Command, Fort Eustis, Virginia, December 1962.

47. Levi H. and Forsdyke A.G. "Steady motion and stability of a helical vortex", Proc. Roy. Soc. A, Vol 120, 1928, pp 670-690.

48. Ollerhead J.B. and Lowson M.V. "Problems of helicopter noise estimation and reduction", AIAA Paper 69-195, February 1969.

49. Leverton J.W. "The noise characteristics of a large 'clean' rotor" Paper 25 in AGARD CPP 111 "Aerodynamics of rotary wings", September 1972.

50. Tanna H.K. and Morfey C.L. "Sound radiation from point sources in circular motion", J. Sound Vib., Vol 16, pp 337-348, June 1971.

51. Ffowcs-Williams J.E. and Hawkings D.L. "Theory relating to the noise of rotating machinery", J. Sound. Vib., Vol 10, No 1, pp 10-21, 1969.

52. Sharland I.J. "Sources of noise in axial flow fans", J. Sound Vib., Vol 1, No. 3, pp 302-322, 1964.

53. Sears W.R. "Some aspects of non-stationary airfoil theory and its practical application", J. Aero. Sci., Vol 8, pp 104-108, 1940.

54. Lowson M.V., Whatmore A. and Whitfield C.E. "Source mechanisms for rotor n ise radiation", Loughborough University of Technology Rep. TT 7202, March 1972.

55. Bull M.K., Wilby J.F. and Blackman D.R. "Wall pressure fluctuations in boundary layer flow, and response of somple structures to random pressure fields", Southampton University Rep. AASU 2 43, July 1963.

56. Lighthill M.J. "Sound generated aerodynamically, Bakerian Lecture 1961", Proc. Roy. Soc. (London), A, Vol 267, pp 147-182, 1962.

57. Schoemer H.H. "Effects of pressure gradient on turbulent boundary layer wall pressure fluctuations", J. Acoust. Soc. Amer., Vol 42, 93-113, 1967.

58. Mugridge B.D. "Turbulent boundary layers and surface pressure fluctuations on two-dimensional aerofoils" J. Sound Vib. Vol 18, pp 475-486, October 1971.

59. Hickey D.H. "Some developments in noise reduction in ducted propellers and fans", pp 104-119, in Rep. FAA No. 69-1, January 1969.

60. Richards E.J. and Fahy F.J. "Turbulent boundary layer pressure fluctuation over two-dimensional surfaces and delta wings", pp 39-62, in "Acoustic fatigue in aero-space structures" Eds. W.J. Trapp and D.M. Forney, Syracuse University Press, 1965.

61. Barry B. and Moore C.J. "Subsonic fan noise", J. Sound Vib., Vol 17, pp 207-220, 1971.

62. Leverton J.W. "Noise of rotorcraft", Westland Aircraft, RP 365, March 1969.

63. Kramer M. "The aerodynamic profile as acoustic noise generator", J. Aero. Sci.. Vol 20, pp 280-282. 296, April 1953.

64. Tu B.J. "Experimental investigation of turbulent velocities in a sub-sonic circular jet", Wyle Laboratories WR 70-2, February 1970.

65. Widnall S.E. "A correlation of vortex noise data from helicopter main rotors", J. Aircraft, Vol 6, No 3, pp 279-281, May-June, 1969.

66. Brown D. and Ollerhead J.B. "Propeller noise at low tip speeds, US Air Force Aero Propulsion Laboratory, AFAPL-TR-71-55, 1971.

67. Davidson I.M. and Hargest T.G. "Helicopter noise", J. Roy. Aero. Soc., Vol 69, pp 235-336, May 1965.

68. Deming A.F. "Noise from propellers with symmetrical sections at zero blade angle" I NACA TN 605, 1937, II NACA TN 679, 1938.

69. Hawkings D.L. and Lowson M.V. "Theoretical investigation of supersonic rotor noise" Loughborough University of Technology, Ref TT 7213, December 1972.

70. Ffowcs-Williams J.E. and Hall L.H. "Aerodynamic sound due to a source near a half-plane", J. Fluid Mech., Vol 40, pp 657-670, 1970.

71. Heller H. and Widnall S.E. "The role of fluctuating forces in the generation of compressor noise, NASA CR 2012, 1972.

72. Jones J.P. "Rotor aerodynamics, retrospect and prospect", Paper I AGARD Adv. Rep. 13, September 1967.

73. Spencer R.H. et al "Tip vortex core thickening for application to helicopter noise reduction", Vertol Division, The Boeing Co., USA AVLABS Technical Report 66-1, September 1966.

74. Spivey W.A. and Morehouse "New insights in the design of swept tip rotor blades", 26th Forum of Am. Hel. Soc., 1970.

75. Arndt R.A. and Nagel B. "Effect of leading edge serrations on noise radiation from a model rotor", AIAA Paper, 72-655, 1972.

76. Leverton J.W. "The sound of rotorcraft", The Aeronautical Journal, Vol 75, pp 385-397, June 1971.

77. Leverton J.W. "Helicopter noise" in AGARD Conf. Proc. No. 31, June 1968.

78. Pollard J.S. and Leverton J.W. "Effect of blade tip planform on the noise and aerodynamics of a helicopter rotor", Westland Helicopters, RP 414, April 1972.

79. Maekawa Z. "Noise reduction by screens", App. Acoust. Vol 1, p 157, 1968.

80. Kinney W.A., Pierce A.D., and Ricklye E.J. "Helicopter noise experiments in an urban environment", J. Acoust. Soc. Amer., Vol 52, pt 1, p 1316, November 1972.

81. Tedrick R.N. "Propagation of low frequency sound near the earth's surface", J. Acoust. Soc. Amer. Vol 36, p 1991, 1964.

82. Mani R. "Diffusion of radiation patterns due to scattering by random inhomogeneities", J. Sound Vib., Vol 17, pp 95-104, 1971.

83. Evans L.B., Bass H.E. and Sutherland L.C., "Atmospheric absorption of sound: theoretical predictions" J. Acoustic Soc. Amer., Vol 51, pp 1565-1575, May 1972.

84. Bass H.E., Bauer H.J., and Evans L.B. "Atmospheric absorption of sound: analytical expressions", J. Acoust. Soc. Amer. Vol 52, pp 821-825, September 1972.

85. Ingard K.U. "On the reflection of a spherical sound wave from an infinite plane", J. Acoust. Soc. Amer., Vol 23, pp 546-549, 1951.

86. Hubbard H.H. and Maglieri D.J. "An investigation of some phenomena relating to aural detection of airplanes" NACA TN 4337, December 1958.

87. Faulkner H. "The cost of noise reduction of helicopters" M.I.T., FTL Rep R71-5, November 1971.

88. Ollerhead J.B. "Estimating community annoyance due to airport noise", Loughborough University of Technology, Rep. TT 7203, February 1972.

89. McLachlan N.W. "Bessel functions for engineers", 2nd ed., Oxford, Oxford University Press, 1961.

90. White R.P. and Balarak J.C. "The nemesis of the trailed tip vortex - is it now conquered?", A.H.S. Preprint 624, May 1972.

91. Ward J.F. and Young W.H. "A summary of current research in rotor unsteady aerodynamics with emphasis on work at Langley Research Center", Paper 10 in AGARD CPP111 "Aerodynamics of rotary wings", September 1972.

APPENDIX: SUPPLEMENTARY BIBLIOGRAPHY OF EARLIER WORK ON PROPELLER NOISE

1. Fage A. "An experimental study of the vibrations in the blades and shaft of an airscrew", Proc. Roy. Soc. A, Vol 107, pp 451-469, 1925.

2. Hart M.D. "The aeroplane as a source of sound", A.R.C. R & M 1310, May 1929.

3. Stowell E.L. and Deming A.F. "Noise from two-blade propellers", NACA TR 526, 1935.

4. Ernsthausen W. The source of propeller noise, NACA TM 825, May 1937.

5. London A. Principles, practice and progress of noise reduction in airplanes, NACA TN 748, January 1940.

6. Deming A.F. Propeller rotation noise due to torque and thrust, NACA TN 747, 1940.

7. Ernsthausen W. "Der Einfluss aerodynamisher Eigenshaften auf Schallfeld und Strahlungsleistung eine Luftschraube" Akustiche Zeit, pp 245-261, July 1941.

8. Shirokov M.F. The sound of a moving aeroplane propeller, Comptes Rendus Acad. Sci. URSS, Vol XLIX, No 8, 1945.

9. Theodorsen T. and Regier A.A. "The problem of noise reduction with reference to light airplanes", NACA TN 1145, 1946.

10. Fleming N. The silencing of aircraft, Journal of the Royal Aeronautical Soc., No. 50, 1946.

11. Stüper J. and Ginzel I. Airscrews, AVA Monographs H4.4-4.7, Reports and Translations 913, 1947.

12. Hubbard H.H. "Sound measurements for five shrouded propellers at static conditions", NACA TN 2024, April 1950.

13. Ernsthausen E.W. "Der rotierende Tragfluegel als Strahlungsproblem", Z.A.M.M., pp 20-35, January/February 1951.

14. Hubbard H.H. and Lassiter L.W. Sound from a two-blade propeller at supersonic tip speeds, NACA Report 1079, 1952.

15. Von Gierke H.E. Physical characteristics of aircraft noise sources, Journal of the Acoustical Society of America, Vol 25, No 3, May 1953.

16. Regier A.A. and Hubbard H.H. Status of research on propeller noise and its reduction, Journal of the Acoustical Society of America, Vol 25, No. 3, May 1953.

17. Arnoldi R.A. "Propeller noise at compressible forward flight velocities", United Aircraft Corp., M-12610-2, 1953.

18. Hubbard H.H. and Lassiter L.W. "Oscillating pressures near a static pusher propeller at tip Mach numbers up to 1.20 with special reference to the effects of the presence of the wing", NACA TN 3202, July 1954.

19. Diprose K.V. "Some propeller noise calculations showing the effect of thickness and planform", R.A.E. Tech. Note M.S. 19, January 1955.

20. Kurbjun M.C. "Noise survey of a 10-foot four-blade turbine-driven propeller under static conditions", NACA TN 3422, 1955.

21. Arnoldi R.A. "Propeller noise caused by blade thickness", United Aircraft Corp., Rep. R-0896-1 (see also Rep. R-0896-2), 1956.

22. Watkins C.E. and Durling B.J. "A method for calculation of free-space sound pressures near a propeller in flight, including considerations of the chordwise blade loading", NACA TN 3809, November 1956.

23. Kurbjun M.C. "Noise survey of a full-scale supersonic turbine-driven propeller under static conditions". NACA TN 4059, July 1957.

24. Dodd K.N. and Roper G.M. "A deuce programme for propeller noise calculations", R.A.E. TN M.S. 45, January 1958.

25. Kurbjun M.C. and Vogeley A.W. "Measurements of free-space oscillating pressures near propellers at flight Mach numbers to 0.72", NACA Rep. 1377, 1958.

26. Kurbjun M.C. "Noise survey under static conditions of a turbine driven transonic propeller with an advance ratio of 4.0", NASA Memo 4-18-592, May 1959.

PROBLEMES DE TRAINEE DES APPAREILS A VOILURES TOURNANTES

par

Paul FABRE

Divieion Hélicoptèree S.N.I.A.S

13 221 - MARSEILLE - Cédex 1

France

RESUME :

Bilan de trainée : part importante due à la trainée du rotor et aux trainéee parasitee.

Influence du décrochage et de la compreeeibilité eur la trainée du rotor

Diminution des trainéee paraeitee en caréanant par exemple la tête rotor

Limitatione en vol hélicoptères : moyens de lee retarder par le vol en aütogyre avec le ralentieeement de la vitesee de rotation du rotor.

NOTATIONS PRINCIPALES :

X Traction ou trainée du rotor, poeitive en trainée
Z Portance du rotor, poeitive vers le haut
W Puissance moteur
$N = W \frac{R}{U}$ couple moteur
U Vitesee périphérique du rotor
V Vitesee d'avancement
$\underline{X}$ Coefficient de traction = $100 \times / \frac{1}{2} \rho S \sigma U2$
$\underline{Z}$ Coefficient de portance = $100 Z / \frac{1}{2} \rho S \sigma U2$
$\underline{N}$ Coefficient de couple = $100 N / \frac{1}{2} \rho S \sigma R U2$

1 - INTRODUCTION :

Depuie un quart de eiècle ou l'hélicoptère eet entré en utilieation opérationnelle, on entend communément dire que celui-ci a atteint le plafond de eee poeeibilitée. On e'aperçoit pourtant que durant ce lape de temps lee performancee lee plus eignificativee, vitesee, altitude, distance franchieeable, n'ont ceeeé de progreeeer. Le record de viteeee n'eet-il pae paeé de 178 à 355 km/h en février 1970 avec le S 67 de Sikoreky; le record d'altitude de 6468 m à 12 440 mètree avec le Lama de l'Aéroepatiale en juin 1972 et le record de dietance franchieeable de 1132 km à 3600 km avec le Hughes OH6A en avril 1966 ? Cee records, battus généralement par dee appareile epécialement préparée en vue du record, traduieent plus lee poeeibilitée maximalee du moment que lee performancee courantee dee appareile en eervice. Toutefoie lee hélicoptèree actuels ont dee viteeeee maximalee en vol horizontal compriiee entre 270 et 320 km/h, dee plafonde pratiquee de l'ordre de 6000 mètree et franchieeent dee dietancee de 600 à 800 km et même plus. Cette amélioration dee performancee n'a pu s'obtenir que par une meilleure compréheneion du fonctionnement du rotor d'ou recul de eee limitatione, l'affinement général dee cellulee, une technologie améliorée conduieant à dee etructuree plus légèree et également l'avènement déjà ancien maintenant dee turbinee.

2 - BILAN DE PUISSANCE :

Pour un hélicoptère claeeique le bilan de puieeance en vol de palier etabilieé peut se décompoeer en puieeance coneommée par la trainée des palee, puissance pour vaincre lee différentes trainéee paraeitee, puiesance dépeneée par le rotor de queue pour aeeurer la fonction anticouple, puiesance pour annuler lee pertee duee aux frottemente de tranemieeion et puieeance induite due à l'effort propulsif du rotor lui-même. La figure 1 montre l'évolution de ces puiseances en fonction de la vitesse d'avancement. Lee deux grande consommateure de puieeance eont donc dus à la trainée dee pales et aux trainées paraeitee. A elles deux, elles repréeentent les 87 % de la puissance totale à une vitesee d'avancement de 300 km/h. Aux vitesees élevéee, c'eet donc eur cee deux poetes qu'il convient d'agir et qui ee partagent pratiquement moitié moitié au point de vue importance.

3 - TRAINEE DU ROTOR :

Avant de voir l'influence dee caractéristiquee aérodynamiquee dee profils eur la trainée du rotor en vol d'avancement, il eet intéreeeant d'analyeer le comportement d'un rotor de profile claeeiquee grâce aux résultats obtenus dane la grande Soufflerie de Modane-Avrieux de l'ONERA sur un rotor tripale. Celui-ci de 4 mètree de diamètre, à palee rectangulairee de 250 mm de corde et de vrillage théorique 8°, avait pour profil le claseique NACA 0012 qui équipe la plupart dee rotors actuele.Les réeultate fournie ne eont pae corrigée de l'effet des paroie, la théorie en veine circulaire n'étant pae suffieamment avancée. Il eemble toutefoie qu'avec un rotor dont le diamètre n'est que 50 % de celui de la veine, lee correctione eoient faiblee surtout aux paramètree d'avancement élevée. Par contre le moyeu relativement important conduit à dee correctione non négligeablee qui ont été déterminée grâce à dee peeées de celui-ci eane palee maie en rotation.

.../...

Les essais ont été effectués en fonction du pas pour différentes inclinaisons de l'arbre, le rotor ne comportant pas de plateau cyclique. Cette représentation, figure 2, n'est pas facilement exploitable en ce qui concerne l'analyse des traînées. Une représentation plus commode pour le calcul des performances élimine toutes références au pas et à l'inclinaison de l'arbre rotor, figure 3. Cependant pour une analyse de la traînée il est intéressant de retrancher de la puissance totale nécessaire pour assurer la portance et la traction, la puissance de traction ainsi que la puissance induite. Il ne reste donc ce cas que la puissance de profil

$$\bar{N}_o = \bar{N} + \Lambda \bar{X} - \frac{\sigma \bar{z}^2}{400 \Lambda}$$

en écrivant que la vitesse induite

$$v_i = \frac{Z}{2\rho S V} = \frac{\bar{z}\sigma}{400} \frac{U}{\Lambda}$$

$\bar{N}_o$ n'est autre que la part de puissance qui ne procure directement ni portance ni traction, c'est donc une approximation de l'énergie dégradée en chaleur et en bruit et c'est ce qui constitue la traînée parasite de la pale.

Nous avons tracé figure 4, l'influence du paramètre d'avancement sur les polaires de profil, puissance de profil portance, à traction nulle du rotor. On peut constater que pour une portance donnée, la puissance de profil augmente d'une façon régulière avec le paramètre d'avancement, qu'elle augmente tout d'abord peu avec l'augmentation de la portance du rotor puis rapidement dès que l'on atteint le début du décrochage du rotor. Par ailleurs le décrochage se produit d'autant plus vite que le paramètre d'avancement est plus élevé.

Figure 5, nous avons porté les polaires de profils pour différentes valeurs de la traction exercée par le rotor et pour le paramètre d'avancement de 0,4. A même portance, la différence de puissance de profil entre une traction donnée et la traction nulle, caractérise le rendement de propulsion du rotor. En première approximation on peut admettre que ce rendement de propulsion est voisin de 0,9 ce qui correspond à un très bon rendement d'hélice. On peut également se rendre compte que le décrochage du rotor arrive d'autant plus vite que la traction demandée au rotor est plus forte.

On peut donc espérer diminuer la puissance de profil du rotor en cherchant des profils qui aient une traînée plus faible, un Mach de traînée de divergence plus élevé et des Cz de décrochage plus grands que ceux du NACA 0012.

C'est ainsi que nous avons essayé en soufflerie transsonique bidimensionnelle trois sortes de profils (figure 6)

- Le NACA 0012 comme base de comparaison
- Un NACA 0012 à bord d'attaque cambré, calculé par l'ONERA et se rattachant à la famille des profils dits "peaky" pour améliorer le Mach de traînée de divergence et les Cz maximaux.
- Un profil de 11 % d'épaisseur relative de la famille NACA 0012 mais à rayon de bord d'attaque augmenté et à faible cambrure donnant un moment théorique au 1/4 de la corde nul, destiné à améliorer le Mach de traînée de divergence tout en ayant des Cz maximaux au moins aussi bons que ceux du NACA 0012.

Les maquettes de ces profils de même corde que la corde du rotor expérimental de 4 mètres furent essayées aux mêmes nombres de Reynolds et de Mach que les profils du rotor dans la Soufflerie S3 de Modane de l'ONERA également.

La figure 7 fournit les Cz maximaux en fonction du nombre de Mach, Comme on peut le voir, le NACA 0012 à bord d'attaque cambré est supérieur dans la plage correspondant aux Mach de pale reculante entre 0,3 et 0,4; au delà de Mach 0,6 le profil développé par l'Aérospatiale devient le meilleur. Par contre le NACA 0012 pur est le plus mauvais dans toute la plage des Mach.

La figure 8 donne pour les 3 profils également le Mach de traînée de divergence en fonction du Cz. Dans la plage utile, c'est à dire aux faibles Cz de fonctionnement, le profil développé par l'Aérospatiale est le meilleur. Il permet en effet d'atteindre un Mach de divergence de traînée à Cz faible de 0,83 contre 0,82 au NACA 0012 à bord d'attaque cambré et 0,78 au NACA 0012 pur.

A notre point de vue, le profil de l'Aérospatiale SA 13 109-1,58 présentait les avantages suivants :

- stabilité dynamique plus grande au voisinage de la portance nulle
- inversion des moments plus tardive
- divergence de traînée aux forts Mach reculés

Ce profil devait donc permettre un gain de performance dans la zone de la pale avançante. Par contre le NACA 0012 à bord d'attaque cambré ayant des Cz maximaux plus importants surtout aux faibles Mach, devait améliorer le fonctionnement du rotor lorsque celui-ci est en limitation par la pale reculante. Un des inconvénients de ce profil était, pour nous, son moment non négligeable au 1/4 de la corde.

Pour vérifier le bien fondé de ces résultats sur rotor, deux autres jeux de pales de mêmes caractéristiques géométriques mais de profils différents furent également essayés à S1 Modane. Un jeu avait pour profil le NACA 0012 à bord d'attaque cambré sur toute l'envergure de la pale et était destiné surtout à vérifier le recul du décrochage sur la pale reculante, l'autre jeu avait un profil évolutif le long de l'envergure de la pale ; NACA 0012 jusqu'à 0,7 R, le 11 % de l'Aérospatiale à 0,85 R et pour finir à un 6 % de même famille que le 11 % en extrémité de pale et était destiné avant tout à reculer les phénomènes de compressibilité.

La comparaison des polaires de profil des trois rotors est donnée figure 9 à traction nulle et pour le paramètre d'avancement de 0,3. On peut voir l'amélioration apportée par le NACA 0012 à bord d'attaque cambré sur le décrochage du rotor qui ne se fait sentir qu'à des portances plus élevées que pour les deux autres rotors. Par contre pour des portances en dessous de celles correspondant au décrochage, les trois rotors sont pratiquement équivalents. Le gain de puissance que l'on aurait pu attendre du rotor avec profils évolutifs ne se retrouve pas pour ce paramètre d'avancement. Il faut dire que l'on est à la limite de précision des mesures; en supposant en effet un gain de 0,003 sur la traînée entre le profil à 12 % et celui à 6 %, le gain sur la puissance de profil est de l'ordre de 0,03. Aux paramètres d'avancement plus élevés, 0,6 par exemple, le profil NACA 0012 à bord d'attaque cambré perd tout intérêt comme on peut le voir figure 10. D'une façon générale l'extension du bord d'attaque recule le décrochage en pale reculante et améliore la manoeuvrabilité aux basses vitesses jusqu'à des paramètres d'avancement de l'ordre de 0,4 ; au delà il perd tout intérêt.

.../...

Par contre on retrouve bien un net recul de l'influence de la compressibilité en utilisant des profils évolutifs à faible épaisseur en bout de pale. Nous avons peu de résultats aux grands Mach sur le rotor avec profils NACA 0012 car les vibrations étaient trop fortes pour aborder le domaine décroché.

La figure 11 montre cependant cette influence au paramètre d'avancement de 0,5 pour les rotors à profils NACA 0012 et à profils évolutifs. On peut voir :

- que le rotor à profils évolutifs décroche plus tard que le rotor à profil NACA 0012 ; environ $\Delta \overline{Z} = 1$ à égalité de Mach
- qu'alors que l'influence de la compressibilité commence à Mach 0,85 pour le rotor à profil NACA 0012, elle ne se fait sentir qu'à partir de Mach 0,92 - 0,94 pour le rotor à profils évolutifs.

D'une façon générale il faut dire toutefois que quelque soit le paramètre d'avancement et le rotor considéré, la compressibilité abaisse la portance d'apparition du décrochage.

Pour fixer les idées sur l'importance de la compressibilité, un rotor de 15 mètres de diamètre de plénitude 0,1 et ayant 210 m/s comme vitesse périphérique, ne serait pas pénalisé à un paramètre d'avancement de 0,5 et un Mach en extrémité de pale avançante de 0,91 - 0,92 avec des profils évolutifs tels que ceux essayés, tandis qu'avec profil NACA 0012 constant sur toute l'envergure il serait pénalisé d'une centaine de kilowatts par la compressibilité. A Mach 0,94 le rotor à profils évolutifs ne serait pénalisé que de 35 KW contre 280KW pour le rotor à profil NACA 0012.

D'après ces essais, on voit que l'on peut reculer les phénomènes de compressibilité en adaptant le profil aux Mach et Cz locaux tout le long de l'envergure de la pale, de même on peut dans un certain domaine reculer également les phénomènes de décrochage en jouant sur les profils. On ne peut par contre espérer gagner énormément dans la plage où ces phénomènes n'interviennent pas.

4 - TRAINEES PARASITES :

L'autre partie importante de la puissance nécessaire au vol d'avancement provient des traînées parasites. La figure 12 montre l'évolution avec le tonnage des traînées parasites pour les hélicoptères et les avions. D'une façon générale la traînée des différentes catégories d'appareils varie moins rapidement que leur masse. Il est cependant intéressant de voir comment se décompose cette traînée parasite pour les hélicoptères. Le tableau ci-dessous donne cette décomposition en % de la traînée parasite totale.

Appareil	Gazelle SA 341	Puma SA 330
Fuselage et protubérances	21	39
Empennages et tête rotor arrière	7	6
.Train ou carénage	23	6
Carénage BTP et moteur	9	19
.Tête rotor	40	30

La traînée relative du fuselage augmente avec le tonnage de l'appareil ; par contre celle de la tête rotor diminue avec celui-ci. Si l'on considère la traînée de la tête rotor et des carénages BTP et moteur et en ramenant arbitrairement la traînée de train à la valeur arbitraire de 6 % on trouve :

Pour la Gazelle près de 60 %
le Puma près de 50 %
le CH 53 près de 45 % *

On voit l'importance que peuvent avoir tête rotor, carénages BTP et leurs intéractions réciproques sur la traînée parasite totale. Des essais en Soufflerie ont été entrepris à l'Aérospatiale sur une maquette partielle pour chiffrer le gain qu'apporterait un carénage de ces parties (figure 13). En hélicoptère nous en sommes arrivés à caréner par un ellipsoïde la tête rotor, ellipsoïde s'étendant jusqu'à la partie profilée des pales. De nombreux essais ont montré qu'il était fort difficile de diminuer la traînée d'une tête rotor d'hélicoptère en carénant au plus près la tête rotor par un ellipsoïde et en carénant par des manchettes la partie non profilée des pales. La variation d'incidence entre pale avançante et pale reculante sectelle en fonctionnement hélicoptère du fait du pas général important et de l'inclinaison de la tête rotor sur le vent que l'on ne peut trouver une forme de carénage qui ne décroche pas, attaqué qu'il soit par l'avant ou par l'arrière. Par contre on peut concevoir un tel carénage pour un fonctionnement en autogyre déchargé par une voilure ou la tête rotor est pratiquement dans le lit du vent et ou le pas général est très faible. Dans le cas de l'hélicoptère on trouve que caréner seulement la tête rotor n'apportait aucune amélioration sensible sur la traînée, ne caréner que la partie en dessous de la tête rotor n'apportait qu'une amélioration de l'ordre de 20 % et caréner le tout apportait un gain de l'ordre de 35 %. Un carénage identique mais encore amélioré fut monté sur la Gazelle lors de son record de vitesse (figure 14). Les gains totaux obtenus en soufflerie en affinant également le train furent confirmés par le vol, de l'ordre de 0,36 m2 soit près de 40 % de diminution des traînées parasites.

* AGARD : Recent developments in circulation control rotor technology by Robert M. Williams, September 1972.

.../...

5 - CONCLUSION :

On peut affirmer d'après les essais en Soufflerie sur rotor effectués à l'ONERA à Modane, que des hélicoptères pourraient voler actuellement à un peu plus de 400 km/h en palier etabilieé. Mais les puissances pour atteindre ce but sont telles que l'on ne réaliserait finalement qu'un hélicoptère de pur record sans utilité pratique. Par contre ces mêmes essais ont montré que pour un rotor au voisinage de l'autorotation, le polaire rotorique était pratiquement indépendant du paramètre d'avancement (figure 15). En conséquence portance et trainés d'un rotor ne dépendent dans ce cas de fonctionnement que de la vitesse de rotation ou de la vitesse en extrémité de pale. Ceci est fort intéressant pour le vol en autogyre avec voilure auxiliaire ou le rotor est déchargé de sa fonction de traction et également d'une grosse partie de sa fonction de portance. Comme on n'est plus limité par les phénomènes de décrochage sur pale reculante, on minimise d'autant la trainés du rotor que l'on diminue sa vitesse en bout de pale. Deux tendances à l'heure actuelle pour le réalisser, soit diminuer la vitesse de rotation du rotor, soit retracter le rotor lui-même. En poussant à l'extrême dans cette voie on en arrive à escamoter le rotor. Mais en restant dans le domaine exploré et encore avec un rotor dont le vrillage n'était pas spécialement adapté pour le fonctionnement en autorotation, puisqu'il était de 8°, autrement dit en fonctionnant à un paramètre d'avancement de 0,87 et sans dépasser un Mach de 0,92 un calcul rapide montre que l'on peut atteindre des vitesses de plus de 500 km/h par simple réduction de la vitesse du rotor sans grosses difficultés techniques.

Fig.1 - PUISSANCE NECESSAIRE EN VOL HORIZONTAL

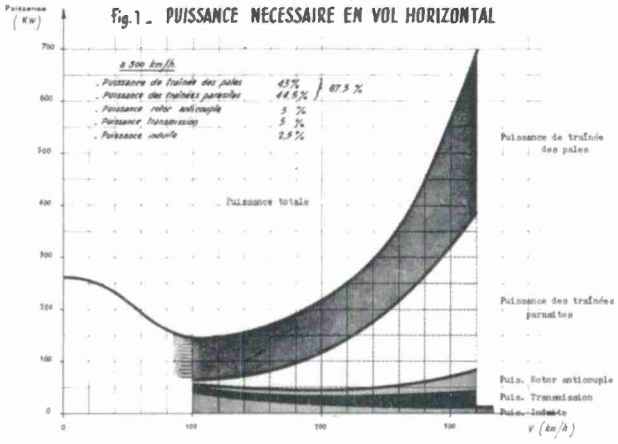


Fig 2 DONNEES DE SOUFFLERIE Λ=0.4 M=0.835

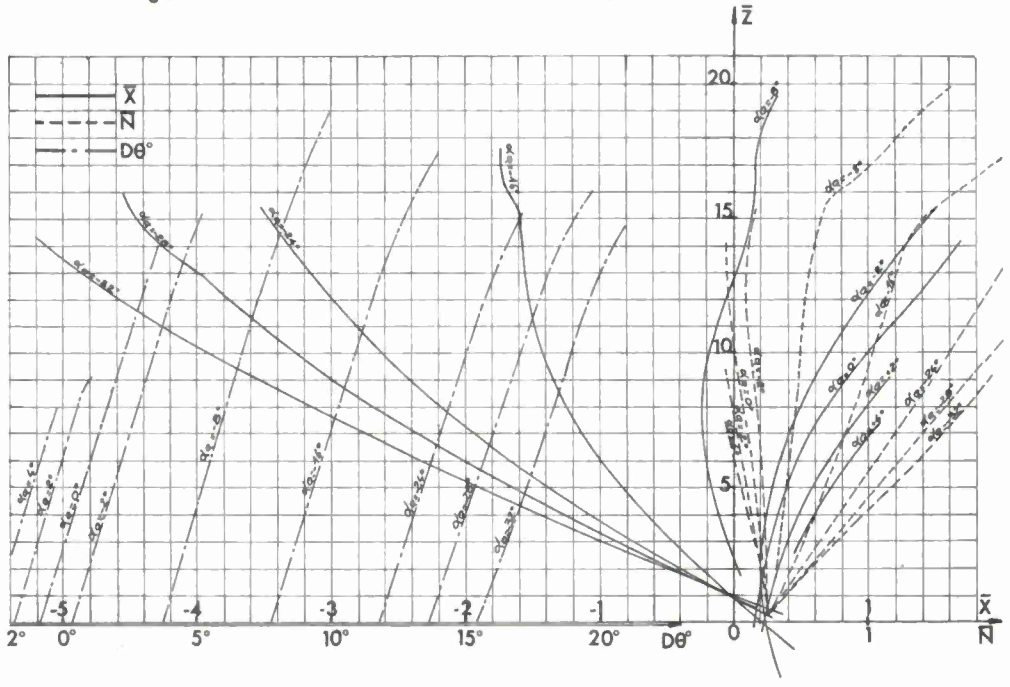


Fig3 POLAIRES INTRINSEQUES Λ=0.40 M=0.835

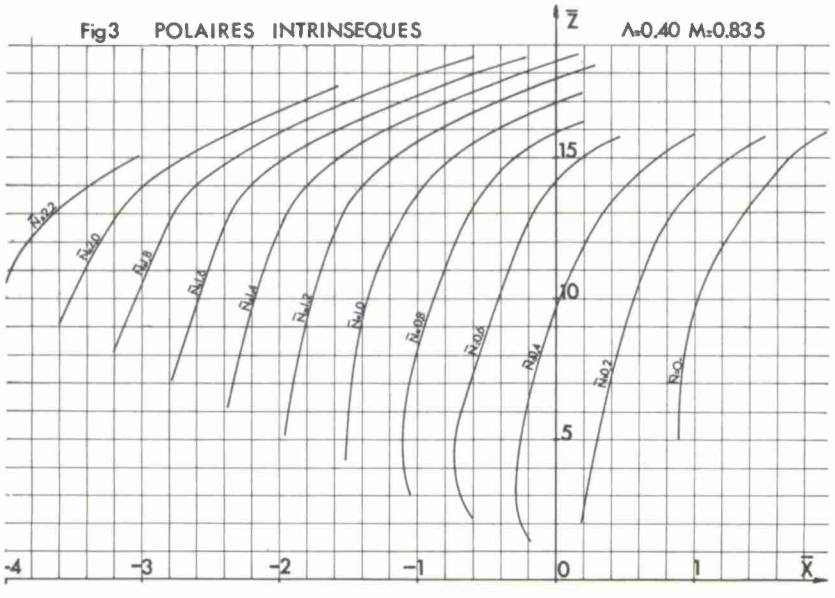


Fig12 INFLUENCE DES TRAINEES SUR LE TONNAGE

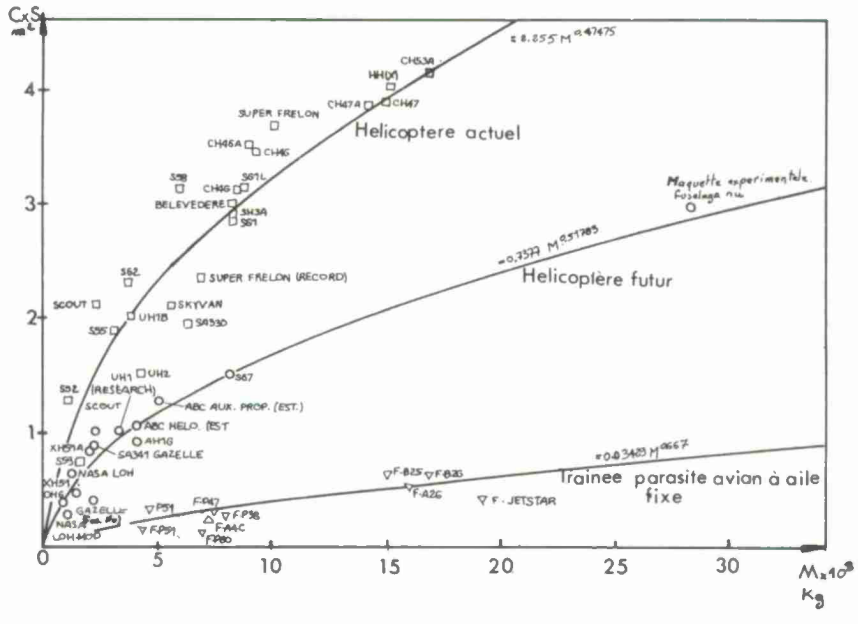


Fig. 13. INFLUENCE du CARENAGE de la TETE ROTOR

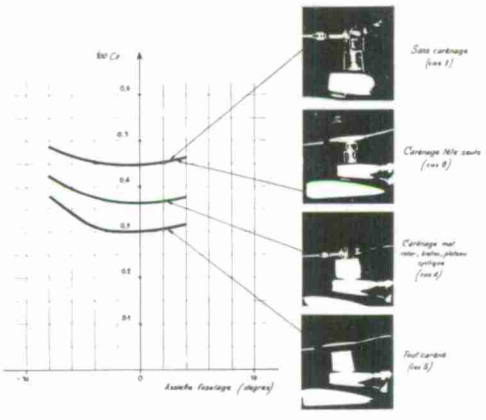
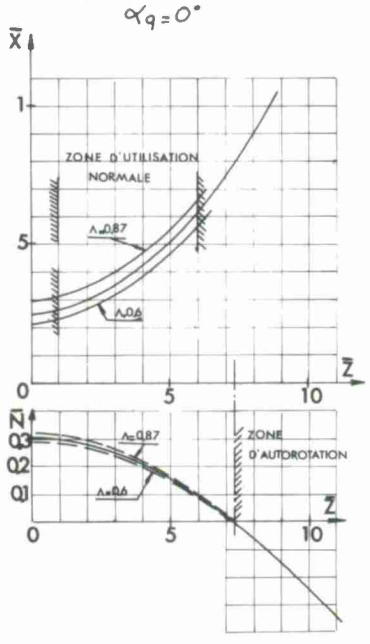




Fig 14 GAZELLE RECORD

Fig 15 INFLUENCE DE Λ SUR LA POLAIRE ROTORIQUE EN AUTOROTATION

$\alpha_q = 0°$



DRAG PROBLEMS ON ROTARY WING AIRCRAFT

by

Paul FABRE

Division Hélicoptères S.N.I.A.S.
13221 - MARSEILLE - Cédex 1
France

(English Translation of Original French Text)

ABSTRACT:

Drag analysis: considerable part due to rotor drag and parasite drags.

Influence of stall and compressibility on rotor drag.

Reduction of parasite drag, by fairing the rotor head, for example.

Helicopter in-flight limitations: means for delaying them by flight in autogyro configuration, with reduction of rotor rotational speed.

MAIN NOTATIONS:

X	Rotor thrust or drag, positive in the case of drag.
Z	Rotor lift, positive upwards.
W	Engine power.
$N = W \frac{R}{U}$	Engine torque.
U	Circumferencial speed of rotor.
V	Forward flight speed.
$\underline{X}$	Thrust coefficient = $100\ X / \frac{1}{2} \rho S \sigma U^2$
$\underline{Z}$	Lift coefficient = $100\ Z / \frac{1}{2} \rho S \sigma U^2$
$\underline{N}$	Torque coefficient = $100\ N / \frac{1}{2} \rho S \sigma R U^2$

1 - INTRODUCTION:

Helicopters became operational a quarter of a century ago and, since that time, one has kept repeating that they had reached their maximum capabilities. However, their most significant performance characteristics - speed, altitude, range - have never ceased to progress. The speed record was increased from 178 to 355 km/hr in February 1970, with the Sikorsky S 67; the altitude record, which was previously 6468 m, reached 12,440 m. with the Aerospatiale "Lama" in June 1972; the range record rose from 1132 to 3600 km. with the Hughes "OH6A" in April 1966. Evidently, such records, usually broken by aircraft especially prepared for the record attempt, reflect the maximum capabilities of the moment rather than the common performance of aircraft in service. However, the maximum level flight speeds of present helicopters range from 270 to 320 km/hr; their service ceiling is of the order of 6000 m, and their ranges reach - and sometimes exceed - 600 to 800 km. Such performance improvements could only be achieved through a better understanding of the operation of the rotor, hence higher limits, a general refining of the airframe, improved technology leading to lighter structures, and the advent of turbines, which already dates back to some time ago.

2 - POWER ANALYSIS:

In the case of a conventional helicopter, the stabilized level flight power can be broken down into: the power absorbed by blade drag; the power required to counteract the various parasite drags; the power absorbed by the tail rotor to ensure the anti-torque function; the power required to cancel the losses resulting from drive frictions, and the induced power due to the propulsive force of the rotor itself. Figure 1 shows the variation of these powers versus forward speed. Therefore, the major power consuming factors are the blade drag and parasite drags. They amount to 87% of the total power for a forward speed of 300 km/hr. At high speeds, it is therefore these two factors which have to be controlled; their practical importance is approximately similar.

3 - ROTOR DRAG:

Prior to considering the influence of the aerodynamic characteristics of the profiles on rotor drag in forward flight, it is interesting to analyze the behaviour of a rotor with a conventional profile, on the basis of the results provided by tests carried out on a three-bladed rotor in the large ONERA wind-tunnel, at Modane-Avrieux. This 4 m. diameter rotor had rectangular 250 mm. chord blades, a theoretical twist of 8° and

the conventional NACA 0012 profile, which is to be found on most present rotors. Wall corrections were not made, as the circular test section theory has not yet reached a sufficiently advanced stage. However, it seems that, in the case of a rotor whose diameter is only 50% of the test section diameter, such corrections should be small, especially for high tip speed ratios. On the other hand, the relatively large hub necessitates non negligible corrections which were determined by weighing this hub without the blades, but in rotation.

Tests were conducted as a function of the pitch, for various shaft tilts as the rotor did not include a swash plate. This representation, which is shown on Figure 2, is not easily utilizable in drag analysis. A representation better suited to performance computation rules out any reference to pitch and rotor shaft tilt (Figure 3). However, for drag analysis purposes, it is advantageous to deduct the thrust power as well as the induced power from the total power necessary to provide lift and thrust. In this case, only the profile power remains:

$$\overline{N_0} = \overline{N} + \lambda \overline{X} - \frac{\sigma \overline{Z}^2}{400 \lambda}$$

by writing that the induced speed

$$v_i = \frac{Z}{2 \rho S V} = \frac{Z \sigma}{400} \frac{U}{\lambda}$$

$\overline{N_0}$ is the fraction of the power which does not provide directly lift or thrust; therefore, it is an approximation of the energy dissipated into heat and noise, and makes up the parasite drag of the blade.

Figure 4 shows the influence of the tip speed ratio on the profile polars, profile power and lift, for a rotor thrust equal to zero. It can be noted that, for a given lift, the profile power rises regularly with the tip speed ratio; to start with, it grows very slightly as the rotor lift increases; then, it increases rapidly as soon as the early stall phase of the rotor is reached. On the other hand, stall takes place all the more rapidly as the tip speed ratio is higher.

On Figure 5, the profile polars have been plotted for various values of the thrust generated by the rotor, and for a tip speed ratio of 0,4. For an identical lift, the profile power difference between a given thrust and zero thrust characterizes the propulsive efficiency of the rotor. As a first approximation, it can be assumed that the propulsive efficiency is close to 0,9, which reflects a very satisfactory propeller efficiency. It is also obvious that the rotor stall occurs all the more rapidly as the thrust required from the rotor is higher.

Therefore, one can hope that the rotor profile power can be reduced through the design of profiles with a lower drag, a higher divergence drag Mach number, and stall lift coefficient (Cz) higher than those of the NACA 0012 profile.

On the basis of these conclusions, three sorts of profiles were tested in a transonic two-dimensional wind-tunnel (Figure 6):-

- The NACA 0012, as a reference basis.
- A NACA 0012 with a cambered leading edge, designed by ONERA and belonging to the so-called "peaky" profile family, to improve the divergence drag Mach number and the maximum lift coefficient (Cz).
- A 11% relative thickness profile, belonging to the NACA 0012 family, but with an increased leading edge radius and a small camber, yielding a zero theoretical moment at $1/4$ of the chord, and designed to improve the divergence drag Mach number while achieving maximum lift coefficient (Cz) at least as good as those of the NACA 0012.

The models of these profiles, whose chord is the same as the chord of the experimental 4 m. rotor, were tested at the same Reynolds and Mach numbers as the rotor profiles in the ONERA S3 wind-tunnel, at Modane.

Figure 7 gives the maximum lift coefficient (Cz) versus the Mach number. From this Figure, it is evident that the cambered leading edge NACA 0012 is preferable within the range corresponding to a retreating blade Mach number of 0,3 to 0,4; beyond Mach 0.6, the profile developed by "Aérospatiale" becomes more efficient. On the other hand, for the whole range of Mach numbers, the unmodified NACA 0012 is the worst.

For the three profiles, Figure 8 gives also the divergence drag Mach number versus the lift coefficient (Cz). Within the useful range, that is to say at low operational lift coefficients, the profile developed by "Aérospatiale" is the best, as it makes it possible to achieve a divergence drag Mach number of 0.83, at low lift coefficient whereas the corresponding value is 0.82 for the cambered leading edge NACA 0012, and 0,78 for the unmodified NACA 0012.

In our opinion, the profile of the "Aérospatiale" SA 13 109-1,58 offered the following advantages:

- higher dynamic stability in the vicinity of zero lift.

- delayed inversion of moments.
- delayed divergence drag at high Mach numbers.

Therefore, a performance gain should be achieved through the use of this profile in the advancing blade zone. However, as the cambered leading edge NACA 0012 permits achieving higher maximum lift coefficients, especially at low Mach numbers, it should improve the operation of the rotor when the latter is subject to a limitation imposed by the retreating blade. From our viewpoint, one of the drawbacks of this profile was its non negligible moment at $^1/_4$ of the chord.

In order to establish the value of these rotor test results, two more blade sets offering the same geometric characteristics but different profiles were also tested in the S1 Modane wind-tunnel. The profile of one of the sets was the NACA 0012, with a leading edge cambered along the whole span of the blade; this set was especially intended to check the delay of the stall on the retreating blade. The other set had an evolutive profile along the span of the blade; NACA 0012 up to 0.7 R, the 11% profile of the "Aérospatiale" at 0.85 R and finally a 6% profile of the same family as the 11% profile at the blade tip; it was essentially designed to delay compressibility phenomena.

A comparison of the profile polars of the three rotors is given in Figure 9 for a zero thrust and for a tip speed ratio of 0,3. It clearly reveals the improvement brought by the cambered leading edge NACA 0012 as regards rotor stall which is only felt at higher lift values than in the case of the other two rotors. However, for lift values below those corresponding to stall, the three rotors are practically equivalent. The power gain which might have been expected from the evolutive profile rotor is not achieved for this tip speed ratio. It should be stated that the limit of accuracy of the measurements has been reached; in fact, if we assume that the 12% profile permits a drag reduction of 0,003 over the 6% profile, the profile power gain is of the order of 0,03. At higher tip speed ratios, such as 0,6, for example, the cambered leading edge NACA 0012 profile loses its interest, as demonstrated by Figure 10. Generally speaking, the extension of the leading edge delays the stall of the retreating blade and improves manoeuvrability at low speeds up to a tip speed ratio of about 0,4; beyond this value, it is no longer advantageous.

However, we observe a marked reduction of the influence of compressibility when we use evolutive profiles with thin blade tips. Few results on the NACA 0012 profile are available at high Mach numbers, as vibrations were too intense to approach the stalled condition envelope.

Nevertheless, Figure 11 reveals this influence for a 0,5 tip speed ratio for rotors with NACA 0012 and evolutive profiles. We can note:

- that the stall of the evolutive profile takes place later than in the case of the NACA 0012 profile; approximately $\Delta\overline{\nabla} = 1$ for the same Mach number.
- that, while the influence of compressibility begins to be felt at Mach 0,85 for the NACA 0012 profile, it is not felt until Mach 0,92 - 0,94 in the case of the evolutive profile.

As a general rule, it should be stated that, whatever be the tip speed ratio and the rotor considered, compressibility decreases the lift value at which the stall occurs.

To clarify the importance of compressibility, a 15 m. diameter rotor having a solidity ratio of 0,1 and blade tip speed of 210 m/s would not be subjected to a penalty for a 0,5 tip speed ratio and a Mach number of 0,91 - 0,92 at the advancing blade tip if using evolutive profiles like those tested, whereas, with a NACA 0012 profile constant along the whole span, it would be subjected to a penalty of a hundred of kilowatts due to compressibility effects. At Mach 0,94, the penalty on the evolutive profile rotor would be 35 kilowatts only, whereas it is 280 kilowatts for the NACA 0012 profile rotor.

According to these text results, compressibility phenomena can be differed by adapting the profile to the local Mach numbers and lift coefficients along the whole blade span; stall phenomena can also be delayed, within a given range, through profile modifications. However, no considerable gain can be anticipated within the range where such phenomena do not take place.

4 - PARASITE DRAGS:

The other considerable fraction of the power necessary to forward flight is absorbed by parasite drags. Figure 12 shows the variation of parasite drags with the size, for helicopters and fixed-wing aircraft. Generally speaking, the drag of the various categories of aircraft varies less rapidly than their weight. However, it is interesting to consider how this parasite drag is broken down in the case of helicopters. This breakdown, in % of the overall parasite drag, is given in the following table.

Aircraft	"Gazelle" SA 341	"Puma" SA 330
Fuselage and prominences	21	39
Tail unit and tail rotor head	7	6
Landing gear or fairing	23	6
Main gear box and engine fairing	9	19
Rotor head	40	30

The relative fuselage drag increases with the size of the aircraft; on the other hand, the rotor head drag decreases with the latter. If we consider the drag of the rotor head, main gear box and engine fairings, and if we take arbitrary the landing gear drag as being 6%, we find:

For the "Gazelle" : nearly 60%
For the "Puma" : nearly 50%
For the "CH 53" : nearly 45%*

This demonstrates the possible importance of the rotor head and the main gear box fairings and their mutual interaction on the overall parasite drag. Wind-tunnel tests were undertaken at "Aérospatiale" on a model to evaluate quantitatively the gain which could be achieved through fairing these components (Figure 13). As far as helicopters are concerned, we have been led to fairing the rotor by means of an ellipsoid which extends as far as the streamlined section of the blades. Many tests have demonstrated that it is extremely difficult to reduce the drag of a helicopter rotor head by shrouding the latter with a closely fitting fairing, and by surrounding with cuffs the non-streamlined section of the blades. Due to the considerable collective pitch and to the rotor head tilt into the wind, the incidence variation between the advancing and the retreating blade is such, as far as helicopter operation is concerned, that it is impossible to design a fairing shape which does not stall, whether it is attacked from the front or the rear. However, such a fairing can be designed for the operation in the autogyro mode relieved by a wing unit, with the rotor head practically in the wind's eye and a very low collective pitch. In the case of helicopters, it is believed that fairing the rotor head only, brings no marked improvement as far as the drag is concerned; fairing the components located below the rotor head brings only an improvement of the order of 20%; and a complete fairing results in a gain of the order of 35%. An identical, but still improved fairing was mounted on the "Gazelle" when it broke its speed record (Figure 14). The overall gains obtained in wind-tunnels through an improved design of the landing gear were confirmed in flight: approximately $0.36m^2$, that is to say nearly a 40% reduction of parasite drags.

5 - CONCLUSION:

On the basis of the results of rotor tests carried out in the ONERA Modane wind-tunnel, it can be stated that some helicopters could now fly at a speed slightly exceeding 400 km/hr, in stabilized level flight. However, the power required to reach this objective is such that, finally, only a helicopter without any practical utility, merely designed for breaking records, could be developed. Nevertheless, these tests demonstrated that, for a rotor, near the autorotation r.p.m., the rotor polar is practically independent of the tip speed ratio (Figure 15). Consequently, for this type of operation, the lift and drag of a rotor depend only on the rotational speed or on the blade-tip speed. This is extremely interesting for flight in the autogyro mode with an auxiliary wing relieving the rotor from its thrust function, as well as of a large part of its lift function. As one is no longer limited by the stall phenomena of the retreating blade, the rotor drag is minimized to the same extent as its blade tip speed is reduced. There are, at present, two trends to reach this target: either reduce the rotational speed of the rotor, or draw in the rotor proper. In carrying this trend to the extreme, one is led to retract completely the rotor. However, while remaining in an explored field, and even using a rotor having a twist not especially suited to operation in auto-rotation, since it is 8°, or, in other words, operating at a tip speed ratio of 0,87 and without exceeding Mach 0,92, quick calculations show that speeds exceeding 500 km/hr. can be reached, merely by reducing the rotor speed, without great technical difficulty.

* AGARD : "Recent Developments in Circulation Control Rotor Technology" by Robert M. Williams, September 1972.

AERODYNAMIC AND DYNAMIC ROTARY WING MODEL TESTING IN WIND TUNNELS AND OTHER FACILITIES

By
FRANKLIN D. HARRIS, MANAGER, BOEING V/STOL WIND TUNNEL
THE BOEING VERTOL COMPANY, PHILADELPHIA, PA. 19142

SUMMARY

While fundamental aerodynamic experimentation using the wind tunnel led the airplane's evolution, both the autogyro and the helicopter evolved by the sheer tenancity of mechanically inclined inventors. For example, considerably more fundamental, non-flight experimentation would have helped Cierva in developing the autogyro. His first, second, and third full-scale prototypes had rigid, fixed pitch blades and upon takeoff were rolled over by the assymetrical lift. Cierva finally solved the problem using rubber band powered model autogyros. His fourth full-scale prototype used an articulated blade attachment concept and flew successfully. The goal of today's experimenter is to do the fundamental and configuration testing that at least ensures that our rotary wing progress is not marred by such an oversight as Cierva made. Stated most simply, today's rotary wing experimenters' goal is "TRY BEFORE YOU FLY."

Major rotary wing experimental facilities and models all simulate full-scale flight in one or the other of two ways suggested by John Smeaton in 1759. Three notable facilities that "cause the machine to move against the air" are the NASA-Langley Control Line Facility, the Cornell University CART, and the Princeton University Dynamic Model Track. These facilities are used primarily for flying qualities study in hover and transition flight. The wind tunnel which "causes the air to move against the machine" was developed in 1871. Today the NASA-Ames 40' X 80', 200 knot wind tunnel and the ONERA S1MA 26' diameter, transonic tunnel provide the maximum rotary wing testing envelope. Wind tunnels providing variable density and/or pressure or use water or Freon as the test fluid are available. Two approaches to the scaling of models for any of these facilities appear to be evolving. The first approach studies primarily rotor blade loads, noise and aircraft performance. The model in this approach has aeroelastically scaled, full-scale tip speed blades, a geometrically scaled hub, and a fuselage shell that geometrically simulates the airframe. These Mach-scaled models when tested in an air wind tunnel are high-powered and heavily loaded. The second approach to rotary wing modeling is evolving from Froude-scaling techniques commonly used in airplane flutter models and ensures that deflections due to gravity are geometrically scaled. In the Froude-scale approach, the model tip speed is reduced from the full-scale by the square root of the scale factor so that dynamic system stresses, rotor system stresses and power requirements are substantially reduced. The resulting Froude-scaled models achieve scaled inertia and weight which permits free and semi-free flight testing necessary to aeroelastic stability and flying qualities studies. The testing of Froude-scaled models in a Freon wind tunnel at reduced pressure can regain the Mach number simulation lost when the reduced tip speed model is tested in an air wind tunnel. Virtually every member of the NATO rotary wing community has developed rotor models. This combined effort is showing that rotor models, though very much more sophisticated than typical fixed wing models, can reliably provide enormous experimental insight and substantially lower the risks in full-scale prototype development. Today's successful contribution of rotor models can be made substantially more effective in the future by (1) improving and creatively using the structural dynamic data acquisition, reduction and presentation system, and (2) by more thorough preparation of the model prior to test.

The question of model/facility size and cost has become increasingly important because reliable test results at low speed/high lift are as needed as test results at high speed. In the transition region, data is influenced by the facility enclosure and reliably translating these model test results to appropriate full-scale data is, today, done only approximately. Even considering both the upwash flow about the model due to the flow interference of the wind tunnel test section and the recirculation of the rotor wake back through the rotor after it impinges on the floor, the testing of rotor models down to advance ratio of .08 and up to thrust coefficient of .015 should still be conducted regardless of the ratio of model size to facility size. Informative results, even when the model lifting system spans 2/3 to 3/4 of the wind tunnel test section width, will still be obtained. The current understanding of rotor stall and limited analysis of Reynolds number effects on rotor stall suggest that simulating this model scaling parameter costs too much for the reduction in technical risks it might provide. The trend of model cost with model size indicates that costs are reduced by roughly the scale factor squared reaching a minimum at 1/15 size for Mach-scaled models and 1/40 size for Froude-scaled, two degree of freedom models. Small models that simulate (1) advance ratio, (2) aeroelasticity, and (3) Mach number and are tested in present facilities provide the most cost-effective, risk reducing contribution the rotary wing experimenting community can make today. For the future, consideration can be given to (1) medium size models tested in a new, larger Freon wind tunnel which would achieve the complete full-scale simulation desired during the preliminary design phase and (2) full-scale vehicle testing in a new, very large wind tunnel.

Successful rotary wing testing with sophisticated powered models depends heavily on the experimenter being knowledgeable enough to ask the key searching questions and knowledgeable enough to concisely display the answers. With that knowledge in hand, the rotary wing experimenting community is capable today of interfacing the experimenter with the model through a remote control system and an on-line data system. This close interface, used in an approach where the experimenter "interrogates" the model with direct questions and "flys" the model to find the answers, can produce 90 percent of the test results in 10 percent of the time.

1.0 OVERVIEW OF EXPERIMENTING

It is particularly appropriate to start this paper on rotary wind model testing by recounting the monumental role that experimentation historically played in the achievement of powered flight. The first wind tunnel, I am convinced, was the key to the successful experimenting that resulted in powered flight. And, interestingly, all of today's goals and reasons for testing can be found in the words of the early experimenters. In this overview section of the lecture, I want you to see again the lessons learned from history, to appreciate the major goal of the experimenter, and to broadly review the many reasons for testing.

1.1 HISTORY

While it can be said that no scientific paper can ignore the countless hypotheses of the Greek philosopher Aristotle or the secretative notebooks and inventive genius of the Italian daVinci, historians[1] agree that Galileo performed the first aerodynamic experiment when he dropped various objects from the top of the Tower of Pisa to find their resistances. He concluded that this resistance or drag varied directly as the velocity, a rather accurate statement in the low velocity range of the experiment and for the year 1590. This creative aerodynamic research initiated by Galileo was moved ahead by tentative, chancy, inspired steps taken by many men over many years. The steps culminated in a successful powered airplane flight in 1903, a successful autogyro flight in 1923, and the demonstration of a practical single rotor helicopter in 1941.

There can be no more enjoyable or informative history of the pioneering instruments used in aerodynamic research than that found in the paper given by J. Laurence Pritchard entitled "The Dawn of Aerodynamics.[2]" In Figure 1, I have cronologically graphed the early accomplishments Pritchard so eloquently describes in his paper. It took us 2100 years to reach our first controlled aerodynamic experiment, as Figure 1 so clearly shows. This period starts with the birth of Aristotle in 389 BC and ends with Benjamin Robins' description to the Royal Society of the first whirling arm test rig in 1746 AD. In another 125 years, we had the first wind tunnel which was described by the Aeronautical Society of Great Britain in its Annual Report for 1871. And in 32 more years, controlled power flight was demonstrated by the Wright Brothers.

In tracing these origins of today's aerodynamic efforts as illustrated by Figure 1, I have concluded that aeronautical progress has been paced more by our experimental successes (and failures) than perhaps all our theoretical efforts put together. While this conclusion is supported by nearly all of the early experimenters (as Mr. Pritchard's paper so delightfully relates) one statement, by the Aeronautical Society of Great Britain in 1870, deserves to be quoted again here:

> "The first great aim of the Society is the connecting of the velocity of the air with its pressure on plane surfaces at various inclinations. There seems no prospect of obtaining this relation otherwise than by a careful series of experiments. But little can be expected from the mathematical theory; it is a hundred and forty years since the general differential equations of fluid motion were given to the world by d'Alembert; but although many of the greatest mathematicians have attempted to adduce from them results of practical value, it cannot be said that any great success has attended their efforts. The progress made has been very slight in the case of water, where the analysis is much simpler than for an elastic fluid like air; and the theory of resistance, which is part of hydromechanics which has most direct bearing on aerial navigation is, perhaps, the part of the subject about which least is known."

The intensive aerodynamic research permitted after the wind tunnel became available in 1871 clearly accelerated our progress towards powered airplane flight as Figure 1 suggests. In stark contrast, the aerodynamic experimentation leading to both the autogyro and the helicopter was miniscule in comparison,as any literature search will show. It appears that fundamental aerodynamic experimentation accompanied prototype configurations in our development of the airplane, but both autogyro and helicopter configurations evolved by the sheer tenancity of mechanically inclined inventors. It could be argued that the airplane relies most heavily on aerodynamics and the autogyro/helicopter on the structural, dynamic, mechanical disciplines. However, considerably more fundamental experimentation would have helped Cierva (as an example) in developing the autogyro. Cierva did use a wind tunnel to determine that a rotor in horizontal flight would produce lift,[3] but his first, second, and third full-scale autogyros had rigid, fixed pitch blades and upon take-off, were rolled over by the assymetrical lift. Cierva finally solved the problem using rubber band powered model autogyros.[4] His fourth full-scale prototype used an articulated blade attachment concept and was successfully flown in early 1923. But this concept had actually been suggested by Charles Renard, a Frenchman, in 1904 and more thorough experimenting prior to flight would most certainly have illuminated the impending catastrophy of Cierva's first prototype.

1.2 GOAL OF EXPERIMENTOR

The goal of today's experimenter is to do the fundamental and configuration testing that at least ensures that our rotary wing progress is not marred by such an oversight as Cierva made. To illustrate this goal, Figure 2 shows several paths[5] from concept to prototype we might take with today's technology. The path selected depends primarily on our assessment of the risk versus the number and size of the steps we take. Many examples in both fixed wing and rotary wing progress can be found where the giant step from concept to prototype was taken without benefit of intermediate analysis or experiment. But the disastrous results far outweigh the successful results in this extremely high risk path, as history so clearly shows. The lowest risk path, on the other hand, requires so many steps that both our patience and our money may be gone before we reach a prototype configuration.

My suggestion of a trade in costs to achieve a successful prototype versus the number of steps we care to take is presented in Figure 3. History notes that Cierva built four machines over a span of three years before he achieved a successful prototype.[4] I am, therefore, suggesting that costs in Figure 3 be measured in number of machines. Also, I suggest that the risks be measured in number of steps where more steps produce a lower risk.

The curve drawn in Figure 3 is my opinion of just how beneficial experimentation can be in reducing the cost to achieve success. If you plan on going from a new concept directly to a demonstrable prototype with virtually no experimentation and little analysis, I consider this path a one to one and one-half step program - and very, very high risk. Cierva's experience suggests that, for this case, you could quite reasonably expect to incur the cost of three machines before rolling out a successful prototype. The addition of experimentation in any of its several forms or combinations will substantially lower the risk. In my opinion, the four or five step program will produce the lowest total cost to achieve a successful prototype. Thereafter, the costs should be expected to rise. As the number of steps approaches infinity, the program cost in equivalent machines will also approach infinity and our patience will run out. We will be "researching it to death."

Perhaps our very nature is to be optimistic and underestimate the total risk, but the rotary wing field has never achieved the balance between experimentation and prototype development that has been practiced in the fixed wing field since 1871 or that is suggested by Figure 3. Stated most simply, today's rotary wing experimenters' goal is "TRY BEFORE YOU FLY."

1.3 TEST OBJECTIVES

The objectives or reasons for doing a test may appear as widely diversed as the many disciplines involved in the rotary wing field. However, Bob Lowey proposed a list of categories of test objectives[6] which quite comprehensively groups the reasons for testing. They are repeated here with some examples I have selected from history:

a) To evaluate hypothesis, theory, or law: Benjamin Robins, often called the "Father of Gunnery", presented a paper on 12 June, 1746 describing his ballistic pendulum shown in Figure 4. The state of the ballistic art in 1746 was well summarized by Robins when he declared, "If it were necessary, a large catalogue of geometers of note might be here produced, who have asserted in their works that, in the operation of gunnery, the resistance of the air was too minute to merit attention. I am fully satisfied that the resistance of the air is almost the only source of the numerous difficulties which have hitherto embarrassed that science." Robins explained that he had carried out many experiments to evaluate the V^2 law of resistance.

b) To study known phenomena: In his lecture of 19 June, 1746 Robins described the experiments which he made with his whirling arm shown in Figure 5. These experiments were carried out not only to check his theory of the drag of cannon balls but because of the difficulties in persuading fellow mathematicians to accept his ideas. On this subject, Robins said, "I have only now to add, that, as I suspected, the consideration of the revolving motion of the bullet, compounded with its progressive motion, might be considered as a subject of mathematical speculation, and that the reality of any deflecting force, thence arising, might perhaps be denied by some computists upon the principles hitherto received of the actions of fluids. To prevent a too hasty discussion of this kind, I thought proper to annex a few experiments with a view of evincing the strange deficiencies of all theories of this sort hitherto established, and the unexpected and wonderful varieties which occur in these matters."

c) To look for unexpected phenomena: Several whirling arm experiments Robins reported in his 19 June, 1746 lecture provided the first experimental evidence that differently shaped bodies, though presenting the same frontal area to the air stream, did not necessarily have the same resistance. He finally tested an oblong flat plate at an angle-of-attack of 45° to the air stream, with the long and short sides, in turn, as the leading edge and found the resistance differed considerably. On this unexpected result, Robins said, "As to cause of this extraordinary inequality, it is not my business at present to enlarge nor have I indeed yet completed all the experiments I have projected on this subject. However, thus far may be easily concluded, that all the theories of resistance hitherto established, are extremely defective, and that it is only by experiments analogous to those here recited, that this important subject can ever be completed."

d) To optimize configurations: In 1759, John Smeaton reported to the Royal Society his experimental results for windmill testing using the whirling arm approach created by Robins. Figure 6 illustrates the apparatus that Smeaton used and could, in fact, be thought of as the first rotor test. About the time he made his experiments on wind sails, there were some 10,000 windmills in England alone. Recognizing the inefficiency of the then current configuration, Smeaton, from his many experiments, determined the power output for a given wind velocity, size of sail and setting of the sails. In summing up the experiments, Smeaton made these observations[2]:

"1) That when the wind falls upon a concave surface, it is an advantage to the power as a whole.
2) That a broader sail requires a greater angle; and when the sail is broader at the extremity, than near the center, this shape is more advantageous than a parallelogram.
3) That beyond a certain degree, the more the area is crowded with sail, the less effect is produced in proportion to the surface."

e) To confirm the performance or integrity of specific designs: The Wright Brothers, while capturing the above four reasons for testing, placed the overwhelming emphasis of their testing on confirming their wing configurations. In December, 1901, they reported to Octave Chanute their conclusions from several thousand readings of force data from more than 200 model wing configurations. Still, however, no direct measurement of the actual forces to be expected on the full size wings was available. The Wright Brothers corrected this short coming in their work by using results from a glider tested in 1902. Lewis noted in his Wilbur Wright Memorial Lecture of 1939 from which I quote, "The glider had a wing scaled up from one of the models tested in the wind tunnel and by means of glide tests in winds of known velocity it was possible to determine the lift and drag as actual forces. These tests in effect calibrated one of the wings tested in the wind tunnel for full-scale conditions, and, since the relation of the other wings to this wing was known from the wind tunnel measurements, the characteristics to be expected from all the wings when flown full size were directly indicated by the wind tunnel data." [7]

These five reasons for testing form an interrelated matrix with the many engineering disciplines that participate in the development of rotary wing aircraft. I have prepared Figure 7 to more comprehensively illustrate this matrix. Unlike the fixed wing field where wing aerodynamics virtually dominate the approach to flight, the rotary wing field has found that the elasticity of the lifting rotor blade is a major factor in the success of a helicopter. For this reason, I place aeroelasticity as the key discipline and suggest that aerodynamics, dynamics, and structures play the supporting roles. The disciplines of flying qualities and design are placed on a level with aeroelasticity. From Figure 7, you can see the possibilities of at least 55 objectives to be supported and met by the rotary wing experimenting community.

2.0 THE EXPERIMENTER'S TOOLS

Today, the rotary wing experimenting community has a broad range of tools to bring to bear in furthering the development of V/STOL aircraft. The adaptation of present facilities and construction of new V/STOL facilities to meet the requirements of rotary wing aircraft during the last fifteen years has been an impressive accomplishment. Improvement in electronic and computer technologies during the same period now permits the thorough on-line data acquisition, analysis and presentation necessary to effective testing. Further, major advances in the fidelity and integrity of rotary wing models have come to pass due to 1) the timely evolution of composite material and elastomeric bearing technologies; and 2) the application of a fast-growing experience derived from a multitude of models built and tested. This rapidly expanding use of our tools is providing insight into the relationship between model size and facility size necessary for appropriately accurate test results. Finally, cost trends are evolving that are extremely helpful in achieving the most cost effective reduction in risks possible with our present tools.

In this section of the lecture, I want you to become exposed to several different testing facilities available; to appreciate the sophisticated data system necessary for continuous, aggressive rotary wing testing; to evaluate the state-of-the art of models; to be aware of the constraints in testing big models in small enclosures; to recognize the costs of using today's experimental tools; and to explore the characteristics of a new testing facility.

2.1 FACILITIES

The problem of simulating full-scale aircraft flight with models was carefully addressed by Smeaton in his paper to the Royal Society in 1759. Concerning his windmill experiments (Figure 6) he wrote:

> "In trying experiments on windmill sails, the wind itself is too uncertain to answer the purpose: we must therefore have recourse to an artifical wind. This may be done in two ways; either by causing the air to move against the machine, or the machine to move against the air. To cause the air to move against the machine, in a sufficient volume, with steadiness and the requisite velocity, is not easily put in practice. To carry the machine forward in a right line against the air, would require a larger room than I could conveniently meet with. What I found most practicable, therefore, was to carry the axis, whereon the sails were fixed, progressively round in the circumference of a large circle." [2]

The major facilities available to the rotary wing experimenter today all simulate full-scale aircraft flight in one or the other of the two ways suggested by Smeaton. Let me first discuss three notable facilities that "cause the machine to move against the air." In deference to Benjamin Robbins and John Smeaton, the first of these facilities is a sophisticated, modern day version of their whirling arm test rig. Today's version is shown in Figure 8 and was put into operation by the NASA in 1955 at Langley, Virginia to study semi-free flying VTOL models. The Langley Control-Line Facility[8] shown in Figure 8 consists of a standard crane with its circular track mounted on concrete pillars. The crane is placed in the center of a 130 foot diameter concrete circle which is located in a wooded area that serves as a windbreak and permits testing even when it is fairly windy outside the woods. To provide control stations for the four operators of the facility, the standard cab on the right side of the crane was enlarged and a duplicate cab was added to the left side of the crane. The crane, which has a standard 4-speed transmission, can be rotated at speeds up to 20 revolutions per minute, and even when in high gear can accelerate from a standing start to top speed in approximately one-fourth of a revolution. In addition to having this excellent acceleration, the crane can also be rotated smoothly and accurately enough to follow VTOL models closely in rapid transitions. The point of attachment of the overhead cable at the end of the jib is about 30 feet above the ground and 50 feet from the center of rotation of the crane. The safety cable is led through the jib and down the boom to the safety-cable operator in the cab of the crane. The control lines run from an attachment on the left side of the model at the fore-and-aft location of the center of gravity to attachments on the vertical boom about 15 feet above the ground. In the original setup, differential movement of the two control lines was used to vary the position of the elevator (or other longitudinal control) of the model. This control system did not prove to be entirely satisfactory for flying VTOL models because, in hovering flight, the control lines occasionally slackened momentarily and caused the control of the model to become erratic. This difficulty was eliminated with a revised longitudinal control system which provided for the installation in the models of control actuators and trim motors. In forward flight on the Control-Line Facility, the centrifugal force on the flying model keeps the restraining line taut. In order to keep the line taut in hovering flight (when there is no centrifugal force) VTOL models are flown with the resultant thrust vector tilted slightly outward away from the center of the circle. In some cases, an additional outward force is provided by an inwardly directed compressed-air jet at the center of the gravity of the model. The restraining line is attached to the boom by a device which automatically keeps the line horizontal regardless of the height at which the model is flying. This device consists of a

vertical track installed on the boom and a small motor-drive carriage to which the restraining line is attached. When the restraining line is not horizontal, it operates a switch to an electric motor which runs the carriage up or down the track to make the line horizontal again. In this system, a small amount of dead spot was used to prevent the carriage from overshooting and "hunting." The purpose of this device is to minimize the effective static stability of height which results from centrifugal force. That is, with a fixed attachment point of the restraining line on the boom, the centrifugal force acting on the model tends to make it fly at the same height as the attachment point. With this device, which automatically keeps the restraining line horizontal, models can be taken off the ground and flown at any height up to approximately 30 feet without experiencing an appreciable restraining effect. Before a transition test is started on the Control-Line Facility, a VTOL model takes off vertically and is trimmed for steady hovering flight. Then the pitch pilot operates the model controls to perform the transition to forward flight at any desired rate while the power operator adjusts the model power to maintain the desired altitude (usually about 15 feet above the ground). The crane operator rotates the crane so that the end of the jib is above the model at all times. It should be emphasized that the model flies at whatever speeds are called for by the control movements made by the pitch pilot. The crane merely follows the model so that the crane rotation has virtually no effect on the model motions. To complete the transition tests, the reverse transition from forward flight to hovering is made and the model then lands. Test data on the Control-Line Facility are obtained in the form of motion picture records of model motion obtained with a 16 millimeter camera mounted on top of the cab of the crane. Also, included in the field of view of the camera are indicators of model velocity and control position. The Control-Line Facility has been used in a number of investigations of the characteristics of VTOL airplane models during rapid transitions from hovering to cruising flight and back to hovering. It has been especially valuable for studying very rapid landing transitions in which a pronounced flare is made in order to stop quickly. In addition, the facility has been used to study the short takeoff and landing (STOL) characteristics of VTOL airplane models.

The second approach to a facility that "causes the machine to move against the air" was developed at Cornell University in 1959 and simply transformed the circular path of the Langley Control-Line Facility into a straight path. Cornell developed a tractor-trailer test vehicle,[9] the trailer part being shown in Figure 9. The complete test facility includes a van truck in which the major instrumentation and data recording components are installed. Data is relayed from the model on top of the trailer to the van by telemetering. The test apparatus consists of a large, flatbed trailer which is towed by a tractor at a desired forward speed. The test rotorcraft is mounted atop a single support tower extending upwards from the trailer. The forces and moments on the test rotorcraft are measured by means of a six-component balance system mounted between the top of the tower and the test rotorcraft. The test apparatus has the following capabilities:

1) Test rotorcraft having a gross weight up to 3,000 lbs.
2) Test rotorcraft with rotor diameters up to 17 feet at several heights ranging from in to out of ground effect.
3) Measure the lift, drag, side force, yawing moment, rolling moment and pitching moment.
4) Achieve forward velocities up to 60 mph.
5) Pitch the rotorcraft at rates up to one radian per second.
6) Provide the rotorcraft with 300 usable horsepower from an external source.
7) Provide the balance system with effective isolation from road roughness.
8) Telemeter ten channels of data.

During the preliminary shakedown operations at Niagara Falls Airport in New York, suspension problems were uncovered as one might expect and these problems were quite effectively solved.

The third approach to a facility that "causes the machine to move against the air" is the Princeton Dynamic Model Track[10] located at Princeton University in New Jersey. This unique facility (the only successful one to date) was developed primarily for V/STOL dynamic model, semi-free flight testing, and is illustrated in Figure 10. The Princeton Track Facility is housed in a building 760 feet long with a cross-section measuring 30 feet by 30 feet. Models can be tested up to speeds of 40 feet per second with a maximum acceleration of 0.6g. The helicopter and VTOL models tested to date have weighed about 25 pounds, but models weighing as much as 40 pounds can be tested. Unlike the models tested on the Control-Line Facility, the models tested on the Princeton track are not equipped with controls for flying, so the flight data obtained are limited to stability information and response to pulse disturbances. The data are transmitted from the model to the recording equipment by telemetering. The models are mounted on a servo-controlled carriage which runs along a straight horizontal track 750 feet long. Mounted on this horizontally moving carriage is a vertical track on which runs a vertically moving servo-controlled carriage with the model support boom installed. The model is attached to this boom with angular freedom and also with ± 9 inches of fore-and-aft freedom along a horizontal track and ± 3 inches of vertical freedom. During a test, the propulsion system of the model provides the lift to support the

model weight and the propulsive force to overcome the model drag in forward flight. The model support strut is moved horizontally and vertically by the two servo-controlled carriages in response to signals from position indicators at the model so that the model stays in the center of its small range of horizontal and vertical freedom. The model support strut therefore provides no restraint to the model in the horizontal or vertical direction (unless, of course, it reaches one end of its limited range of freedom in the horizontal or vertical direction). Extensive work was required to develop a system which would respond rapidly and accurately enough to keep the model motions from being affected to an unsatisfactory extent by the support boom. Although the facility was designed primarily to conduct dynamic testing, certain features make it well suited for static stability research of V/STOL vehicles for the hover to transition speed range. This form of testing is similar to conventional wind tunnel testing (though perhaps not as efficient) but with the advantage of a 30' X 30' test section, precise airspeed measurement, and a uniform flow condition free from turbulence.

You can see from these three examples of facilities that "cause the machine to move against the air" that they are used primarily for flying qualities study in the hover and transition regions. Of the three approaches, the Princeton Track Facility has been found most successful and is continually in use.

Now, let me turn your attention to facilities that "cause the air to move against the machine." Quite probably, Smeaton knew that this approach to a test facility would be better than the whirling arm rig and, perhaps, he envisioned today's wind tunnel. However, the experimenting community did not get its first wind tunnel until 1871. Sponsored by the Aeronautical Society of Great Britain, an experimental committee was appointed in July 1870 and included two Fellows of the Royal Society, Charles Brooke and James Glaisher and four engineers of standing, F. H. Wenham, E. W. Young, D. S. Brown, and W. H. le Feuvre. The following paragraphs are taken from Mr. Pritchard's exciting discussion[2] of the historic work carried out by these men:

> In the Annual Report for 1871, there was published an account of the investigations on the pressure on the surfaces in a stream of air.
>
> The experiments had been carried out in the engineering works of Messrs. Penn at Greenwich, under the supervision of Wenham and other members of the Experimental Committee. A wind tunnel for the purpose, the first of its kind as far as is known, had been designed by Wenham and Browning. It was a foot and a half square section and some ten feet in length. The current was provided by means of a fan driven by a steam engine. The horsepower was not stated. Four flat plates, one a foot square, a second a circular one also of one square foot area, an oblong 4-1/2 inches by 18 inches and another 9 inches by 18 inches were tested.
>
> "The plane to be acted upon was fixed to the long end of a horizontal arm, which vibrated like the beam of a balance, and bore upon its shorter end a sliding counter weight so as to balance the weight of any plane which might be fixed at the opposite extremity. The horizontal or direct pressure was read off by a spring steelyard, which was connected to the end of a lever from a vertical spindle close to the base of the machine. The vertical or raising force due to the various inclinations was read off by an upright spring steelyard."
>
> Measurements were made at angles of 15, 20, 45, 60 and 90 degrees, one observer taking the vertical reading and one the horizontal. Wenham declared at a meeting of the members of the Society that the measurements would have been more accurate if they could have been self-recorded simultaneously. "The experimenter would then have nothing else to attend to but to see that all other conditions were acting properly."

Mr. Pritchard notes that the Society stated that "these first experiments were somewhat crude and incomplete, but it is desirable that these important experiments should be verified and continued." Later in 1896, Wenham declared "that he would have liked to have built a large tunnel which would provide currents from a gentle breeze up to a tornado that could rip the clothes off your back."[2] Clearly, a pattern of never being quite satisfied with the experiment, the model, the data system, or the wind tunnel was established.

Since 1871, many wind tunnels have been built, used, discarded, re-opened and upgraded. Until recently, the best survey of operating wind tunnels was contained in the book "Wind-Tunnel Testing" written by Alan Pope.[11] In November 1971, NASA[12] provided an inventory of United States wind tunnels. From these two works, plus additional research reported in References 13 and 14, I have prepared in Figure 11 a summary of the world's wind tunnel capability for helicopter testing in the form of

maximum speed versus a test section reference dimension, the square root of width times height. The NASA-Ames 40' X 80' and the ONERA S1MA 26 foot diameter transonic tunnel at Modane, France provide the maximum helicopter testing envelope today and these wind tunnels are in constant use. As discussed by Mark W. Kelly, Chief of the 40' X 80' NASA-Ames tunnel, a need exists for a much larger testing envelope.[15] Figure 12 shows an artist's rendition of a proposed NASA wind tunnel having a high speed test section 150 feet wide by 75 feet high and capable of speeds to 300 knots combined with a low speed test section 200 feet wide by 133 feet high capable of 150 knots. This would provide a significant capability to do full-scale aircraft wind tunnel testing (also see article in October 30, 1972 issue of Aviation Week). What an extraordinary increase in the experimenting community's capability when you think that in 1871 our first wind tunnel had a test section 1-1/2 foot by 1-1/2 foot and a maximum speed of perhaps 15 to 20 knots.

Because I am most familiar with the Boeing V/STOL Wind Tunnel, I will discuss this facility as a representative example of "causing the air to move against the machine." This wind tunnel was conceived as a rotary wing testing facility.

The Boeing V/STOL Wind Tunnel was designed as a completely autonomous test facility. As shown in Figure 13, the complex includes, besides the wind tunnel itself, an engineering support building and complete model shop.

The shop is large and well equipped. It has the tools and staff to do machining, woodworking, composite material bonding, instrumentation work, and model assembly and inspection. In this shop, we have the capability to do 85% to 90% of the work necessary to build a model. Nearly all of the models we build are powered by either electric or pneumatic motors and an overwhelming percentage of them are partially or completely dynamically scaled. We also build rotor test stands for isolated rotor testing. As component parts of these models and stands, we manufacture our own drive systems, rotor blades, force and moment measurement equipment, and the instrumentation and control systems.

The engineering building is located adjacent to the model shop and in front of the wind tunnel test section. The front half of this two-story building contains office area for the people who design and test the models and for those who operate and maintain the wind tunnel.

The model assembly area is located on the first floor of the back half of the engineering building. In the back of this room is a large pressure door through which models can be transported into the wind tunnel. On the aft second floor are located an instrumentation lab, small model preparation room and portions of the tunnel data system.

Up a small flight of stairs from this area is the wind tunnel control room, situated so that test personnel are at eye level with the test section. In this room are housed the wind tunnel speed and auxiliary equipment controls, the model attitude and control system controls, safety-of-flight monitoring equipment, and the remainder of the tunnel data system, including an on-line IBM 1800 computer and associated input/output equipment.

The data system is capable of handling approximately 128 channels of information, half quasi-steady-static or "static" data and the remainder dynamic data. On-line, final data output on listings and drum plotters is generally used.

The wind tunnel itself is shown in planform in Figure 14. It is a conventional closed, single return type typical of most low speed tunnels with one major exception. It was conceived from the start as a V/STOL testing facility.

During the design stage of this tunnel, we looked at numerous design variables that have been used or proposed such as 1) return-open versus closed; 2) test section configuration - single, tandem, insert; 3) throat configuration - open, closed, slotted; 4) cooling methods - turning vane versus heat exchanger with either water or Freon as a cooling method; 5) construction materials - steel, poured-in-place concrete, pre-cast concrete. The possible suitable configurations are almost infinite. In the period that this wind tunnel was designed, a number of other design teams were working on tunnels for the same general purpose. There was a considerable exchange of ideas among these teams. Three of these tunnels besides our own were built: NASA-Langley, Lockheed-Georgia, and NRC-Ottawa, Canada - and while they are very similar in some aspects (the general test section size and speed range are the same) they are markedly different in most areas. Each group chose a configuration that best fit their needs, and each can give convincing arguments on why they went that way. We chose a closed return tunnel with a single test section. The closed return seemed to offer the best chance to obtain a controlled test environment with the flow quality we wanted and the single test section reduced the amount of test section equipment needed and would keep test duration to a minimum.

The Boeing V/STOL Wind Tunnel is constructed of steel and concrete. The contraction cone/test section area and the fan section are steel - partly because they are formed sections (the labor involved in making the forms for poured-in-place concrete can be very expensive) and partly because Boeing experience had shown that these

sections are the most likely to be changed during the life of a wind tunnel. The remainder of the shell is concrete, with the walls and ceilings of flat, pre-cast concrete panels to keep the cost down. The wind tunnel is powered by a 15,000 HP package with both electric motors located in the nacelle. The 1500 HP DC motor, forward of the fan, powers at low speed. A 13,500 HP AC motor with a liquid rheostat drives the tunnel at medium speeds with the DC motor in a motor/generator mode acting as a vernier speed control. At high speeds, both motors drive in a load-sharing combination. This system provides excellent speed control through our test section speed range of 0 to 235 knots. For cooling, we use air exchange - primarily because the maintenance is less than liquid systems and has the added advantage of being able to purge the tunnel of engine exhaust/gases or other fumes. The air inlet is located just downstream of the test section and the exit upstream of the contraction cone. At maximum air exchange opening, about 10% of the air is exchanged which keeps the tunnel to within approximately 20°F of ambient temperature at maximum tunnel speed. The location of the air exhaust imposes the condition that the static pressure in that area be roughly atmospheric and, therefore, the static pressure in the test section goes down with increasing velocity, approximately as the dynamic pressure. Since there is a flow quality screen between the air exchange and the test section, there is also a small decrease in total pressure with a corresponding additional decrease in static pressure. The decrease in static pressure requires that the test section be enclosed with a pressure vessel or plenum - the cylindrical, domed structure that can be seen in Figures 13 and 14. Entrance to the plenum is gained through pressure doors with the main model entrance through the model assembly area door as mentioned. Personnel enter the test section through a door on the control room level during testing. In addition, there are air locks on both levels for personnel entrance to the plenum while the tunnel is running.

In the design of the test section, we tried to provide as versatile a test tool as possible. Since we felt that there was a large unknown in V/STOL and low speed rotor testing, particularly in the area of the effect of the test section boundaries, we included the capability of either open or closed throat testing. The basic dimensions of the closed test section are 20' X 20' square by 45' long. An excellent flow quality exists over an 18 foot square by 25 foot long volume of the test section. To convert to the open throat, the aft 29 feet of the test section ceiling, walls, and floor can be removed and stored. The insertion of a 6 foot collector at the aft of the test section provides an open jet test length of 23 feet. The ability to remove the walls, floor and ceiling provides another desirable capability; hover testing of rotors can be conducted while in the tunnel in a greatly increased volume.

In addition to the open and closed throat capability, we also included a slotted wall configuration. The basic effect of the solid wall is to constrain the flow about the model, the open jet allows the flow to overexpand. Wall corrections for open and closed jet are therefore of opposite sign - though not necessarily of equal magnitude - and it is theoretically possible to design a porous boundary which results in a true simulation of free-air conditions. Our slotted wall configuration was based on limited small scale experimental tests conducted in a model tunnel and on a theoretical investigation of the effects of various slot configurations. We feel that this configuration best simulates the free-air situation, as long as the model size remains reasonable.

Model support in test can be provided in a variety of ways. The majority of our models are sting-mounted with internal balances, like the rotor mounted on our Dynamic Rotor Test Stand in Figure 15. The main sting/strut system can automatically maintain a nominal model location in pitch through a substantial vertical/longitudinal envelope. A yaw adaptor is available with additional pitch capability. Models can be strut-mounted by attaching directly to the main floor or by mounting on a turntable that is inserted in the main floor. A second insert with a portable external balance can be interchanged. Models with internal balances can also be wall-mounted and dynamically similar models with multiple degrees of freedom can be mounted on a floor-to-ceiling wire support.

Takeoff and landing in "ground effect" testing can be done over a fixed ground board that can be installed at a number of test section heights; this ground board doubles as a splitter plate for half models mounted on the external balance. We do the majority of our ground effect testing, however, over a Moving Belt Ground Plane. This ground plane replaces the main floor in the test section and is used in conjunction with the sting support described earlier. It consists of an endless belt 17 feet wide, suspended on two rollers 26 feet apart, and driven by the aft roller. When mounted in the tunnel, it sits above the nominal floor line with a scoop in front to remove a majority of the floor boundary layer. At matched tunnel/belt speeds, the minimum velocity in the residual boundary layer is greater than 95% of free-stream velocity. Its present top speed is 100 knots, but we have plans to increase this further.

One of the main concerns in experimental rotor testing is safety. We have firm rules prohibiting the presence of personnel in the test section and plenum during rotor and high pressure air tests. During tests of small rotors and air models, the control room crew are protected by steel plate and double bullet-proof windows in the control room wall. For larger rotors with higher energy levels, we suspend a 5/8 inch thick armor plate barrier between the control room and test section. For power-on checkouts outside the test section, we have recently activated a test cell adjacent to the model assembly room. This 20' X 20' X 35' room has 9 inch thick reinforced concrete

walls and ceiling and an armor plate entrance door. In this room, models can be completely assembled and checked out in safety prior to installation in the tunnel.

Wind tunnels providing variable density, or variable pressure, or wind tunnels using water or Freon rather than air as the test fluid, are available. One excellent example of a Freon facility is the NASA Transonic Dynamic Tunnel located at the Langley Research Center, Virginia. As discussed in Reference 16, Freon as a test medium, provides a lower speed of sound ($\sim$ 510 ft/sec), higher density (~ 0.008 slug/ft^3) than air and lower kinematic viscosity ($\mu/\rho = \nu \sim 3.38 \times 10^{-5}$). The ratio of specific heats of Freon is about 1.13 as compared to 1.40 for air, but this does not appear to be of major importance[6]. The Freon medium permits closer simulation with models of several significant rotor parameters, not the least of which is high Mach number simulation[17] at high advance ratio with improved Reynolds number simulation.

The several facilities I have discussed above represent a cross-section of approaches that make non-flight testing both comprehensive and efficient. Of course, any testing program may well have short comings, but the appropriate use of these available experimental facilities will become more necessary if the improvements in rotary wing aircraft we all seek are to be made.

2.2 MODELS

While a facility to "cause the machine to move against the air" or to "cause the air to move against the machine" is necessary, the key to experimental knowledge lies within the models we use for testing. The last decade has seen enormous progress in the design, fabrication, and testing of rotary wing models. An overwhelming number of these past models have just studied the rotor system and the rotor blades but during the last several years a stronger effort has been made to model the full aircraft. By necessity, all rotary wing models have become more reliable and, hence, test results more abundant.

Two approaches to the scaling of models appear to be evolving. The first approach emphasizes rotor blade loads and aircraft performance. The model in this approach has aeroelastic scaled, full-scale tip speed rotor blades, a geometrically scaled hub, and a fuselage shell that geometrically simulates the airframe. Because testing is conducted at full-scale tip speed, Mach number, advance ratio, and rotor downwash (the disc loading is at the full scale level) can be exactly matched. These Mach scaled ($M_{model} = M_{full\text{-}scale}$) models are high-powered and heavily loaded. While model fidelity to its full-scale version is the desired objective, the overriding consideration in a Mach-scaled model design must be mechanical and electrical integrity. The number one design criteria for a Mach-scaled model is

"THOU SHALT NOT BREAK."

Because of the advances in composite materials and availability of Nomex honeycomb, economical aeroelastic model blades satisfying this criteria at full-scale tip speed are well within today's state-of-the-art. The application of lamiflex/elastomeric bearings, "mini" antifriction bearings and "mini" wire-ply packs for blade retention has made hub scaling possible at reasonable cost. Little attempt is made, in the Mach-scaled model, to dynamically simulate the airframe. To illustrate the advances made in Mach-scaling, let me contrast two tandem rotor helicopter models designed at the Boeing V/STOL Wind Tunnel. The key features of the first model, completed in early 1963, are shown in Figure 16. The model is referred to as the Universal Helicopter Model, or UHM-I. Although this 5-1/2 foot diameter model was originally designed for continuous full-scale tip speed operation, limitations of the two 20 horsepower electric motors, the needle bearings in the flap and lag articulated hinges, and the overweight pitch housing all contributed to reduced tip speed testing in the 400 to 500 ft/sec region before satisfactory model operation was reliably achieved. A new set of rotor blades, aeroelastically scaled for 450 ft/sec tip speed, were made in 1969 and the UHM-I has been used in over 26 test programs since 1963. Now, contrast the UHM-I with the UHM-II, a new tandem rotor helicopter model, designed in 1972 and to be tested in late 1973. The key features of the UHM-II are shown in Figure 17. The 90 horsepower air motor provides a noteworthy starting point for the complete dynamic system, while the total model balance provides the best solution for on-line testing at specific flight conditions. The knowledge gained from 70 Mach-scaled, powered models designed, fabricated, and tested over the thirteen year period since Boeing began serious rotary wing modeling in 1959 are incorporated in this UHM-II.

The second approach to rotary wing modeling is evolving from Froude-scaling techniques commonly used in airplane flutter models. This aeroelastic scaling approach to a helicopter model ensures that deflections due to gravity are geometrically scaled. In addition, because the model tip speed is reduced from the full-scale by the square root of the scale factor, dynamic system stresses, rotor system stresses and power requirements are substantially reduced. The resulting models, designed to a Froude approach, achieve scale inertia and weight which permits the free and semi-free flight testing necessary to aeroelastic stability and flying qualities studies. A recently tested, powered, aeroelastically similar, two degree of freedom (pitch and roll) model is shown in Figure 18. A single 6 horsepower electric motor provides adequate power for this 5-1/2 foot diameter model. Other key features of this Froude-scaled model are shown on Figure 18.

Virtually every member of the NATO rotary wing community has developed rotor models as even the briefest of literature searches will uncover. This growing application of both successful (and unsuccessful) models is showing that rotor models, though very much more sophisticated than typical fixed wing models, can reliably provide enormous experimental insight. In October 1972, the Mid-East Region of the American Helicopter Society sponsored a symposium reviewing the Status of Testing and Modeling Techniques for V/STOL Aircraft. At that symposium, Carl O. Albrecht, Assistant Manager of the Boeing V/STOL Wind Tunnel, presented a paper dealing with the "Factors in the Design and Fabrication of Powered, Dynamically Similar V/STOL Wind Tunnel Models." I have included his paper as an appendix to this lecture to provide you with more details of what we at Boeing found necessary to produce reliable, cost-effective, high integrity rotary wing models.

2.3 DATA ACQUISITION AND PRESENTATION

In reporting to the Royal Aeronautical Society in 1871 the first test results from the first wind tunnel, Wenham declared that "the measurements would have been more accurate if they could have been self-recorded simultaneously. The experimenter would then have nothing else to attend to but to see that all other conditions were acting properly."[2] James Glaisher emphasized that "the measurements made were only accurate to the extent to which the instrument would measure them, and that certainly some of the measurements were uncertain, as those of the wind speed, for example, as the only instrument available, a Lind's Anemometer, was not very satisfactory."[2] These comments are just as commonly heard today as they must have been one hundred years ago, for rotary wing testing is so unique that the demands on model instrumentation, data acquisition and data presentation are extremely high. What has happened, of course, is that our experimental questions continue to be more far reaching and sophisticated than the state-of-the-art of our instrumentation. The most acceptable recourse for this situation is to achieve flexibility in the overall data management.

Rotary wing testing today is dominated by strain gage instrumentation (and Reference 18 is a very good book on the subject). Further, because so much of our desired information, such as blade motions and loads, comes from the rotating system, our data acquisition is complicated by a slip ring (i.e., commutator) used to transfer the data to the stationary world. While the normal force and moment data providing aerodynamic performance characteristics is commonly available on-line, acquiring and presenting the structural dynamic data on-line is of equal importance for successful testing. In addition, rotary wing models should be remotely controlled to enhance their testing capability. Finally, in rotary wing testing, the model can experience severe fatigue loading so that safety of flight monitoring is a prime consideration.

I do not know of any model/facility that has achieved a data acquisition and presentation system that is entirely satisfactory including the Boeing V/STOL Wind Tunnel system with which I am most familiar. However, I would like to present to you the key features of this wind tunnel's data acquisition and presentation system as a measure of what is required for aggressive, continuing rotary wing testing. This data management system was conceived from inception primarily for rotary wing testing and was developed around an 1800 digital computer and strain gage bridge transducers.

There are three major elements in the Boeing V/STOL Wind Tunnel data acquisition and presentation system. In order of importance, they are:

1) Safety of Flight Monitor Element
2) Static (Force and Moment Data Element)
3) Structures/Dynamic Data Element

and I will discuss them in that order.

The Safety of Flight Monitor Element, a pure, real time analog computer system, is outlined in Figure 19. The normal electronics to power a strain gage bridge and amplify the data signal are neatly housed and hardwired to key terminals in the wind tunnel control room. Oscillographs are on-line should a particularily interesting vibration or loads phenomena require an immediate record. Oscilloscopes continually display waveforms of critical rotor system loads. These waveforms appear as a standing wave because the horizontal sweep frequency is keyed to the rotor shaft once-per-rev signal. The 100% meters are somewhat unique and have proven to be the most effective part of the safety monitor element. These meters display the alternating (i.e., peak-to-peak divided by two) magnitude of all critical rotor system loads as a percentage of the calculated fatigue allowable load. The pointer on these 100% meters turns the color red when a 75% load level is reached. And, at a 100% load level, a quiet bell sounds. In addition to the safety of flight data as shown in Figure 19, the model control panel has a bank of thermocouple meters to continuously present the temperature signature of a model's motor, gearbox, swashplate, etc.

The Static Data Element is common to nearly all testing facilities. As illustrated in Figure 20, rotary wing models at the Boeing V/STOL tunnel all have one or more six-component strain gage balances. The signal condition equipment again is the first interface between the control room and the model. The amplified data signals in analog form are digitized by the IBM 1800 computer and averaged over a one second data acquisition period (for most models) to ensure a high quality, steady force or

moment signal expressed in digital counts. (There are 16,383 counts per 5 volts). Conversion to engineering units of pounds or foot-pounds is made, corrections for wind tunnel wall effects (if any) are applied, rotary wing aerodynamic coefficients are calculated, and the data is recorded on magnetic tape or disc. From the recorded data bank, data is continually presented on a normal flight monitor where any non-dimensional coefficient (or dimensional force or moment) can be selected by the test manager using a typewriter input instruction to the computer. Any quantity of data can be selected for on-line print-out and, using three drum plotters, on-line plotting of key data is made. The position of the model's fly-by-wire control system such as collective pitch, longitudinal and lateral cyclic pitch inputs of the swashplate are presented and recorded as part of the Static Data Element. Finally, the vibratory fatigue loads from the balance(s) are continually displayed on safety of flight 100% meters.

The Structures/Dynamic Data Element of the Boeing V/STOL tunnel data acquisition and presentation system has been - and continues to be - in a state of constant improvement and refinement as real needs have dictated. As illustrated by Figure 21, data signals from a blade strain gage bridge, for example, are keyed to the blade azimuth position before entering the multiplexer and passing on to be converted from analog to digital counts at the rate of 8,191 counts per 5 volts. The high speed multiplexer/A to D converter is an electronic parallel to a scanner valve/pressure meter system, or perhaps more appropriately, a parallel to a selector switch tied to a volt meter. After conversion to digital counts, a data channel waveform covering 360 degrees of blade rotation is transformed to engineering units in the IBM 1800 computer. Considerable flexibility in the extent of waveform analysis to be done in the computer is available to the test engineer. To begin with, he can record several 360 degree waveforms from any or all data signals and have the computer calculate an averaged waveform for that data channel. Normally, 3 to 5 rotor cycles are acquired and averaged (in a typical test) for 15 channels of data. Next, the test engineer can call for any or all of several levels of waveform analysis. He can have the computer calculate the harmonic coefficients implied by a Fourier series curve fit from one harmonic up to 10 harmonics. He can have the peak-to-peak divided by two amplitude of the waveform. He can call for maximum and minimum values in the waveform and the azimuth location for each, and he can change his selection of the scope and depth of the data from test run to test run. But regardless of what choice he makes, all digitized data is stored on magnetic tape for possible post-test processing. The data processed on-line, in real time, then passes on to be recorded on disc. From disc storage, the data is printed and can be plotted.

A summary overview of the management of the three elements of this data acquisition, reduction, and presentation system is provided by Figure 22. The value of the completely dedicated IBM 1800 computer (integral to the wind tunnel facility) is overwhelmingly evident. Without this computer (or a better one), the on-line data analysis in the scope and depth required for penetrating rotary wing experimenting on a cost effective basis would not be possible. During the four years that I have been associated with the Boeing V/STOL Wind Tunnel, replacement of this computer with a bigger and better one has been brought up more than once. I personally can not support, at least within the foreseeable future, leap-frogging up and up in computers because a computer change is too traumatic of an experience. The system has been developed and refined to execute what looked like an impossible task in mid-1969, thanks to some very creative system programming plus a chance to fully exploit the computer's hardware potential. Today, even in a comprehensive data acquisition, reduction and presentation format (on the order of 25 structural/dynamic data channels harmonically analyzed and 25 static data channels corrected and in coefficient form) a data point is provided to the experimenter, on-line, in under two minutes.

2.4 MODEL SIZE/FACILITY SIZE TECHNICAL CONSIDERATIONS

As more and more rotary wing testing has been accomplished and the need for new testing facilities has become more apparent, the question of model size and facility size has become more of an issue than a consideration. The issue appears to me to be four-fold. First, the testing of any model, regardless of size, in an enclosure such as a wind tunnel or a Princeton Track will raise the point that the walls, ceiling and floor create a flow interference - of some magnitude. Second, the model helicopter rotor at operating thrust produces a significant downwash that will recirculate through the rotor itself - to some degree. Thirdly, while a small rotor in relation to a given enclosed facility is accepted as goodness, small rotors will be influenced by the out of scale Reynolds number - by some amount. And, the fourth point, the above three parts of the issue can be removed - with some quantity of money.

Let me delay the fourth point on money until the next section of the lecture and take up the first three parts of the issue here. While there is precious little theoretical and experimental data to put on the table, there is enough to develop an initial quantitative engineering opinion. I intend to do this by first providing some background on the points, and then examining some rotor experimental data obtained at low speeds. In this part of the discussion, I will only be talking about square test sections to illustrate trends.

The first point of flow interference on the model due to the testing facility boundaries has received considerable attention over the years as you will see by reading Chapter 6 of Pope's book[11], "Wind Tunnel Testing." The extension of wall

(and floor and ceiling) correction theories to account for a highly deflected downwash wake behind a lifting surface contained in a testing enclosure is being given serious attention, particularily by Harry Heyson[19] of NASA, and Bill Rae[20] and Bob Joppa at the University of Washington. The major rotary wing wall corrections in this regard come when the normal thrusting rotor is tested at low speeds from hover up to the speed for minimum power required. In this speed/thrust region, the testing enclosure induces a non-uniformily distributed upwash that makes the rotor think it is not tilted as far forward as the geometric shaft tilt indicates. Thus, the immediate influence in neglecting this induced upwash is to create an overly optimistic experimental impression of the rotor propulsive force. The key facet of this first point is that testing of any size rotary wing model in a wind tunnel, for example, will provide data that is not representative of free-air conditions because the tunnel walls will induce an upwash that is large at low speed/high thrust conditions but more importantly, is not uniformly distributed over the rotor disc.

Sufficient theoretical calculations[19] of this first point have been made to obtain an engineering order of magnitude of the averaged upwash as a function of the rotor diameter, the enclosure dimensions, the rotor loading conditions, and the flight conditions of the test. A measure of the trend magnitude in the averaged flow upwash angle as a function of the four major parameters is presented in Figure 23. For this illustration, I have conveniently grouped the rotor loading and flight conditions into the approximately correct parameter C_T/μ^2 so that I can draw your attention to the influence of the model size to tunnel size ratio on this flow upwash angle. A potential mid-transition flight situation is noted on Figure 23 for a .1 solidity rotor spanning 50% of the wind tunnel test section width and operating at a $C_T/\sigma = .15$, $\mu = .08$ where test results would be very important to helicopter development. Clearly, even the magnitude of the averaged upwash angle in itself can be very large. Again, neglecting this upwash will lead to an incorrect translation of the model data to a corresponding free-air flight condition.

The second point of downwash recirculation through the rotor because of the test enclosure has been under study by Bill Rae[20] and Bob Joppa at the University of Washington for several years. This recirculation phenomena in a wind tunnel is referred to as flow breakdown and is caused by the model's wake, at large downwash values, impinging on the floor of the wind tunnel. At some low speed/high thrust condition, the leading edge of the rotor wake strikes the tunnel floor and flows upstream. This forward flowing portion of the model's wake interacts with the main tunnel flow, and the two flows roll up into a vortex-like flow. Once the vortex-like flow has formed, any manner of recirculation may occur depending to considerable extent on the particular wind tunnel test section shape, position of the rotor in that test section, and the rotor thrust/speed conditions.

Today, the studies of the flow breakdown phenomena suggest that it represents no less than the beginning of a low speed/high thrust region in which theoretical wall corrections for upwash angle can not be applied with confidence. (Let me interject that at the Boeing V/STOL Wind Tunnel we routinely operate our model rotors and collect data in this regime with no operational problems such as model failure or tunnel speed control.) The flow breakdown experimental data has been used to develop trends in wind tunnel geometry and V/STOL aircraft operational characteristics that can precipitate flow breakdown.[20] In Figure 24, I have illustrated the rotor trend magnitude for the flow breakdown region onset in terms of C_T and μ showing the influence of the model size to tunnel size ratio when a rotor is tested in a square wind tunnel test section. The trends provided by Figure 24 do not encourage the testing of large rotors in small wind tunnels.

The testing of small rotors in large wind tunnels, however, brings up the question of Reynolds number, the third part of the model size/facility size issue as I see it. Reynolds number is an aerodynamic parameter that measures the non-dimensional state of the boundary layer on any surface exposed to air (or any fluid) flow. It is derived from the ratio of a fluid's inertial force to its viscous force and is generally thought to be a key parameter in simulating proper fluid dynamics by both the rotary and fixed wing experimenting communities. While the dependency, for example, of an airfoil's drag[21,22] (such as the skin friction component) on Reynolds number is an important aspect in model testing, the dependency of an airfoil's maximum lift coefficient ($C_{\ell max}$) on Reynolds number is the major point of the Reynolds number issue. The experimenting community illustrates the Reynolds number issue with airfoil $C_{\ell max}$ data as shown in Figure 25. For the sake of completeness, I have shown the trends for several Mach numbers. The fixed wing experimenting community is very concerned in model testing by these $C_{\ell max}$ versus RN trends because the stalling process of a three-dimensional wing closely follows the aerodynamic stalling characteristics of its two-dimensional airfoil. The Reynolds number issue in the rotary wing experimenting community, appears to me, nothing more than a carrying over of the fixed wing worries under the assumption that the three-dimensional rotor stalling process closely follows the characteristics of its two-dimensional airfoil. If this assumption were reasonably correct, the uncorrected application of model rotor data taken in the stalled regime to full-scale flight conditions would be as incorrect for rotary wing model testing as it is for fixed wing model testing.

The $C_{\ell max}$, Mach number, Reynolds number trends of Figure 25, when applied to the rotary wing case, actually lead to a considerably more favorable model/full-scale relationship than they do in the fixed wing case. To illustrate this, let me work out for you the classical interpretation of Figure 25 using a practical situation in effect today. The situation is this: The Boeing Company is currently developing a very large, tandem rotor Heavy Lift Helicopter, under contract with the United States Army. At present, the helicopter has a rotor diameter of 92 feet, 4 blades per rotor, and each blade has a chord of 40 inches or 3-1/3 feet. The rotor system is expected to operate at a tip speed of 700 feet per second. Now, the classical interpretation[3] of Figure 25 for rotary wing aircraft is that retreating blade tip stall represents a practical limit to the gross weight/speed envelope of any helicopter. As you know, when a helicopter increases its speed from hover, the dissymetry in local blade element velocities laterally across the rotor disc are made up by a dissymetry in local blade element angle-of-attack so that there is no rolling moment developed on the total helicopter. Achieving this rolling moment equilibrium at all speeds and gross weights requires that the local blade element angle-of-attack ($\alpha_{1,270}$) at the tip ($r/R = 1.0$) of the blade when on the retreating side of the disc ($\psi = 270$ degrees) grows for increases in speed, propulsion, and thrust. When this $\alpha_{1,270}$ equals the stall angle, onset of separated flow with the rotor disc has classically been expected. This classical interpretation does not provide one shred of quantitative data as to the impact of the separated flow on the aeroelastic, flying qualities, or design characteristics of a rotor. To emphasize: the classically used criteria of $\alpha_{1,270}$ equal to some allowable value has been only a <u>crude measure</u> of separated flow onset within the rotor disc.

Now, using the situation of a 92 foot diameter, 3-1/3 foot chord, 700 ft/sec tip speed rotor controlled by Reynolds number, Mach number and angle-of-attack conditions at $r/R = 1.0$ and $\psi = 270$ degrees, let me map out several model rotors from 6 foot diameter to full-scale on Figure 25 for flight at sea level on a standard day. Reynolds number and Mach number at the retreating tip are given classically by

$$RN_{1,270} = \frac{V_t \, c \, (1-\mu)}{\bar{\mu}/\rho}$$

$$M_{1,270} = \frac{V_t}{a_s} (1-\mu)$$

and you will note that Mach number lines become advance ratio (μ) lines when all models are designed to the same tip speed (i.e., Mach scaled modeling). The results of this rather straight forward exercise is presented in Figure 26. For speeds ranging from hover to 200 knots ($\mu = .5$), the full-scale rotor and models thereof operate in a very much smaller region of the $C_{\ell max}$, RN, MN trends than we normally think of for today's fixed wing aircraft. The speeds above 200 knots or $\mu = .6, .7, .8$ etc., appear reserved for compound helicopters which should automatically preclude retreating blade stall since that is one of the objectives of the compound configuration. The example presented by Figure 26 leads me to the conclusion that a considerably more favorable model/full-scale Reynolds number situation exists in the rotary wing modeling case than exists in the fixed wing modeling case.

To ensure that this background of the Reynolds number issue is complete, you must appreciate in some magnitude, at least in terms of rotor thrust and speed, what the separated flow onset $C_{\ell max\ 1,270}$ implies. To construct this implication, the simple theories of Gessow and Myers[3] are quite adequate. The $C_{\ell max\ 1,270}$ data of Figure 26 can be used to define conditions for the retreating tip at which separated flow onset may be expected. Consider the helicopter as having a gross weight to equivalent flat plate area drag ratio of GW/fe = 582 lbs/sq. ft. and operating at 700 ft/sec tip speed. Use the simple aerodynamic theories[3] for rotor C_T/σ, local blade element angle-of-attack, and let rotor propulsive force define the rotor tip path plane tilt as

$$\alpha_{TPP} = - \frac{f_e \, q_t \, \mu^3}{GW}$$

With a little arithmetic you will find for $\mu > .1$, that

$$C_T/\sigma \approx \left(\frac{1}{8} - \frac{1}{6}\mu\right) C_{\ell 1,270} - \frac{\mu^3}{2} (1-\mu-\mu^2) \, q_t \, \frac{f_e}{GW}$$

when solidity = .0872 and airfoil lift curve slope = 5.73 per radian.
The results of this exercise are shown in Figure 27 where I chose to plot the C_T/σ for separated flow onset at the retreating blade tip against the Reynolds number of the retreating blade tip for advance ratios from 0 to .4.

The results of this simple example, as presented by Figure 27, illustrate what I feel is the importance of Reynolds number simulation in the rotary wing community's effort to model our full-scale helicopter. While Reynolds number appears important at the higher advance ratios, the simulation of advance ratio (and hence, Mach number) appears considerably more important and should be considered first. Of course, this is the approach we do take today and I believe it is a correct approach.

I have not introduced any issue with regard to Mach number because rotary wing models that operate reliably at full-scale tip speed can be built today at reasonable cost. However, several full-scale rotor tests conducted in the NASA 40' X 80' wind tunnel have had to test at reduced tip speed (thus losing Mach number simulation) in order to acquire experimental data at high advance ratio. This situation has, on at least one occasion[2,3], led to a false sense of security about the aeroelastic stability of a rotor system. Full-scale flight tests reveal that Mach number, at high advance ratio, can create some very undesirable rotor system characteristics. It should be clear to you from either Figure 25 or 26 that a full-scale rotor will experience different retreating blade tip separated flow trends with Mach number than will a reduced scale model operating at the same tip speed. However, I believe that Mach number considerations are more important on the advancing side of the rotor disc. High angle-of-attack separated flow can not be tolerated nor is it expected in this region of the disc, but subtle transonic aeroelastic characteristics such as a propensity towards classical flutter can have a significant effect in achieving a satisfactory helicopter rotor system. To me, consideration of Mach number is primarily an issue of what testing facility speed is required to ensure that advancing tip Mach number influences are discovered.

The several foregoing paragraphs have, I feel, provided you with the background to appreciate the upwash issue, the flow breakdown issue and the Reynolds number issue involved in the technical consideration of model size/facility size. Now, I want to show you rotor experimental data that illustrates where, in the rather large gross weight/velocity envelope of a helicopter, the need for testing prior to full-scale flight is most required.

The experimental trend of rotor characteristics with forward speed at a normal operating gross weight is a most natural starting point. To illustrate these trends, I have selected some 12 foot diameter model rotor data acquired in the Boeing V/STOL Wind Tunnel. The model itself had a Mach-scaled, aeroelastically similar rotor of an early Heavy Lift Helicopter design. The testing was conducted by "flying" the model (remotely) at nearly constant C_T/σ and propulsive force coefficient, $X/qD^2\sigma$, to provide equilibrium flight data over the advance ratios from hover to $\mu = .4$. Four channels of data of particular interest to this model size/facility size discussion were illuminated in this experiment, namely: (1) power required, (2) lateral flapping, (3) alternating blade root flap bending moment, and (4) alternating blade root torsion.

The trends with advance ratio of the selected four aeroelastic rotor characteristics are shown in Figure 28. I am sure you are familiar with the trend of the first characteristic of power required (C_P/σ) and the experimental results presented in Figure 28 do not suggest anything startling over the speed range. The second characteristic of lateral flapping (b_1) shows that low advance ratio on the order of .1 creates a situation of greatest lateral flapping. This trend of lateral flapping was also studied in Reference 24. The third characteristic of alternating blade root flap bending moment shows that blade loads during transition flight could be as large or larger than the loads incurred at high speed. The fourth characteristic of alternating blade root torsion loads shows high speed to be most important. Thus, the data of Figure 28 define that experimental study in the low speed transition regime requires as much, if not more, attention than the very high speeds. In view of the complex downwash patterns developed by the rotor in transition flight which, today, can not be adequately studied by theory, the need for experimental data in this regime of flight is even more pressing.

Since the data of Figure 28 shows $\mu = .1$ to be an important region for experimental study when developing a helicopter, let me show you additional results from this 12 foot diameter model test. First, we will look at the influence of climbing and descending expressed in terms of the rotor drag/lift ratio at this low speed and secondly, look at increasing thrust. Testing to illuminate the influence of climbing and descending was accomplished by varying the shaft tilt of the rotor model at constant wind tunnel speed while adjusting the collective pitch to hold constant rotor lift coefficient (C_T'/σ).

The results of this experiment are shown in Figure 29 where the four selected aeroelastic characteristics are plotted against the rotor drag to lift ratio expressed in degrees. The alternating blade root flap bending moment is extremely sensitive to the descending or climbing situation. This data very clearly indicates that the upwash induced, for example, by wind tunnel test section walls must not be neglected or the equilibrium flight conditions used to determine blade moments might create a totally incorrect impression of the full-scale rotor design problem. If the wall induced upwash created an interference angle on the order of 5 degrees equivalent to descending, the blade root flap bending moments could be influenced by 50 percent when translating the model results to full-scale equilibrium flight conditions. While the whole wall induced upwash could be dismissed by designing the full-scale rotor blade to the maximum measured flap bending moments, the non-uniformity in the distribution of the upwash must surely increase the maximum moments. This could lead to a pessimistic full-scale design.

Now, let me show you the trends in the four selected aeroelastic characteristics developed as a function of rotor thrust, but still in the transition speed region of $\mu = .1$. These data are shown in Figure 30 and were developed by testing the 12 foot diameter model rotor at constant shaft tilt and varying collective pitch. In this

experiment, all four aeroelastic parameters exhibit effects of operating at what is equivalent to overload gross weight. The blade root torsion moment particularly indicates that the extent of separated flow within the rotor disc is significant.

Finally, let me show you the trends in the four selected aeroelastic characteristics plus the longitudinal flapping angle as they vary with rotor thrust at a high speed condition of $\mu = .4$. These data were developed by testing a 6 foot diameter rotor at constant propulsive force coefficient using remotely controlled collective pitch and shaft tilt. The results are shown in Figure 31. The effects of rotor stalling become evident in all the aeroelastic parameters to some degree at $C_T/\sigma = .105$.

With this experimental data and the background provided earlier in the discussion now in your hands, I want to establish the ratio of model size to facility size expressed by rotor diameter ÷ test section width (D/W) that is required for acceptable rotary wing testing. This model size to facility size ratio is defined from the transition flight regime information. From the experimental results of Figure 28, testing down in speed to an advance ratio of $\mu = .08$ is clearly required to ensure that experimental, transition speed, aeroelastic characteristics are available. From Figure 30, testing up to thrust levels of $C_T/\sigma = .15$ (and certainly no less than overload gross weight) is clearly required to establish the onset of rotor stall. In addition, high solidity rotors of $\sigma = .1$ do not seem very far off, particularly since the HLH is now at $\sigma = .0925$. Finally, the experimental data, blade load data for example, must be translatable to the full-scale equilibrium flight condition in a reasonably correct fashion. To me, this last point is the same as saying the model size to facility size ratio must be such that flow breakdown will not occur above $\mu = .08$. Therefore, using $C_T/\sigma = .15$ (at $\sigma = .1$) as the maximum thrust condition where correctable data must be acquired and $\mu = .08$ as the lowest advance ratio that correctable data must be acquired, you can see from Figure 24 that the ratio of rotor diameter to wind tunnel test section width is

$$\frac{D}{W} = 1/3$$

There is one additional factor, besides changing to a rectangular test section which I will discuss later, that can favorably alter this engineering opinion of model size to facility size. This factor is to change the tunnel test section from a solid wall, ceiling and floor configuration to a slotted configuration. This test section flexibility was included in the Boeing V/STOL Wind Tunnel on the basis of model wind tunnel test results. Data[25] acquired in a 10 inch by 10 inch test section model wind tunnel showed that slotting the test section by removing 10 percent of the walls, floor and ceiling created porosity. Uncorrected for upwash model rotor test results in the test section of 10 percent porosity agreed well with corrected test results for the same model in the solid test section. Figure 32 illustrates this in the form of rotor thrust coefficient versus shaft angle-of-attack at $\mu = .113$. Because of the improved low speed testing environment provided by test section porosity, all rotor tests at the Boeing V/STOL Wind Tunnel are conducted with 10 percent slotted test section and no wall corrections are applied at all. Also, we believe that the slotted test section permits testing of larger than D/W = 1/3 models in the 20'x20' test section at $\mu = .08$ by delaying flow breakdown.

To complete the discussion of what the model size should be - in short, the Reynolds number issue - you need to appreciate that all of the background on the subject given above is rapidly becoming obsolete. The rotary wing community is reassessing its understanding of the blade stall phenomena. Because the airfoil in a rotor blade is really operating in a highly swept or yawed flow that varies as the blade rotates and undergoes no less than once-per-rev angle-of-attack changes, fixed wing static airfoil characteristics such as those presented in Figure 25 for $C_{\ell max}$ as a function of Reynolds number and Mach number are completely inadequate. However, airfoil characteristics that more realistically represent the rotor blade aerodynamics are available. These more correct airfoil trends are in use in several rotor aeroelastic theories and have permitted the rotary wing community to successfully predict rotor characteristics even with the rotor operating well into the stalled regime[26]. At the October 1972 AHS Symposium reviewing the Status of Testing and Modeling Techniques, Bill Hardy, of the Boeing V/STOL Wind Tunnel staff, presented a paper[27] dealing with the effects of Reynolds number on rotor stall. This theoretical study was conducted using the most up to date three-dimensional, unsteady, aerodynamic approach to the rotor problem available in The Boeing Company and I have included his work as Appendix II to this lecture. This paper shows that rotor blade aeroelastic response to airfoil pitching moment characteristics is far more important than airfoil lift characteristics even in determining the rotor stalling behavior as it effects C_T/σ. For this lecture, Bill Hardy extended his computations to show the effect of Reynolds number on the maximum lift potential of a rotor. The results of the computation are shown in Figure 33 where C_T/σ is analytically varied by increasing collective pitch at a shaft tilt of -14 degrees, $\mu = .3$ and tip speed of 750 feet per second. The data shows that Reynolds number effects are first apparent at about C_T/σ of .08, but onset of stall is delayed until a C_T/σ well over .1 and differs only slightly for the extremes of the Reynolds number case. Lastly, even the predicted maximum C_T/σ for the two cases differ very little.

While this more current understanding of rotor stall and more correct, but limited, analysis of Reynolds number effects suggest Reynolds number must be of concern,

technically, its effects place it much further down on my list of parameters to be simulated in rotor testing. From the discussion, the experimental data, and the theoretical data, my order of importance for models reads today as follows: (1) advance ratio, (2) aeroelastic similar model, (3) Mach number, and (4) Reynolds number. To me, the actual model size then becomes a question of cost, not Reynolds number.

2.5 MODEL/FACILITY COST CONSIDERATIONS

Mr. Pritchard's paper[2] notes that the 1871 Annual Report of the Aeronautical Society of Great Britain published the first recorded use of a wind tunnel. Unfortunately, I have not been able to find out how much this first wind tunnel and model cost. However, in doing some homework for this lecture, Bill Dixon, Assistant Manager for the Boeing V/STOL Wind Tunnel Facility, and I studied the evolution of twenty wind tunnels in the United States. With the help of members of the Subsonic Aerodynamic Testing Association, we uncovered the quantity of testing done by these wind tunnels in the period from 1930 through to 1971. We concluded that the average wind tunnel conducts 22 tests each year. In addition, our study also uncovered a trend in the cost to build a wind tunnel as a function of its size. This data is shown in Figure 34. Making allowances for inflation and normalizing the available data to 235 knots design speed, Bill Dixon and I concluded[14] that a wind tunnel should cost

$$\$70{,}000 \left[\text{TEST SECTION WIDTH X HEIGHT} \right]^{.79}$$

Perhaps Wenham had unlimited funds to construct the first wind tunnel in 1871. However, the cost of wind tunnels today is high and I submit this data to you for our discussion. With respect to models, Wenham reported tests results for an inclined flat plate in that first wind test of 1871. Since then, our wind tunnel models, even for conventional airplanes, have become increasingly complex. And, in the V/STOL field where rotors and prop/rotors are key elements of the lifting system, we are compounding the modeling tasks. However, with the advances in designing and building V/STOL models illustrated by Appendix I, the cost of these complex models has been kept down to a level that gives a high return for monies spent.

During the past twelve years, Boeing-Vertol has designed and built over 70 rotary wing models. In recent years, we have been able to gather some comparative data of what scaled prototype models cost relative to their full-scale prototype counterparts. Drawing upon this data, I have shown in Figure 35 the ratio of model cost to full-scale cost as a function of model diameter ratioed to full-scale diameter. The basis of cost for the full-scale is all costs up to the day the first aircraft rolls out of the hanger. The basis of cost for the model is all costs up to the day the model is placed in the wind tunnel. All the full scale costs, of course, must be recognized as estimates, but this is the best data I have come up with.

The trend of model cost with model size shown by Figure 35 indicates that costs are reduced by roughly the scale factor square. In addition, as Carl Albrecht reported in Appendix I, building a powered, full-scale tip speed helicopter model at 1/20 scale is feasible. Both Carl Albrecht and I have the intuitive feeling, however, that model costs will increase again if smaller than 1/20 scale models were desired. We suspect that the minimum cost model falls at about the 1/15 scale size. I am, therefore, suggesting two trend lines that approximate model costs. The trend for Mach-scaled helicopter models has a minimum of .65 percent of full scale cost at 1/15 scale; the other trend is for Froude-scaled helicopter models having two degree of freedom which, I will guess, reaches a minimum cost of .2 percent of full-scale cost at 1/40 scale. With such small scale models in a conventional wind tunnel, the only scaling parameter that can not be matched is Reynolds number. Offsetting this technical objection is the technical advantage (never mind the lower cost advantage) of testing a small model in a reasonably sized wind tunnel which permits testing to lower transition speeds before flow breakdown occurs.

Because considerable study on building new wind tunnels throughout the NATO community is presently being conducted, there is an additional study made for this lecture that I can transmit to you. The question is this: As a function of model/facility size, what is an order of magnitude cost trend including both model construction costs and intial facility costs (but not including facility operation costs) over a twenty-five year period? The assumptions I made to find the answer to this question were:

1) One facility will be built. It will be a square, solid wall test section wind tunnel having a 235 knot speed capability and use ambient air as the test fluid.
2) The wind tunnel will provide correctable test results for helicopter models down to an advance ratio of .08 and up to $C_T/\sigma = .15$ for rotors having solidity up to $\sigma = .1$. Therefore, the ratio of model diameter to wind tunnel test section width of 1/3 will be invoked.
3) The industry will develop one new prototype helicopter every 5 years. Each prototype will cost \$100,000,000 and have a rotor diameter of 100 feet.

4) Each full-scale prototype helicopter will have a corresponding Mach-scaled model and a corresponding Froude-scaled model.
5) After the initial model testing program, each model will be modified twice each year for five years making a total of ten modifications per model. The ten modifications will conservatively, equal the cost of the original model.
6) The cost trend data of Figures 34 and 35 are reasonably correct.

The results of this rather crude order of magnitude study are presented in Figure 36. The sum of costs for the models plus cost of the facility over the twenty-five year period are shown versus model diameter. The first interesting suggestion is that twenty-five year costs will be minimized by making all models at 4 foot diameter and testing them in a wind tunnel having a 12 foot by 12 foot solid wall, test section. The scale factor of the model would be 1/25 which is possible today with Froude-scaled models. But 1/25 scale factor is not,in my opinion, within the state-of-the-art for Mach-scaled helicopter models,not so much because of model blades and hub retention,but because the industry needs to simulate the control system in future models. At the Boeing V/STOL Wind Tunnel, we have achieved control system simulation at a scale of 1/6.6 in a 14 foot diameter model of the 92 foot diameter full-scale as discussed in Appendix I. We were not successful with a 12 foot diameter model.

The second interesting point that can be made from this "rough cut" cost study deals with the model size issue in regards to Reynolds number. You will recall that technical considerations alone could not provide an overwhelming argument to simulate Reynolds number in our model testing. I concluded that cost to simulate Reynolds number would decide the issue. On Figure 36, I have illustrated the size range corresponding to the low Reynolds number region, the transition Reynolds number region, and the full-scale Reynolds number region using the $C_{\ell max}$, Reynolds number, Mach number trends from Figure 26. From 1 foot to 16 foot diameter, all models will operate sub-critically and the selection of model size is simply one of cost and practicality. This says that the 4 foot model is best from the twenty-five total cost point of view - if you can build it. But, it looks to me that 14 foot diameter, full-scale tip speed is a practical limit today if the control system is modeled. The region from 16 foot diameter to 48 foot diameter (you know, most of today's helicopters are in this range!) is not an attractive range at all in which to simulate future, large full-scale helicopters because the Reynolds number effects are likely to be highly non-linear. From 48 foot diameter up to full-scale diameter of 100 feet, the models simulate full-scale Reynolds number effects. Thus, the cost to simulate Reynolds number - in my twenty-five year example - approach $485,000,000,or virtually the cost of the five (5) prototype to be developed. And this would mean building 1/2 scale "models" of 100 foot diameter full-scale helicopters to achieve Reynolds number simulation in air. Frankly, that appears rather ridiculous to me. I do not believe that a large scale facility, solely to provide Reynolds number simulation, is justifiable by the rotary wing community. In this twenty-five year cost example, the evidence suggests that considerably more emphasis should be placed on using our present facilities and applying our money to building the models we really want.

If the influence of Reynolds number is established by additional experimental and theoretical work to be more important than it appears today, then a wind tunnel using a fluid other than air (such as Freon-12 to retain Mach number simulation) must be considered. The use of Freon in a wind tunnel, as demonstrated at the NASA-Langley Transonic Dynamic Facility, provides an immediate capability to simulate Mach number with many of our present and all of our future Froude-scaled models. This benefit occurs because the gas properties of Freon[28] permit, by reducing the pressure at constant temperature in the wind tunnel, a reduction in Freon density from a normal .008 slug/cubic foot at atmospheric pressure to the value of air, .002378 slug/cubic foot. The speed of sound, which remains dependent primarily on the Freon temperature even at reduced pressure, can be taken as 500 ft/sec. As an example then, a 1/5 Froude-scaled model of a 100 foot diameter, 700 ft/sec tip speed full-scale helicopter would operate at 312 ft/sec tip speed in either air or Freon. But the blade tip Mach number of the model at hover would be only .28 in an air wind tunnel as contrasted with .625 (or full-scale) in a Freon wind tunnel. This capability to simulate Mach number with Froude-scaled models is of enormous value in itself to study high Mach number, aeroelastic stability of rotor systems prior to building a full-scale rotary wing aircraft. This single feature of a Freon wind tunnel should, in itself, demand much higher utilization of the NASA facility.

But, to continue. To achieve both Mach number and Reynolds number simulation requires only a slight variation in our present Mach-scaled (in air) aeroelastically similar rotary wing models, and the testing of these models in a Freon wind tunnel, but at atmospheric pressure where the density returns to .008 slug/cubic foot. Continuing the example, a 1/5 Mach-scaled model of a 100 foot diameter, 700 ft/sec tip speed, full-scale helicopter would operate at 312 ft/sec just as the previously discussed Froude-scaled model would because Mach number simulation is desired. The retreating blade tip Reynolds number at an advance ratio of .4, for this 20 foot diameter model, would be approximately 5×10^6 as contrasted to the value 1×10^7 for the 100 foot diameter, full-scale helicopter. While not at full-scale Reynolds number, you can see from Figure 27 that the C_T/σ for separated flow onset would be well simulated by this 20 foot diameter model.

A 20 foot diameter model helicopter, based on Boeing experience, would be a very, very practical size at which to work. Considering the Froude-scaled like properties such as low tip speed of a model when designed for a Freon testing fluid, it would also be very cost effective. The wind tunnel itself could have a square test section (I will discuss the rectangular test section shortly). A model diameter to test section width of 1/3 would ensure the low speed/high thrust results. This means the wind tunnel test section would be 60 foot by 60 foot. If we stay within our cost example, the maximum speed of the Freon wind tunnel would be roughly 235 knots for the same installed horsepower that is required to drive an air wind tunnel at 235 knots. Because either type of model designed for Freon would operate at 312 ft/sec, testing at advance ratio of 1.25 with advancing blade tip Mach number of 1.4 could be performed.

2.6 CONSIDERATIONS FOR A NEW FACILITY

The possibility of achieving improved simulation of rotary wing model characteristics using Freon as the test fluid in a wind tunnel is clearly impressive. A detraction to the scheme that is brought up is the limited operational accessibility to the test section should model repairs or changes be required. With respect to this, I firmly believe that today's rotary wing models, which operate (at the Boeing V/STOL Wind Tunnel) at one-fourth the testing efficiency of fixed wing models, can and will rapidly achieve both the mechanical integrity and functional reliability that will make testing in a limited access environment cost effective. Whatever the impediment to operational testing that a Freon wind tunnel implies, a Freon wind tunnel provides one very overwhelming advantage over an air wind tunnel. In a Freon wind tunnel, a Froude-scaled model and a Mach-scaled model can be achieved with just one model.

To study the cost of Reynolds number simulation in Freon and rough-out the characteristics of a new Freon wind tunnel for your consideration, two factors must be brought into play. They are:

1) Defining what aeroelastic scaling parameters are to be met by this one model, and then getting this one model to be smaller than a 20 foot diameter version of the 100 foot diameter full-scale by varying the Freon density and speed of sound with pressure and temperature; and

2) Increasing the rotor diameter to test section width ratio from one-third by considering other than a square, solid wall test section.

The study of model scaling parameters can be very simply understood if approached from a practical direction with rotor parameters commonly used in our helicopter work. Figure 37 summarizes ten rotor parameters which, when all are simultaneously met, will ensure that one model will achieve aeroelastic and flying qualities objectives. And, from the ten parameters, we only need to achieve an acceptable level of Reynolds number, define a typical full-scale rotor to be modeled, and work with four of the rotor parameters in order to determine the model scale and desired Freon gas conditions.

Let me use the Heavy Lift Helicopter full-scale prototype as the helicopter to be modeled since it is a current situation and can provide a real example. My criteria for an acceptable Reynolds number for the model is taken from Figure 27 as a range of $4.6 \times 10^6 \leq RN_{1,270} \leq 9.0 \times 10^6$ at $\mu = .4$ or in hover $7.67 \times 10^6 \leq \rho V_T c/\bar{\mu} \leq 14.9 \times 10^6$.

The full-scale HLH rotor system has geometry of

$R = 46$ Feet
$c = 40$ Inches
$b = 4$
$\sigma = .0924$
$\mathcal{R} = 13.8$
$\Omega R = V_T = 700$ Ft/Sec

To start with, we want to achieve Froude number simulation which means the tip speed of the model is scaled from the full-scale as $V_{t_m} = V_T (R_m/R)^{1/2}$ and to achieve thrust simulation of any model at equal disc loading further requires that $(\rho V_T^2)_m = \rho V_T^2$. Therefore, the density of the Freon must be

$$\text{Freon } \rho_m = \rho_{air} \, R/R_m$$

To achieve Mach number simulation, the speed of sound in Freon must be

$$\text{Freon } a_{s_m} = a_{s_{air}} \, (R_m/R)^{1/2}$$

These two gas properties immediately define the pressure that a new Freon wind tunnel must be designed to. Since, to the first approximation, $a_{s_m} = (\gamma \bar{R} T°)_m^{1/2} = (\gamma P/\rho)_m^{1/2}$

$$\text{Freon } P_m = \frac{a^2_{s_m} \rho_m}{\gamma_m} = \frac{a^2_{s_{air}} \frac{R_m}{\bar{R}} \rho_{air} \frac{R}{R_m}}{\gamma_m} = \frac{a^2_{s_{air}} \rho_{air}}{\gamma_{Freon}} = \frac{1115^2 \times .002378}{1.14}$$

$$= 2590 \text{ pounds per square foot}$$

As you can now see, the pressure will be roughly the same regardless of model size and only the temperature that the wind tunnel is going to operate at is a variable. This temperature (in degrees Rankine = 459.6° minus degrees Fahrenheit) is

$$\text{Freon } T_m{}^{\circ R} = \frac{a^2_{s_m}}{\gamma_m \bar{R}_m} = \frac{a^2_{s_{air}}}{\gamma_{Freon} \bar{R}_{Freon}} \left(\frac{R_m}{R}\right) = \frac{1115^2 \left(\frac{R_m}{R}\right)}{1.14 \times 411.5}$$

Lastly, the Reynolds number will be computed as

$$RN = \frac{\rho_m V_{T_m} c_m}{\bar{\mu}_m} = \frac{\rho_{air} V_T R}{\mathcal{R} \bar{\mu}_{Freon}} \left(\frac{R_m}{R}\right)^{1/2}$$

With these scaling parameters now available, we can investigate what can be done to achieve a smaller than 1/5 scale model. The arithmetic is straight forward and the table below provides a summary of the computations:

MODEL SCALE	FREON GAS PROPERTIES					MODEL PROPERTIES		
R_m/R	$T° F$	p	ρ	a_s	$\bar{\mu}$	D	ΩR	RN
1/10	-195	2590	.02378	352	1.66×10^{-7}	9.2	222	10.6×10^6
1/6.67	-63		.01582	432	2.10×10^{-7}	13.8	271	10.3×10^6
1/5	+69		.01188	499	2.55×10^{-7}	18.4	313	9.7×10^6
1/4	202		.00952	557	3.00×10^{-7}	23.0	350	9.3×10^6
1/3.33	334	2590	.00792	610	3.43×10^{-7}	27.6	383	8.9×10^6

The first two columns of this table immediately show us that a refrigerated Freon wind tunnel is required before any significant reduction in model size can be achieved. Secondly, any of the models will achieve Reynolds number simulation. Paradoxically, the Reynolds number goes down as model size goes up because of the increase in absolute viscosity and decrease in density with increasing model size.

Therefore, my conclusion is that Reynolds number simulation in Freon is achieved with a smaller model than would be in air. But you can not significantly further reduce model size by varying pressure and temperature. However, Freon does permit us to build only one model, whereas in air, both a Froude and a Mach scaled model would be built and neither would achieve Reynolds number simulation. This one model for the Freon wind tunnel would be 1/5 scale and somewhat under 20 feet in diameter. Its aeroelastic structural properties are derived from Figure 37 using Lock number to define blade weight per foot (w) and rotating blade frequencies to define stiffness (EI) as

$$w_m = (R_m/R) w \sim \text{pounds per foot}$$

$$EI_m = EI\ (R_m/R)^4 \sim \text{pounds-square foot}$$

At a 1/5 scale, this model is well within today's state-of-the-art. And the wind tunnel is too. The only major difference between the NASA Transonic Dynamic Facility (besides being too small) and the facility under consideration here, is the requirement to operate at 1-1/4 atmospheric pressure which infers that the facility should be designed to something like 3000 pounds per square foot pressure. In concluding this discussion on the first factor to be considered in a new facility, let me say that if a better fluid than Freon can be found that will allow the model to be made smaller, then I am all for it.

Now, let me go on to the second factor to be considered in a new wind tunnel facility. This factor deals with finding what test section rectangularity will improve the ratio of model diameter to test section width and achieve a reduction

in facility cost. In the discussion so far, I have used theoretical and experimental data for a square test section to illustrate trends. However, there is experimental evidence that a square test section is not the best shape for isolated rotor testing when avoidance of flow breakdown is the technical objective. Bill Rae, in his experimental investigation of flow breakdown, tested an isolated rotor in test sections of different cross-sectional shape. The conditions of rotor thrust, tunnel speed, and test section configuration that lead to flow breakdown were summarized[20] in the format of model disc area divided by test section area plotted against a simple momentum theory computed downwash angle for the several test section width to height ratios studied. Harry Heyson[19] later found that the experimental data expressed in terms of impingement distance (X) divided by rotor diameter (D) provided at least a first order non-dimensionalization of model area divided by test section area and the computed downwash angle. The impingement distance is calculated from the simple momentum theory downwash angle and measures the horizontal distance from the rotor center to where the horizontal wake impinges on the floor. With the data available, the impingement distance divided by rotor diameter was adequately determined solely by the test section width (W) to height (H) ratio. The data at the time suggested that a tall, narrow test section would lead to the same rotor conditions for flow breakdown as its reciprocal which would be a short but wide test section (i.e., X/D would be the same for H/W = .5 or W/H = 2) even though the rotor remains horizontal. In my recent communication with Bill Rae, additional data does not now suggest this interchangeability. I intend to use the data as presented in Figure 38 as the criteria for rotor conditions (measured by impingement distance divided by rotor diameter) that lead to flow breakdown as a function of test section width to height ratio. The criteria is developed only on the basis of changes in rotor thrust and test section tuft flow visualization trends due to flow breakdown. I personally believe that rotor thrust is much too insensitive to adequately define the onset of flow breakdown and would recommend that an aeroelastic blade load such as root flap bending be used as the measure of flow breakdown onset. This recommendation comes from the trends in rotor aeroelastic parameters versus advance ratio in Figures 28 and 29. In that data,root flap bending data and rate of descent appear most influenced by how the rotor is operated at low speed. Since large sums of money would be spent on a new wind tunnel designed to a flow breakdown criteria, considerably more theoretical and experimental work should be done to ensure that the criteria as defined in Figure 38 is very correct.

My objective now is to minimize the cost of the wind tunnel facility which will test the defined 20 foot diameter isolated rotor model down to $\mu = .08$, up to $C_T = .015$ and not incur flow breakdown. From the wind tunnel cost trend data of Figure 34, you can see that the test section area of width times height must be made as low as possible. The immediate step to be taken is to minimize the test section height as test section area expressed as $(W/H)\ H^2$ shows. With Figure 38 available and with the model diameter and operating conditions fixed, the problem is simply one of geometry. Regardless of test section dimensions, the model will have the downwash angle of $\chi = 48.7$ degrees at $\mu = .08$, $C_T = .015$ and zero drag. Figure 38 provides the impingement distance as a function of W/H so that the test section height and area are simply

$$H = 2\frac{\left(\frac{X}{D}\right) D}{\tan \chi} \quad \text{(Assumes rotor in center of tunnel)}$$

$$W \times H = \frac{W}{H} H^2 = \frac{4D^2}{\tan^2 \chi} \left(\frac{X}{D}\right)^2 \left(\frac{W}{H}\right)$$

To minimize the test section area, the size parameter $(X/D)^2\ (W/H)$ must be made small regardless of the model size or flight conditions under consideration. Figure 39 shows this size parameter of $(X/D)^2\ (W/H)$ as it varies with the width to height ratio. Note that for $\mu = .08$ and $C_T = .015$ which gives $\chi = 48.7$ degrees, the width to height ratio can not be smaller than .37 because the rotor diameter equals the test section width. Other test section configurations that have less area than a square test section become very apparent when the problem is studied from this viewpoint as Figure 39 shows. Within the experimental data available, it appears that the extremes in width to height ratio will provide the lowest cost wind tunnel for single rotor model helicopter testing. Cost reduction, at least by a factor of 2, should be expected by going away from a square test section.

I have applied the fundamentals just discussed to our example of a 20 foot diameter model and illustrated the results in Figure 40. In addition to relating the several test section configurations studied to the appropriate point on the flow breakdown curve, each configuration has tabulated the informative data of model diameter to test section width, upwash angle, test section area, and wind tunnel cost. The cost of each Freon wind tunnel, as you will note from Figure 34, is extrapolated from one point - the NASA Transonic Dynamic Facility - trended in parallel to the data for an air wind tunnel. This gives the cost-size equation

$$\text{Freon Wind Tunnel Cost} = \$390{,}000\ (\text{Test Section Width X Height})^{.79}$$

The tall, narrow test section is clearly favored when single rotor testing is to be done.

Since a side-by-side rotor system as applied, for example, in a tilt rotor aircraft is receiving considerable attention today, this new wind tunnel must be sized to accommodate that possibility. A flow breakdown criteria is not available for the tilt rotor configuration, so, with a few assumptions, I will construct one from the single rotor helicopter data. The guessed criteria for tilt rotor aircraft flow breakdown is shown in Figure 41. It was constructed assuming that the center line of the tilt rotor aircraft is a plane of symmetry and each rotor is an isolated rotor centered in its half of the test section width. This is equivalent to doubling the W/H scale of Figure 38 which is exactly what I did to arrive at the tilt rotor aircraft flow breakdown criteria shown in Figure 41.

The test section size parameter of $(X/D)^2$ (W/H) is constructed next and is shown in Figure 42 with a comparison to the previous data for the single rotor helicopter. Staying above the envelope of the two curves is required when thinking about a wind tunnel designed for at least the testing of these two rotary wing configurations. Note that the test section width to height ratio can not be less than .75 because at that point, the two rotors together span the full test section width for the conditions of $\mu = .08$ and $C_T = .015$ and the rotor blade tips are just touching. Figure 42 shows that either of two test section configurations would be capable of testing the two rotary wing configurations. One is somewhat higher than it is wide having a W/H = .85; the other is somewhat wider than high having a W/H = 1.3.

The application of this tilt rotor flow breakdown criteria to the specific model rotors, each being 20 foot in diameter, is shown in Figure 43. Again, data has been tabulated, this time for the ratio of two (2) model diameters to test section width, the upwash angle for the individual rotor, the test section area, and the wind tunnel cost per the equation previously developed.

The conclusions I draw from this brief discussion of a new facility are that

1) The practical, cost-effective test section for single rotor testing has a W/H = .667 = 2/3 and, for 20 foot diameter model testing, would be 45 feet high and 30 feet wide. As a Freon wind tunnel, it would cost $111,000,000, in contrast to an air wind tunnel which would cost $21,000,000. The twenty-five year costs, following the cost example but with only one model per prototype which achieves Reynolds number simulation, would be $131,000,000. This contrasts to the air wind tunnel solution taking credit for a non-square 45 foot by 30 foot test section testing a 20 foot diameter model but building two models per prototype and giving up Reynolds number simulation on both, of $61,000,000.

2) The practical, cost-effective test section for tilt rotor testing has a W/H = 1.33 = 4/3 and, for 20 foot diameter model testing, would be 45 feet high and 60 feet wide. As a Freon wind tunnel, it would cost $182,000,000. The twenty-five year costs with one model per prototype would be $202,000,000.

3) With the twenty-five year single rotor cost example, achieving Reynolds number simulation in Freon will cost $131,000,000 by the first conclusion. Achieving Reynolds number simulation in an air wind tunnel would require a 50 foot diameter model, a test section 110 feet high and 75 feet wide and require $432,000,000 over the twenty-five year period.

4) The flow breakdown criteria are presently inadequate with respect to the task of defining the size of a new wind tunnel that could cost $100,000,000 to $200,000,000.

5) The cost to simulate Reynolds number in models of future large, prototype rotary wing aircraft is still very high even with a fluid of Freon-12 properties. A better fluid permitting smaller models and hence, a smaller wind tunnel is required.

3.0 PREPARING A ROTARY WING MODEL FOR WIND TUNNEL TEST

One of the most important steps in the testing of a rotor system is the preparation of the test equipment. It is impossible to place enough emphasis on a methodical, meticulous model preparation and checkout. Many a well designed test program was washed out through oversights in the preparation phase. In this section, I want you to become exposed to several key steps that must be accomplished prior to test and to see the impact on your test program if you rush through or skip this important phase of model preparation.

3.1 ASSEMBLY

The initial stage of preparation starts at the final assembly of the test equipment. At this stage, great care must be exercised in the mechanical preparations to assure that all preloads, clearances, torques, etc. are to the specifications as determined by component testing at a prior stage. Special attention should be paid to the installation of any balances even to the extent of having an SR4 meter attached to the balance bridges during the installation to ascertain that no undesired strains are included in the assembly. Other areas requiring careful observation are the cooling water, lubrication oil, and hydraulic fluids - their flow direction and rates as well as checks for any possible leaks or pinching that might occur at some point of model travel. On the electrical side, there should be the usual continuity checks that all wiring is as identified, especially those pertaining to bridges, thermocouples, and other measuring devices that are going to be inaccessible after assembly.

A further step that should be included at this stage is checks on the available motions of all moving parts. Although these checks should be routine (having been verified in the sub-assembly stage) there may be a possibility of interferences not apparent until all units are assembled together.

3.2 CAN I T RUN?

Having been carefully assembled, the model is now ready to be prepared for running and taking data. Since a certain amount of data is required for model safety during checkout running, some channels have to be calibrated (even if only roughly) especially the critical components. This will include checking bridge voltages, amplifier gains, oscilloscope, oscillograph or safety meter sensitivities and once again, the thermocouples. These selected channels will allow the model to be rotated safely up to its operating speed (without blades). Checks have to be made now for such items as model vibrations and load amplifications to identify possible resonances between model frequencies and blade natural frequencies. At the same time, a check can be made on the stability of all force and moment channels relative to time, temperature, torque, and RPM.

3.3 CAN I T GATHER DATA?

Once the stand gets through this proof of usability, it is ready to acquire data. The next stage is to establish the accuracy with which this data will be obtained. Each channel must have its calibration checked for prime sensitivity completely through whatever data acquisition system is to be used for the test. If there are any interferences between any of the measuring channels, a suitable combined load should be applied which will verify the cross-relationships.

The controls and safety monitoring system can now be set up to enable the equipment to be operated safely. Set angle measuring devices to provide the maximum resolution over the full required range of travel. Use alternating voltages of known dimensions to represent the alternating loads based on the statically acquired sensitivities of each channel being used to monitor for alternating allowables. Check scopes against peak-to-peak meters, oscillographs and data printout. Clearly identify the pre-selected allowable limits in all data presentation media.

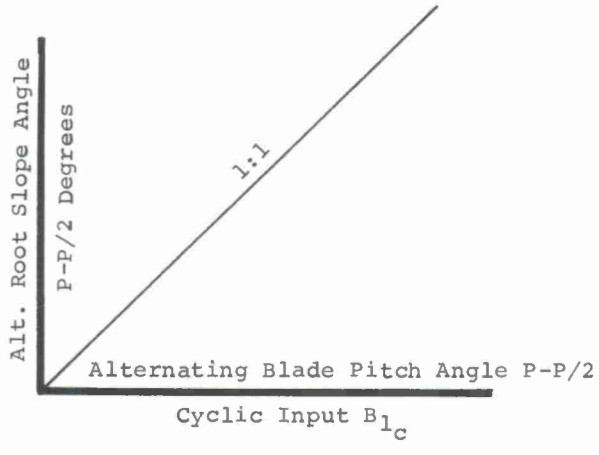
With the equipment now operable, the rotor system can be fine-tuned for track and dynamic balance to minimize the alternating loads stemming from a system unbalance in order to neither mask any aerodynamic effects that may occur, nor use up unnecessarily any of the fatigue allowables of the system components.

Remember that where possible, the rotor system should be statically balanced during assembly taking account of blade weights and CG locations. Moreover, the hub assembly should be dynamically balanced before the addition of any blades. The tracking and balancing can be accomplished by utilizing the data acquired from the harmonic analysis of the inplane forces and moments (as verified initially by the oscillograph traces). Records will be kept of the variation of the alternating loads as functions of $(RPM)^2$ to identify any resonances that may exist in the model. Also, the intercept of the blade collective and coning calibrations should be adjusted such that zero thrust occurs at 0° collective and provides 0° coning. At this stage, also, the inplane shaking forces can be utilized to check the peak-to-peak safety meters and the stress analysis program. The final dynamic balance at the desired test RPM should be ideally 5% (or less dependent on test requirements) of the corresponding balance alternating allowable. Moreover, the track should be within half a blade thickness or 1/4 inch, whichever is less, over the range of test RPM and over a range of thrust levels where such adjustment of the blade flying properties is available.

3.4 HOW GOOD IS THE DATA?

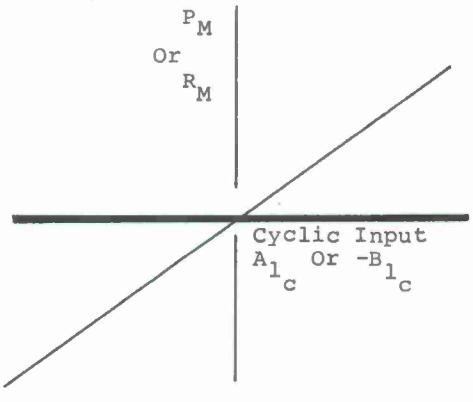
The system is now ready for aerodynamic verification of the data acquisition and reduction system. A suitable check is to input certain blade controls and review the reactions recorded. Place the model in the best hover location where minimum interference will be felt and select a running RPM at or close to the desired test RPM (keeping in mind the results of the natural frequency study conducted earlier). Adjust the cyclic inputs to zero (compare with the visual records in the appropriate blade pitch angle and blade flapping oscilloscopes) and set the collective for zero thrust (should be zero blade pitch angle θ). Data collected at different RPM's during this flat pitch run-up to the selected test RPM will render a comparison between the measured rotor torque and the expected torque due to the rotor profile drag.

Now make a five-point data run taking data at zero and the maximum usable positive and negative inputs for both longitudinal and lateral cyclic. (Beware of possible droop stop pounding at high cyclic angles due to low collective setting). From the data acquired, prepare plots of the peak-to-peak value of the alternating root slope (flapping) as compared to both the cyclic input and the measured peak-to-peak of the alternating blade angle. Theoretically, these items should bear a 1 to 1 relationship with each other in a rotor that has its flapping hinge at the center of rotation.

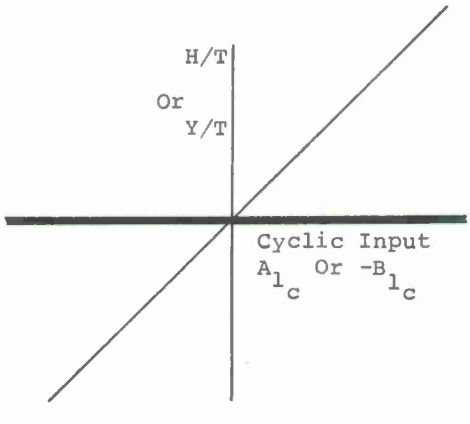


Prepare a further comparison of measured hub moments (both pitch and roll) with the input cyclic. The theoretical relationship in this case is $P_M = \frac{C_F.\varepsilon.b}{2} \times \frac{(-B_{1_C})}{57.3}$

or $R_M = \frac{C_F.\varepsilon.b}{2} \times \frac{(A_{1_C})}{57.3}$ where C_F is the centrifugal load due to the blade outboard of the flapping hinge, ε is the radial location of the flapping hinge in feet and b is the number of blades.



Repeat the above sequence at a positive thrust value on the linear portion of the C_T versus collective pitch relationship. The above plots can again be used but in addition, a plot should be made of the displacement of the thrust vector (H Force/Thrust or Side Force/Thrust) compared with the cyclic inputs. This, again, would be expected to be a 1 to 1 relationship. Comparisons of A_1 and B_1 cyclic inputs with the 1st harmonic of the blade root slope (flapping β) can be used to adjust the cyclic inputs to the correct input azimuth location.



One additional check at this stage is the check for Control System Hysteresis. Repeat the previous run but fill in more data points on the cyclic sweeps around the zero degree input. Similar plots as before can be used for the analysis.

If the facility is such that all these checks to date have been accomplished in a test cell (or checkout area) the model may now be considered a test vehicle and transferred to the test section of the wind tunnel. If this is done, then the main safety items must be repeated (i.e., oil and water direction and flow rates; temperatures; combined loads checks; spot check calibrations on all bridge circuits; control angle movement and position indicators; etc.) back through to this same point in the checkout program. However, before the blades are added, it may be convenient to run hub tare runs at several values of tunnel dynamic head corresponding to the expected test range.

Further runs that can be recommended for data checkout in comparison with previously prepared theoretical estimates are: at a constant advance ratio and collective, run a shaft angle sweep; and at a constant C_T/σ and tip speed, run a μ sweep.

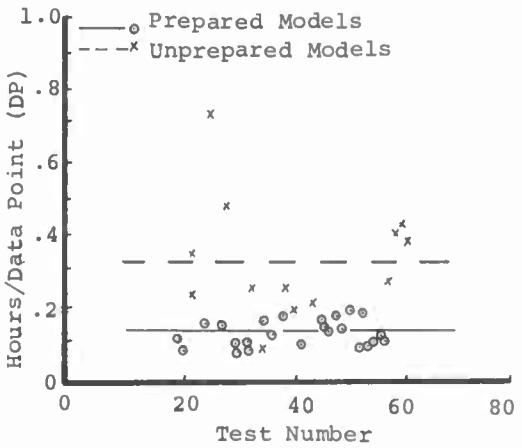
3.5 HOW DO WE KEEP A CHECK ON THE SYSTEM?

Finally, provide a quick check that can be applied on a daily basis to identify any mis-setting of data channels or changes in rotor characteristics either due to expended life or other causes. Select a forward flight run at relatively low power but with sufficient output on the alternating channels to be clearly identified and recorded. Suggested sequence would be: Apply 5° of longitudinal cyclic to the control system and tilt rotor forward until the control axis is at -29°. Bring rotor speed up to that value of RPM which corresponds to a $\mu = 0.2$ (keeping in account any model resonances previously noted) at an optimum speed of the tunnel which is recommended for motor power conservation, adjust thrust throughout to a small positive value as tunnel speed comes up from zero to that corresponding to $\mu = 0.2$. At test conditions, adjust collective to give zero thrust, alter shaft angle to -12° and take records of all scopes, peak-to-peak meters, oscillographs and data printout. Compare these results with each other and preserve for comparison with themselves on a day to day basis.

At this stage, the rotor model can be considered to be operational and ready to be used for rotor experiments.

3.6 WHAT CAN HAPPEN IF THESE RECOMMENDATIONS ARE IGNORED?

Two areas can be affected by not complying with the above recommendations: test economy and data accuracy. A study of typical wind tunnel operational records will show a pattern similar to that presented in the adjacent figure, namely, the average cost of each DP (in hours or other cost units) is much higher on models that have not been previously checked out than on those that have. This stems not only from taking a longer period of time to get the vehicle installed and get to a DP, but also from continuing difficulties arising throughout the test period.



The second area, data accuracy, is not clearly presentable but nevertheless, is an even more severe problem because it can throw doubt on even the minimal amount of runs that are achieved. There will always be that nagging doubt - were the sensitivities and matrices used really valid? Without the specified checks, no one will really know.

4.0 ROTARY WING EXPERIMENTS

There is no facility of which I am aware that sees so continually the contrast between fixed wing model testing and rotary wing model testing than does the Boeing V/STOL wind tunnel. While fixed wing STOL models have, in fact, become more complex, the rotary wing model offers a challenge 10 times that of any fixed wing model. On the more positive side, the rotary wing model features extensive remote control which permits many more model changes to be made while the tunnel remains operative. The results are that the efficiency in rotary wing model testing is, today, only 1/4 that of fixed wing model testing. While it may take 160 hours of rotary wing testing to accomplish what can be done in 40 hours of fixed wing model testing, rotor models generally acquire at least aerodynamic and structural load data with one model in one test, which is twice as much data as in fixed wing testing. A fair conclusion, then, is that we are only half-way from achieving historically accepted levels of productive testing. Considering our present deficit, however, rotary wing testing must be more carefully planned to include "work around" schemes when the model developes mechanical/electrical problems. And most importantly, the testing must be conducted in a way that directly answers the questions asked.

The number of testing objectives to be met with our rotary wing models was discussed in the first section of my lecture and summarized by Figure 7. The matrix of reasons for testing and the several interested engineering disciplines leads to a rather classical situation. In creating and conducting a complete wind tunnel model test program, a minimum of 11 highly motivated, technically competent engineers having many, if not all, of the reasons for doing the test shown in Figure 7 are likely to be involved - and each one desperately needing the experimental data. In this situation, the number of channels of data required from the model can be overwhelming, the number of flight conditions to be studied can rapidly exceed what is possible within allocated time and monies, and certain flight conditions will be desired that can destroy the model, to the dissatisfaction of all. With rotary wing models today, a well prepared model, a realistic/honest appraisal of the experimenting community's capability - and compromise - must prevail. The greatest conflict in need seems to continually occur between the research engineer who tests for trends in non-dimensional coefficients and the design engineer who tests for trends in specific, dimensional parameters. My experience favors the design engineer approach with the data available on-line, in both non-dimensional and dimensional form. A minor corollary to this diversity in approach comes about in deciding whether to test over a range of advance ratios and Mach numbers or specific speeds and RPM. My preference is for the latter. A major corollary to this conflict in approach comes about in deciding whether the design points should be examined first and the off-design points gathered second in a broad matrix of test conditions or whether the design points are just part of the broad test matrix and will be gathered as the test proceeds. On this point I feel very strongly that rotary wing test results should be gathered at the design points first for three reasons. The prime reason is that rotary wing models in general have less than an iron-clad guarantee against failure during a long test program which strongly suggests that the very most key data be acquired first. The second reason is that the initial data acquired helps show where, in the broad matrix of possible test conditions, the key off-design data falls and this can be very helpful if theory is not providing that insight. The third reason is that broad matrix testing provides too much data, which, in my experience, is not included in the final reports.

In this section of the lecture, I want you to see how to anticipate the quantity of data that can realistically be acquired in a given test period, to acknowledge the quality of data you can expect today, to appreciate the use of the models' remote control features in approaching rotary wing experimenting along the most direct path that answers the test question, and to be exposed to a number of rotary wing experiments that address key technical questions.

4.1 DATA QUANTITY AND QUALITY

With regard to the quantity of data, Mr. Pritchard describes the efforts of the Wright Brothers during the latter part of 1901 as follows:

> "In the autumn of 1901 the brothers built a wind tunnel, 22 in. square section, 5 ft. long. A fan provided an air speed of 25 to 35 m.p.h., a wire mesh and sheet-iron honeycomb being used to straighten the current.
>
> More than 200 aerofoils were made and tested. They were constructed from 20 gauge sheet steel, with aspect ratios of from 1 to 10, spans up to 12-1/2 in., camber 1/6 to 1/20, flat plates and curved ones, turned up trailing edges, square and rounded wing tips, bird wing section, square, oblong and elliptical shapes, monoplane, biplanes of various gaps. The aerofoils were tested at angles of 0, 2-1/2, 5, 7-1/2, 10, 12-1/2, 15-1/2, 20, 25, 30, 40 and 45°, a very astonishing achievement.
>
> Several thousand readings were made in a little more than two months." [2]

Today, of course, fixed wing experimenters acquire much more data in two months. Because of the nearly absolute reliability of a fixed wing model, it is not unreasonable to expect that "several thousand readings" would be made in two weeks.

But quantity of data, per se, is a very poor measure of either the success or progress the experimenting community is making. The rotary wing field has not in the past, nor does it today, enjoy the financial support provided to the fixed wing field. And this situation exists despite the fact that our rotary wing technical questions are considerably more numerous and complex. Because of this, I believe that our experimenting efforts must be measured by

$$\frac{\text{Objectives Met}}{\text{Monies Spent}}$$

The efforts of the experimenter and the people that help him do the experiment are illuminated by this measuring parameter. At the Boeing V/STOL Wind Tunnel, we express this measure of experimenting economics in a sentence and an equation. The sentence is

a wind tunnel objective to "answer the most testing questions for the least dollars in the shortest time." The equation is

$$\frac{\text{Objectives Met}}{\text{Monies Spent}} = \frac{\text{Test Questions Answered}}{\text{Dollars Spent}} = \frac{\text{Questions Answered}}{\text{Questions Asked}} \times \frac{\text{Questions Asked}}{\text{Experimental Data Acquired}} \times \frac{\text{Experimental Data Acquired}}{\text{Wind Tunnel Occupancy Time}} \times \frac{\text{Wind Tunnel Occupancy Time}}{\text{Dollar}}$$

The four factors in this equation provide four key guidelines for rotary wing testing:

1) Our standard can be nothing less than to answer all questions asked.

2) We must become more knowledgeable and creative in the way we ask our questions so that we get our answer in the most direct way with the least quantity of data acquired. The answer to such questions as "are we using the model's remote features to advantage?" and "what channels of data are REQUIRED to meet each particular test objective?" need to be scrutinized by the experimenter and the test engineer.

3) We must continue to develop the simplest, most reliable, thoroughly prepared model that can acquire the data to answer our test questions, know this model's limitations, and acquire that data in the quickest way possible. The answer to such questions as "are we being realistic about how much data we can acquire in the time and monies available?" and "are we designing a model more complicated and heavily instrumented than our experience says we can test?" need to be scrutinized by the experimenter and the test engineer.

4) We must match the model and test program to a facility best suited to the job.

The first and fourth factors in this equation require little discussion. I will discuss the third factor dealing with the quantity of data acquired per time along with the quality of this data, first. Then, you will have a better perspective of the second factor which is the need to answer the test questions with the least data.

Historically, data quantity is measured in the wind tunnel by a RUN. A RUN consists of a series of DATA POINTS investigating one variable with all other test conditions held fixed. The best example of a RUN is to vary the rotor shaft angle of attack over some range at fixed control positions and fixed wind tunnel conditions. The recording of data at a discrete shaft angle provides a DATA POINT. Another example of a RUN would be recording data over a range of wind tunnel speeds where each discrete speed would provide a DATA POINT. At the Boeing V/STOL Wind Tunnel, we have kept testing economics records for all tests conducted in the facility since it became operational in March 1968. This historic information has shown us (1) a wealth of trends that point to areas where testing economies can be improved; (2) how rapidly we have learned to competently and efficiently conduct both fixed and rotary wing testing; (3) the impact of an unprepared model; (4) the influence of model complexity; and (5) how to anticipate the quantity of data that will be acquired in a given period of wind tunnel occupancy. It is this last historic piece of information that I want to transmit to you.

For rotary wing testing, the quantity of data should be measured in DATA POINTS, not in RUNS as is normally done within the fixed wing experimenting community. There are at least four reasons for this. The first reason is that the remote control features of a helicopter model generally can be used to avoid stopping for a model change. For example, rotor collective pitch is the equivalent of the fixed wing flap angle in that it changes the angle-of-attack for zero lift. With the fixed wing models I have experienced, flap angle changes are not made remotely so that distinct periods of model downtime occur to hand-set the flaps and this gives rise to a new RUN. On the other hand, when the rotary wing model operates as reliably as the fixed wing model and the experimenters have timely relief, no stopping is required at all. The second reason is that, today, few rotary wing models are that reliable, and planning a test program by DATA POINT helps to ensure the scrutinizing of how the test objectives are to be met with the least quantity of data. The third reason is that the specific definition of what channels of data are required for each DATA POINT becomes more readily apparent. The fourth reason is that not all DATA POINTS will require that every channel of data from the model be operational - or recorded - and the acquiring of those channels of required data without stopping the test to fix unrequired data channels that "have been lost" significantly improves testing progress.

To anticipate the quantity of DATA POINTS we can expect during a rotary wing test program, the Boeing V/STOL Wind Tunnel uses the data shown in Figure 44. The complexity of the model and its test program has come to be measured by the average number of data channels required which includes operating condition channels such as speed, pressure, temperature, RPM, shaft angle, control positions, etc. The wind tunnel occupancy period includes the hours to install and make the model operational, the

the hours in which maintenance is done on the model and facility and data system, the hours for model changes, and the hours when the model is running for checkout and data acquisition. It has been our experience that the average rotary wing model test program extends over a 160 hour wind tunnel occupancy period, requires an average of 43 channels of data, and acquires an average of 880 DATA POINTS.

The data of Figure 44 shows that installing a rotary wing model into a wind tunnel and bringing it to operational status can be very time-consuming when the number of channels of data required is large. Figure 44 also shows that once the rotary wing model is running well, it does provide data in an economical manner. In contrast to fixed wing models where the wind tunnel and data acquisition system can impede the rapid and economical gathering of data, the rotary wing model installation and shakedown is the dominate problem. Anticipating the quantity of data that will be acquired during the test period requires very thorough understanding of both the test objectives and the model by both the experimenter and test engineer. To fulfill that anticipation requires agreement on the what and how aspects of the program by all concerned.

Now, let me go on to the subject of data quality. The state-of-the-art in acquiring aerodynamic performance data with a strain gage balance and associated electronic data reduction systems is more than sufficient to achieve the accuracy we need in fixed wing testing. In applying this fixed wing technology to the rotary wing model, one (or all) of four problems can arise that completely overshadow such mundane things as balance hysteresis, data system noise or other .1 percent of full-scale load worries. The four problems are:

1) Providing less than rigid end fixity of the balance mounting due to insufficient room in the model for the balance.

2) Transmitting rotor torque across the balance.

3) Locating the balance in close proximity or attached to such heat producers as electric motors, gearboxes, etc., due to model size.

4) Designing the balance to be stiff so that it will measure rotor hub vibratory loads with high fidelity but achieving this at the expense of aerodynamic performance load sensitivity which magnifies the three problems above.

Every one of the above problems can be licked during a several-day model preparation period, but if they are not solved before the model is put in to test, they can create a very annoying situation. The first problem arising from not rigidly mounting the balance becomes difficult primarily when the balance has significant interactions between measuring elements. Between thrust and drag would be a good example. With interactions of this type, the magnitude of the interaction will change every time the balance (even though bolted and pinned in place) is "touched". Non-rigidly mounted balances lead to the equivalent of second order interactions which are not tolerated in fixed wing model balance design. The magnitude of this first problem can easily approach the 5 percent level. An immediate assessment of this first problem can be made by measuring the weight of everything sitting on the balance with the balance as the rotor shaft is tilted through the widest shaft angle range possible. Recalibrating the model with the balance in its final installed configuration is the only effective way of solving this first problem.

The second problem is not associated with all types of models because the rotor drive system can be placed on the balance. But when torque is carried across the balance, you must (until proven otherwise) expect torque to produce interactions in all the balance elements. An immediate assessment of this problem is obtained by spinning the rotor over by hand and recording the balance signals on an oscillograph. A harmonic sinusoidal output in thrust, for example, is sufficient notice that "zeros" at zero rotor speed will be a function of what azimuth position the rotor is in when at rest. With a data reduction system that averages the data over some period of time, non-rotating zeros for the balance taken at a rotor speed of 10 to 25 RPM provide the most appropriate zero to be used in data reduction. But this is just the initial step to solving this second problem. The accounting for a torque interaction must be made at all levels of torque. This can be done by whirling short tubes in place of blades. The tube diameter and span is selected to load the system to full torque and the interaction of torque uncovered from recorded data for all balance elements. The magnitude of this second problem can create errors that approach 10 percent of full-scale load. The data from this simple calibration provides corrections that account for the interaction of torque on the balance elements.

The third problem is created by a difference in temperature across the balance which the balance sees as a thermal induced strain. An immediate assessment of this problem can be made by rapidly bringing the model, with blades off, to the operating RPM starting from a cold or ambient condition. Balance data is recorded with time holding the RPM fixed. If the model is operating normally, the temperature environment of the model will stabilize and so will the balance readings. Then the model is brought to zero RPM, and the balance data continues to be recorded with time. Performing this simple test for several rotor speeds will provide a reasonable assessment of RPM interactions on the balance elements due, for example,to flexible couplings. Performing

this simple test with short tubes or blades will normally increase the temperature environment. While the magnitude of this problem between zero RPM, ambient temperature conditions and normal operating RPM and temperature conditions can easily approach 10 percent full-scale loads, the errors introduced after the model is "warmed up" are more on the order of 2 percent or less. With a steel balance, a warm-up run for 15 to 20 minutes is generally sufficient to solve this problem. Aluminum balances transfer heat much too quickly and are not acceptable for rotary wing models.

The fourth problem is really only a problem in that it makes the magnitude of the three previously discussed problems greater. The task of combining in one balance the ability to measure rotor hub vibratory loads with high fidelity while retaining satisfactory steady load signal levels is difficult at best. In 1972, the Boeing V/STOL Wind Tunnel designed, built and tested a "dynamic balance" for the four-bladed, 14 foot diameter rotor model shown in Figure 2 of Appendix I. The balance center was located 17.8 inches (21 percent of diameter) below the rotor center. The balance had its first natural frequency at 15 per rev because of the stiff flexural elements. At this natural frequency, the 4 per rev hub loads were amplified by 1.07 and the 8 per rev hub loads were amplified by 1.37. In operation, the normal temperature environment (created by the bearing housing bolted and pinned to the top of the balance as shown in Figure 24 of Appendix I) led to thermal induced strains, primarily in the balance drag flexures, that were of the same order of magnitude as the steady aerodynamic drag to be measured. No adequate solution to the problem was found in the time available. In 1973, the lessons learned from this failure were applied to the design of a "dynamic balance" shown in Figure 22, Appendix I to be used in the four-bladed, 10 foot diameter single rotor helicopter shown in Figure 28, Appendix I. In this 1973 effort we moved the balance closer to the rotor center (9.4 inches or 15.6 percent of rotor diameter) and we selected the flexural stiffness to give the first natural frequency at 6.3 per rev. This amplified the 4 per rev hub vibratory loads by 1.7. Measurement of 8 per rev hub vibratory loads was not considered. This somewhat less ambitious objective has proven to be a very successful compromise. Steady hub loads are measured with errors less than 3 percent of full load and vibratory hub loads are easily corrected for dynamic amplification effects.

4.2 APPROACH TO ROTARY WING EXPERIMENTING

Now let me go back to the second factor:

$$\frac{\text{Test Questions Asked}}{\text{Experimental Data Acquired}}$$

In this section of the lecture, I want you to consider an approach to rotary wing experimenting that helps to maximize this factor. In advocating this approach, my frame of reference is one in which the quantity of data estimated by Figure 44 is about 1/4 of what I really want based on standards used in fixed wing testing. Secondly, I will remain pessimistic about the reliability of my rotary wing model today and be prepared for a model failure at any time. In this frame of reference, you can appreciate the need to acquire the key data first and fill in the blanks in a matrix of test conditions second - for as long as the model runs productively. Please note that I am not suggesting that a matrix not be filled in. I am only recommending what is to be done first because of data quantity and model limitations.

The philosophy of the approach that I am suggesting to you is as applicable for the testing questions that a research engineer might ask as it is for the testing questions a design engineer might ask. Using hover testing of a rotor as an example, let me first illustrate the philosophy of the approach as it would apply in a research engineering situation, then re-emphasize the approach by using a design engineering situation.

The situation for the research engineer is this. A new, theoretically derived airfoil shows a potential to significantly improve existing helicopter hover performance capability because it expands the envelope of operating lift coefficient versus Mach number at reduced drag over all presently known airfoil families. Feasibility studies show practical application, enthusiasm developes, financial support is gained and a model rotor is designed, built and successfully prepared for test. The objective of the hover test is to provide experimental data that justifies further consideration of the airfoil. Of course, all five of the reasons shown in Figure 7 for doing the test underscore the objective. To satisfy the objective, the prime output data required from the model are rotor thrust, torque and blade root torsion steady moment which reflect the airfoil characteristics of C_ℓ, C_d, and C_m, respectively.

The prime input variables in the test are immediately obvious. They are collective pitch and rotor speed. A broad matrix in these two variables is clearly called for. The comprehensive matrix that historically has evolved appears on the following page.

COLLECTIVE PITCH	ROTOR SPEED MACH NUMBER .2	.3	.4	.5	.6	.65	.70	.75	.80
0									
1									
2									
4									
6									
8									
10									
12									
14									
16									
18									
20									
22									
24									

It is at this point that I have found the greatest need to advocate a rotary wing testing approach of asking the model direct questions and getting direct answers. As you can see, the classical test question posed by the above matrix is to obtain 126 DATA POINTS or, in short, fill in the blanks. Implicitly, within this matrix, lies the data that leads to the objective. This classical test plan format puts "the cart before the horse." I view this classical approach as one saying, "First, give me the data. Then, give me your questions. Then, I will set about answering the questions." I believe that classical approach is unacceptable as a general approach to rotary wing experimenting because:

1) There is, today, inadequate assurance that the model can safely acquire all data points;

2) No evidence is given that the researcher senses or has considered model limitations;

3) Monies and time may only permit the acquisition of 31 DATA POINTS (126÷ 4);

4) No evidence is given that remote control features and on-line data acquisition/analysis/display capabilities are to be used creatively.

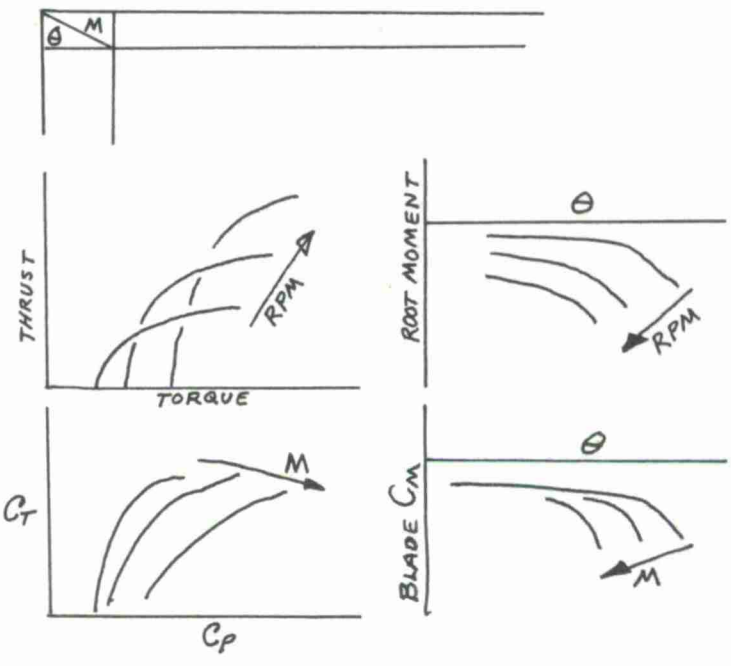
The approach to rotary wing testing I am advocating evolves by following the data from the initial matrix through to the graph(s) the research engineer ultimately intends to use to display the potential of the newly discovered airfoil. This key question and how the answer is displayed define the first set of DATA POINTS to be acquired. Further, knowledge of how the answer is to be displayed can be used to operate the model and use the data system creatively. To illustrate this point, think your way through the proposed hover test to one possible key display like this:

Step 1 - Create matrix

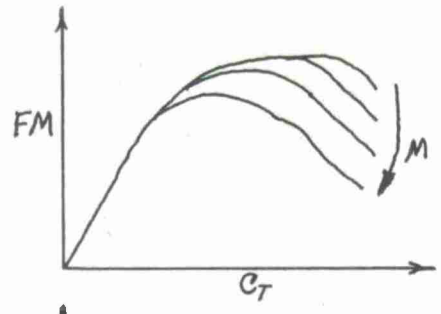
Step 2 - Acquire 126 DATA POINTS by varying collective pitch holding RPM constant

Step 3 - Plot raw data

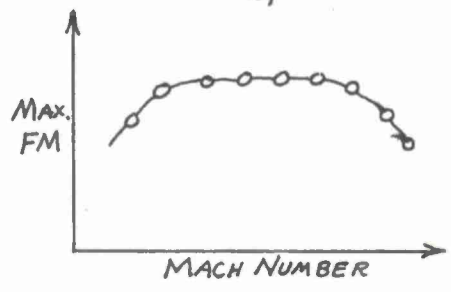
Step 4 - Plot non-dimensional data



Step 5 - Analyze data for a rotor Figure of Merit question



Step 6 - Display answer



The question I pose to you now is this: If the key technical question is what maximum Figure of Merit will the airfoil provide as a function of tip Mach number-and it can be answered with only nine (9) DATA POINTS, then why not get the answer with the first nine (9) DATA POINTS? Then continue the acquisition of the other 117 DATA POINTS guided by what you learned from the first 9. If the model fails in less time than it takes to get 9 DATA POINTS, you would never get the answer anyway. Model failure at the 9th DATA POINT will provide the answer to the key technical question. After that, the data base can be expanded for as long as the model is productive or until time or money run out. In this example, you can see that acquiring the first 9 DATA POINTS is quite easy. At the Boeing V/STOL Wind Tunnel, we would instruct the computer to provide a continuous display of Figure of Merit and Mach number in two of the digital light meters shown as part of the Monitor Display in Figure 20 (Static Data Acquisition). Then the model would be "flown" by remote collective pitch control, while holding Mach number constant, to the condition where Figure of Merit visually appeared to maximize. That one condition would be permanently recorded. Holding that collective pitch, the Mach number would be increased, changes in Figure of Merit by varying collective pitch would be studied visually, and that maximum value permanently recorded. And so on.

The application of the approach I am advocating to the design engineering situation emphasizes the point. The design engineer would expect this newly discovered airfoil to significantly improve helicopter payload, for example. If applying the airfoil to a helicopter currently in service, he could quite logically ask the question, "What increase in gross weight over our present blade can we get considering that the installed horsepower and operating RPM are fixed?" Or, if applying the airfoil to a helicopter that is in the preliminary design phase, he could logically ask, "What minimum torque/RPM point can we get to at the design gross weight so we can reduce rotor system and drive system weight?" Either of these two questions could be answered with data developed in the classical approach shown by the broad matrix of 126 DATA POINTS for collective pitch and rotor speed conditions to be tested. But each question can be first answered directly using the remote collective pitch control and visual data display features available to today's experimenters. The first question of thrust at fixed horsepower and RPM could be answered with one (1) DATA POINT! The approach is to "fly" the model with collective pitch up to the condition where the visual display reads the given horsepower holding the RPM constant and permanently record that one (1) DATA POINT. This is somewhat more austere than I would recommend but it does illustrate the point. The second question suggests that the trend in torque with RPM at fixed thrust would provide the appropriate answer. The approach in this case would be to display both thrust and torque data visually and "fly" the model at constant thrust. As rotor RPM is increased, permanently record the data at selected RPM's and pay particular attention to the RPM region where the visual display shows torque is minimizing. Nine (9) DATA POINTS spent here would surely provide the data to answer such a simple question and the program could be continued to acquire the other 117 DATA POINTS.

By now I suspect you understand the need, the philosophy, and the execution of the approach to rotary wing testing I advocate. The approach depends heavily on the experimenter being knowledgeable enough to ask the key searching questions and knowledgeable enough to concisely display the answer. With that knowledge in hand, the rotary wing experimenting community is capable today of interfacing the experimenter with the model through the remote control system and the on-line data system. This close interface, used in an approach where the experimenter "interrogates" the model with direct questions and "flys" the model to produce the answer, can produce 90 percent of the test results in 10 percent of the time.

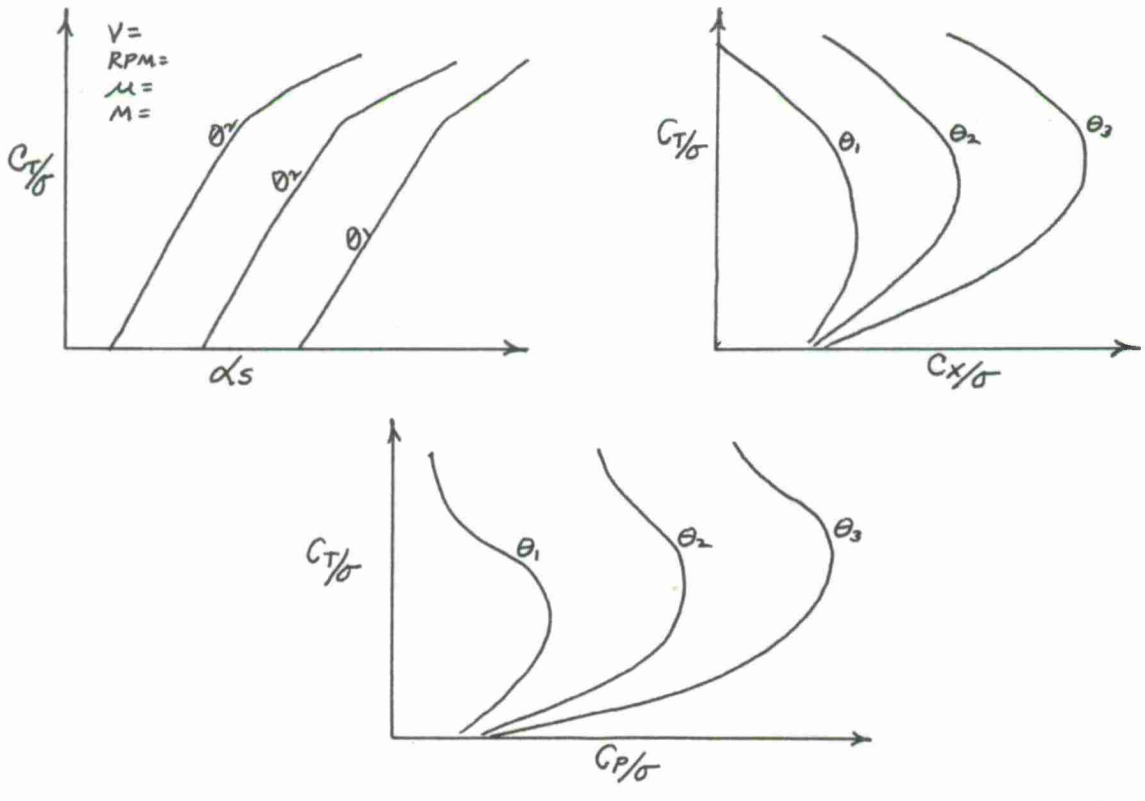
4.3 KEY EXPERIMENTS

The literature on rotor test results is so extensive that this single lecture could not possibly capture the overwhelming progress made by the rotary wing experimenting community over the last fifteen years. The Boeing V/STOL Wind Tunnel alone has contributed over 10,000 hours of wind tunnel time to the study of helicopter, tilt rotor and tilt wing aircraft in the five years since becoming operational in March 1968. The total contribution of all community members is surely staggering. While this total community contribution is far less than that made in the development of fixed wing aircraft, we are approaching the capability to fulfill rotary wing testing needs. With this growing momentum, theoretical answers to key technical questions are now receiving the supporting experimental attention that is required for substantial improvement in our rotary wing aircraft. In this section of the paper, I want to pose two technical questions for you, discuss how a model was used to answer each question with an appropriate number of DATA POINTS, and briefly convey the answers.

4.3.1 Question 1 - Will increased blade twist delay retreating blade stall?

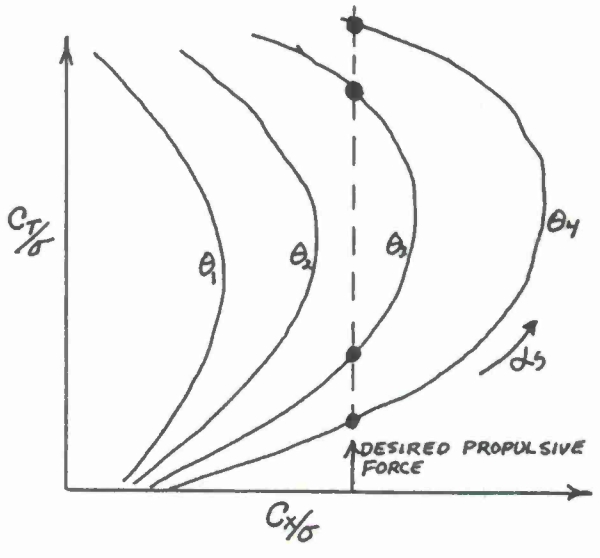
An overwhelming number of helicopters have been built that have a linear blade twist on the order of -8 degrees. The concept of blade stall as classically presented by Gessow and Myers[3] in 1959 suggests that blade twist is a means for delaying blade stall in helicopter design. Using a criteria of retreating blade tip angle-of-attack ($\alpha_{1,270}$) simple theory shows that "twisting the blade so as to lower the pitch at the tip with respect to the root pitch tends to distribute the lift more evenly along the blade and therefore avoids the high angle-of-attack region at the tip."[3] Flight test results are reported[3,29] for blades having no twist and blades having -8 degrees of twist. A twist of -8 degrees is calculated to reduce the retreating tip angle-of-attack by 2-1/2 degrees over zero twist at constant airspeed. Corresponding theoretical calculations with an experimental correction for blade stall show a reduction in profile power for the twisted blade. The question, as posed, suggests that a further increase in blade twist from -8 degrees to a higher value will further delay blade stall.

To answer the question, the testing of several rotor blades each of different twist, is,of course, required. But let me first discuss how a model has been and should be used to answer the question. The non-flight testing of a rotor in forward flight has much too commonly been conducted by adhering to a classical matrix of collective pitch/shaft angle sweeps at selected speeds or advance ratios and a particular rotor RPM. Performance data, for example, is usually plotted from the test results in the form shown below at each speed:

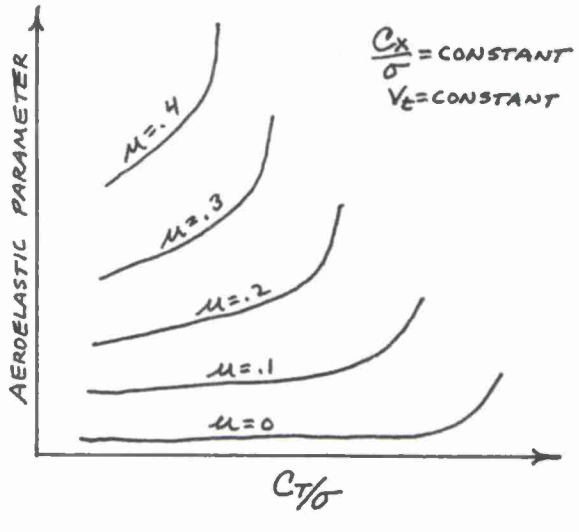


The appearance is given that a great deal of important data has been acquired in a very logical way by this classical matrix approach and the resulting graphical display. However, nothing could be further from the truth. To point this out, let me pose the question a little more specifically: Will increased blade twist delay retreating blade stall AND THUS let the helicopter rotor develop more lift while still maintaining a propulsive force for trimmed level flight?

By the addition to the original question, data with lift varying at a constant propulsive force simulating the trimmed flight condition is required first. If you try to answer this more specific question with the data collected from a classical matrix approach, you can very easily find yourself quite short of data. Look at the little sketch here showing the trends in lift and propulsive force as shaft angle is increased at fixed collective pitch, tunnel speed and rotor RPM and you will see what I mean. The question calls for data at a trimmed level flight propulsive force plotted versus rotor lift, but from the sketch, only four (4) DATA POINTS are immediately available and only 2 of these will be at high lift. All other data points come, hopefully, from interpolation and not extrapolation. In short, with ten (10) DATA POINTS for each shaft angle sweep at four collective pitch angles, you have acquired forty (40) DATA POINTS at one speed/RPM condition and still can not answer the question with more than 2 key DATA POINTS! Further, this approach at advance ratios of 0, .1, .2, .3, and .4, for example, would create 200 DATA POINTS, just at one blade twist, of which only 8 to 12 would be of immediate value!!



If you tackle the specific question directly, you can answer it with very few data points by "flying" the model at constant propulsive force while increasing rotor lift. This testing approach at several advance ratios provides raw data in the form shown here. About 50 DATA POINTS are acquired and all contribute immediately to defining a rotor lift at which separated flow effects begin to appear important in such aeroelastic parameters as power and blade root torsion moment.



In studying this question of delay in blade stall due to increased twist, the Boeing V/STOL Wind Tunnel built two 3-bladed, 6 foot diameter rotor blade sets. One set had blades twisted to -7 degrees and the other set twisted to -13 degrees. Each blade was constructed as shown in Figure 6, Appendix I for the 6 foot diameter HLH UHM rotor. A 600 DATA POINT total test plan was created, of which 150 DATA POINTS were devoted to "flying" the model with increasing rotor lift at constant propulsive force for advance ratios of 0, .1, .2, .3, and .4. Both rotor sets of -7 degrees and -13 degrees followed this test approach.

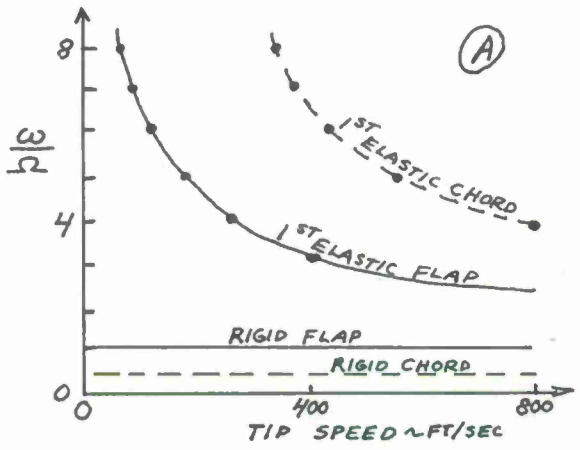
The answer to the question was that increased blade twist did not delay the onset of blade stall as the data shown in Figure 45 confirms. Two envelopes of C_T/σ versus μ based only on the trends of alternating blade root torsion moment with increasing rotor lift are shown in Figure 45. Supporting data at $\mu = 0$ and $\mu = .3$ for two aeroelastic parameters of alternating blade root torsion moment and power are also shown in Figure 45. This supporting data shows why the root torsion moment is the best indicator of blade stall. The two alternating root torsion envelopes in C_T/σ versus μ come from two criteria applied to the root torsion moment data. The lower envelope in C_T/σ versus μ is subjective and qualitative because it is based on an opinion of the rotor lift where root torsion moment "sharply" increases. The higher envelope in C_T/σ versus μ is quantitative because it is based on that C_T/σ where alternating blade root torsion moment equals 15 inch-pounds which is roughly three times the unstalled load.

The test results for the two blade twists create virtually identical envelopes in C_T/σ versus μ and so the answer to the question is - no, increased blade twist will not delay retreating blade stall and let the helicopter rotor develop more lift while still maintaining a propulsive force for trimmed level flight. The data strongly suggests increasing the strength of selected control system components to gain a significant expansion in the C_T/σ versus μ envelope.

4.3.2 Question 2 - What blade rotating natural frequencies should be avoided in the design of an articulated, four-bladed rotor system?

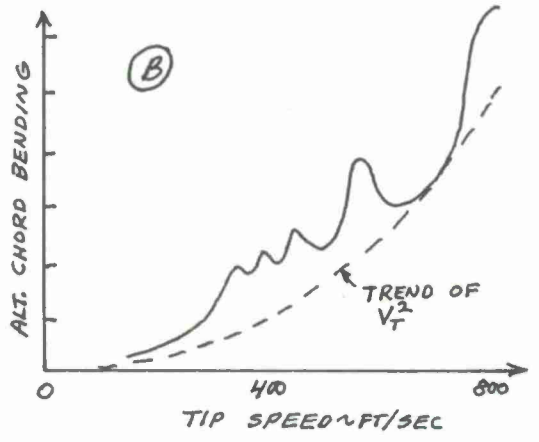
A set of rather universally applied "rules of thumb" for rotating blade natural frequencies have come about through experience in the helicopter field. These "rules of thumb" suggest the avoidance of blade frequencies equal to integers of blade number, for example, if blade and hub vibratory loads are to be minimized. Gessow and Myers[3] provide an introduction to helicopter vibration problems. In that book, periodic airloads at least up to 4 per rev flapwise and higher chordwise, are made apparent even if the rotor blade was non-flexible. For the flexible blade, these periodic loads "excite the blade flexing modes and the blade responds with an amplitude of motion depending on how near the excitation frequency is to the blade natural frequency. When excitations occur at the blade natural frequency, these forces are only opposed by damping forces because by definition, the spring and mass forces in the blade are in equilibrium. Thus the forces, when applied near resonance, produce amplitudes much greater than would be expected if the forces were applied statically to the blade. This dynamic amplification is important in conventional rotor blades because the exciting forces at 2/rev and 3/rev are near enough to the natural bending frequency to cause large amplifications. The 2/rev and 3/rev flexings of the blade are important, not only because of the input forces they may transmit to the rotor hub, but also because of the high alternating blade stresses and accompanying possibilities of fatigue failure. Conventional blades are stiffer in the in-plane direction than in the flapping direction and the natural bending frequencies are correspondingly higher. The first bending frequency is often about four times the rotational speed. Considerable amplification of 4/rev inputs may, therefore occur."[3] In discussing the blade and moment forces transmitted to the rotor hub, the assumption is generally made that all blades are identical. Then the governing fundamental rule is one that says "the only alternating forces and moments which the blades may transmit to the rotor hub are those which are integral multiples of the number of blades."[3]

The question, as posed, defines that blade rotating natural frequency is of primary concern. An approach in which blade rotating natural frequencies are directly varied can be expected to provide the answer most directly. The approach is suggested from the knowledge that blade rotating natural frequencies, when expressed on a per rev basis, are very dependent on what the rotor speed is. Sketch A shown here illustrates this typical dependency of both rigid and first elastic bending modes on rotor RPM or tip speed. (The correct aeroelastic variable is $EI/w\Omega^2R^4$ as noted in Figure 37). There are many places (or V_T's) on the diagram as shown by Sketch A, where resonance might occur. Therefore, operating a given model over a wide range in rotor speed should produce conditions of high blade loads and high vibratory hub loads. Because the airloads also vary with rotor speed, the model must be "flown" in such a way that the aerodynamic environment is constant, at least in a non-dimensional sense.

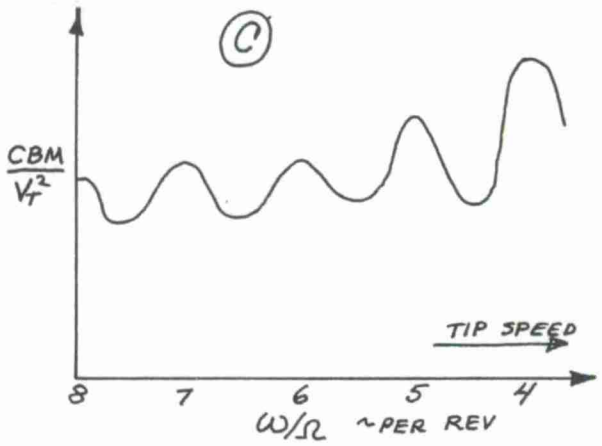


The experimental approach is quite simple. The rotor RPM is varied, but advance ratio is held constant which means wind tunnel speed is varied as rotor RPM is varied. By holding constant the rotor shaft angle-of-attack, collective pitch and cyclic pitch, the rotor stays in a constant non-dimensional rotor aerodynamic environment. Such typical rotor aerodynamic parameters of μ, λ, C_T/σ, C_P/σ, β_o, a_1, b_1, etc. are all constant. To the first approximation, the periodicity of airloads is constant, but the airload strength is changing as RPM^2.

In essence, the airloads are used as a forcing function that is linear with RPM^2. If the blade loads and hub vibratory loads, when divided by V_T^2, do not remain constant with V_T, then a resonance natural frequency can be suspected. To illustrate this point, imagine the raw data for alternating blade chord bending moment being acquired at increasing RPM and when plotted versus V_T looking like Sketch B. The trend, if no resonances occurred, would be in proportion to V_T^2 and the load would faithfully follow the forcing function. This raw data, when



divided by V_T^2, would look like Sketch C where each peak corresponds to a particular V_T which is in turn related to a rotating blade natural frequency. If a particular aeroelastic parameter does not show a peak in the format of Sketch C, then avoidance of that particular rotating blade natural frequency could be reassessed and might lead to a much improved rotor system.



In studying this question of blade rotating natural frequencies that should be avoided, I have selected test results from a 14 foot diameter HLH model rotor test. This model is shown in Figure 2, Appendix I. The rotor system was tested using a very stiff balance so that hub vibratory loads up to the 9th harmonic would be measured with a minimum of of amplification. The balance first natural frequency was 204 cycles per second for vertical loads and 240 cycles per second for inplane and moment loads. The model was "flown" to the following nominal aerodynamic trim condition:

μ	= .20	a_1	= 0°
α_s	= -6.00°	b_1	= 0°
$\theta_{.75}$	= 7.83°	C_T/σ	= .077

At this flight condition, the rotor tip path plane remains nearly perpendicular to the rotor shaft. Blade load and balance vibratory load data were then acquired at tip speeds from 249 to 752 feet/second. Mid-span blade flap bending moment, mid-span chord bending moment, 4/rev longitudinal vibratory load and 4/rev vertical vibratory hub load data are presented on Figure 46 to answer this question. The presented results confirm our experience that at operating rotor speed the blades should have rotating natural frequencies between integers of rotor speed.

The question I leave you with then is this: If the desired frequencies are 1-1/2, 2-1/2, 3-1/2, 4-1/2, 5-1/2, 6-1/2, 7-1/2, etc., at which ones should the blade be designed to achieve the lowest vibration level? the lightest blade? the best compromise? the best helicopter?

5.0 CONCLUSION

The rotary wing experimenting community now has the capability to effectively participate in the future development of VTOL aircraft.

REFERENCES

(1) Henry Margenau, David Bergamini, "The Scientist", Time Incorporated, New York, 1964

(2) J. Laurence Pritchard, "The Dawn of Aerodynamics", Journal of the Royal Aeronautical Society, Vol. LXI January-December 1957, Page 149

(3) Alfred Gessow, Garry C. Myers, Jr., "Aerodynamics of the Helicopter" Frederick Ungar Publishing Company, New York 1952 (3rd Printing)

(4) Charles Gablehouse, "Helicopters & Autogiros, A Chronicle of Rotating Aircraft", J.B. Lippincott Co., Phila., Pa., 1967

(5) Jan M. Drees, Bell Helicopter Co., Panel Discussion Notes, Proceedings, AHS Mideast Region Symposium, "Status of Testing and Modeling Techniques for V/STOL Aircraft", October, 1972

(6) Robert E. Loewy, University of Rochester, "An Overview of the Status of Aerodynamic and Dynamic Modeling", Proceedings, AHS Mideast Region Symposium, October 1972

(7) Dr. G. W. Lewis, Wilbur Wright Memorial Lecture, 1939, "Some Modern Methods of Research in the Problem of Flight", Journal of the Royal Aeronautical Society

(8) John P. Campbell, "Free and Semi-Free Model Flight-Testing Techniques Used in Low-Speed Studies of Dynamic Stability and Control" AGARDograph 76, October 1963

(9) Edward M. Sullivan, "A Test Apparatus For Small Rotorcraft" Cornell Aeronautical Lab Report No. SG-1195-S-3, (Volume I) Buffalo, New York, November 1959

(10) H. C. Curtiss, Jr., W. F. Putman, J. J. Traybar, "General Description of the Princeton Dynamic Model Track", USAAVLABS Technical Report 66-73, November 1966

(11) Alan Pope, M. S., "Wind-Tunnel Testing", John Wiley & Sons, Inc., New York, Copyright 1947, 1954 (Second Edition)

(12) C. J. Pirrello, R. D. Hardin, M. V. Heckart, K. R. Brown, "An Inventory of Aeronautical Ground Research Facilities" NASA CR-1874, (Volume I - Wind Tunnels) November 1971

(13) W. J. Dixon, "Low Speed Wind Tunnel Construction Cost Evaluation", The Boeing Vertol Company Interoffice Memorandum 8-7890-4-54, July, 1972

(14) W. J. Dixon, "Low Speed Wind Tunnel Test Survey", The Boeing Vertol Company Interoffice Memorandum 8-7890-4-60, October, 1972

(15) Mark W. Kelly, Panel Discussion Notes, Proceedings, AHS Mideast Region Symposium, October 1972

(16) Langley Working Paper No. 799, "The Langley Transonic Dynamics Tunnel", NASA-Langley Research Center, September 1969

(17) Charles Lee, Bruce Charles, David Kidd, "Wind-Tunnel Investigation of a Quarter-Scale Two-Bladed High-Performance Rotor in a Freon Atmosphere", USAAVLABS Technical Report 70-58 February 1971

(18) C. C. Perry, H. R. Lissner, "The Strain Gage Primer", McGraw-Hill Book Co., Inc., New York, 1955

(19) Harry H. Heyson, "Linearized Theory of Wind Tunnel Jet Boundary Corrections and Ground Effect for VTOL-STOL Aircraft", NASA TR-R-124, 1962

(20) William H. Rae, Jr., Limits on Minimum-Speed V/STOL Wind-Tunnel Tests", Journal of Aircraft, Volume 4, No. 3, May-June, 1967, Pages 249-254

(21) Ascher H. Shapiro, "Shape and Flow, The Fluid Dynamics of Drag", Doubleday & Co., Inc., New York, 1961

(22) R. E. Gormont, "Scale Effects on Model Rotor Performance", The Boeing Vertol Company Interoffice Memorandum 8-7441-1-410, June 1970

(23) Evan A. Fradenburgh, Sikorsky A/C Div., United A/C Corp. Panel Discussion Notes, Proceedings, AHS Mideast Region Symposium, October 1972

(24) F. D. Harris, "Articulated Rotor Blade Flapping Motion at Low Advance Ratio", Journal of the American Helicopter Society, Vol. 17, No. 1, January 1972

(25) C. Bobo, M. Cull, "Progress Report on Experimental Program to Investigate Various Test Section Configurations in Conjunction with Development of Boeing V/STOL Wind Tunnel" The Boeing Vertol Company Report D8-0696, June 1967

(26) F.D. Harris, "Rotor High Speed Performance, Theory Vs. Test", Paper Presented at V/STOL Technology & Planning Conference, Sponsored by Air Force Flt. Dyn. Lab., 1969 (J. of AHS, July 1970, Vol. 15, No. 7)

(27) W.G.S. Hardy, The Boeing-Vertol Company, "Reynolds Number Effect on Rotor Stall", Proceedings, AHS Mideast Region Symposium, October 1972

(28) Paul W. Huber, "Use of Freon-12 as a Fluid for Aerodynamic Testing", NACA TN-1024, April 1946

(29) Alfred Gessow, "Flight Investigation of Effects of Rotor-Blade Twist on Helicopter Performance in the High-Speed and Vertical-Autorotative-Descent Conditions", NASA TN-1666, August 1948

ACKNOWLEDGEMENT

This paper is dedicated to the men and women of the Boeing V/STOL Wind Tunnel. In five years, their combined effort has accomplished more to advance the art of rotary wing model designing, building, instrumenting and testing than any group I know.

FIGURE 1 THE HISTORY OF AERODYNAMIC TESTING

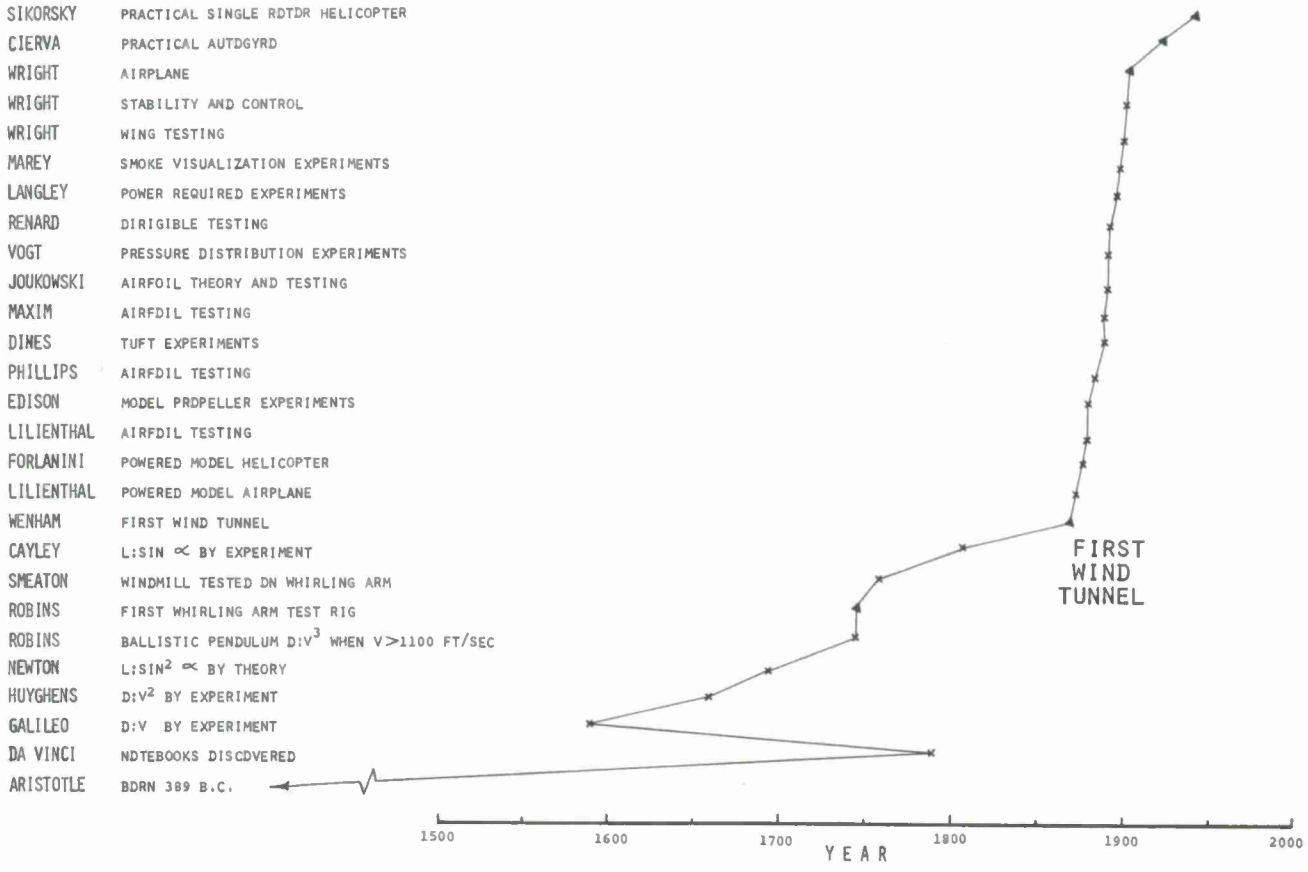


FIGURE 2 STEPS THAT CAN BE TAKEN TO REDUCE THE RISKS IN ROTARY WING AIRCRAFT DEVELOPMENT

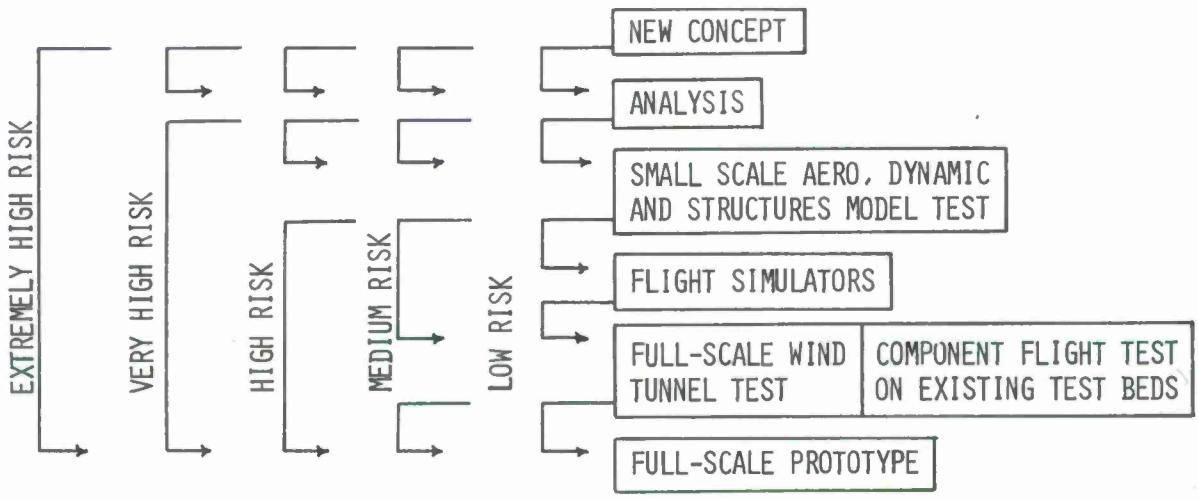


FIGURE 3 USING OUR TOOLS WILL REDUCE RISK AND COSTS

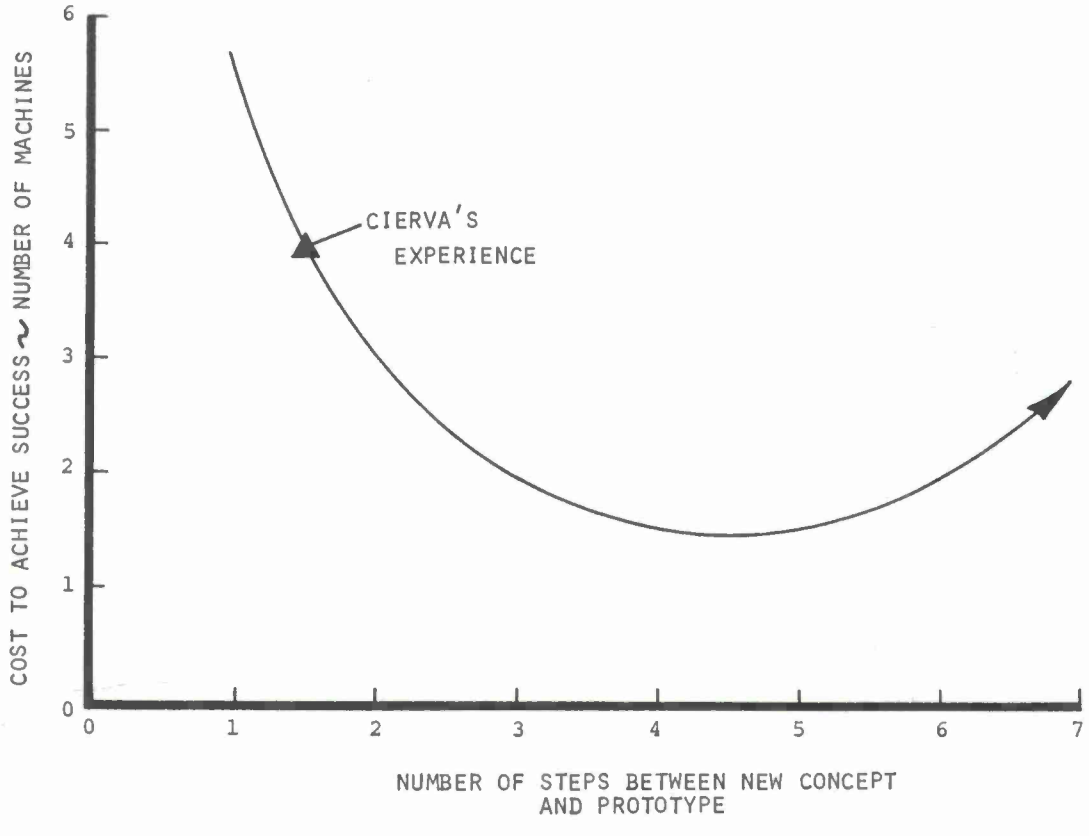


FIGURE 4

ROBINS' BALLISTIC PENDULUM

JUNE 1746

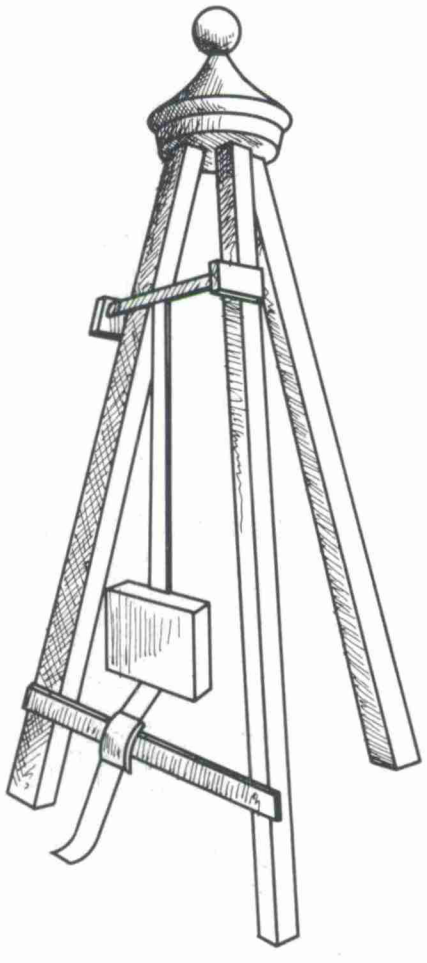


FIGURE 5 ROBINS' WHIRLING ARM
TEST RIG JUNE 1746

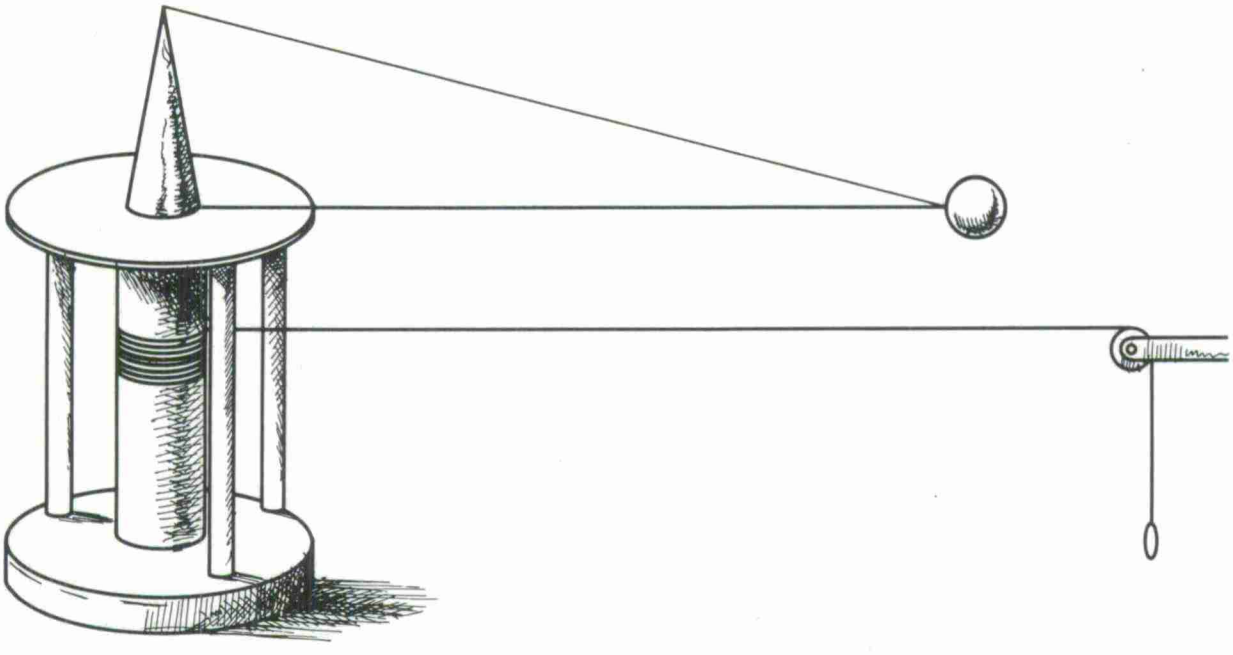


FIGURE 6 SMEATON'S WIND MILL TEST RIG JUNE 1759

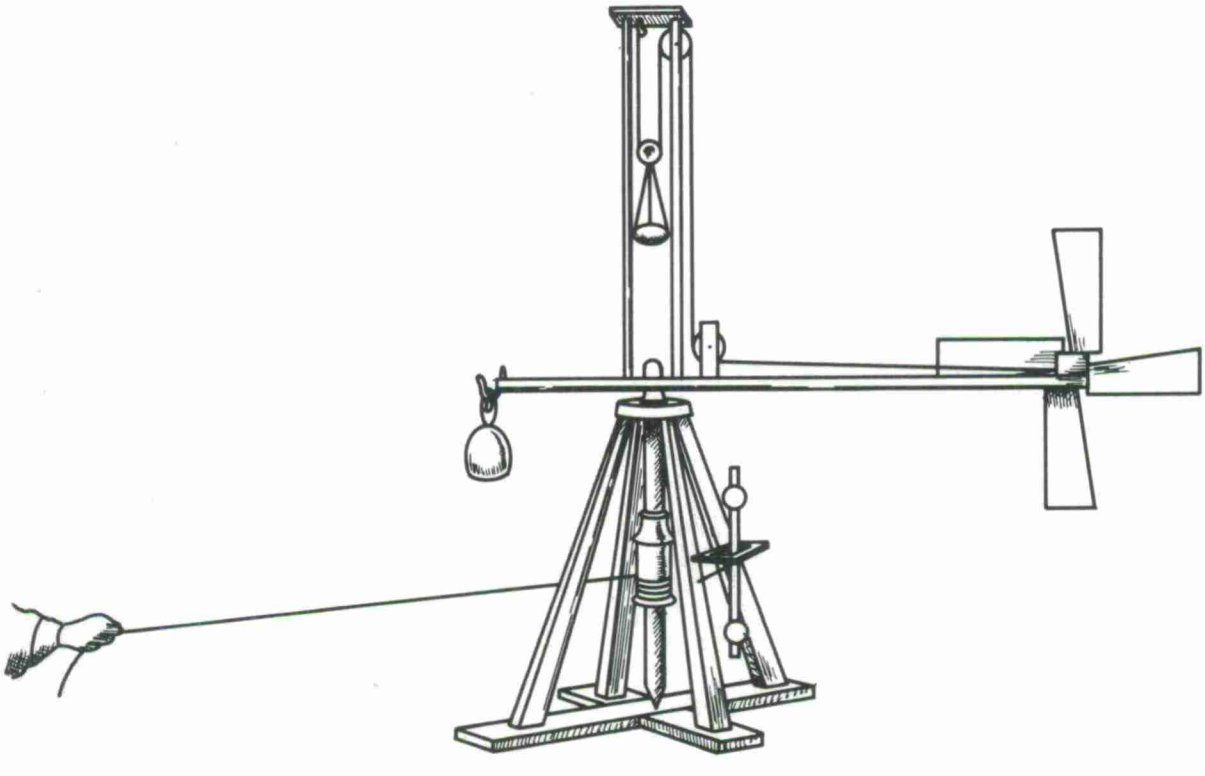


FIGURE 7 A MATRIX OF TEST OBJECTIVES

	ENGINEERING DISCIPLINES										
	AEROELASTICITY			FLYING QUALITIES				DESIGN			
REASONS FOR TESTING	AERODYNAMICS	DYNAMICS	STRUCTURES	STABILITY	CONTROL	ACOUSTICS	VIBRATION	CONFIGU-RATION	COMPONENTS	PROPULSION	WEIGHTS
TO EVALUATE HYPOTHESIS, THEORY OR LAW											
TO STUDY KNOWN PHENOMENA											
TO LOOK FOR UNEXPECTED PHENOMENA											
TO OPTIMIZE CONFIGURATIONS											
TO CONFIRM THE PERFORMANCE OR INTEGRITY OF SPECIFIC DESIGN											

FIGURE 8 THE NASA LANGLEY CONTROL-LINE FACILITY

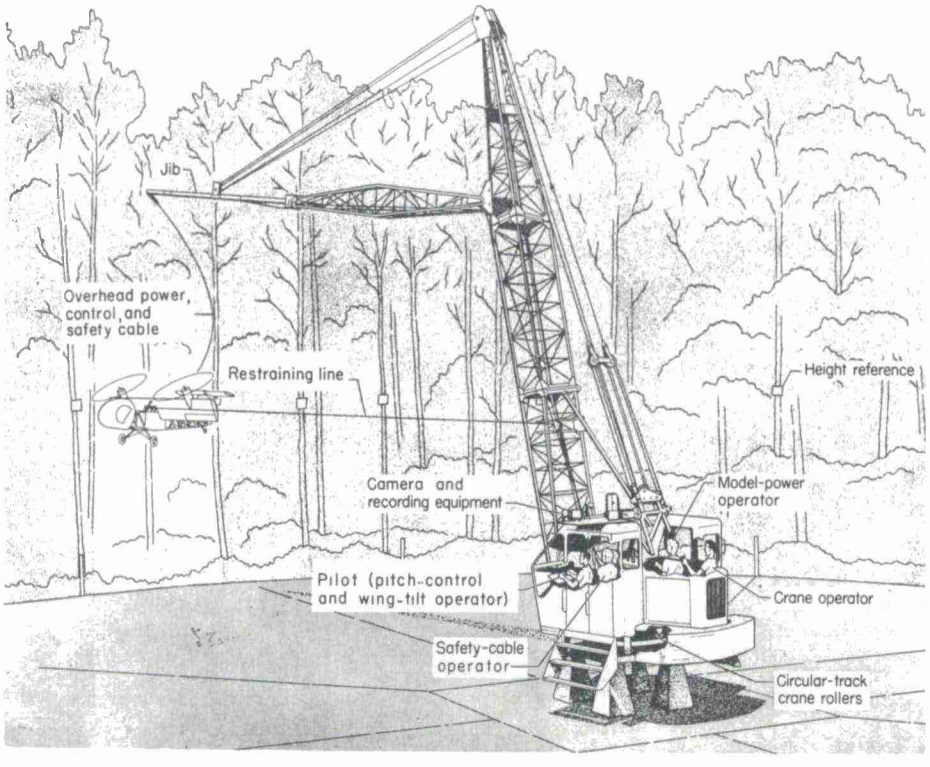


FIGURE 9 THE CORNELL C.A.R.T. TEST FACILITY

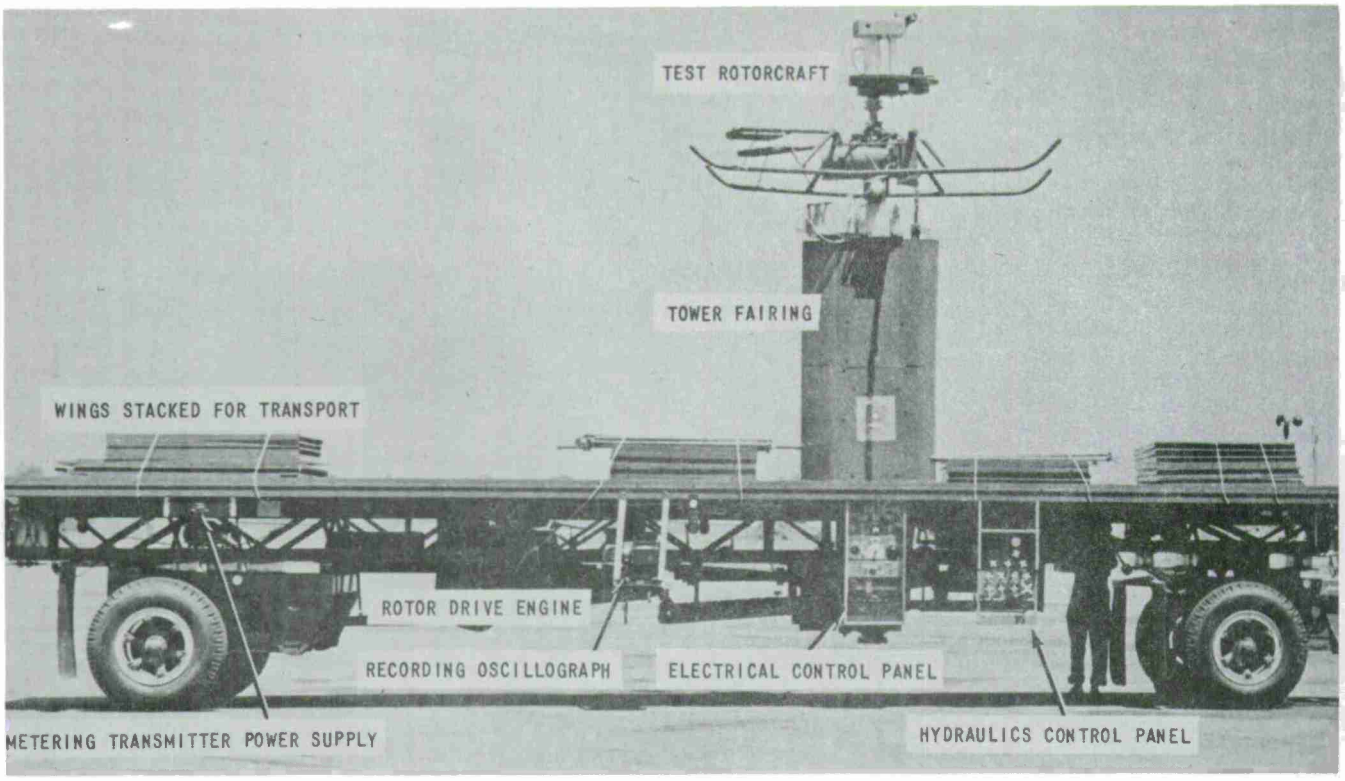


FIGURE 10 THE PRINCETON TRACK TEST FACILITY

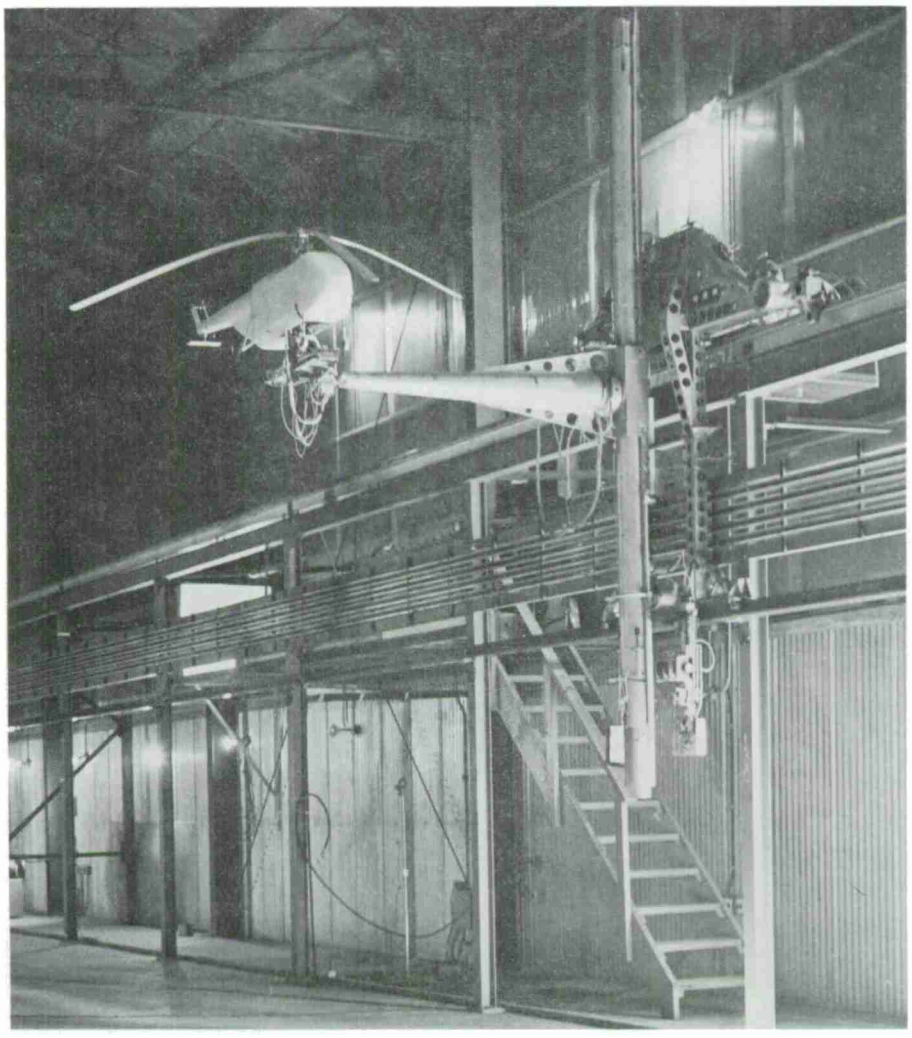


FIGURE 11 ROTARY WING FACILITY TESTING ENVELOPE

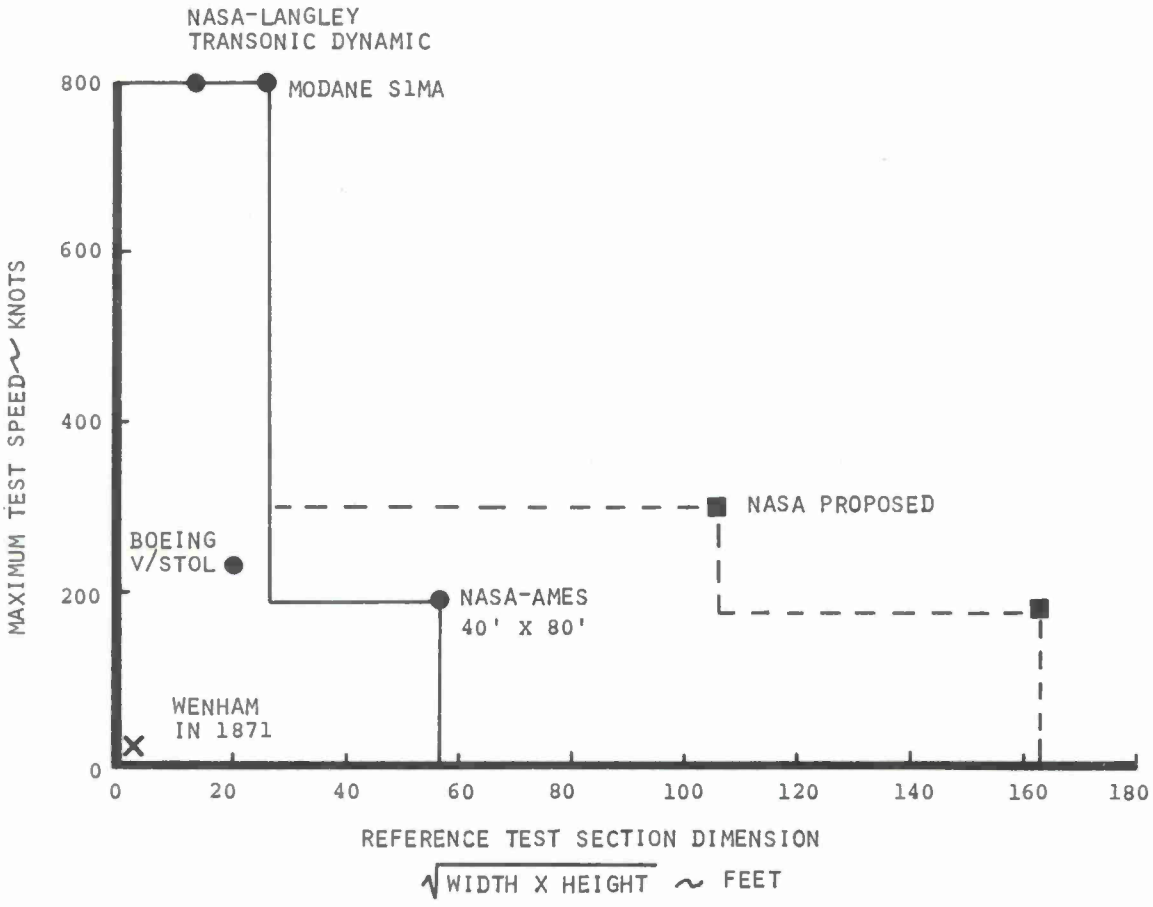


FIGURE 12 NASA PROPOSED FULL-SCALE SUBSONIC WIND TUNNEL

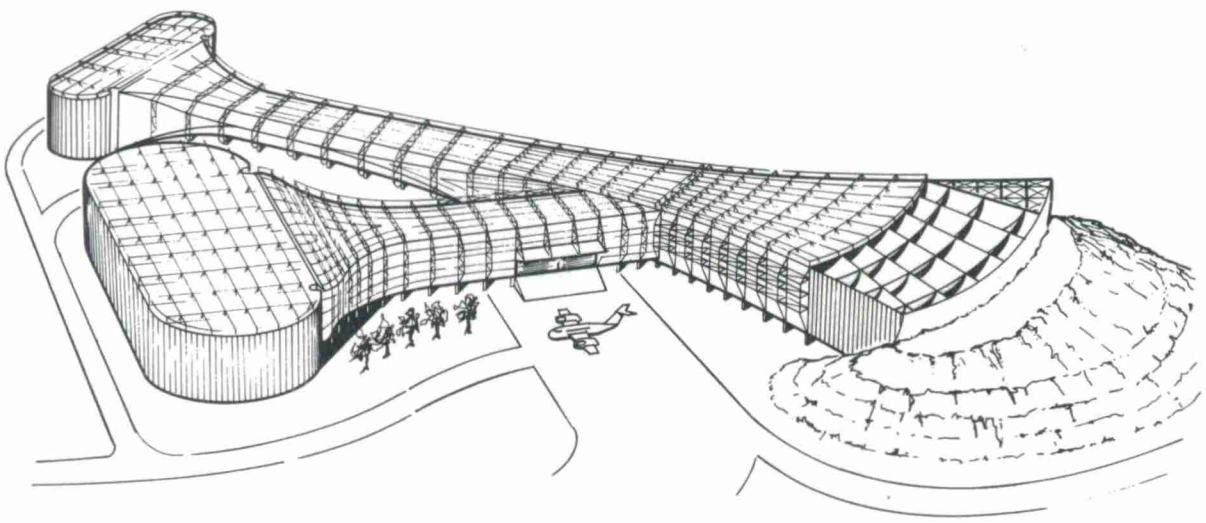


FIGURE 13 OVERVIEW OF BOEING V/STOL WIND TUNNEL

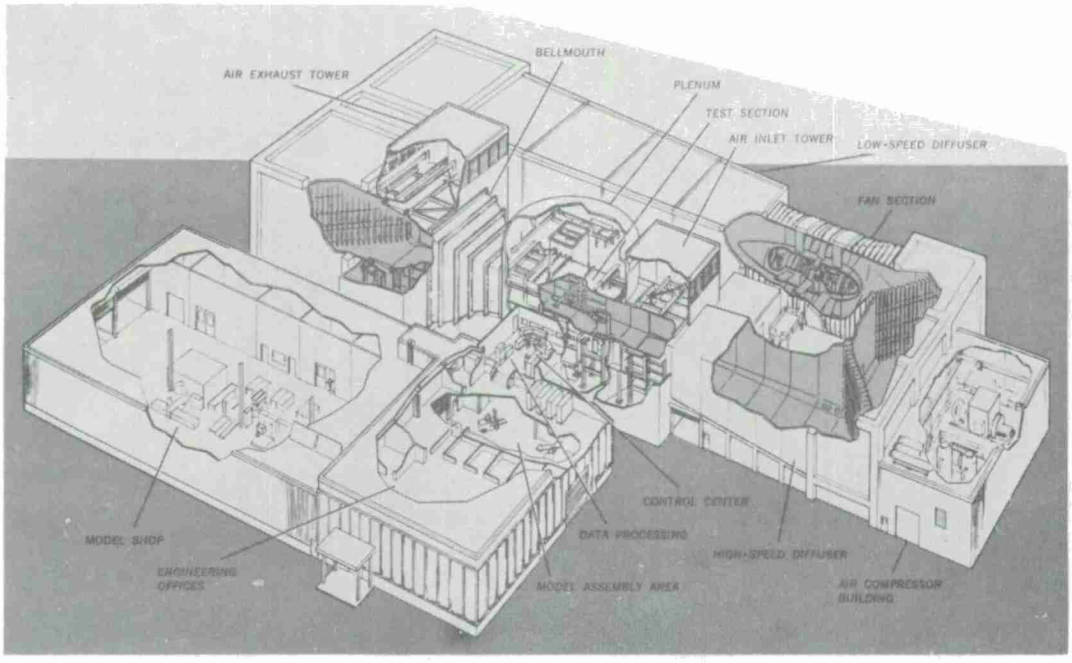
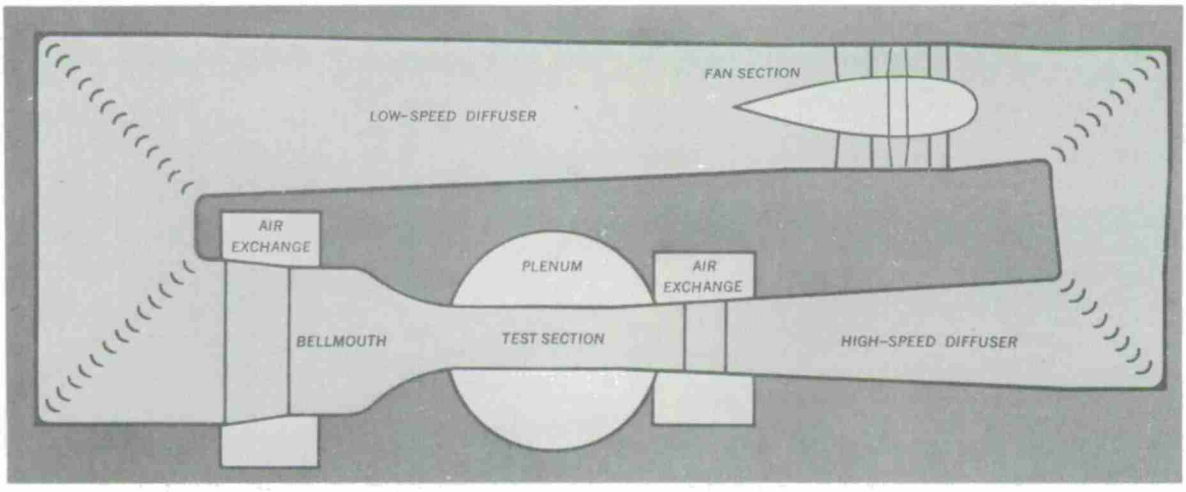


FIGURE 14 BOEING V/STOL WIND TUNNEL CIRCUIT LAYOUT



TEST SECTION FEATURES

- 20x20 ft.cross section
- 45 ft.long
- contraction ratio =6.0
- diffuser angle =6°equiv.cone
- maximum tunnel velocity v=240knots

FIGURE 15 BOEING V/STOL WIND TUNNEL TEST SECTION
WITH 16-FOOT DIAMETER MODEL ROTOR

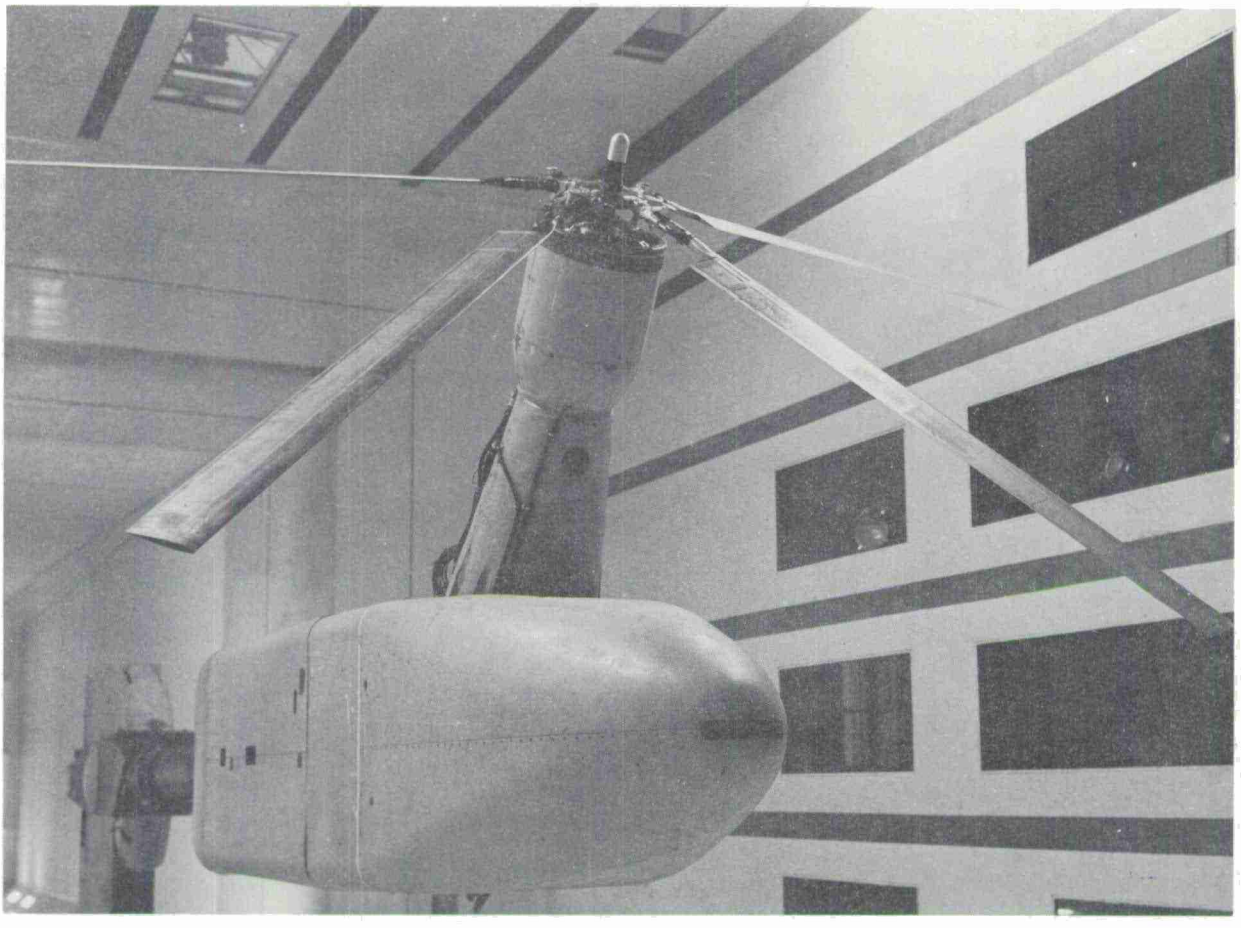


FIGURE 16 BOEING UNIVERSAL HELICOPTER
MODEL, OR UHM-I 1963

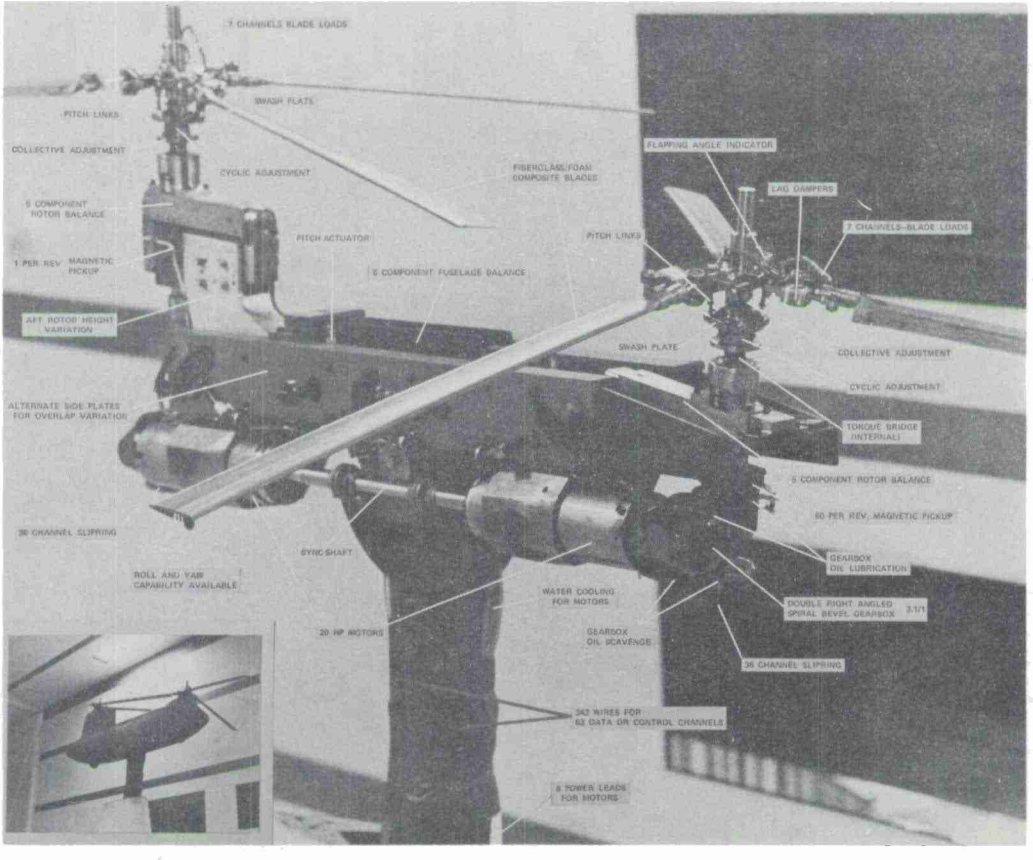


FIGURE 17 BOEING UNIVERSAL HELICOPTER
MODEL, OR UHM-II 1973

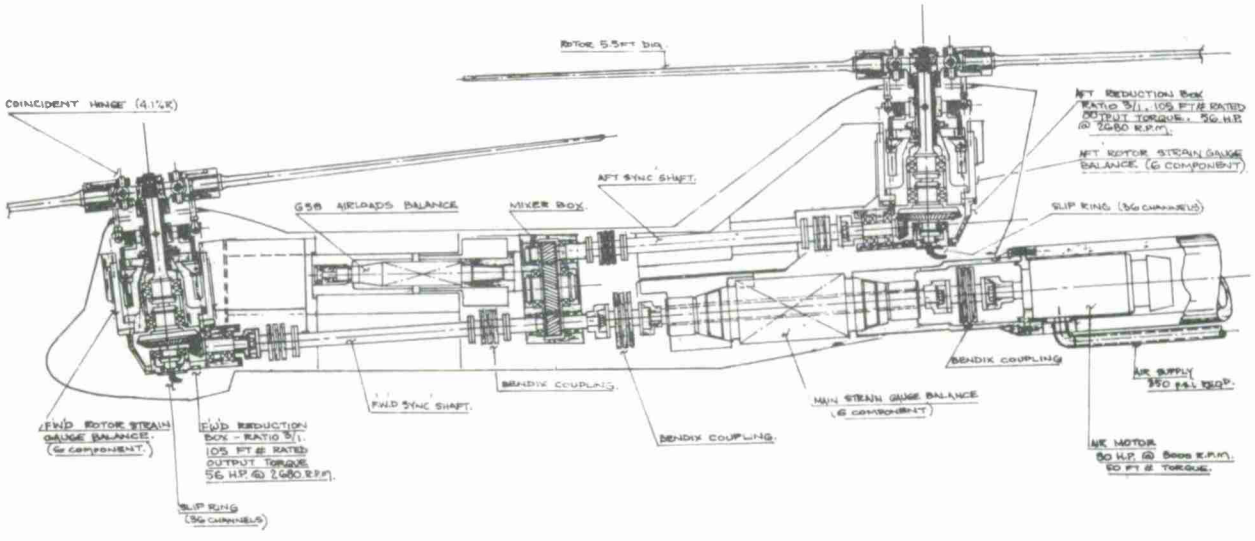


FIGURE 18 PITCH/ROLL FREEDOM FROUDE SCALED
SINGLE ROTOR HELICOPTER

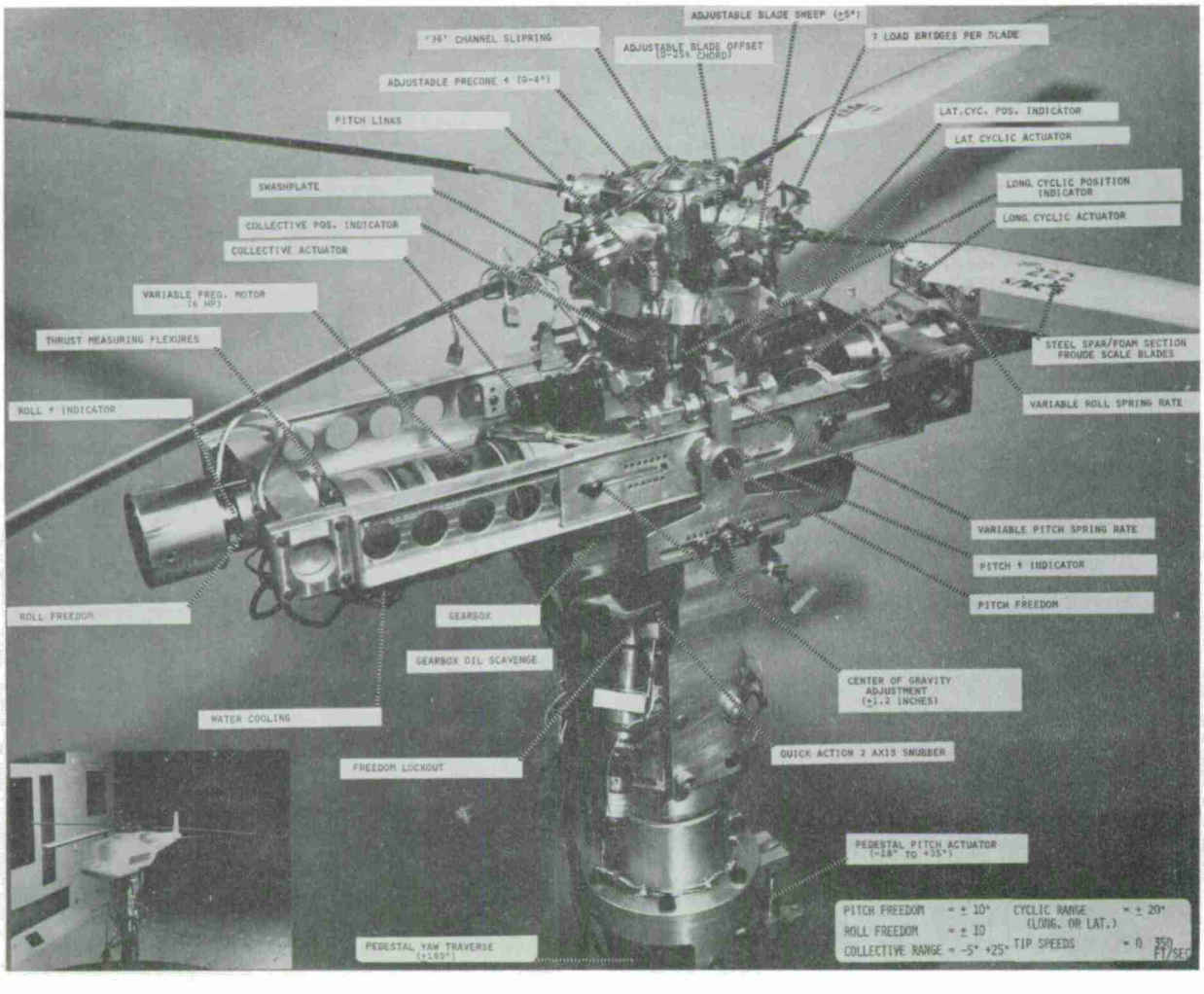


FIGURE 19 SAFETY OF FLIGHT MONITOR

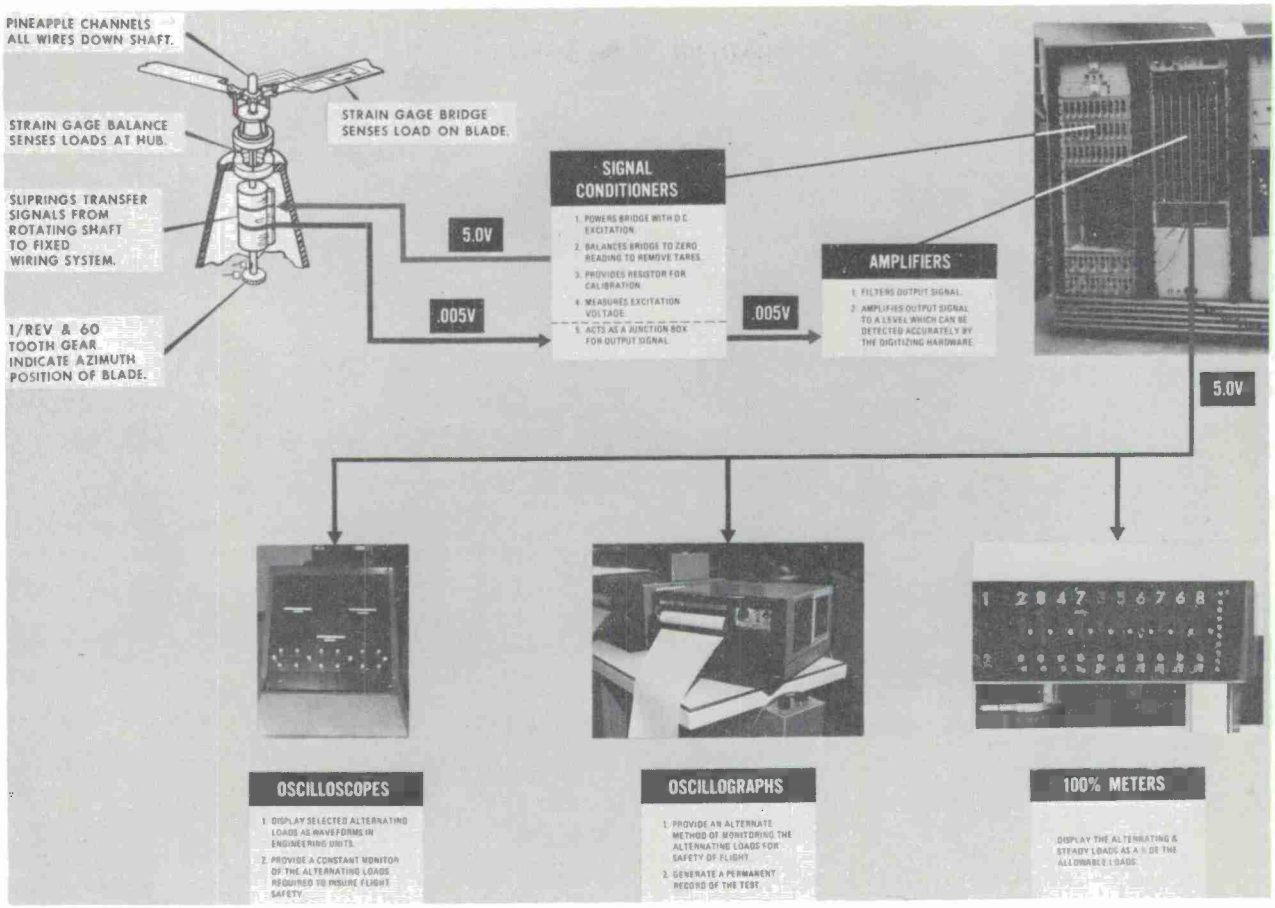


FIGURE 20 STATIC DATA SYSTEM

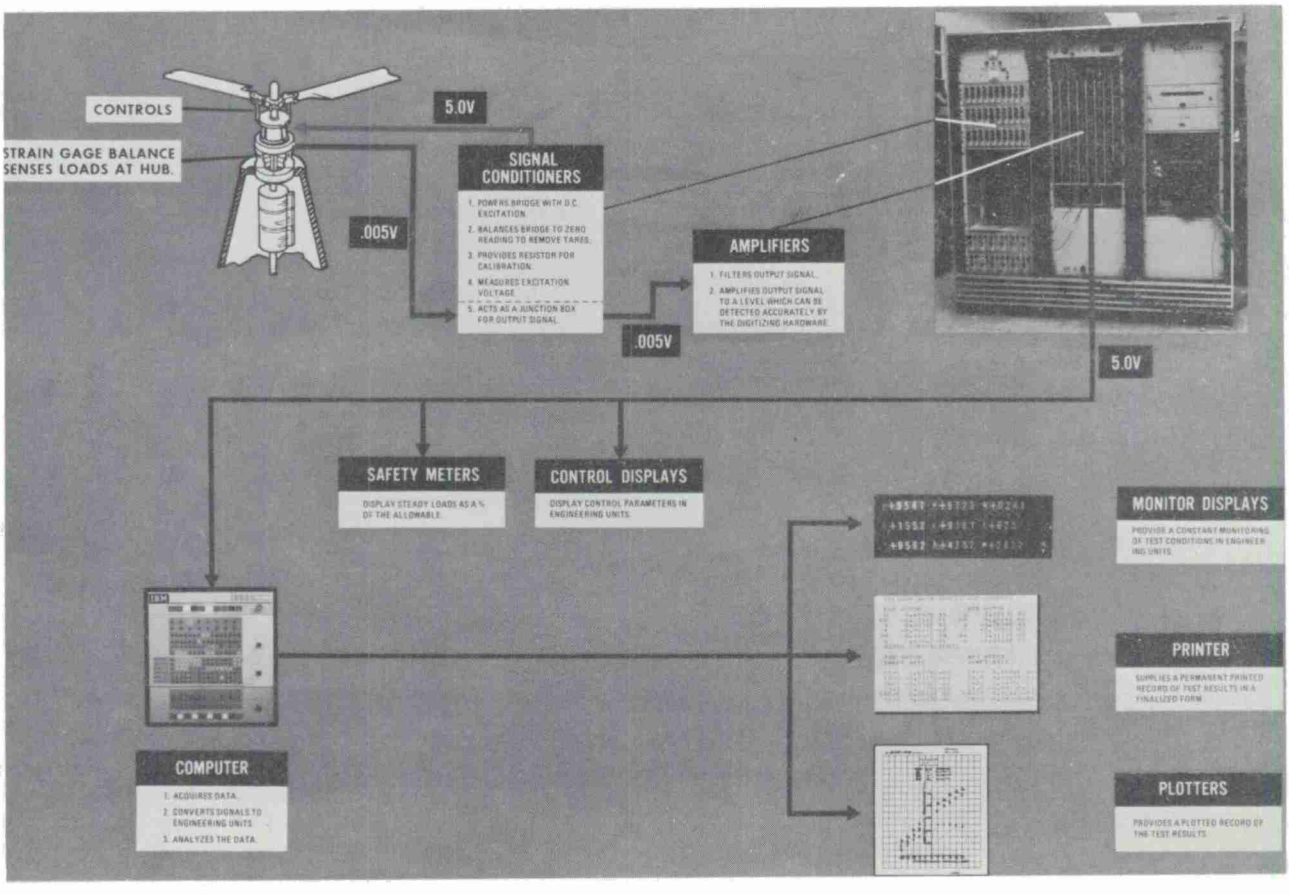


FIGURE 21 STRUCTURAL/DYNAMIC DATA SYSTEM

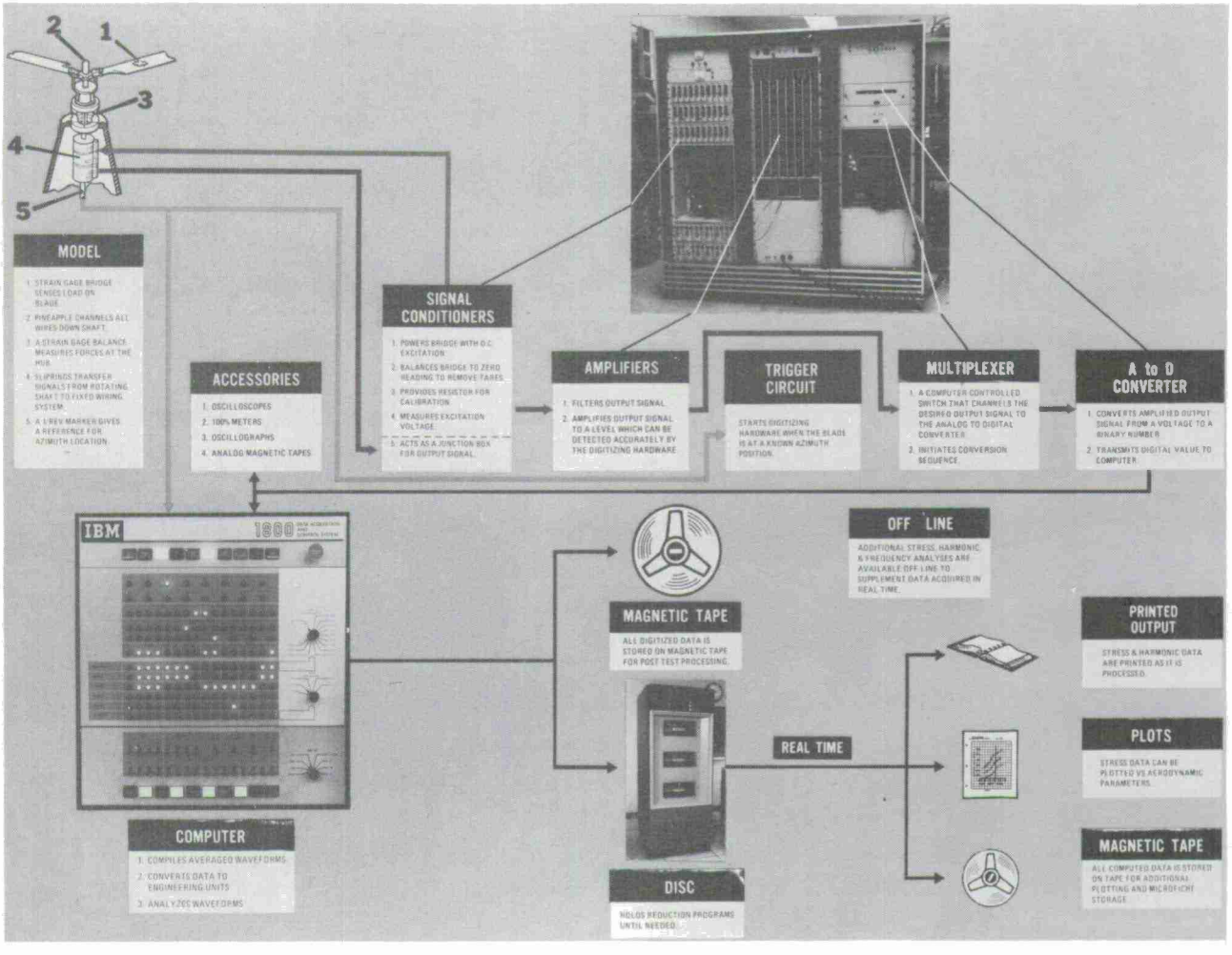


FIGURE 22 BOEING V/STOL WIND TUNNEL
DATA MANAGEMENT SYSTEM

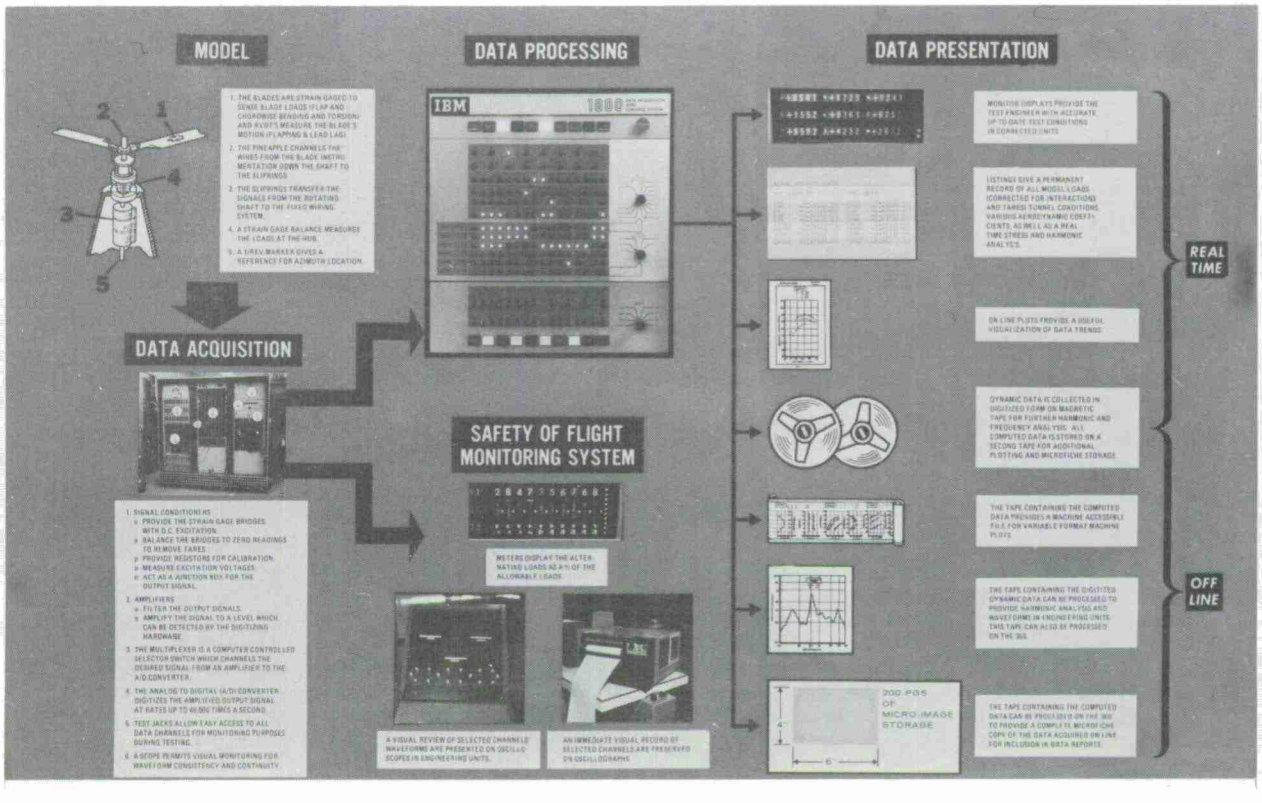


FIGURE 23 UPWASH ANGLE DUE TO WIND TUNNEL WALL INTERFERENCE FOR SQUARE TEST SECTION

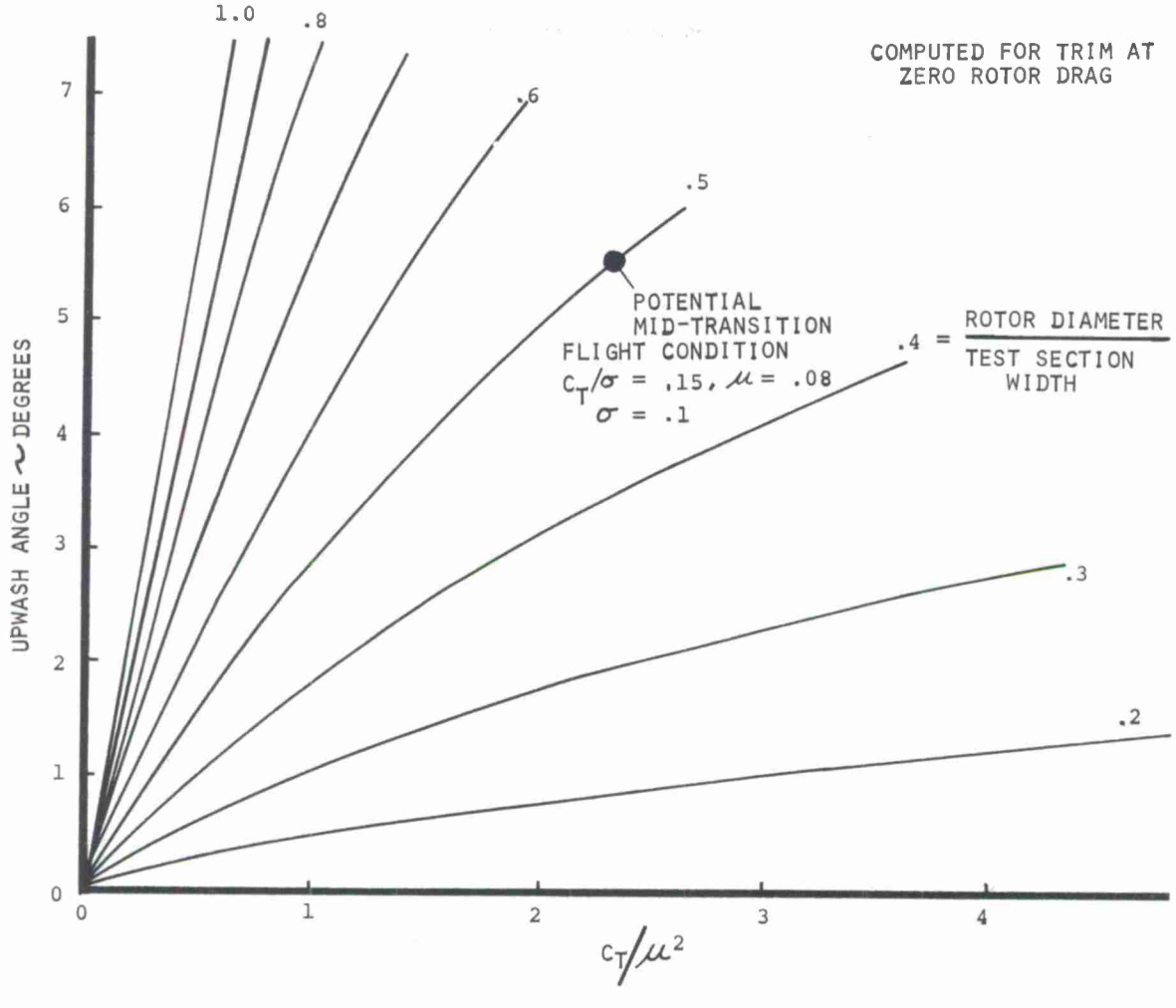


FIGURE 24 ROTOR THRUST/SPEED CONDITIONS FOR FLOW BREAKDOWN IN A SQUARE TEST SECTION WIND TUNNEL

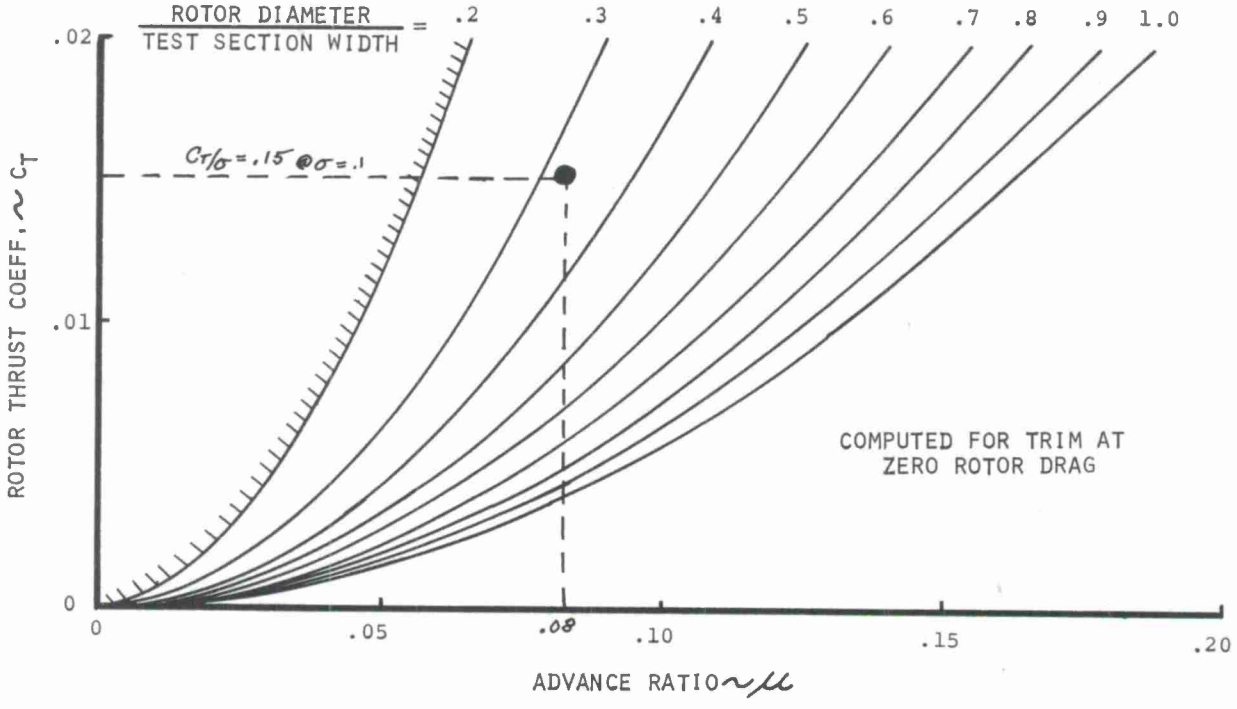


FIGURE 25 TYPICAL AIRFOIL STALLING CHARACTERISTICS

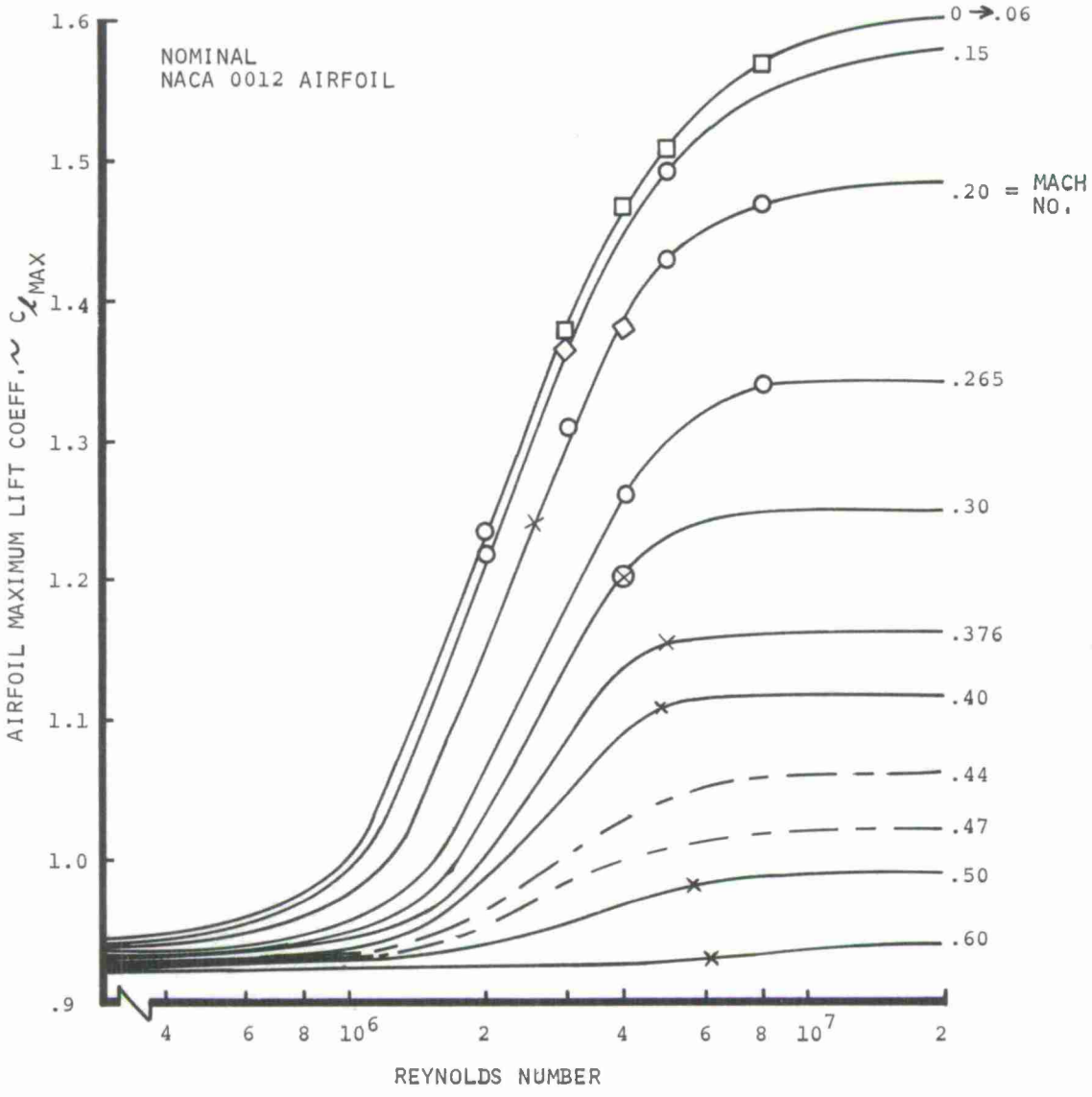


FIGURE 26 RETREATING BLADE TIP LIFT COEFF. FOR SEPARATED FLOW ONSET IN ROTOR DISC

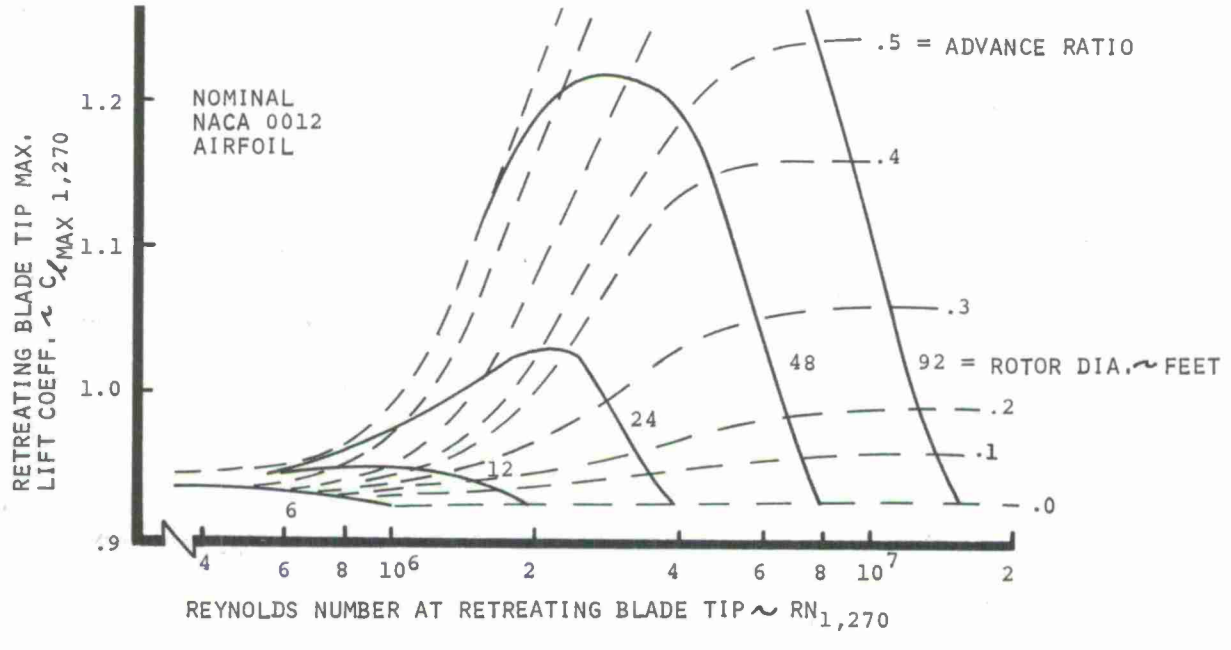


FIGURE 27 ROTOR C_T/σ FOR ONSET OF SEPARATED FLOW

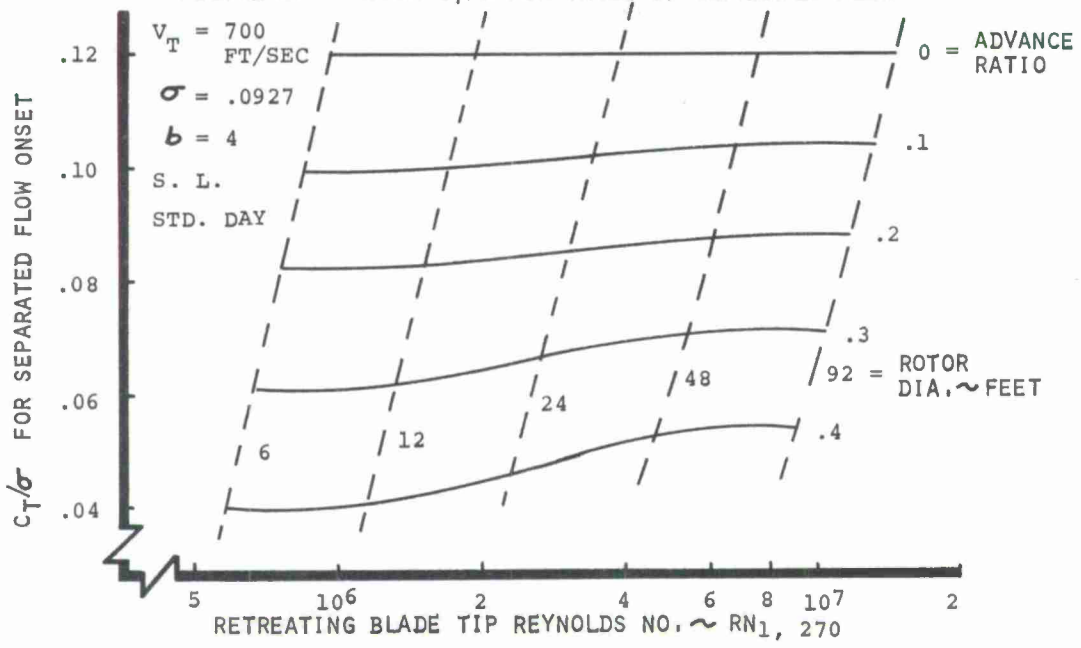


FIGURE 28 ROTOR AEROELASTIC CHARACTERISTICS WITH ADVANCE RATIO AT C_T/σ = .09, $X/qD^2\sigma$ = .25, V_T = 695 FT/SEC

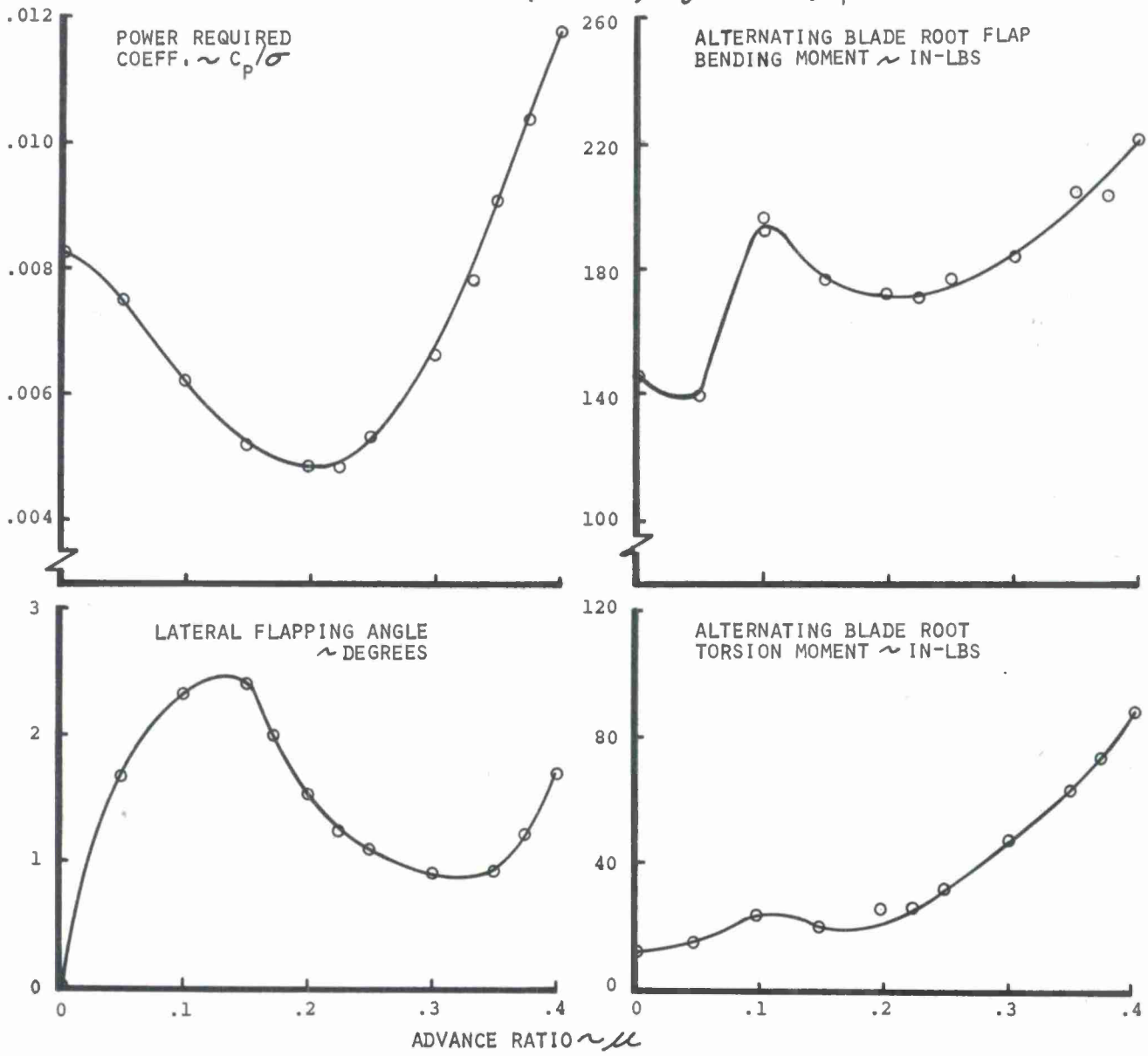


FIGURE 29 ROTOR AEROELASTIC CHARACTERISTICS WITH ROTOR DRAG/LIFT RATIO AT ADVANCE RATIO = .1

$$\frac{L}{\rho b C R V_T^2} = .0806 \quad V_T = 695 \text{ FT/SEC}$$

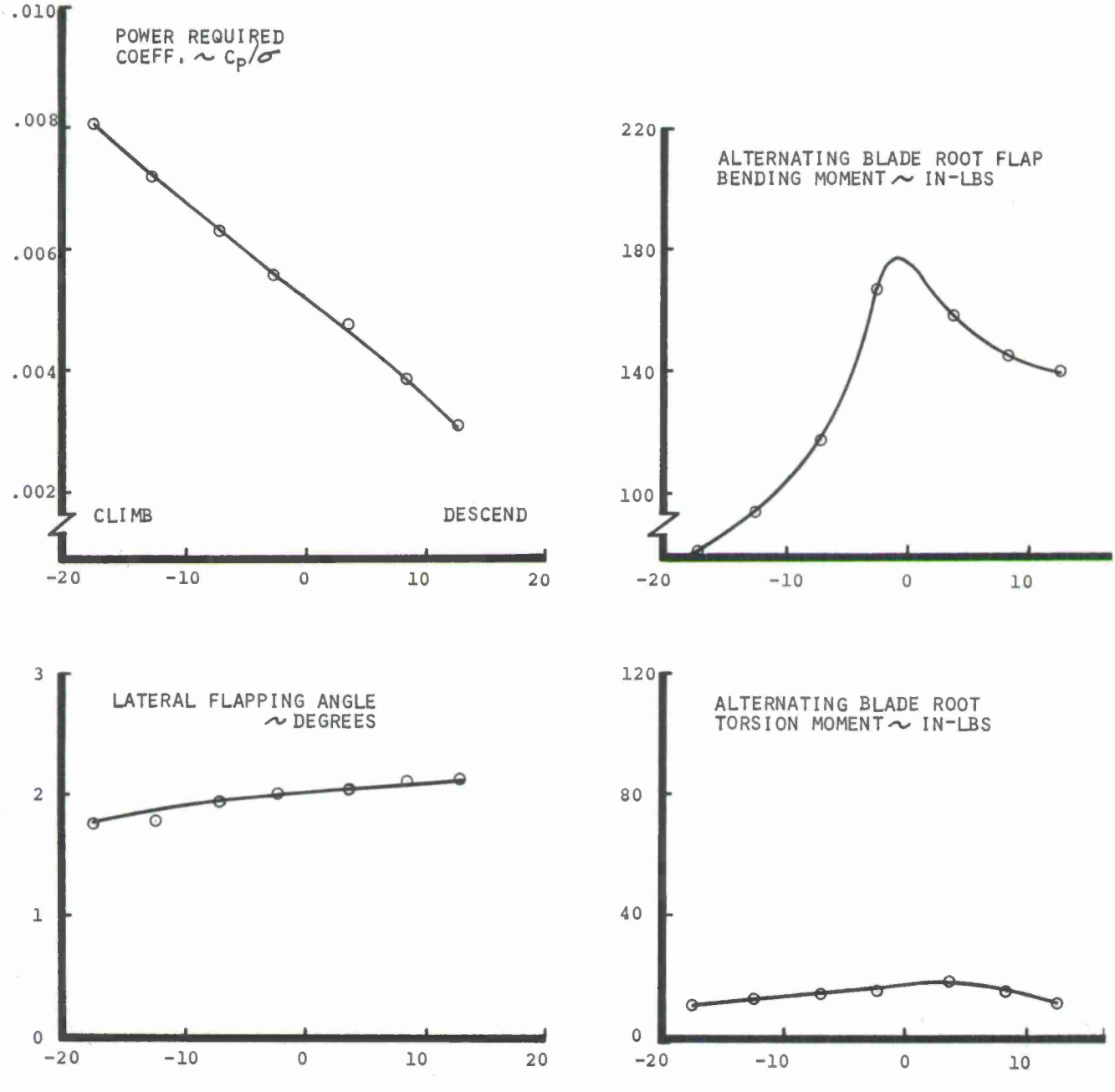


FIGURE 30 ROTOR AEROELASTIC CHARACTERISTICS WITH ROTOR THRUST AT ADVANCE RATIO = .1

$\alpha_S = -4.62°$, $V_T = 695$ FT/SEC

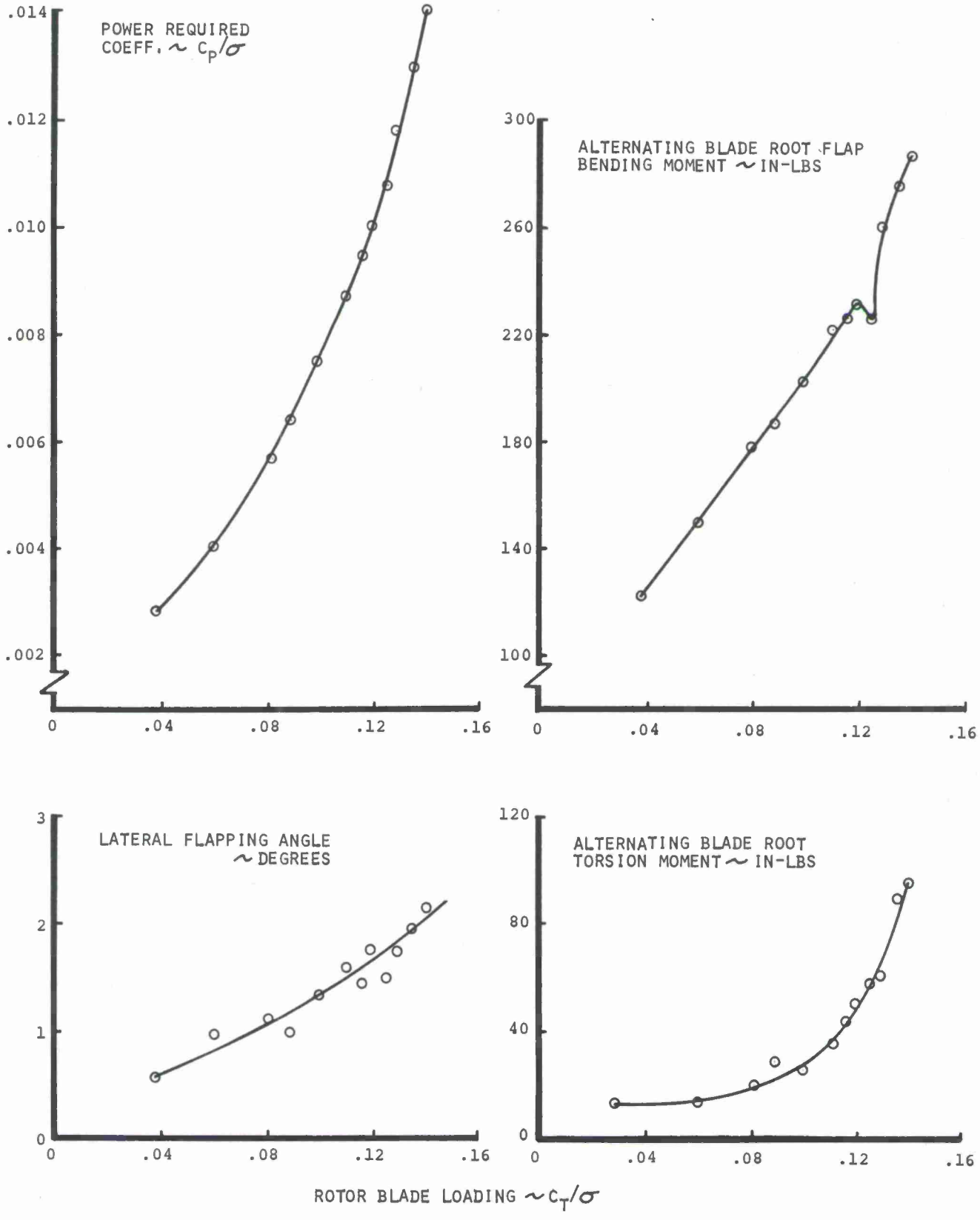


FIGURE 31 ROTOR AEROELASTIC CHARACTERISTICS WITH ROTOR THRUST AT ADVANCE RATIO = .4
$X/\rho D^2\sigma$ = .1, V_T = 765 FT/SEC

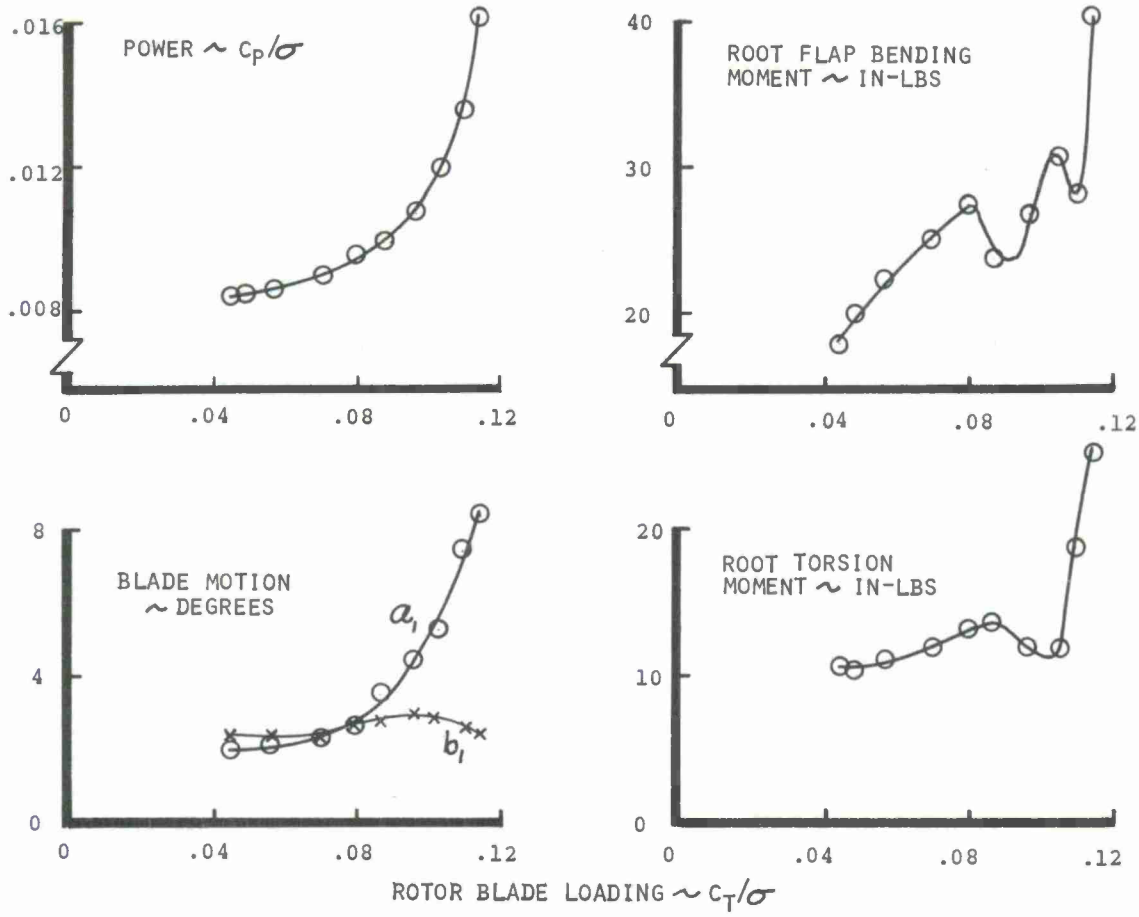


FIGURE 32 EFFECT OF WIND TUNNEL TEST SECTION POROSITY ON MODEL ROTOR THRUST AT ADVANCE RATIO = .113

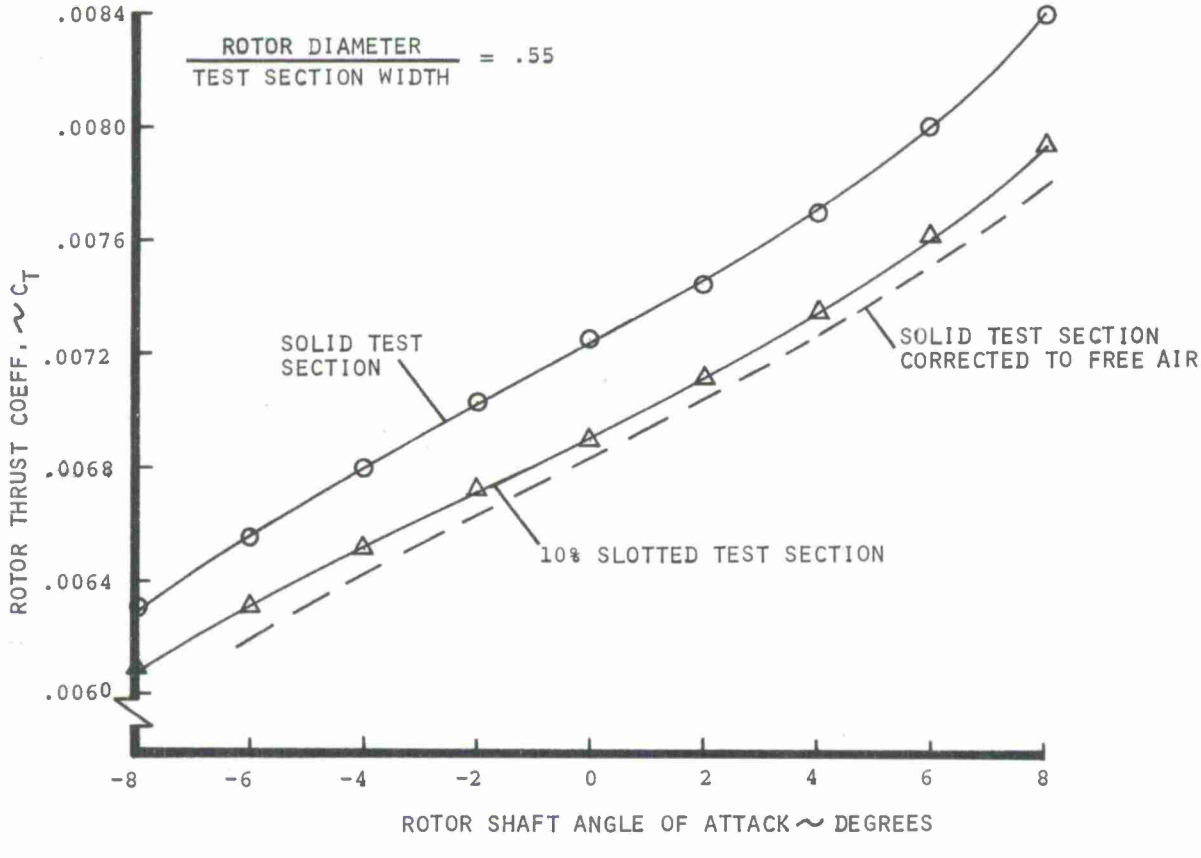


FIGURE 33 THEORETICAL EFFECT OF REYNOLDS NO. ON ROTOR STALL

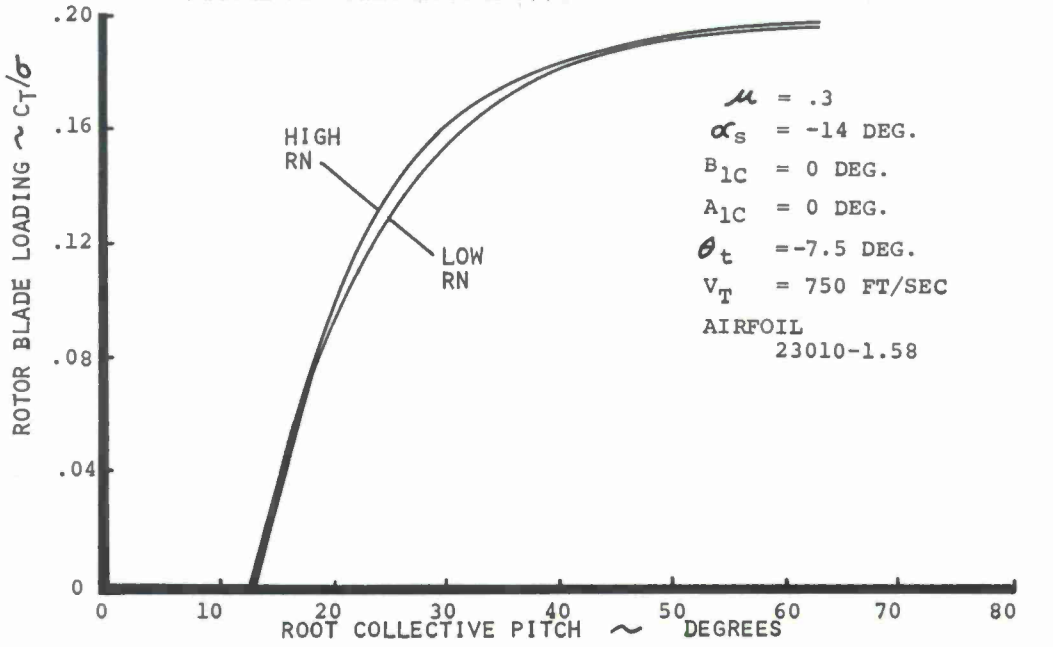


FIGURE 34 LOW SPEED WIND TUNNEL COSTS

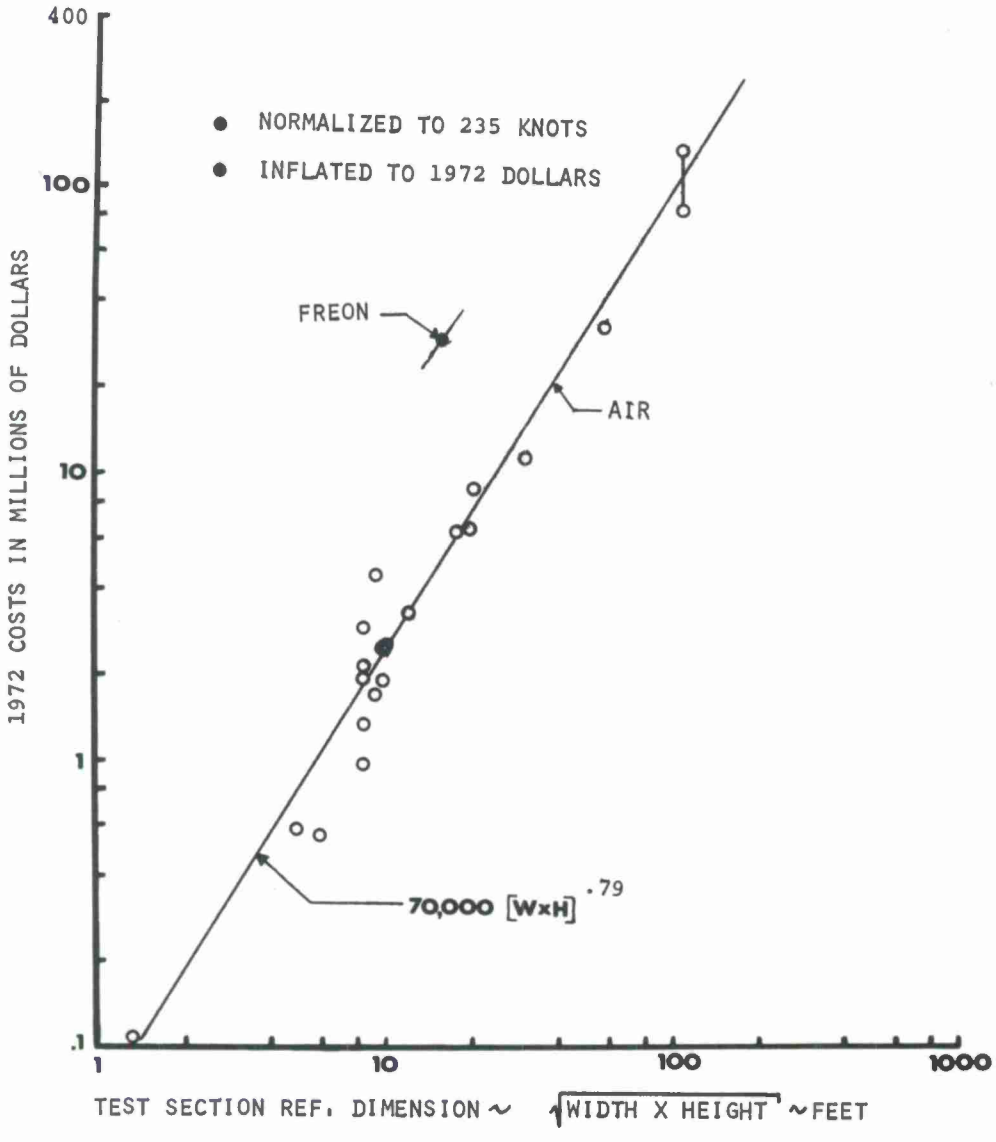


FIGURE 35 MODEL COSTS RELATED TO FULL-SCALE COSTS AS A FUNCTION OF SIZE

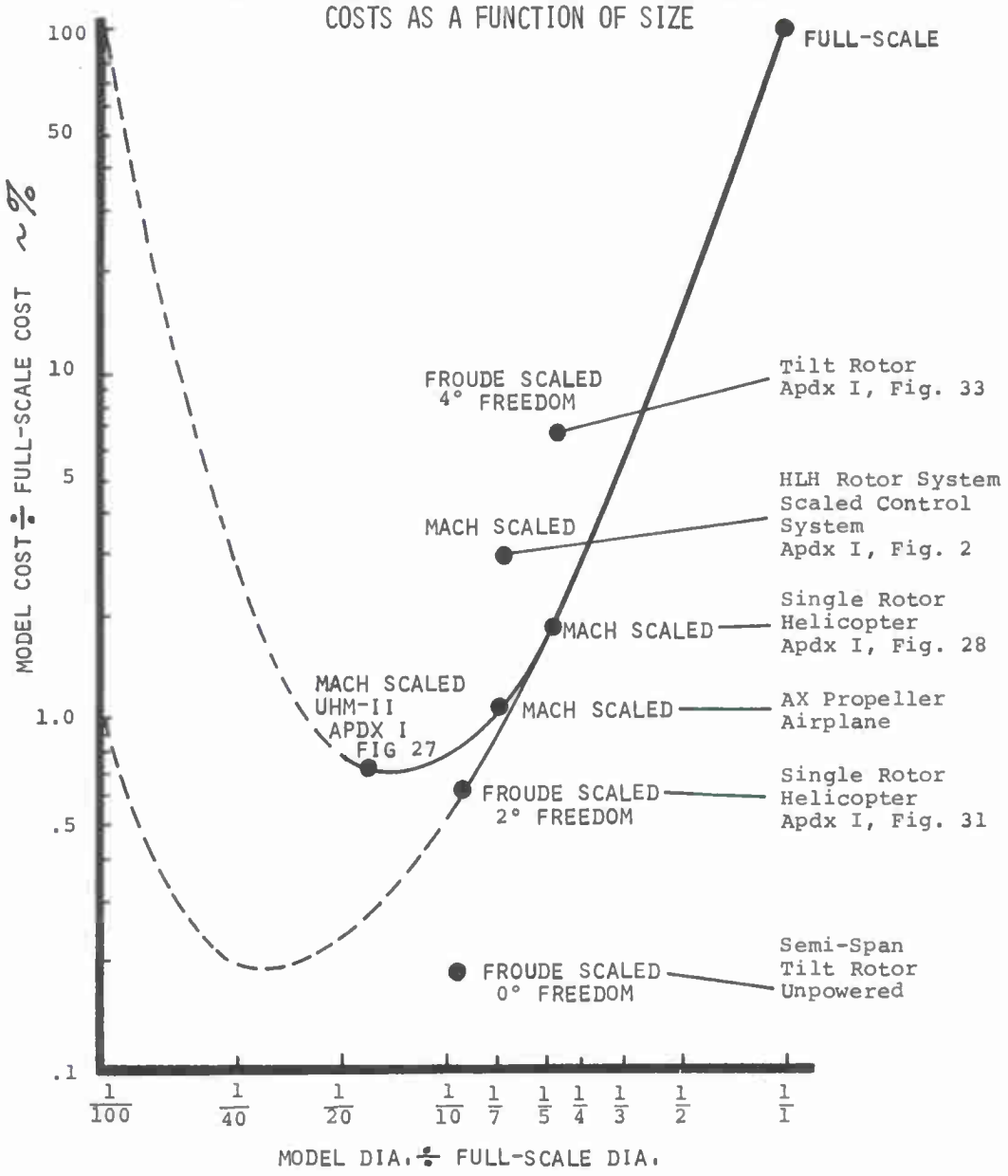


FIGURE 36 MODELS PLUS WIND TUNNEL COSTS OVER 25 YEARS TO SUPPORT DEVELOPMENT OF 5 FULL-SCALE PROTOTYPES

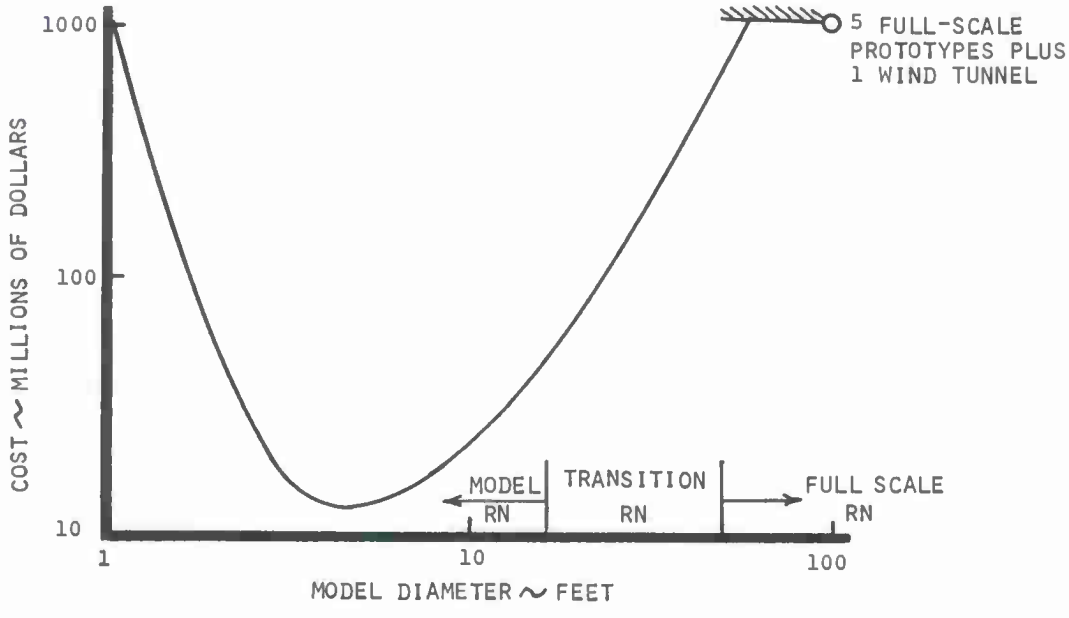


FIGURE 37 MODEL ROTOR SIMULATING PARAMETERS

TO SIMULATE	ROTOR PARAMETER	EQUATIONS (UNIFORM BLADE)	SCALING RELATIONSHIPS
SPEED	ADVANCE RATIO	$\mu = V/\Omega R$	$V_m = (\Omega R)_m/\Omega R \; V$
COMPRESSIBILITY	MACH NUMBER	$M = \Omega R/a_s$	$(\Omega R)_m = (a_{sm}/a_s)\; \Omega R$
STRUCTURAL DYNAMICS	BLADE FREQUENCY	$\frac{\omega_n}{\Omega} \propto \frac{EI}{w\Omega^2 R^4}$	$EI_m = \frac{w_m}{w} \frac{(\Omega R)^2_m}{(\Omega R)^2} \left(\frac{R_m}{R}\right)^2 EI$
AERO MOMENT / CENTRIFUGAL MOMENT	LOCK NUMBER	$\gamma = \frac{3\rho acRg}{2w}$	$w_m = \frac{(\rho cR)_m}{\rho cR} \; w$
WEIGHT MOMENT / CENTRIFUGAL MOMENT	FROUDE NUMBER	$\mathcal{F} = 3g/2\Omega^2 R$	$(\Omega R)_m = (R_m/R)^{1/2} \; \Omega R$
THRUST	THRUST COEFFICIENT	$C_T = \frac{T}{\rho \pi R^2 \Omega^2 R^2}$	$(\Omega R)_m = \left(\frac{\rho}{\rho_m}\right)^{1/2} \Omega R$
DOWNWASH	DISC LOADING	$D.L. = T/\pi R^2$	$T_m = (R_m/R)^2 \; T$
BLADE STALL	REYNOLDS NUMBER	$RN = \frac{\rho \Omega R c}{\bar{\mu}}$	$c_m = \frac{\bar{\mu}_m}{\bar{\mu}} \frac{\rho \Omega R}{(\rho \Omega R)_m} c$
GEOMETRY	BLADE ASPECT RATIO	$\mathcal{AR} = R/C$	$c_m = (R_m/R)\; c$
GEOMETRY	SOLIDITY	$\sigma = bc/\pi R = b/\pi \mathcal{AR}$	$b_m = (\mathcal{AR}_m/\mathcal{AR})\; b$

FIGURE 38 FLOW BREAKDOWN CRITERIA FOR SINGLE ROTOR

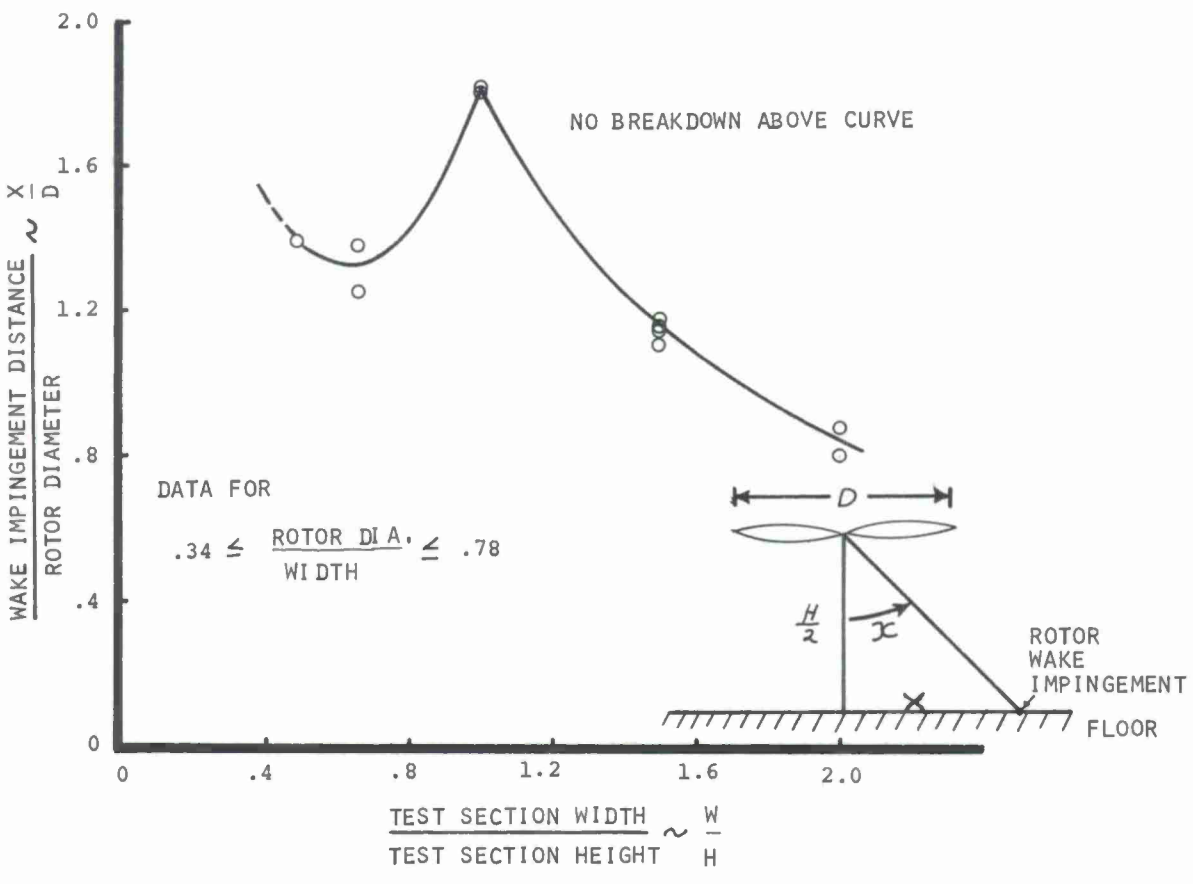


FIGURE 39 TEST SECTION SIZE PARAMETER FOR SINGLE ROTOR

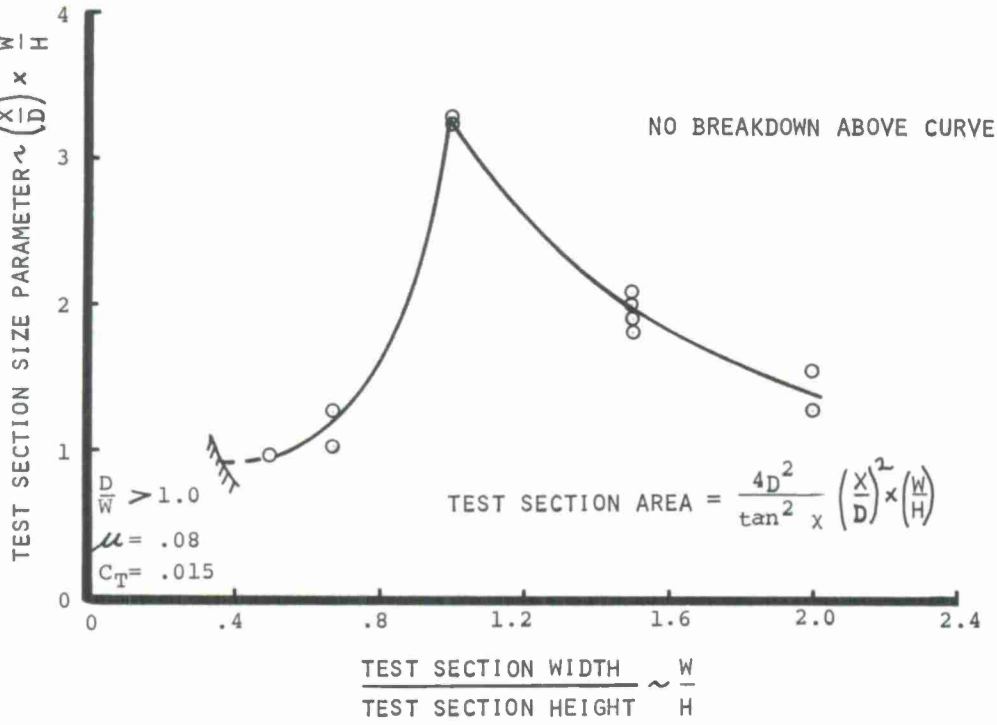


FIGURE 40 TEST SECTION SIZE THAT AVOIDS FLOW BREAKDOWN AT μ = .08, C_T = .015 FOR 20 FOOT DIAMETER SINGLE ROTOR MODEL TESTING

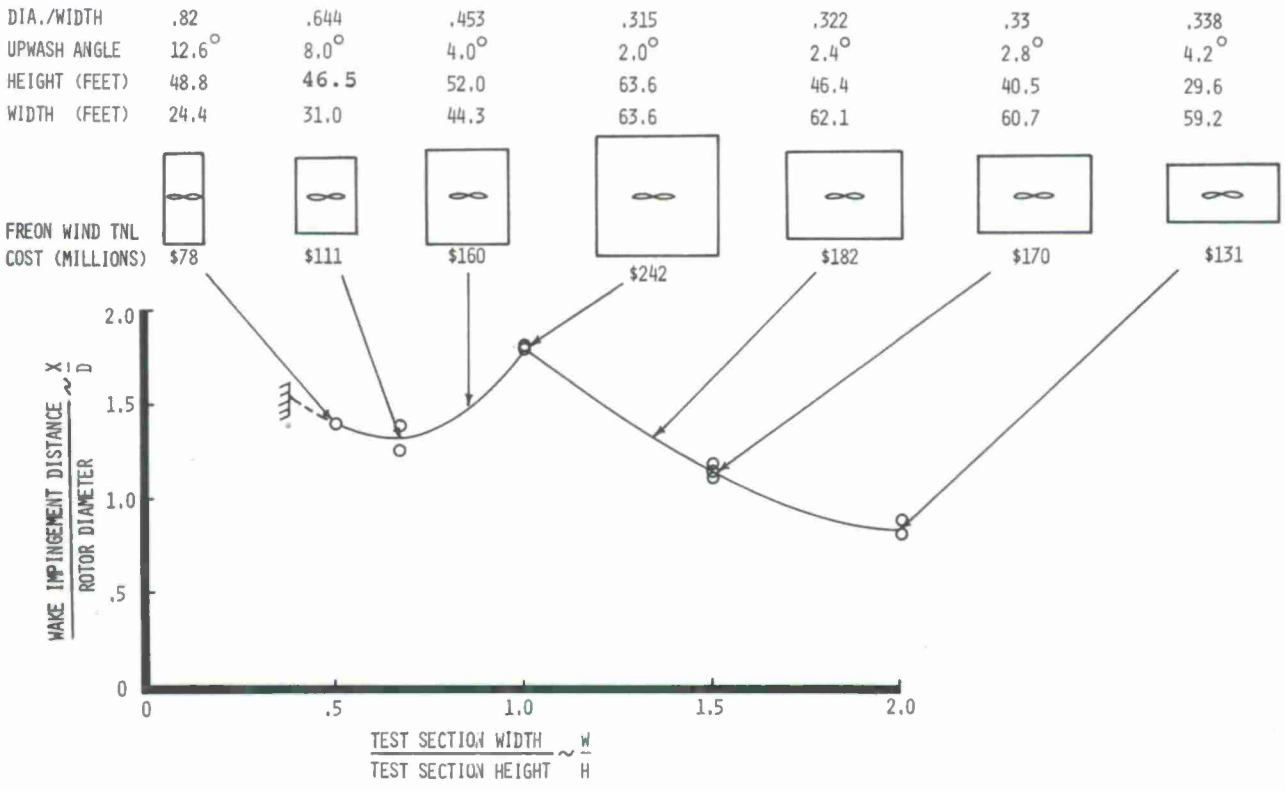


FIGURE 41 GUESSED FLOW BREAKDOWN CRITERIA FOR TILT ROTOR

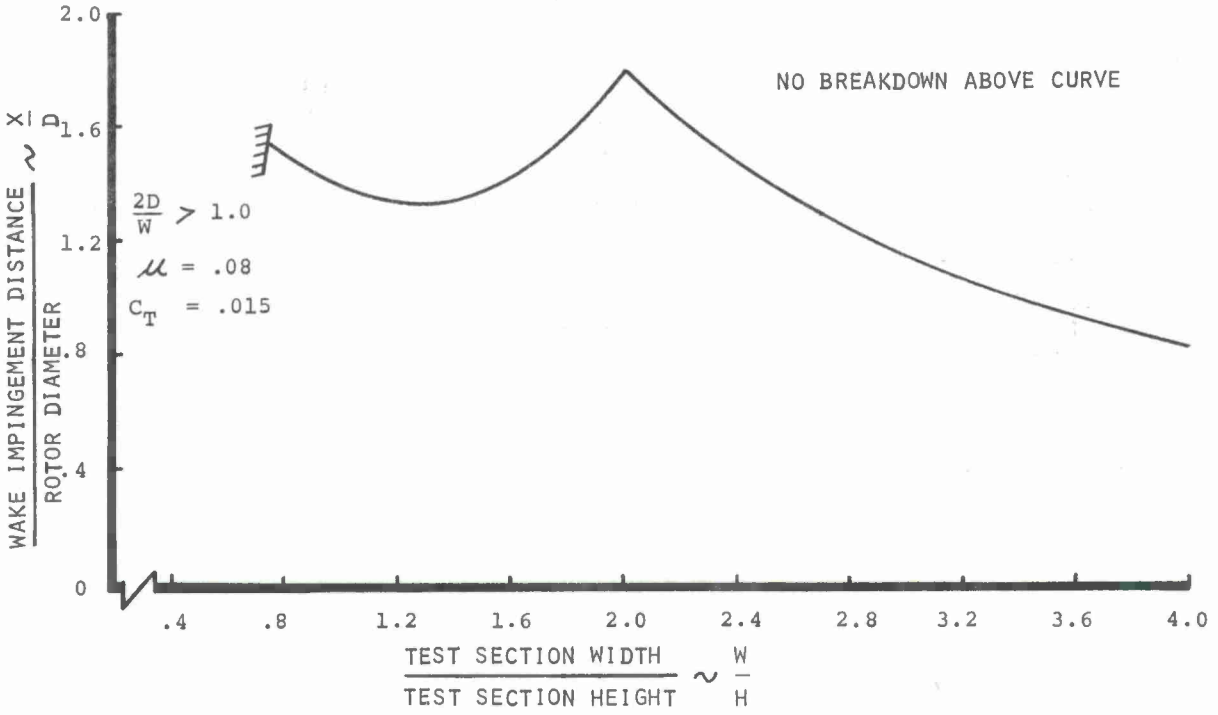


FIGURE 42 TEST SECTION SIZE PARAMETERS FOR TILT ROTOR AND SINGLE ROTOR

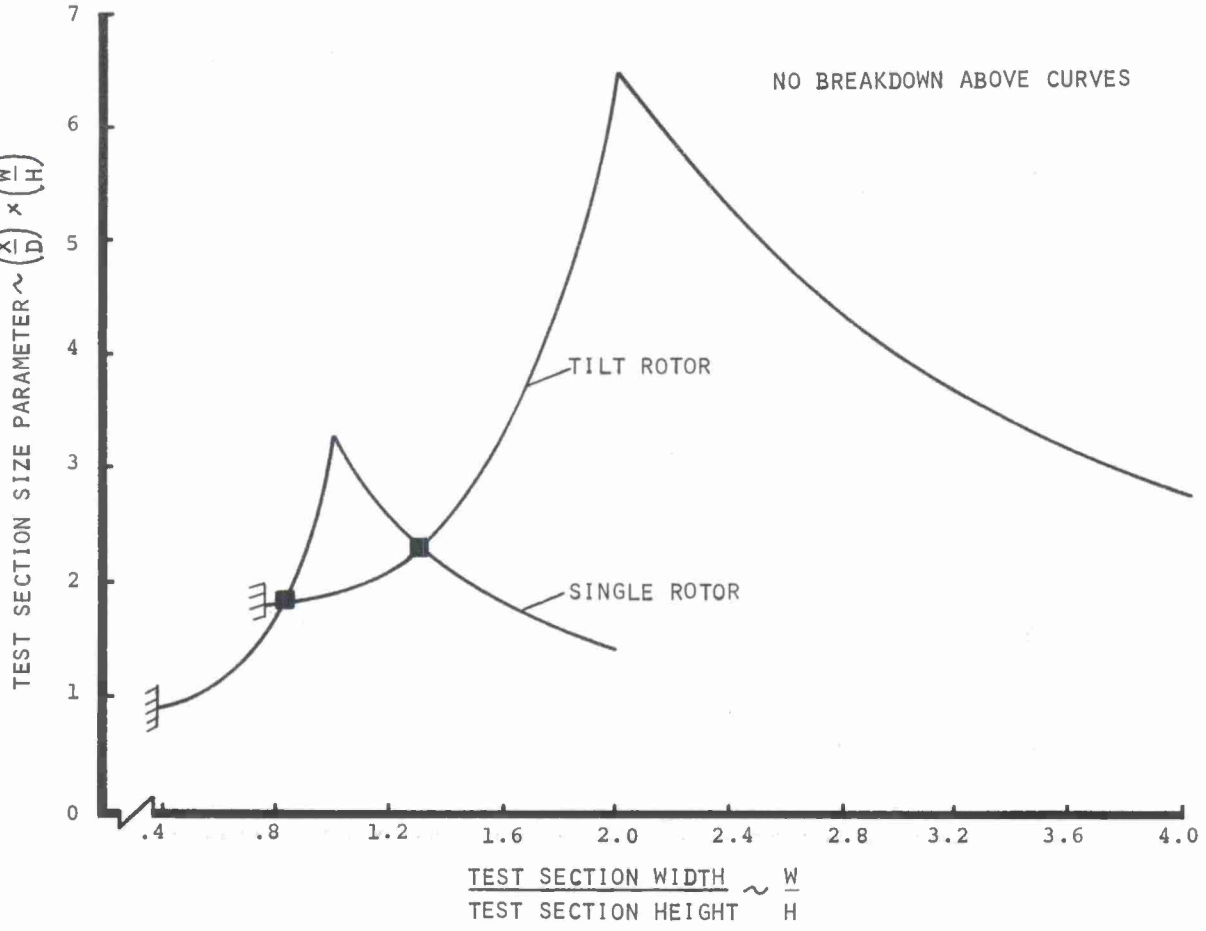


FIGURE 43 TEST SECTION SIZE THAT AVOIDS FLOW BREAKDOWN AT μ = .08 C_T = .015 FOR 20 FOOT DIAMETER TILT ROTOR

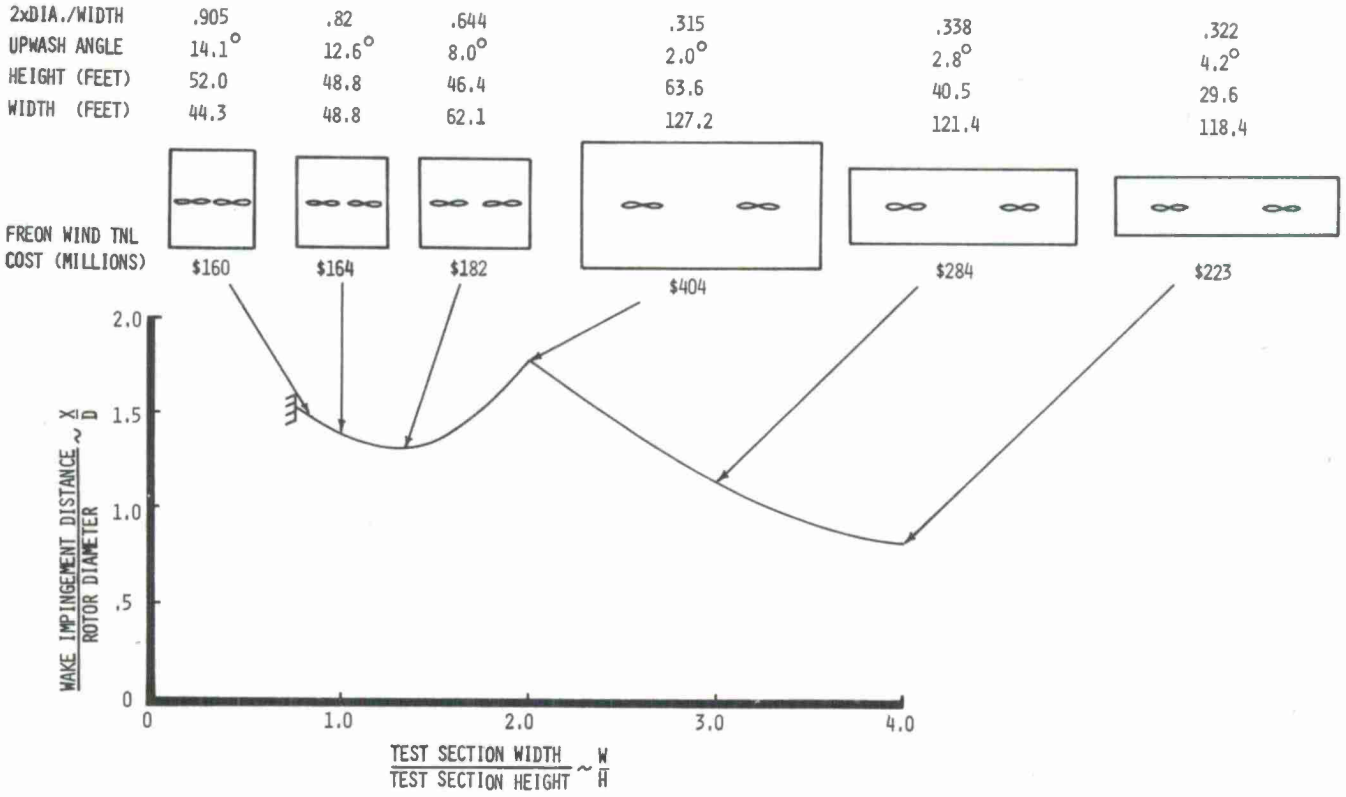


FIGURE 44 ANTICIPATING THE QUANTITY OF DATA

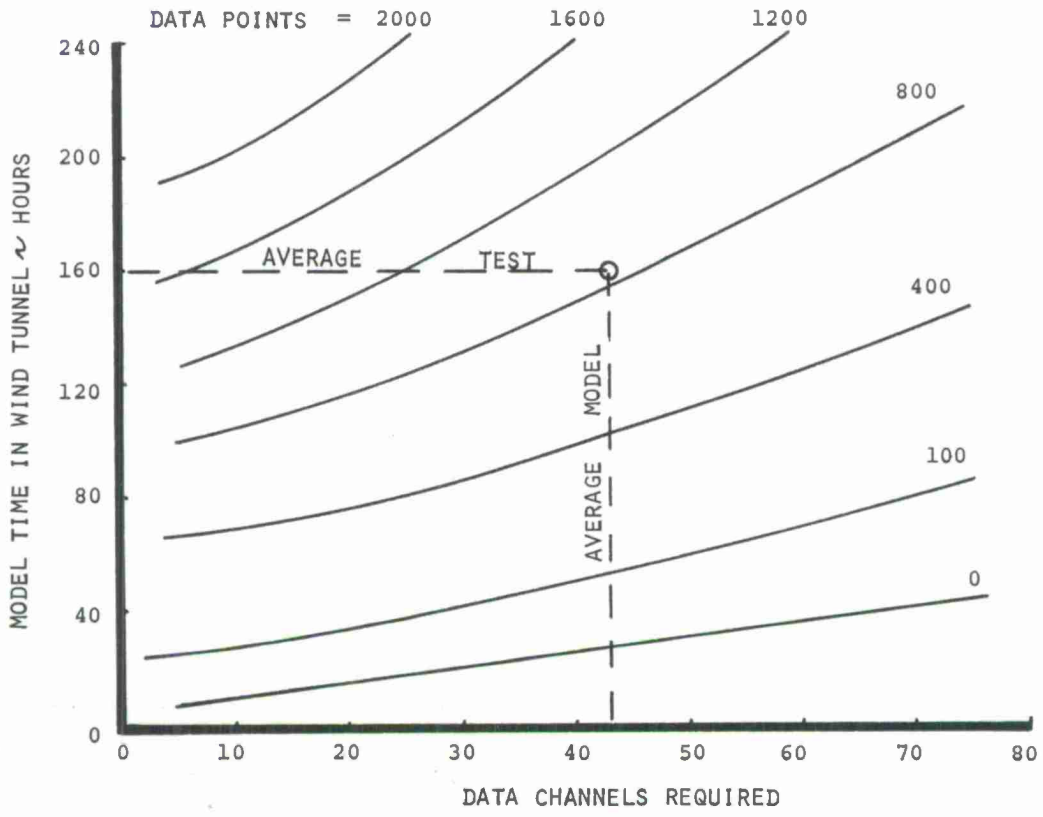
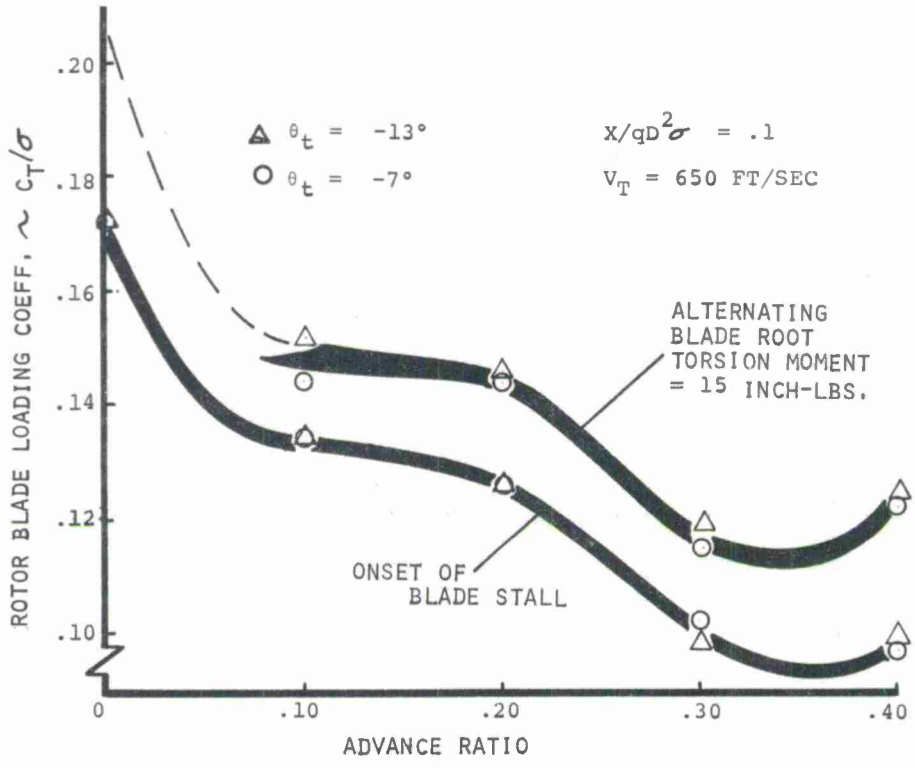
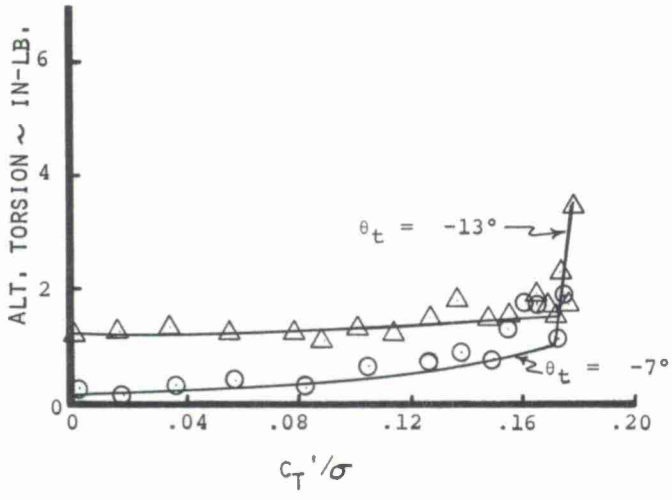
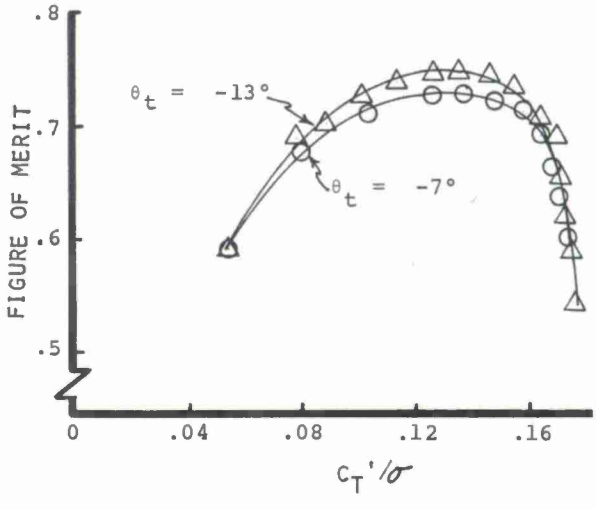
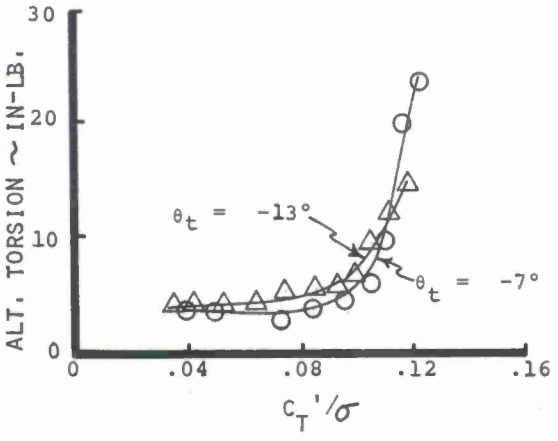


FIGURE 45 QUESTION - WILL INCREASED BLADE TWIST DELAY RETREATING BLADE STALL? ANSWER - NO









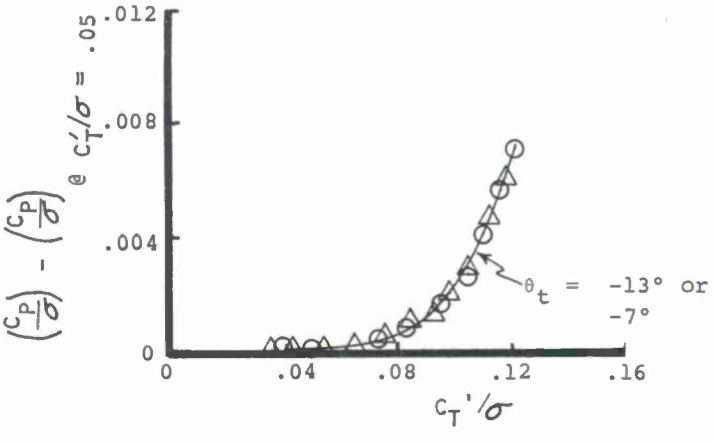


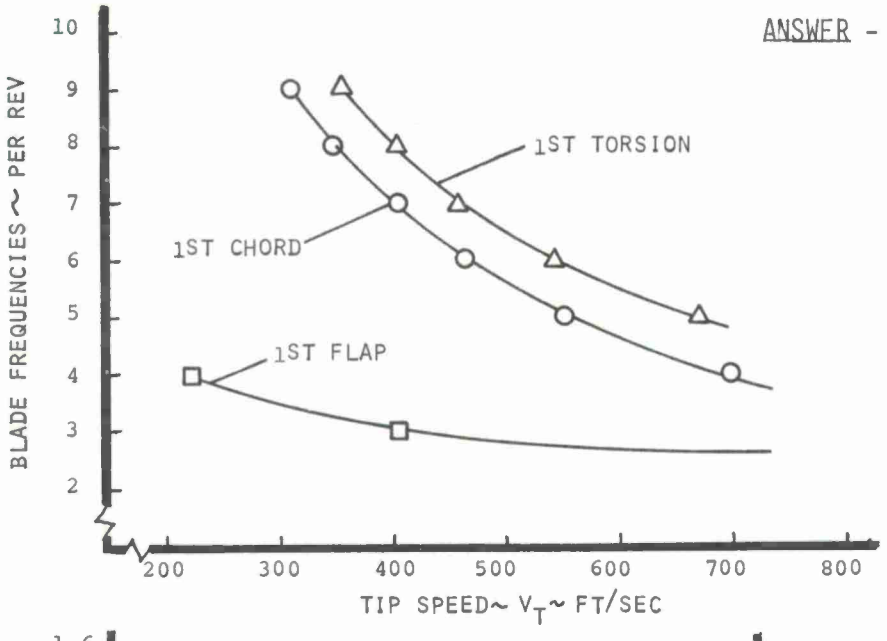
FIGURE 46 QUESTION - WHAT BLADE ROTATING NATURAL FREQUENCIES SHOULD BE AVOIDED IN THE DESIGN OF AN ARTICULATED, FOUR-BLADED ROTOR SYSTEM?

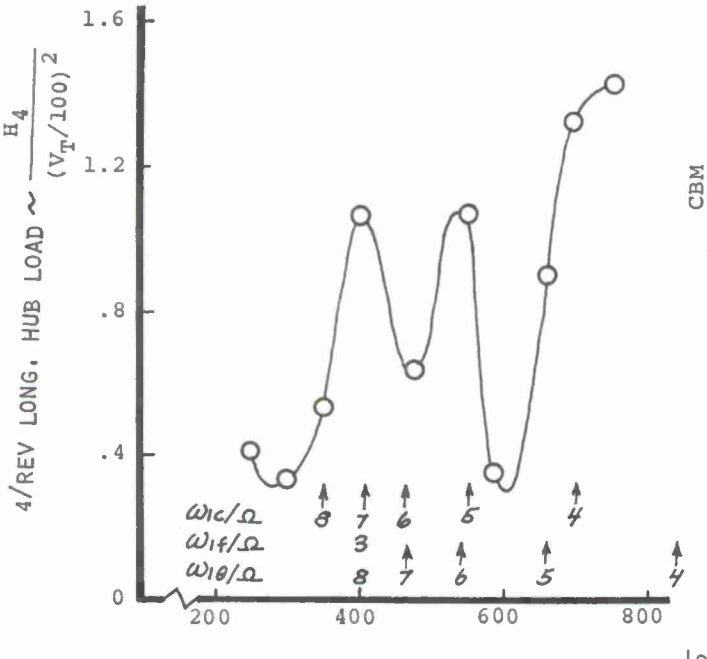
ANSWER - AVOID

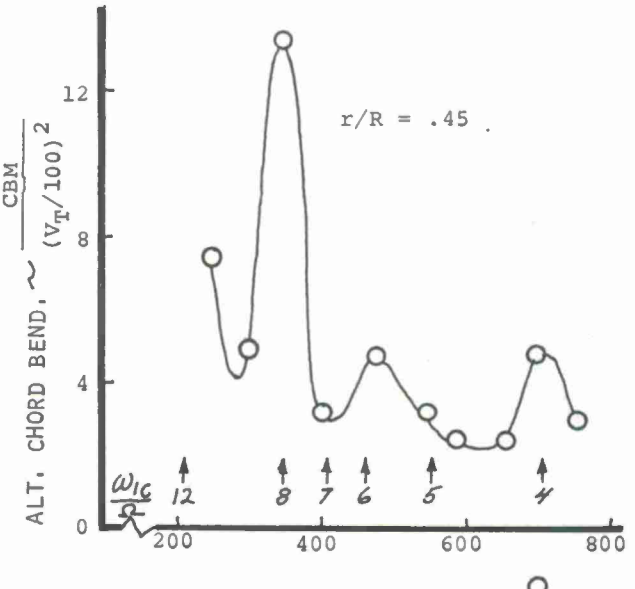
1ST FLAP = 4/REV

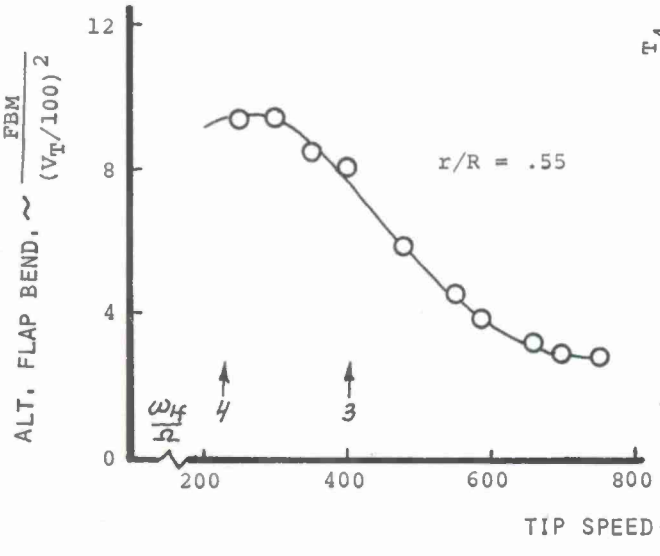
1ST CHORD = 4/REV
5/REV
6/REV
7/REV

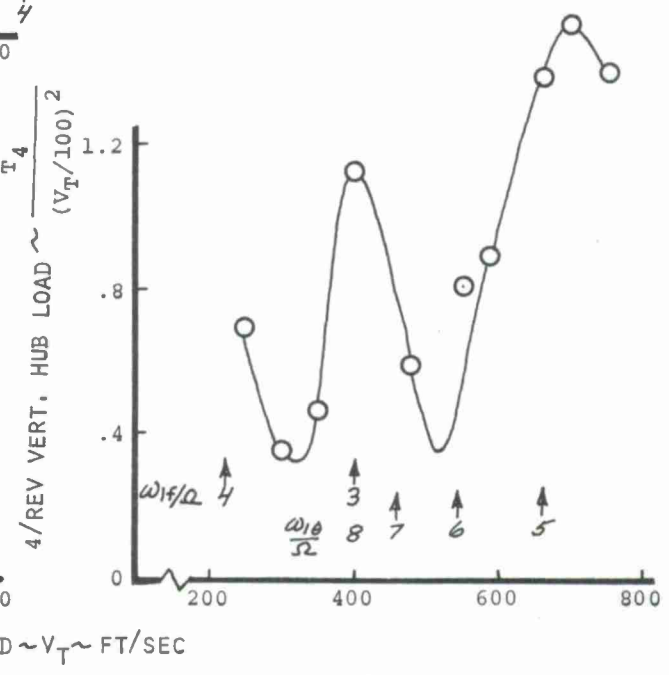
1ST TORSION = 5/REV
6/REV
7/REV
8/REV











A P P E N D I X I

FACTORS IN THE DESIGN AND FABRICATION OF POWERED DYNAMICALLY SIMILAR V/STOL WIND TUNNEL MODELS

By

Carl O. Albrecht

ASSISTANT MANAGER

BOEING V/STOL WIND TUNNEL

THE BOEING VERTOL COMPANY

FACTORS IN THE DESIGN AND FABRICATION OF POWERED DYNAMICALLY SIMILAR V/STOL WIND TUNNEL MODELS

BY

CARL O. ALBRECHT
ASSISTANT MANAGER
BOEING V/STOL WIND TUNNEL

SUMMARY

A few years ago most model designers would say that it was not practical, within reasonable cost limitations, to design and fabricate dynamically similar Mach-scaled V/STOL models of small sizes because of minimum thickness or physical size limitations of materials available. In a short period of time, however, these limitations have nearly disappeared. With a little ingenuity and inventiveness, dynamic Mach scaling of models down to six-foot rotor diameter is within our grasp. The ability to accomplish this feat is one that starts with proper blade scaling and then progresses through the remainder of the model.

The factors affecting those areas of model design where significant gains have been made over the past few years are discussed. For example, the availability of Nomex honeycomb and advanced composites has made economical blade scaling possible. The application of lamiflex/elastomeric bearings, "mini" antifriction bearings and "mini" wire-ply packs for blade retention has made hub scaling possible at a reasonable cost.

Our cumulative experience plus state-of-the-art developments have been applied recently to a Mach-scaled 14-foot diameter dynamically scaled rotor system designed for the Heavy Lift Helicopter. A detailed review of this system is included in the discussion and is followed by a review of the developmental steps that led to this configuration.

INTRODUCTION

The Boeing Company believes in the philosophy of "try before you fly". In support of that belief, in 1964 it committed itself to the testing of V/STOL models by initiating design of a large V/STOL wind tunnel. In 1968, a 20' by 20' V/STOL Wind Tunnel was completed and began to support the increasing need for performance and dynamic load data. The experience gained in models designed and fabricated since 1964 has shown that these V/STOL model test programs add roughly 1% to a full scale prototype program cost and much less to the costs of a full scale production program.

Since 1959, the number and quality of V/STOL models designed and fabricated at Boeing-Vertol has increased significantly and knowledge on dynamic scaling has steadily increased. This trend is illustrated in Figure 1. The current end points of our experience are shown by two models, one Mach-scaled and one Froude-scaled. These models are the most recently designed and tested in the Boeing V/STOL Wind Tunnel.

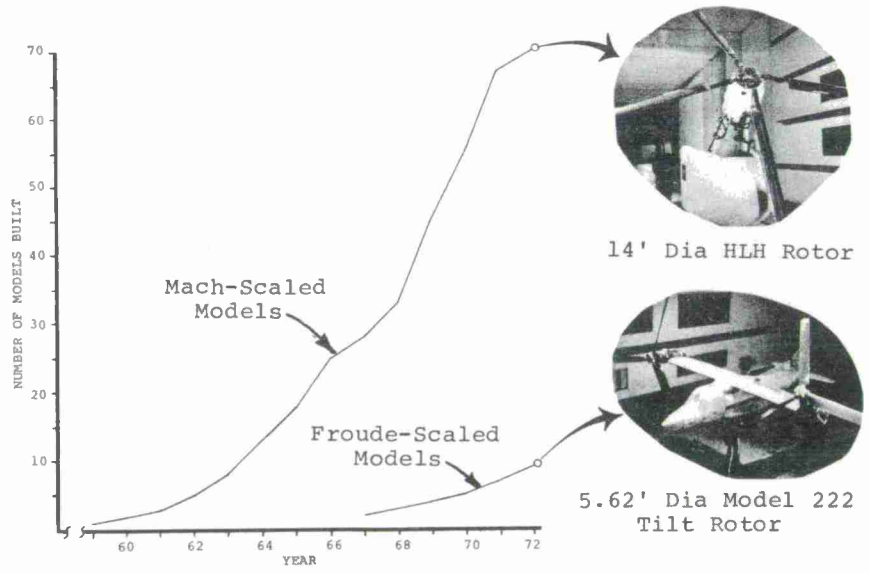


FIGURE 1
POWERED V/STOL MODELS BUILT DURING PAST EIGHT YEARS

The ensuing discussion will cover Boeing-Vertol efforts towards dynamic scaling primarily over the past four years. Mach-scaled rotor systems are first discussed. The 14-foot diameter H.L.H. dynamically similar rotor system is first briefly reviewed. The steps and knowledge gained that led up to this system are then covered. Each element of the system; the rotor blades, the rotor hub, the rotor controls (rotating and stationary), are discussed since they each play an important part relative to dynamic scaling. This discussion is followed by a review of the stand considerations necessary when trying to test and obtain dynamic data from Mach-scaled rotors. The discussion immediately following stand considerations covers dynamic modeling efforts at Boeing-Vertol using Froude-scaling techniques.

As background, at this point, a brief review of Mach-scaling and Froude-scaling is in order. Froude scaling and Mach scaling are two modeling techniques currently used at Boeing-Vertol. Although the differences are fundamentally keyed to the relationship between aerodynamic and gravity loading, we have come to the following simplified definition for V/STOL models. The Froude approach is used when deflections due to weight and airloads are to be directly scaled. The Mach approach is used when blade loads due to airloads are to be most correctly measured. The differences between Froude and Mach scaling in terms of scaling factors are shown in Table 1 (see Appendix).

What these scaling approaches really mean to the model designer, however, are tabulated below:

Mach Scaling Advantages

- Scaling to full scale loads = Model Loads x (Scale Factor)^2 This is considerably more accurate than Model Loads x (Scale Factor)^3 as used for Froude-scaled models.
- A higher Reynolds number exists with Mach scaling by the $\sqrt{\text{scale factor}}$.
- Mach No. effect on blade loads is exactly represented.
- More accurate hub loads because blade loads are exactly represented.
- With a Mach-scaled, full model, the dynamic interaction between fuselage response characteristics and properly represented hub excitations is more realistic.

Froude Scaling Advantages

- Lower loads and stresses on structural components which have a secondary effect of allowing weight reduction while still meeting strength and dynamic scaling requirements.
- Reduced power requirements, which has a secondary effect of reducing motor weight and thereby makes weight scaling easier.
- For desired C_T/σ and μ conditions the required tunnel speed is reduced.
- Static deflections are properly scaled; i.e., transient blade deflections during start up and shut down and ground resonance studies are properly represented.
- Reduced model temperature problems in comparison to Mach-scaled models.

MACH SCALED ROTOR MODELS

The 14-foot diameter H.L.H. rotor model and supporting rotor test stand structure, as installed in the Boeing V/STOL tunnel, are shown in Figure 2. The pertinent features of this model are:

- Full scale tip speed.
- Dynamically scaled rotor (five modes).
- Dynamic blade loads measurement capability.
- Scaled pitch housing and retention system mass and inertia.
- Scaled spherical elastomeric bearing retention system.
- Scaled hub mass and inertia.
- Vibratory hub loads measurement capability.
- Scaled control system mass and inertia.
- Variable swashplate support stiffness simulating swashplate actuators (magnitude and azimuth position variable as well).
- Variable swashplate damping (magnitude and azimuth position variable as well).
- Dynamic control loads measurement capability.

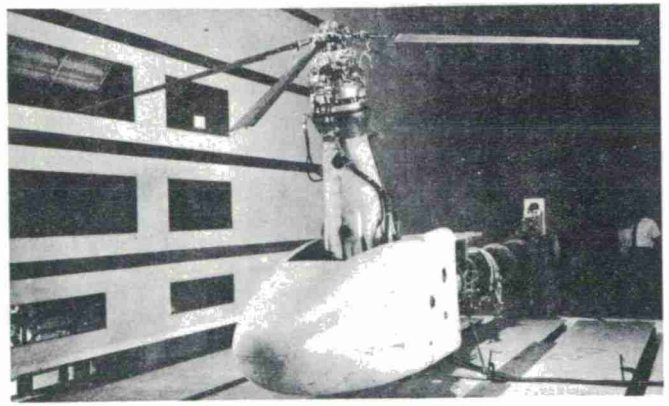


FIGURE 2
14-FOOT DYNAMICALLY SCALED HLH ROTOR SYSTEM

A. BLADES

Some of the features of the 14-foot H.L.H. rotor blade as shown in Figure 3 are:

- o VR-7 and VR-8 cambered airfoils with 12° twist.
- o Composite materials construction - fiberglass and PRD-III* with a Nomex honeycomb core.
- o Torsionally rigid "D" spar construction.
- o Matched physical properties along the entire span.
- o Trimmable trailing edge tabs that do not affect chordwise blade frequencies.
- o Overbalance weight pocket buried at blade outboard section.

*(PRD - Dupont organic fiber)

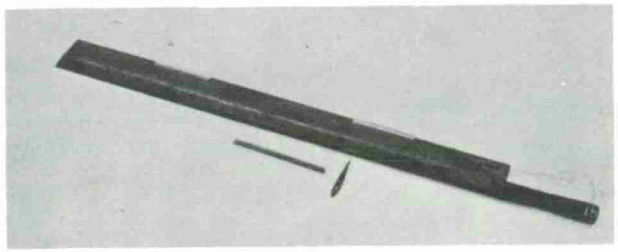


FIGURE 3
14-FOOT DIA DYNAMICALLY SCALED HLH ROTOR BLADE

The search for a quick, economical means of designing and fabricating dynamically similar Mach-scaled model rotor blades over the past few years has been a difficult one. Limitations in available materials, thicknesses, model shop capabilities, etc., would have led one to say that dynamic Mach scaling of small rotors (down to 6-foot diameter) was not practical. As a matter of fact, only a few years ago our own thinking was limited to fairly large rotor sizes such as 16-foot diameter model rotors.

However, with the advancements in the state-of-the-art over the past years, our outlook has changed to the extent that we feel confident in saying that Mach scaling of rotors down to 6-foot diameter is possible. Figure 4 shows four dynamically similar blades from 6-foot diameter to 16-foot diameter fabricated and tested at full scale tip speeds during the past three years.

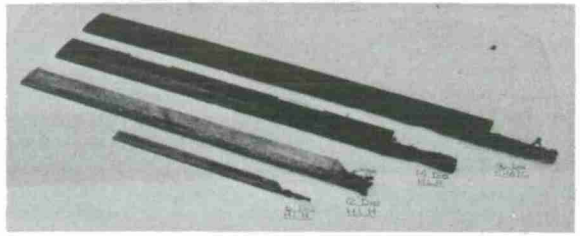


FIGURE 4
MACH-SCALED ROTOR BLADES 6' TO 16' DIA

1) TRAILING EDGE BOXES

The most difficult restraint in designing dynamically similar blades is not the spar as one might think but really the trailing edge boxes. If the box weights are not precisely scaled, the requirement for chordwise balance will result in heavy spars and excessive blade weight. A required trailing edge box weight can be as low as 4 #/Ft^3. The lightest possible balsa or foam available, covered with a structural skin, weighs about 6 #/Ft^3 and, therefore, is much too heavy.

The use of aluminum honeycomb, illustrated in Figure 5a, to meet the required weight objectives in the 16-foot diameter rotor was successful but had the following drawbacks. Because of "hard" tooling, extremely accurate machining of the honeycomb was required (accomplished using EDM techniques). A closed mold technique was used rather than bagging for accuracy reasons. The aluminum honeycomb had a tendency to cut the thin fiberglass skin during bonding and the large cell size (3/16 inch) resulted in a dimpled appearance of the skins after bonding.

A later attempt using built-up box construction shown in Figure 5(b) accomplished weight objectives, gave a smooth aerodynamic surface and was relatively inexpensive to fabricate. The 12-foot diameter blade shown in Figure 4 used this type of construction. However, because of the hollow construction, blade handling damage resulted in frequent, but minor, repairs. And so, research for a better way to make boxes continued.

Our most recent and most successful step in trailing edge box design has come with the use of Nomex honeycomb shown in Figure 5(c). This is available at weights as low as 2 #/Cu-Ft. Machining tolerance is not as critical when

compared to aluminum honeycomb since the Nomex can be machined slightly oversize and crushed to shape in the molds. The small cell size (1/8 inch diameter) has virtually eliminated any dimpled skin effect and the construction is not susceptible to handling damage. With structural skin thicknesses of .002, box weights of 4-5 #/Ft^3 can be fabricated for a blade chord as small as 2.3 inches.

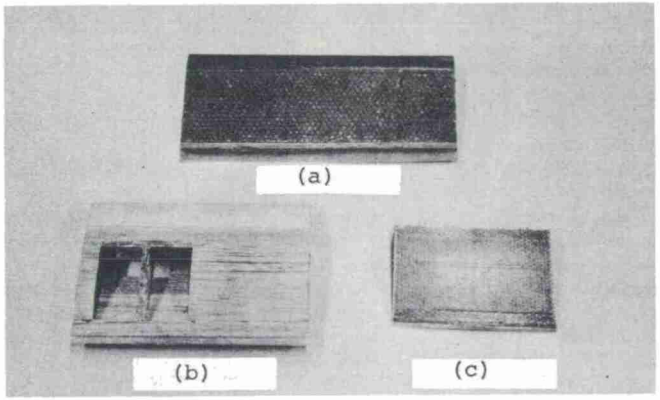


FIGURE 5
TRAILING EDGE BOX CONSTRUCTION CONCEPTS

2) BLADE SPARS

The most time consuming aspect of designing blade spars is in the station by station matching of all of the physical properties (Wt/In, EI_{Flap}, EI_{Chord}, $GJ_{Torsion}$, C.G., Neutral Axis and Shear Center). Direct substitution of scaled thickness of the same material used in the full scale blade may not be practical or desirable. For example, the 16-foot diameter rotor (Figure 4) used a scaled thickness steel spar. The cost of fabrication of the .010 inch thick spar wall with an integral root end was very expensive and this experience directed us towards other less expensive means of fabrication.

The use of identical materials also results in allowables that are no greater than those of the full scale vehicle. This can result in a less than desired wind tunnel flight envelope. The higher strain allowables associated with many composites encouraged us to concentrate our efforts in that direction. Over the past three years the appropriate use of composites (fiberglass, boron, carbon filament, PRD, etc.) has enabled us to match desired properties of virtually any blade configuration requested. Figure 6 shows typical material combinations used in matching required properties.

Production techniques for applying pressure during spar fabrication are not readily adaptable to model blade fabrication. We have found that the use of either foam or balsa mandrels, that are left in the blade spar, has resulted in a much simpler and less expensive means of providing pressure in the mold during the curing operation. This assures a structurally sound blade.

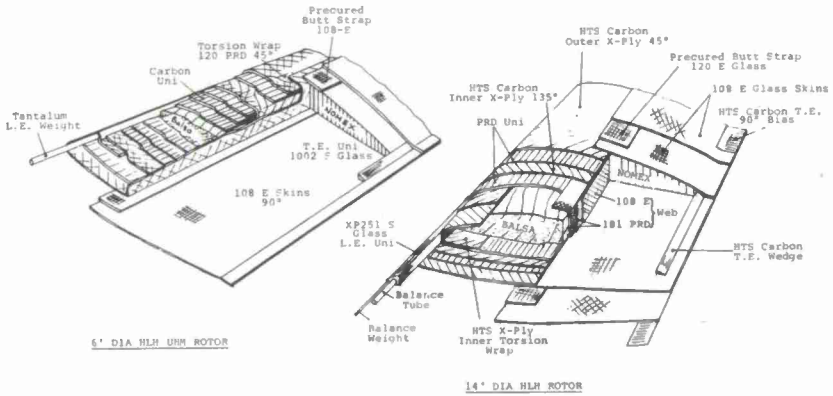


FIGURE 6
MODEL BLADE SPAR CONSTRUCTION

One would be rather naive, however, to believe that desired properties can be matched with the first blade out of the mold. It invariably requires some ply alterations or material change so that the second blade can come within 5% of the requirements. A closer match might perhaps require that even additional proof blades be made.

3) BLADE ROOTS

The blade root retention elements and hub hardware are designed primarily by blade centrifugal force and by inertia loads resulting from their own weight. It is therefore necessary that the blade be properly scaled first. If this is not done, the result is heavier and stiffer root elements which result in increased blade loads which in turn requires more blade structure for

strength considerations. It is a converging process, but disasterous from a dynamic scaling viewpoint.

Although it is possible to scale blade frequencies without precisely matching inboard masses, the weights must be kept low in order to minimize inboard blade moment "humps". Figure 7 illustrates the degree to which inboard mass has varied over the years and the degree to which it is now controlled. Yes, the one that sticks out like a sore thumb (TR-31) did turn out to be a problem.

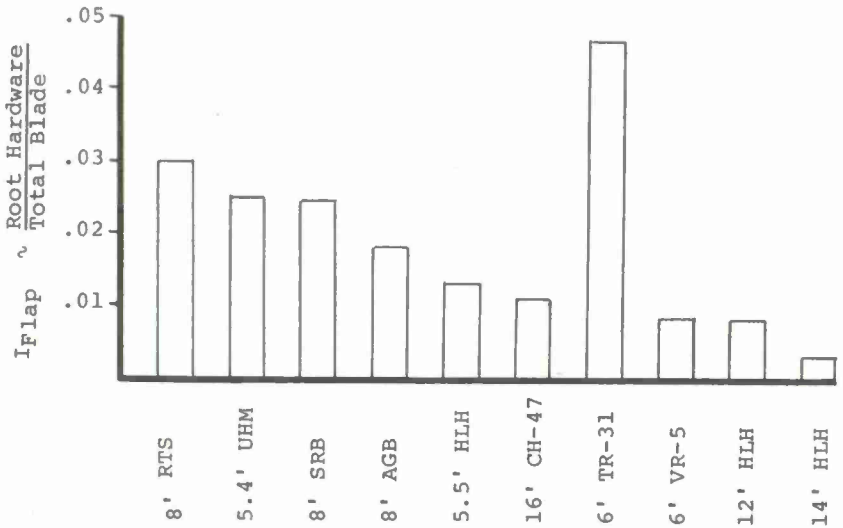


FIGURE 7
INBOARD ROOT MASS SUMMARY

Three basic blade root retention concepts have been used over the past years on all of our composite blade designs. These concepts which are representative of their full scale counterparts are shown in Figure 8 and have been used successfully with no problems.

A typical fabrication problem encountered on full scale hardware is to achieve adequate material compaction around the fittings. On model rotors, however, the problem is lessened considerably because of the relatively small amount of material involved. - A scaling problem in reverse.

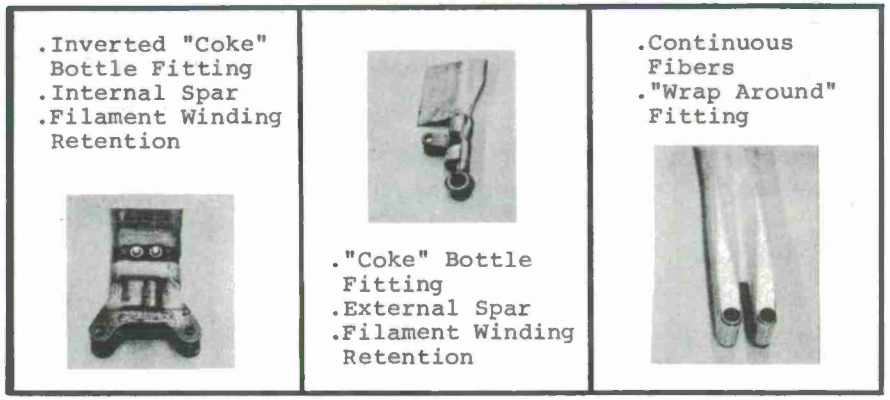


FIGURE 8
BLADE ROOT RETENTION CONCEPTS

4) BLADE TOOLING AND FABRICATION

Of significant importance in fabricating any model blade is a mold that will produce identical blades with an external contour and twist distribution that are within 1% of the requirements. Figure 9 shows a mold used in fabricating a 6-foot diameter blade where not only the close tolerances were satisfied, but where changes in airfoil shape and nonlinear twist along the span was achieved.

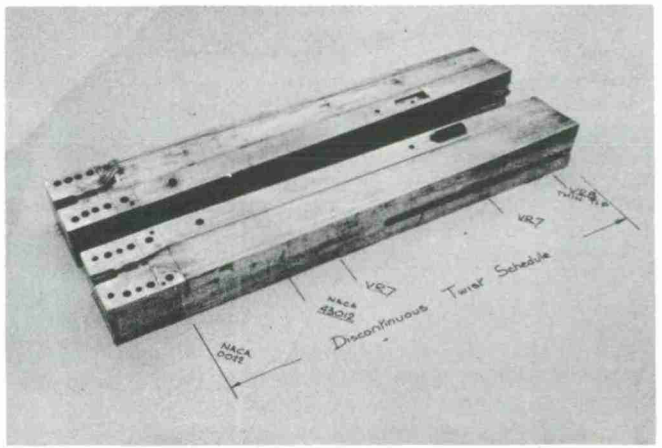


FIGURE 9
6-FOOT DIA VARIABLE AIRFOIL BLADE MOLD

Early development of such molds started with fiberglass tooling. The mold distortions, even though small, that occurred with each cure cycle were unacceptable and we turned to the development of solid aluminum molds. Either single-point cutters that "shave" the airfoil or numerical control machines together with subsequent hand finishing has produced the desired results. Problems expected from thermal loads induced because of the material differences (fiberglass-aluminum) have never materialized.

The use of aluminum molds has had several secondary beneficial effects. Because of the high thermal conductivity, the mold heats uniformly and very rapidly. Where mold size exceeds our oven capacity, built-in heating elements in the mold permit rapid heat buildup and accurate control of blade curing temperatures.

Where distortions from desired tolerances on items such as twist have occurred because of fiber quantity or orientation, we have found that a "stress-relieving" process can be applied. In this process a jig with built in spring-back capability holds the blades in a corrected position while they are subjected to a repeat of the cure cycle. No physical damage has been noted nor has there been any indication of strength reduction resulting from this process.

5) BLADE INSTRUMENTATION

The increased use of composites has resulted in higher allowable fatigue strains. Initially the blade instrumentation wiring and gages could not withstand these higher strains without frequent failure. During the past few years the use of higher strength, .007 diameter (with insulation) wiring has provided acceptable life. The wiring is installed in the blade during fabrication as close to the flap and chord neutral axis as possible. High fatigue strength gages (μ = 2200 @ 10^7 cycles) currently available, have all but reduced gage failure to a relatively few number of occurances. Where size permits, the gages are preferably placed externally on the blade surface although blades with internal instrumentation can easily be built by gaging the balsa or foam spar mandrel prior to installation in the blade mold.

6) BLADE MATERIAL ALLOWABLES

The advanced composite materials used on model rotor blades have not had the benefit of allowables that were established from a large number of fatigue test specimens. The flow time required from model design to test does not permit such luxuries. Allowables are set initially based on the best knowledge available from published literature and company-available data. Over the years, however, the allowables have been supported or corrected as a result of actual wind tunnel test experience. In order to justify their use and to gain operating experience and minimize the possibility of component failure, all model test programs are flown with some means of monitoring blade stresses or moments.

Table 2 (see Appendix) presents model blade material allowables proven satisfactory by actual operating experience. The S_e/E, S_e/W_t, etc. relationships are used to guide the selection of optimum materials to satisfy the physical property requirements.

7) TEST CONSIDERATIONS AND POINTERS

An item for consideration in the testing of dynamically scaled blades is the closeness which blade spar span moment and the dynamic balance axis are matched from blade to blade prior to flying. Although we have not seen how this impacts test results, it certainly speeds up rotor balancing and tracking during the test checkout period.

Blade instrumentation can be costly and time consuming. Keeping the quantity down can however, control these factors. Safety monitoring gages are usually the same ones that are requested by the customer. Since the desired data is usually flap moment and chord moment at a specific location, we have devised a means to take full advantage of the allowables in each plane while properly accounting for their interaction. The use of a scope, shown in Figure 10, where say flap moments are on the vertical axis and chord moments on the horizontal axis, results in a Lissajous curve that should be contained within the allowables band shown on the scope. This permits the test engineer to maximize his test envelope with respect to allowables. The technique can be applied to other areas such as balance load monitoring as well.

4) SPHERICAL BEARINGS

The most recent hub designs on the full scale H.L.H. incorporate a spherical elastomeric bearing that takes the place of horizontal, vertical and pitch bearings. The ability to scale such a bearing to small sizes has already been proven. Figure 15 shows the comparison of the full scale HLH bearing, a scaled bearing for the 14-foot diameter dynamically similar H.L.H. rotor and a bearing for a 6-foot diameter H.L.H. Universal Helicopter Model utilizing a scaled rotor system. All are designed to retain the blade at full scale tip speed centrifugal forces.

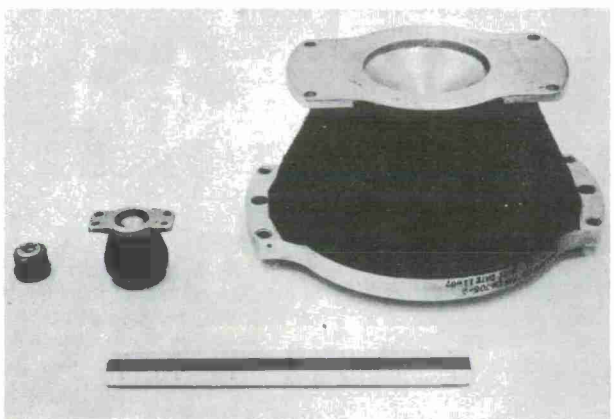


FIGURE 15
SPHERICAL ELASTOMERIC/LAMIFLEX BEARINGS

It is important that trade studies be conducted on bearing size early enough in the design to obtain maximum possible margin, minimum maintenance and maximum life potential. The two major factors affecting the bearing design are compression "column" stability and oscillation life. In the past we have allowed the envelope available (after designing everything else) to design the bearing. We have learned that a bearing designed first to meet growth and margin requirements does not compromise the envelope requirements that much. This is illustrated in Figure 16 for a bearing selected to be used in the 6-foot diameter UHM-II. For the bearing shown it is evident that when the bearing diameter increases from .65 inches to .80 inches the P critical increases 100% and life increases by 40%. The selection of a stack height of .35 provides a factor greater than two for both the centrifugal force loading and the bearing life.

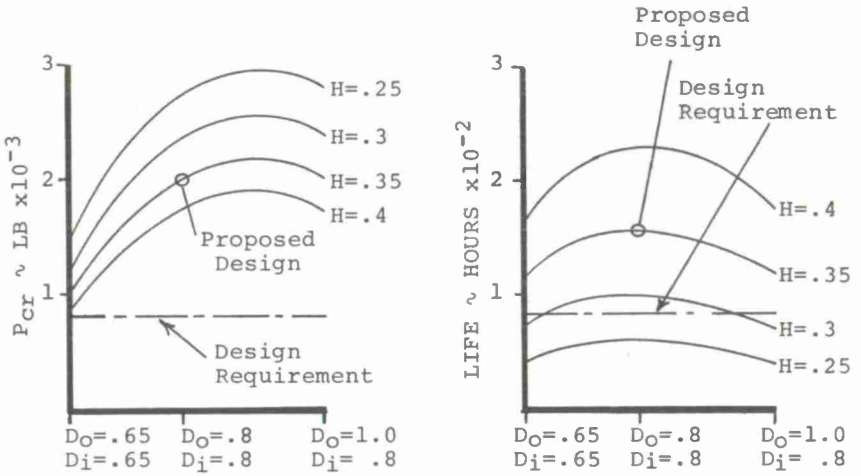


FIGURE 16
SPHERICAL BEARING TRADE STUDY FOR 6-FOOT DIA ROTOR

5) WIRE-PLY RETENTION SYSTEMS

Another means of reacting blade centrifugal force loads is through the use of a wire-ply retention system. Figure 17 shows a model pack compared with a full scale unit. The model pack was built for a 10-foot diameter rotor model. The pack represents the smallest unit made to date by Bendix for blade retention purposes. There is every indication that even smaller sizes are feasible. A fatigue test evaluation is currently underway and if it is successful, this retention system will be used in a rotor test to be conducted in November.

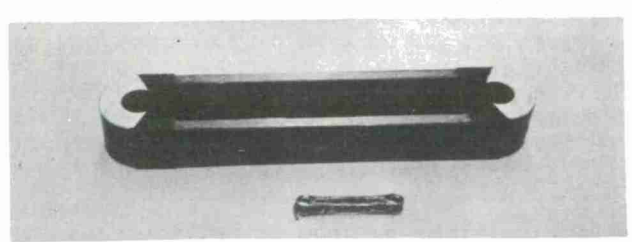


FIGURE 17
BENDIX "WIRE-PLY" C.F. STRAPS (FULL SCALE & MODEL)

6) LAG DAMPERS

The "mini" viscous lag dampers used on dynamically scaled models have always been and continue to be a source of trouble. Their effectiveness is short lived and they require frequent recharging. Their necessity in preventing rotor system mechanical instability, even in models, has been proven: so, lag damping per se cannot be eliminated. In two rotor models where damping obtained from vertical pin lamiflex bearings was significant, dampers were eliminated completely without any evidence of mechanical instability.

Our experience with mechanical viscous dampers has shown that if any loads other than axial piston loads are present, damper rate deterioration is extremely rapid. The 14-foot diameter H.L.H. rotor utilizes viscous lag dampers that are positioned and supported in such a manner on the hub that bending moments across the damper piston, due to centrifugal field effects, are minimized. It can be seen in Figure 11 that the damper body C.F. loads are reacted by the trunnion which is basically located at the damper body center of gravity.

Experience has also shown that damper rate characteristics obtained quasi-statically are very optimistic when compared to results from a dynamic load test (shake test) at model frequencies. Therefore, care must be taken to perform a proper dynamic damper calibration.

7) HUB DESIGN AND FABRICATION

As part of an overall plan to use wind tunnel models to measure hub vibratory loads, the most recent 14-foot diameter H.L.H. rotor model utilized a lightweight (twenty pound) scaled rotor hub illustrated in Figure 11. This was done to properly represent the effective mass on the balance and so that the rotor/balance system natural frequency was above 8Ω. The weight scaling was accomplished with less difficulty than we expected and without compromising the structural integrity.

The unusual-shaped hub, shown in Figure 11, required because of the three degrees of freedom provided by the spherical bearing, was in fact very easy to fabricate. This part (and others like it) was made in the "Linemaster" machine shown in Figure 18. The machine, although initially procured for template fabrication, can be and is used extensively for any complex shape two-dimensional part. A scaled-up engineering layout is traced by an electric eye follower that moves the milling head cutter to the complex pattern desired.

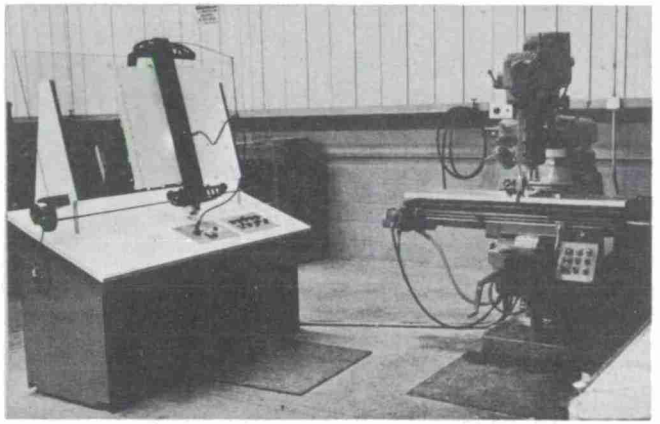


FIGURE 18
"LINEMASTER" MILLING MACHINE

8) MOTION TRANSDUCERS

As in all rotor models the blade motions, flap and lag, must be accurately measured. The problem becomes more difficult, however, when a spherical bearing retention concept is used. The motions are coupled and are difficult to separate. The 14-foot diameter H.L.H. system utilizes the lag damper axial stroke as a measurement of lag and the motion about the damper body pivot axis as a measurement of flap (see Figure 11). Kinematic error calculations are then used to correct measured data.

In the past, numerous types of RVDTS, which use A.C. power, were tried in the attempt to measure blade motions. Each had problems which were usually related to the centrifugal force field. About a year ago, "Hall" effect devices were tried that were more successful in the centrifugal force field and utilized D.C. power which removed the electrical interference from A.C. sources. During the past six months, however, we have been using conductive plastic strips together with a spring follower to read these motions. To date we have found this system to be the most reliable, inexpensive, lightweight and conveniently adaptable system available and should certainly be considered a breakthrough in steady state and dynamic motion measurement.

C. UPPER CONTROL SYSTEM (ROTATING)

Most performance models are built with as rugged a control system as is reasonably compatible with space and to some extent weight limitations. Conventional swashplate systems have been used with success and an absolute minimum of problems.

The 14-foot diameter H.L.H. model rotor is the first system in which we have dynamically scaled the control system weights and stiffnesses. The requirements specified that the entire control system from the pitch links to the stationary actuator be scaled to a weight of two pounds. The system as designed and fabricated weighed 2.8 pounds. Table 3 (see Appendix) shows a detailed weight breakdown that compares desired weights versus actual weights achieved. The actual weight, although eight tenths of a pound heavier than desired was an intentional compromise. The compromise was made in the swashplate bearing selection. Although a lighter bearing was available it was marginal with respect to life and stiffness requirements. The assembled control system is shown in Figure 19.

It was not practical to scale down the full scale swashplate dimensionally because of the very thin sections that would have resulted. We compensated for this by: (1) designing a swashplate of a smaller pitch line diameter than the full scale, (2) minimizing the offset loads that result in high swashplate torsional stresses and (3) introducing and reacting loads as close to the bearing ball path as possible. Through the use of aluminum and the addition of lightening holes throughout, sufficient bearing cooling existed so that operating temperatures never rose above 100° even though only grease lubrication was provided.

Metal-on-metal rod end bearings (steel ball - brass housing) have never proven satisfactory for Mach-scaled models because of the excessively high wear rate which results in a "sloppy" control system. The increasing availability of teflon/fiber-lined rod end bearings from various vendors has made tight and reliable control systems possible. These bearings are expensive but worth it when considering model maintenance costs.

There are still minimum size limitations on these bearings; but where weight is a consideration, special bearings made of aluminum and teflon/fiber-lined are available. This type of rod end bearing was used in the 14-foot diameter H.L.H. rotor control system shown in Figure 19.

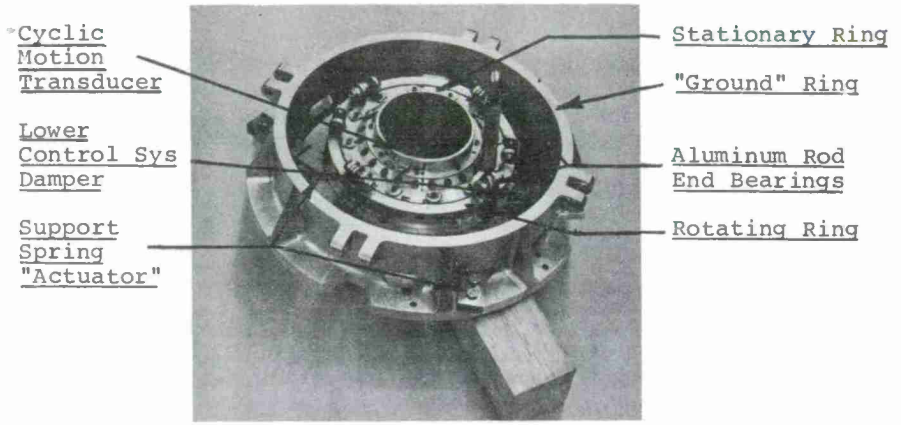


FIGURE 19
14-FOOT DIA HLH ROTOR CONTROLS

On many occasions a situation arises where the requirements cannot be met by direct scaling, however, we have found that by simulation nearly anything is possible. An example of this was a requirement to study the effects on stall flutter of blade torsional stiffness and root spring stiffness together with root damping. Figure 20 shows a model configuration called the "birdcage" control system. It represented a mathematical model of a mass/spring/damper system as closely as possible. By adjusting the support ring, the length of the fingers is changed and a root stiffness variation change of over 10 to 1 can be achieved. Blades were designed to be flown on this system so that the total torsional frequency range test capability was from 2/rev to 6/rev. The larger ring surrounding the birdcage is a centrifugal force friction damper in which the active portion can be changed by altering the weight.

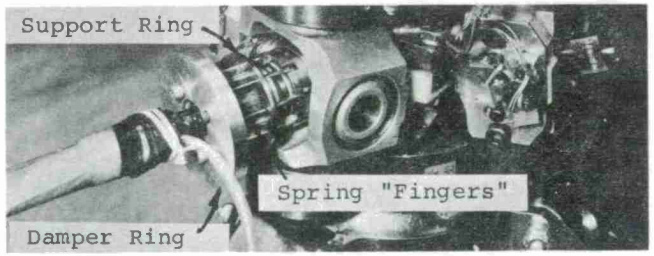


FIGURE 20
"BIRDCAGE" CONTROL SYSTEM SIMULATION

D. LOWER CONTROL SYSTEM (NON-ROTATING)

Virtually all systems designed for use in the Boeing-Vertol Wind Tunnel utilize remote controls to permit rapid test condition changes without shutting down the tunnel to adjust the model.

Lower control systems utilizing various remote control concepts have been tried over the years. One unusual variation was used in the 14-foot H.L.H. rotor system and is shown in Figure 19. The non-rotating swashplate is supported by leaf springs that are fastened to a rigid "ground ring". These leaf springs represent actuators and their support structure stiffness. The spring elements can be replaced in order to alter stiffness and relocated azimuth-wise with respect to support location. Viscous dampers can also be attached between the swashplate and ground ring at various locations and the magnitude of damping varied. The ground ring is rigid and is attached by means of stiff hydraulic cylinders to the test stand. The hydraulic cylinders provide the desired remote collective and cyclic capability. All components of the system discussed above are shown in Figure 21.

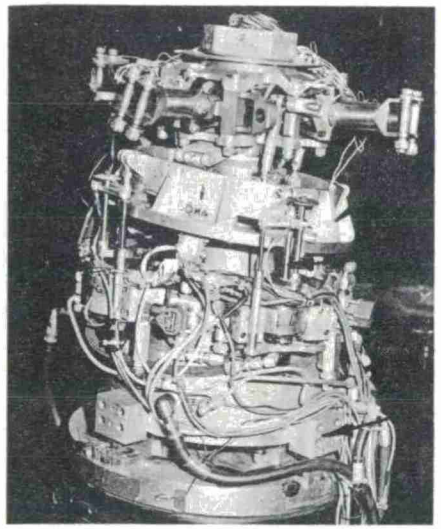


FIGURE 21
14-FOOT DIA HLH DYNAMICALLY SCALED ROTOR SYSTEM

Based on all the experience acquired over the past years and the problems associated with each of the various systems, we have concluded that the best swashplate actuator concept is that shown in Figure 22. By isolating collective and cyclic motions the reliability and accuracy by which control positions can be established and placed is increased significantly.

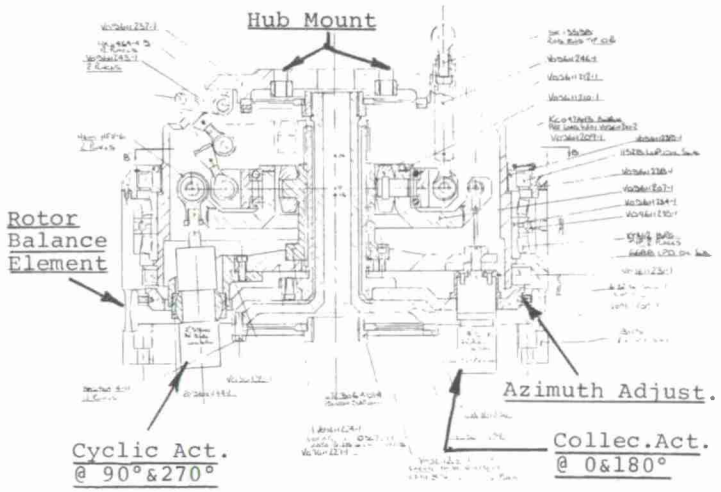


FIGURE 22
SINGLE ROTOR HELICOPTER CONTROL SYSTEM

TEST STANDS FOR MACH SCALED ROTOR MODELS

To obtain dynamic data from a Mach-scaled rotor system such as described previously, we must consider also the dynamic characteristics of the force measurement element (balance) and the rotor test stand itself. A discussion, on the three major elements of the stand - the balance, the drive system package, and all supporting structure back to ground - follows.

A. DRIVE SYSTEM

The Achilles' heel in Mach scaling of dynamic models is the drive system. Although water cooled electric motors have been used in most powered models, their weights, though light by air cooled motor standards, are still too heavy by dynamic scaling standards. If, for example, the drive system were placed on the "live" side of the load balance, weight tares with respect to rotor loads would be significantly out of proportion.

Figure 23 shows the weight-to-power relationship for most available reciprocating engines, electric, hydraulic and air motors. It is evident that electric motors are much too heavy and what we really need is an inexpensive, lightweight model turbine engine.

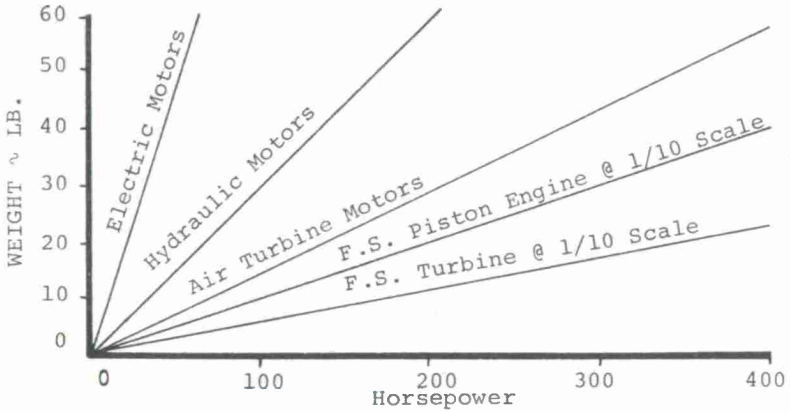


FIGURE 23
MODEL POWER PLANTS - WEIGHT/POWER RELATIONSHIP

The only current means we have found to achieve dynamic scaling weight objectives is by mounting the drive system external to the rotor model in a manner such as used for the 14-foot diameter H.L.H. rotor and shown in Figure 24. The concept of an external power supply is typical of rotor test stands. "Bendix" flex couplings have been designed and fabricated to have the desired torque capability and yet are soft enough axially, laterally and moment wise so that loads across the balance are not greater than 1/4 of one percent of the loads to be measured.

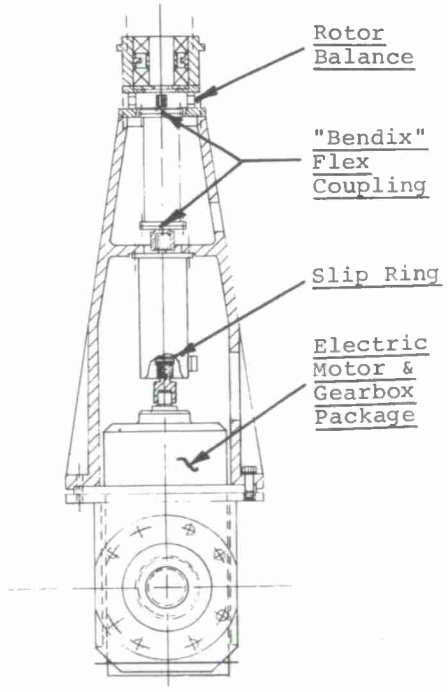


FIGURE 24
EXTERNALLY MOUNTED DRIVE SYSTEM

B. LOAD BALANCES

The proper design of a rotor balance for a dynamic model is one of the most difficult tasks we encounter because of the apparently conflicting requirements. The task is difficult but not impossible. The items to be considered are:

- Accurate steady-state load measurement.
- "Thou Shalt Not Break" fatigue strength requirements.
- High frequency requirement of mass on balance.
- Minimal steady load drift due to thermal environment.

The first and prime requirement of all balances is to measure accurate (<1%) steady-state loads such as lift, drag, pitching moment, etc. In conflict with this is the structural requirement to withstand vibratory hub loads that may be as high as the steady state loads. This requires the use of strain allowables that are roughly 10-15% of the static strength. To minimize this conflict, it is our standard practice to maximize fatigue allowables by using large fillet radii to minimize stress concentrations, shotpeen all critical balance elements, and make the balance integral wherever possible.

If good dynamic load data is desired up to 4 and 8 per rev, the natural frequency of the hub, stack and control system mass on the balance should be at least six to twelve times rotor frequency. This can be accomplished to some extent by minimizing hub mass and placing it as close to the balance reference center as possible. But, because of the desired proximity of the balance as close to the rotor head as possible, it invariably falls close to heat generating sources such as swashplates, hub bearings, stack bearings, etc. Even where water cooling is used to reduce these temperatures, there still exists temperature differences across the balance, front to back, top to bottom, etc., due to cooling in and out locations and because of tunnel wind. A temperature difference of as little as 3°F on a very stiff balance can result in an unacceptable, nonrepeatable balance drift. This interaction is most prevalent with very stiff elements and not as forgiving as the more flexible, steady-state load only, balance. We have found that even the use of steel bolts holding an aluminum balance and support structure together is a source of drift because of the small but significant structural distortions resulting from thermally induced loads.

Another very significant factor in the design of a one-piece integral balance is the effect of the body stiffness of the balance, the stiffness of the structure to which the balance is being attached and the method of attachment. On many occasions a balance that is calibrated on a rigid support needs recalibration when installed in the actual model.

Other factors to be considered are higher frequency excitations such as second mode blade chord, flap and blade torsion resonances and drive system excitations. These high frequency loads can be filtered out for steady state and N per rev load measurement purposes but are real when considering the fatigue load environment on the balance.

Our recent experiences have enabled us to finally close our arms around the total balance design task. We now feel that our future model balances will be capable of reading both aerodynamic and dynamic loads with high fidelity and without the excessive loads that minimize the test envelope.

C. ROTOR MODEL SUPPORTING STRUCTURE (TEST STAND)

Last, but not least important in the testing of Mach-scaled rotors and measurement of dynamic blade loads and hub forces, is the basic stand on which the test is conducted. The primary stand built for this purpose and for testing at the Boeing-Vertol V/STOL tunnel is the Dynamic Rotor Test Stand (DRTS) shown in Figure 25.

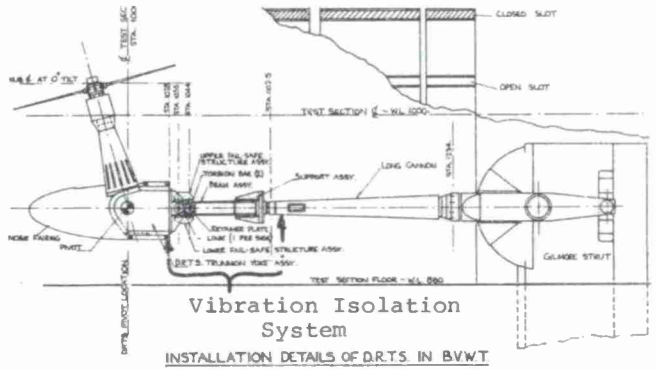


FIGURE 25
DYNAMIC ROTOR TEST STAND

Conceptually the system uses a large seismic mass supported at the end of the sting, a passive isolation system consisting of soft torsion bars for vertical/longitudinal motions and a torsionally soft I-beam for lateral and roll motions. Stand excitations from whatever source are not transmitted to the rotor hub and are not felt by the rotor balance. A curve showing the forced response characteristic on the balance for in-plane hub loads is presented in Figure 26.

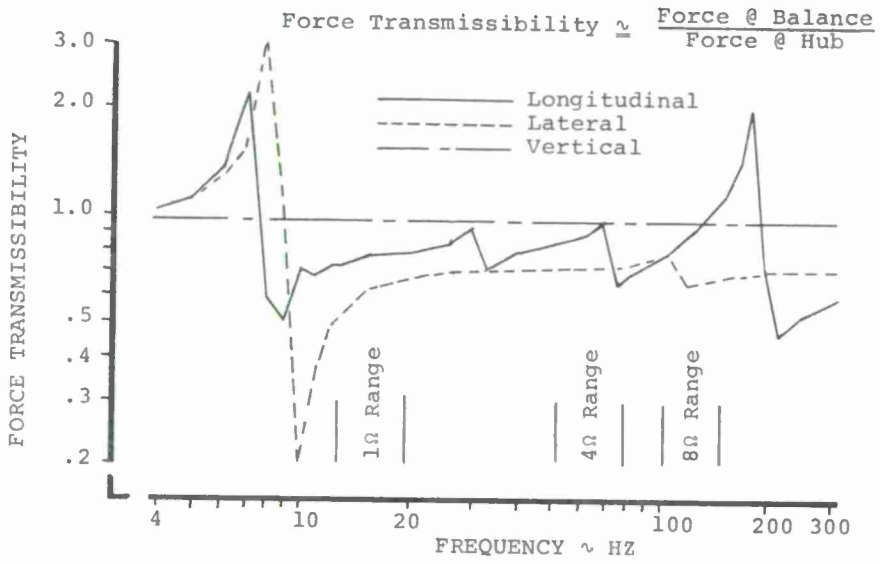


FIGURE 26
DRTS DYNAMIC RESPONSE CHARACTERISTICS

When designing such systems, consideration must be given to low frequency requirements as well. These can present a problem when balancing the rotor system and can result in a mechanical instability (ground resonance) if inadequate damping exists at rotor speeds where a stand natural frequency plus the rotor blade "in-plane" frequency adds up to one. A more detailed explanation of this phenomenon can be obtained from Reference 4.

PERFORMANCE MODELS
USING MACH-SCALED ROTOR SYSTEMS

Several full performance models have been built by Boeing-Vertol over the years. Even though the design philosophy on such models is aimed at ruggedness and durability with ample power instead of dynamic properties scaling, the same factors that are critical in the design of isolated rotor test stands discussed so far in this paper are critical here as well.

Examples of two full performance models using Mach-scaled rotor systems presently being designed and fabricated at Boeing-Vertol are shown in Figures 27 and 28.

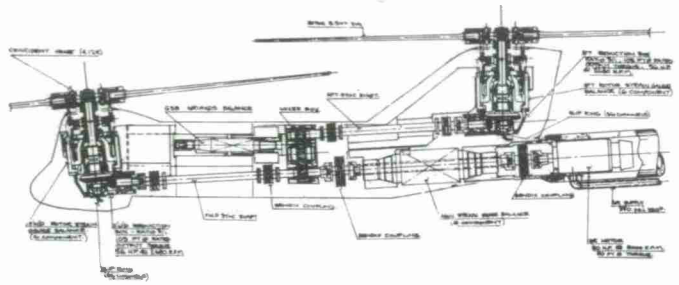


FIGURE 27
UNIVERSAL HELICOPTER MODEL-II (6-FOOT ROTOR)

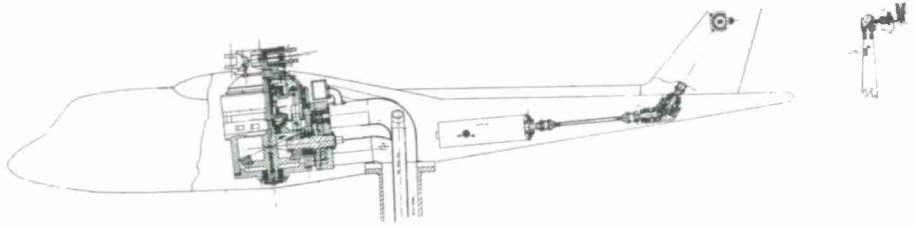


FIGURE 28
SINGLE ROTOR HELICOPTER MODEL-I (10-FOOT DIA)

Figure 27 shows an engineering layout for a tandem rotor Universal Helicopter Model (UHM-II). Significant features are:

- Six-foot diameter Mach-scaled and fully instrumented H.L.H. rotor blades.
- Simulated and/or actual coincident hinge configuration.
- Remote collective and cyclic actuation.
- Four six-component balances:
  - Forward rotor
  - Aft rotor
  - Fuselage
  - Total model
- 90 horsepower externally mounted air motor with compatibly designed gearboxes and shafting.
- Rotor overlap variation capability.
- Rotor vertical spacing variation capability.
- Sting mounted for in-ground effect Moving Belt Ground Plane testing, remote controlled attitude adjustment, and convenience in positioning model at a working level for maintenance purposes.

Although the UHM-II currently weighs three times as much as the scaled H.L.H., we are looking into the feasibility of modifying the design to make it, in fact, a totally Mach-scaled dynamically representative model.

Figure 28 shows an engineering layout for a Single Rotor Helicopter model (SRH-I). Significant features are:

- Ten-foot diameter Mach-scaled and fully instrumented UTTAS rotor blade.
- Scaled hub and blade retention system.
- Remote collective and cyclic actuation.
- Four six-component balances:
  - Main rotor
  - Tail rotor
  - Fuselage
  - Total model
- Three, 90-horsepower internally mounted air motors with 300-horsepower gearboxes and shafting for the main rotor drive.
- One, 52-horsepower internally mounted electric motor for the tail rotor drive.
- Scaled/simulated "flex-strap"tail rotor blade and retention system.
- Rotor system package is mechanically adaptable for running in the Dynamic Rotor Test Stand.

No consideration has been given to full model Mach scaling but the rotor system including the rotor balance has been designed so that dynamic blade and hub load data can be obtained.

FROUDE-SCALED DYNAMIC MODELS

Although many Froude-scaled full dynamic models have been successfully designed and fabricated for fixed wing aircraft, the extension to helicopters was not direct and in fact did require considerable development. Our experiences in adapting these techniques are discussed in the following section.

A. BLADE CONCEPTS

The first Froude-scaled VTOL model flown by Boeing-Vertol was designed and fabricated by Dynamic Devices and utilized a blade construction concept that had been used quite successfully on fixed wing flutter models. The blade is shown in Figure 29(a). The spar provided the required stiffnesses and a segmented aerodynamic shell satisfied airload and weight distribution requirements. This blade had quite a few shortcomings such as a relatively poor aerodynamic surface because of the many spanwise breaks in continuity, a large number of parts requiring considerable assembly time, and easily damaged structure while handling requiring frequent rework, existance of stress concentrations in critical structural member resulting from point attachment of airfoil boxes, a large portion of the weight not contributing to the structural integrity, and a surface material that was susceptible to leading edge abrasion.

Different concepts have been tried over the past several years that have successfully overcome the above-mentioned drawbacks. The most successful of these are shown in Figures 29(b) and 29(c). The blade shown in Figure 29(b) utilizes an I-beam shaped shotpeened titanium spar with local tantalum balance weights covered by a 6 #/Cu-Ft continuous foam envelope. The blade shown in Figure 29(c) utilizes advanced composites (PRD) for the basic shell with a balsa spar mandrel and Nomex trailing edge box construction. PRD-III was used for this blade because of the large torsional stiffness required. Boron was used on the full scale blade, but is not feasible on a model of this size because of the small leading edge radius around which a boron fiber cannot be curved without snapping. Both methods of construction have resulted in an excellent continuous aerodynamic surface, minimum number of parts and assembly time, reduced handling damage susceptibility, maximum strength-to-weight or stiffness relationships, virtually all of the weight is structural and leading edge abrasion both with and without a polyurethane finish protection is minimal.

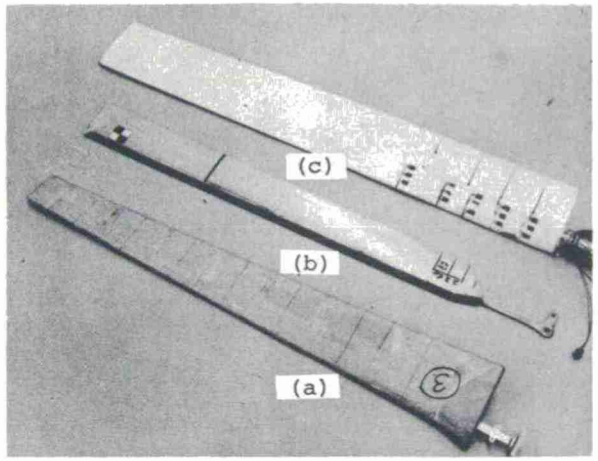


FIGURE 29
FROUDE SCALED MODEL ROTOR BLADES

B. HUB CONCEPTS

Blade retention systems for Froude-scaled models are virtually no problem when compared to Mach-scaled models. Almost every system that we have tried, whether it was a deep groove ball bearing, angular contact bearing, needle roller bearing, or a lamiflex bearing, has worked successfully. This can be attributed to the fact that lower loads and speeds result in scaled bearing lives that are approximately equal to the full scale life x (scale factor)$^{3.3}$.

C. CONTROL SYSTEM

As in the case of the hub, control systems pose virtually no structural problems when compared to the Mach-scaled models.

Occasionally some unique model requirements result in a control system that is "different". An example of this is the system used on the Model 222 dynamic model. The collective and cyclic system was required to move $\pm$ one degree at a rate of 26 CPS, which is equivalent to 1.3 per rev. The design utilized a drive motor/gearbox combination that was continuously spinning at 2000 RPM which was then engaged by a rapid acting clutch resulting in a movement of these controls to the proper position where they are held by a brake. All of this hardware is contained within the rotor

nacelle and together with rotor drive system and balance hardware was fabricated to within 15% of the nacelle weight requirements. A picture of this system is shown in Figure 30.

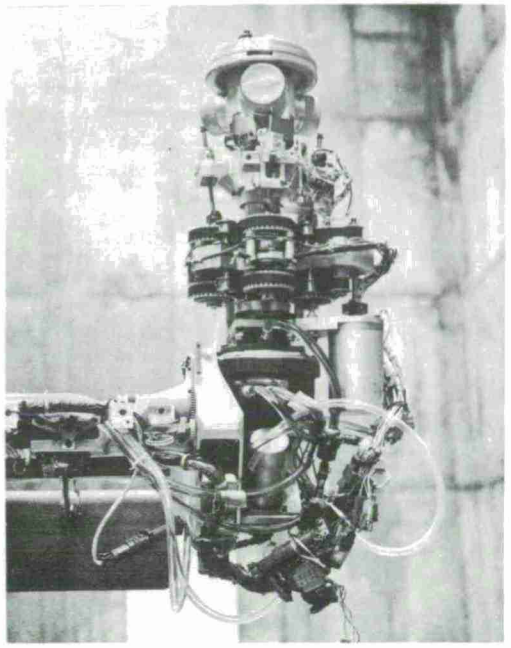


FIGURE 30
MODEL 222 TILT ROTOR "HIGH SPEED" ROTOR CONTROL SYSTEM

D. DRIVE SYSTEM CONCEPTS

The power requirements for a Froude-scaled model are equal to the full scale Horsepower ÷ (Scale Factor) $^{7/2}$. This can be compared to Mach-scale requirements of full scale Horsepower ÷ (Scale Factor)^2. Because of this relationship we have found it possible on two degree of freedom models to live with motor weights when they are mounted within the model at a preferred location.

The development of lightweight power plants permitting proper weight scaling is a must for the future if additional degrees of freedom are to be obtained with ease.

E. FULL MODELS

Our success in designing and fabricating Froude-scaled models is illustrated in Figures 31, 32 and 33.

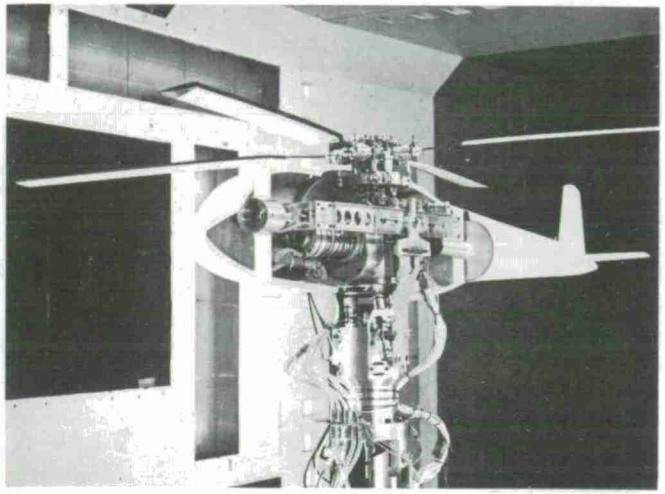
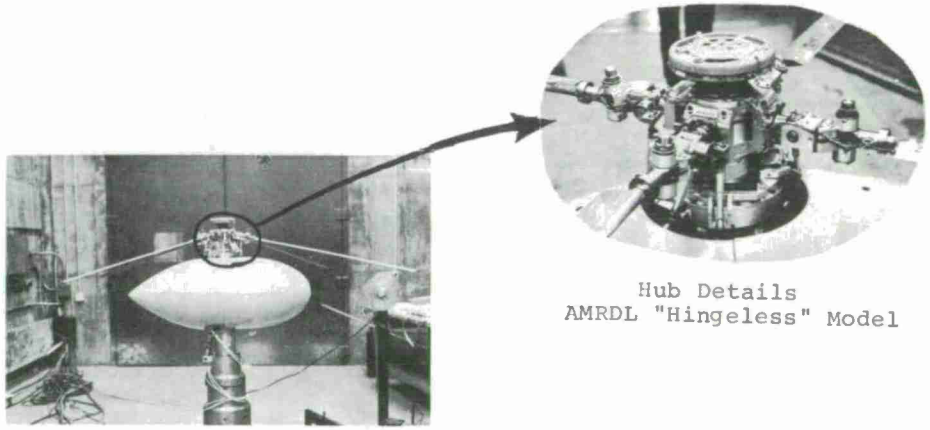


FIGURE 31
UTTAS DYNAMIC MODEL



Hub Details
AMRDL "Hingeless" Model

FIGURE 32
USAMRDL DYNAMIC "HINGELESS" MODEL

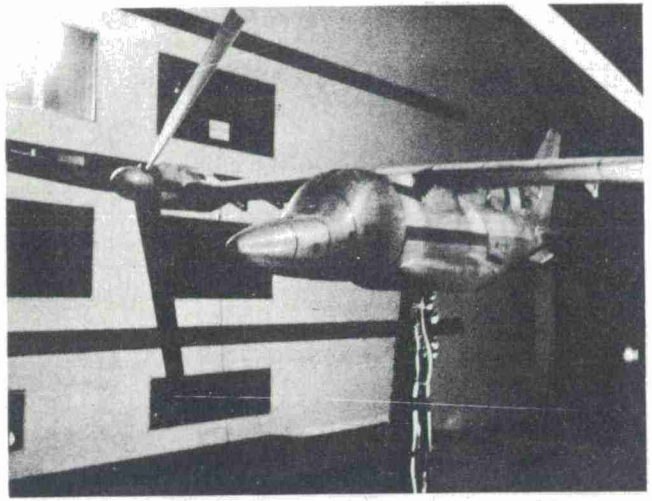


FIGURE 33
MODEL 222 DYNAMIC TILT ROTOR MODEL

Figure 31 shows a Froude-scaled 5.5-foot diameter UTTAS dynamic model. Some of its significant features are:

- Dynamically-scaled instrumented rotor blades.
- Variable hub precone, blade offset, blade sweep.
- Remote control collective and cyclic.
- Two degree of freedom gimbal mounting with scaled pitch and roll inertias.
- Variable vertical and longitudinal "CG"/pivot axis position.
- 6-horsepower internally installed electric motor.
- "Stick" controls for flying model in the tunnel.

Figure 32 shows a Froude-scaled 5.5-foot diameter "Hingeless" rotor model built for United States Army Air Mobility Research and Development Laboratory (USAAMRDL). Some of the significant features are:

- Stiffest possible rotor blades with respect to Locke number.
- Replaceable hinge springs that allow the following rotor frequency ranges:

$$1.07 \leq \omega_{flap} \leq 1.29$$
$$.52 \leq \omega_{chord} \leq 1.56$$
$$2.00 \leq \omega_{torsion} \leq 12.20$$

- Variable lag hinge damping
- Variable hub precone, blade offset, blade sweep.
- Hub balance for measurement of rotor loads.
- Remote control collective and cyclic.
- Variable amplitude and frequency cyclic excitation system.
- Two degree of freedom gimbal mounting with representative pitch and roll inertias.
- Variable vertical and longitudinal "CG"/pivot axis position.
- Two, 6-horsepower internally installed electric motors.
- "Stick" controls for flying model in tunnel.

Figure 33 shows a Froude-scaled 5.62-foot diameter tilt rotor Model 222. Some of the significant features are:

- Dynamically scaled, instrumented rotor blades.
- Hub balance for measurement of rotor loads.
- Remote control collective and cyclic.
- High speed collective and cyclic (26 CPS) which is equivalent to $\pm$ one degree motion in less than one rotor revolution.
- Remote control nacelle pitch mechanism.
- Weight and inertia scaled nacelles.
- Variable nacelle pitch stiffness.
- Weight, inertia and stiffness scaled wing spars.
- Remote controlled inboard and outboard wing flaps.
- Weight, inertia, and stiffness scaled fuselage spars.
- Frequency scaled vertical and horizontal stabilizer.
- Remote controlled ailerons and rudder.
- One, 20-horsepower electric internally mounted motor.
- Pitch, roll, yaw and vertical degrees of freedom when mounted on the "Monkey Pole" installation.
- Dynamically scaled landing gear springs and dampers for ground instability studies.
- Combination dynamic and performance model.

This model without a doubt, has been our most ambitious task to date. Weight scaling although normally not a problem on a Froude-scaled model was a problem here. Although the design model weight was 125 pounds, the combined weights of all fifteen (15) motors (main drive, flap motor, pitch motors, etc.) totaled 50 pounds or 40% of the desired model weight.

The extensive electrical control system such as that used on the Model 222 Tilt Rotor Model is worthy of discussion.

A complete autopilot system controls both flight surfaces, and rotor settings to maintain a given attitude in hover, transition and forward flight modes. Additional features of the system are easily programmable feedback schedules

for the transition mode, auto-minimization capability for either blade or wing loads, and the ability to enter step disturbance while under auto-control. Manual override is available at all times and the autopilot system is cut out whenever an excessive error signal (i.e., component or wire failure) occurs.

A separate control panel encompassing all of the controls mentioned was built to permit the model to be flown by a model "pilot". Figure 34 shows a picture of the control panel. This type of panel is typical of those used for the control of dynamic models.

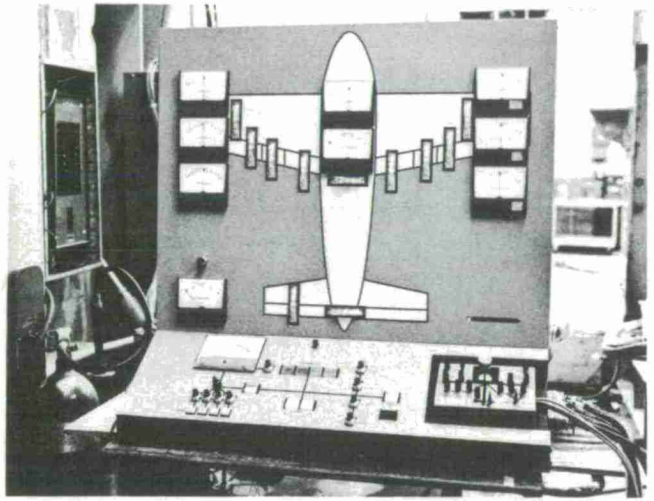


FIGURE 34
MODEL 222 FLIGHT CONTROL PANEL

MISCELLANEOUS DESIGN FACTORS

(MACH & FROUDE SCALED MODELS)

A. HEAT SCALING

An item mentioned only briefly before but which plays a large part in dynamic model scaling is heat. It can be shown that on Mach-scaled models the temperature rise due to surface area convection is identical to full scale. The temperature rise due to conduction is equal to the full scale divided by the scale factor. If cooling is needed on the full scale article, then similar cooling is required on the model. It is our practice to install thermocouples at points of concern to provide a thorough temperature signature of the model. On Froude-scaled models, however, the heat generated is significantly less and, therefore, temperature problems rarely exist.

B. WEIGHT SCALING PROBLEMS

In the process of trying to keep model hardware weights down to a prescribed value, we have concluded that the following design philosophy should be enforced wherever feasible.

- Minimize parts required and number of joints.
- Use magnesium unless structurally inadequate then,
- Use aluminum unless structurally inadequate then,
- Use titanium unless structurally inadequate then,
- Use steel.

Although aluminum, titanium and steel are in relatively good supply, we found magnesium lacking in immediate availability. Since the required flow time to acquire magnesium can be long, we do some stockpiling. A similar stockpiling of rod end bearings and small anti-friction bearings has been necessary to provide programs with this hardware in a relatively short time period.

C. FABRICATION COSTS

A continuing goal of the V/STOL Wind Tunnel Engineering/ Manufacturing team is the reduction of model costs. Many parameters have been studied over the years to establish just what drives the cost of a model. We were pleased to find that the simplest of parameters - number of parts - provides the best correlation. Complexity of parts and size of parts (from a one-foot rotor diameter model to a 16-foot rotor diameter model) seem to average out costs

due to set-up times, duplications, assembly times, etc. A curve demonstrating cost correlation for many models built over the past four years is shown in Figure 35.

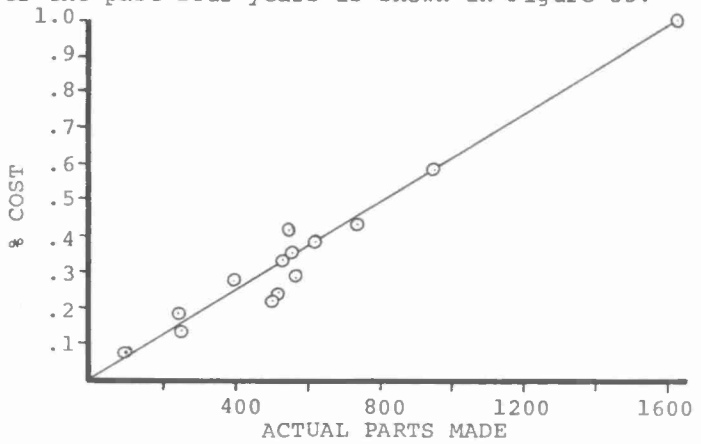


FIGURE 35
MODEL PART/COST RELATIONSHIP

POINTS TO PONDER

What then is the next step in the design and fabrication of Mach-scaled models?

Can all of this lead to a free flight Mach-scaled dynamic model?

Is it possible to design and fabricate an "all singing, all dancing" model that satisfies both static and dynamic data requirements within a reasonable cost and schedule?

By working hard at a solution to the power plant scaling problem and establishing a suitable means to transmit steady state and dynamic data from the model without wires, and developing a means of cooling heat generating items, a free flight Mach-scaled dynamic model should be possible within the next ten years.

The Froude-scaled V/STOL dynamic model with four degrees of freedom is within the state-of-the-art. To investigate the feasibility of adding the lateral and longitudinal degrees of freedom, a reduced tip speed radio controlled helicopter model was designed and fabricated by Gene Rock, a Boeing-Vertol model designer. The model was successfully flown in the Boeing V/STOL Wind Tunnel. Figure 36 shows the model helicopter representing a full scale helicopter with a gross weight of 12,000 pounds in free flight carrying a weight that would be the equivalent of a 1,200 pound telephone pole flying up to full scale speeds of 57 MPH.

It is interesting to note that as far back as 1956 feasibility of a six degree of freedom system that utilized an "umbilical" cord for power and data requirements was established for a free flight Froude-scaled model of the V-76 Tilt Wing aircraft. This model was designed by Vertol, built by NASA and flown successfully in the NASA Langley 30' by 60' tunnel. The model and the program are described in Reference 7. These successful efforts on Froude-scaled models give us the confidence that equal success can be achieved with Mach-scaled models.



FIGURE 36
FREE FLIGHT RADIO CONTROL HELICOPTER MODEL
IN BOEING V/STOL TUNNEL

CONCLUSIONS

The state-of-the-art in modeling has been advanced significantly over the past four years. Mach scaling of rotor systems down to the stationary swashplate support structure is completely feasible and practical. Froude-scaled full V/STOL models down to a 5-foot diameter are feasible and practical. Feasibility of a Mach-scaled full V/STOL model is within our grasp. Our thinking at the Boeing V/STOL Wind Tunnel is limited to no less than a Mach-scaled full V/STOL free flight model within the next 10 years. With this long range objective, intermediate steps (significant in their own right) become a little easier to achieve.

ACKNOWLEDGEMENTS

I would like to thank Bob DiRusso, Pete Dixon, Frank Harris, Joe Mayer, Ed McGee, Harry Parkinson and Kathy Trapp for their participation in the preparation of this paper.

REFERENCES

1) The Application of Models to Helicopter Vibration and Flutter Research,
Brooks, G.W. NACA AHS Paper, May 1953.

2) The Development of Dynamic Model Rotor Blades in High Speed Helicopter Research,
Fradenburgh, E.A., and Kiely, E.F. Sikorsky Aircraft Symposium on Aeroelastic and Dynamic Modeling, September 1963.

3) Results of Experimental Investigation of Small Viscous Dampers
Silveira, M.A., Maglieri, D.J., and Brooks, G.W.
NACA - NACA TN 4257

4) Theory of Self Excited Mechanical Oscillation of Helicopter Rotors with Hinged Blades
Coleman, R.P., and Fiengold, A.M.
NACA TR1351, 1958

5) Low-Speed Wind Tunnel Testing,
Pope, Alan and Harper, John J.
Wiley & Sons, Inc. - 1966

6) Aeroelasticity
Bisplinghoff, R.L., Ashley, H., Halfman, R.L.
Addison-Wesley Publishing Company

7) Flight Investigation of the Stability and Control Characteristics of a 1/4 Scale Model of a Tilt Wing Vertical-Take-Off-And-Landing Aircraft
Tosti, L.P., NASA Memo 11-4-58L

SCALE FACTOR SUMMARY

MODEL = FULL SCALE/S^N

S> 1.0

PARAMETER	SCALING (S^N) MACH	FROUDE
Linear Dimensions	S	S
Mass or Weight	S^3	S^3
Time	S	$S^{1/2}$
Frequency	S^{-1}	$S^{-1/2}$
Linear Deflection due to Gravity	S^2	S
Linear Displacement - Dynamic	S	S
Linear Velocity	1	$S^{1/2}$
Linear Acceleration	S^{-1}	1
Angular Deflection due to Gravity	S	1
Angular Displacement - Dynamic	1	1
Angular Velocity	S^{-1}	$S^{-1/2}$
Angular Acceleration	S^{-2}	S^{-1}
Viscous Damping Coefficient	S^2	$S^{5/2}$
Stiffness	S^4	S^5
Linear Spring Rate	S	S^2
Mass Moment of Inertia	S^5	S^5
Force	S^3	S^3
Strain	1	1
Moment and Torque	S^3	S^4
Power	S^2	$S^{7/2}$
Heat (Generated)	S^2	$S^{7/2}$
Heat (Convected)	S^2	S^2
Heat (Conducted)	S	S
Natural Frequencies	S^{-1}	$S^{-1/2}$
Per Rev Frequencies $\frac{\omega n}{\Omega}$ $\frac{\text{(Natural Frequency)}}{\text{Rotor RPM}}$	1	1
Disk Loading	1	S
Mach No. (1 = F.S. Tip Speed)	1	$S^{1/2}$
Froude No. (1 = F.S. C.F./Gravity Force)	S^{-1}	1
Lock No. (1 = F.S. Coning Angle)	1	1

TABLE 1

MATERIAL PROPERTIES USED IN MODEL DESIGN

	S_{et}	S_{es}	S_{et}/E	S_{es}/G	S_{et}/ρ	S_{es}/ρ	E/ρ	G/ρ
	@ R=0 ~±PSI		x10^6 ~±PSI/PSI		~±PSI/LB/IN^3		x10^-6 ~PSI/LB/IN^3	
METALS								
Magnesium	2880	1680	443	700	48000	28000	108.00	40.00
Aluminum	5550	3223	555	805	55800	32230	100.00	40.00
Steel	23700	13862	817	1260	81724	47800	100.00	37.90
Titanium	17420	10028	1088	1620	108875	62675	100.00	38.70
Tantalum	23840	-	1135	-	39210	-	34.50	11.50
FIBERGLASS								
E-1002 Uni @ 0°	9875	1000	1795	1667	141071	4285	78.57	8.57
E-1002 X-Ply @45°	2737	3330	1710	1959	39100	47571	22.86	24.29
E-181 WOV. @0°±90	7875	1877	2540	2317	112500	26814	44.29	11.57
E-181 WOV. @45°	3515	4493	1598	3328	50214	64185	31.42	19.29
S-1002 Uni @ 0°	17450	2035	2727	2907	249285	29071	91.42	10.00
S-1002 Uni @45°	4638	5992	2493	2853	66257	86600	26.57	30.00
XP-251S Uni @ 0°	17974	2035	2392	2907	246220	27877	102.70	9.58
XP-251S X-Ply @45°	3271	6882	1363	2867	44800	94270	32.90	32.90
CARBON								
HTS @ 0°	40000	1500	2000	3000	774000	2900	386.00	9.67
HM @45°	3500	6100	1590	871	63640	111000	40.00	127.00
BORON								
Boron @ 0°	16120	1027	448	1070	217838	13880	486.50	12.97
Boron @45°	2500	3914	714	444	33800	52891	47.30	118.90
PRD								
PRD Uni @ 0°	17325	1200	1386	3000	327000	22600	235.00	7.50
PRD X-Ply @45°	2888	3400	2888	1214	54500	64150	18.80	53.00
FILLS								
Foam 605 (6#)	39.6	20	7857	10416	11314	5714	1.44	.55
Foam 610 (12#)	55.6	36	4365	6666	7857	5143	1.80	.77
Balsa 6 #/Ft^3	260.0	29	810	1600	7430	6857	91.40	4.28
Balsa 12 #/Ft^3	780.0	64	920	1778	11143	9143	121.40	5.14
Nomex 2 #/Ft^3	17.0	10	3777	3571	14655	8620	3.90	2.40

TABLE 2

14-FOOT DIA HLH SCALED CONTROL SYSTEM WEIGHTS

ITEM	REQUIRED SCALED WEIGHT (#)	ACTUAL COMPONENT WEIGHT (#)
Pitch Arms (4)	.13	.16
Pitch Links (4)	.16	.18
Swashplate - Rotating	.70	.80
Swashplate Bearing	.20	.54
Swashplate - Stationary	.58	.64
Drive Scissors (2)	.16	.15
Slider Assembly	.08	.15
Spring/Damper (Active Portion)	-	.16
TOTAL WEIGHT CONTROL SYSTEM	2.01	2.78

TABLE 3

APPENDIX II

THE EFFECTS OF REYNOLDS NUMBER ON ROTOR STALL

By

WILLIAM G.S. HARDY
BOEING V/STOL WIND TUNNEL
THE BOEING VERTOL COMPANY

THE EFFECTS OF REYNOLDS NUMBER ON ROTOR STALL

by
William G.S. Hardy
The Boeing Company
Philadelphia, Pennsylvania

INTRODUCTION

The effects of Reynolds number have been associated with the scaling of model data to full scale data. However, today's fixed and rotary wing aircraft experience large changes in Reynolds number due to variations in speed and altitude which could effect the performance of both unless they are anticipated.

The importance of Reynolds number in considering flow similarity has been established in fixed wing aerodynamics. Its effect on rotary wing aerodynamics is not as well understood. Model rotor data is available to today's rotorcraft aerodynamicist, but comparative full scale data is lacking. In this situation, we are forced to turn to mathematical models of the rotor to explore the influences of Reynolds number.

The theoretical foundations of rotary wing mathematical models lie in fixed wing aerodynamics. Thus, our basic hypotheses about the effects of Reynolds number have been drawn from this discipline. The study outlined below utilizes an existing mathematical model to relate our fixed wing knowledge of Reynolds number effects to the rotary wing and gain an understanding of the effects of Reynolds number on rotor stall.

THE MATHEMATICAL MODEL OF THE ROTARY WING

The mathematical models of rotary wing aircraft have evolved by applying fixed wing aerodynamics to the relatively complex problem of rotors. The "wing" is rotated at some speed, inducing flow over it. This creates a lift, drag, and pitching moment which are computed using the appropriate two dimensional airfoil section characteristics. These aerodynamic forces are reacted by the blade weight, the centrifugal force, and inertia force. The forces are computed locally and then used to solve the equations of motion of the blade. For forward flight conditions, the external flow is imposed on the rotating wing, but the procedure of solution still utilizes the two dimensional section characteristics to compute the local aerodynamic forces.

More sophisticated mathematical models now include

i. non-uniformities in the flow encountered locally by the blade by introducing the effects of the local downwash from each blade section,

ii. the effects of changes in the lift, drag, and moment characteristics due to the three dimensional, oscillatory motion of the blade by adjusting the steady airfoil characteristics for these effects, and

iii. variations in the assumed blade position induced by the elastic deformation of the blade under load.

The mathematical model used in this study included all of these effects and is described in Reference 1.

A REVIEW OF FIXED WING REYNOLDS NUMBER EFFECTS

Before proceeding with a discussion of the effects of Reynolds number on rotary wing aircraft, a review of the classical fixed wing effects is in order. Consider the two dimensional airfoil section characteristics of a 23010 airfoil at two different Reynolds numbers (Figure 1). One Reynolds number corresponds to a full scale CH-47 sized blade, and the second to a 6 ft. diameter, CH-47, wind tunnel model. These data show the well known reduction in the maximum lift coefficient as Reynolds number is reduced. Associated with this reduced $C_{L_{max}}$ is a decrease in the angle of attack at which the airfoil stalls and at which moment curve breaks.

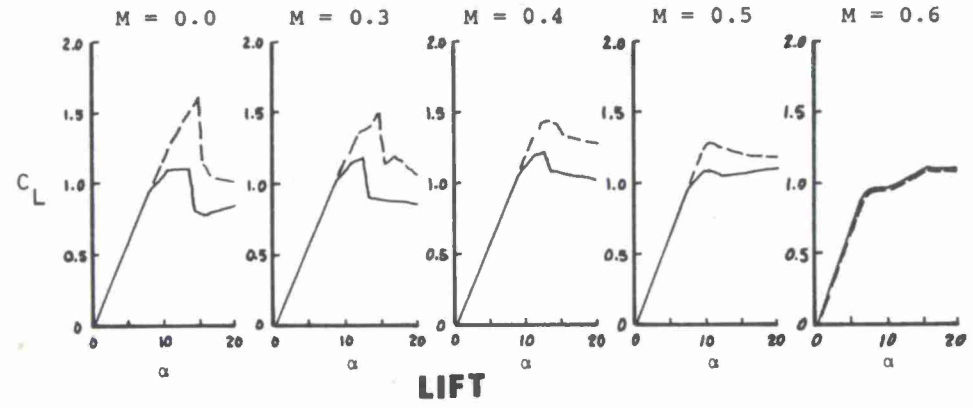
THE COMPARISON OF THE MATHEMATICAL MODEL TO EXPERIMENTAL DATA

The experimental data necessary for this paper came from a single wind tunnel test run in which a 6 foot diameter, 3 bladed rotor model was pitched through a range of shaft angles. A detailed description of the model is contained in Reference 2. During this run, no changes were made to the model except in shaft angle. The longitudinal cyclic pitch, B_{1_c}, and the lateral cyclic pitch, A_{1_c}, were zero. The root collective pitch was held constant at 20.6 degrees. The advance ratio was constant, and a full scale tip speed was maintained throughout. The experimental rotor thrust curve is shown in Figure 2. The inception of stall is at a C_T/σ around 0.10.

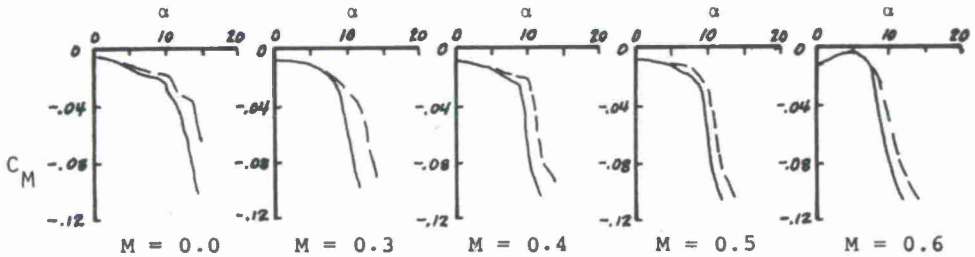
23010-1.58 AIRFOIL SECTION CHARACTERISTICS

— — — FULL SCALE REYNOLDS NUMBER

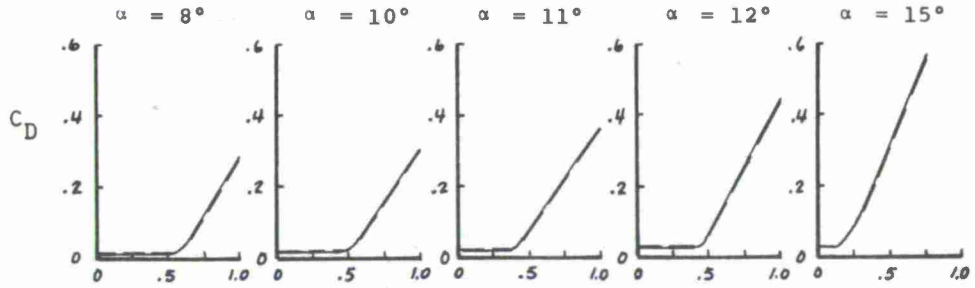
——— MODEL SCALE REYNOLDS NUMBER



LIFT



PITCHING MOMENT



DRAG

FIGURE 1

6 FOOT DIAMETER
MODEL ROTOR DATA

$V/\Omega R$ = 0.3
A_{1_C} = 0.0°
B_{1_C} = 0.0°
V_{TIP} = 750 FT/SEC
θ_{ROOT} = 20.6°
θ_{TWIST} = -7.5°

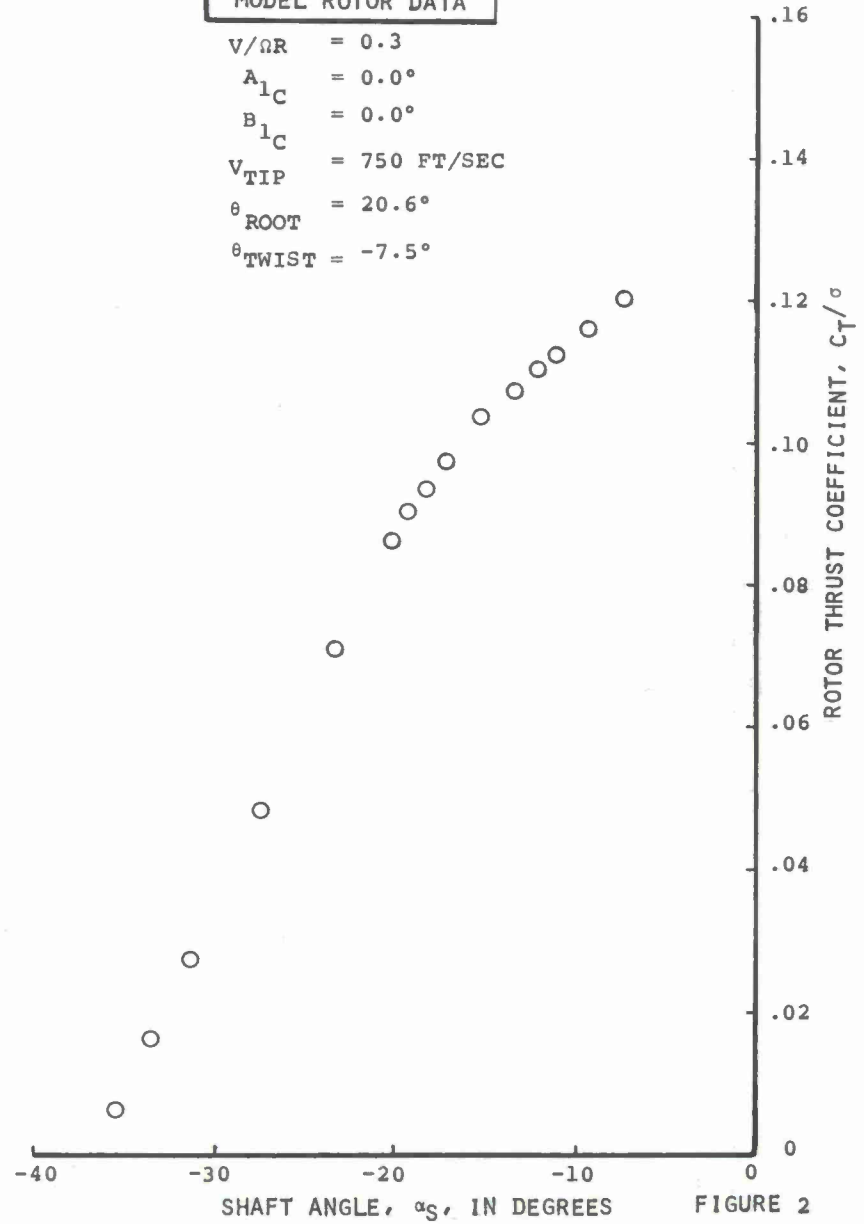


FIGURE 2

Using these test results as a basis for our investigation, the mathematical model, using the model scale airfoil section characteristics shown in Figure 1, first matched the low thrust test results to establish the theoretical root collective pitch of 20.9 degrees. With this theoretical root collective pitch held constant, the mathematical model of the rotor was then used to determine the thrust variation over the same range of shaft angles as the wind tunnel model. These data are compared in Figure 3. The agreement between the theory and the test results is good over the entire thrust range both before and after stall.

From these results it was concluded that we could proceed with the theoretical study of the effects of Reynolds number.

THE AERODYNAMIC EFFECT OF REYNOLDS NUMBER

Since the aerodynamics of a rotor are so complex, we approached the investigation in two phases. The first phase aimed at isolating the pure aerodynamic effect of Reynolds number on rotor stall as related to our fixed wing background. This effect is the stalling characteristic of the airfoil section and the associated variation of $C_{L_{max}}$ with Reynolds number. To accomplish this, the ability of the blade to elastically twist under aerodynamic loading was removed from the mathematical model. For comparison purposes with the test data, we re-established the required collective pitch at the low thrust conditions and generated the remainder of the data at that collective pitch.

Two Reynolds number cases were considered. One case used the airfoil section characteristics of the model scale blade, and the second used the section characteristics of the full scale blade. In both cases the blade was infinitely rigid in torsion. Figure 4 shows the results of these cases.

A finite $C_{L_{max}}$ and the non-linear stalling of the local airfoil section characteristics introduce non-linearities into the thrust curve of the rotor. Without real airfoil section characteristics, the rotor thrust curve should be expected to continue along a straight line as indicated. Altering these characteristics to account for Reynolds number changes the stalling character of the rotor, but the reduction in rotor thrust does not begin to approach in magnitude the reduction in section lift. The two dimensional $C_{L_{max}}$ was reduced by 18%, but the rotor thrust curve shows only a 3% reduction in thrust at the highest

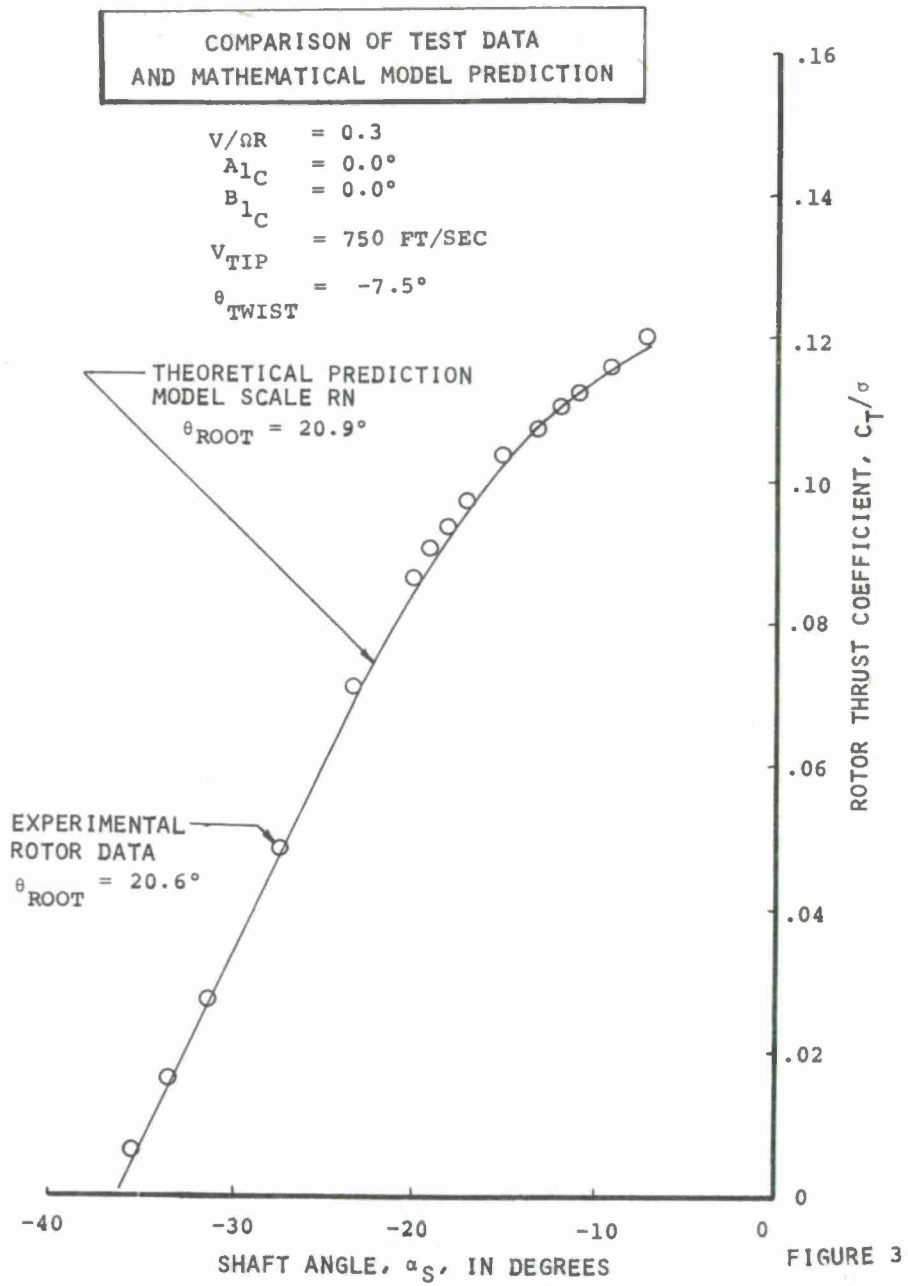


FIGURE 3

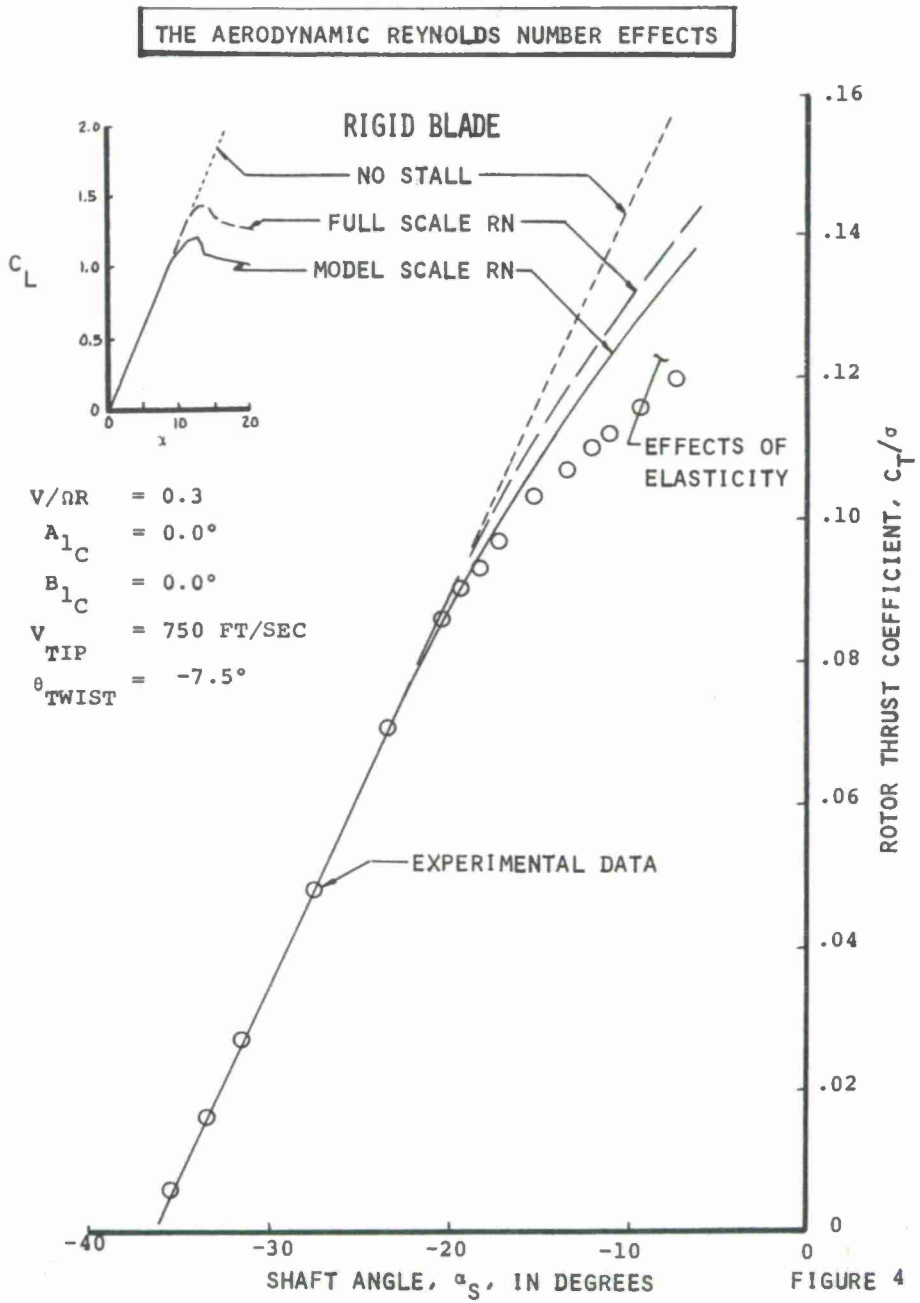


FIGURE 4

thrust coefficient considered. The rotor does not stall completely and therefore cannot be expected to show all of the loss indicated by the local section characteristics. In addition, just accounting for $C_{L_{max}}$ - Reynolds number trends is not sufficient to bring the theory into agreement with the experimental data.

AEROELASTIC EFFECTS DUE TO REYNOLDS NUMBER

Thus far in the study, we have only considered a rotor with inelastic blades. The combined effects of aerodynamics and aeroelasticity can be seen in Figure 5. With the addition of elasticity, the theoretically predicted rotor thrust curve has fallen into agreement with the experimental data. This fact emphasizes the importance of understanding the interaction of pitching moment and the elastic twisting of the blade. The effect of Reynolds number on this interaction is also evident in Figure 5. The full scale blade does not feel the effects of the reduced pitching moments until a higher angle of attack. Therefore, the full scale blade is able to develop more local lift before the moments twist the blade and reduce the local angle of attack. It is evident that the effect of elasticity is a major factor after the onset of stall. Before stall, however, the rotor thrust characteristics remain essentially the same because the airfoil section lift curve slope dominates the aerodynamics of the blade.

The relationship between lift and elasticity is straight forward. The elastic twisting of a wing is caused by the aerodynamic moment on it locally. In fixed wing aerodynamics, these moments are usually considered important in determining the stability and control of the aircraft, but have little influence on the performance. The reason for this is that the lift level is only slightly coupled to the aerodynamic moment because the fixed wing is relatively rigid. If the fixed wing did twist, the local angle of attack would change and the lift level would become a function of the local moment.

On the other hand, in rotor aerodynamics, the blade is twistable. It is a rotating, elastic wing, and the lift level is related to the local moment. In our case, the aerodynamic moment twists the blade nose down and reduces the local angle of attack. This in turn reduces the thrust developed by the rotor as indicated in Figure 5. From this we see that the airfoil pitching moment characteristics and resulting blade twisting are important in determining the rotor's performance.

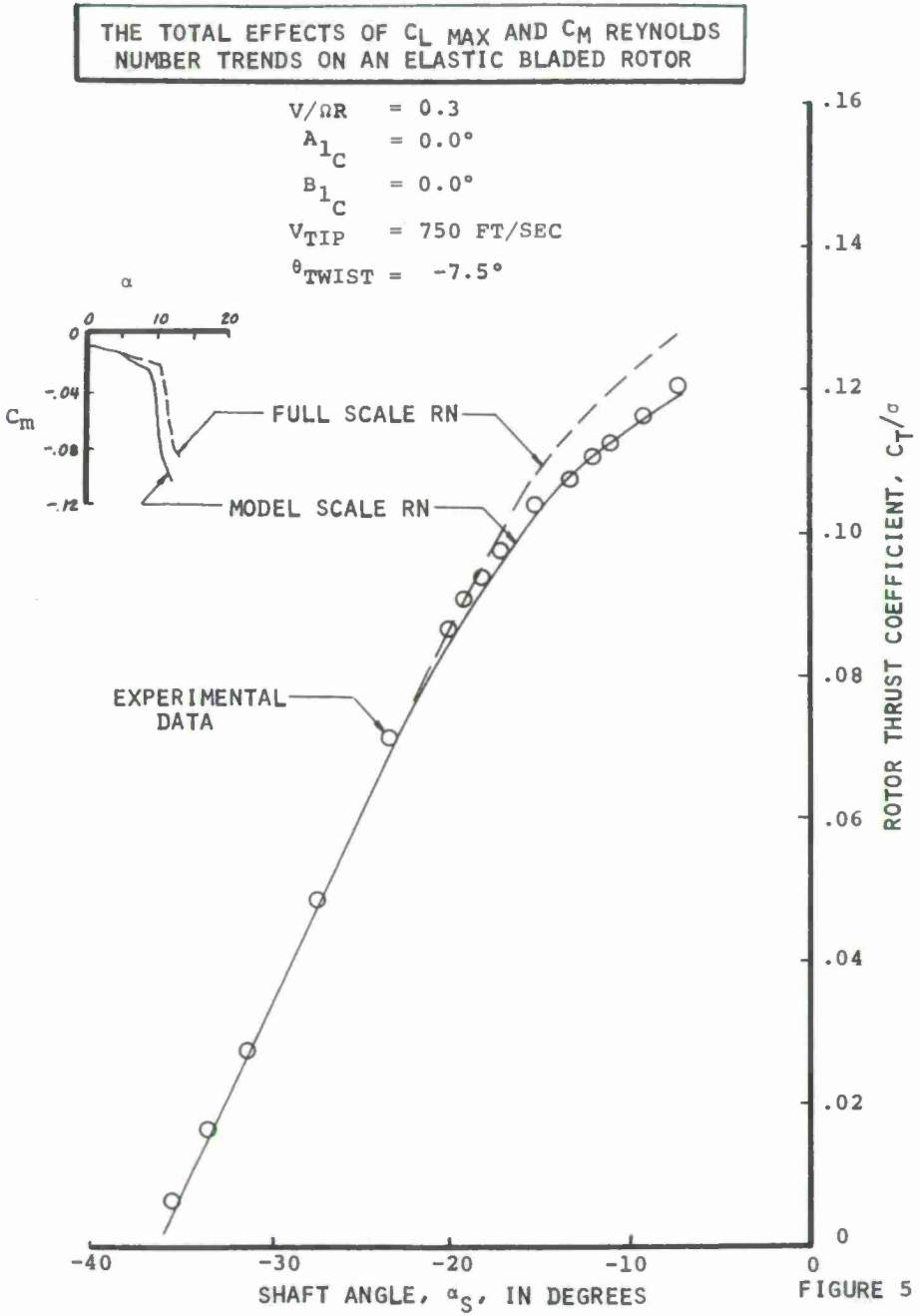


FIGURE 5

Figure 5 indicates that the effects of Reynolds number have been accentuated when $C_{L_{max}}$, C_m, and torsional deflection characteristics are considered. Where the thrust loss due to Reynolds number for the torsionally rigid rotor blade was 3%, it is now nearly 8%. This change is due primarily to the effects of pitching moment twisting the blade.

It is interesting to separate the aerodynamic effect from the aeroelastic effect. This is done in Figure 6. The pure aerodynamic effect, indicated by the dashed line in Figure 6, is the difference between the curves in Figure 4 and represents the decrement in thrust due to reductions in $C_{L_{max}}$ assbciated with changes in Reynolds number. The total Reynolds number influence, represented by the solid curve in Figure 6, is the difference between the curves in Figure 5 and represents the combined effects of reduced $C_{L_{max}}$ and the aeroelastic twisting of the blade in response to increased pitching moment. The difference between the curves in Figure 6 is the aeroelastic effect due to Reynolds number. It can be seen that for this rotor the aeroelastic effect of Reynolds number further reduces the rotor thrust and is of the same magnitude as the aerodynamic effect associated with $C_{L_{max}}$.

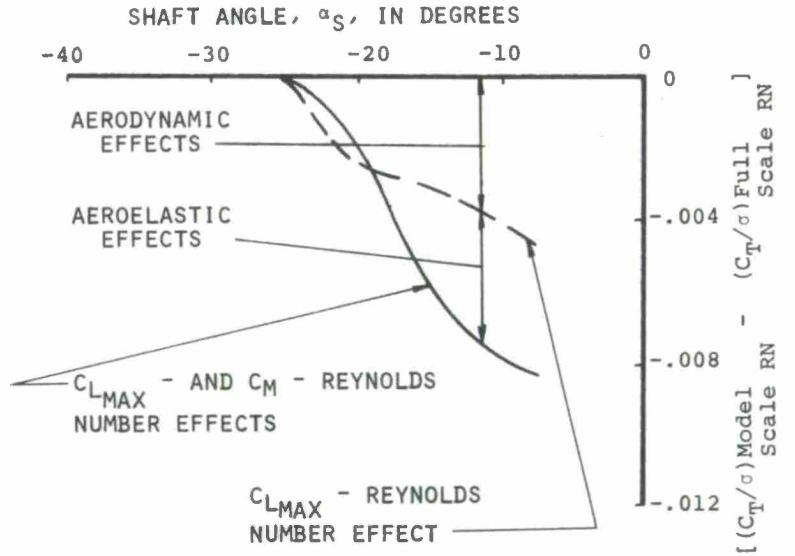


FIGURE 6: Comparative Influences of Reynolds Number

This aeroelastic reduction in thrust is derived from differences in pitching moment between the full scale airfoil section pitching moment and the model scale airfoil section pitching moment. As was noted in discussing these differences, the model scale pitching moment characteristics evidence a marked reduction in moment coefficient at angles of attack which are lower than the full scale's. Therefore, the model scale case will not only experience a lift loss at lower angles but will also experience a large nose down moment which will reduce the local blade pitch angle and further reduce the local lift.

The blade elastic twist in response to pitching moment is both a steady and a cyclic phenomenon. It can be represented as a harmonic series with a steady term and sine and cosine terms.

$$\theta_{e_t} = \theta_{e_{t_s}} + \theta_{e_{t_{1_s}}} \sin\psi + \theta_{e_{t_{1_c}}} \cos\psi$$

The steady term is the aeroelastic equivalent to the geometric twist of the blade. The sine and cosine terms are aeroelastically induced longitudinal and lateral cyclics. As in the case of classic rotor aerodynamics, the sine harmonic is seen directly in the thrust and longitudinal flapping whereas the cosine harmonic shows up as a change in the blade lateral flapping.

FURTHER COMMENTS ON AEROELASTIC EFFECTS

To comprehensively review the effects of elasticity on this rotor performance problem, consider the progression of the theory to the prediction of the test results using the simple theoretical approach as a base. This progression, outlined by Figure 7, starts with the linear aerodynamic equation for rotor thrust given in Reference 3.

Curve I is the simple theory's prediction at a root collective pitch of 20.9 degrees. Curve II is the current method's prediction for the rigid blade rotor and represents the influence of stalling, non-uniform downwash, and unsteady aerodynamics. Curve III is our mathematical model's complete solution for the true aeroelastic problem. It is evident that the effect of aeroelasticity alone is at least equivalent to the combined effects of stall, non-uniform downwash and unsteady aerodynamics and emphasizes the importance of the interaction of pitching moment and torsional rigidity.

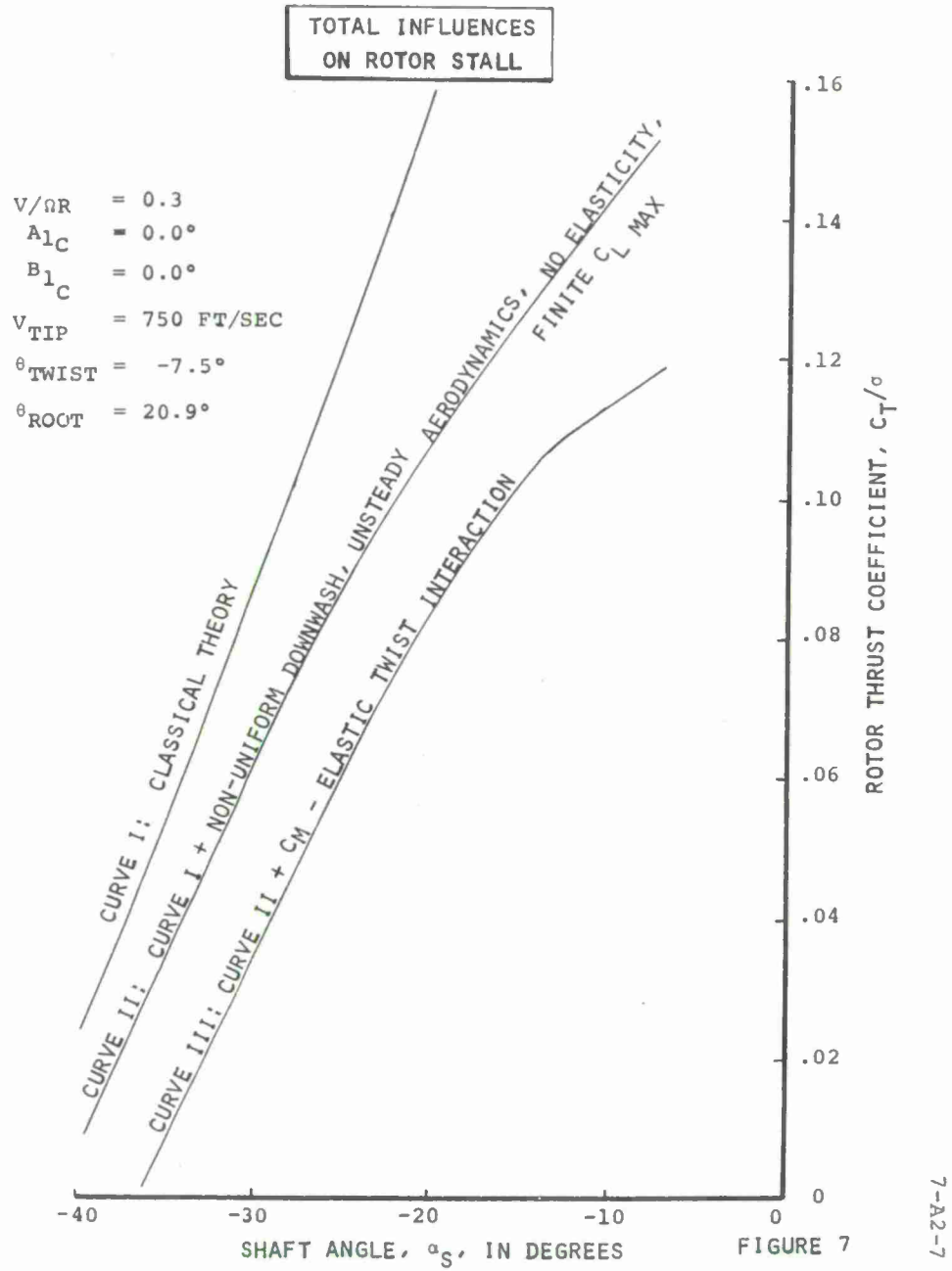


FIGURE 7

CONCLUSIONS

The plight of the rotary wing aerodynamicist is not as great as the fixed wing aerodynamicist with regard to Reynolds number influences. Although these influences are more difficult to isolate, the variations on rotor thrust due to changes in Reynolds number are small when compared to fixed wing lift variations.

In analyzing the effects of Reynolds number, however, we must break away from the fixed wing approach and consider not only lift effects on lift but moment effects on lift. We must be more critical of the aerodynamic pitching moment characteristics of the airfoil, the variation of these characteristics with Reynolds number, and the structural properties of our elastic blade. If this is done meaningful predictions can be made for each rotor under consideration and the effects of Reynolds number on stall can be anticipated.

REFERENCES

1. Davenport, F.: Rotor Airloads and Performance Analysis with Non-Uniform Induced Flow
The Boeing Company Document D8-0312, January 1968.

2. Gabel, R. & Tarzanin, F.: Blade Torsional Tuning to Manage Rotor Stall Flutter
AIAA Paper 72-958; 2nd Atmospheric Flight Mechanics Conference; September, 1972.

3. Gessow, A. & Myers, G.C.: Aerodynamics of the Helicopter
Fredrick Ungar Publishing Company - 1952

PARAMETRIC TRENDS & OPTIMIZATION — PRELIMINARY SELECTION OF CONFIGURATION — PROTOTYPE DESIGN & MANUFACTURE

by

H. Huber
Messerschmitt-Bölkow-Blohm GmbH
8012 Ottobrunn, Germany

OUTLINE

This lecture is intended to show how all aerodynamic and dynamic inputs contribute to the design systhesis, with the main emphasis placed on rotor problems.

Aerodynamic rotor design is concentrated on disc loading, tip speed and solidity selection. Rotor airfoil design is discussed under the aspects of compressibility and stall problems. Some advanced profile shapes with thickness and tip geometry variations are shown.

Fundamental flapping and inplane frequencies are shown to be the two basic parameters in dynamic rotor design. A selection of these two parameters must consider flight dynamics behaviour, rotor blade stability and blade stresses. Higher harmonic blade tuning and blade torsional effects are of similar importance. Hub geometry design must not only regard static blade deloading aspects but also bending-torsion coupling effects.

Ways of developing various trend curves and their interpretation is supplemented by formal and iterative optimization techniques. Iterations of preliminary design, showing crystalization of the configuration most responsive to the customer's requirements are presented.

New materials are shortly described under the aspect of advanced rotor design.

Some test programs (wind tunnel, structures and subsystem testing) are shown to be important during the prototype development.

1. INTRODUCTION

The development of an aircraft from the first ideas to the production stage is a really complex process. Manpower, time and money are necessary to get the aircraft from the paper into the air. Roughly the total process can be divided into four essential phases, which are connected to each other. A final success depends on the quality of the individual steps. The four essential phases can be stated to be:

- preliminary concept studies
- project studies and definition
- development, design and manufacture of a prototype, flight tests
- preparation of the production stage, series tests and certification.

In this process the points of transition between the individual phases are of great importance. Here the design people must come to the decision about the technical and economical chances of the development and hence of the final product.

The development of helicopter concepts with respect to their practical use is large. In the development of these types of VTOL-aircraft one can clearly distinguish two trends: the quantitative trend concerned with size and lift capacity of the aircraft and the qualitation trend concerned with improvements of the tactical and economic features of the helicopter. Simultaneous with these trends a general wish for increase in flight comfort for pilots and passengers - such as reduction of noise and vibrations - can be observed in the modern helicopter development field.

The main impulses for a new development can either arise from market-studies of companies or institutes or can be produced by civilian or military announcements. They must give the basic informations about the application and the use of the aircraft (for example executive aircraft, wounded person rescue and transport or economical intercity-traffic), the region of use and operation (military, civil), the time of introduction and the scope of series demand.

In general, the peculiar requirements for the employment and the performance characteristics must be specified by the following criteria :

1.1 Mission Criteria

Design criteria for the general concept can only be developed on the basis of the knowledge of the main tasks of the helicopter. The definition of the missions itself can be done again, when the knowledge of technical possibilities is present. Hence, the development of the specific mission of a new helicopter system is an iteration process. Some characteristic input data are flight range, speed, useful load, start and landing-conditions and some special requirements, such as max. load factors, for example. One main result from these mission-studies is the gross weight of the aircraft.

1.2 Performance Criteria

Essential inputs to the helicopter design are provided by the classical performance characteristics. Of primary interest is the determination of the performance data of the helicopter, i.e. the limiting flight regimes. First, hover performance at all altitudes is to be considered. As rotor power requirements and engine power available are contrary values over flight altitude, the start- and hoverconditions are of great influence on the maximum grossweight, as shown in Figure 1.

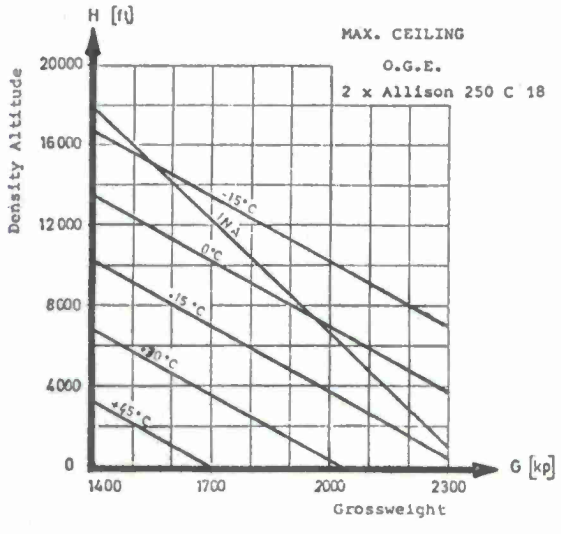


Figure 1 Maximum Take-Off Weights

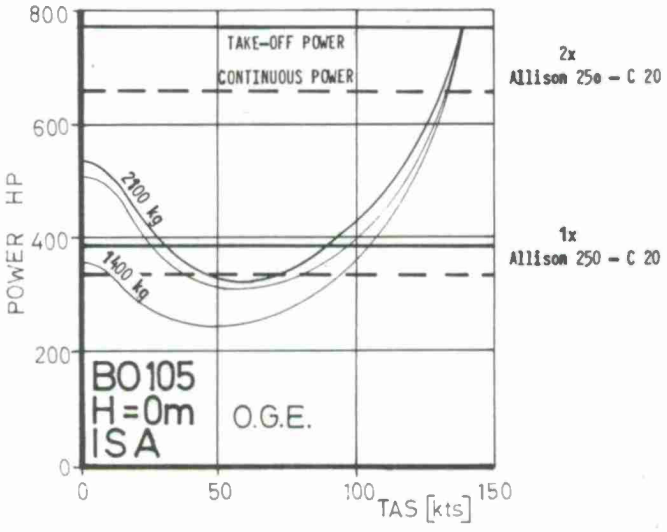


Figure 2 Helicopter Performance

Other important parameters are the minimum and maximum horizontal flight speed and the resulting maximum rates of climb at all altitudes. In Figure 2 power requirement is shown versus flight speed for an example helicopter. Here the minimum power of horizontal flight and the vertical rate of descent at this speed are two essential performance characteristics. In Figure 2 the power available with only one engine on is sufficient for a safe flight over a large speed even with climbing flight.

Reconversion from high speed flight without power and autorotational landing from any flight mode are two more performance criteria, as indicated by the hight-velocity diagram in Figure 3.

For modern helicopters the question of maximum rotor loading becomes more and more important. Improvements of the maneuverability with high load factors over the whole flight speed range are desirable especially for military aircrafts (Figure 4). Constant or even increasing load-factors over flight speed are opposed to the physical engagement of rotors, so that these requirements can normally not be fulfilled by conventional helicopter concepts. Additional wings and/or auxiliary thrust is necessary to meet them.

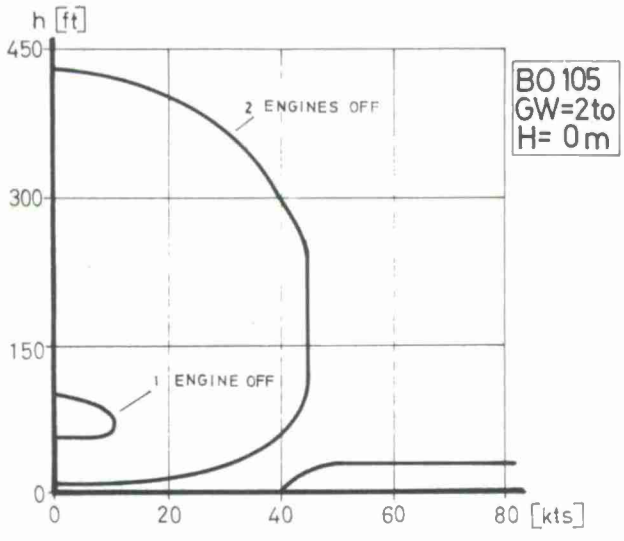


Figure 3 Height-Velocity Diagram

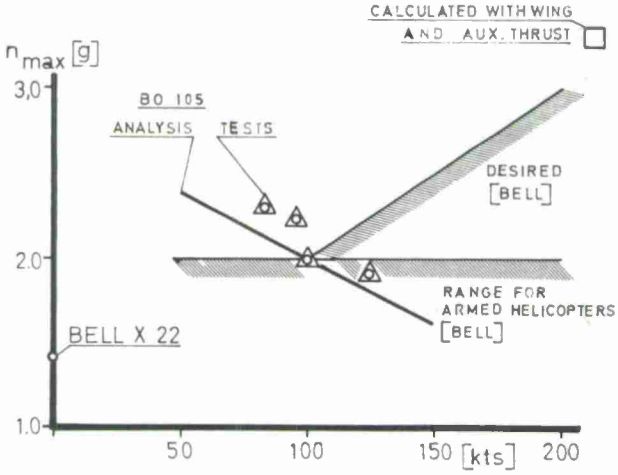


Figure 4 Maximum Load Factor-Velocity Envelope

1.3 Flying Qualities Criteria

From the beginning of helicopter developments the concepts and design principles were governed only by the basic aerodynamic requirements. Hover and forward flight performance was the main goal for all developments (2). The handling characteristics and the flying qualities of these helicopters were poor, which was nearly not noticed. With progress in the VTOL-technology the demand for improvements of handling qualities and stability characteristics increased rapidly. Today's modern helicopters are judged not only by the performance characteristics but also by handling and flying qualities.

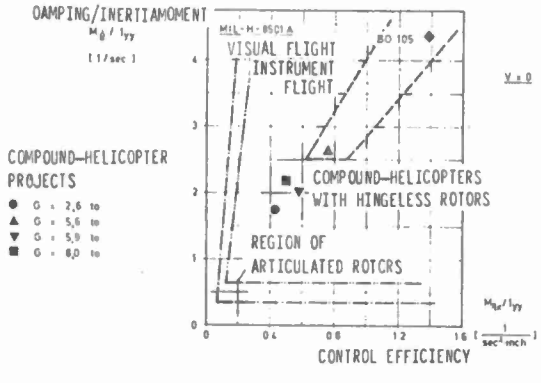


Figure 5 Control Characteristics (Pitching)

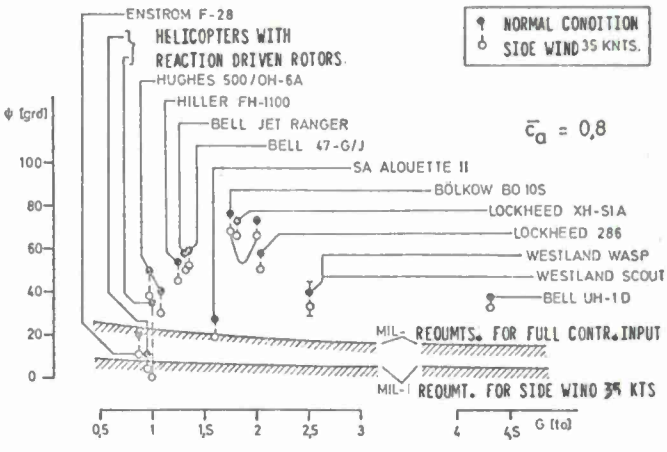


Figure 6 Control Characteristics (Yaw)

With this progress requirements and recommendations were developed to give a support in the development. The MIL-H-8501A General Requirements (3) were made 20 years ago with respect to the state of the technology of that time. Today they are too moderate in many aspects, as might be indicated by the pitch and yaw control characteristics in Figure 5 and 6. In addition, recommendations were made especially for armed helicopters by Edenborough and Wernicke (4). All these requirements and specifications are in further development, they are adapted to the special flight missions of the various types of V/STOL aircraft (5), (6), (7).

The requirements for inherent stability can normally not be fulfilled by helicopters over the whole flight regime. In this respect it seems to be more important to have high damping in all directions, which will provide satisfactory control behaviour and flying qualities (8), (9). Artificial stability augmentation systems (SAS) result in additional advances in this field.

1.4 Noise and Vibration Criteria

With the general environment problems all over the world the noise generation of helicopters and V/STOL-aircrafts is considered critically too. Users of present-day helicopters are beginning to demand an acoustical environment which is comparable to that found in other airplanes. Hence, acceptable noise levels inside and outside are now essential requirements in V/STOL-aircraft design.

Criteria for inside noise limits are based in part on empirical standards, with consideration of general comfort, speech, communication and psychological factors. One method commonly used is based on an average speech interference level (SIL), as is shown in Figure 7 (10). External noise level limits are defined for example by the 95 PNdB FAA guideline level for V/STOL-aircrafts.

SIL (db)	Required Voice Levels
65	Raised voice at 1.5-3 feet; loud voice at 3-6 feet.
70	Raised voice at 1-2 feet; loud voice at 1.5-3 feet.
75	Raised voice at 0.5-1 feet; loud voice at 1-2 feet.
80	Raised voice at less than 0.5 feet; loud voice at 0.5-1 feet, very loud voice at 1-2 feet.
85	Loud voice at less than 0.5 feet; very loud voice at 0.5-1 feet.

Figure 7 Speech interference level (SIL) and required voice levels for reliable conversation

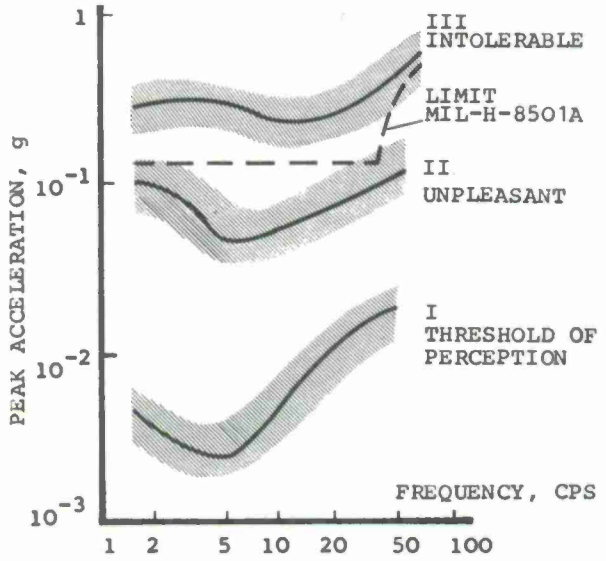


Figure 8 Subjective perception of vibrations

Besides of noise problems the vibration level of helicopters is of great importance. Both are produced by the same aerodynamic forces. They lead to negative effects on structures and to a reduction of passengers' comfort. Figure 8 shows the result of investigations of the subjective effects of vibrations in terms of frequency and amplitude. Vibration limits for steady state and transient motions are defined, for example, in military specifications (2). It seems to be no secret, that these minimal requirements are not accomplished by many helicopters in all flight conditions. In general, the vibration problem on helicopters is so complex that higher harmonic blade bending must be considered already in the early design phase.

2. AERODYNAMIC ROTOR DESIGN

Before aerodynamic rotor design work can be started, the general configuration of the aircraft must be known. This includes the basic configuration features, such as number and location of rotors, type of rotor systems, drive and propulsion systems and unloading devices. Considering the desired total lift capacity of the rotor, usual values of power/weight ratios and load ratios, the flying gross weight and the average amount of installed power may be determined. With all these basic questions answered, the helicopter design engineer is supplied with the most important design parameters. The main problem is now to tailor the rotor to the specific mission requirements.

During the initial phase of aerodynamic rotor design, there are a few parameters which basically are connected with the physical properties of the lifting system itself. The principal characteristic of a rotor is to produce thrust independent from the magnitude of its flying speed. When considering this phenomenon in the view of the most simple performance analysis of the hovering rotor, the thrust is produced by the momentum change of the air mass passing through an actuator disc. That means that one determining factor in the hovering thrust capability is given by the magnitude of the rotor disc. The airflow through the rotor disc is basically produced by the totality of blade elements rotating with a certain speed and at certain angles of attack. Hence, two other major factors in the rotor thrust production are the rotational speed and the total blade area.

One can derive from this simplified relationships that the aerodynamic rotor layout must start from the three essential parameters of

- rotor disc loading
- rotor tip speed
- blade area (solidity).

A full treatment of these parameters would require a total lecture series alone. Since the intent of this section can only be to show the basic aerodynamic inputs into rotor layout, only a broad characterization of the influencies and parametric trends in design will be given.

2.1 Rotor Disc Loading

The first question in rotor layout is: How does one select disc loading? The basic reason for the dominance of low-disc-loading VTOL-aircraft is their superior vertical lifting efficiency. Generally this capability can be defined by the expression of

$$M = \frac{\text{minimum possible power required in hover}}{\text{actual power required in hover}} ,$$

which is called the figure of merit. This characteristic value can be expressed by terms of rotor thrust T, power P and the rotor radius R:

$$M = 0.707 \cdot \frac{T}{P} \sqrt{\frac{T}{\rho R^2 \pi}} .$$

From this expression a direct relation can be seen between rotor efficiency and disc loading: Rotor figure of merit is proportional to the square root from disc loading. Derivations of rotor performance expressions can be found in references (35) for instance.

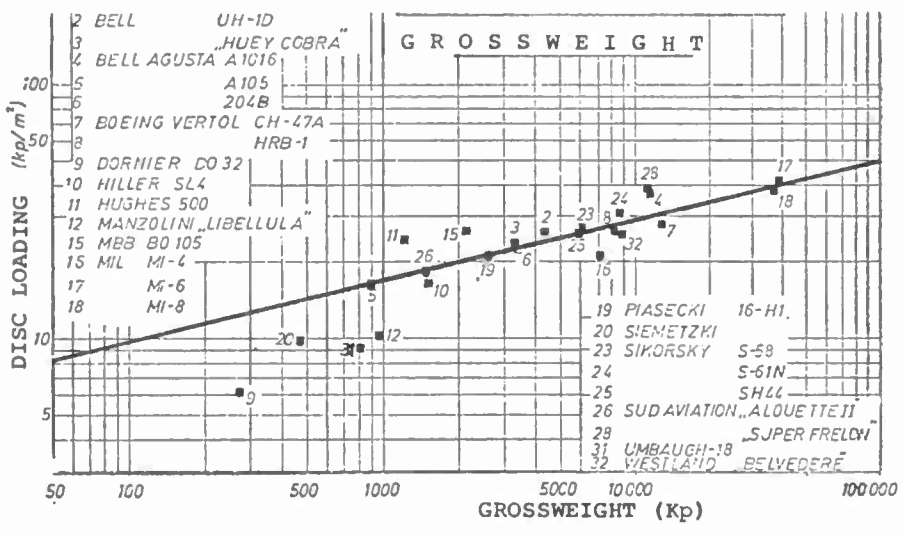


Figure 9 Rotor disc loadings of different helicopters

Statistics show that the general trend in rotor design is toward higher disc loadings, the values doubled in the period of the past twenty years. The optimum range of disc loading of a certain helicopter depends on many influencing factors. Commercial users interests will normally differ from military users interests and light utility helicopters will show other requirements than heavy-lift-transport helicopters. The statistics show a general increase of disc loading with higher design gross weights (Figure 9). Disc loadings vary from 10 to 50 kp/m^2 when considering light and superheavy helicopters. Disc loading influences not only the power requirements and, hence, fuel consumption but is a parameter, which affects the rotor downwash and all corresponding effects. This includes autorotation characteristics, the effects on the surrounding downwash environment and noise, for instance.

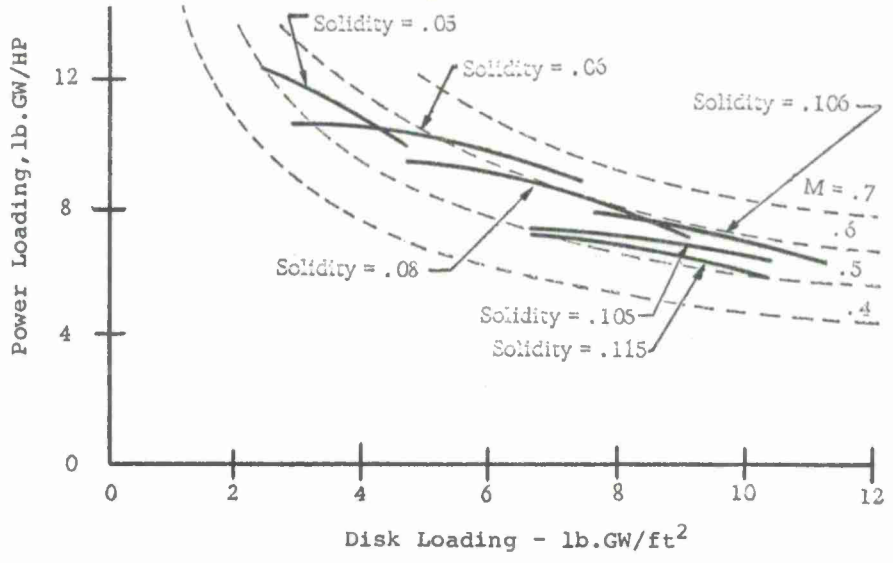


Figure 10 Power loading versus disc loading

The influence of rotor disc loading on the power requirement per unit thrust have been shown by many investigations, so that this basic relationship shouldn't be discussed here in more detail. The general power loading diagram of Figure 10 , drawn from (34), may indicate the general trend of decreasing figure of merit with increase of disc loading. When considering other effects of disc loading, the autorotation characteristics can be stated to be an important factor for determining the design. The behaviour following total power failure are largely affected by the aerodynamic configuration and by the size of the rotor. A direct relation can be observed between disc loading, the solidity and the mass moment of inertia of the rotor about the axis of rotation. The rate of descent without power is proportional to the square root of disc loading and, moreover, great rotor disc result in long blades and this in a high rotor moment of inertia. High kinetic energy is present in this case, so that there is only a moderate decrease in rotational speed. Further advantages are lower sink rates and advantages during the landing flare. The design principle from that would be to select a rotor span as great as possible. One limiting factor in doing this is,of course, the weight of the rotor system, which increases approximately proportionally with the cube of its span. Another aspect is given by high flight speed efficiency. Although rotor disc loading becomes less important for forward flight performance, it is an important parameter in rotor drag. The increase of rotor drag with flight speed is nearly proportional to the rotor disc area and comes up to a significant factor especially on high speed helicopters with low fuselage drag. Hence, typical high speed rotor designs will select smaller rotors and thus higher values of disc loading. More details about disc loading selection with special consideration of load and power/weight ratios are given in (11).

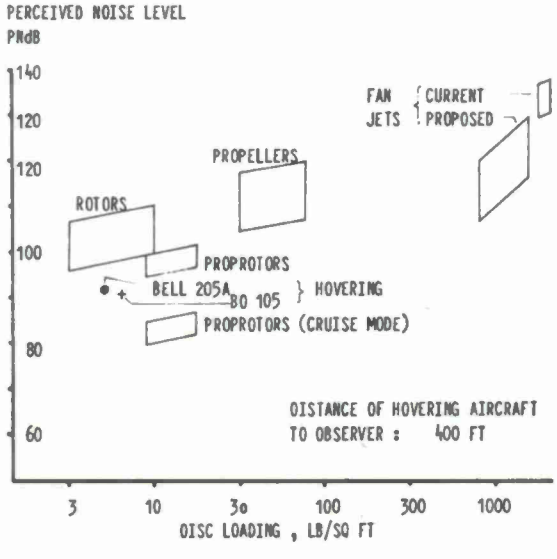


Figure 11 VTOL aircraft subjective noise characteristics

Another - environmental - characteristic of V/STOL aircrafts, which is influenced by disc loading is rotor noise. Figure 11 , which has been extracted from (36), summarizes estimated perceived noise levels from various 80,000 lb-aircrafts in hover as a function of disc loading. A helicopter is considerably less noisy than propeller and - of course - jet-lift VTOL-types. Low disc-loading proprotor aircraft will be still more quiet , especially due to a large reduction in blade tip speed in the cruise mode.

2.2 Rotor Tip Speed

The second main parameter in rotor layout is the rotor tip speed. There are different aspects influencing the choice of this parameter, such as

- rotor efficiency
- compressibility effects
- stall and reverse flow effects
- aeroelastic instabilities
- gearbox and transmission weight
- noise.

It seems to be clear, that there are quite a lot of condradictory influences involved and the difficulty for the design engineer is to individual effects. It is impossible for him to find a tip speed that would meet all the requirements,and the question is, how the tip speed should be selected to obtain the optimum design.

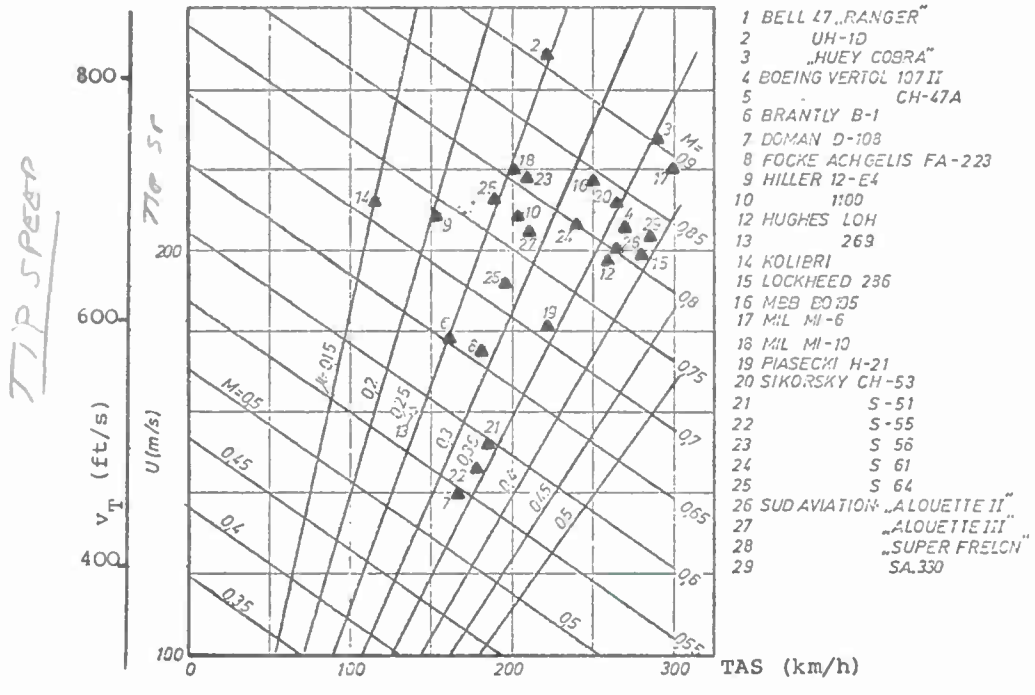


Figure 12 Rotor tip speed versus flight speed

A first selection can be done by considering the well known plot of tip speed versus flight speed as shown in Figure 12 . For example, considering a maximum design speed of 250 km/h and a maximum Mach-number of .85 on the advancing blade will result in a tip speed of 220 m/s (720 ft/s). This would be a tip Mach number of about Ma = 0.65 in hover and an advance ratio of $\mu = 0.3$ at maximum design speed. In general, the performance optimization of the rotor tip speed depends largely on the mission requirements and will give different results for a heavy-lift helicopter with long hovering phases or a high speed armed helicopter, for example. The one will primarily need best hover performance, which can be obtained by lowering the tip Mach-number and thus the rotor power. The other will be focussed on minimum drag and favourable aeroelastic stability qualities and will thus have a higher disc loading with somewhat increased tip speed.

There are different aerodynamic problems arising from the nonsymmetric distribution of velocity and dynamic pressure over rotor disc area (Figure 13). The advancing blade tip is exposed to transonic flow and is operating beyond the drag divergence boundaries. As the high values of drag coefficients are weighted by the excessive dynamic pressure (Ma > 0.9), the advancing blade tip contributes to an excessive rotor power increase at high speeds. Other problems connected with compressible flow are the alternations of chordwise pressure distributions: By exceeding the critical Mach-number the transonic field is extended to the trailing edge with increasing compressibility effects. It is quite clear that a change of pressure distribution will influence the airfoil lift, drag and moment characteristics. Moreover, the subsonic-transonic change are nonsteady (12), (13). The aerodynamic effects resulting from these types of flow patterns can be an excessive increase of blade control loads and compressible flutter effects, in general.

The physical reasons for all these effects were largely unknown over a long time and, therefore, for many years the rule has been to keep away from compressible effects on the advancing blade. An advancing tip Mach-number of .8 was considered to be the limit

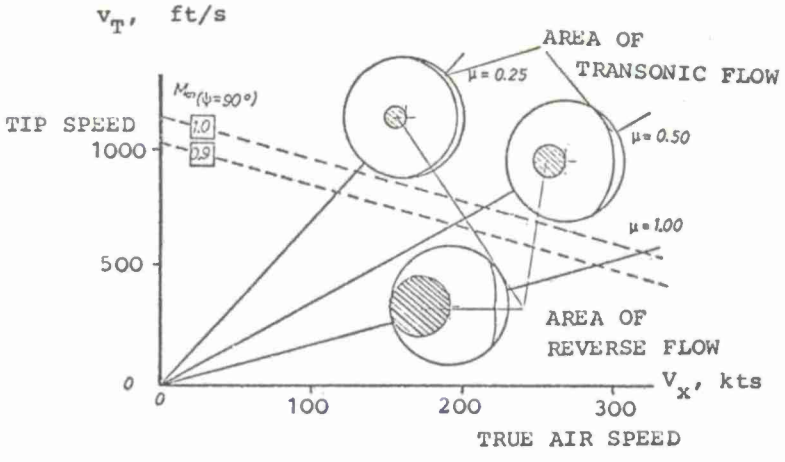


Figure 13 Flow conditions on rotors with different advance ratios and tip Mach-numbers

of helicopter operation. Later investigations and experience have modified this rule and at present rotors are operated at tip Mach-numbers beyond .95. The ability to operate with supercritical areas on the rotor disc will brinq benefits, if the adverse compressibility effects can be controlled. Therefore, the advancing blade problems must be considered in dependency of airfoil development, and progress in this field will give more freedom in tip speed layout. This will be discussed in section 3. in more detail. Another limitation of rotor operating conditions is indicated in Figure 13 by reverse flow and retreating blade stall. In this region the blade is exposed to low dynamic pressure and high angles of attack. In these conditions much of the blade is beyond airfoil stall boundaries. As this condition occurs only over a small azimuth range, the effect on total rotor lift is not very large. However, the more adverse effects are the typical stall phenomena, which can lead to the typical stall flutter problems ((14) to (18)). Under these conditions the blade is exposed to large control loads, power increase and high levels of vibration. Figure 14 from reference (34) shows one more summary diagram of the rotor limits in high forward speed flights. In the plot of advance ratio versus flight speed various limitations for rotor operation are shown. It can be seen that the practical selection of rotor tip speed is limited in both directions by Much number limits, flutter limits and blade instability and resonance limits.

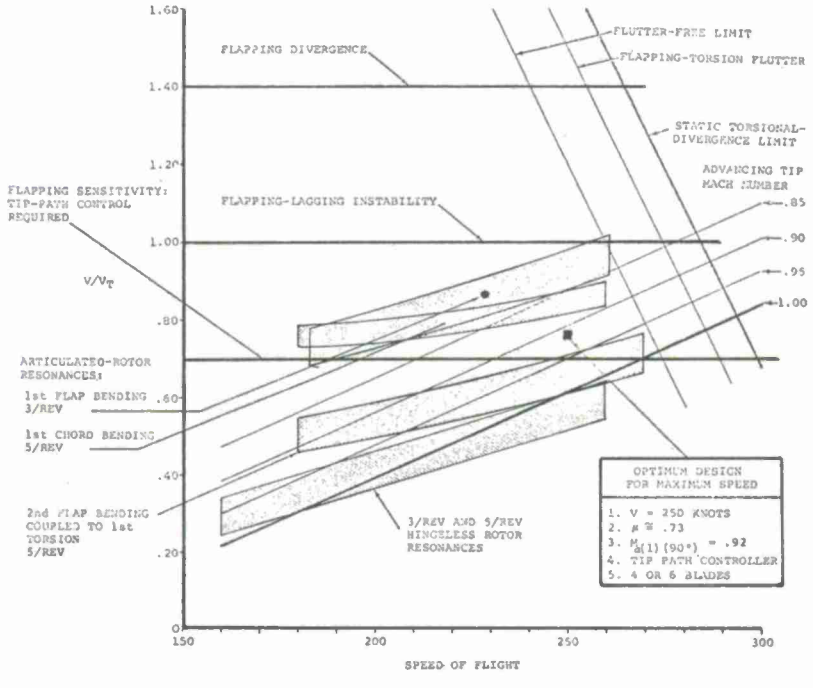


Figure 14 Unloaded rotor operating limits

It must be noted, that all high speed problems on a helicopter rotor cannot be considered independently from each other. Means for improving the speed and maneuver limitations can always only be a compromise with favourable effects on the one side but with unfavourable effects on an other side. This is, in general, due to the physical addition of rotating and translation speeds on the rotor. In the optimization process with respect to tip speed selection, there are two contradictory effects: The one, reducing the rotor tip speed would reduce the compressibility problems of the advancing blade but but will worsen the stall problems on the retreating side. On the contrary, an increase of rotor speed will normalize the retreating blade flow but will cause the advancing blade tip to operate in the transonic region. As it looks at the present time, the latter seems to be the more promising design solution, as the compressibility problems can pro-

bably be handled easier than the dynamic nonsteady stall problems. Blade leading edge treatment and blade thickness reduction are two helpfull means of doing this. With special tip sections an advancing tip Mach-number of .95 can be used as a design value, where no compressibility effects are encountered. Even supersonic blade tip operation ($M_{1,0,90}$ = 1.1) seems possible with large efforts in aerodynamic design work.

In this respect another factor becomes quite important, the noise-environment of the rotor. In the past few years noise considerations have become more and more prominent also in helicopter design. In the literature ((19), (20), (21), for example)) three aerodynamic sources of rotor noise are distinguished: The rotational noise, the vortex noise and the so-called blade slap. Theoretical investigations and measurements show that all these aerodynamic noise spectra depend on the rotor tip speed. The blade slap phenomenon seems to be produced by fluctuating aerodynamic forces and by local transsonic flow. It can be observed nearly in all flight conditions, especially at high forward flight speeds and during high rotor load maneuvers. Investigations at Boeing-Vertol have shown that blade slap noise is produced at high speeds, when the advancing blade tip is beyond a certain critical Mach-number. Figure 15 shows that the blade slap noise is nearly proportional to the difference of tip Mach-number and critical Mach-number of the profile (22). Influences of tip modifications are shown in this diagram, too.

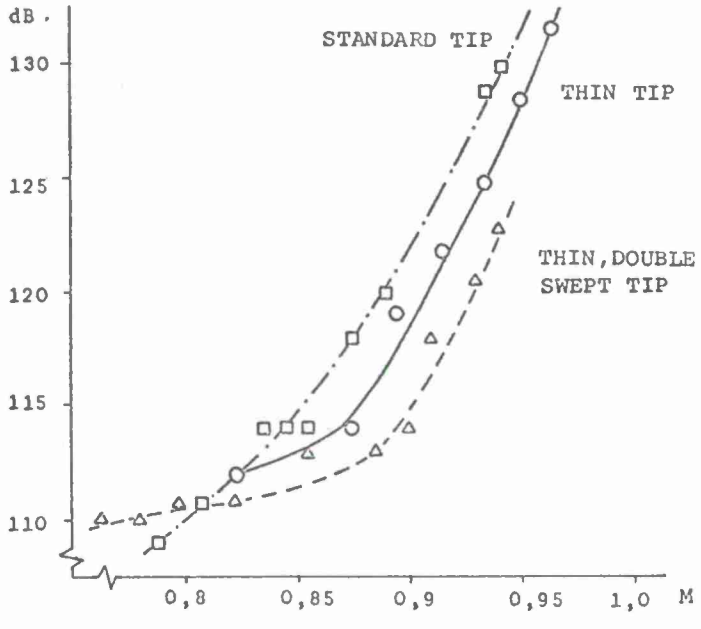


Figure 15 Effect of advancing tip Mach-number, blade thickness and tip sweep angle on noise pressure level

The sources of vortex noise seems to be fluctuating aerodynamic forces (turbulence effects) and periodical forces due to vortex separation. As it is indicated by measurements and by theoretical investigations ((20),(23)), the acoustical intensity of vortex noise is proportional to the 6th power of tip speed, so that a tip speed reduction is the most powerful means for reducing rotor noise. Other noise reductions can be obtained by a proper selection of the blade geometry (taper, twist and chord) as well as by the number of blades. Those effects will be discussed later.

It can be seen from all these diagrams that there are many contradictory considerations that the designer must weigh, when he has to decide about the magnitude of rotor tip speed. Words like compressibility effects, critical Mach-number and stall behaviour indicate, that the selection of this parameter is essentially connected with the profile design. Much progress in rotor-airfoil-development (increase of maximum lift coefficients and of drag divergence boundaries, for example) is necessary to enlarge the possible design field in this respect.

2.3 Number of Blades and Solidity

The third main parameter to define a rotor aerodynamically is the total blade area, i.e. the product of the single blade area and the number of blades. The effective blade loading is determined by the ratio of total blade area and the rotor disc area, which is called the solidity factor σ. This is indicated by the relationship

$$\bar{c}_L = 3.2 \cdot k_n/\sigma \quad ,$$

where $\bar{c}_L$ is the average lift coefficient and k_n the thrust coefficient in hovering flight. The choise of blade loading is a new optimization process, where different flight conditions must be considered. First aim will normally be an optimum of rotor efficieny. In this the effect of solidity is coupled primarily to the profile losses. Under this consideration a rotor should operate at the mean lift coefficient close to the stalling condition of the blades. Figure 16 gives a plot of rotor efficiency versus mean blade loading and one can see that maximum values are obtained almost in the range of $\bar{c}_L \approx 0.7$ with nearly no further increase at higher blade loadings. Average lift coefficients are normally tailored to the range $\bar{c}_L \approx 0.4 \div 0.6$, the lower values being used on high speed/high maneuverability helicopters, as they provide high thrust capability at high forward speeds. Excellent "g"-capability is necessary to accomodate the maneuvering requirements of mo-

dern helicopters. However, increase of blade area results in an increase of the rotor's drag/weight ratio. Basic theory for hover shows that performace should normally be improved with more blades, but experience has low speed and high solidity, but there are certain lower limitations on rotor speed, for example, kinetic energy considerations for the autorotation characteristics. Moreover, this philosophy is contradictory to the high forward speed requirements.

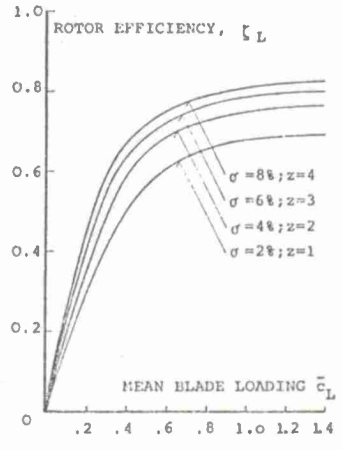


Figure 16 Rotor efficiency versus mean blade loading

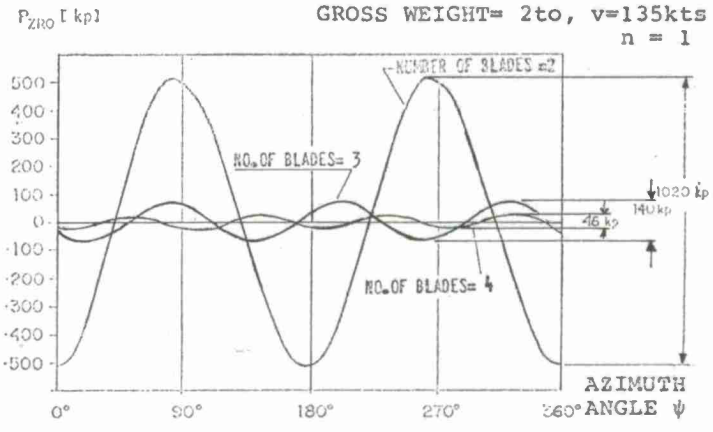


Figure 17 Oscillating vertical forces on rotors with two, three and four blades

The question of the number of blades must also be seen under the aspect of vibratory loads. The oscillating aerodynamic forces of the individual blades are superimposed in the rotor hub section. With increase of blade number more rotor harmonic loads are subpressed and therefore the vibratory loads on the fuselage are considerably reduced. In Figure 17 the oscillating vertical forces during a 140 knots horizontal flight are shown for rotors with different numbers of blades. The z-forces vary between 1000 kp and 50 kp, depending on the number of blades. In addition the basic blade passage frequency is much lower on the two-bladed rotor, which is another unfavourable effect on the aircraft vibrations. A second reason for the substantial vibratory improvements with a higher number of blades is that the blade passage frequencies normally get outside of the body resonance frequency regions, so that the exciting forces cannot come through into the airframe. For example, on the NH-3A research helicopter from Sikorsky , a vibration reduction of 50 percent was encountered in the cockpit when the five bladed rotor was replaced by a sixbladed rotor.

3. AERODYNAMIC BLADE DESIGN

In the past, the prime rule in aerodynamic rotor blade design was to use relatively conservative profiles and to keep away from the limitations due to Mach number and stall effects, for instance. Hence, most of the helicopters in use are fitted with symmetric profiles of the NACA OO-series. The 0012 profile for example has already been chosen in the early beginnings of the development of helicopters. The maximum lift capacity of this profile is relatively low and the lift curve slope is increasing with higher Mach-numbers. Although the aerodynamic problems are far more complex than on fixed wing aircraft, relatively simple profiles are used up to now.

However, with increase of the helicopter operation range the need for improved airfoil profile characteristics became apparent and in the past years much progress was made in special helicopter airfoil design. For example, some of them were developed by the Boeing-Vertol-Company on the basis of NACA 5-digit series. These airfoil sections provide the designer with some 15 to 20% more usable lift coefficient than available with the symmetric 0012 blade. In addition, special blade tip airfoils were developed by transonic tunnel tests, allowing the penetration of the sonic region on the advancing blade side. The favourable results can be a reduced blade area, significant weight reductions due to higher tip speeds and improvements of rotor efficiency in general. The importance of airfoil characteristics and the resultant design criteria are indicated very vividly in reference (25), for instance.

3.1 Aerodynamic Requirements

A main precondition for new profile design work is of course,a founded knowledge of the requirements the airfoil should meet. As it has become distinct yet before, the extreme profile requirements are basically fixed by the aerodynamic environment in high speed flight and in maneuver conditions. In these conditions the rotor limits become apparent. Figure 18 shows typical aerodynamic environment conditions for the total blade of a helicopter flying at 136 knots. The curves describe the operating conditions at different spanwise positions. It is important to note that the blade is exposed to high lift co-

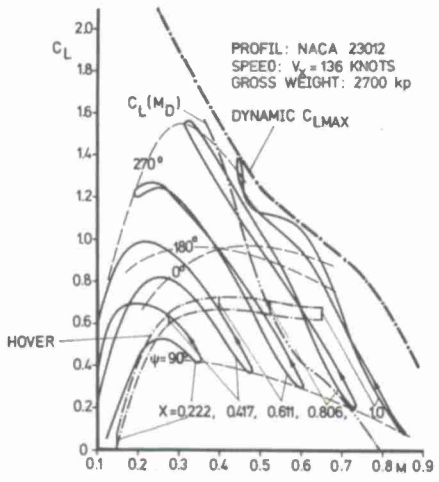


Figure 18 Rotor blade airfoil working environment in forward flight

efficients at medium subsonic Mach-numbers and to low C_L-values at high subsonic Mach-numbers. These are the two critical design quantities for rotor sections in the helicopter use. With increase of flight speed these two operating regions become still more extreme.

The two limiting lines describe the maximum dynamic lift capacity and the region, where the drag divergence Mach-number is exceeded. This is one example for a rotor operating region, other flight conditions are showing quite different characteristics. Since critical rotor load conditions almost always are found in extreme operating regions, a way must be found for weighing the different and contradictory flow characteristics. To date, both the maximum lift and the compressibility problem seems to be of paramount importance. However, some progress in other rotor design fields could shift the priorities.

3.2 Need for High Lift Capability and Favourable Moment Characteristics

The rapid variations of aerodynamic flow over rotor disc culminates in excessive angles of attack on the retreating blade. The onset of stall with increase of speed and rotor thrust is a limiting factor for rotor operation. Therefore, in airfoil design a great deal of attention must be directed towards maximum lift capability.

As it is well known, a substantial gain in lift coefficients can be achieved by the introduction of cambered airfoils. However, cambered airfoils normally show large pitching moment coefficients, which would cause a rapid growth of pitch link loads at increasing flight speeds. Therefore, only slight camber or a pure leading edge camber can be applied on helicopter profiles. The droop-snoot airfoil 23010-1.58 developed by the Boeing-Vertol Company was already mentioned (25). The main effect of introducing leading-edge camber is that the maximum lift coefficients are increased in the medium Mach-number region, without adversely affecting the other characteristics.

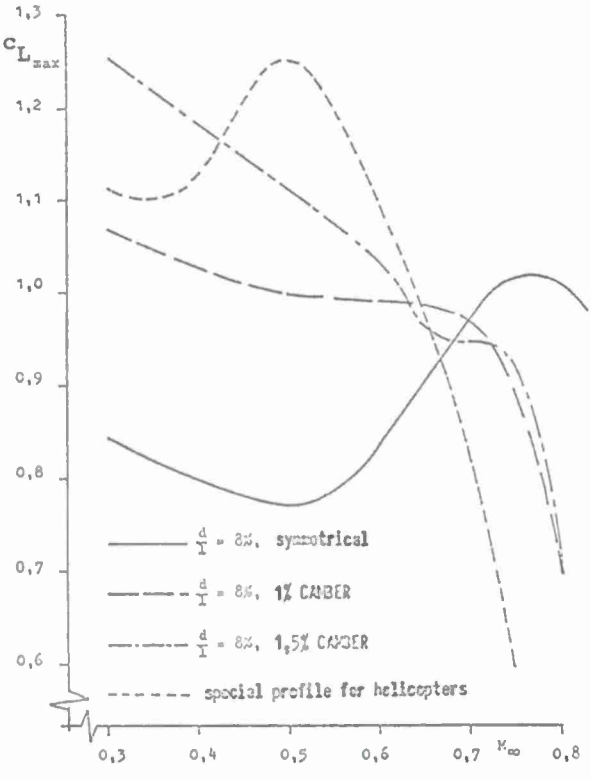


Figure 19 Effect of Mach-number and airfoil-camber on maximum lift coefficients

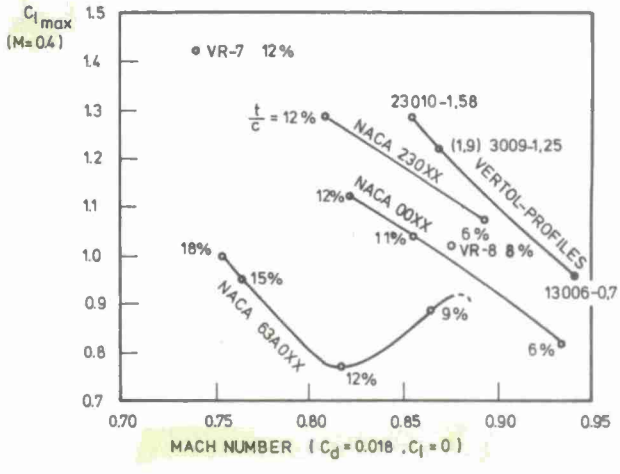


Figure 20 Summary of stall and drag rise characteristics for several airfoil families

The effect of leading-edge camber is shown in Figure 19 for airfoils of 8% thickness (24). The maximum lift coefficient is increased just in the right region and decreases at higher Mach numbers. The special helicopter airfoil shown in this picture has an almost optimum shape of the lift curve, but has unfavourable compressibility characteristics that indicate no promise for high speed application. It may be derived from this example, that it is necessary to modify the profile shapes and to combine the advantages of certain airfoils. Figure 20 shows a summary of different airfoil families on the basis of maximum lift and drag divergence characteristics. The profile family with best stall characteristics are the droop snoot profils, which were developed by the Boeing-Vertol Company by changing the leading edge radius (25). Whereas the NACA six series airfoils show poor characteristics and will not promise improvements in helicopter operation.

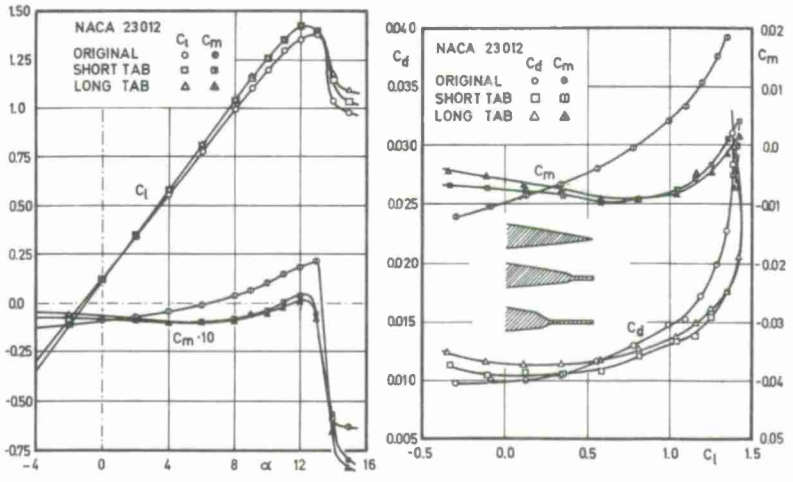


Figure 21 Effect of trailing-edge modifications on the characteristics of a NACA 23012 profile at M = 0.4

Other modifications can be applied at the profile's trailing edge. The changes of the characteristics of a NACA 23012 profile caused by modifications of tabs at the trailing edge are shown in Figure 21 , which is extracted from reference (37). In comparison to the lift characteristics which nearly are not influenced by trailing edge modifications, essential changes can be observed in the pitching moment characteristics: The positive c_m/c_L-slope of the original profile is turned into slight negative slope, i.e. that the aerodynamic center is shifted rearward. Considering the normal torsional flexibility of rotor blades, a positive (rearward) shift of the a.c. is stabilizing, because the effective pitch angle of the blade is reduced, when lift is increased. If there is sufficient torsional flexibility, the elastic deformations act as substantial control inputs. Theoretical studies of aeroelastic phenomena have indicated (27), (28) that a substantial gain in rotor performance and flying qualities can be achieved by the aerodynamic characteristics in combination with aeroelastic effects of torsionally flexible blades. The most important characteristics proved to be

- the section maximum lift coefficient
- the section lift curve slope
- the a.c.-position of profile section.

One effect resulting from increased stall limits is indicated in Figure 22 . It is a peculiar effect of rotor trim that the maneuver stick position per g characteristic may become unstable at high load factors. The reason is that the lift of the retreating blade is limited by the onset of stall. Typically, with symmetric profile section with poor stall characteristics the stick reversal over g is reached within a maneuver range as low as 1.5 g and the maximum trimmable load factor is limited to about 1.9 g. By use of non-symmetric airfoil section this stick instability is postponed and steady load factors up to 2.4 g are obtained. According to the more favourable stall characteristics of this airfoil, pitch link loads are reduced at all flight speeds and moreso in maneuver flights (27).

Research work in the past few years has shown that the aerodynamics of the profile are influencing the stability characteristics and handling qualities as well. Figure 23 shows the inherent dynamic stability of the BO 105 helicopter with a hingeless rotor for the longitudinal motion (27). The time to double amplitude and the period are shown over flight speed. It is indicated by calculation and by flight tests that significant improvements in dynamic flight behaviour can be obtained with proper blade design. In this way the speed of equivalent stability is increased considerably. The improvements shown here emanate mainly from a slight reduction of the lift curve slope and a 1% rearward aerodynamic center. The blade modifications included small changes in the dynamic characteristics too, which will be explained later.

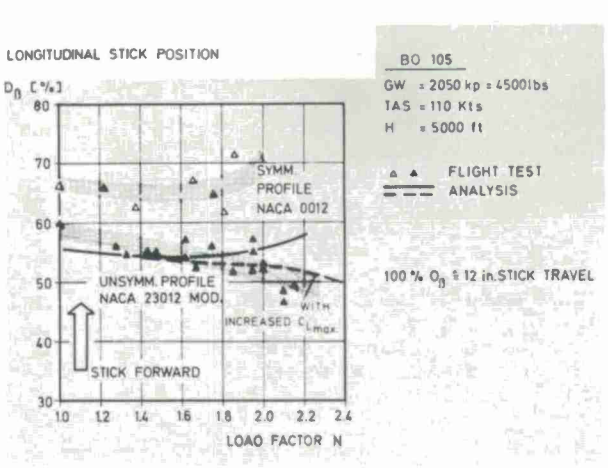


Figure 22 Longitudinal control stick position in maneuver flight

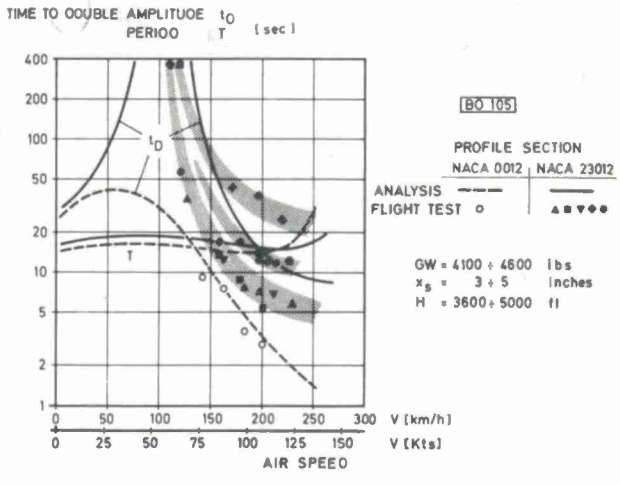


Figure 23 Dynamic stability in forward flight with blades of different airfoil sections

Other effects of aerodynamic blade modifications can be observed in the control characteristics of the rotor (27). This is indicated in the control-damping diagram of the pitching motion in Figure 24 . There is an essential change in the correlation between control efficiency and rotor damping, when the a.c. of the profile is displaced from the 25% position. In general, the control power recommendations for armed helicopters (4) in this diagram can be well obtained by a hingeless rotor system, which is considered in this case. It seems to be an essential effect that this range can be enlarged by aeroelastic effects. In this respect the increase of damping is the more important effect, whereas the slight decrease of control power is nearly insignificant at a hingeless system and can be compensated by adapting the control ratio.

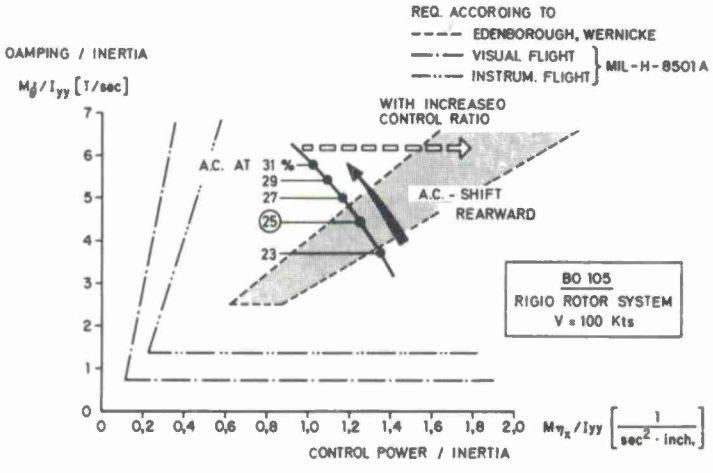


Figure 24 Effect of blade a.c.-offset on control-characteristics (pitching)

It seems to be of utmost importance, that by airfoil design improvements gains cannot be obtained only in the rotor performace field, but also in the field of handling qualities and general flight characteristics. It is shown in reference (27), that substantial improvements can be made, promising quite a new era of helicopter design. However, aerodynamic and aeroelastic research work must be coordinated and considerable effort is necessary to govern the more complex design problems.

3.3 Compressibility Characteristics

It was shown in Chapt.2.2that the choice of rotor tip speed becomes quite severe a problem, when an increase of flight speed is considered. The different aerodynamic problems arising from the nonsymmetric flow distribution over the rotor disc culminate in the two opposite regions of the retreating and the advancing blade. Both conditions are quite different from the aerodynamic standpoint, but they are strongly connected by the laws of rotor operation. The retreating side problems have been treated in the foregoing section and some requirements have been shown for the aerodynamic airfoil design. There is no doubt from the aerodynamic standpoint that gains in rotor operating cabability can be expected from stall behaviour improvements.

However, postponing only the stall problems cannot substantially enlarge the general limiting factors on speed and lifting capacity. For this the compressibility problems occuring on the advancing rotor blade are of paramount importance. Therefore, an optimization of rotor design must be focussed to this side, as well. What means are present today to reduce the unfavourable effects of transonic flow and to provide the designer with more freedom in the advancing tip problems?

3.3.1 Influence of Relative Profile Thickness

As it is well known, the compressibility effects of profiles depend on the ratio of slenderness. The critical Mach-number is increased with slender profiles and with a reduction of lift (29). This drag divergence due to compressibility is postponed just in the region of the advancing blade tips. As was noted in section 2.2, one of the require-

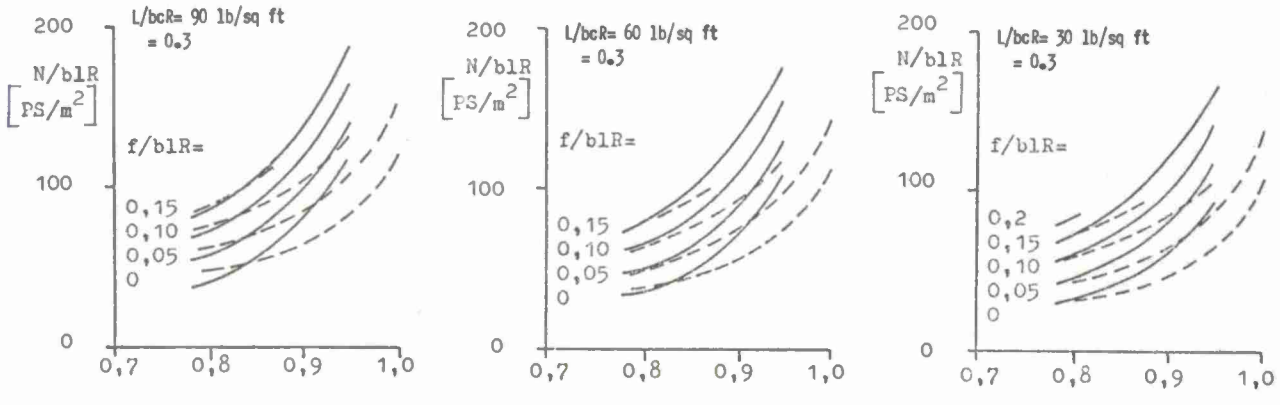


Figure 25 Performance comparison of standard and thin-tip rotors

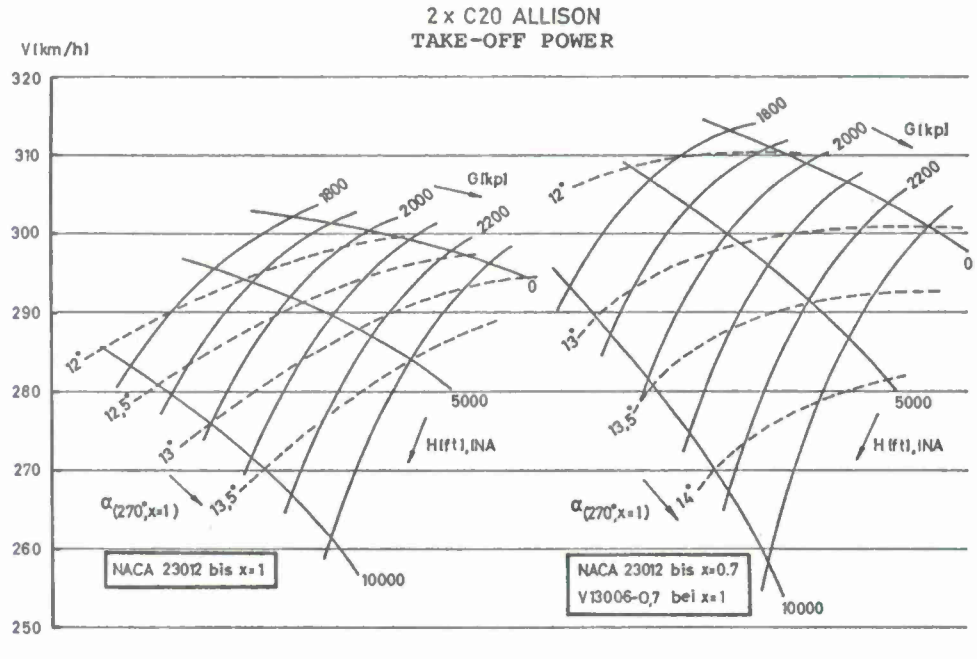


Figure 26 Effect of thinned blade tips on forward flight performance

ments for an airfoil suitable for utilization on helicopter rotors is that the drag at high Mach-numbers and low lift coefficients must be as low as possible. The favourable effects of thinned blade tips on the critical Mach-number are well known for a long time, and are used in rotor airfoil design (24), (25). Some results of wind tunnel tests, Bell conducted on a UH-1D rotor with tip Mach-numbers over 1.0, are shown in Figure 25 (24). It should be noted, that the normal blades' rotor power is increased by about 100%, when the tip Mach-number is raised from 0.85 to 0.95, which compares to a speed increase of only 15 knots in forward flight. With thinned blade tips the unfavourable compressibility effects are strongly reduced. A further benefit of the thin tip blades was, that even at hover a small power reduction occured. Figure 26 shows the increments of maximum horizontal flight speed of the BO 105 by using modified blades with thinned tips. An increase of about 6 knots is obtained.

Other effects of compressible flow can be observed in the chordwise pressure distribution, which may result in a substantial change of lift, drag and pitching moment characteristics. Pitch-link loads normally show a μ^2 relationship increase with speed due to dynamic pressure. Pitching moment change due to compressibility will suddenly produce high moment coefficients and will worsen the torsional dynamic behaviour of the blade. Under these circumstances blade control loads increase and the blade can be involved in compressible flutter problems (14). Thin-tip blades can markedly reduce these effects, as the formation of shock waves on the advancing tip is delayed.

Although the advantages of thinned profiles in postponing the compressibility effects are obvious, their application is not without problems. Thinned profiles must have sharper leading edges which cause adverse stall characteristics on the retreating side. Therefore, simple thickness reduction on the blade tips will improve the compressibility behaviour, but will worsen the "g" maneuverability of the rotor. From this it becomes obvious that airfoil design must have a look on both critical quantities, and the optimum profile must combine leading edge treatment and thickness reduction (34).

3.3.2 Blade Tip Geometry

In the fixed wing aerodynamics much attention is paid to the tip shapes since a long time. The effects of threedimensional flow, shock build-up and tip vortex are largely explored (32) and proper solutions are well known today. In contrast to that, most of todays helicopter rotors are fitted with normal rectangular blades, although their blade tips are operating partly in the sonic region. This conservativity partly comes from tradition and partly from production considerations: Nonuniform blade geometry is a compli-

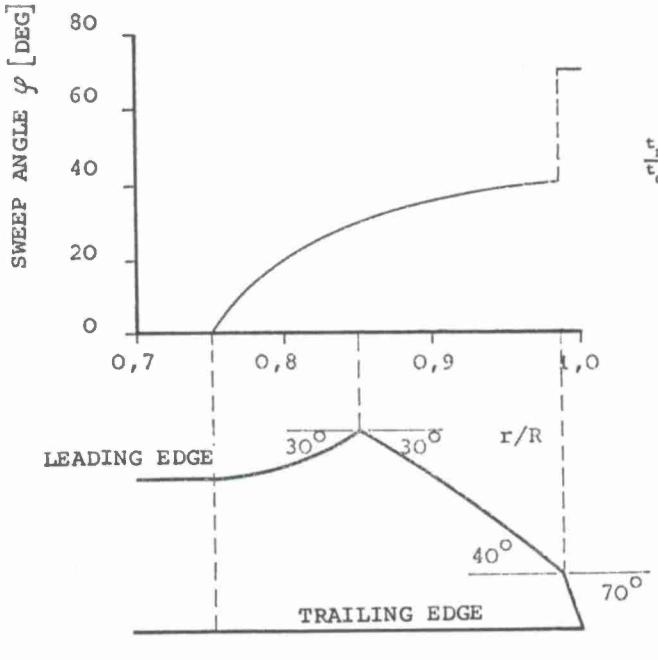


Figure 27 Spanwise optimum sweep angle distribution and resultant blade tip shape on a typical rotor

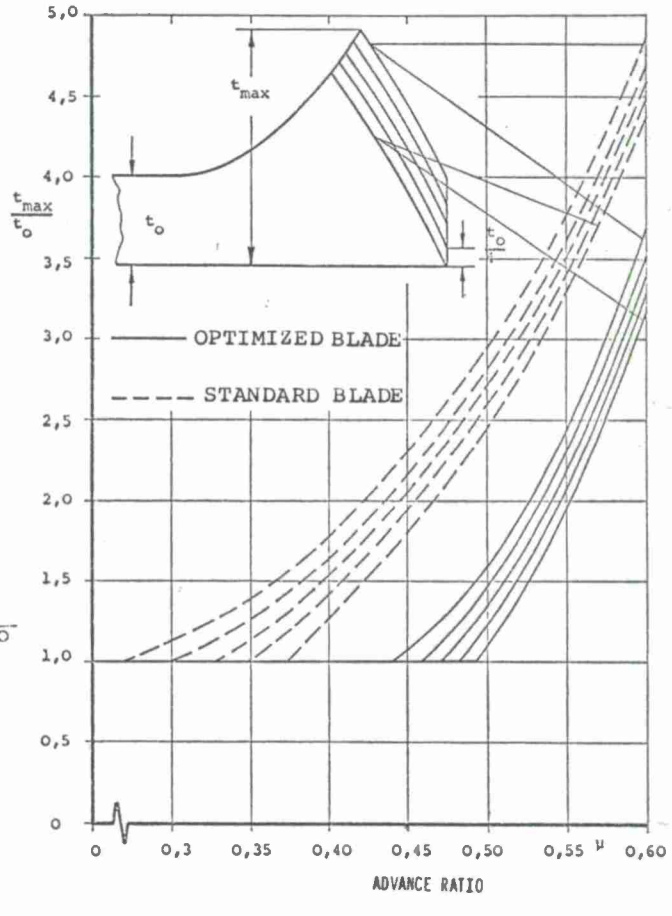


Figure 28 Maximum blade chord of swept tips as a function of design advance ratio

cating factor. In this respect the fiberglass offers new possibilities, as the blade shapes can be modified easily and cheaply (30). The use of all plastic rotor blades on the BO 105 helicopter is a significant step into this technology.

The experimental investigations on fixed wing were extended to rotors with normal rectangular blades and finally with a variation of blade tip shapes (24). Some modifications with different sweep angles of the leading and trailing edges have resulted in considerable gains in rotor efficiency. It was recognized that the local pressure peaks caused by vortex proximity can be reduced considerably and that the unfavourable compressibility effects can be postponed by leading edge sweep like on fixed wing aircraft. Reference (33) indicates that tip modifications could be used to reduce the peak vortex velocities by as much as 80%. Hence, it became obvious to use the beneficial effects in rotor blade geometry design too. As it is indicated in (28), the effective Mach-number can be reduced by cos $^1/_2$ of the leading edge sweep angle. Hence, the optimum sweep angle φ can be determined by using the maximum design tip Mach-number (M_D), the tip Mach-number in hovering flight ($M_{\Omega R}$), the advance ratio μ and the blade spanwise position:

$$\phi = \arccos \left\{ \left(\frac{M_D}{M_{\Omega R}} - \mu \right) \frac{1}{x} \right\}^2$$

In Figure 27 the optimum leading edge shape is shown for a typical high speed flight condition (24). Presweep and aft sweep are combined in this case in order to reduce the pitching moment of the blade section. As the maximum design Mach-number M_D should normally be related to the drag divergence Mach-number of the profile, it becomes clear that the optimum sweep angle distribution will depend on the profile thickness. In general, thinned blade tips will need smaller sweep angles to obtain the same favourable characteristics. This seems to be quite important, as sweeping the blade leading edge increases the local blade chord, which must be limited of course to a certain amount. This relationships are indicated by Figure 28 showing the maximum blade chords as a function of advance ratio for two different blades (43). Applying optimum sweep angles on the normal blade (23012) would result in large local blade peaks even for low advance ratios. In comparison to that only a small blade chord increase is necessary on the optimized blade version with a V13006-0,7 airfoil on the blade tip. This blade version seems to be acceptable up to 0.5 advance ratio. From that it becomes obvious that an optimum blade tip design can be obtained only by a combination of leading edge treatment and reduction in blade thickness.

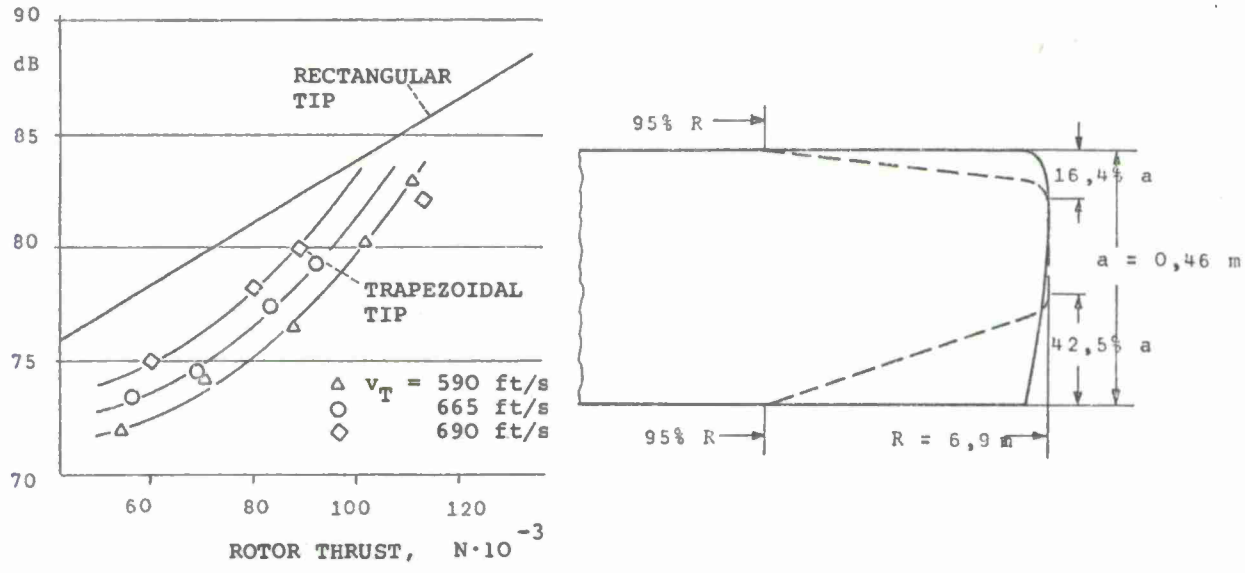


Figure 29 Effect of blade tip shape on rotor vortex noise

In the previous section discussion centered around blade tip shape effects which relieve the advancing tip compressibilty problems. In general, these modifications are quite favourable in lowering the acoustic level of rotors. It is indicated by the tests of reference (20) that noise level reduction is primarily due to a reduction of tip vortex noise. The two blade tip modifications shown in Figure 29 differ by about 7 dB in their noise environment at design rotor thrust. Swept tip blades are applicated today on several modern helicopter designs, for instance on the Sikorsky S-67 "Black-Hawk" - armed helicopter (Figure 30) and on the Bell AH-16 "King Cobra" helicopter.

The list of aerodynamic design inputs, of course, could go on and there are many other areas which need continued attention. It is interesting to note, that although the helicopter is an aerodynamic device, improvements in helicopter techniques up to now have come more from other design possibilities, such as advances in propulsion, structural



dynamics and stability and control. To date, the current limitations on operational capabilities of helicopters are mainly related to aerodynamics and hence, a strong effort in aerodynamic research and development has begun. The major challenge is now to increase the basic knowledges and to apply the results to the total system design . The aerodynamic research work is only of value if we can translate it into hardware design. All these aerodynamic problems and their influencies on the helicopter and V/STOL aircraft design are discussed in detail in session 2 of this lecture series. Moreover, excellent summaries of current aerodynamic research work are given in (34) and (63), for instance.

Figure 30 Advanced blade tip shapes on the Sikorsky S-67 "Black Hawk" Helicopter

4. ROTOR SYSTEMS

One important step in the helicopter and V/STOL-aircraft development is the definition of the general configuration. The number of rotors and rotor location, the type of rotor system, the drive and propulsion system, wings and auxiliary thrust equipment are the basic parameters in this phase. The final decision about the overall configuration is mainly influenced, of course, by the mission requirements. But there are also other points of view, which influence the final selection of the configuration. Among these are, for example,

- use of existing components
- utilization of special technological "know-how"
- tradition
- general trends.

Today rotor systems may be divided into four concept groups: the fully articulated rotor, the semirigid rotor, the hingeless rotor and the "rigid" rotor system.

4.1 The Articulated Rotor

On the fully articulated rotor each blade is attached individually to the rotor hub normally by three hinges: a flapping hinge, a lagging hinge and a feathering hinge. The main advantage of this completely articulated design is that each blade is allowed to flap independently and to follow the aerodynamic and dynamic forces. By this the effective bending loads are reduced essentially. There are a lot of disadvantages adherent to this system. The rotor is a very complex thing with a lot of hinges, bearings, dampers, and the total number of components is about three times higher than on hingeless rotors. Regarding this complexity only a lesser degree of reliability can be expected, moreover the effort of maintainance is high.

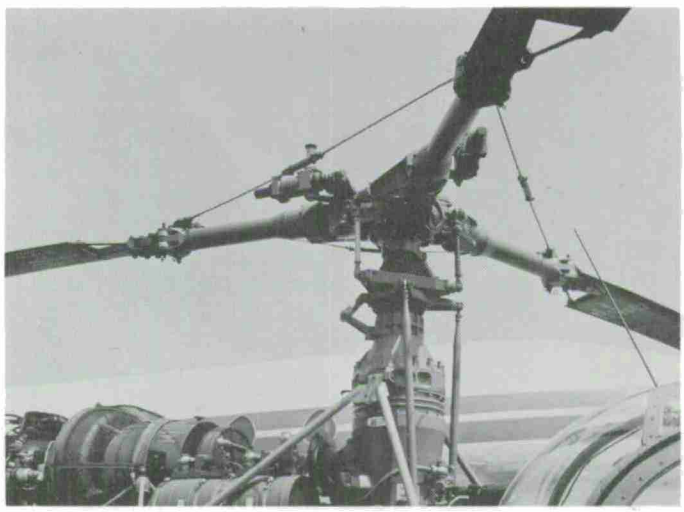


Figure 31 Articulated rotor (Alouette II)

Another drawback of the articulated system stems from its poor moment capability (39). With only small hinge offset nearly no moments can be transmitted from the blades into the rotor hub. The control is managed in the main by the tilt of the rotor disc providing a thrust vector component perpendicular to the rotor shaft.

The poor moment capability results in low control efficiency, low rotor damping and poor dynamic stability behaviour, especially in hover and at low flight speeds (8), (9). These handling qualities demand high sensibility and attention from the pilot.

4.2 The Semirigid Rotor

The name of this rotor type is somewhat misleading, since it could be associated with the rigid rotor trend. However, the semirigid concept is by nature an articulated rotor with a common central hinge and is thus usually applied only on two bladed rotors (see-saw rotors from Bell, Hiller). The construction is relatively simple, the total number of components is reduced in comparison to the articulated rotor. As the blades cannot flap independently on a two-bladed seesaw rotor and as there are normally no lagging hinges, the blade bending loads are high.

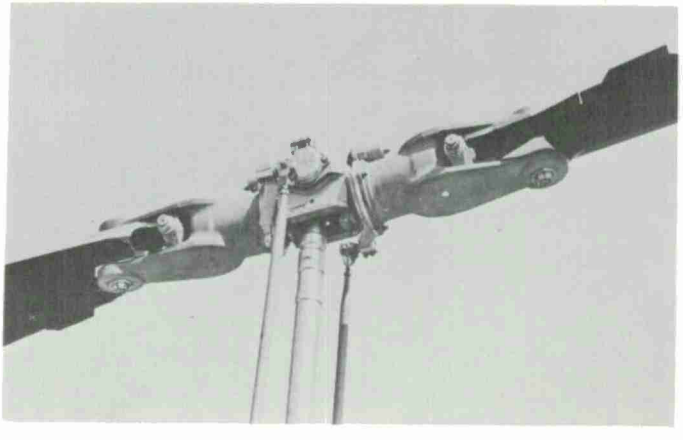


Figure 32 See-saw rotor (Bell 206A Jet Ranger)

By the central flapping hinge the rotor hub moment is nullified so that the total control is only provided by the tilt of the rotor disc. By this the control power and damping moments are further reduced and helicopters with this type of rotor show very poor stability and control characteristics. In addition, the oscillating aerodynamic forces increase with

decreasing number of blades, which results in large oscillating superpositions on the rotor hub. Therefore, seesaw rotors are normally subject to higher vibration levels at more unpleasant, lower frequencies.

4.3 The Hingeless Rotor

The hingeless rotor system is sometimes denoted to a "rigid rotor" system. This is not correct for modern rotor designs, because a high degree of flexibility is involved in the blade or in the attachment structure. There are no flapping and no lagging hinges, only the control of the rotor is done in the conventional manner by using feathering bearings (30). The function of the flapping and lagging hinges is replaced by the corresponding elastic deformations of the blades. The design and development of this type of "elastic" rotor was only possible in the last few years, where materials were available, which could meet the requirements of high elasticity, low specific weight and high fatigue strength (30). The dynamic behaviour of the rotor blades is nearly comparable to articulated blades, but there is a difference in the blade bending loads. Due to lack of real hinges the blades and the rotorhub are loaded with high static and oscillating bending moments. In order to achieve a good design, the blade stiffness must be optimized with respect to desired and detrimental effects.

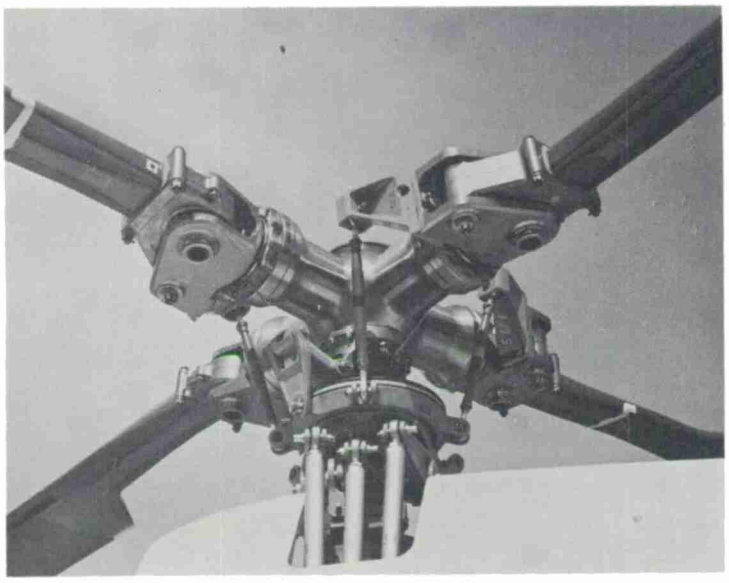


Figure 33 Hingeless rotor (Bölkow Bo 105)

Compared to an articulated rotor the hingeless rotor concept causes a mechanical simplification, achieved by elimination of hinges, dampers and blade stops, for example. This additionally results in aerodynamic clean rotor design with reduced drag. Only low maintainance is needed too.

Theoretical and experimental work over about ten years has shown that the hingeless system offers a significant improvement in handling qualities in comparison to articulated systems (8), (9), (39). These benefits are caused by the flapping behaviour of the elastic rotor blades, which is comparable to flapping of a high offset hinge rotor (39). Thus large moments can be transmitted to the rotor hub, which will allow a more direct control of the aircraft. The control power of the articulated rotor is exceeded by a factor of about four (9). The control action consists nearly of pure moment power and is independant from rotor thrust. For damping similar relations exist, which is of paramount importance. Besides of excellent control characteristics the stability of the helicopter is improved, especially in the hover condition. At higher forward speeds the rotor is more sensitive to external disturbances, which results in a decrease of stability (8), (38). However, the total flying behaviour is judged by means of stability and control. In this respect the hingeless rotors are favoured by all pilots.

4.4 The "Rigid" Rotor and Propeller

When speaking from a "rigid" system, the same restrictions must be made as before with respect to the word "rigidity". Modern rigid rotors represent not a new class but can be denoted as hingeless rotors with increased stiffness. For this type of rotor high blade thickness is normally used in the blade sections and the total geometry can already become similar to propellers. The blades showing only low flexibility are exposed to extremely high bending loads, which can only be tolerated with highly qualified materials. Such types of rigid rotors are usually designed for aircraft configurations, which are somewhat different from the classical helicopter. Sikorsky has done pioneering work in this field with its ABC-rotor (advanced blade concept), two of which are used in a coaxial position. Another concept is used in helicopters with side-by-side rotors. To provide the advantages of such advanced rotary wing concepts, rotor systems are necessary which can support large moments and which are stiff enough to prevent any danger of instabilities in stop or other conversion modes.

The description made above should only give a short synopsis on the most important features of different rotor concepts. The comparison is related to basic constructions and on the scope of flight dynamic behaviour. It will be shown later that all rotor dynamics can be characterized by a few fundamental parameters, such as flapwise, inplane and torsional stiffness, and the corresponding frequencies, as well as some more important hub parameters.

5. DYNAMIC ROTOR DESIGN

In chapter 2. a discussion was carried out of all the basic considerations influencing the aerodynamic configuration of the rotor. The determining parameters to be defined were rotor size, rotor tip speed, number and area of blades, and the aerodynamic profile section. It was shown that there is a lot of inputs contributing to the design synthesis. The final selection can only be a compromise between quite different and even contradictory effects.

When this phase is concluded successfully, the second essential design phase can be started: The phase of dynamic rotor design. The fact that the rotor is not only a hypothetic aerodynamic thing but consists of real mass and material, results in the need of a thouroughly dynamic treatment. Of course the term "dynamic design" has a complex meaning and can only characterize the totality of the rotor behaviour. What is included in this term, what are the basic centers in this design phase?

5.1 Basic Considerations about Blade Mass

Assuming that the aerodynamic configuration and the geometry of the rotor is known, the first question the designer must answer is, how the blades are to be built. A first lead for the total blade weight can be derived from the inertia characteristics the rotor should have. The determining factor for the kinetic energy involved in a rotating rotor is the total mass moment of inertia of all blades about the rotor axis. This is an indication for the autorotation characteristics of the helicopter in the case of power failure. An investigation of the descent and landing characteristics of helicopters with engines off shows that these characteristics can be expressed by an energy/time factor, the so-called "Katzenberger"-factor (44). Figure 34 shows the relationship and the values for a lot of current helicopters (45). The qualities in the engine -out condition are indicated by the mass moment of inertia (I_{Ro}/G), the rate of descent depends on the disc loading (G/F), whereas the rotor rpm breakdown is characterized by the parameter γ_1. High values of F_K denote good autorotation characteristics and it can be seen from Figure 34 that small helicopters have, in general, poor autorotation characteristics, while large helicopters are excellent.

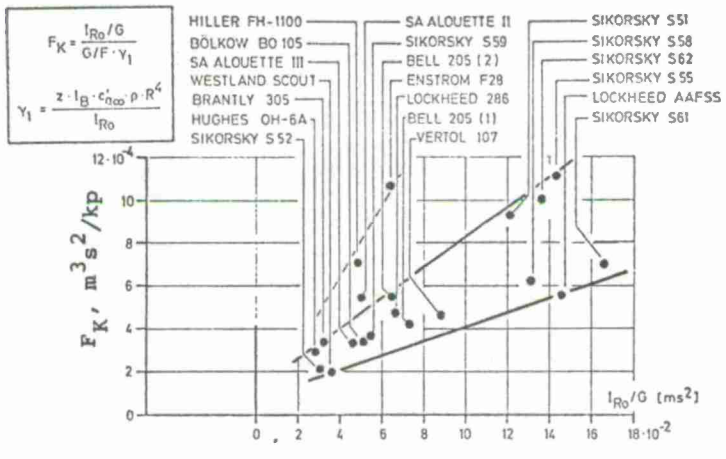


Figure 34 Autorotation-factor F_K (Katzenberger) for several helicopters

Helicopter	τ, sec	Pilot Rating
Bell UH-1A	2.46	Excellent
Hiller 12E	2.31	Excellent
Sikorsky S58	2.12	Good
Vertol H21-D	1.93	Fair
Hughes 269	1.73	Poor

Figure 35 Time to maximum acceleration and pilot ratings for several helicopters

Another rational blade design criterion for satisfactory engine-out performance was derived by Sadler and Crimi (46), who define the time to maximum acceleration and relate it to pilot ratings. Excellent autorotational characteristics are shown by those helicopters, whose total rotor mass of inertia is large. Fundamental relationship like the Katzenberger-factor (Figure 34) or the time-constant (Figure 35) can be used to get a first idea of the total inertia of the rotor and hence of the minimum blade masses. This is an essential step, because the poor autorotational capability cannot be improved later with disc area and blades committed.

5.2 General Research and Design Areas on a Rotor

The purpose of the next Figure 36 is to illustrate qualitatively the most important problem areas in the further dynamic rotor design work. They are indicated by the example of a hingeless type of rotor, other rotor systems would show just the same scope of research and design areas.

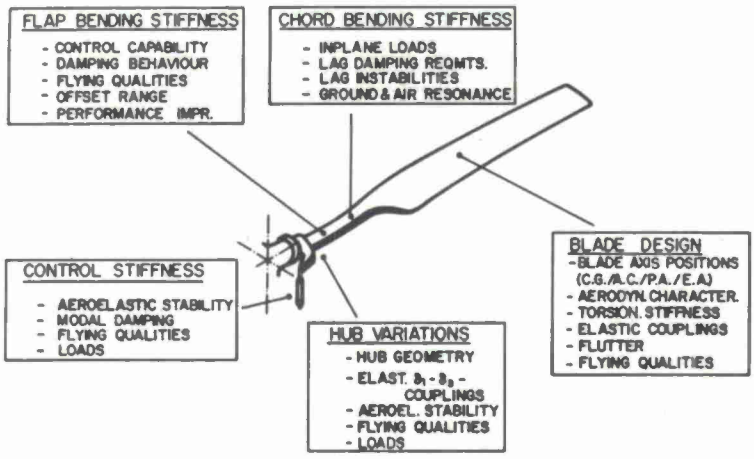


Figure 36 Research areas on hingeless rotors

As it can be seen, the problem areas can roughly be divided into several centers. They are indicated in terms of stiffness parameters and of certain geometries and are thus largely considered under dynamic aspects. A short summary of the main dynamic effects is given, they are influenced by the individual design parameters. The effects are related mainly to the flight dynamic and aeroelastic field and of course cannot represent the total range of design inputs.

5.3 Flapping Frequency Selection

In a foregoing section a description was made of different rotor concepts, which are the most common ones used or designed today. It can be shown that all these concepts can be collected under one essential parameter, the first flap natural frequency of the blades. It proves to be the determining parameter for the dynamic and flight dynamic characteristics of all types of rotors. The following investigations will show this influence and will give a guideline for an optimal selection of this parameter. Of course, it is a difficult task to obtain a technical compromise as an optimum. Normally the aspects are too different and in part contradictory.

In order to give a first insight into the characteristics of the different rotor systems, some typical rotor groups are collected in Figure 37. They are characterized by the fundamental rotating frequencies of their blades in flapwise and inplane directions. At this time only the abscissa should be looked upon. It shows the first flapping frequency in relation to the rotor frequency.

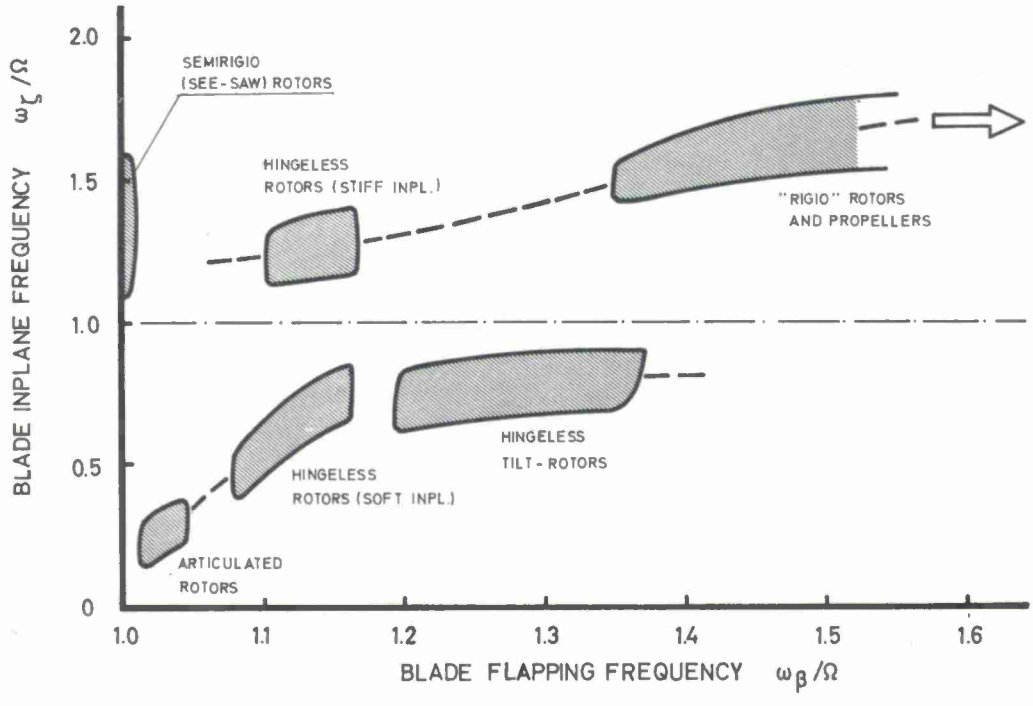


Figure 37 Typical rotor characteristics in the flapping / inplane frequency plot

This is the normal way to characterize rotor stiffness. The rigid body flapwise mode of conventional articulated rotors can have a natural frequency as small as 1.02 per rev if the hinge offset is small. Hingeless rotors generally can be designed over a wide frequency region, depending on the geometric and material properties. The todays hingeless rotors lie in the range around 1.1 to 1.2. The hingeless rotor of the Bölkow helicopter BO 105, which is the first hingeless system built in production series, uses a frequency ratio of 1.12, for instance, (27). Rotors for tilting prop/rotor aircrafts are focussed to somewhat higher frequencies, they are generally being designed to have flapwise frequencies of about 1.2 to 1.3 per rev. "Rigid" rotors and propellers for VTOL-aircrafts are usually hingeless rotor designs. In order to achieve light weight, rotors are usually designed under the aspect of maximum specific stiffness. Here the frequency ratios depend on the size of the rotors. From the standpoint of aeroelastics, propeller and rotor blades should be considered flexible if the first mode natural frequency is less than 1.8 per rev (47).

When classifying the different rotor systems into stiffness rubrics, only the flaping stiffness is considered, while the inplane stiffness is not taken into account here. Inplane considerations and their input to the design synthesis will be discussed later.

5.3.1 Basic Relationships

The first flapping natural frequency of a rotating hinged blade is defined by

$$\bar{\omega}_\beta = \frac{\omega_\beta}{\Omega} = \sqrt{1 + \frac{a_\beta M_S}{I_A} + \frac{c_\beta}{I_A \Omega^2}} \quad .$$

This formula is representative for all types of rotors. The frequency depends on the flapping hinge offset a_β, the static moment (M_S), the moment of inertia (I_A) and a spring constant c_β. This spring constant is, of course, zero on articulated rotors but may become an important factor on rotors without flapping hinges. Hingeless rotors can indeed be calculated in the same way as articulated rotors. For this the real hinged blade is replaced by an equivalent blade system including virtual hinge offset and flapping restraint. This was first devised by Young (39) and developed further by Ward (48), for instance. This equivalent system technique was refined more and more, and the systems were improved with time. Figure 38 shows a newer one with hinges in flapping, inplane and torsional directions (27). Ways of determining and using such types of equivalent systems have been discussed in session 3 of this lecture series (53).

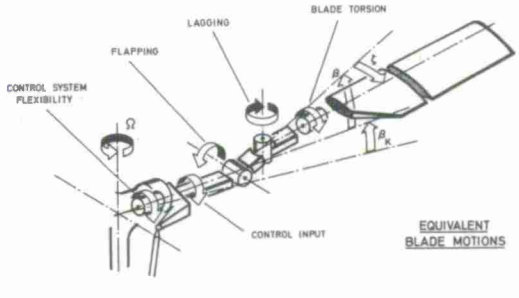


Figure 38 Analytical model of rotor blade with elastic deflections

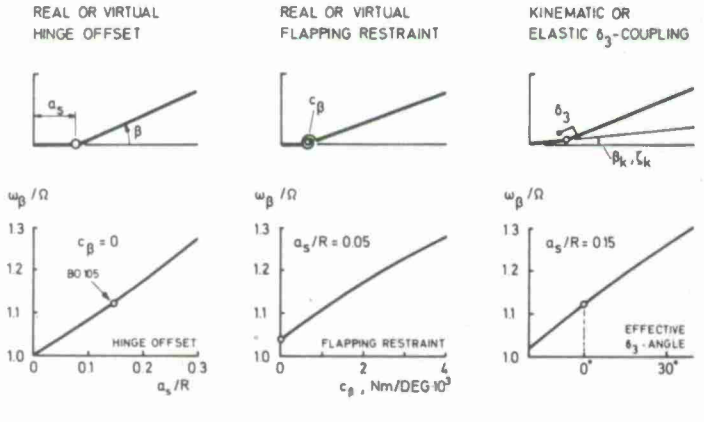


Figure 39 Basic influencies on the flapping frequency of rotor blades

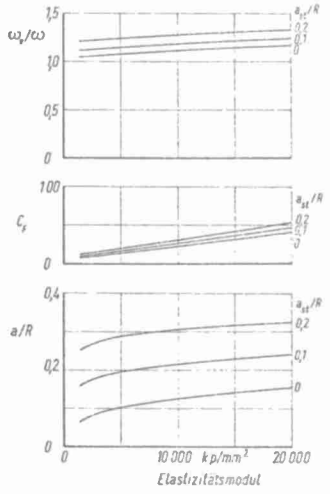
Returning to the task of designing a rotor, a first determination of the (real or virtual) hinge offset can be made by assuming constant blade mass:

$$\frac{a_e}{R} = \frac{\bar{\omega}_\beta^2 - 1}{\bar{\omega}_\beta^2 + \frac{1}{2}}$$

Figure 39 shows the most important relationships in the flapping dynamic behaviour (38). Frequencies above unit can be obtained either by means of hinge offset or by blade root restraint. The cantilevered elastic blade of the BO 105 rotor, for instance, results in an equivalent hinge offset of about 15% radius and a zero or slightly negative hinge restraint. A third way to influence the flapping behaviour is the use of pitch-flap coupling (δ_3). But it must be recognized in this case that the change of flapping frequency due to δ_3-effects is not entirely comparable to real stiffness frequency changes, because

there is no change in the specific moments per degree of flap angle. These effects will be discussed later.

It can be concluded from Figure 39 that three principal means of influencing the natural frequency are available to the rotor designer



- real or virtual hinge offset
- real or virtual flapping hinge restraint
- kinematic or elastic pitch-flap (δ_3) coupling.

In general, these effects are interchangeable and can be handled by the design engineer by means of blade stiffness optimization. This might be indicated by the relationships in Figure 40 , where first mode flapping frequency, hinge stiffness and the equivalent "hinge" offset are shown as a function of the materials stiffness (49). All these parameters are increased with the modulus of elasticity and with the radial distance at the point of support.

Figure 40 Flapping characteristics as a function of material stiffness

5.3.2 Cyclic Moment Capability

On helicopters the rotor is used for generating the control and trim moments of the aircraft during hover and all other flight conditions. This eliminates the need for additional control devices. Therefore, the capability of producing moments is an essential characteristic of rotors. However, this capability is not fully present on all types of rotors, as it was indicated before.

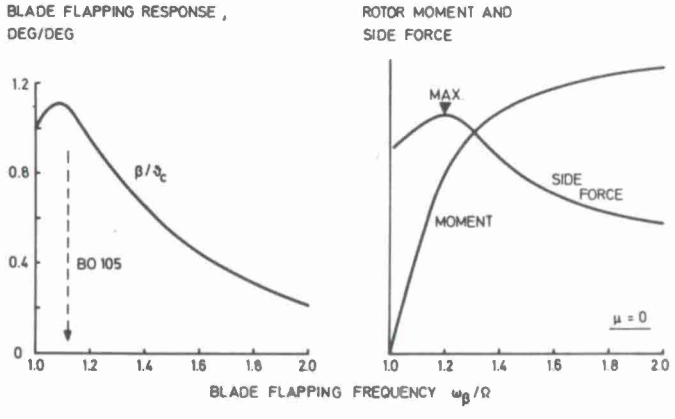


Figure 41 Blade flapping, rotor forces and momentsdue to cyclic pitch in hover flight

To illustrate this in more detail a variation in the cyclic control moment with blade flapping frequency is illustrated in Figure 41 ; these calculations are for a one degree cyclic pitch setting in hover (38). It should be noted that the flapping amplitude response - on the left part - of a typical hingeless rotor is very nearly the same as the response of a fully articulated rotor ($\bar{\omega}_\beta = 1.0$), but is decreasing with higher frequencies. In contrast to the similarity in the amplitudes of blade motion, the magnitude of the resulting moments increases with flapping stiffness. It is shown to vary by a factor of about 3.0 as the stiffness is increased from the typical hingeless range ($\bar{\omega}_\beta \approx 1.1$) to the "rigid" rotor range. However, it must be mentioned by the designer that the main increment of control moment is already obtained at relatively low flapping frequencies and a further increase of blade stiffness will bring nearly no additional control power. Even a completely rigid rotor cannot produce infinitive moments. The relative stiffness of a rotor can be expressed by the factor:

$$c_{rel} = \frac{\text{cyclic moment (effective)}}{\text{cyclic moment (stiff rotor)}}.$$

This relative stiffness factor approaches to 1.0 with increase of rotor stiffness. Plots like that of Figure 41 can also be used to determine the control angle requirements for trimming and controlling the helicopter. A rotor with a flapping frequency of 1.2 will need less than 25% of the control angles required for a rotor slightly above unit frequency. In forward flight there is an increase of all other derivatives too. That means that the same amount of cyclic pitch is required for the aerodynamic compensation of pitch attitude, inflow angle and forward speed, for instance. Only the direct portion to trim center of gravity or external moments is reduced. Therefore, articulated rotors and hingeless rotors are quite similar in their forward flight trim angles (Figure 42). Similar control range must be provided at these two systems.

Another parameter in control system design is the phase behaviour. Rotors with 1.0 flapping frequency are characterized by a 90° phase lag between control and flapping

response (49). This phase lag is reduced with higher frequencies so that phase angles of about 50 to 70° are typical for the normal hingeless rotor range. The optimum control phase angle is a compromise between different flight conditions and must be found for the special stiffness characteristics of the rotor system.

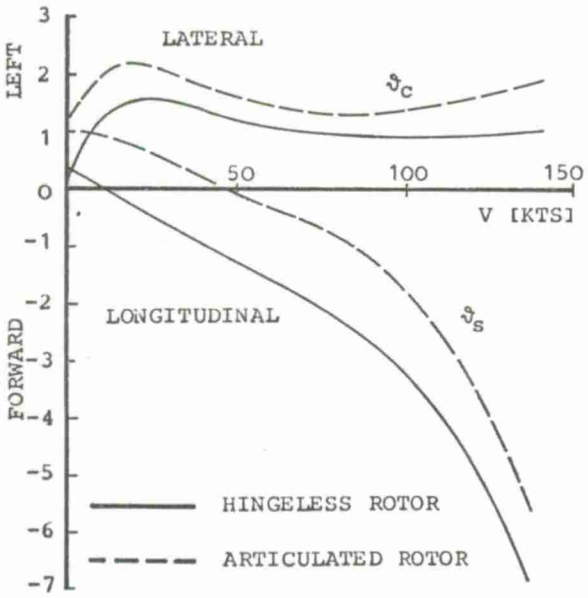


Figure 42 Cyclic control in forward flight for different rotrors

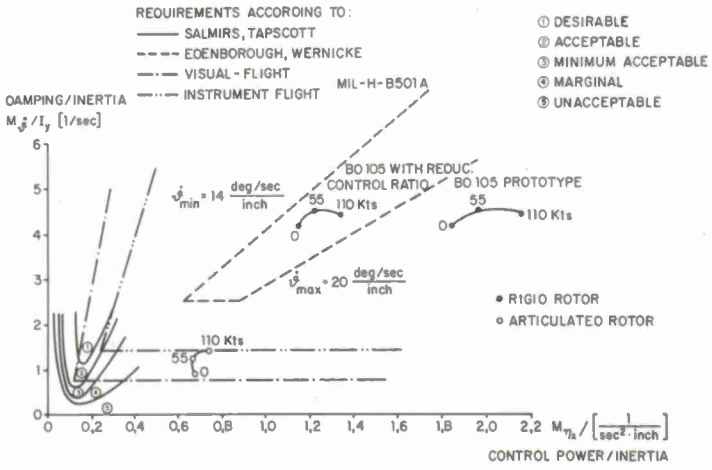


Figure 43 Control characteristics (pitching)

In order to judge the control characteristics completely, control inputs must be considered with respect to the corresponding time behaviour. Usually the control efficiency will be expressed by the initial acceleration per unit stick deflection, the time behaviour is expressed by the damping moment, referred to the inertia moment of the aircraft (Figure 43). Limits of satisfactory properties, established by Salmirs and Tapscott (50) and even the Military Specifications (3) seem to be too moderate for todays controls.Recommendations made by Edenborough and Wernicke especially for armed helicopters (4) seem to be more true for todays modern helicopters. They can be a guideline for rotor design with respect to handling qualities. The comparison of an articulated rotor and a hingeless rotor on the same helicopter shows that both control power and damping is increased with flapping frequency. Both values are about three to four times that of the articulated rotor, which is an essential improvement in the control behaviour. This is fully demonstrated by the experience with the Bölkow hingeless rotor helicopter BO 105. It must be noted, however, that a further increase of flapping stiffness must not necessarily improve the control characteristics still more.

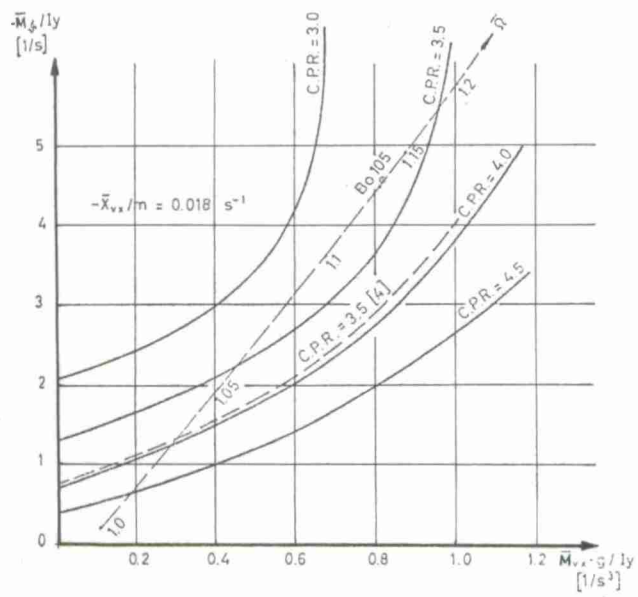


Figure 44 Pilot ratings in the plot of damping / speed stability derivatives

More information about these problems can be gained by a dynamic control simulation study including the pilot's reactions (51). These ratings are shown in Figure in a plot of the rotor damping versus forward speed derivatives of the pitching moment (52). The corresponding values gained by a rotor frequency variation are shown in this picture and can be compared with the C.P.R.-values. Low C.P.R.-values indicate proper control behaviour. The optimum pilot rating is obtained in this case at a flapping frequency ratio of 1.11, although the intersection is relatively flat (52). A strong decay of pilot rating happens, when the rotor stiffness is decreased, but nearly the same decay can be observed with increase of rotor stiffness. This shows that the control sensitivity can also be overdone by too high a frequency. Of course, optimization processes in that way depend on a lot of parameters and must be considered with certain restrictions. However, they can provide a guideline for a proper selection of the flapping frequency, which seems to be very important in the first design phase.

5.3.3 Dynamic Stability

Helicopters normally show an unstable flight behaviour without pilot actions. This stick fixed instability is produced by the rotor, which represents quite an unstable disc with respect to changes of altitudes and velocities (49). The only stabilizing effect is provided by the rotor moment, which results from the roll or pitch rate of the rotor disc. This rotor damping moment tries to slow down the motion. Regarding the influencies on the moment characteristics, shown before, one can expect that an increase of moment power will affect the instability quantitatively. It was mentioned just before that the damping moment increases almost linear with an increase of the relative rotor stiffness (see Figure 44).

Variations in the dynamic stability with flapping frequency of the blades are illustrated in Figure 45 for a hover flight condition. The longitudinal motion of the helicopter, indicated by the time to double amplitude t_D and the period, shows an unstable characteristic over the whole stiffness range. However, the time to double amplitude of about 4 sec with the 1.0 frequency ratio (seesaw rotor, for example) is increased over 30 sec with a 1.15 hingeless rotor. In the Military Requirements (3) a minimum t_D of 10 sec is demanded, which can only be met with a rotor frequency beyond 1.04 in this case. But this limit proves to be quite moderate and seems not to describe the ideals of modern "good to fly" helicopters. Stability values beyond 20 sec., for instance, can only be obtained by typical hingeless rotor frequencies (1.1 ÷ 1.2). Interesting to note that the stability improvements due to flapping stiffnes is limited as well: The optimum stability value would be obtained in this case with a completely stiff rotor at about $t_D \approx 40$ sec. A similar effect of saturation could be observed already with the control-characteristics (Figure 41). It indicates that selecting the flapping frequency for the purpose of flying qualities improvements, an optimum must be found in the medium range.

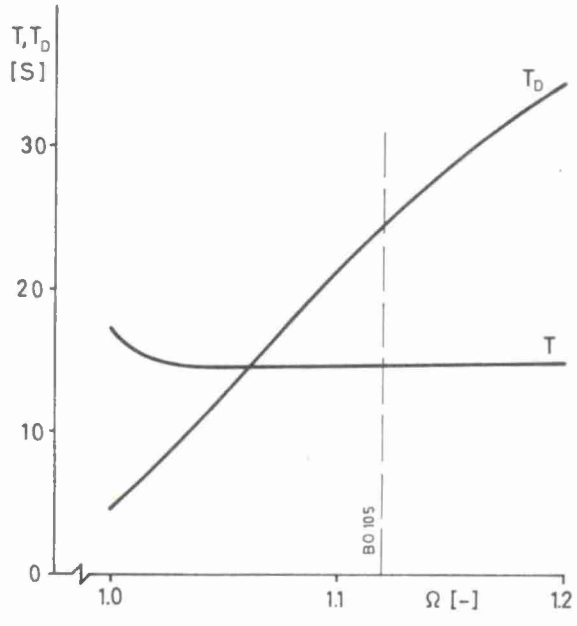


Figure 45 Inherent dynamic stability in hover flight as a function of the blades first flap frequency

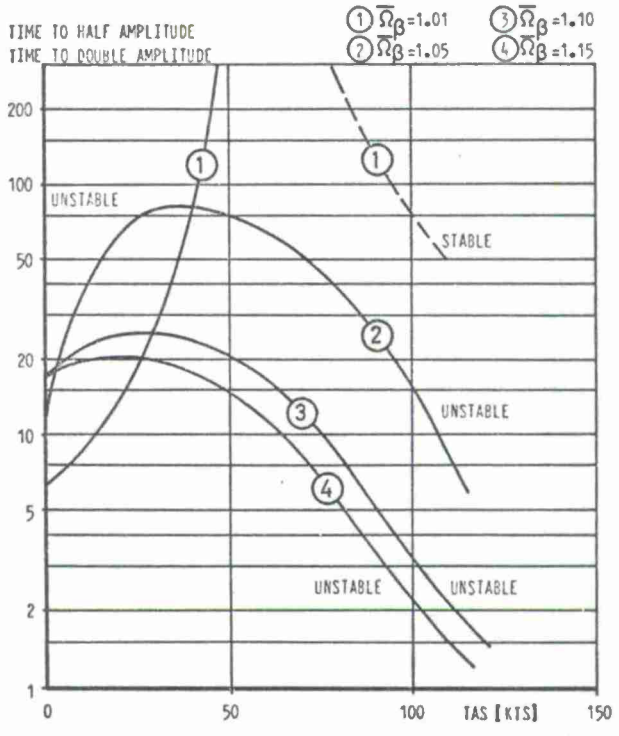


Figure 46 Inh erent dynamic stability in forward flight for rotors with different flapping frequencies

New inputs into these considerations are obtained from a forward flight stability analysis. It can easily be shown, that in forward flight there is another dominating stability parameter, the pitching moment - angle of attack derivative (9). Hingeless rotors produce - compared to the articulated rotor - a higher destabilizing moment. With the same fuselage shape and the same horizontal tail the resultant angle of attack stability is worse with stiffer rotors. The variation of the dynamic stability of a helicopter with different rotors is shown in Figure 46. Starting from unfavourable stability qualities in hovering flight the low frequency rotor ($\bar{\omega}_\beta = 1.01$) is more and more governed by the stabilizing horizontal tail, which is large enough to get stable conditions for higher speeds. With increase of flapping stiffness a destabilizing trend can be observed over flight speed. At extremely high speed conditions times to double amplitude just below 1 sec. are obtained for the stick fixed longitudinal motion. It appears that the destabilizing character with higher stiffness blades comes to a limitation too (compare with Figure 45).

Investigations and flight tests have shown that one way for counteracting the

forward flight instability is to increase the horizontal tail volume (8). But, to obtain really stable conditions large stabilizer areas would be necessary, which results in increased rotor moments and blade bending loads again.

These considerations must be supplemented by the real stability feeling of the pilots. Pilots flying the BO 105 with a hingeless rotor do not feel any unstable character of the aircraft, even with stability values of t_D = 1 sec, for example (9). The discrepancy can be explained when considering the total aircraft-pilot system. The pilot is always controlling the aircraft by small inputs, even without noticing it. These automatic control inputs can be extremely small because of the high control power of hingeless rotors. Therefore , a critical examination of the dynamic behaviour must consider totality of three essential parameters: inherent stability, control efficiency and ride qualities in general. Pure stability requirements are not sufficient for doing this.

5.3.4 Structural Loads

With all these flapping stiffness considerations the question of blade loads must be noticed. It was shown before that high flapping stiffness rotors are capable to produce high hub moments. But high rotor moments can only be achieved with high blade bending moments in the inner parts of the root section. Figure 47 shows a typical moment distribution over blade span. It can be seen that the moment rises mainly in the very stiff parts of the root section and the rotor hub. The amount of bending moments in these parts can be derived from the amount of the total rotor moment. An articulated rotor and a hingeless rotor will show quite different hub moments in a normal steady trim condition, because they manage the trim problem in quite a different way. When considering flight maneuvers or gust penetration at high forward speeds the hub moments will differ still more. For a proper layout of the rotor components all practical ground and flight operating conditions must be studied in detail which may result in high structural loads. They are usually first harmonic loads, caused primarily by the flow dissymmetry.

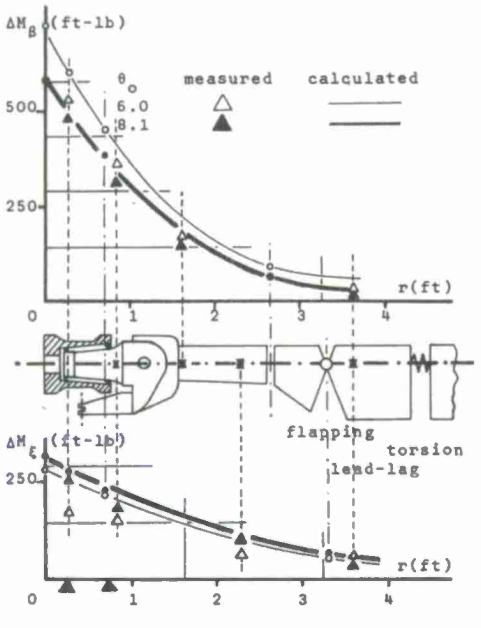


Figure 47 Typical spanwise moment distributions of a hingeless rotor (forw. flight)

In general, the amount of blade bending loads in the critical inboard section is almost proportional to the total moment capacity of the rotor. When selecting the optimum flapping stiffness, all effects must be regarded, which were shown before. During this process the question of the structural loads will necessarily become secondary, because they cannot be changed without changing the moments desired. In contrary, the rotor layout should prevent from overdoing the stiffness increase, because the additional moment power will not improve the rotor qualities still more, so that the bending loads on the rotor components would be useless.

5.4 Inplane Frequency Selection

In the development history of the helicopter serviceable concepts could only be obtained by means of introducing flapping and inplane hinges. Only in this way the structural loads could be reduced to a controllable limit. At hingeless rotors the function of the hinges is replaced by a flapwise and chordwise flexibility, thus reducing the structural moments by bending the blades. The importance of the flapping hinge or the flapwise flexibility respectively, is discussed in (53). First flap natural frequency proves to be the determining parameter for the blade flapping response and for the rotor moment characteristics. So the flight dynamic characteristics of all types of rotors can be derived from the flapping frequency parameter.

The second essential parameter describing the rotor dynamic behaviour in the first natural frequency of the inplane motion. In contrast to the flapping loads the inplane bending loads of the blades must be characterized as pure parasite loads which nearly not contribute to the active characteristics of the rotor. In general, inplane motions are not submitted to such definite demands, like the flapping motions, and can thus be treated with more freedom by the designer. Of course, he must understand the physical connections and must identify the conditions which require most detailed study.

5.4.1 Basic Relationships

For a better understanding of the dynamic inplane behaviour of rotor blades, some basic relationship should be considered. Similar to the flapping frequency the first inplane natural frequency of a rotating blade can be expressed by

$$\bar{\omega}_\zeta = \frac{\omega_\zeta}{\Omega} = \sqrt{\frac{a_\zeta \cdot M_S}{I_A} + \frac{c_\zeta}{I_A \Omega^2}} \quad .$$

In contrast to the flapping frequency, which can never be smaller than the one per rev rotor frequency, the inplane frequency can be located over a wide range. A small hinge offset, for instance, results in a very low inplane frequency, because the influence of the centrifugal force is much smaller for the inplane motion (53). Two means of influencing the inplane frequency can be seen: the amount of hinge offset and the amount of hinge restraint.

In order to get more insight into the inplane frequency relationships, Figure 37 should be considered again. Different rotor systems are shown there in a plot of first natural frequencies of flapping and inplane motion. The systems were discussed with respect to their flapping frequency yet before; so we can concentrate now on the ordinate axis. In general it appears, that the inplane frequencies of the different rotor concepts are not in that clear correlation as observed with the flapping frequencies. The total possible range of inplane frequencies extendsfrom 0.0 up to 2.0, which is a wide range, when comparing to the flapping frequencies. Hingeless rotor concepts can practically be handled with ratios from 0.3 up to 1.5, depending on the flexibility of the root and of the blade section. It is proved by these facts that the inplane stiffness of a rotor system is not a concept parameter, which must follow a physical sequence unconditionally. However, as it was mentioned before, it is a parameter with most important secondary effects.

5.4.2 Danger of Lead-Lag Instabilities

When considering a helicopter under the aspects of dynamics, it consists of a complex system of an elastic fuselage and the rotating rotor. They represent an oscillating system which can be liable to self-excited oscillations under certain circumstances (54). They can occur either on ground or in the air and are called the classical "ground and air resonance" phanomena (57). Instabilities of this type were encountered during ground operations with hinged rotor systems, but can also occur with hingeless rotor systems. A theoretical treatment of the problem is possible with the classical ground resonance theory development by Coleman and Feingold (57). An extensive theoretical analysis of the phenomena for the hingeless rotor has been carried out in references (54), (55), (56).

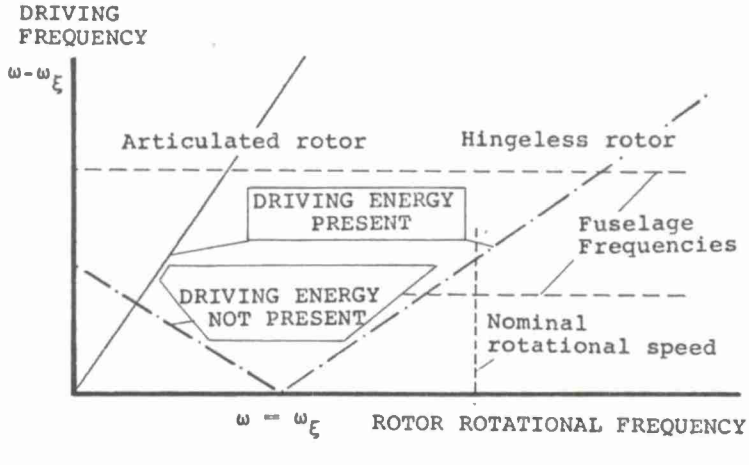


Figure 48 Ground resonance - frequency diagram

In order to design a rotor system which is safe from any lead-lag instabilities the design engineer, of course, must have an insight into the physical problems and into the various parameters affecting the phenomena. The main source of potential instability are represented by the blades. Unstable conditions can be excited when blade's oscillations go in their inplane natural frequency. This results in an unbalance on the helicopter with the nonrotating frequency of $|\Omega \pm \omega_\zeta|$. With an inplane frequency $\omega_\zeta > \Omega$ the oscillating energy is absorbed by the driving system. With $\omega_\zeta < \Omega$ an energy transport occurs from the driving system to the oscillation (54). Figure 48 shows the different regions of energy transport for an articulated and a hingeless rotor. As the inplane frequencies of fully articulated rotors are normally low ($\bar{\omega}_\zeta \approx 0.3$), the critical frequency $\Omega - \omega_\zeta$ is high, so that much driving energy is present for exciting the system. Soft inplane hingeless rotors lie around ≈ 0.7, so that the critical air-resonance frequency and the corresponding driving energy are lower. Finally, on rotor systems with first inplane frequency $\omega_\zeta > \Omega$ the energy transport is adverse, as mentioned before. Hence "stiff" inplane hingeless rotors are safe from any danger of lead-lag instability. For the time being this is a reason for designing hingeless rotors with an overcritical inplane frequency. However, there are other adverse effects, as will be discussed later.

5.4.3 Rotor Damping

Whether a resonance condition results in a real instability, depends on the total damping involved in the system. In general, there are four essential sources of damping: blade damping, aerodynamic damping, damping of the airframe and damping due to aeroelastic coupling effects (38). Blade damping can be provided either by artificial dampers or by "material" damping in the blades. Aerodynamic damping results from direct aerodynamic force acting and from the flapping motion of the blades. The damping involved in the airframe consists of structural damping effects and of damping in the landing gear. Finally, additional damping effects can be obtained from aeroelastic coupling of the blade motions.

This seems to be a great palette of damping sources, which the design engineer can make use of. In this respect the two decisive questions during the design phase are: How much damping is required and how much damping is present? In order to get an answer to the damping requirement problem, much theoretical work is necessary involving different ground and air resonance flight conditions.

Figure 49 shows some typical results of a ground resonance study which must be conducted during the design phase (38). The figure shows the modal damping of the inplane motion (rotating system) as a function of inplane frequency. Inherent blade damping, which can consist of structural or viscous damping, is used as a parameter. On hinged rotors with low inplane frequencies ($\approx$ 0.3) much blade damping is required to avoid ground resonance conditions. On typical hingeless rotors with an inplane frequency of about 0.7 the damping required for stability is much less. It should be mentioned that the damping requirements of these two rotors differ by a factor of 5. Similar results are shown in (41), for instance. Supercritical rotors with $\omega_\zeta > \Omega$ are not considered here, as they are not subject to ground and air resonance problems.

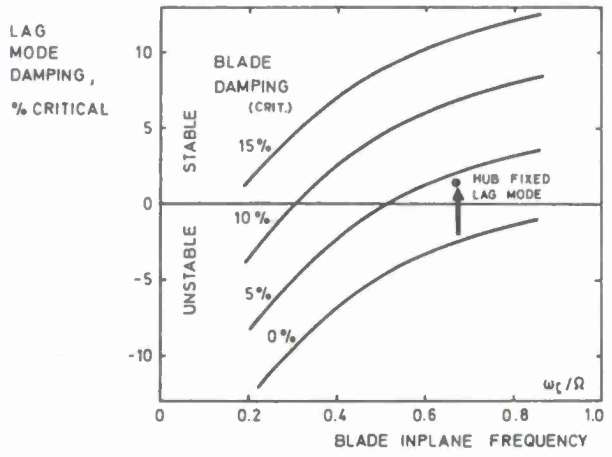


Figure 49 Effect of blade inplane frequency and damping on ground resonance stability (calculated)

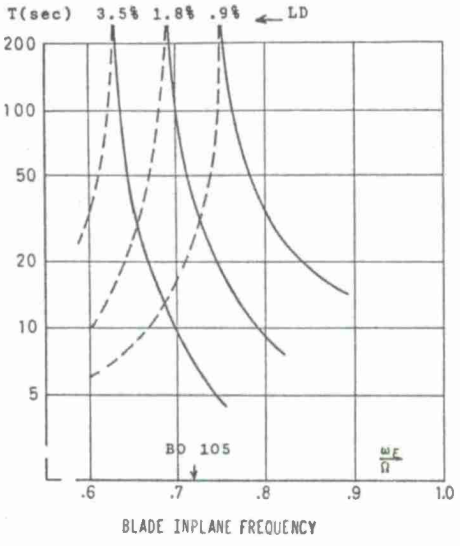


Figure 50 Air resonance map in hover

The phenomenon of mechanical lead-lag-instability may also occur in the air, as mentioned before. Figure 50 illustrates results of a simple study done for hovering (56). It is shown, that damping is a very strong stabilizing effect in general, but the more important conclusion is that reducing the inplane frequency acts in a destabilizing sense so that more damping is required for air resonance stability. This corresponds to the effects shown for the ground resonance problem.

Additionally, differencies in the ground- and air-resonance behaviour result also from the inplane frequency itself. It was indicated before, that the magnitude of the ground/air resonance frequency is much higher for normal articulated rotors. Hence, in the case of a potential instability the excitation is more explosive for articulated rotors On the other side, the $(\Omega-\omega_\zeta)$-frequencies of hingeless rotors tend to be located in the range of the flight dynamics frequency of the helicopter (see Figure 48). As they are the dominating frequencies in the air, hingeless rotors must be investigated especially with respect to the air resonance phenomenon. Of course, these frequencies depend largely on the size of the rotor and the helicopter. It is demonstrated by the flying helicopter BO 105 that there are no problems of air resonance instability. Enough damping is provided, first, by the flapping stiffness (increase of flight dynamic damping) and secondly by the structural damping in the blade and the blade attachment. There is no mechanical damper applied (30).

In general, the design engineer can only consider these effects, if he knows the different damping factors. This seems to be a most important question when structural blade damping is considered. Intensive test programs were conducted, for instance, during the development of the hingeless rotor of the MBB company. It was experienced that the blade's structural damping depends on a lot of parameters, the most inportant ones being

the way of blade attachment, the centrifugal force and the moment amplitudes.

5.4.4 Structural Loads

Another important question connected with the inplane frequency considerations is the question of structural loads. Tests of several rotor configurations have shown in early time, that especially on hingeless rotors the inplane or chordwise bending moments became very large and were sensitive especially to maneuvers (58).

As we have seen, the question of flapwise structural loads is somewhat in the background, as they cannot be changed without changing the moments desired. In contrast to that, the chordwise bending loads do not directly contribute to the active characteristics of the rotor. So the designer should focus attention to a reduction of these loads in order to increase the blade life. The tests of (58) have shown that the chordwise bending moments could largely be reduced by using a flexible drag link at the blade root (Figure 51). An even greater reduction in the loads was achieved by matching the chordwise stiffness to the flapwise stiffness along the entire blade. The physical reason for this effect is that a flexible blade is able to bend away under airloadings and to develop a centrifugal relieving moment. With a real hinge located in the inboard section of the rotor hub the blade inplane motion can compensate nearly all blade bending moments. Therefore, on articulated rotors with low inplane frequencies only small bending loads appear. The opposite condition can be observed on "stiff" inplane rotors with nearly no flexibility over the entire blade.

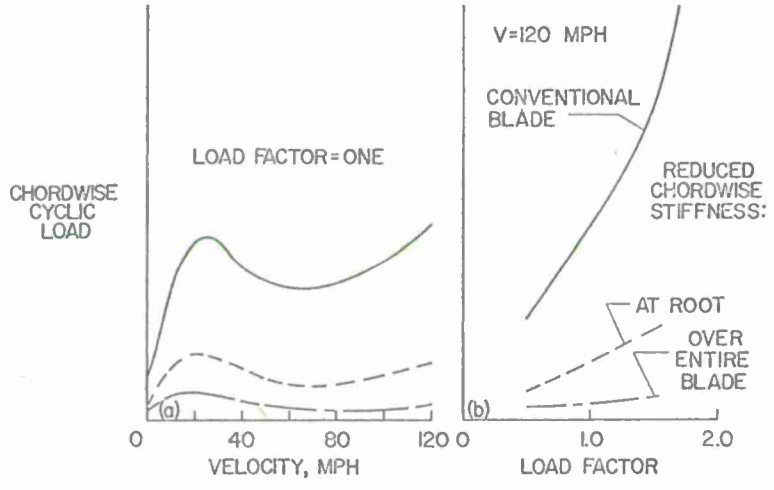


Figure 51 Effect of chordwise stiffness on blade chordwise cyclic load

In general, to avoid high cyclic chordwise bending moments the chordwise stiffness should be reduced. This can either be done by using a real hinge in the inboard section or by providing high flexibility on the blade, as is done on the BO 105 and WG-13, for instance. In general, the introduction of inplane flexibility is the only way to offer a solution to the problem of high cyclic chordwise moments on hingeless rotors. However, care must be taken to achieve the reduction in stiffness without a substantial reduction in chordwise modulus of elasticity. This can be handled by proper selection of materials and of weight and stiffness distributions along the blade. This is realized, for instance, on the BO 105 soft inplane rotor showing an inplane frequency of about 0.65 (30). The requirements were met by using an all fiberglass material which offers the highest fatigue strenth by having the lowest stiffness per weight.

5.4.5 Optimum Blade Design

In general, the choice of lead lag frequency is governed by a trade-off between stability and blade inplane stresses. Structural loads and stability considerations have resulted in two essential conclusions, both of which are illustrated in Figure 52 : The one, in order to reduce the blade structural inplane loads, the chordwise natural frequency should be as low ad possible. This may be achieved by hinges or by high blade flexibility. The second, in order to avoid mechanical instabilities of the ground and air resonance type, the inplane stiffness must not be placed below a certain lower limit. In this region damping requirements become more critical. This is a severe impact to the design of hingeless rotor systems, which normally are assigned to use no auxiliary blade dampers. If it is possible, the amount of damping necessary to guarantee ground and air resonance stability should be drawn only from the blade structural damping. The BO 105 soft inplane rotor was aimed for that and is flying successfully.

One precondition for designing a soft inplane rotor without use of auxiliary blade dampers is a well founded knowledge of the material qualities with respect to strength behaviour and damping characteristics. The main questions are how much damping is basically present in the blades material and what are the factors influencing the amount of damping. Since only small damping is required to insure the avoidance of ground and air resonance instability a high level of accuracy is needed for a theoretical calculation of the damping requirement.

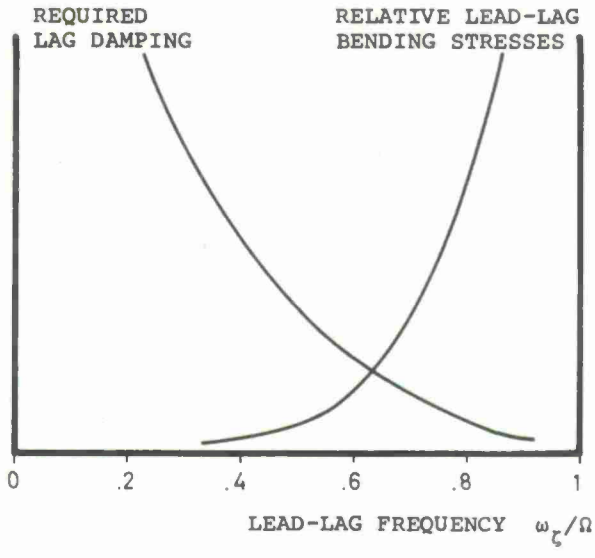


Figure 52 Lag damping requirement and bending stresses as a function of inplane frequency (qualitatively)

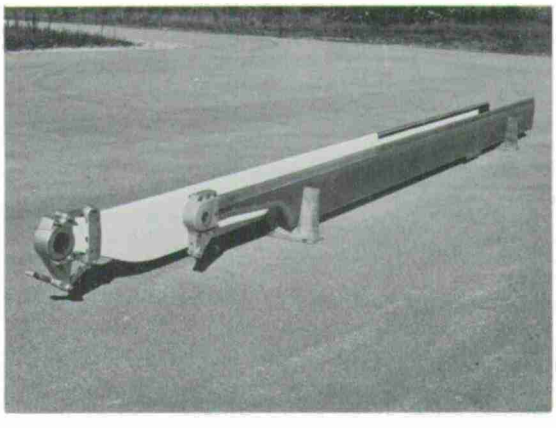


Figure 53 Fiberglass rotor blades with different inplane stiffness

The structural development process used by MBB in designing the BO 105 main rotor may be a good example for illustrating the optimization process in selecting the basic lead-lag frequency. During the initial runs of the test rotor the real first inplane frequency proved to be higher than calculated ($\bar{\omega}_\zeta \approx 0.85$) and too near to first harmonic resonance. Hence, chordwise bending moments were high and would have decreased the structural fatigue limit of the blade root section. Therefore, the inplane frequency was reduced by matching the blade's stiffness near the root. This could easily be achieved by reducing the chord of the blade in the root section (Figure 53). In addition a smaller rotor head built from titanium gave a further reduction in inplane stiffness with a final frequency ratio of 0.65. This ratio was found to be a good compromise. For this reduction a parametric analysis of all important flight conditions had to be conducted to insure that the reduced chordwise stiffness blades remained free from any ground and air resonance problems.

Recent analyses and experiments (38) indicate that additional effects on blade stability and rotor response can be produced by using the elastic coupling effects on rotor blades. There are many parameters, which influence the bending-torsions coupling and provide an additional source of blade damping. As an example, the use of low precone angle of the feathering axis can be highly stabilizing for a soft-inplane hingeless rotor (38). In general, elastic coupling effects will be useful in a rotor design if there is a complete understanding of the effect and if the design variables are tailored specifically. These effects will be discussed in section 5.7 in more detail.

5.5 Blade Tuning with Respect to Higher Harmonic Frequencies

Besides of the two fundamental parameters of first flapwise and inplane frequencies higher mode's frequencies must be considered too. It is indicated by measurements of aerodynamic forces and bending moment distributions (59), (60), that the blades are loaded with higher harmonic forces, which may excite higher natural bending modes. In general, the frequencies found are multiples of the rotor speed and can normally be observed up the 10th or 15th harmonic order. It can be derived from simple frequency considerations that higher harmonic blade bending moments occur if the exciting forces lie near to or are coincident with natural frequencies of the blade. In critical flight conditions, such as transition speed or landing flares, the contribution of higher order moments to the total bending moment may be as great as the sum of steady and first harmonic terms, or even greater. Thus higher harmonic stresses may considerably exceed the original value from conventional design criteria and may reduce the fatigue life of blades and rotorhub. One more inconvenient effect is a high vibration level in the helicopter. Figure 54 may prove that there is a direct connection between certain higher harmonic hub bending moments (rotating system) and the corresponding frequency vibrations in the fixed system.

First developments of helicopter rotors were actually done without considering higher harmonic stresses in flight. It was mainly the use of computational methods that permitted a blade design with refined selection of stiffness and mass distributions. To get a first feeling for the higher harmonic blade frequencies a "resonance" diagram should be used, as shown in Figure 55. This diagram is constructed by plotting the curves of uncoupled bending frequencies against the rotational speed of the rotor. A family of straight lines radiating from the origin indicates the harmonic order numbers. The intersection of any natural frequency curve with any order line notifies a possible resonance

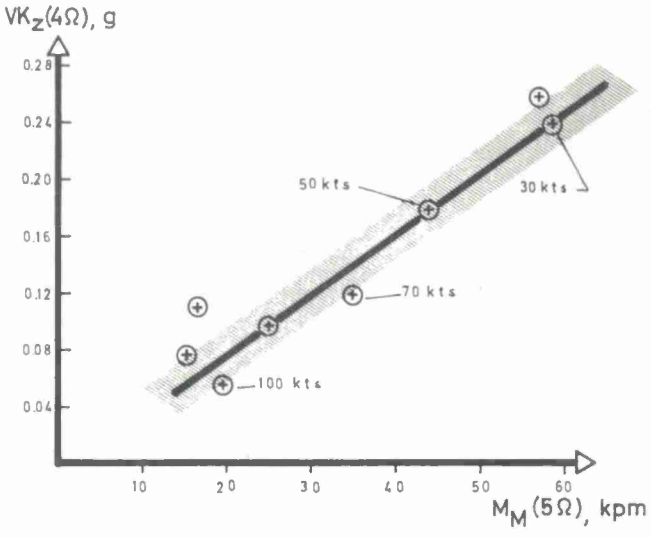


Figure 54 Crossplot of 4Ω-Vibrations (non-rotating system) versus 5Ω-Bending moments (rotating system)

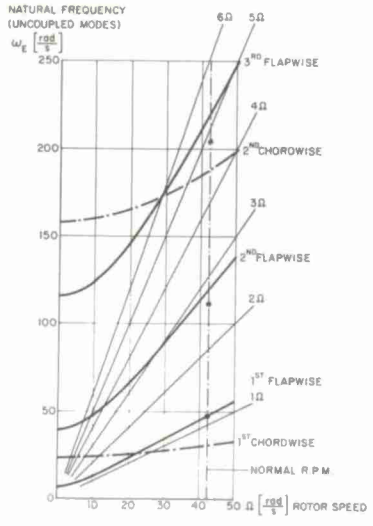


Figure 55 Resonance diagram

point. A fundamental design rule says, that no resonance point should be located in the normal operating speed range of the rotor. It can easily be seen from Figure 55 that it is difficult or even impossible to avoid higher mode resonance effects for all operating conditions.

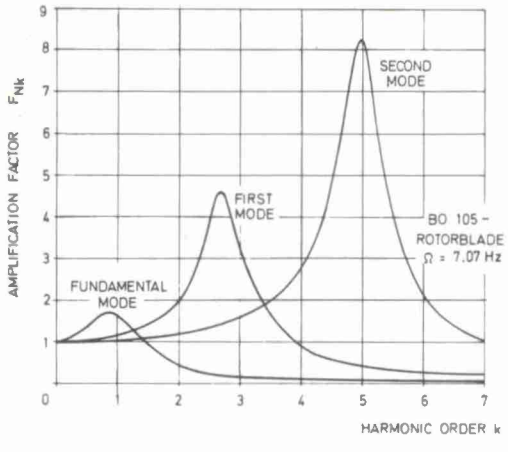


Figure 56 Dynamic amplification versus harmonic order

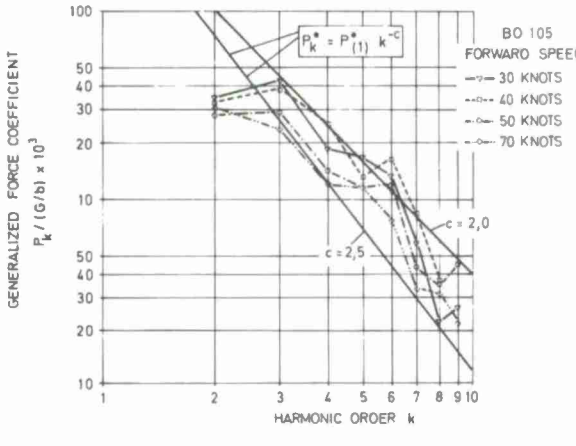


Figure 57 Generalized force coefficients versus harmonic order

5.5.1 Dynamic Amplification

Bending moments of a given harmonic order can be expressed by the static moment due to airloads and by an amplification factor by which the static moment is multiplied. While the resonance diagram permits an estimation of the natural frequencies separation from excitative frequencies, the amplification diagram is of interest when estimating the extent of amplitudes. Figure 56 presents plots of the amplification factors for the first three bending modes of a hingeless helicopter rotor blade (BO 105-blade). The curves show the amplification of blade forces of different harmonic order in different bending modes. There is an excessive increase of dynamic amplification with higher harmonic orders. It can be seen that when a 5th harmonic loading is in resonance with the third mode, the third mode static moments are amplified 16 times more than the second mode static moments produced by the same harmonic loading. Even higher amplifications occur on higher modes and higher harmonic loadings. One can see that higher order bending moments are very sen-

sitive to the higher harmonic airloads. This relationship becomes still more complex, when variations of the rotor speed are considered (61).

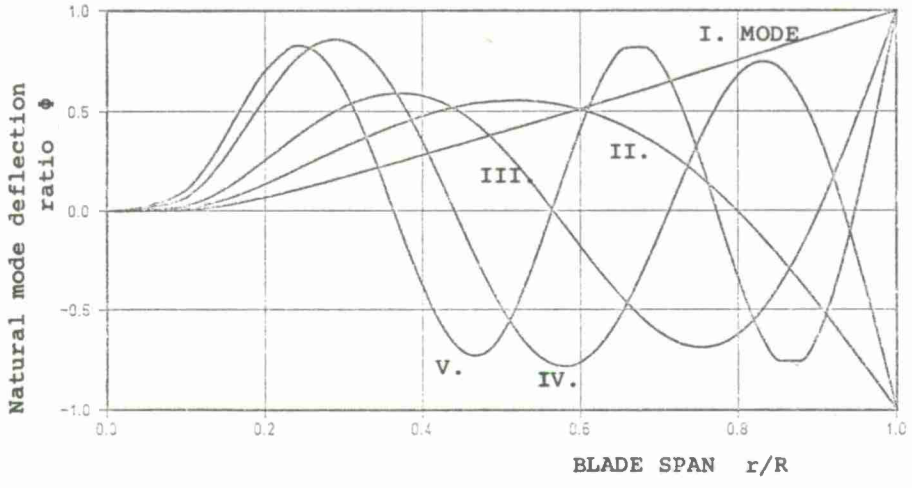


Figure 58 Flap bending mode shapes (I. to V. mode)

In order to get a rough estimation of higher harmonic blade bending during the preliminary design phase a relatively simple method for calculating the natural frequencies and bending modes can be used (62). With advance in the design phase the final blade mass and stiffness distributions are known, so that the exact frequencies and bending mode shapes and moment distributions can be calculated (Figure 58). With these values known the amplification factors and all other parameters, such as the equivalent mass and stiffness and the aerodynamic damping of the different bending mode can be determined (61). In this way an optimization of the blade design with respect to higher harmonic resonances can be performed. One difficulty in doing this is that the aerodynamic exciting forces are normally not known. Classical rotor theories are incapable of predicting higher harmonic blade loadings. Progress was made in the rotary wing aerodynamics in the recent years (34) (63), but up to now the wake and vortex problems and the nonsteady flow environment can not be treated satisfactorily. The existing theories are too complex to use them in the design phase. One proper means for the designer is to use empirical functions of higher harmonic airloads. Figure 57 shows a typical distribution of aerodynamic forces obtained at low transition flight speeds (64). It is noted that the magnitude of the generalized forces decrease with harmonic order number. Although the generalized forces exciting the higher modes are considerably smaller than those exciting the first and second mode, the resultant higher harmonic bending moments are of similar magnitude because of the larger amplification of the higher mode static moments (compare Figure 56).

5.5.2 Means for Reducing Higher Harmonic Blade Bending

In general, during the structural development process of the blade, attention must be focussed to avoid higher harmonic/higher mode resonance effects. This becomes more difficult with increasing harmonic order, as it was indicated by the resonance diagram (Figure 55) and by the amplification factor diagram (Figure 56).

A highly effective way of detuning certain blade natural frequencies is to change the blade mass and/or stiffness distribution. As an example, the proximity of the second flap bending mode to the 3P rotor harmonic can be reduced by increasing the blade mass locally at the loop of the corresponding blade oscillation. The frequency separation is indicated in Figure 55. Second and third bending mode frequencies are displaced from the resonance points with the 3P and 5P excitation frequencies, and, hence, the amplifications are reduced considerably. In addition, the corresponding natural bending moments are reduced providing a further reduction of vibration bending moments on the rotor hub. However, when tailoring the dynamic response characteristics of a certain natural bending mode, careful attention must be given to insure that no other bending mode is affected adversely. Figure 56 shows that reducing the second mode frequency too much would increase the amplification of the second harmonic order. One example of an optimized blade mass distribution with respect to favourable higher harmonic bending oscillations is shown in Figure 59 (BO 105-blade). A typical local mass increase can be seen at 40% spanwise position.

Question may arise, if the vibratory moments and therefore the vibration problem is influenced by the type of rotor hub itself. In general, it should be noted that increasing the first flapping frequency will also increase the higher mode frequencies. Therefore, hingeless rotors in the typical range of flapping frequency usually tend to have a

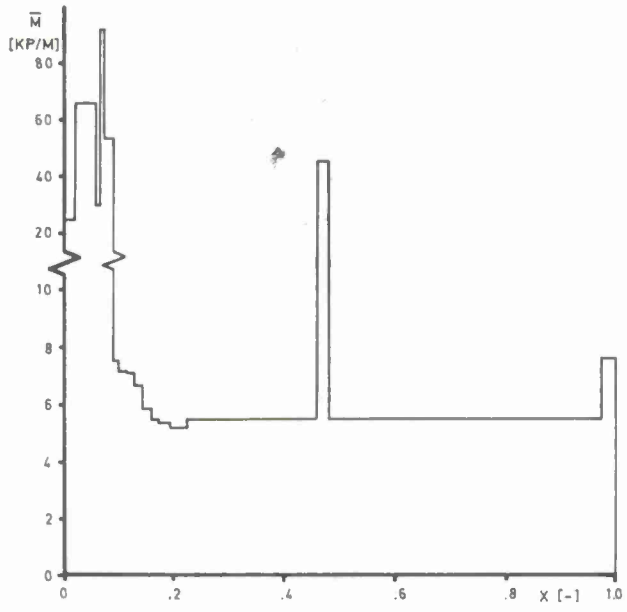


Figure 59 Blade mass distribution

proximity of the second flap bending mode to the 3P rotor harmonic order and eventually a similar condition at the point of 3th mode/5P exciation frequency (Figure 60). This tendency should be considered by the designer from the begin of blade design work, especially on four bladed rotors. In comparison, articulated rotors are characterized by a somewhat lower first mode frequency, which results in a similar reduction of the higher mode frequencies too. Therefore, there is a corresponding tendency to a second mode/2P resonance and a third mode/4P exciting frequency respectively. These resonance points must be treated very thoroughly especially on three bladed articulated rotors.

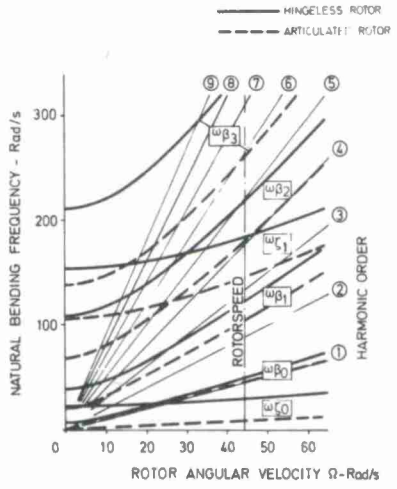


Figure 60 Resonance diagram

It is indicated by these results, that blade tuning with respect to higher harmonic resonances is a difficult task for the designer. The optimum blade design can - by nature - be only a compromise. Higher harmonic bending shows almost excessive parameter sensitivities. On one side this is an unfavourable fact, because several parameters can not be determined quite exactly with theoretical tools. On the other side this is good reason for optimism, because the designer is presented with means for improving the blade design. However, higher harmonic blade tuning must be started still in the beginning of design phase. It is much more difficult and very expensive, to modify the blades in the test or series production stage.

5.6 Blade Torsional Considerations

5.6.1 Rotor Blade Instabilities and Control Loads

The variable flow conditions over the rotor disc can result in a number of possible aeroelastic instabilities on the rotor blades ((15), (65), for instance). The most important phenomena can be collected as the classical flutter, static divergence, pitch-lag-instability, stall flutter, compressibility flutter and flap-lag-instabilities.

Considering fixed wing aircrafts, the classical aeroelastic instabilities are influenced mainly by the torsional stiffness of the wings. Helicopter rotor blades show even greater aspect ratios and they can normally not be mounted rigidly to the hub because of the control inputs. In addition the aerodynamic environment is far more complex in comparison to the fixed wing. In Figure 61 the stability margin's of the classical blade flutter are shown for the BO 105 over flight speed. With all axes concentrated to the 25% line the torsional frequency necessary to provide stable operating is relatively low. Tor-

sional frequency ratios of about 1.2 are normally far exceeded by the actual blade frequencies which lie about 3.0 to 5.0. An analysis of the torsional motion indicates that the elastic torsion of rotor blades is mainly influenced by the chordwise center of gravity position. The classical flutter and the static divergence phenomena depend on this mass center position (Figure 62). From these effects proper rotor blade designs should always be focussed to c.g. position at 25% or even forward ; some restriction can be made if high torsional stiffness is provided by special blade structures (thick profiles, for instance).

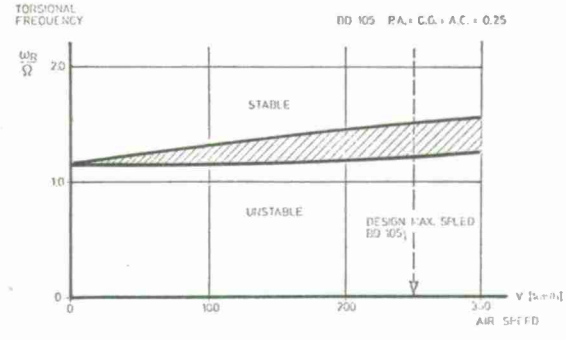


Figure 61 Stability limit for classical flutter

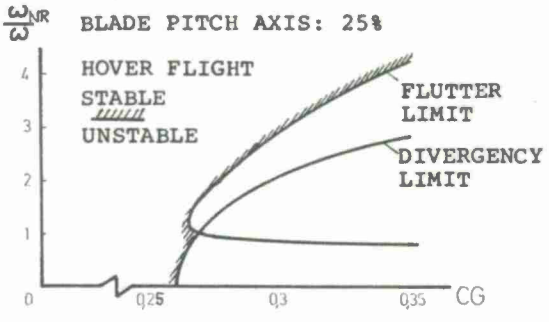


Figure 62 Effect of blade c.g. location on stability limits

Another severe problem of helicopter flight can be the stall flutter phenomenon. A rapid growth of control loads is observed when airspeed, gross weight or altitude are increased over a certain limit. The large control loads result from "stall flutter" which is a consequence of high angles of attack on the retreating blade side. This phenomenon became more and more important with increase of advance ratio and with highly loaded rotors. The normal way to encounter these difficulties and to withstand high torsional moments was thought to be an increase of the torsional stiffness. In contrast to that it was found by analytical investigations (17), (66) and by wind tunnel and flight tests that reducing the blade torsional frequency may reduce stall flutter control loads significantly.

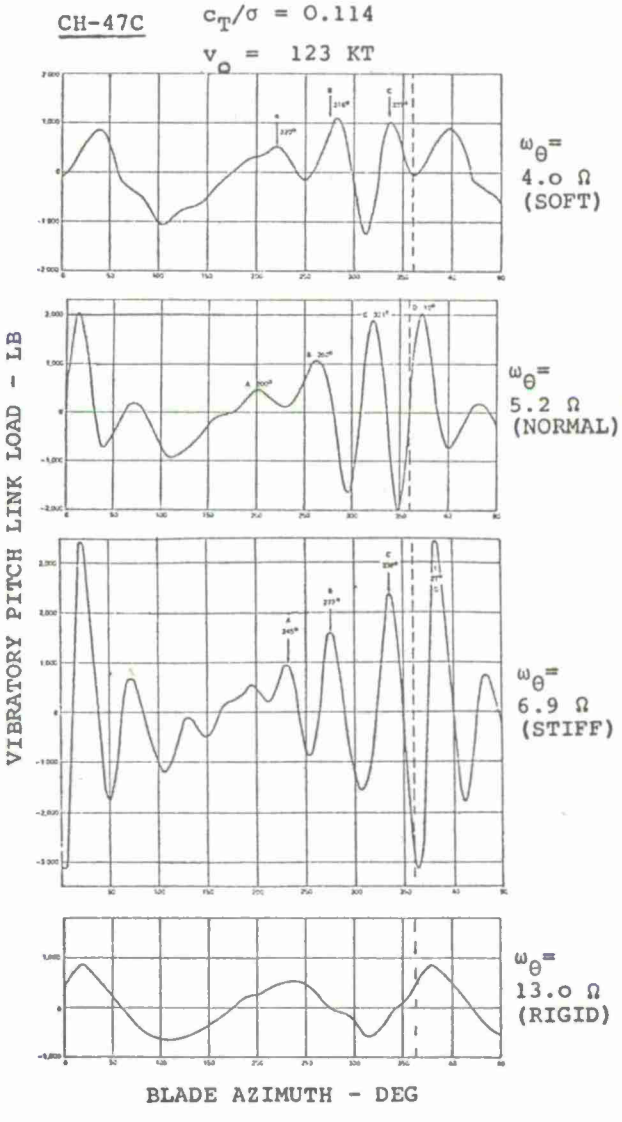


Figure 63 Pitch link load waveforms for rotors with different torsional natural frequencies (calculated)

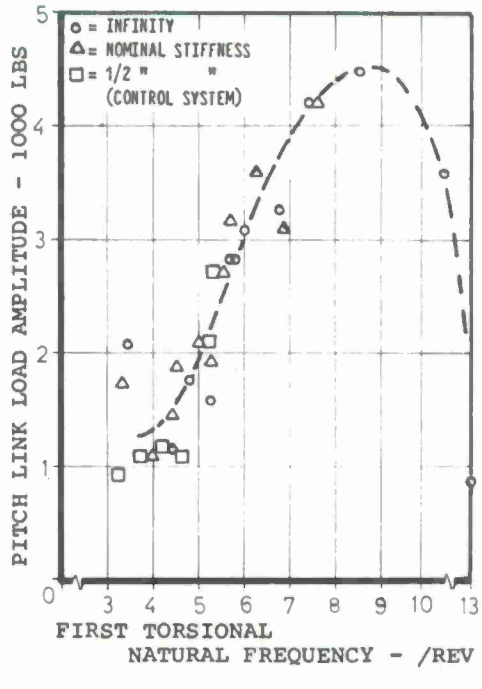


Figure 64 Stall flutter control load variation versus torsional natural frequency

To study this reduction in control loads Gable and Torzanin (18) have investigated pitch link load wave forms at different torsional natural frequencies from 3.1 to 13.0 Figure 63 taken from (18) shows that the higher torsional frequency blade can develop more pitch oscillations within the critical azimuth range. If the torsional frequency is very large, the elastic angles of attack may become too small to enter stall so that the pitch link loads are reduced again.

All these theoretical results are collected in Figure 64. Stall flutter control loads are reduced on both sides of the maximum region of about 8/rev torsional frequency. Natural frequency ratios of about 4/rev., which are typical for many rotor systems, are favourable in this respect. Increasing the torsional stiffness would amplify the control loads. A further reduction could only be gained with very high torsional frequencies which are not practicable on normal blade designs. The results of these investigations of (18) are of utmost interest to the design engineer. He seems to get more freedom in blade torsional tuning.

5.6.2 Influence of Torsional Elastic Coupling on Handling Qualities

In addition to the blade stability and blade load problems there are other torsional dynamic effects, which are of great influence on performance and flying qualities of a helicopter. The flight characteristics can be improved by elastic coupling effects using the coupling of the aeroelastic blade deflections in flapping, inplane and torsional directions. Regarding the moment capability, substantial gains can be obtained especially on hingeless rotor systems (27).

Some of the effects were already shown in connection with the aerodynamic blade design considerations (section 3.). The pitching moment characteristics (a.c.-position) proved to be of utmost influence on control and stability characteristics. In addition, the torsional elastic motions of the blade are equally influenced by the chordwise massdistribution (c.g.). In main, a coupling exists between the flapping motion and torsion, when the blade is unbalanced in chordwise direction (27). Considering a blade with the c.g. shifted forward towards the leading edge, the centrifugal forces produce a nose-down twist, if the blade flaps up. In fact, this is a blade integrated feedback system, if there is sufficient torsional flexibility in the blade.

As an example, Figure 65 shows the impact of the blade's c.g. position on vehicle angle of attack stability, which is a direct indication of the dynamic stability. The derivatives are shown for the isolated rotor and for the total helicopter. Shifting the blade c.g. forward by about 5% the angle of attack instability is reduced essentially to neutral stability. It is interesting to note that there are only small stabilizing effects with an articulated rotor. The reason is the low moment capability which makes it nearly insensible to the small elastic control inputs (27).

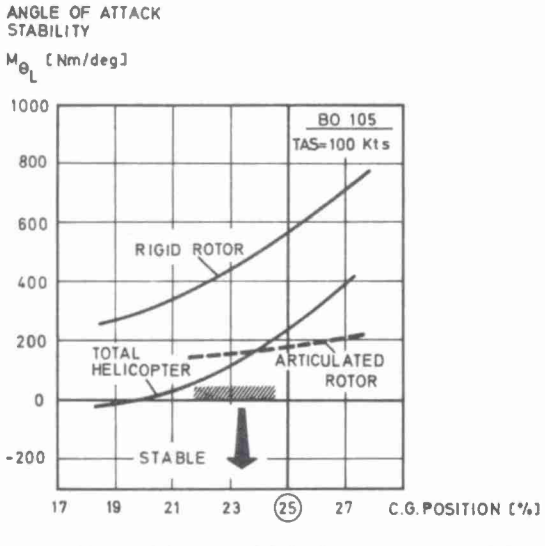


Figure 65 Effect of blade c.g. position on the angle of attack stability

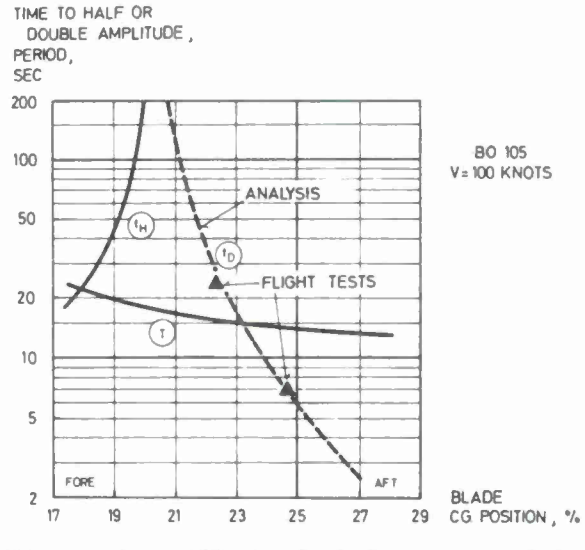


Figure 66 Effect of blade c.g. position on longitudinal dynamic stability

A blade design with c.g. forward of the quarter chord axis will influence the dynamic stability too. A broad variation of the c.g. position is shown in Figure 66, illustrating the time to double amplitude and the period of the critical longitudinal helicopter motion. A forward blade c.g. position provides the blade with positive stability and hence dynamic stability is improved with forward c.g. locations. Normal torsional flexibility of fiberblades are considered here and therefore the improvements seem to be remarkable. There is good correlation between analysis and flight test data, which were achieved by adding a concentrated 7-pound weight on the blades leading edge (38). The improvements in flying characteristics consist not only of increasing times to double amplitude, but also of increasing oscillation periods. This is a favourable effect which results from the im-

provements in damping behaviour. The period is increased over the 20 sec point, which is an important criterion in the MIL-H-8501A specification (3), for example. In general, the favourable parameter trends are in accordance to the requirements of blade stability and control loads (c.g. forward, only moderate torsional stiffness). In blade torsional tuning the fiberglass technique proves to be most advantageous. Blades can normally be modified to include high c.g. offsets and a wide range of torsional natural frequencies.

5.7 Hub Geometry Design

One main task in rotor layout is the design of the rotor hub. There are many parameters in this area which might influence the final construction. Naturally, the basic hub design is determined by the rotor concept, which is - by nature - quite different for articulated rotors, semirigid rotors, hingeless rotors and "rigid" rotor systems. A short description of the most important features of these different rotor concepts was given before. In general, all types of rotors can be summerized in their dynamic behaviour by only a few fundamental parameters. Flapwise, inplane and torsional frequencies have already been discussed. In comparison to these parameters other more geometric parameters are of paramount importance. In the following part the most important design parameters and some of the major problem areas affecting the design of the rotor will be discussed. It should be noted that rotor hub design aspects are more important for hingeless rotors than it is the case for conventional articulated rotors. There is a much higher degree of interrelation between the various elastic couplings, and at the same time the effects obtained, are much more effective.

5.7.1 Hub and Blade Unloading

One basic principle in designing the rotor hub geometry is to provide unloading effects on the structure. This can be done, for instance, to a certain degree by preconing the hub arms in flapping direction. This simple relationship is illustrated in Figure 67, where the root moments of a hingeless rotor are shown for a 1° cyclic hover condition. Precone offers the advantage of cancelling the steady moments caused by blade lift. Normally the precone angle will be chosen with respect to the design rotor thrust. Other thrust conditions and alternating thrust of the blades will result in corresponding moments at the hub. The reduction of steady moments in the blade root and rotor hub section is quite important on hingeless rotors as they produce moments which are an order of magnitude greater than on articulated rotors.

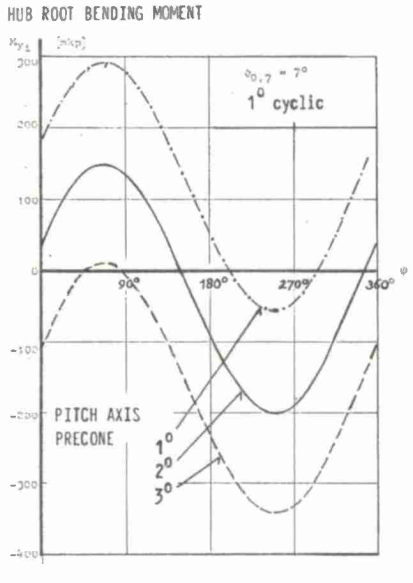


Figure 67 Effect of precone angle on medium hub root bending moment

Similar relieving effects can be obtained in the inplane direction by blade sweep angles. By sweeping the blade's spanwise axis forward or aft the centrifugal force is permitted to cancel the blade moment caused by the rotor driving torque. However, similar to precone blade sweep may also change the relative blade position with respect to the pitch axis and may produce higher control moments. This is again followed by a change of the pitch-flap-lag-coupling behaviour of the elastic blade. It can be concluded from that, that precone and blade sweep angle cannot only be selected from the blade loads standpoint but must be considered also under the aeroelastic aspect.

5.7.2 Torsion due to Blade Bending

When looking on several rotor hub/blade constructions one may observe considerable differences in the type and location of hinges or in the mode of flexibilities of blades and hub. Recent investigations (27), (67), (68) of the basic design concepts have indicated that there is quite a lot of kinematic or elastic coupling effects depending on the blade and hub configurations. At the present time rotor research work is largely concentrated on these effects in many companies and the understanding of the elastic coupling behaviour is growing. This development was stimulated largely by the development of hingeless rotor systems as they show a coupling behaviour which is much more pronounced than is the case for articulated rotors.

Using the relationship between the flapping and inplane moments and the elastic reactions in the blade, the local pitching moment can be expressed by the formula (11)

$$\frac{dM_{\Theta}}{dr} = M_{\beta} \cdot M_{\zeta} \left(\frac{1}{EJ_{\beta}} - \frac{1}{EI_{\zeta}}\right) .$$

It can be derived from this relationship that blade torsional moments are determined by the flapping and inplane moment distributions along the blade and by the corresponding

stiffness distributions. Local torsional moment can be procuded only in those sections, where flapping and inplane bending moments are present and where flapping and inplane structural stiffness are unequal. On hingeless rotors the first condition is fulfilled especially in the inboard region of blade span where the moments rapidly increase. These relationships are shown qualitatively in Figure 68. Flapping and inplane stiffness are "matched" in the inboard region up to that point, where the airfoil section begins. The product finally results in a local torsional moment distribution as illustrated. It should be noted that the maximum torsion-flap-lag coupling is in the region of the blade root, hence, all inboard blade sections and the control system are affected by the torsional moment due to aeroelastic coupling. The magnitude of the resultant coupling depends on the torsional flexibility of these parts, which is normally determined by the relatively flexible kinematics of the control system. Therefore, the coupling characteristics of a hingeless rotor system is largely determined by the spanwise location of the pitch bearing in comparison to the blade location, where the bending moments and hence the torsional moments are high.

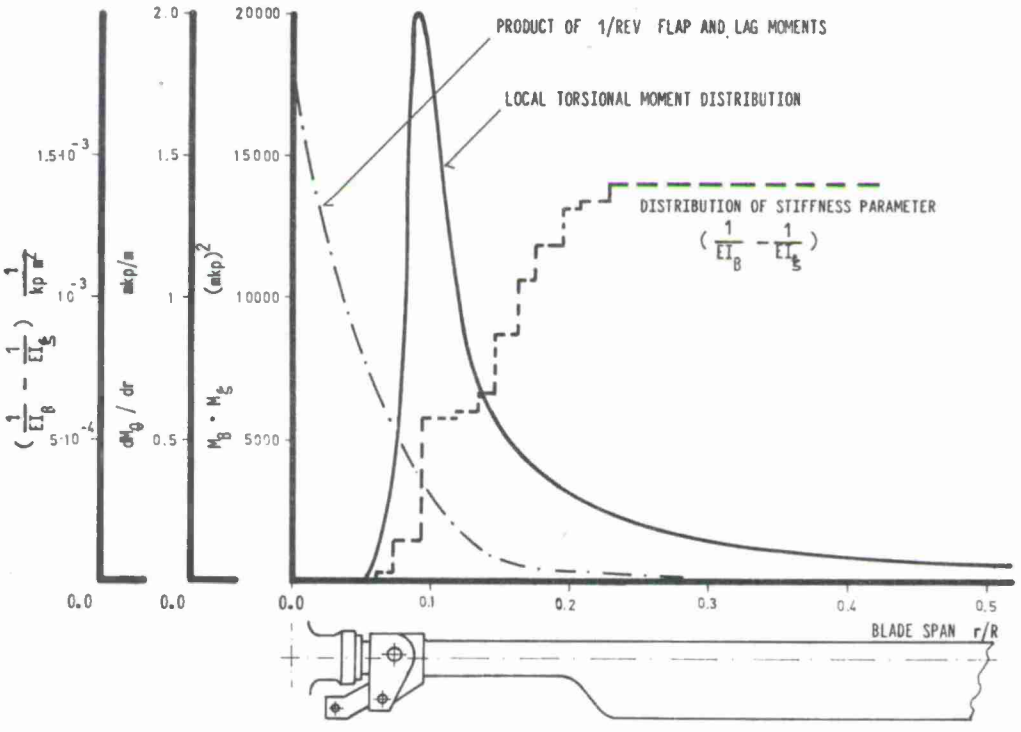


Figure 68 Typical torsion - flap - lag coupling on a hingeless rotor blade (Bo 105)

It can be derived easily from the above relationship that the coupling characteristics of a rotor system can also be described by the blade's rotating frequencies: To eliminate all torsional moments from blade bending the condition $1 + \bar{\omega}_\zeta^2 - \omega_\beta^2 = 0$ must be satisfied (matched stiffness). Considering a typical hingeless rotor with a flapping frequency of $\bar{\omega}_\beta = 1.12$ (BO 105) the inplane frequency ratio must necessarily be $\bar{\omega}_\zeta = 0.5$, if an elimination of all torsional coupling is desired. However, there is a lower limitation in inplane frequency choice dictated by the ground and air resonance phenomena (see Chapter 5.4.2).

Ormiston (67), summarizes the different parameter influences very vividly by introducing an elastic coupling parameter R. This parameter represents the division of blade flexibility inboard and outboard of the pitch bearing and gives a good indication of the magnitude of the elastical coupling characteristics of a rotor blade. An example of a rotor configuration with nearly negligible torsion-flap-lag coupling effects is given by the WG-13 rotor of the Westland company (Figure 70 from (67)).

The quite opposite design philosophy is to use the substantial torsional deflection effects positively and to introduce benefitial effects into the rotor system. This technique is realized in the BO 105 hingeless rotor system of MBB (Figure 69). In this concept the pitch bearing is located in the most inboard section of the rotor hub so that the blade bends away from the pitch axis, showing a powerful elastical pitch-flap-lag coupling. Frequency matching ($1 + \omega_\zeta^2 - \omega_\beta^2 = 0$) is not desired in this rotor design and therefore, the inplane frequency selection could be done with more freedom ($\bar{\omega}_\zeta \approx 0.65$).

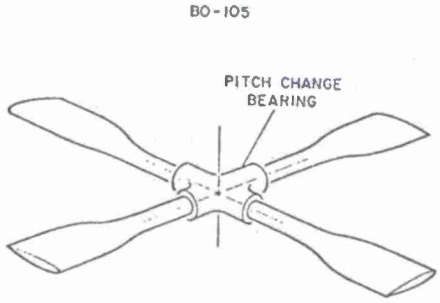


Figure 69 Sketch of Bo 105 rotor hub, elastically coupled

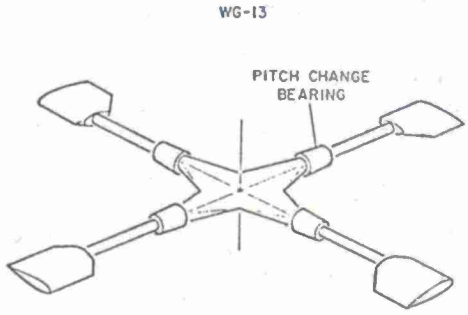


Figure 70 Sketch of WG-13 rotor hub, elastically uncoupled

5.7.3 Parameter Sensitivities

Recent analyses and experiments (38), (68) have shown that the benefits especially of hingeless rotors can be further enhanced to a high degree by using aeroelastic coupling effects. The improvements may be extensive, including the rotor response in general, flight dynamics behaviour and even ground- and air-resonance stability as well. Naturally, a complete understanding of all the important parameter influences is necessary, to make a good rotor design.

5.7.3.1 Influence on Flight Dynamics Behaviour

Two essential hub parameters with influence on the flight dynamics behaviour are blade precone and sweep angles. When analyzing their effect one should consider the importance of the blade root moments again, as was indicated in Figure 67. Both steady flapping and steady inplane root moments can largely be changed by precone and sweep angle and it is quite evident that these angles will influence the torsion-flap-lag coupling. Figure 71 shows some results of a study, illustrating the effect of the sweep angle on the elastic pitch torsion. The coupling is strongly influenced by blade sweep, and can be related directly to an equivalent δ_3-angle. Forward sweep results in negative δ_3-angles, rearward sweep in positive δ_3-angles (negative pitch-flap-coupling). Considering normal flexibility a δ_3-effect of 10^o is obtained per one degree of sweep angle. In this case, similarly the elastic δ_3-behaviour is influenced by precone of the feathering axis and by the inplane stiffness of the blade .

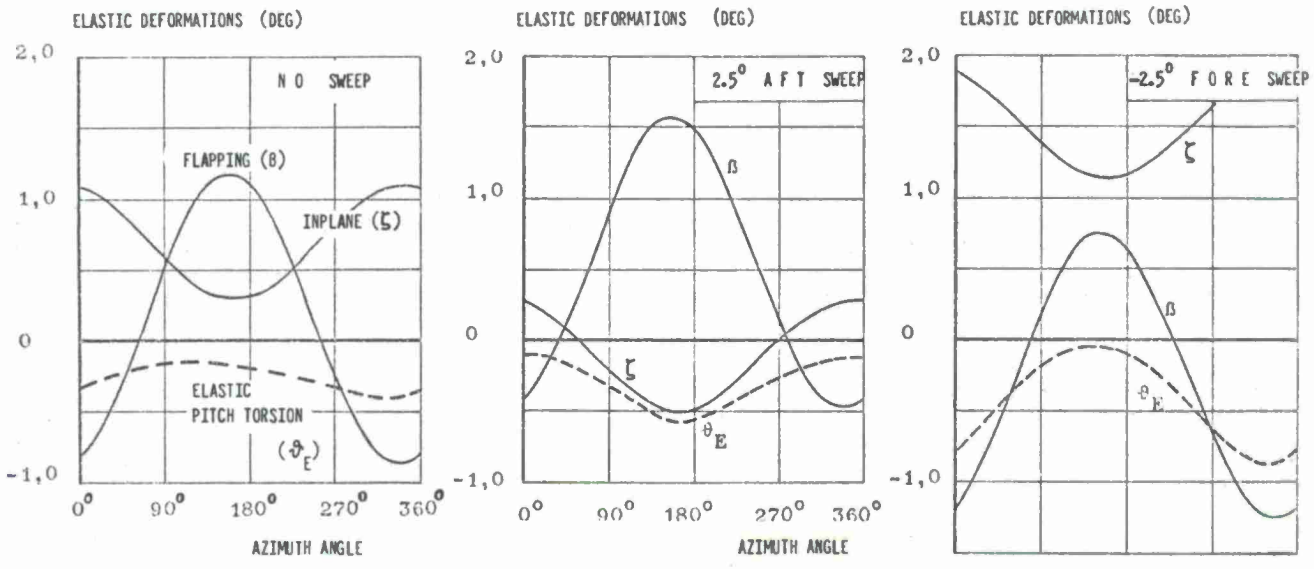


Figure 71 Influence of blade sweep angle on the elastic pich-flap-lag coupling

The effects of sweep angles are in accord with the typical δ_3-behaviour, which might be seen from Figure 72 . There are illustrated the angle of attack stability and the pitch damping moment of an isolated rotor in forward flight (27). The large pitch-up destabilizing moments, which can be a serious problem for hingeless rotors at high speed

flight, can significantly be reduced by introducing blade rearward sweep angle. However, as a second effect, the rotor damping is reduced too, so that the longitudinal dynamic stability can only be slightly improved by sweep angle. It should be noted that both effects are gained by lowering the fundamental flap frequency. Thus the hingeless rotor shows a trend towards the articulated rotor in its general rotor hub moment response, when blade sweep back is applied. Similar impacts are obtained by various other coupling parameters, such as precone angle of feathering axis and torque offset. It is an important conclusion from these effects that hub geometry design must not only consider requirements of steady moments, but must regard dynamic effects too.

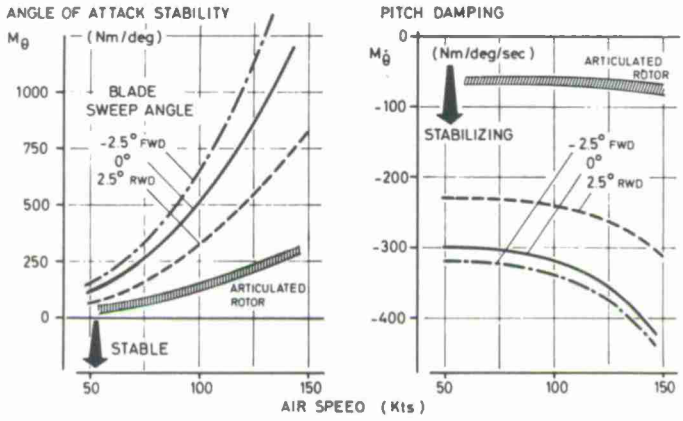


Figure 72 Effect of blade sweep angle on piching moment derivatives in forward flight (isolated rotor)

When considering all these benefitial aeroelastic effects it can be stated that the powerful influences of rotor hub parameters can be used to change the flight dynamics behaviour and to tailor the rotor characteristics in general. This might be indicated by the control characteristics diagram (Figure 73). It is shown there that the possible range of a hingeless rotor can be highly enlarged by using the aeroelastic coupling effects. First, control power and damping can be changed unidirectionally by increasing or reducing the flapping stiffness. It should be noted that the same effects can be obtained by a proper selection of the main hub parameters. This seems to be of utmost importance, because the selection of the flapping frequency is normally subject to certain limitations and is often impractical beyond a certain point. Hence, flapping frequency is, to a certain degree, interchangable with coupling effects. In contrast, by varying the c.g.-a.c. offset of the rotor blades a change of control characteristics is provided which is perpendicular to the normal slope: A c.g.-forward blade will increase damping and will reduce control power. Therefore, by properly combining the flapping stiffness and torsional-elastic coupling effects a wide range of control characteristics can be obtained and the rotor design can be tailored exactly to the customers requirements. This counts not only for the control behaviour but also for all flight dynamics characteristics. It should be noted in Figure 73 that applying the same effects on articulated rotors would only result in small variations.

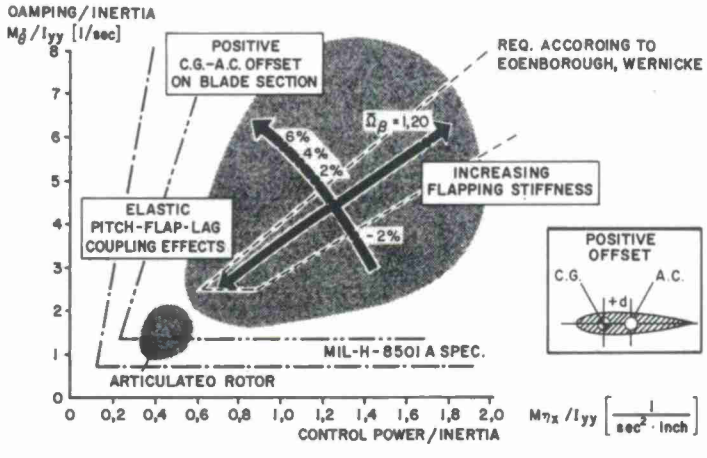


Figure 73 Possible range of control characteristics with a hingeless rotor system

5.7.3.2 Influence on Rotor Blade Stability

As discussed above, the blade stability problems can be significant determining factors in the general rotor design. Ground and air resonance was shown to be one main

phenomenon in this field. The choice of lead-lag frequency was governed by the rotor blade stability and the question of blade structural damping was an essential one for soft inplane hingeless rotors.

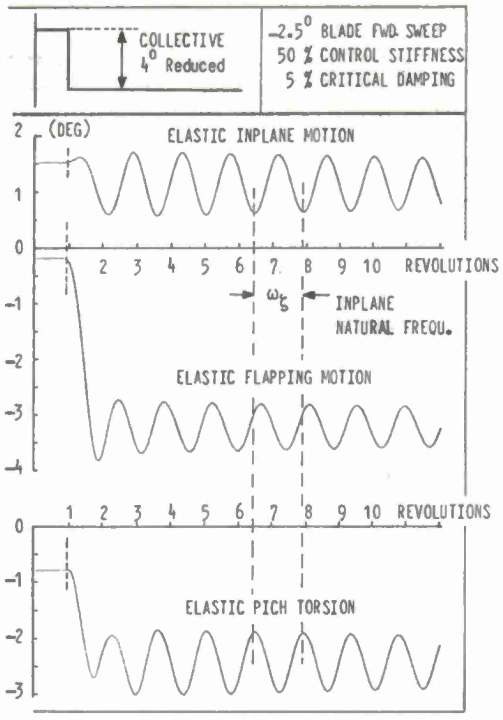


Figure 74 Time history of a typical pitch-flap-lag coupling motion

Furthermore, advances in understanding the aeroelastic behaviour of rotor blades permits the blade stability problems to be treated more intensively. As it is well known, kinematic pitch-lag coupling can highly influence blade stability. As an example, pitch-lag instability was encountered during tests of a model rotor (70). The origin of the oscillations could be shown to be the kinematic properties of the blade linkage that caused pitch to be reduced as the blade lagged back. It became apparent by these tests and by analysis (70), (71) that negative pitch coupling shows the tendency of increasing blade oscillations and may cause blade instabilities.

A typical case of elastic pitch-lag coupling is illustrated in Figure 74. After lowering the collective pitch from hover setting, a coupled oscillation in the inplane natural frequency starts, although there is no further excitation (hover condition, no cyclic!). The oscillation is nearly undamped. This seems to be somewhat surprising when considering the high aerodynamic flap damping and the 5% structural inplane damping involved in the system in this case. The exploration of this phenomenon can be derived from the elastic coupling of the pitch and lag motions, which is a pure case of negative pitch-lag-coupling (lag forward, pitch up). The curves are for a special case of an unfavourable rotor design (38).

In Figure 75 some more results are collected showing the elastic pitch-lag-coupling factors as a function of collective pitch (rotor thrust). These factors were obtained from calculating time histories as shown in Figure 74. In general, higher collective pitch setting results in negative factors, which stands for positive pitch-lag coupling. This is a stabilizing effect on the system stability. In addition, the feathering axis precone angle is varied in this diagram and it can be seen that this parameter will definitely affect the type and amount of pitch-lag coupling. High precone angles result in destabilizing effects and with 5° precone, for instance, an elastic coupling factor of about 1 degree torsion per 1 degree lagging occurs. This means a quite severe unfavourable coupling, which affects the rotor stability extremely bad. Conversely, a zero precone angle results in improved coupling behaviour and will act highly stabilizing.

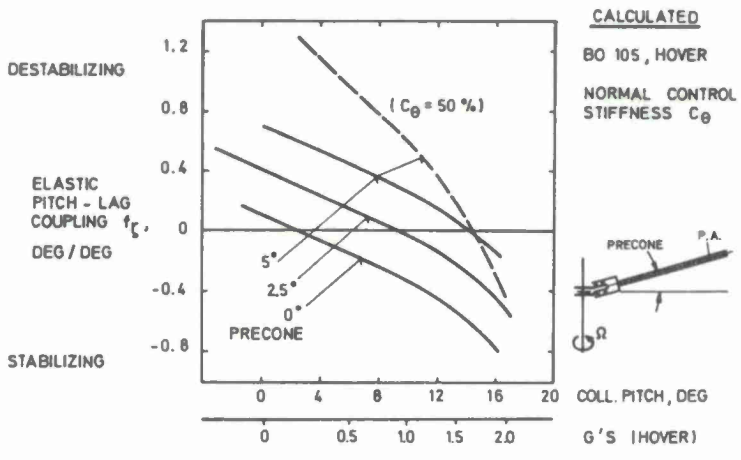


Figure 75 Effect of pitch axis precone on the amount of pich-lag coupling

Now, what are the influences on blade damping and ground- and air resonance stability? Figure 76 shows the stability characteristics of the blade over collective range (38). There is illustrated the lead-lag mode damping with all degrees of freedom of the hub fixed. This will give an indication of the isolated blade damping behaviour.

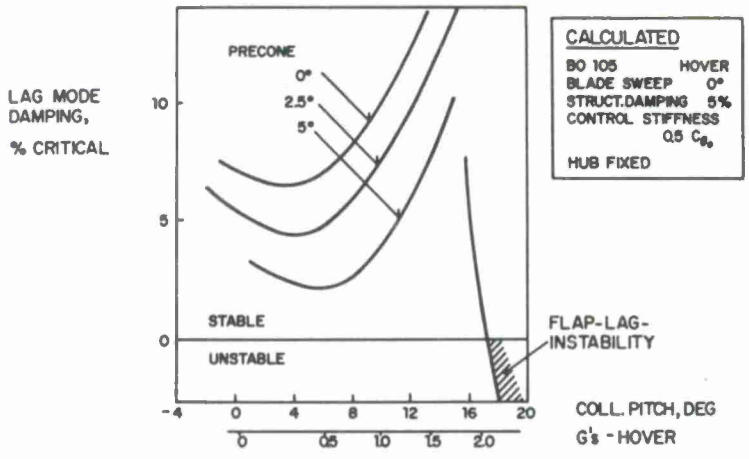


Figure 76 Effect of pitch axis precone on lag mode damping (rotating system)

A minimum of damping occurs in the low thrust region and with increase of collective pitch, damping is increasing, too. The elastic pitch-lag coupling efficiency of precone angle is indicated in this Figure by a highly stabilizing effect on the lag motion. The deterioration of lag damping with high precone angles is evident, showing that a 5° precone hub is acting against the structural damping of the blades. Conversely, a zero precone angle increases the blade damping.

Similar effects are provided by other hub parameters, such as blade sweep and control stiffness (27). The trends shown here are in full agreement with model testing carried out with a BO 105 soft inplane hingeless rotor model (28" rotor diameter) by the Boeing-Vertol Company (68). They are further confirmed by the findings in (67), (69).

It becomes apparent from these few examples that elastic coupling effects might be of significant benefit. The powerful influences of precone, blade pre-sweep and control stiffness, for instance, can be used by the designer to improve the rotor damping behaviour and to tailor certain rotor characteristics. This seems to be of utmost importance expecially for soft inplane hingeless rotors, which may have problems with inplane damping. Elastic coupling effects are most helpful for the designer in compensating a lack of structural damping by a proper hub geometry.

6. OPTIMIZATION TECHNIQUES

6.1 Formal Techniques

Even until today there is to realize a certain rejection against the full application of electronic computers in the practice of an aircraft designer. The explanation for this astonishable circumstance may to be found in the first generation of electronic computers which were proclaimed as the philosophers' stone but which were available only for a limited class of problems, i.e. those with exact solutions. Contrary to that class of problems direct solutions are no more possible in modern aircraft design. Therefore a designer is forced to apply an approximiation method, e.g. an iteration procedure. Appropriate for this type of calculus he can work now with the new generation of computers. Another reason for the past somewhat deeply-rooted rejection in the circles of designers may have been that there was only few or actually no applicable optimization software. The steep ascending tendency in the rotor aircraft design and development concepts is to integrate numerical methods more and more in order to optimize several parameters. The aim is at first to find certain algorithms which can be translated in digital computer language.

The research can generally be divided in two different types. The first one includes the cases, where the problems can be expressed as a function of variables, here parameters. Mathematically seen, those n parameters in the objective function

$$I = f(x_1, \ldots x_n)$$

can be expressed as the components of a vector belonging to a n-dimensional space with the well-known Eucledian distance between two points. More detailed information about this mathematical problem is given in references (72) and (73).

The second circle of problems can be described in a system of ordinary differential equations. The investigation here tends to a variation problem. The task now can be defined as the selecting of a variation (e.g. within a certain time interval) with given initial and boundary conditions, so that the integral (e.g. over time) becomes an optimum.

Often used procedures in this circle are those of Ritz and Galerkin (74),(75) to get an approximate solution. It may be emphasized that the only difficulty in applying those numerical methods - besides the computer's costs, of course - is to define the optimization goal and to select the real representative variables.

The next step will be to develop a proper mathematical model using all those selected variables or parameters x_i. The following step will be the development of a system model. Especially in this part the experienced engineer and designer can influence the development with his knowledge. This is a wide, often untouched field. The rest is fixed by the computer's narrow ways. Neither the already mentioned direct method nor the direct enumeration scheme will be satisfactory, especially because of the computing costs. There are, of course, many programs which could be used for optimization, but often they are only applicable for a certain class of functions. Hence, for problems with a multiparameter function, refering to the first type of problem, really efficient search methods (e.g. multidimensional) are required. In the U.S., for example, a multisearch method like AESOP (Automatic Engineering and Scientific Optimization Program, developed by the Boeing Comp.) was used which contains nine various numerical optimization methods (for example "Quadratic Search", "Random Point Search" or "Pattern Search").

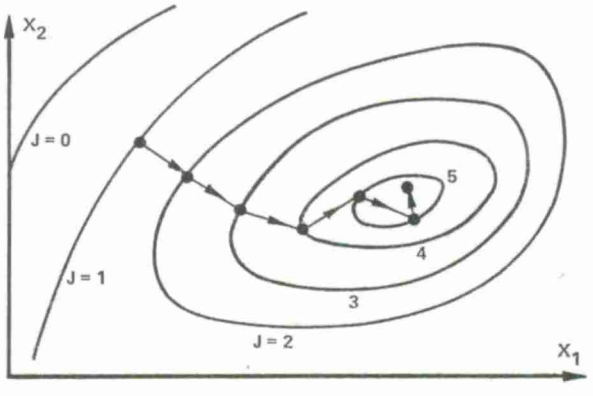


Figure 77 Typical steepest descent search

In reference (72) W.Z. Stepniewski describes the various search techniques and some of their applications. One technique, the "Steepest Gradient"-method, may be quoted here as an example. The idea is, as shown in Figure 77, to crystalize the direction of the greatest change of the function I which will indicate the way to the desired extremum. Beginning with a certain initial value of I the partial derivatives, simply shortened with the Nabla-Operator ∇I, are to be computed. With that, the direction of the gradient is obtained. Then you have to follow this direction in a certain length s. Repeating this procedure, a point must be reached where $\nabla I = 0$, which means that an extremum, either minimum or maximum, is reached.

In AESOP all nine search-techniques are combined as preprogrammed algorithms so that a multivariable search is formed. Figure 78 indicates schematically how AESOP is linked with an engineering model.

Maximum and minimum variable values are inputted in a name-list format to AESOP, along with the search or combination of searches desired. AESOP automatically feeds various combinations of the parameters to the model. After the desired number of performance evaluations, AESOP reports the best performance found.

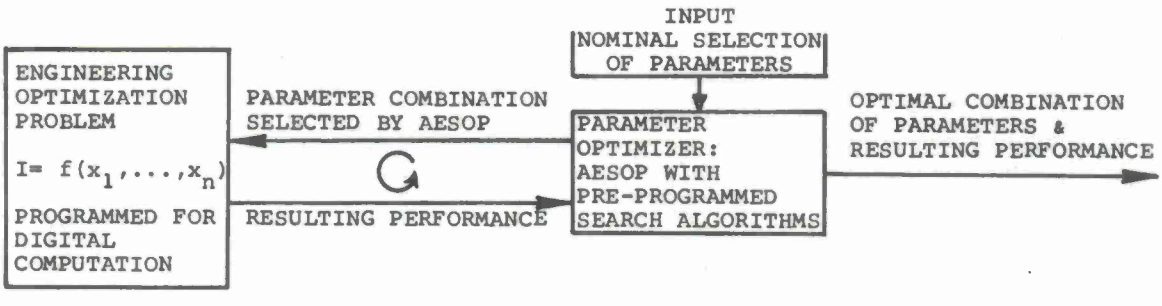


Figure 78 Scheme of optimization process with AESOP

A similar application of numerical optimization methods in Germany was aimed on the development of better aerodynamic design of rotors and propellers. Figure 79 may show schematically the propeller design procedure, applicated to the propeller of the VC 400, a German VTOL-aircraft (76). Contrary to the concept of Stepniewski characteristical flight conditions were set. As Figure 79 shows, there is a main optimization program including the

different subprograms, as needed. Parallel to thrust- and power-calculation the blade weight is computed. Out of these dates a goal function is analysed. With the computed value of the goal function new blade dates are determined. This iteration process is running as long as the optimum is reached.

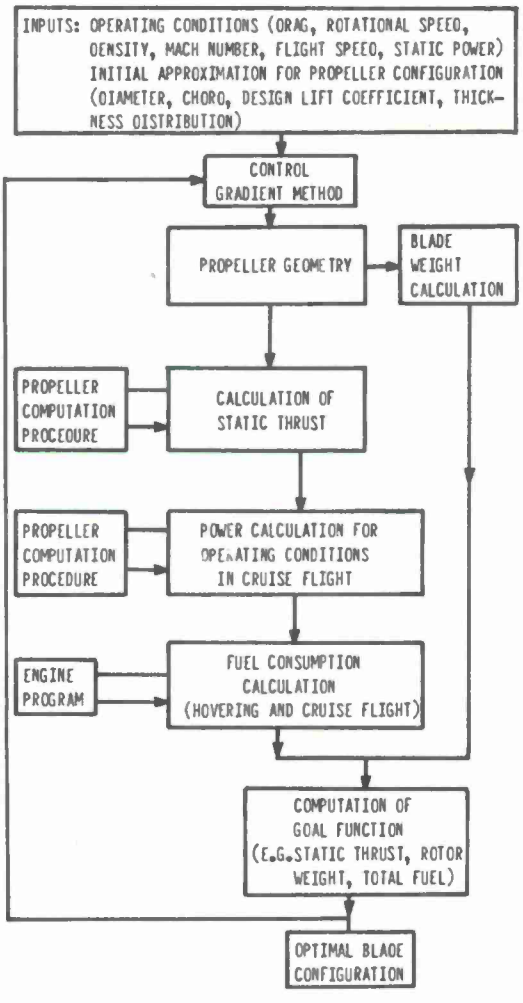


Figure 79 Automated V/STOL propeller design program

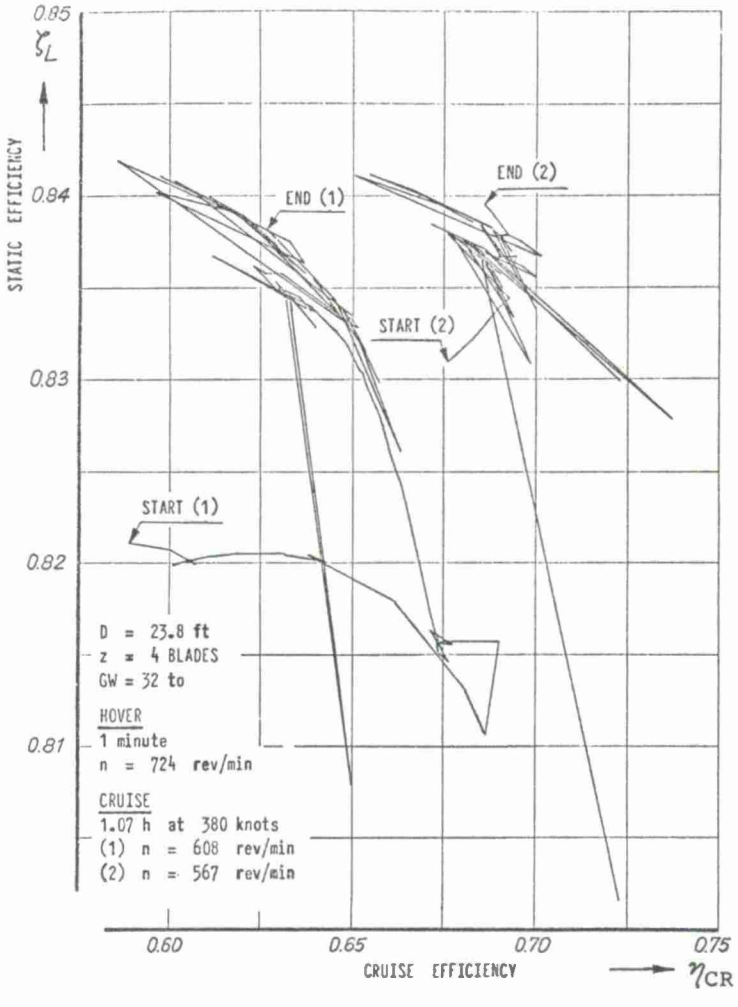


Figure 80 Typical program steps in the performance envelope during the optimization process

Applying all these conditions several VTOL-Rotors were optimized for typical missions. Figure 80 shows the - sometimes erronious - ways of the procedure in the plot of static rotor efficiency (ζ_L) versus cruise flight efficiency (η_{CR}). The goal is to get an optimum somewhere in the upper right corner. A second start was done during this process as the initial rotor tip speed proved to be too high for getting acceptable cruise flight efficiency. The typical performance envelope shape can be observed. The optimum of the prop/rotor configuration is defined by the point of tangency of the last step.

In conclusion, the following important points should be noted:

1. A clear definition of the optimization goal and of all interesting accessory conditions is of utmost importance.

2. The analytical methods for predicting rotor performace are decisive, because they basically influence the useful load, of course.

3. In optimizing rotors/propellers for high cruise speeds the transonic profile characteristics are of utmost importance.

6.2 Iterative Design Processes

In the preceding section the application of formal optimization techniques in aircraft design was described. Multisearch programs, as exemplified by AESOP, appear most suitable for some types of optimization problems encountered in the design and operation of aircraft. As a typical example of application,the maximization of a propeller with respect to static and cruise efficiency was shown. In contrast to conventional engineering practice, this design task can be solved by multisearch programs within minutes or hours, rather than in weeks or month.

Other examples of application are discussed in (72) in the field of aerodynamic prop/rotor design for tilt-wing and tilt-rotor aircraft and in helicopter design. This problem is much more complicated than that of the figure of merit maximization, because the preconditions have to be much more developed. In the case of a prop/rotor optimization a basic compromise is already required. In a helicopter rotor design optimization the cruise conditions are characterized by the edgewise translation with rather excessive variations in the flow conditions. Of course, cruise flight theories and computer programs can be included and can be handled by the total program as well. Stall flutter limits, comprised by C_T/σ boundaries could be introduced as additional constraints on the solution.

However, formal optimization techniques always depend on the quality and simplicity of the mathematical and analytical models used.Constraintslike stall flutter, maximum lift boundaries and dynamic blade properties are complicating factors which make the whole process longer and less clear. The problem is that, although hovering figure of merit and general performance are still main design criteria, modern helicopter and rotor designs will come more and more to the real physical boundaries, where the limitations on operational capability are mainly related to the rotor dynamics/aerodynamics. They will define the scale of the real problems and will finally determine the design. Formal optimization processes are less suitable to handle these special problems.

In addition, today's helicopter developments are characterized by great efforts in the structural field. Much progress in rotary wing technology has come from advances in structural dynamics, vibration control and in materials and fatigue life. It is recognized that the total design process is an iterative one involving elements of geometry, mathematical analysis, constructive inputs and manufacturing constraints.

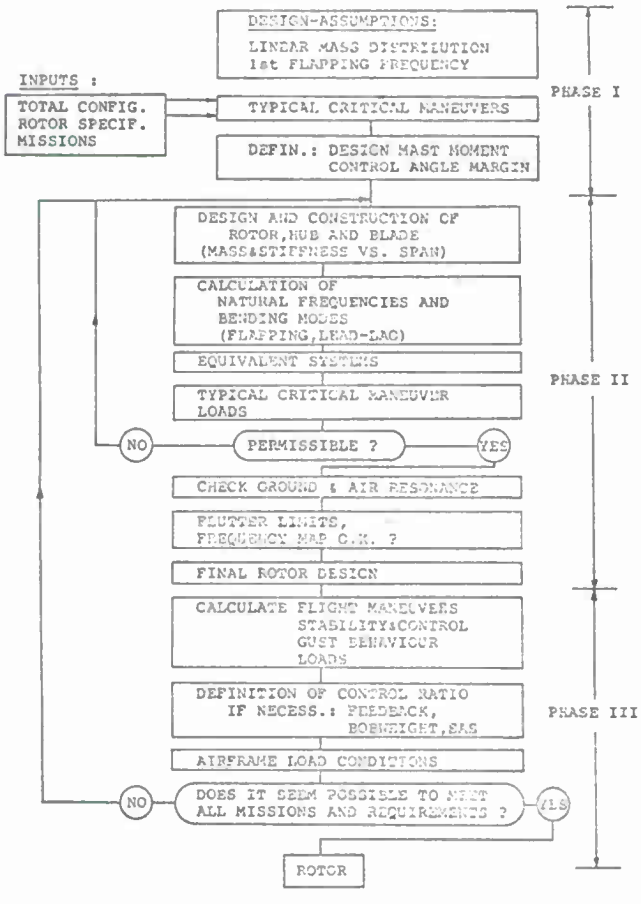


Figure 81 A way to design a rotor system

A schematical flow chart in Figure 81 shows the way of an aerodynamic-dynamic and constructive iteration process. The stress is layed on the dynamic-constructive field in this case (78). There are basically three phases involved. The first serves to elaborate a design specification using assumptions appearing reasonable, as well as simple considerations. The alternate bending moment on the rotor mast is used as a reference point for all considerations in this case. By fixing the geometry and force conditions for the junction of rotor head and blade, phase II is started. A sufficiently accurate head and blade construction is prepared in order to be able to perform exact frequency and strength calculations. Equivalent systems can now be defined in a more accurate manner, and a recalculation of critical flight conditions can be done. The preliminary load conditions, determined by simple considerations,are compared with the results of strength calculations. If a sufficiently high strength level seems to be reached, the dynamic problems must be investigated. Rotational speed resonances, classical and stall flutter,and dynamic rotor-fuselage interactions will be considered in this step. If a satisfying result is likewise obtained for this case, the final design will be fixed. From this final rotor design, it is assumed with reasonable probability that even accurate calculations do not result in substantial corrections of the rotor.

Phase III serves to recalculate the design very accurately. This includes also flight dynamic characteristics, which may give an input to the stability and control system considerations. If necessary, required feedback or other servocontrol systems can be defined now, in order to reach the desired characteristics of the rotor-heli-

copter system. Further, the dynamic problems are investigated in more detail, and the most important boundary conditions to be kept with respect to the fuselage are defined. In the event that the desired characteristics cannot be obtained or that they would require too great an amount of additional expense, it is necessary to go back to phase II or - in the most fatal case - even further.

7. MATERIALS FOR ADVANCED ROTOR DESIGNS

It has been explained in the preceding sections that intensive dynamic design work is necessary to make the helicopter usable. It can be stated generally that dynamic rotor design is closely connected to the question of materials. In the past years new materials did play a part in this development and - undoubtedly - much of the progress in the helicopter field was caused by progress of new materials. Roughly speaking, advanced materials cannot only be used to improve fatigue strength or to reduce weight, for instance, but can also be employed to improve the dynamic behaviour and even handling qualities of the helicopter. Examples of this have already been discussed in this paper. It has been explained that torsionally flexible blades with a chordwise offset c.g. can be used to improve stability and control; and it has been explained how to obtain the proper values of flapping and lagging stiffness, needed not only to improve response and maintainability but to keep low inplane stresses and to avoid ground resonance.

7.1 Application of Fiber-Reinforced Plastics

One evolution of rotor and propeller blade design during the last 20 years has been the adaption of hollow constructions and the introduction of fiberglass and other fiber-materials and of titanium. They have made truly lightweight blade constructions practicable. Most recent developments utilizing the boron/alumininum metal matrix composite materials promise blade weight fractions, less than 25% of the earlier solid constructions (Figure 82, drawn from (77)). Hamilton Standard has done pioneering work in this field.

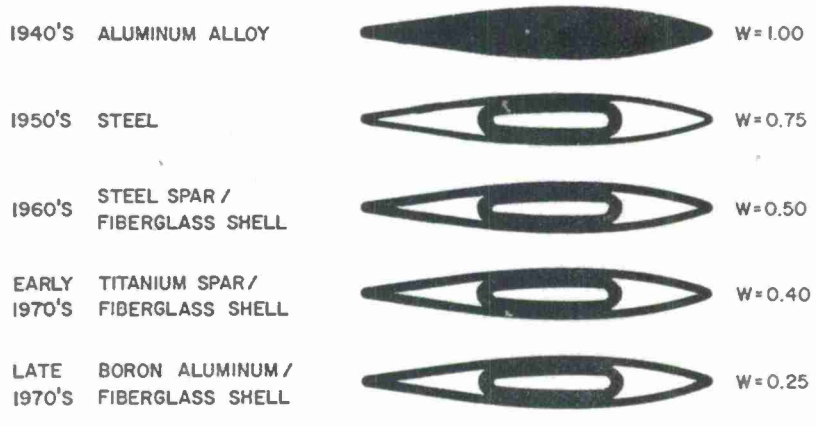


Figure 82 Evolution of basic propeller blade structures (Hamilton Standard)

In 1948 rotor blades were constructed, for example, from steel tubes with wood and fabric covering. These designs were costly to manufacture in man-hour content, were not robust and suffered badly under poor conditions of environment. Figures 83/84 may illustrate the changes in blade design over the years. The increased knowledge of the aerodynamic of airfoils for rotor systems has necessitated rotor blade construction which can provide changes in profile over the length of the rotor blade. In addition, dynamic considerations of hingeless rotors have required precise control over mass and stiffness distributions along the blade length. Both these requirements have led to the development of advanced blade designs, such as shell-core blade construction (WG 13) or fiber reinforced plastic constructions (BO 105, SA 341).

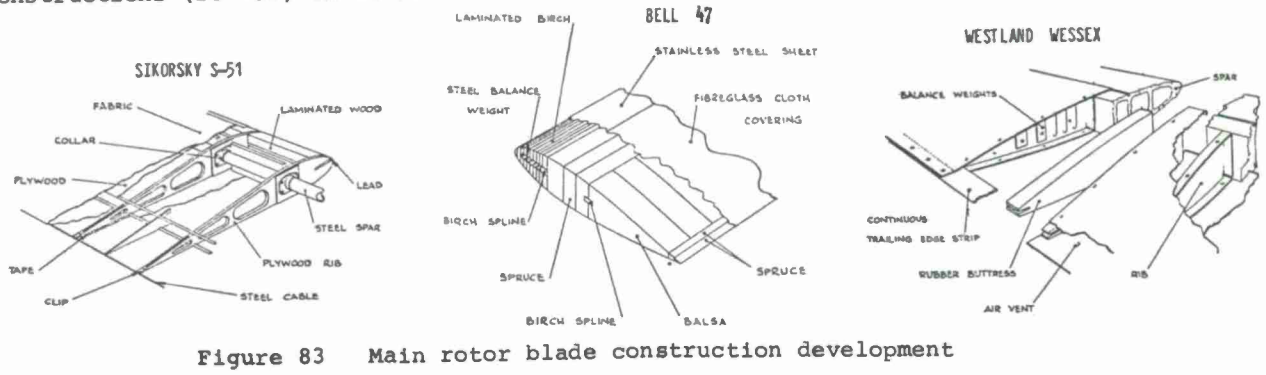


Figure 83 Main rotor blade construction development

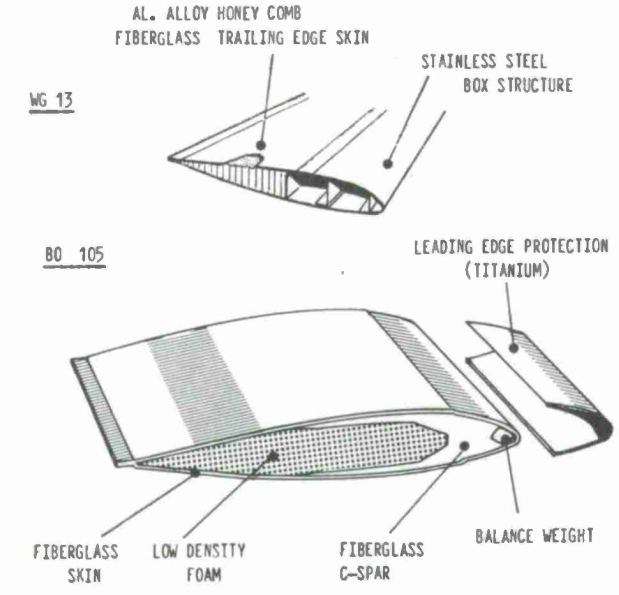


Figure 84 Main rotor blade construction development (continued)

Our knowledge of the blade stresses has increased considerably over the past years and together with advanced materials, blade can be designed with high safe fatigue lifes and fail safe properties. Plastic constructions are of significance in this respect since they normally are composed of millions of single fibers. Simulated lightning strikes and gun fire tests have shown fiber-reinforced plastic blades to be superior to metal blades. The blade shown in Figure 85 which was subjected to gun fire, didn't show any damage increase after a one million cumulative bending cycles, which would be comparable to about 4o flight hours.

In general, the mechanical properties of fiber-reinforced plastics (F.R.P.) cannot be simply defined because they depend upon different effects. But a few generalisations are possible. Strength and stiffness advantages can be seen best from their ratios to the corresponding densities. As Figure 86 shows, there is only little difference between the metal and fiber materials from the standpoint of specific stiffness. However, fiber materials do have strength to weight ratios four times as high as titanium or dural. Of paramount importance is the extremely high fatigue strength. For further description see (87).

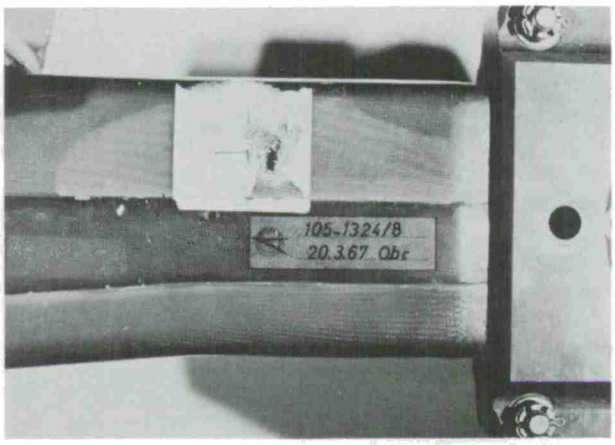


Figure 85 FRP Blade root subjected to gun fire

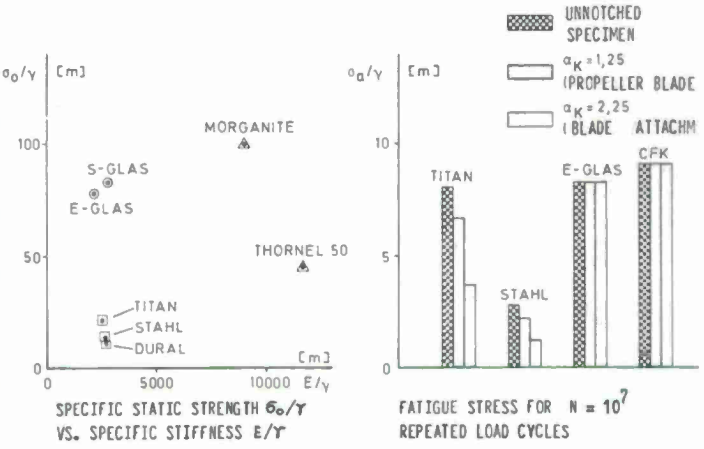


Figure 86 Material properties comparison

Moreover, to maximize the advantages, fiber materials can be changed in their fiber orientation, distribution and content and the constitution of the resin. By this means the modulus of elasticity and the shear modulus can be manipulated within a large range. Both values are shown for the "Thornel 50" material in Figure 87 as a function of the fiber orientation angle (78).

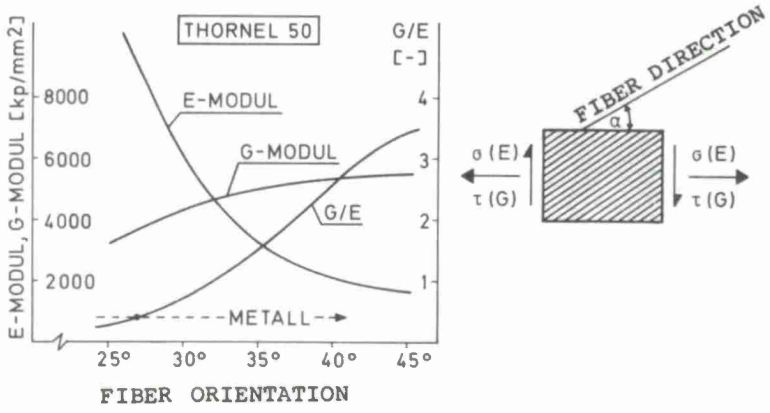


Figure 87 Coefficients of elasticity of a fiber structure

Broadly speaking this effect is most useful for those structures whose design is governed by stiffness or aero-elastic requirements. Hence, one main advantage of the fiber-technique is, that the fiber orientation can be chosen to provide any desired stiffness distributions. Blade designs can use unidirectional fibers oriented spanwise for optimum bending strength and stiffness and unidirectional fibers oriented at 45° to the span (i.e. crossply) in order to provide torsional stiffness. In this way the amounts of flapping, inplane and torsional stiffness can be coordinated individually and the blade frequency pattern can be tailored to the specific requirements. Coupling, for example for δ_1/δ_3-purposes, and uncoupling of the various vibratory modes can be provided.

All this is based on the possibility of combining different fiber materials, and of laying the fibers in any required direction. Advanced manufacturing methods, such as the filament winding process (82), enable any desired airfoil or blade shape to be produced. Blades with a chord up to 25" and a span of up to 10 m have already been made at the MBB-Company (Figures 88,89).

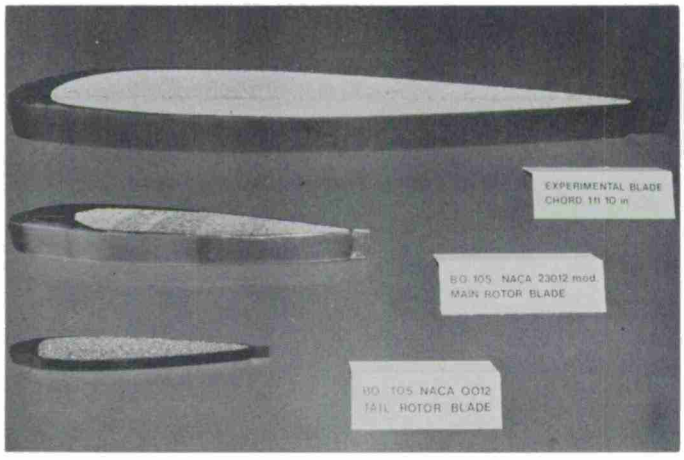


Figure 88 FRP blade cross sections with different chord

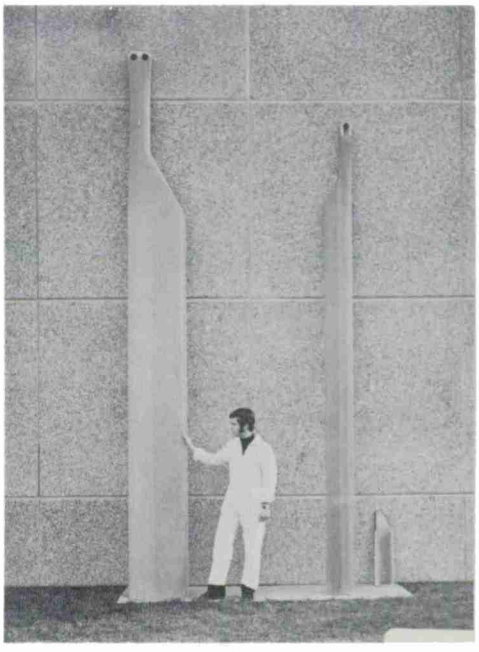


Figure 89 Fiber reinforced plastic blades

7.2 Structural Blade Design

In order to show the superiority of the fiber-technique in blade design, some constructive possibilities will be discussed. Figure90 shows a plot of bending stiffness versus torsional frequency for three types of cross sections. Different contents and distributions of glass fiber and carbon fiber material are shown.

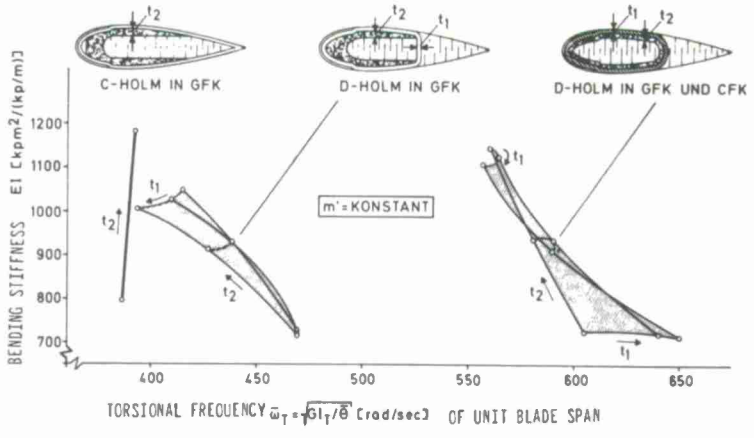


Figure 90 Possible stiffness range with different fiber plastic structural designs

On the first blade design in the left part the exterior blade skin is used for torsional stiffening. As an increase of skin thickness will increase both, torsional stiffness and torsional moment of inertia, there is nearly no possibility of changing the torsional frequency of this cross section. In comparison to that an essential improvement is obtained by using a closed type of D-spar, as shown in the medium cross section of Figure 90 . If it is desired to achieve an extremely high torsional stiffness, the D-spar construction can be supported by an additional skin of carbon fiber material (right blade section). In this design the fiber orientation is optimized for providing a proper torsional and bending stiffness combination. As can be seen, a torsional stiffness increase can only be obtained at the cost of bending stiffness.

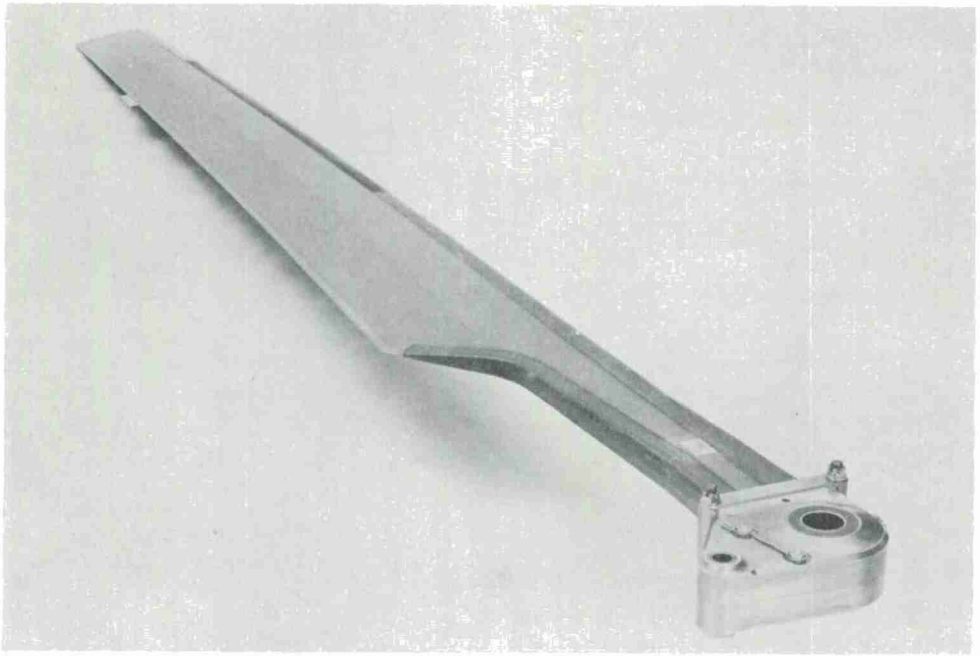


Figure 91 Fiber glass rotor blade (BO 105)

At the MBB-Company a glass fiber/epoxy resin system is used to fabricate the rotor blades for the BO 105 hingeless rotor, as shown in Figure 91 . The cross section consists of an open C-spar of unidirectional fibers to withstand the centrifugal forces and bending moments. The core is made of low-density foam. The torsional moments are absorbed by the skin made out of woven fiberglass material. For erosion protection a titanium alloy strip is bounded at the outer portion of the blade. For the inner section polyurethane is used. The blade has a nearly constant mass distribution (with only small tuning mass), constant chord and constant thickness ratio with a nonsymmetric airfoil section (NACA 23012 modified). The blade inboard section chord is reduced to the socalled "swan-neck" providing the desired inplane first natural frequency (compare chapter 5.4).



Figure 92 Tail rotor blades and horizontal stabilizer made from carbon fiber plastics (BO 105)

Blade construction methods and fabrication techniques are developed further on, and in the past years carbon fiber reinforced plastic have become prominent. For example, blades for main and tailrotors have been built and flight-tested at MBB (86). In Figure 92 carbon fiber blades can be seen mounted on the BO 105 tail rotor. Sikorsky, for example, uses a boron fiber/epoxy resin to fabricate typical blade sections for the ABC-rotor (79).

J.P. Jones summarizes the promises of new advanced materials in reference (80). His conviction is that radically new materials will be the key for transforming the conventional helicopter to an advanced aircraft. One exciting prospect is to use of materials not only for reducing structure weight but also for providing better handling qualities. However, Jones mentiones, that considerations of economy, durability and lack of design experience will make the practical adoption "a slow process".

8. PROTOTYPE DEVELOPMENT

This section's title includes quite a lot of problems, and it seems to be clear that to work this task completely - if actually possible - would be enough subject for a new lecture series. All what can be done here is only to show some specific activities connected with this last phase of development.

Each individual development process will start from quite specific preconditions, will be determined by quite different exterior requirements, will be handled by quite different engineer teams with special knowledges and will - last not least - be determined by the factors of time and money. From this somewhat simplified facts it may become quite obvious, that it is impossible to give a general prescription of the total aircraft design and manufacture process. Impulses can always only be drawn from actual examples.

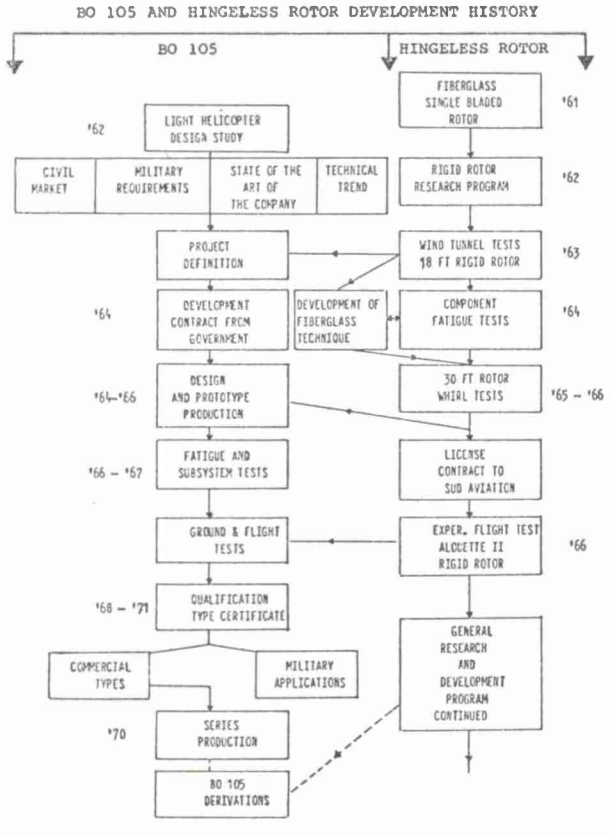


Figure 93 Bo 105 development history

Figure 93 illustrates, as an example, the development history of the BO 105 helicopter, showing some of the key milestones. Two parallel programs were started, the one concerning the BO 105 development itself, and the other concerning the hingeless rotor research program. It can be seen from this example that besides of the direct design work there is another center during the development process, the phase of tests.

8.1 Modell and Full Scale Wind Tunnel Tests

The need for wind tunnel tests is, of course, obvious. New types of rotor and aircrafts must be tested to check the performance predictions or to define operational flight envelopes. Much of test work can be done by model tests, especially when particular problems are to be investigated. Simons (81) summarizes some objectives and problems associated with model testing. Several advantages over full scale and flight testing are obvious such as cheapness, easier instrumentation, more controllable experiments, ability to test difficult or dangerous flight regiones and to test individual components of aircraft, for example. Model scaling is one of the first and most difficult problems that is encountered in conducting model tests. The difficulties in achieving similarity between full scale and model rotor are well known, especially when full aerodynamic and dynamic similarity is desired.

Full scale testing of a rotor system is, of course, preferable. It can eliminate the doubts and risks often associated with theoretical predictions and with extrapolation of small scale test data. Naturally, full scale tests are a question of time and money. In this respect the development effort of a full scale test rotor is nearly not different from the real rotor development. Tooling and manufacturing methods are normally not consistent with quantity production methods, which is a complicating factor in addition. All these problems were discussed in section 7 of the lecture series.

8.2 Laboratory Test Programs

8.2.1 Structures Testing

In order to achieve the desired reliability of the components and to get the required safety for the prototype flight testing, structure's testing is indispensable. According to the fact that new rotor and helicopter developments are - normally - connected

with the utilisation of new materials and new production techniques, a structural test program becomes necessary. A large variety of tests has to be done to determine such things as materials' properties and processing requirements and environmental characteristics.

Throughout the development program of the BO 105 hingeless rotor extensive hub and blade tests were conducted. Blade fatigue tests were divided into two sections, specimen tests and full scale components tests (82), (83). Structural tests had to be concentrated especially on the blade and rotor head because they were made from relatively new materials (fiber reinforced plastics, titanium (Ti A16 V4), and employed advanced fabrication techniques. Different types of specimens were used and for the purpose of comparison to the full scale tests all specimens were cut from full scale blades. To cover the full range of ambient temperatures, low and high temperatures tests were made, in addition. The aim of such types of specimen tests is to establish materials' properties curves (e.g. S-N-Curves), and to prove that the material will be able to withstand all practical enviromental conditions.

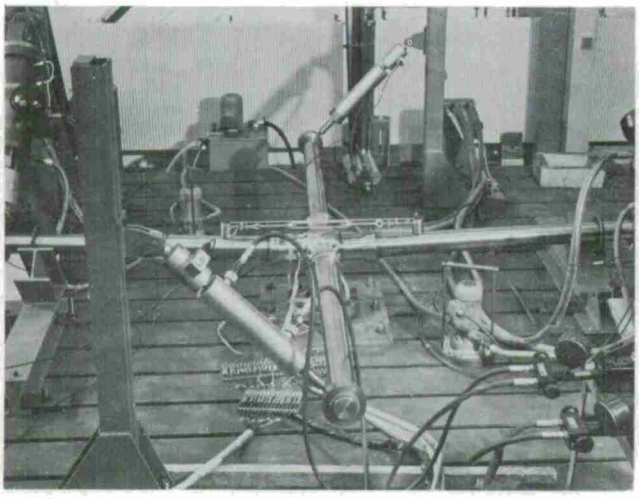


Figure 94 Test bench for rotor hub testing

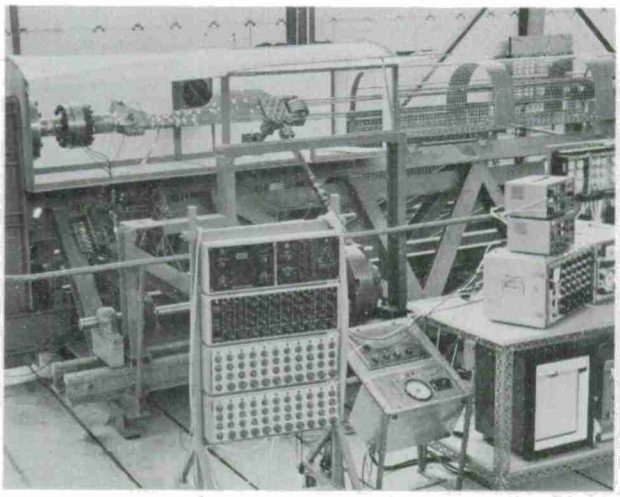


Figure 95 Test bench for blade root testing

An advanced step of structures' testing is the full scale components test . The main rotor hub, the blade attachment and root section, the blade outboard section, as well as the tail rotor hub and blades are typical components to be selected for early development testing. The dynamic components must be divided into separate test setups. Some typical setup installations are shown in Figures 94 and 95 . On the test bench of Figure 94 various types of fatigue tests were done for the rotorhub of the BO 105 hingeless rotor. The structural requirements for the hub are defined by the centrifugal forces and by the moments that are transferred from the rotor blades to the shaft and the fuselage. The central part housing was tested under alternating bending loads, which were induced by hydraulic actuators. The same test conditions were applied to the pitch change bearings in the pitch housing under cyclic pitch inputs. In general, there were similar conditions for the allowable moments of hub and blades, with respect to the fatigue loads. That means that the aim of structurally matching hub and blade design was fully achieved (84).

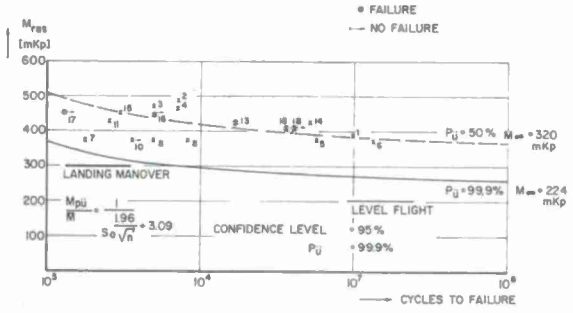


Figure 96 Allowable blade bending moment (root section)

The full size component testing of the blade included the blade inboard and root section with the blade attachment, and the outboard section. A typical test setup for such tests is shown in Figure 95 . It is a test bench for blade root testing under flapwise and chordwise alternating bending and simulating centrifugal force. The blade outboard section was tested on resonance test benches, where the blade is suspended on soft springs and is excited in its first-free mode by an excenter. This type of resonance test is for extreme fatigue test purpose and may bring a great number of individual failures.

Figure 96 illustrates the results of 18 blade root tests (84). For the regression curve a standard deviation of 1.1 is used to establish permissible moments. This value was the result of small specimen tests. Usually the first cracks were detected in these tests

after about 1.5 to 2.0 million cycles under extremely high loading conditions. In Figure 96 the curve with a survival probability of 99.9 percent is compared with flight loads. Extremeley high speed flight values are considerably below the 224 mkp fatigue limit.

An important question in component testing is related to the type of loading spectra. In general, the most critical components should be tested under real flight-by-flight loading conditions, which can be prerecorded on magnetic tapes and programed through individual servo loops (85).

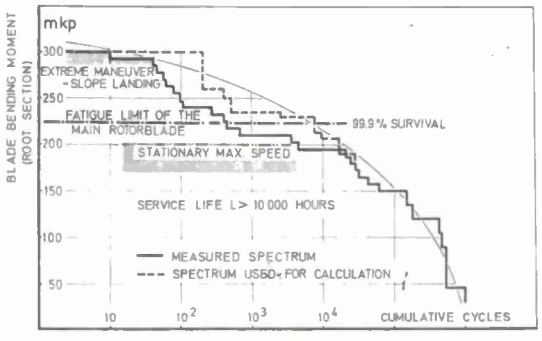


Figure 97 Flight load spectrum BO 105

A typical flight loading spectrum consists of different loading distributions from take-off, forward flight and flight maneuvers, to maximum and minimum power flight and landing. Figure 97 shows a typical full flight spectrum with measured data (84). For life time calculation the highest values of the flight conditions considered were used for the total time of the corresponding flight condition. According to Miner's rule a service life of more than 10 000 hours is obtained for this blade.

8.2.2 Subsystem Test Programs

Laboratory test of subsystems are of similar importance and are normally conducted for each major subsystem. They can use either full-scale functional mockups or real elements. Control system tests may be shortly discussed as an example. Figure 98 shows a complete control system test bench including swashplate , pitch linkage, mixing unit, mechanical and the complete hydraulic servo system (30). Collective and cyclic stick are operated mechanically, with servo control system on and off. In addition to the normal proof and operational tests, the stiffness constants of the control system can be determined, which is an important value for the flutter behaviour of the rotor system. In this way components test can be used to get basic informations for a better theoretical treatment, too.

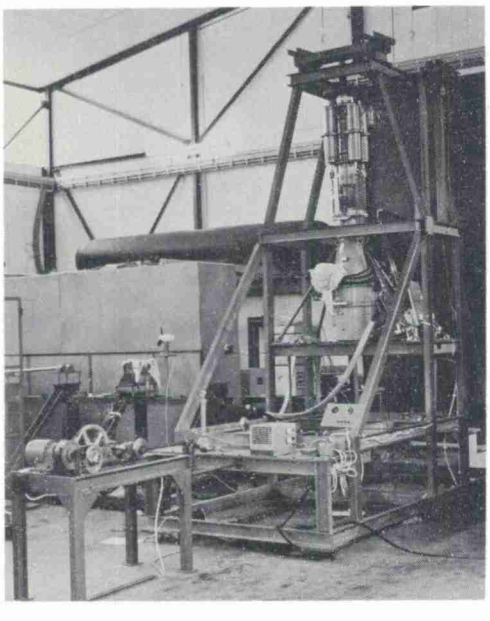


Figure 98 Control system test bench

Subsequent laboratory testing will involve more subsystems. Actual components are the mechanical power train elements including gear-boxes, transmissions, flexible couplings and clutches. Full scale mockups are usually used for functional testing of the hydraulics, of electrical and of the avionic equipment systems. In general, adequate laboratory subsystem and integration testing is a tool for minimizing development flight testing and the risk, connected with it.

9. CONCLUSION

In conclusion, it should be noted that helicopter design and development is, of course, an extremely large theme and it is impossible to treat it completely in one lecture like this. Here, helicopter aerodynamics and dynamics are discussed with the main emphasis on the rotor field, but this should not be understood as the only problem area. Tail rotor design, airframe, wing and stabilizer's layout, for example, is of utmost importance, as well, and it is not secret, that just these components have been somewhat neglected in the helicopter design up to now. To get the helicopter more widely usable, will undoubtedly mean success just on these areas too.

10. REFERENCES

1. Jonischkeit, R.: "Auslegung von Drehflüglern", Lehrgang der Carl-Cranz-Gesellschaft e.V., Oberpfaffenhofen, 1972

2. Georgi, H.: "Drehflügler-Entwicklungsrichtungen", Lehrgang der Carl-Cranz-Gesellschaft e.V., Oberpfaffenhofen, 1972

3. Anon.: "Helicopter Flying and Ground Handling Qualities; General Requirements for Mil. Specification, MIL-H-8501A, 1961

4. Edenborough, H.K., Wernicke, K.G.: Control and Maneuver Requirements for Armed Helicopters, AHS, 20th Annual National Forum, 1964

5. Anon.: "AGARD V/STOL Handling Qualities Criteria", AGARD TR-408B

6. Anon.: "Suggested Requirements for V/STOL-Flying Qualities", AVLABS TR 65-45

7. Anon.: "A Proposed Military Spezification for V/STOL-Flying Qualities", Cornell AFFDL Report

8. Reichert, G., Oelker, P.: "Handling Qualities with the Bölkow Rigid Rotor System", AHS, 24th Annual National Forum, 1968

9. Huber, H.: "Das Stabilitäts- und Steuerungsverhalten des gelenklosen Rotors System Bölkow", Deutsche Gesellschaft für Luft- und Raumfahrt, DLR-Mitt. 71-12, 1971

10. Cox, C.R.: "Design Considerations for Acceptable Cabin Noise Levels in Light Helicopters", AHS Joint Symposium, Arlington, Texas, 1970

11. Mil, M.L., et al.: "Helicopters - Calculation and Design. Volume I, Aerodynamics", NASA TT F-494, 1966

12. Holder , D.W., Pearcey, H.H., Gadd, G.E., Seddon, J.: "The Interaction between Shock Waves and Boundary Layers, with a Note on the Effects of the Interaction on the Performance of Supersonic Intakes", A.R.C., C.R. 180, 1954

13. Pearcey, H.H., Holder, D.W.: "Simple Methods for the Prediction of Wing Buffeting Resulting from Bubble Type Separation", 14th Meeting of the AGARD Structural and Materials Panel, Paris, July 1962

14. Reichert, G.: "Schwingungs- und Betriebsfestigkeitsprobleme bei Hubschraubern", Lehrgang der Carl-Cranz-Gesellschaft, Oberpfaffenhofen, 1972

15. Ham, N.D.: "Stall flutter of Helicopter Rotor Blades: A Special Case of the Dynamic Stall Phenomenon", JAHS, Vol. 12, No. 4, October 1967

16. Ham, N.D.: "Aerodynamic Loading on a Two-Dimensional Airfoil During Dynamic Stall", AIAA Journal, Vol. 6, No. 10, October 1968

17. Carta, F.O., et al.: "Analytical Study of Helicopter Rotor Stall Flutter", AHS, 26th Annual National Forum, June 1970

18. Gabel, R., Tarzanin, F.Jr.: "Blade Torsional Tuning to Manage Rotor Stall Flutter", AIAA 2nd Atmospheric Flight Mechanics Conference, Palo Alto, September, 1972

19. Gutin, L.: "On the Sound Field of a Rotating Propeller", NACA TM-1195, October 1948

20. Schlegel, R.G., King, R.J., Mull, H.R.: "Helicopter Rotor Noise Generation and Propagation", USAAVLABS TR 66-4, 1966

21. Lowson, M.V., Ollerhead, J.B.: "Studies of Helicopter Rotor Noise", Wyle Laboratories, WR 68-9, 1968

22. Cox, C.R.: "Rotor Noise Measurements in Wind Tunnels", Bell Helicopter Company, 1969

23. Stuckey, T.J., Goddard, J.O.: "Investigation and Prediction of Helicopter Rotor Noise, Part I - Wessex Whirl Tower Results", Journal of Sound and Vibration (1967) 5-(1)

24. Spivey, R.F.: "Blade Tip Aerodynamics Profile on Planform Effects", AHS, 24th Annual National Forum, Mai 1968

25. Davenport, F.J., Front, J.V.: "Airfoil Sections for Rotor Blades - A Reconsideration", AHS, 22th Annual National Forum, May 1966

26. Benson, R.G., Dadone, L.U., Gormount, R.E., Kohler, G.R.: "Influence of Airfoils on Stall Flutter Boundaries of Articulated Helicopter Rotors", AHS, 28th Annual National Forum, May 1972, Preprint No. 621

27. Reichert, G., Huber, H.: "Influence of Elastic Coupling Effects on the Handling Qualities of a Hingeless Rotor Helicopter", 39th AGARD Flight Mechanics Panel Meeting, Hampton, Virginia, September, 1971

28. Spivey, W.A., Morehouse, G.G.: "New Insights into the Design of Swept-Tip Rotor Blades", AHS, 26th Annual National Forum, June 1970

29. Göthert, B.: "Profilmessungen im DVL-Hochgeschwindigkeits-Windkanal", Forschungsbericht FB 1490, 1941

30. Weiland, E.: "Development and Test of the BO 105 Rigid Rotor Helicopter", AHS, 24th Annual National Forum, 1968

31. Fradenburgh, E.A., Chuga, G.M.: "Flight Program on the NA-3A Research Helicopter", Journal of AHS, Volume 13, No. 1, January 1968

32. Hoerner, S.F.: "Fluid dynamic drag", Midland Park, New Jersey, 1965

33. Mc Cormick, B.W., Spencer, R.H. and Sternfeld, H.Jr.: "Tip Vortex Core Thickening for Application of Helicopter Rotor Noise Reduction", USAAVLABS TR 66-1, September 1966

34. Yaggy, P.F.: "The Aerodynamics of V/STOL Aircraft, Part B: Pure and Compound Helicopters", AGARD-VKI Lecture Series 9, May 1968

35. Jenny, D.S., Olson, J.R. and Landgrebe, A.J.: "A Reassessment of Rotor Hovering Performance Prediction Methods, AHS Forum, May 1967

36. Lichten, R.L.: "Design problems and Solutions for Five Types of Low-Disc-Loading, High-Speed VTOL Aircraft", 7th congress of ICAS, September 1970

37. Reichert, G., Wagner, S.N.: "Some aspects of the Design of Rotor-Airfoil Shapes", AGARD Specialist's Meeting on "The Aerodynamics of Rotary Wings", Marseille, 1972

38. Huber, H.: "Some Objectives in Applying Hingeless Rotors to Helicopters and V/STOL-Aircraft", AGARD Specialist's Meeting on the "Aerodynamics of Rotary Wings", Marseille, 1972

39. Young, Dr. M.I.: "A simplified Theory of Hingeless Rotors with Application to Tandem Helicopters", AHS, 18th Annual National Forum, May 1962

40. Gallot, J.: "Effets Aéroelastiques sur les Qualités de vol d'un Rotor Rigide", AGARD CP46, 1969

41. Richardson, D.A.: "The Application of Hingeless Rotors to Tilting Prop/Rotor Aircraft", AHS, 26th Annual National Forum, June 1970

42. Tiller, F.E. Jr., Nicholson, R.: "Stability and Control Considerations for a Tilt-Fold-Proprotor Aircraft", AHS, 26th Annual National Forum, June 1970

43. Wagner, Dr. S.,: "Aerodynamische Untersuchungen zur Profil- und Blattgestaltung für Hochleistungshubschrauber", MBB, TN D127-4/71

44. Katzenberger, E.F.: "An Investigation of Helicopter Descent and Landing Characteristics Following Power Failure", Journal of the Aeronautical Sciences, 1956

45. Huber, H.: "Ermittlung des Autorotationsverhaltens von Hubschraubern am Beispiel des BO 105", DGLR-Symposium, Stuttgart, Nov. 1969

46. Sadler, G., Crimi, P.: "The effects of rotor inertia and aerodynamic configuration on Helicopter Autorotational Characteristics", RASA Report No. 66-11, Dec. 1966

47. Magee, J.P., Pruyn, R.R.: "Prediction of the Stability Derivatives of Large Flexible Prop/rotors by a Symplified Analysis", AHS, 26th Annual National Forum, June 1970

48. Ward, J.F., Huston, R.J.: "A summary of Hingeless Rotor Research of NASA-Langley", AHS, 20th Annual National Forum, May 1964

49. Reichert, G.: "Flugmechanische Besonderheiten des gelenklosen Hubschrauberrotors", WGLR Jahrbuch 1965 (translated by NASA-Langley)

50. Salmirs, S., Tapscott, R.J.: "The Effects of various Combinations of Damping and Control Power on Helicopter Handling Qualities during both Instrument and Visual Flight", NASA TN D-58, 1959

51. Cooper, G.E.: "Understanding and Interpreting Pilot Opinion, Institute of Aero. Soc. Preprint No. 683, 1957

52. Mühlig-Versen, B.: "Variation der Rotorsteife der BO 105", MBB GmbH, Bericht DF 33, 1966

53. Reichert, G.: "Basic Dynamics of Rotors Control and Stability of Rotary-Wing-Aircraft Aerodynamics and Dynamics of Advanced Rotary-Wing Configerations", VKI/AGARD Lecture series No. 63, April 1973

54. Kanno, J.S., Lundgren, S.: "Equations of Motion for the Dynamic Analyses of a Hovering Rotor Including Gyro Control System", Lockheed California Company, LR 17185, June 1961

55. Lytwyn, R.T., Miao, W., Woitsch, W.: "Airborne and Ground Resonance of hingeless rotors", AHS, 26th Annual National Forum, June 1970

56. Woitsch, W., Weiß, H.: "Dynamic Behaviour of a Hingeless Fiberglass Rotor", AIAA Paper No. 69-204, Febr. 1969

57. Coleman, R., Feingold, A.: "Theorie of self-excited mechanical oscillations of helicopter rotors with hinged blades", NACA Report 1351, 1958

58. Ward, J.F.: "A Summary of Hingeless Rotor Structural Loads and Dynamics Research", Symposium on the Noise and Loading Actions on Helicopter V/STOL Aircraft and Ground Effect Machines", Southampton UK, Sept. 1965

59. Hirsch, H., Kline, J., Daughaday, H.: "H-5 Variable Stiffness Blade Program", AFTR-6329, Parts 1-6

60. Hirsch, H.: "The Contribution of Higher Mode Resonance to Helicopter Rotor Blades", Journal of Aeronautical Sciencies, Vol. 15, No. 8, 1948

61. Daughaday, H., Kline, J.: "An Approach to the Determination of Higher Harmonic Rotor Blades Stresses", AHS, 9th Annual National Forum, 1953

62. de Guillenschmidt, P.: "Calculation of the Bending Stresses in Helicopter Rotor Blades", NACA TM 1312, March 1951

63. Yaggy, P.F., Statler, I.C.: "Progress in Rotor-Blade Aerodynamics", 39th AGARD Flight Mechanics Panel Meeting, Hampton, Virginia, September 1971

64. Huber, H.: "Ermittlung von höherharmonischen Erregerkräften und Blattbiegemomenten am BO 105-Rotor", MBB-GmbH, TN D126-7/72

65. Strehlow, H., Habsch, Dr. H.: "Untersuchungen aeroelastischer Probleme von Drehflügelflugzeugen", MBB GmbH, UD TNA D12-5/69

66. Tarzanin, F.J., Jr.: "Prediction of Control Loads Due to Blade Stall", AHS, 27th Annual National Forum, May 1971

67. Ormiston, R.A., Hodges, D.H.: "Linear Flap-Lag Dynamics of Hingeless Helicopter Rotor Blades in Hover", AHS Journal, April 1972

68. Burkam, J.E., Miao, W.: "Exploration of Aeroelastic Stability Boundaries with a Soft In-Plane Hingeless Rotor Model", AHS, 28th Annual National Forum, May 1972

69. Ormiston, R.A.: "Some Comments on Dynamics of Hingeless Rotor Helicopters", U.S. Army, Airmobility R&D Laboratory, Moffet-Field, California

70. Mc Kee, J.W.: "Pitch-Lag Instability as Encountered during Tests of a Model Rotor", IAS Preprint No. 807, 26th Annual Meeting, January 1958

71. Chou, Pei Chi: "Pitch-Lag Instability of Helicopter Rotors, IAS Preprint No. 805, 26th Annual National Forum, January 1958

72. Stepniewski, W.Z., Kalmbach, C.F. Jr.: "Multivariable Search and its Application to Aircraft Design Optimization", RAS-Journal, Vol. 74, 1970

73. Hague, D.S., Glatt, C.R.: "An Introduction to Multivariable Search Techniques for Parameter Optimization", NASA CR-73200, April 1968

74. Collatz, L.: "Numerische Behandlung von Differentialgleichungen", Berlin 1951

75. Michlin, S.G.: "Variationsmethoden", Leipzig, 1962

76. Ebeling, P.: "Probleme der aerodynamischen Auslegung von V/STOL-Propellern", DLR-Mitteilung 71-18, Dezember 1971

77. Jackson, A.: "Meeting Propulsion Needs of Future High Performance V/STOL", DLR-Mitteilung 71-18, Dezember 1971

78. Huber, H., Weiß, H.: "Moderne Technologien in der Entwicklung von V/STOL-Propellern und Rotoren", DLR-Mitt. 71-18, Dezember 1971

79. Burgess, R.K.: "Development of the ABC-Rotor", AHS, 27th Annual National Forum, May 1971

80. Jones, J.P.: "Materials for advanced Rotorcraft", 39th AGARD Flight Mechanics Panel Meeting, Hampton, Virginia, September 1971

81. Simons, I.A.: "Some Objectives and Problems Associated with Model Testing", RAS-Journal, Volume 74, No. 715, July 1970

82. Jarosch, E., Stepan, A.: "Fatigue Properties and Test Procedures of Glass Reinforced Plastic Rotor Blades", AHS, 25th Annual National Forum, 1969, Paper No. 370

83. Pfleiderer, K., Arendts, F.J.: "Comparing the Classification of the Fatigue Strength Behaviour of small Specimens and Large Scale Components", 7th Congress of the International Council of the Aeronautical Sciences, Rome, September 1970, Paper No. 70-34

84. Reichert, G.: "Review of German Activities in Helicopter Structures and Dynamics", 31st Meeting of the Structures and Materials Panel of AGARD, Nov. 1970, Norway

85. Theriault, P.W.: "Status Report on Design Development of the AH-56A Cheyenne", AHS, 24th Annual National Forum, May 1968

86. Bongers, Brunsch, K., Jonda, W.: "Development and Test of Carbon Epoxy Fiber Composite for Helicopter Tail Rotor Application", 7th International Reinforced Plastics conference, October 1970, Brighton

87. Wetter, R.: "Kunststoffe der Luft- und Raumfahrt mit besonderer Rücksicht der Faser-Verbundwerkstoffe", MBB-Bericht UD 57-70/ö

FLIGHT TESTING FOR PERFORMANCE AND FLYING QUALITIES

by

Kieran T. McKenzie
Chief Technician
Westland Helicopters Limited
Yeovil, Somerset.
U.K.

SUMMARY

A review is presented of the required approach to flight testing in the major areas of Performance and Flying Qualities. Programme philosophies, problem areas, techniques of measurement, recording and analysis are examined and discussed. Some sample measurements and procedures are examined to illustrate approaches. The need for objectivity in proportion to value concept is predominant.

1.0 FLIGHT TESTING

Amongst the essentials of flight testing are objective observation accompanied by objective reporting and sufficient testing with appropriate accuracy for the purpose of the flight test programme. Value concepts have to be applied to flight testing as well ae most branches of engineering.

The purist may recoil at the suggestion that we do not necessarily seek absolute knowledge by flight testing. In the main we are concerned with probability concepts in subsequent operation and we have to try to assess them on a limited sample in a limited time scale with a limited experience.

With these limitations it is important that we do not produce false solutions by having preconceived notions and allowing test results appear to be consistent with them. It is essential to devise test procedures which genuinely sample the attendant possibilities. Paradoxically it is equally essential to have a good knowledge of possible critical or problem areas so as to ensure an adequate coverage in testing. This is the balance that must be struck to achieve "value" Flight Testing.

In such a limited session as this it is difficult to be fully formal and systematic, and this talk leans more to considering approaches to and pitfalls in testing rather than absolute detail and techniques.

2.0 PERFORMANCE TESTING

If we start again with essentials, we can list

(1) knowledge and understanding of atmospheric effects

(2) adequate instrumentation

(3) adequate stable conditions

(4) basic understanding of performance.

(5) With pilot manoeuvre performance, an awareness of the pilot interference or reaction.

The helicopter or Rotary Wing aircraft is much more complex than the general fixed wing aircraft. It has critical performance in high induced flow conditions, in stall conditions, sometimes in compressible conditions, sometimes influenced by aeroelastic behaviour, always verging on non linear aerodynamics (both because of its complex geometry and its complex behaviour), and in its critical low speed regime suffering from deficiencies in measuring its relative velocities.

2.1 Atmospheric Effects

Since so much of typical helicopter performance is associated with low altitude (below 2000 feet) or hover with its high induced velocity and efficiency criteria, problems of atmosphere frequently spoil the testing.

Basically hover testing is useless in turbulence because the gradient of performance change with velocity is so immense and the methods of measuring velocity are not very effective in turbulence. Effective absolute hover testing is usually defined as requiring winds of less than 5 knots (and stable). But the unexpected variable is a vertical component of air velocity which would be very difficult to assess or quantify. There have been instancee of well conducted hover performance showing different results on successive days. The difference could only be attributed to such an atmospheric variation. Fortunately this variation is infrequent and not very large, but nevertheless it would normally justify carrying out two substantive eets of measurements.

2.2 Instrumentation

The basic aircraft performance instrumentation parameters are in fact what are usually considered as part of the normal pilots instruments Airspeed, Rotor Speed, Torque, Altitude, Temperature.

Usually the normal instruments are accepted for performance provided they have reasonable accuracy and are calibrated. Airspeed and Torquemeter are probably the two that need to be subjected to most

ecrutiny. Airspeed errors can be examined before a main performance programme by airlog measuremente or by flying a measured course. If the errors are not coherent then a epecial airspeed system may be needed for tests.

For low speed performance testing doppler and radio altimeter facilitiee can be extremely useful if availablo.

Torquemetere may be based on a number of principles of which the two most well known are hydraulic (or pressure) and strain-gauge ehaft. On many installations, particularly hydraulic types, apparent torque errors of 10% have been seen. It is important that in the acceptance of euch a system there is an adequate understanding of its susceptibility to variation of its environment and that there is a coherent method of calibration. Typical overall system accuracies for a "good" eystem are 2 - 3% for a hydraulic system and 1 to 1½% for a self test strain gauge system.

Fig. 1 illustrates the variation of production climb tests on a large batch of a particular production helicopter corrected to a standard weight and temperature. Of course the total variation is made up of other factors than torquemeters including atmospheric variability as the tests must be done at a particular time.

The weight of the aircraft throughout the teets must be monitored to an adequate degree of precision during major performance testing. Normally this will be done through a major weighing of the equipped aircraft without fuel at a time close to the test period and then keeping a very careful weight control on all added iteme such as crew, fuel, ballast or payload. An accurate fuel measuring system is essential if a eignificant amount of fuel is used. Fuel gone or fuel contents measurements are equally appropriate provided they are properly calibrated and tested. As a cross check the joint use of both can often be extremely valuable as can also the occasional check of the fuel left at the end of a flight by draining out and weighing or in critical tasks the weighing of an aircraft with its take-off fuel loading.

2.3 Recording

Three main methods of recording are used. The first simply is flight crew observation of the pertinent information with obvioucly various means of logging and transmitting the data including radio transmittal to a flight monitoring team.

The second is a very useful method long used of a photographic sampling of a panel of performance instruments in the aircraft which is then available for detail examination of critical areas of the performance tests. The examination of theee photographe is however very laborious.

The third basic method is to record performance parameters on continuoue trace of which there are a number of variations including magnetic tape.

The choice of methods is not easy and is sometimes dictated by the requirements for other agencies to be able to scrutinise recorded data. Often combinations of the methods are used, eometimes indeed all three methods are used together covering different areae or aepects of the performance parameters.

The first method is generally technically acceptable provided the conditions being tested are well established and etable, the instrumentation is satisfactory, and that there are sufficient teste in the programme to allow cross checking.

2.4 Performance Test Programme

Unless a test is required for a specific limited objective, the purpose of a performance teet programme is to produce a general coverage for all admitted operational usages. Even for one single-rotor helicopter configuration the number of parameters is large e.g. Weight, rotor speed, altitude, temperature power or torque, airspeed and centre of gravity. To test all these parametere comprehensively would be a massive taek as also would be ite subsequent analysie.

It is necessary then to try to rationalise the problem and conceive methods of etudying performance to isolate the significant major relationships and then devise a test programme which utilises this knowledge as a main framework, but which aleo goes on by limited samples cross-check the relationships and confirm that the minor parameters are not significant.

For the single-rotor helicopter, theoretical work shows that level performance can be expressed in non-dimensional forms one without compressibility effects and the second with compreseibility.

For performance purposes on a particular helicopter it ie unnecessary to go back completely to the basic non-dimeneionals and it is eufficient to consider the relationship in a normalised form.

The incompressiblo relationehips can then be expressed in the form $\frac{P}{\sigma n^3} = f\left(\frac{W}{\sigma n^2}, \frac{V}{n}\right)$

where n is the ratio actual rotor speed to nominal reference speed,

P is input transmission or engine power

W is the aircraft weight

σ is atmospheric deneity

V is forward epeed - true airspeed.

The compressible relationship is expressed through the parameter $n/\sqrt{\theta}$ replacing n where θ is the ratio of actual absolute temperature to a standard temperature (usually the ISA Sea Level value.

Two extremes of performance testing are possible one to assume the simpler relationship and add eufficient cross checks to show that these assumptione are valid within the range of variations available to the test facility, subsequently seeking to confirm these by the later availability of say more extreme climatic conditions or the other extreme assume the most complex relationship and test accordingly. The former approach is much to be preferred in a value concept provided it ie treated objectively and critically.

When steady performance other than level performance is required, e.g. climbs or accelerations, or compound configurations are involved, deeper consideration into other non-dimeneional relationships is required and must be tested.

When dynamic performance is required, e.g. flight path and clearance after engine failure is required then non-dimensional performance is not uniquely valid and effects of absolute mass and kinematics are involved and need to be examined. Due to the difficulties of achieving a sufficisnt range of testing variables in a given test facility recourse may be had to a soundly based theoretical study whose validity is demonstrated through experimental testing in the range of variables available.

The theoretical studies producing nom-dimensionalisation are of course fundamentally aero-dynamically orientated and they do not necessarily recognise the influence or rotor kinematics, dynamics or aeroelastic effects. The existence of these imply that there may be minor effects not represented in the basic non-dimensional concepte even in steady performance and so these possibilities have to be critically examined by selective cross-checks of mass and rotor speed variation superimposed on the elemental non-dimensional testing.

2.5 Performanco Testing

On the basis of the principles previously outlined performance testing will proceed. Although this is talked of here as an entity, in practice it will usually take place progressively, in bits and pieces first of all and then later in major segments. Only sample areas can be treated here to illustrate the major elements of the discipline.

2.5.1 Hover Testing

Ae stated earlier hover testing in particular requires stable atmospheric conditions. Three broad groups of hover testing may be defined

(1) Tests in vicinity of ground reference

(2) Tethered hover

(3) Free air tests remote from ground reference

Tests in ground effect can obviously only be done in the first two groups and equally obviously the third group is not technically desirable when in practice the required range of altitude and or compressibility parameters can be readily obtained within the test programme.

For absolute hover measurements in group 1 or 2 it is essential that the relative airspeed is known within 2 or 3 knots. Both groups have their limitations

Group 1 - tests in the vicinity of ground reference - is inhibited by power or torque limitations and the weights at which the aircraft is permitted to fly, unless a wide range of altitude add/or temperature level ground sites are available. It has however the attraction that provided the atmosphere is etablo, testing may be extended to embrace low speed performance by various techniques. Theee include formating on a ground vehicle travelling at various speeds with airspeed measuring equipment, or using flight crew estimated ground speed or airborne doppler speed in conjunction with ground reference measured wind speed. Variation in test weighte have however to be achieved by either ballasting or by consuming fuel.

Tho tethered hovering technique introduces the flexibility of changing the effective weight continuously without interrupting the test so frequently. The aircraft is connected vertically to "earth" and the tension developsd in the connection is measured directly. The effective weight can then increase to permitted aircraft limite and need not be constrained to the permitted aircraft weight. Thie technique however suffers from the lack of flexibility in airspeed. The only means of achieving this ie to sit and wait for stable winds of various speeds. Fig. 2

The third possibility, Free Air Testing, is the most powerful technique provided accurate near zero airspeeds can be obtained as it enables the greatest variation or selection of altitude. A flexible method of obtaining and maintaining near zero airspeed is by formating on smoke puffs fired from the helicopter. The successful achievement of hover requires a good flying technique as airspeed and altitude information may be totally coherent at the airspeeds involved in initiating manoeuvres. More refined methods have been developed and used, such ae for example determining in one location on the helicopter the direction of the rotor downwash. Such methods are however not necessarily flexible and often require experimental datuming for each test configuration.

Fig. 3

2.5.2 Forward Flight Testing

Almost all forward flight steady performance testing is carried out with reference to normal aircraft instruments. Two broad procedures are used, one can be called "non-dimensional datum" and the other "natural datum".

In the first procedure altitude is varied for each test point as the weight changes with time so that normalised weight $\left(\frac{W}{\sigma}\right)$ is kept constant. Sometimes Rotor speed is also varied to keep a constant value of $\left(\frac{n}{\sqrt{\sigma}}\right)$.

The second procedure accepts standard, or free within a band, values of altitude and Rotor speeds and processes the results later in a normalised form which will require cross interpollation.

Both procedures are valid, the first tends to complicate test procedure to simplify analysis, while the second simplifies and makes flexible the test with a consequential complication of analysis.

As a rule each level speed point should be held for about three minutes after achieving the condition, and a procedure followed of obtaining one half of the points in an increasing speed profile and the other half decreasing (e.g. 80, 100, 120, 110, 90, 70 knots). Additional points should be measured where significant changes are encountered or anticipated, e.g. rotor stall, compressibility etc.

Fig. 4

Forward flight climb performance is usually treated as a simple extension of level flight performance, with a factored energy concept i.e. $\frac{\Delta P}{\sigma n^3} = k \frac{W}{\sigma n^2} \times \frac{V_c}{n}$ where ΔP is excess power above level flight. With the increase in transmission ratings, and engine powers, and the increased interest in altitude operations such assumptions must be validate by testing at extreme weights and different levels of power through the available altitude range.

Fig. 5

Factors which can invalidate the simple energy concepts are changes in the pre-stall efficiency of the rotor system, major stall on the main rotor (or tail rotor) or airframe loads at high climb rates.

In dealing with climb performance, it should also be recognised that the measuring unit of pressure altitude is not the same as the energy unit of true altitude except for the International Standard Atmosphere and that the relationship "true" Rate of Climb equals Pressure Rate of Climb multiplied by the ratio of actual absolute temperature to ISA absolute temperature.

In all quasi-steady performance testing, non-dimensionalisation must be challenged. The aero-elastic and kinematic behaviour of the rotor system depends on absolute quantities so variation of mass-dynamic parameters must be tested in conjunction with non-dimensional, e.g. W/n^2 as well as $W/\sigma n^2$.

2.5.3 Dynamic Performance

A specialist area in performance testing has grown up over the last ten to fifteen years - flight path and avoidance techniques associated with engine failures - e.g. the conventional "Dead Mans Curve" or the more recent "Operational procedures for multi-engined rotorcraft".

In earlier days the subject was treated simply by ad-hoc tests. As the importance of safety increased this has given rise to the growth of a more sophisticated need which has been approached by a combination of semi-theoretical computer techniques and an attempt to simulate variations experimentally.

This area is one of the most difficult performance areas to treat satisfactorily for a large number of reasons and yet it looms large in the present and near future definition of acceptability of permitted Take Off Weight operation and therefore VALUE.

Amongst the reasons for these difficulties are:

(1) Mass parameters are involved as well as non-dimensional - exchange of rotor Kinetic Energy (Change of Rotor Speed) into performance energy is related to mass.

(2) Piloting techniques are involved - individual pilot variation, learning phase and variation of pilot response with proximity to obstacles are all significant.

(3) Performance in descent at low airspeeds in possible ground effect and with possible rotor divergence are the least well authenticated areas of performance knowledge.

(4) Such tests by their very nature imply a greater risk of damage than subsequent operation.

(5) Airborne instruments, Airspeed and altitude are not usually coherent in this region.

Present clearance techniques are therefore based on experimental measurements varying power weight and heights and attempting to correlate these with computer studies. The correlation is often poor in absolute terms (due usually to the second reason above), but fortunately most current operations only involve a limited range of atmospheric density and the operational implications can be defended from this mixture of experiment and theory.

Nevertheless there would appear to be a need for more fundamental measurements to be made than currently available in low speed descent and in manoeuvres close to the ground.

2.6 Test Analysis

Test analysis should flow naturally from what has been said in the previous sections. First correct for basic instrument errors, then next for installation errors, e.g. Pressure Error on airspeed etc.

From there the normal procedure would be to reduce the results to the relevant incompressible non-dimensional parameters, attempt to systematize the results on this basis and then question critically the validity of this with mass, rotor speed or temperature, to attempt to isolate kinematic - aeroelastic or compressibility effects. Where any of these are seen to be significant then a much more complex analysis would be required.

3.0 FLIGHT TESTING FOR STABILITY, CONTROL ETC.

Unlike performance testing where flight crew active participation is minimal, in control testing pilot participation is predominant. Paradoxically pilot acceptability is the fundamental criterion, but this acceptability is confused by the exceptional capability of most test pilots to act unconsciously as adaptive stabilizing mechanisms, albeit in often very different modes and prejudices. Control flight testing then must be not only objective but subjective. The ultimate objective is not necessarily stability or controllability in itself, but almost non definable criteria of work load and probability of achievement of operational tasks by operational aircrew and the avoidance of dangerous or catastrophic incidents by such operational aircrew. To this is added the almost abstract concept of the operational aircrew trusting automatic pilots (or stabilizer systems) being in command of the aircraft without the need for continuous monitoring or intervention.

3.1 Measuring Techniques

With this background, the performance acceptability of direct aircraft instrument reporing is not transferable. Although it is possible (and usual) to provide cockpit instruments showing control positions and aircraft attitudes, it is not possible (or permissible) to assume without confirmation that the pilots will leave the controls alone in any conditions except the most stable. Equally when specific pulse type inputs are tested it is not easy for the pilot to ensure that the control is returned to the original datum. Some improvement can be obtained by providing control position indicators or mechanical stops or gates for datumming.

Figs. 6 & 7

There is therefore a general need for recording which usually must have as a final output an analogue form. Suitable methods are airborne trace, airborne tape or telemetry transmission. The advantages of the latter system are threefold. First is that the weight of airborne equipment can be cut down, second that it provides simultaneous observation of the behaviour of the pilot and aircraft with the pilots comments on acceptability criteria for the consideration of specialists on the ground, and three, in the unfortunate event of the loss of the test aircraft, valuable information could be immediately available in a concrete form.

3.2 Flying Qualities Test Programme

The objectives of the test programme can be conveniently classified in the following manner, bearing in mind that these classifications can be further multiplexed by consideration of operational modes, e.g. non-assisted, assisted (automatic stabilizer etc.) failure survival, and emergency,

(1) Measurements of controllability and control availability

(2) Measurements of overall stability

(3) Pilot assessment

(4) Measurement to isolate stability parameters etc.

With rotary wing aircraft it must be remembered that absolute stability although desirable is not an absolute end in itself, but has to be rationalized in terms of "acceptability" for the operational missions of the specific aircraft. Further there are many more stability and response modes that could be significant than with a conventional fixed wing aircraft.

3.2.1 Measurements of controllability and control availability

While controllability cannot be divorced from stability, it is useful to try to separate the effects of stability to identify the basic control mechanisms and to be able to assess possible improvements etc.

Various factors come into the assessment of controllability (either qualitative or quantitative) - these include:

(1) the response in the required mode (angle, direction, acceleration etc.)

(2) proportionality or continuity of response with input

(3) "small" time lag in effective response after input
(depending on circumstances "small" would frequently be in the order a quarter to one second)

(4) minimum unwanted disturbance in other modes or axes

(5) avoidance of excessive or inadequate response in relation to input displacement or force.

Many treatments of helicopter control requirements were couched in terms of response of one motion (e.g. angular) in one axis. The validity of this treatment is not self-evident as translation also occurred in the process and at certain stages the available moment is altered by the effective self-flapping behaviour of the rotor system. We can illustrate this by considering a simple comparison betweeen a small offset flapping rotor and a semi-rigid (large effect offset), both with the same moment about the centre of gravity per inch of stick.

	Small Offset	Semi-rigid
Head Moment per degree cyclic	400	1650
Tilt Moment per degree cyclic	400	350
Total Moment per degree cyclic	800	2000
Gearing, degrees per inch stick	2.5	1.0
Total Moment per inch stick	2000	2000
Degrees cyclic for say 20 knots	3	3

In the same way very great emphasis was laid on the purity of control response to the axis of control input. This may have been because significant size inputs were needed to obtain desired response. More recent experience has shown that in free flying with high control power rotors, lack of purity from cyclic inputs is not self-evident to pilots and carefully contrived control input tests (or comprehensive instrumentation) can be necessary to establish the true relationship. One such series of tests showed that with small displacements a cyclic movement at 45 degrees to the fore and aft axis was required to produce pure motion and yet this was noticed as a significant feature in free flying.

Pilot assessment as such is dealt with later, but as it is involved in controllability in the absence of valid criteria, it is relevant at this stage to note that the concept of acceptability applies to the ultimate operational mission or missions and not simply free flying. Test conditions must be configured to test the appropriate elements of missions and to ensure that testing takes place in representative turbulent conditions and with adequate coverage of "upset" failure and emergency conditions.

Tests for control available are usually construed as steady state or steady maneouvre trims leaving say 10% control margin still unused in the authorised operational flight envelope with authorised loading configurations. While this is a defensible starting point, consideration should be given to the existence of enough control authority for a recovery from an upset.

Enough different conditions must be tested to ensure that no intermediate marginal conditions are overlooked. Taking for example sideways flight, basic theory would predict a linear variation with change of sideways velocity. A test at say 30 knots might be assumed to clear intermediate conditions. However cases have occurred where for example, greater tail-rotor angle was required at 10 to 15 knots than at 30 knots.

Fig. 8

3.2.2 Measurements of overall stability

The most common method of measurement or assessment of stability is to attempt to study the behaviour after disturbance has been created by some form of control displacement and after the controls have been placed in a fixed position (or exceptionally left free). Various forms of disturbance can be used depending on the stability and response of the aircraft and the modes being studied, a step (ramp) a single sided pulse, a double pulse, an impulse and so on. Many motions are complex with many modes in the motion and the different types of input are frequently used to attempt to show these up.

Where absolute definition is required, unless the stability is very positive with a short time to damp or stabilise, turbulence can confuse the test results. A trim condition must be carefully established first before the input Repeat tests must be carried out to endeavour to exclude spurious results due to turbulence.

3.2.3 Pilot Assessment

Part of the purpose of flight testing is to make a valid assessment within a limited period of time of the probability of acceptability of the airoraft in its operational task in its operational environment and with its operational aircrew. Simple criteria of excellent or uncontrollable are helpful during specific tasks in development testing (but sometimes even these descriptions stem from isolated subjective environments). The need for objective standards has been recognised for some considerable time and various so-called scales have been proposed and used.

A very useful review of the subject was made in AGARD Stability and Control Conference September 1966 in the paper "A Revised Pilot Rating Scale for the evaluation of Handling Qualities" by Robert P. Harper Jr. and George E. Cooper which reviews the early Cooper Scale and the Cornell-Ames work leading to the presentation of the revised pilot rating scale reproduced herein:

Controllable Capable of being controlled or managed in context of mission, with available Pilot attention.	Acceptable May have deficiencies which warrant improvement, but adequate for mission Pilot Compensation, if requires to achieve acceptable performance, is feasible.	Satisfactory Meets all requirements and Expectatione, good enough without improvement Clearly adequate for Mission	Excellent, Highly Desirable	A1
			Good, Pleasant, Well Behaved	A2
			Fair. Some Mildly unpleasant characterietics. Good enough for Mission without improvement.	A3
		Unsatisfactory Reluctantly acceptable. Deficiencies which warrant improvemeat. Performance adequate for Mission with feasible Pilot compeneation.	Some minor but annoying deficiencies. Improvement is requested. Effect on performance is easily compensated for by Pilot.	A4
			Moderately objectionable deficienciee. Improvement is needed. Reasonable performance requires considerable Pilot compensation.	A5
			Very Objectionable Deficiencies. Major improvements are needed. Requires beet available Pilot compeneation to achieve acceptable performance.	A6
	Unacceptable Deficiencies which require mandatory improvement. Inadequate performance for Mission even with maximum feaeible Pilot compensation.		Major Deficiencies which require mandatory improvement for acceptance. Controllable. Performance inadequate for mission, or Pilot compensation required for minimum acceptable performance in Mission is too high.	U7
			Controllable with Difficulty. Requiree substantial Pilot skill and attention to retain control and continue Mission.	U8
			Marginally controllable in miseion. Requiree maximum available Pilot skill and attention to retain control.	U9
Uncontrollable Control will be lost during some portion of Miseion			Uncontrollable in Mission	10

REVISED PILOT RATING SCALE

In the words of that paper "The basic pilot rating data on which these decisions are based however must be strictly mission-oriented if the subsequent quality versus cost decisions are to be meaningful".

A concept of the "ecale" as a numerical linear scale of dimensional value is completely misleading. The definitions (or criteria) are more important than the numbers although in the couree of time personnel operating the rating ecale might automatically learn to talk in terms of the number (as it were a short-hand or code).

The teste must be clearly identified as "mission oriented". The normal test pilot is immensely adaptive and his capacity for control is related to the task and the environment. The ultimate judgement is one of what the operational pilot would be capable of doing in his operational environment. Thie judgement must, by the very nature of the facilities for testing, be a synthetic one and the groundwork for such a eynthesis must be laid.

(1) The test programme should ensure the precise definition of the mission concept, and ite elements and provide sufficient test conditions to synthetize them

(2) The pilot must be aware of the full purpose of the programme, and have available to him such technical and other information as he requires. However care must be exercised not to precondition him to a particular solution. Preferably he should be subjected to variations which remove the chances of preconditioning.

(3) The pilot should be asked to state his choice of ratings in relation to each taek or eegment. He should be allowed the facility for half ratings when he cannot clearly decide. He should give or be asked for comments in addition to the ratings to try to identify problem areae, partly to see if they can be improved or partly to later attribute total ratings and total value. Preferably these comments should be made at the time of test and then reviewed after the test.

(4) A running attempt must be made to relate rating concepts in a flight segment to the total mission concept.

(5) Finally the rating in its total mission concept must be established and then evaluated in a value concept, i.e. the evaluation of ratings for different aircraft or alterations against their cost for the given miseion accomplishment.

Even if this type of rating scale is not used in a formal eense, the informal use of this type of categorizing is fundamental to any assessment that is meant to be meaningful and should be applied as widely as possible in helicopter testing and appraisal - not just in controllability.

3.2.4 Measurement to isolate stability parameters etc.

As the operational helicopter moves into a more complex operational field, is more widely used and seeks more acceptability there arises a greater need to know the elements of behaviour more closely so as to provide ultimately more effective solutions.

Some such measurements have been going on for years in the quasi-static field, e.g. balanced sideslip measurements. However even these measurements are not absolute, but only relative in terms of eay aircraft derivative to control derivative. If we assume no spurious cross coupling, the only new requirement here is that the sideslip measuring system is properly calibrated in the aircraft pressure field.

The acquisition of fundamental knowledge in this quasi-static manner is eeverely limited and the simpler dynamic testing can find itself finally confused by the large number of modes or indeed cross couplings that ariee particularly in the pitch channel.

The problem is much more intense than the general fixed wing aircraft and measuring and isolation techniques have to be extended and improved.

In some areas initial work has been going on in this field, some of it by pilot shaped input (extension of the inputs referred to earlier), some by pulse boxes in an electronic AFCS system with electronic changes of added stability, eome by frequency response methods of control excitation. The testing is complex and needs methodical care, preparation and instrumentation, and a specifically justified programme. Although theoretical stability usually postulates linear systems, the helicopter abounds with potential non linearities of possible significance, at large displacements in the rotor output and aircraft behaviour, at small displacements in the effecte of the hydromechanical inputs. Test methods and instrumentation have to be devised to allow for these.

Fig. 9

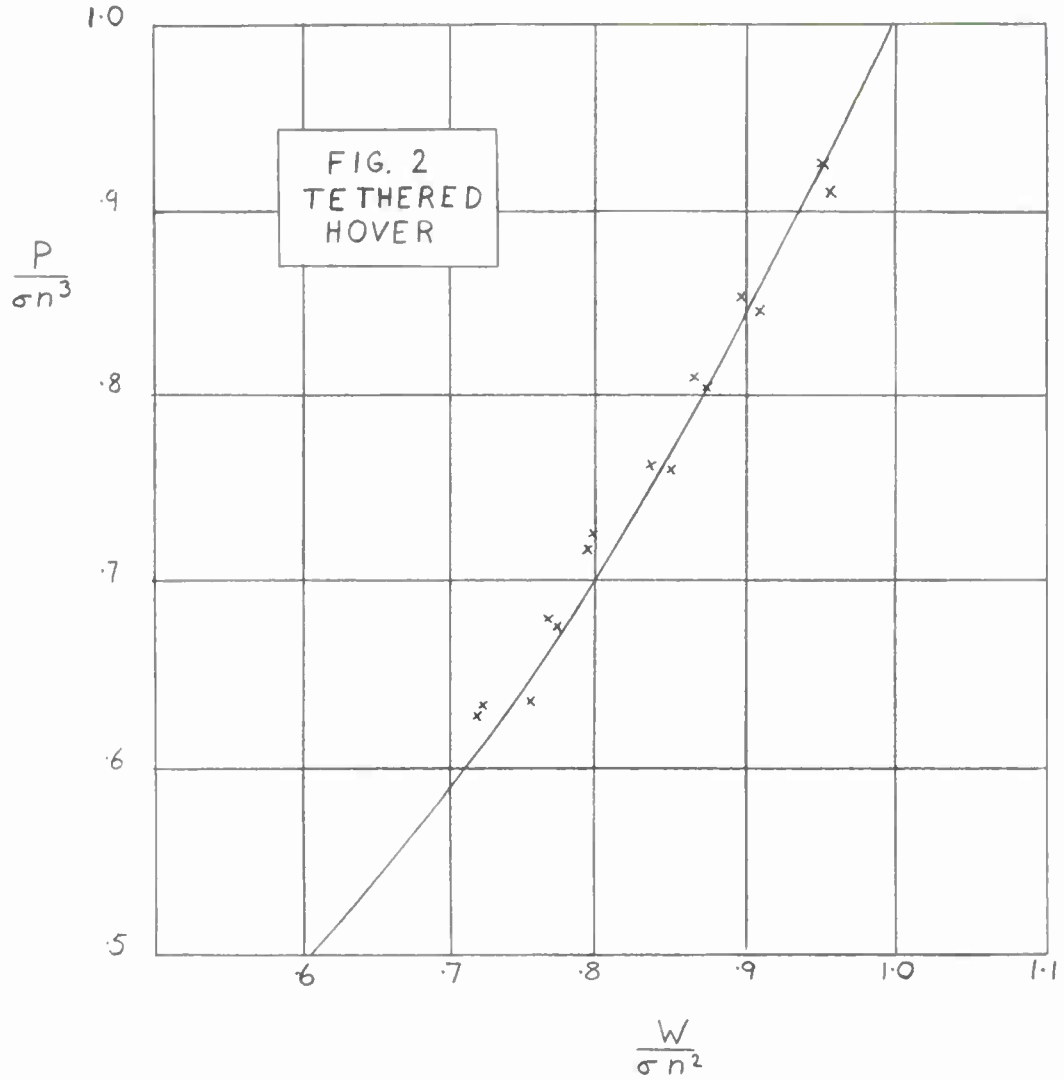
4. THE "WASH-UP"

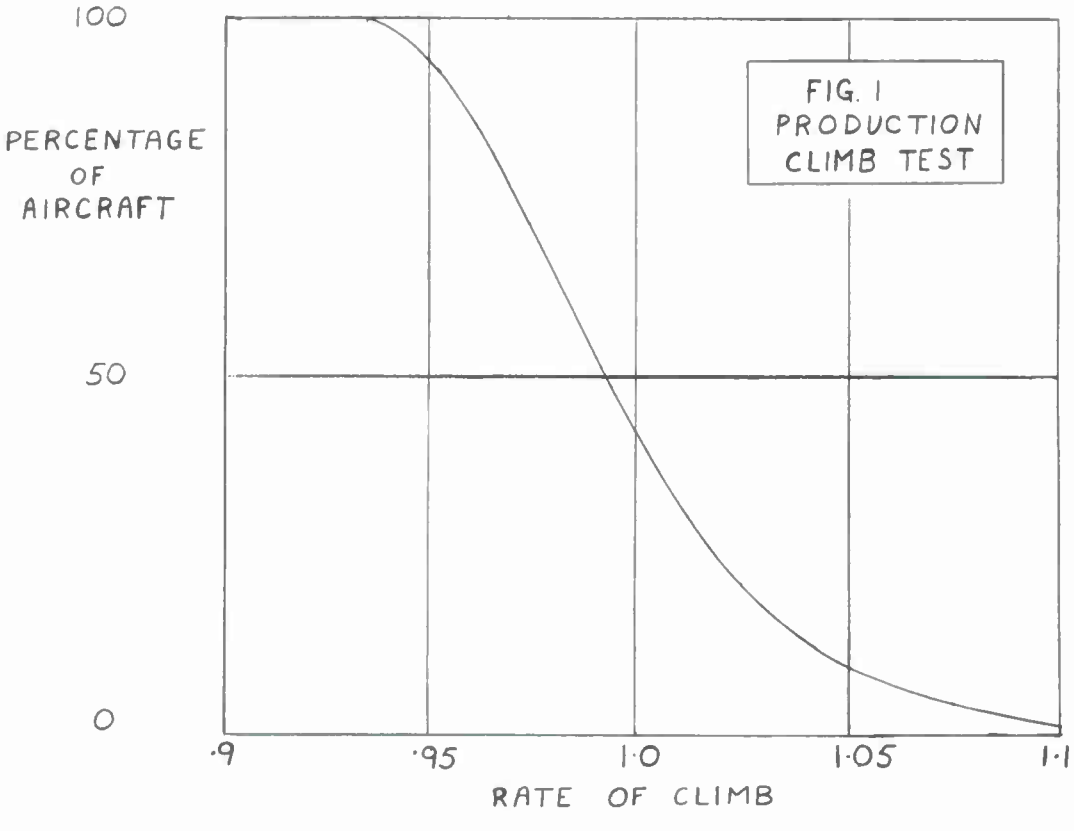
("Wash-up" is a term used particularly in a test programme for a reviow at a convenient point of the results achieved in relation to the programme, of problems encountered, of areas highlighted and indications of future needs.)

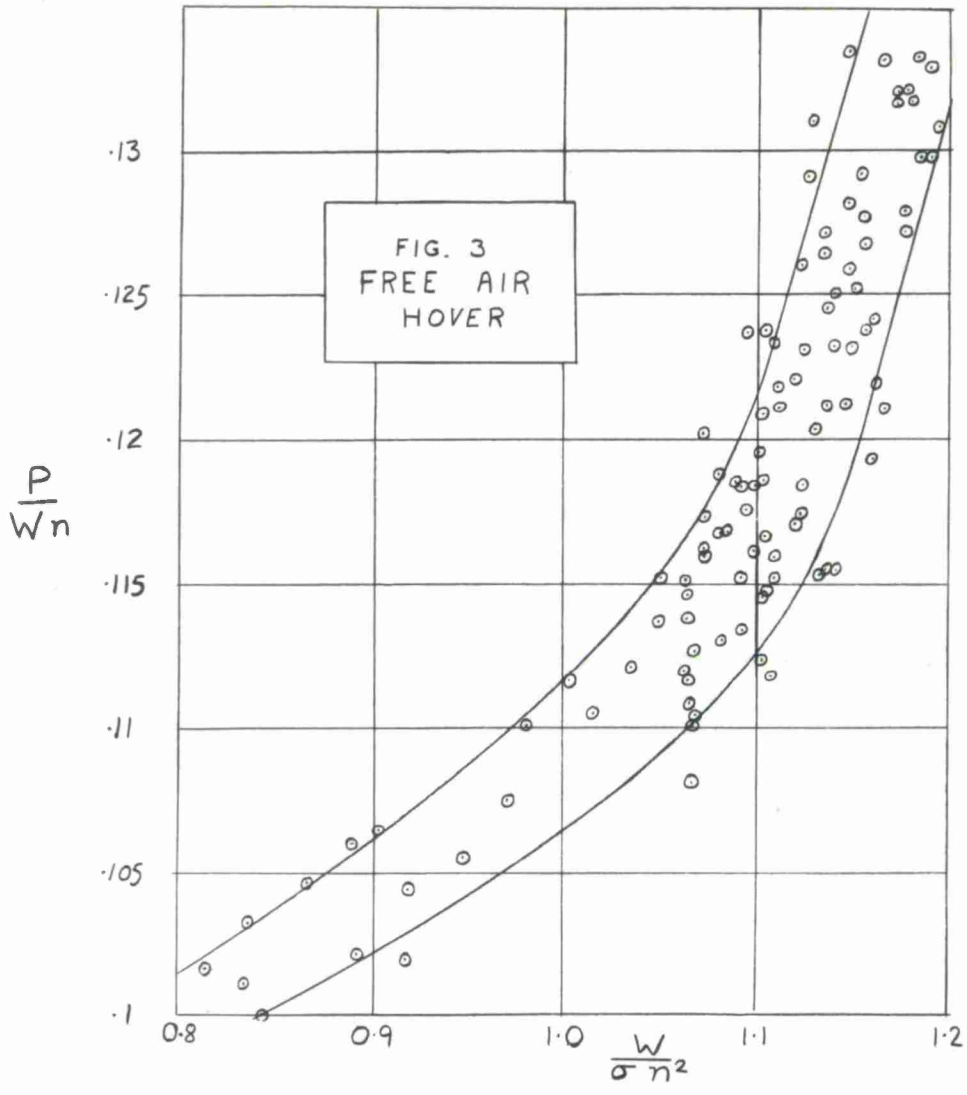
Such a "wash-up" at this point would say that in helicopter engineering theoretical work and flight testing are interrelated and interdependent, but neither should be subordinated by the other. Random flight-testing is useless. There is a need for a basic input of theoretical background in the planning, execution and interpreation of testing - to minimize wasteful testing, to concentrate on critical areas and to assist in the analysis.

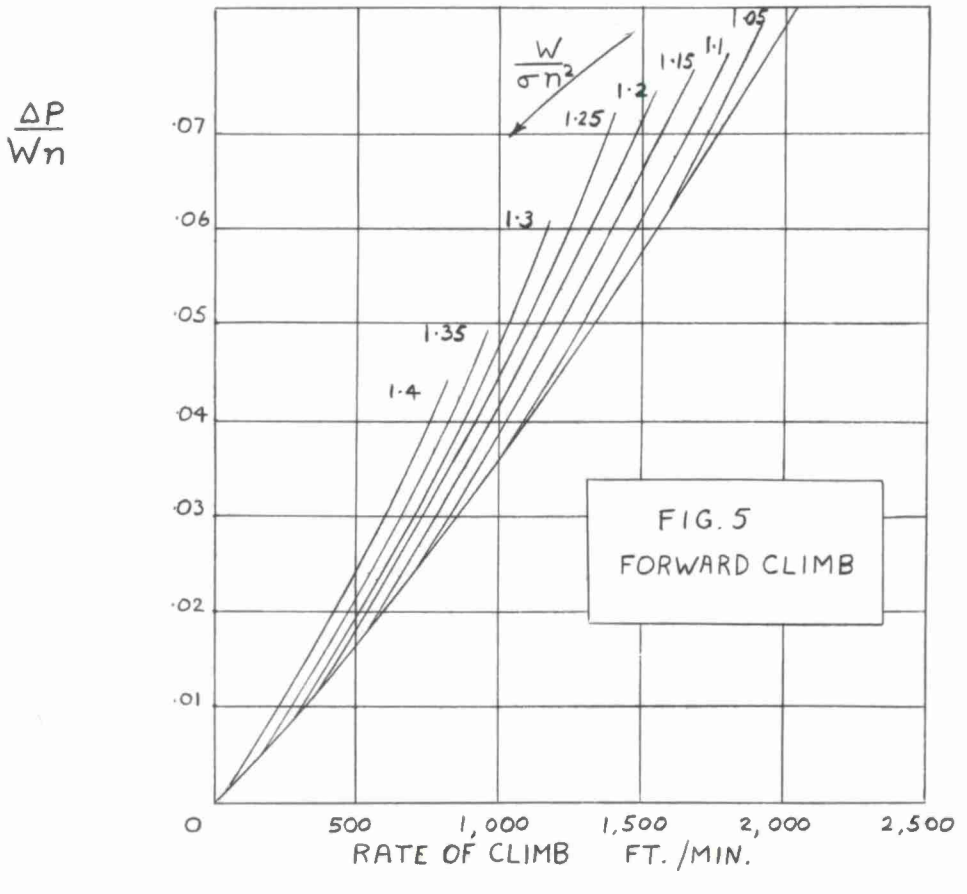
In turn Flight testing must probe the validity of the theory, be open to the possibility of derivation, and feed back into the world of the theoretical and research areae problems which are not adequately covered by existing theory or knowledge.

Helicopter aerodynamic/dynamic engineering is too complex to warrant continuoue use of absolute theoretical knowledge in its own right and too important to be complaisant about simple representation. Flight testing is the bridge between the past and the future - the challenge to do better in cost and operational effectivenees terms. It must be eeen ae such and given the necessary identification.


FIG. 2
TETHERED
HOVER
P/σn³
1·0
·9
·8
·7
·6
·5
·6
·7
·8
·9
1·0
1·1
W/σn²


FIG. 1
PRODUCTION
CLIMB TEST
PERCENTAGE
OF
AIRCRAFT
100
50
0
·9
·95
1·0
1·05
1·1
RATE OF CLIMB


FIG. 3
FREE AIR
HOVER
P/Wn
·13
·125
·12
·115
·11
·105
·1
0·8
0·9
1·0
1·1
1·2
W/σn²


ΔP/Wn
W/σn²
1·05
1·1
1·15
1·2
1·25
1·3
1·35
1·4
·07
·06
·05
·04
·03
·02
·01
0
500
1,000
1,500
2,000
2,500
RATE OF CLIMB FT./MIN.
FIG. 5
FORWARD CLIMB

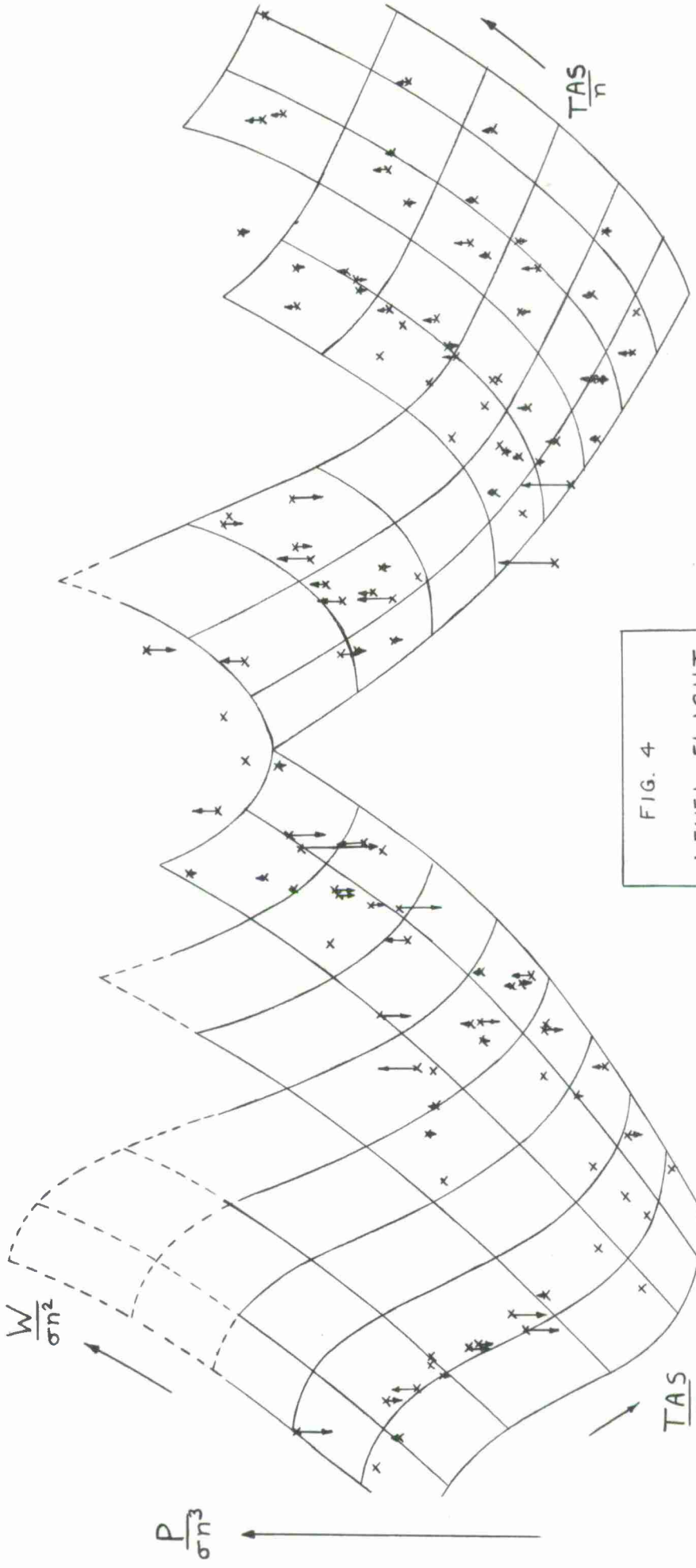


FIG. 4
LEVEL FLIGHT

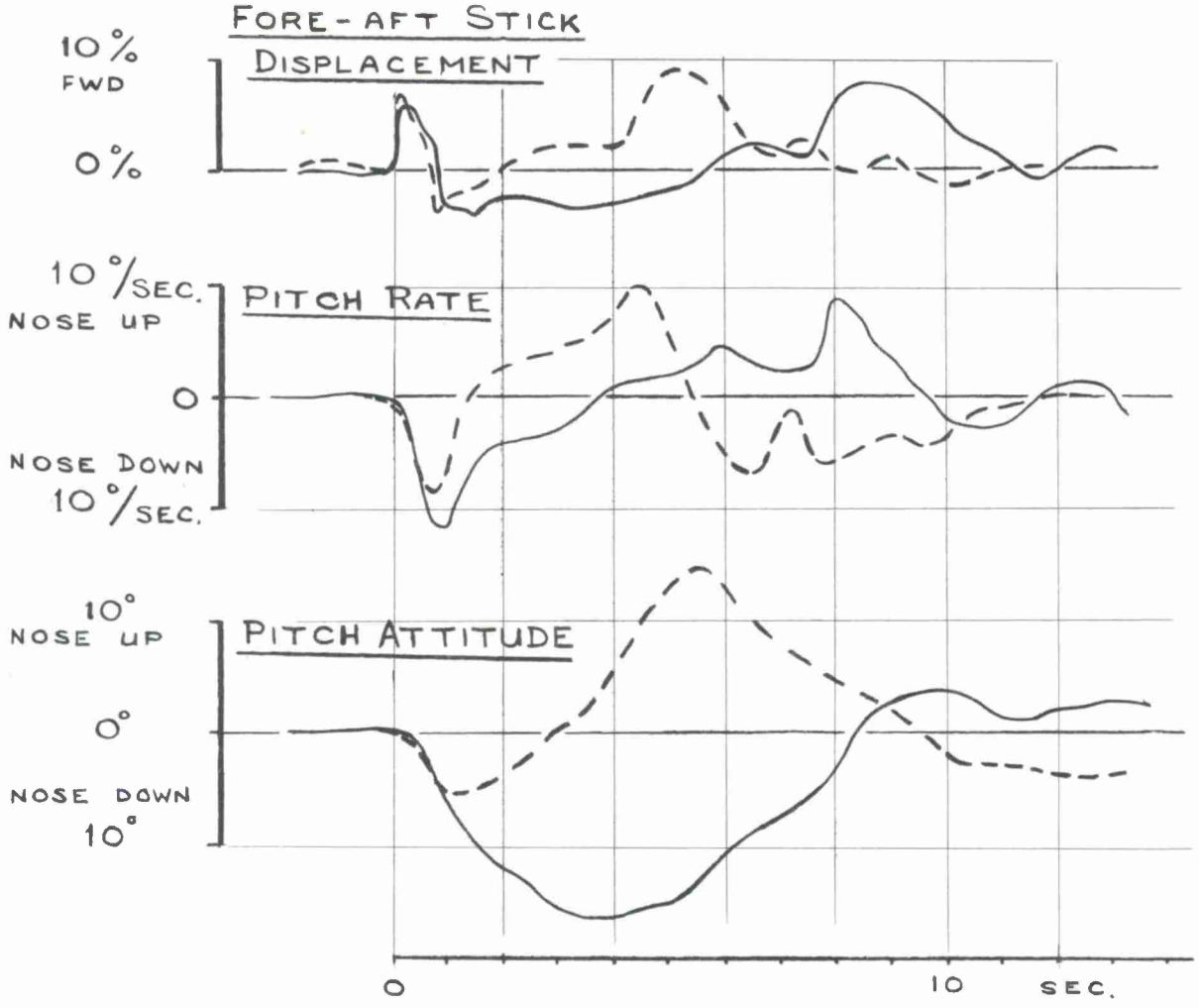


FIG. 6 MANUAL STICK INPUTS

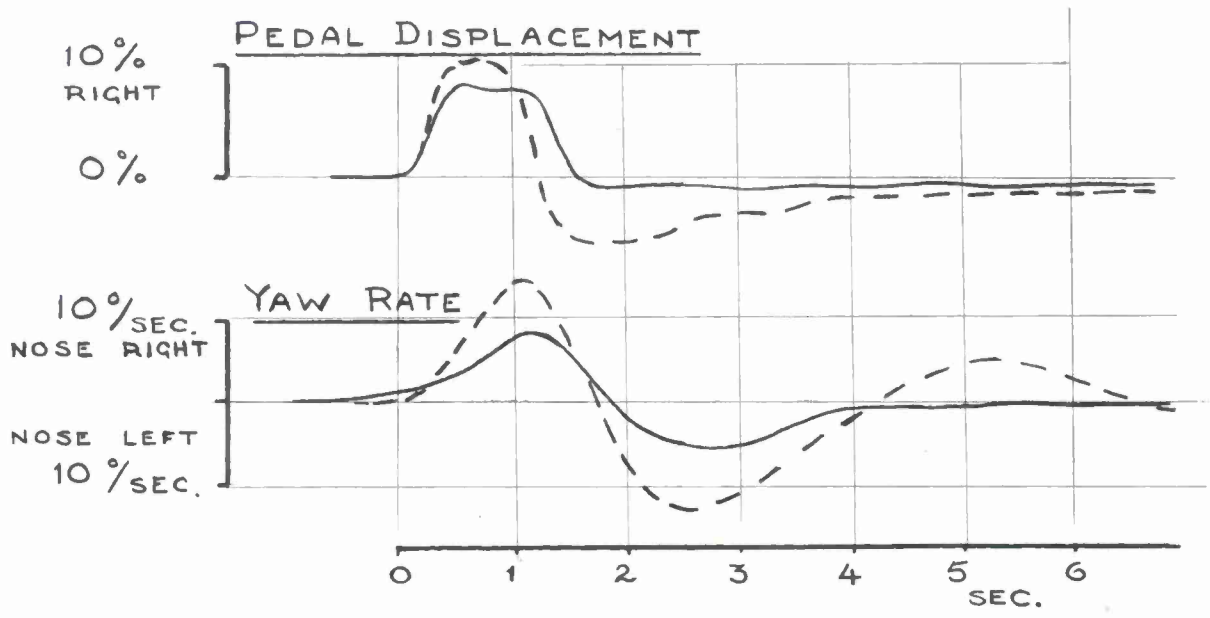


FIG. 7 MANUAL PEDAL INPUTS

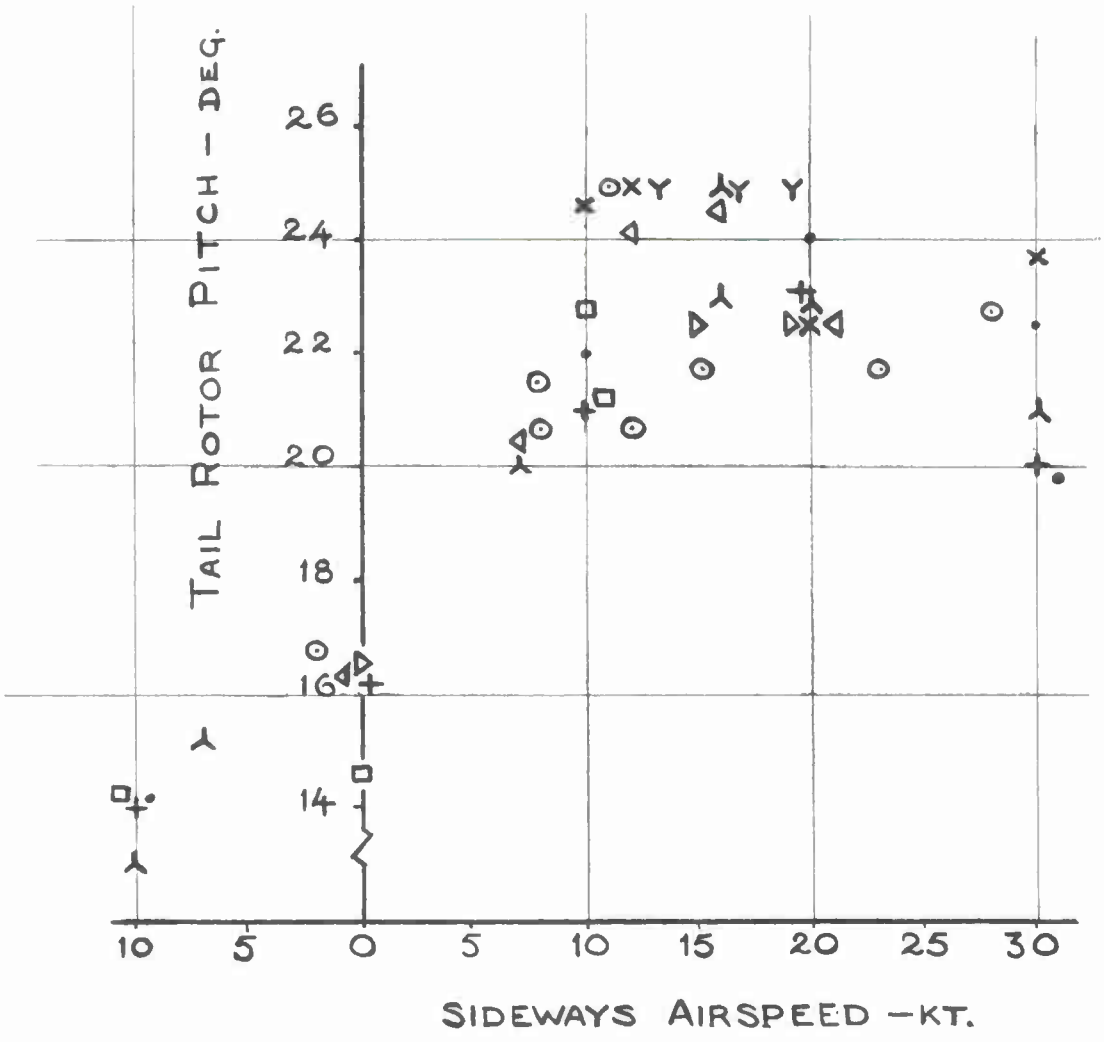


FIG. 8 STEADY SIDEWAYS FLIGHT

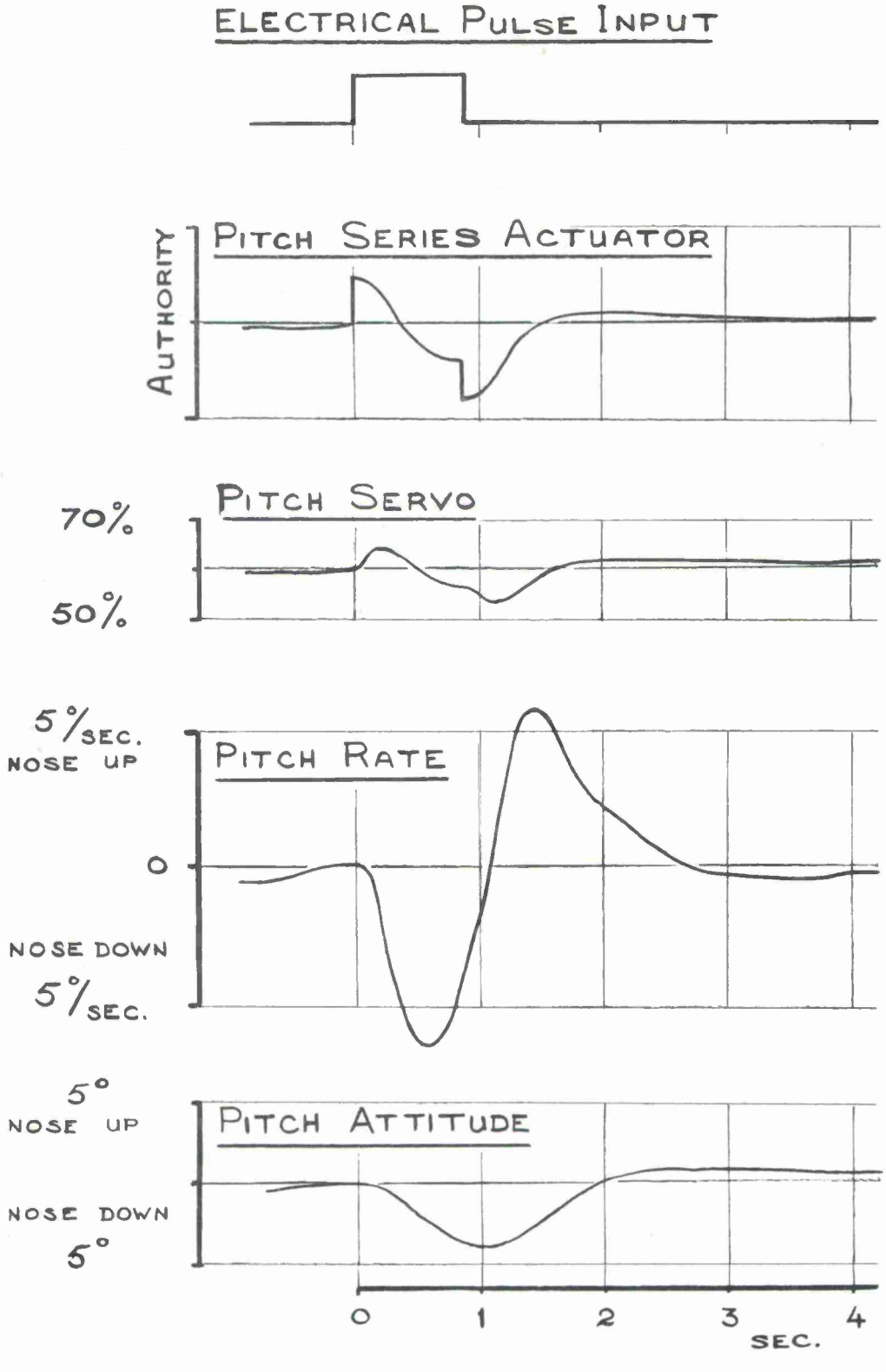


FIG. 9 ELECTRICAL PULSE INPUT
(WITH ASE ENGAGED)